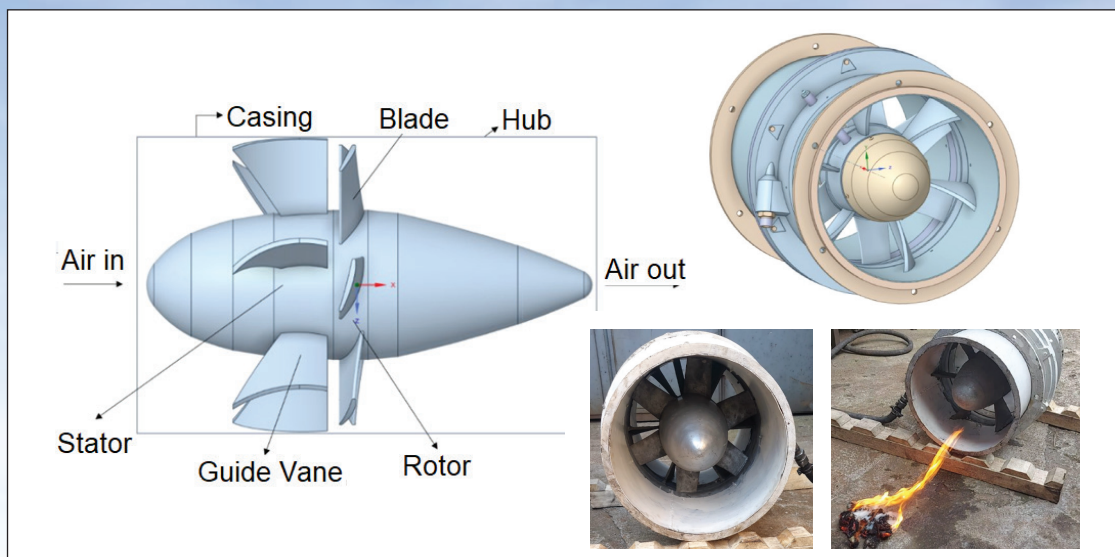




Karaelmas Fen ve Mühendislik Dergisi

Zonguldak Bülent Ecevit Üniversitesi Tarafından Yayınlankmaktadır
Published by the Zonguldak Bülent Ecevit University

Karaelmas Science and Engineering Journal



- New Schiff Base and Its Platinum Complex: Inhibition of Amyloid Aggregation
- Üç Aşamalı Derin Öğrenme Tabanlı Otomatik Araç Plakası Algılama ve Tanıma Sistemi
- Characteristics and Kinetic Analysis of Sorption Performance of Functionalised Biomass by Various Acidic Agents
- An Alternative Approach to Burden Estimation Based on Targeted Mean Fragment Size Using Rock Fragmentation Models
- Techno-Economic Assessment of a Hybrid Renewable Energy Powered Electric Vehicle Charging Station For Shopping Mall in Edirne, Turkey
- Yapım İşlerinde İhale Parametreleri Kullanılarak Makine Öğrenmesi ile Sözleşme Bedeli Tahmini
- Generation of Synthetic Data Using Breast Cancer Dataset and Classification with Resnet18
- Detection of Pipes Decreasing Residual Chlorine Via Wall Reaction Coefficient in Water Distribution Networks
- Forecasting Earthquake Impact Scenarios in İstanbul with Machine Learning Algorithms
- On Convergence in Quaternion-Valued g-Metric Space
- Tire (İzmir) İlçesinin Atmosferik Polenleri
- Determination of Prosulfocarb in Potato Flour Samples by Gas Chromatography-Mass Spectrometry
- Çeşitli Tekrarlayan Sınır Ağları Kullanarak Siber Saldırı Tespiti
- Investigation of a New Blade Design to Improve the Efficiency of an Axial Fan Used in an Underground Mine
- Kestel Bölgesinde (Kadınhanı-Konya) Yetişen Bazı Makromantarların Antimikrobiyal Aktivitelerinin Araştırılması

Cilt / Volume: 14
Sayı / Number: 3
Kasım / November 2024

ISSN: 2146-4987
E-ISSN: 2146-7277



<https://dergipark.org.tr/tr/pub/karaelmasfen>
<https://dergipark.org.tr/en/pub/karaelmasfen>


Karaelmas Fen ve Mühendislik Dergisi

Dergi web sayfası: <https://dergipark.org.tr/tr/pub/karaelmasfen>
 Zonguldak Bülent Ecevit Üniversitesi Yayın Organı
Official Journal of Zonguldak Bülent Ecevit University

Zonguldak Bülent Ecevit Üniversitesi Adına Sahibi <i>Owner on Behalf of Zonguldak Bülent Ecevit University</i>	İsmail Hakkı ÖZÖLÇER Zonguldak Bülent Ecevit Üniversitesi Rektörü
Baş Editör/Editor in Chief	Yılmaz YILDIRIM Zonguldak Bülent Ecevit Üniversitesi, Mühendislik Fakültesi
Sorumlu Müdür/Publishing Manager	Yasin HAZER Zonguldak Bülent Ecevit Üniversitesi, Eczacılık Fakültesi
Yönetim Yeri/Head Office	Zonguldak Bülent Ecevit Üniversitesi, Mühendislik Fakültesi Dekanlığı, 67100, İncivez, Zonguldak
Redaksiyon ve Teknik Destek/ <i>Redaction and Technical Support</i>	Salih ERDEM Zonguldak Bülent Ecevit Üniversitesi Havva KARAHAN Zonguldak Bülent Ecevit Üniversitesi, Fen Fakültesi
Yazışma Adresi/Correspondence Address	Zonguldak Bülent Ecevit Üniversitesi, Fen Bilimleri Enstitüsü, Farabi Kampüsü, İncivez, 67100, Zonguldak Tel : +90 0372 291 11 00
İnternet Adresi/Web Address	https://dergipark.org.tr/tr/pub/karaelmasfen
Yayinevi/Publishing House	Buluş Tasarım ve Matbaacılık Hizmetleri, Bahriye Üçok Cad. 9/1 06500 Beşevler, Ankara, Tel: +90 312 222 44 06 Faks: +90 312 222 44 07 www.bulustasarim.com.tr
Yayın Türü/Publication Type	Yerel Süreli / <i>Periodical</i> Yilda üç sayı yayımlanır: Nisan, Temmuz, Kasım <i>Published three issues per year: April, July, November</i> ISSN: 2146-4987
E-posta /Email	havaatar@beun.edu.tr

Bu dergideki yazıların dergi standartlarına uygunluğunun kontrolü, dizimi, derginin yayına hazır hale getirilmesi BULUŞ Tasarım ve Matbaacılık Hizmetleri San.Tic. tarafından gerçekleştirilmiştir.

Review of the articles in the journal to make sure they conform to publishing standards, typesetting, getting the journal ready for publication and finally the publishing process has been the responsibility of Buluş Design and Printing Services Company.

**Karaelmas Fen ve Mühendislik Dergisi**Dergi web sayfası: <https://dergipark.org.tr/tr/pub/karaelmasfen>

Yılda üç sayı yayımlanır

Published three issues per year



Baş Editör <i>Editor in Chief</i>	Yılmaz YILDIRIM	Zonguldak Bülent Ecevit Üniversitesi, Mühendislik Fakültesi <i>Zonguldak Bülent Ecevit University, Faculty of Engineering</i>
Yardımcı Editörler <i>Associate Editors</i>	Rukiye UZUN ARSLAN Yasin HAZER Salih ERDEM	Zonguldak Bülent Ecevit Üniversitesi, Mühendislik Fakültesi <i>Zonguldak Bülent Ecevit University, Faculty of Engineering</i> Zonguldak Bülent Ecevit Üniversitesi, Eczacılık Fakültesi <i>Zonguldak Bülent Ecevit University, Faculty of Pharmacy</i> Zonguldak Bülent Ecevit Üniversitesi <i>Zonguldak Bülent Ecevit University</i>
İngilizce Redaksiyon <i>English Redaction</i>	Özgür ZEYDAN Can Murat DİKMEN Nizamettin ÖZDOĞAN	Zonguldak Bülent Ecevit Üniversitesi, Mühendislik Fakültesi <i>Zonguldak Bülent Ecevit University, Faculty of Engineering</i> Zonguldak Bülent Ecevit Üniversitesi, Fen Fakültesi <i>Zonguldak Bülent Ecevit University, Faculty of Science</i> Zonguldak Bülent Ecevit Üniversitesi, Mühendislik Fakültesi <i>Zonguldak Bülent Ecevit University, Faculty of Engineering</i>
Sorumlu Müdür <i>Publishing Manager</i>	Yasin HAZER	Zonguldak Bülent Ecevit Üniversitesi, Eczacılık Fakültesi <i>Zonguldak Bülent Ecevit University, Faculty of Pharmacy</i>
Uluslararası Yayın Kurulu <i>International Editorial Board</i>	Ahmet ÖZASLAN Akira HIRAO Baki HAZER Boris NATALIN Claude TOUZET David W. STANLEY Enver DURMUŞOĞLU Ferhan ATICI Figen KAYA Haluk GÜVEN İskender YILGÖR İsmail Hakkı ÖZÖLÇER Kemal BÜYÜKGÜZEL Mahmut ÖZER Martin BOHNER Mehmet KARATAŞ Mehmet YAMAN Melih GENİŞ Mustafa SÖZEN Münevver PINAR Neil CUMBERLIDGE Nursel GÜL Per Nicolai MARTENS Rafat SIDDIQUE Remzi KARAGÜZEL Suna CEBEZOY Şahnaz BOLKENT Ten FEIZI Türkan KOPAÇ Umut TOPRAK Yılmaz YILDIRIM	Zonguldak Bülent Ecevit University, Zonguldak, Türkiye Tokyo Institute of Technology, Japan Kapadokya University, Nevşehir, Türkiye İstanbul Technical University, İstanbul, Türkiye University of Provence, Marseille Cedex, France Agricultural Research Service-USDA, United States Ege University, İzmir, Türkiye Western Kentucky University, United States Yıldız Technical University, İstanbul, Türkiye Zonguldak Bülent Ecevit University, Zonguldak, Türkiye Koç University, İstanbul, Türkiye Zonguldak Bülent Ecevit University, Zonguldak, Türkiye Zonguldak Bülent Ecevit University, Zonguldak, Türkiye Milli Eğitim Bakanlığı, Ankara, Türkiye Missouri University of Science and Technology, United States Necmettin Erbakan University, Konya, Türkiye Bolu İzzet Baysal University, Bolu, Türkiye Zonguldak Bülent Ecevit University, Zonguldak, Türkiye Zonguldak Bülent Ecevit University, Zonguldak, Türkiye Ankara University, Ankara, Türkiye Northern Michigan University, Michigan, United States Ankara University, Ankara, Türkiye RWTH Aachen University, Germany Civil Engineering Thapar University, Paitala (Punjab), India İstanbul Technical University, İstanbul, Türkiye Ankara University, Ankara, Türkiye İstanbul University, İstanbul, Türkiye Imperial College London, United Kingdom Zonguldak Bülent Ecevit University, Zonguldak, Türkiye Ankara University, Ankara, Türkiye Zonguldak Bülent Ecevit University, Zonguldak, Türkiye



AMAÇ ve KAPSAM

Karaelmas Fen ve Mühendislik Dergisi (<https://dergipark.org.tr/tr/pub/karaelmasfen>), Zonguldak Bülent Ecevit Üniversitesi'nin resmi yayın organıdır.

Derginin amacı, Fen Bilimleri, Temel Sağlık Bilimleri ve Mühendislik Bilimleri alanlarında yapılan özgün araştırma makaleleri, derlemeler, kısa makaleler, teknik not, kitap eleştirileri ve bilimsel nitelikli editöre mektupları yayınlayan uluslararası ve saygın bilimsel bir dergi olmaktadır.

Bu dergide yayınlanan makaleler, bağımsız ve önyargısız çift-körleme hakemlik (peer-review) ilkeleri doğrultusunda bir danışma kurulu tarafından değerlendirilir. Makaleler başlıca altı kategoride yayımlanır: (1) "Araştırma Makaleleri", (2) "Derleme Makaleler", (3) "Kısa Makaleler", (4) "Teknik Not ve Vaka Takdimleri", (5) "Editöre Mektuplar", (6) "Kitap ve Yazılım Programı Eleştirileri". Makaleler Türkçe veya İngilizce dillerinde yazılabilir; İngilizce veya Türkçe Özeti ile anahtar sözcükler içermelidir.

Karaelmas Fen ve Mühendislik Dergisi, Nisan, Temmuz ve Kasım aylarında olmak üzere yılda üç kez yayınlanmaktadır ve <https://dergipark.org.tr/tr/pub/karaelmasfen> internet adresi üzerinden takip edilebilir.

Yayın İzni

Bireysel kullanım dışında, Karaelmas Fen ve Mühendislik Dergisi'nde yayımlanan makaleler, şekiller ve çizelgeler yazılı izni olmaksızın çoğaltılamaz, bir sistemde arşivlenmez veya reklam ya da tanıtım amaçlı materyallerde kullanılamaz.

Bilimsel makalelerde, uygun şekilde kaynak gösterilerek alıntı yapılabilir.

Abone İşlemleri

Karaelmas Fen ve Mühendislik Dergisi, Üniversite Kütüphanelerine ve bilim insanlarına düzenli olarak ulaştırılmaktadır. Yayımlanan makalelerin tam metnine, çizelgelerine ve özetlerine çevrim-içi olarak <https://dergipark.org.tr/tr/pub/karaelmasfen> adresinden ücretsiz olarak erişilebilmektedir.

Yazıların Bilimsel ve Hukuki Sorumluluğu

Yayımlanan yazıların bilimsel ve hukuki sorumluluğu yazarlarına aittir. Yazıların içeriğinden ve kaynakların doğruluğundan yazarlar sorumludur. Editör, Yardımcı Editörler, Yayın ve Danışma Kurulu üyeleri ve Yayımcı, dergideki hatalardan veya bilgilerin kullanımından doğacak olan sonuçlardan dolay sorumluluk kabul etmez.

Yazarlarımızın etik ihlalleri ile ilgili tüm iddia ve kesinleşmiş süreçler kendi sorumluluklarında olup, kesinleşen etik ihlalleri durumunda makale otomatik iptal edilir.

AIMS and SCOPE

Karaelmas Science and Engineering Journal (<https://dergipark.org.tr/en/pub/karaelmasfen>), is the official journal of Zonguldak Bülent Ecevit University.

The journal's aim is to be scientific journal publishing original papers, reviews, short communications, technical book reviews and scientific editorial letters of science in the following areas: basic sciences, basic medicine science and engineering fields.

Articles submitted to this journal are evaluated in a double blinded peer-reviewed fashion by an advisory committee. Articles are published mainly in six categories: (1) "Research articles", (2) "Review Articles", (3) "Short Communications", (4) "Technical Notes and Case Reports", (5) "Letters to the Editor" and (6) "Book/Software Reviews". All articles may be written in Turkish or English, and should include English and Turkish abstracts and key words.

Karaelmas Science and Engineering Journal is published three issues per year in April, July and November.

The journal has also been available on-line by a website: <https://dergipark.org.tr/en/pub/karaelmasfen>

Permission Requests

Manuscripts, figures and tables published in the Karaelmas Science and Engineering Journal cannot be reproduced, archived in a retrieval system, or used for advertising purposes, except personal use.

Citations may be used in scientific articles with proper referral.

Subscriptions

Karaelmas Science and Engineering Journal is delivered complimentarily to University Library and scientists Tables of contents, abstracts and full texts of all articles published are accessible free of charge through the web site <https://dergipark.org.tr/en/pub/karaelmasfen>

Scientific and Legal Responsibilities

Scientific and legal responsibilities pertaining to the papers belong to the authors. Contents of the manuscripts and accuracy of references are also at the authors' responsibility. Editor, Associate Editors, Editorial and Advisory Board members and the Publisher decline responsibility for errors or any consequences arising from the use of information contained in this journal.

All claims and finalized processes regarding violations of ethics by our authors are under their own responsibility, and in case of ethical violations, the article is automatically canceled.



YAZARLARA BİLGİLER

Karaelmas Fen ve Mühendislik Dergisi, Fen Bilimleri, Temel Sağlık Bilimleri ve Mühendislik Bilimleri alanlarında yapılan özgün araştırma makaleleri, derlemeler, kısa makaleler, teknik not, kitap eleştirileri ve bilimsel nitelikli editöre mektupları yayınlayan uluslararası bir dergidir. Nisan, Temmuz ve Kasım aylarında olmak üzere yılda üç kez yayınlanır. Dergi, <https://dergipark.org.tr/tr/pub/karaelmasfen> internet adresi üzerinden takip edilebilir.

Dergide yayınlanacak makale türleri aşağıdaki gibidir.

Araştırma makalesi: Makale mutlaka orijinal ve daha önce hiç bir dergide basılmış veya sunulmamış olmalı, makale yayılmasında sayfa sınırı kaynaklar dahil 30 sayfayı geçmemelidir.

Derlemeler: Herhangi bir araştırma alanındaki son yıllarda yaşanan gelişmeleri ve bu konuda son yıllarda yapılmış çalışmaların bir araya getirildiği makale türüdür. 15 sayfayı geçmemelidir.

Kısa makaleler: Küçük çapta yapılan çalışmalar, orijinal araştırma deneylerinin ön sonuçlarından, yeni buluşlar ve klinik deneylerden oluşmalı ve 5 sayfayı geçmemelidir.

Teknik notlar, Olgu sunumları: Bilimsel olarak önemli katkı sunan raporlardan oluşmalı ve 3 sayfayı geçmemelidir.

Editöre mektuplar: Herhangi bir araştırma konusuna ait fikirler, haberleri, önerileri kapsamlıdır ve 2 sayfayı geçmemelidir.

Kitap veya yazılım programlarına ait eleştiriler: Kitap veya yazılım programı hakkındaki kısa ve özet bilgileri içermelidir ve 1 sayfayı geçmemelidir.

YAYIN KURALLARI

Dergide yayınlanacak makalelerin yazım dili Türkçe veya İngilizcedir. Yazım kurallarına uymayan makaleler, hakemlere gönderilmeden düzeltilmek üzere yazarla geri gönderilir. Bu nedenle derginin yazım kuralları dikkate alınmalıdır. Makaleler şekiller ve çizelgeler dahil 20 sayfayı geçmemelidir. Dergiye yayın için gönderilen makaleler iki uzman hakem tarafından değerlendirilir ve yayılmasına editör tarafından karar verilir. Dergiye gönderilen yazılar başka bir yerde yayınlanmamış veya yayımlamak üzere gönderilmemiş olmalıdır. Dergide yayınlanmak üzere kabul edilmiş olan yazıların yayın hakları Karaelmas Fen ve Mühendislik Dergisine aittir. Düzeltilmiş yazılar 3 ay içerisinde editöre gönderilecektir.

DEĞERLENDİRME SÜRECİ

Dergi yönergelerine uymayan yazılar, bilimsel değerlendirme yapılmadan yazarlara iade edilecektir. Dergi yönergelerine uygun olarak gönderilen makaleler, onları hakemlere atayacak olan Baş Editör veya Yardımcı Editör tarafından incelenir. İnceleme süreci tek kórdür. Hakem önerileri, alan editörlerinin görüşleri ve yayının literatüre katkısı doğrultusunda Editör karar mektubunu yazar. İncelenmemiş tüm yazılar 10 gün içinde geri gönderilir ve yazıların karar mektupları 3-6 ay içinde gönderilir.

Makalelerdeki tüm değişiklikler yazarları tarafından yapılır. Son şekli verilen ve yayına hazırlanan makaleler üzerinde yazarlarca bir değişiklik yapılamaz. Her ne nedenle olursa olsun makalesinin yayınlanmasından vazgeçen bir yazar, makalesini dergiye sunum tarihinden itibaren en fazla iki ay içerisinde çekebilir. Hayvan deneylerinde etik kurul izin belgesi gereklidir.

MAKALE SUNUMU

Makaleler elektronik ortamda sunulacaktır.

YAZIM KURALLARI

- Makale A4 boyutlu kağıda, tek yüze, tüm kenarlardan 2.5 cm boşluk bırakılarak bir buçuk (1.5) satır aralıklı ve iki yana yashı yazılmalıdır. Dergimizin yazım kurallarına ulaşmak için lütfen linke tıklayınız.
<https://dergipark.org.tr/tr/pub/karaelmasfen/writing-rules>
- Yazım biçimi tüm metin için **Times New Roman yazı tipi** ve **12 punto** Microsoft Word kullanılarak hazırlanmalıdır. Metnin tamamı siyah-beyaz renkte olmalıdır.
- Satır başları ilk sayfadан itibaren sürekli olarak (şekiller, çizelgeler ve kaynaklar dahil olmak üzere) numaralandırılmalıdır. Sayfa numaraları, sayfaların alt orta bölümlerine konmalıdır.
- Eserin sisteme yüklenen Tam Metin dosyasında kör hakemlikten dolayı yazarla ait bilgiler verilmemelidir. Yazara ait bilgiler Kapak Sayfasında yer almmalıdır.
- Makalenin ana bölümleri, Türkçe Öz, İngilizce Öz (Abstract), Giriş, Geçmiş ve yöntem(ler) (Saha tanımlamaları, çalışılan malzeme vd. Yöntemler kısmının altında alt başlık olarak verilmelidir), Bulgular ve tartışma, Sonuç ve Öneriler ve Kaynaklardan oluşur.
- Latince isimler italic olarak yazılmalıdır.
- Makale yayılmasında SAYFA SINIRI kaynaklar dahil 30 sayfayı geçmemelidir.

Kapak Sayfası: Kapak Sayfası ayrı Microsoft Word dosyası olmalıdır. Kapak Sayfasında başlık, tüm yazarın tam adı, kurumlar ve ORCID'ler; sorumlu yazarın iletişim adresi ve e-posta adresi verilmelidir.

Kapak Yazısı Planı:

- Makale türü
- Türkçe ve İngilizce başlık
- Yazar adları ve adresleri
- Sorumlu yazarın adı, adresi ve e-posta adresi
- Kısa başlık
- Tüm yazarların ORCID'leri
- Etik gerektiren tüm çalışmaların Etik Kurul Kararı eklenmelidir.

Tam Metin Sayfasının Planı

İlk sayfa Özet Sayfasıdır. Özet Sayfasının planı aşağıdaki gibi olmalıdır:

1. Türkçe makalelerde

a) Türkçe Başlık (12 Punto)	d) Anahtar Kelimeler (12 Punto)*
b) İngilizce Başlık (İtalik, 12 Punto)	e) Abstract (12 Punto)
c) Öz (12 Punto)	f) Keywords (12 Punto)
2. İngilizce makalelerde

a) English Title (12 punto)	d) Keywords (12 punto)*
b) Türkçe Başlık (İtalik 12 punto)	e) Öz (12 punto)
c) Abstract (12 punto)	f) Anahtar Kelimeler (12 punto)

*Anahtar kelimelerden sadece ilk anahtar kelimenin ilk harfi büyük diğerlerinin ilk harfleri küçük olmalıdır.



Başlık: Metin ile uyumlu, kısa ve anlaşılır olmalıdır. Ortalanmış olarak, sadece ilk harfi büyük sonraki küçük, 12 punto ve koyu olmalıdır.

Yazar adları ve adresleri: Başlığın altındaki yazar isimleri kısaltması (Akademik unvan kullanılmamalıdır), adı ve soyadı (varsayı ikinci ismi veya soy ismi) küçük harf ile ortalanmış olarak 12 punto ve koyu yazı karakteri ile yazılmalıdır. Yazar isimlerinden sonra adres belirtmek için üst simge olarak rakam kullanılmalıdır (¹²³ gibi). Sorumlu yazar isminde yıldız sembolü olmalıdır (*). Yazarların tam adresleri küçük harfle, ortali ve 12 punto olarak yazılmalı, sırasıyla Üniversite, Fakülte, Bölüm, Şehir ve Ülke belirtilmelidir. Sorumlu yazarın e-posta adresi, adresinin sonunda mutlaka verilmelidir.

Öz ve Anahtar Kelimeler: Özetter 12 punto ile yazılmalı, maksimum 250 kelime olmalıdır. Özetter makaleden elde edilen sonuçları ortaya koymalıdır. Türkçe ve İngilizce özetter altında makale başlığında geçmeyen 3-5 kelimeden oluşan Anahtar kelimeler yazılmalıdır. Anahtar kelimeler alfabetik sıraya göre verilmelidir. Anahtar kelimelerden sadece ilk anahtar kelimenin ilk harfi büyük diğerlerinin ilk harfleri küçük olmalıdır. Anahtar kelimeler virgül ile ayrılmalı ve sonra bir karakter boşluk bırakılmalıdır.

Anahtar kelimelerden sonra arada bir satır bırakılarak Giriş bölümü başlatılmalıdır. Tam metinlerde makaledeki ana başlıklar ve varsa alt başlıklar anlaşılır olmalıdır. Ana metin başlıkları sola hizalı, sadece ilk kelimenin ilk harfi büyük ve koyu renkli olmalıdır. Alt başlıklar küçük ve italik yazılmalıdır. Ana ve alt başlıklara numara verilmelidir.

Giriş: Araştırmının amacı, önemi ve konusunda yapılmış yayınlar arasındaki yeri belirtilmelidir.

Gereç ve Yöntem(ler): Uygulanan yöntemler ve teknikler anlaşılır bir şekilde verilmelidir. Daha önce yapılmış referanslar ile desteklenmelidir. İstatistiksel modeller ve analiz yöntemleri açıkça belirtilmelidir.

Bulgular ve Tartışma: Bu bölümde elde edilen bulgulara yer verilmeli, bulgular gerekirse şekil ve çizelgelerle desteklenmelidir. Elde edilen bulgular ilgili literatürlerle karşılaştırılmalıdır. Bulguların benzer ve farklılıklarını yorumlanarak, çalışmadan elde edilen bulgular özetlenmelidir.

Sonuç ve Öneriler: Sonuçlar özetlenmeli ve öneriler yapılmalıdır.

Teşekkür: Araştırmaya destek olan kişi ve kuruluşlara yapılan teşekkürleri içermelidir.

Her türlü çıkar çatışması, finansal destek, yazarların katkı beyanı, bağış ve diğer editorial (istatistik analiz, İngilizce/Türkçe değerlendirme) ve/veya teknik yardım var ise metnin sonunda sunulmalıdır.

Yazar Katkısı: Yazar A: çalışmaı planlamış ve tasarlamıştır, Yazar B: Çalışma hakkında verileri toplamış ve analiz etmiştir, Yazar C: Çalışmanın analizlerini yaparak makaleyi yazmıştır.

Etik Kurul Onayı: Eğer varsa etik kurul onayı eklenmelidir. Üzerinde etik kurul onayını veren kurum, onay numarası ve tarih yazılmalıdır.

Kaynaklar: Gönderilen makalelerin kaynakça kısmı hariç genel benzerlik oranı %20'yi geçmemelidir. Her türlü intihal içeren makale otomatik olarak reddedilecektir. amış bilgiler kaynak olarak verilmemelidir. Ancak, tamamlanmış ve jüriiden geçmiş tezler kaynak olarak verilebilir. Kaynaklar, makale sonunda alfabetik sıradır (yazar soyadlarına göre) verilmeli, yazar adı ve soyadları, makalenin basım tarihi koyu olarak yazılmalıdır.

İntihal Raporu: Gönderilen makalelerin kaynakça kısmı hariç genel benzerlik oranı %20'yi geçmemelidir. Her türlü intihal içeren makale otomatik olarak reddedilecektir.

Telif Hakkı Devir Sözleşmesi: Sayfada yer alan "Copyright Transfer Form" bağlantısına tıklayarak açılan form doldurulmalıdır, imzalı yüklenmelidir. Dergimizin telif hakkı devir sözleşmesine ulaşmak için lütfen linke tıklayınız.

<https://dergipark.org.tr/tr/pub/karaelmasfen/page/10931>

Kaynakların metin içerisindeki kullanımı aşağıda verilmiştir:

1. Türkçe Makalelerde:

Tek yazarlı çalışma (Aliskan 2021). İki yazarlı çalışma (Yıldırım ve Topaloğlu 2018) şeklinde belirtilmelidir.

Üç ve daha fazla yazar söz konusu ise (Yılmaz vd. 2007, Erdem vd. 2022) şeklinde, aynı yazarın birden fazla makalesi kullanılacaksa (Erdem vd. 2022a, 2022b) şeklinde olmalıdır.

Herhangi bir kaynaktan alıntı yapılmışsa: Karahan ve Çölgeçen (2021)'e göre..... şeklinde olmuştur; Yılmaz vd. (2007)'e göre; diye yazılmalıdır.

2. İngilizce Makalelerde:

Tek yazarlı çalışma (Aliskan 2021). İki yazarlı çalışma (Yıldırım and Topaloğlu 2018). Herhangi bir kaynaktan alıntı yapılmışsa.... according to Ünlü and Gerçek (2023)... şeklinde olmalıdır diye belirtilmelidir.

Üç ve daha fazla yazardan oluşan çalışmalar (Evans et al. 2023, Landen et al. 2021) şeklinde olmalıdır. Alıntı yapılacaksa.... according to Landen et al. (2021)... diye yazılmalıdır.

Kaynak gösterilecek yanında kaç isim varsa, kaynaklar bölümünde tümü belirtilmeli, kısaltma yapılmamalıdır.

Türkçe ve İngilizce makalelerde, yazılım programları metin içerisinde ismi ve yili belirtilerek (IBM SPSS Statistics 2016) şeklinde verilmelidir.

Kaynakların metin sonunda veriliş şekilleri aşağıdaki gibidir:

Kaynaklar alfabetik sıraya göre yazılmalıdır.

Makale:

Tek yazarlı

Işınkaralar, K. 2022. Theoretical removal study of gas BTEX onto activated carbon produced from Digitalis purpurea L. biomass. Biomass Convers. Biorefin., 12(9): 4171-4181. Doi: 10.1007/s13399-022-02558-2

İki yazarlı

Eker Şanlı, G., Tasdemir, Y. 2022. Accumulations and temporal trends of polychlorinated biphenyls (PCBs) in olive tree components. Environ. Geochem. Health., 44(8): 2577-2594. Doi:10.1007/s10653-021-01046-2

Yaralı, O., Duru, H. 2016. Investigation into effect of scratch length and surface condition on Cerchar abrasivity index. Tunn. Undergr. Space Technol., 60: 111-120. Doi: 10.1016/j.tust.2016.08.005

Üç ve daha fazla yazarlı

Erdem, S., Gonca, E., Başoğlu, G., Aydemir, E. 2022. İskemi sonrası verilen kannabidiol reperfüzyon ile uyarılan aritmilere karşı koruyucu etkilidir. Med. J. West Black Sea, 6(1): 16-23. Doi: 10.29058/mjwbs.1016783

Erkaymaz, O., Yapıcı, İS., Uzun Arslan, R. 2021. Effects of obesity on time-frequency components of electroretinogram signal using continuous wavelet transform. Biomed. Signal Process Control, 66: 102398. Doi: 10.1016/j.bspc.2020.102398

Öztürk, Ş., Hazer Y., Kaşkatepe, B., Çölgeçen, H., Kulak, M. 2023. Kırmızı kantaron (*Hypericum capitatum*) bitkisi: fenolik içeriklerinin, antioksidan aktivitesinin belirlenmesi ve klinik izolatlar üzerinde antimikrobiyal etkinliğinin araştırılması. Batı Karadeniz Tıp Dergisi, 7(1): 57-65. Doi: 10.29058/mjwbs.1251370

Aynı yazarın iki veya daha fazla çalışması kullanılmışsa kaynaklar tarih sırasına göre dizilmelidir.

Berndt, T.J. (2022).



Berndt, T. J. (2023)

Yedi yazardan fazla ise ilk altı yazarın adı listelendikten sonra üç nokta koyup son yazarın adı eklenir. Yedi isimden fazlası yer almamalıdır.

Miller, FH., Choi, MJ., Angeli, LL., Harland, AA., Stamos, JA., Thomas, ST.,... Rubin, LH. 2009. Web site usability for the blind and low-vision user. Technical Communication, 57: 323–335.

Kitap:

Reşat, U. 2001. Uygulamalı jeoteknik bilgiler. 4. Basım, TMMOB Jeoloji Mühendisleri Odası Yayınları, Nitelik Matbaacılık, Ankara, 385 s. Sanford, RJ. 2003.

Principles of fracture mechanics, Prentice Hall, Pearson Education, Inc. Upper Saddle River, USA, 404 pp.

Kitapta Bölüm:

Atar, H., Çölgeçen, H. 2020. Bioactive compounds of oregano seeds. Victor R. Preedy, Ronald Ross Watson [eds.], Nuts & Seeds in Health and Disease Prevention (2nd ed.). Oxford: Academic Press is an imprint of Elsevier, London, San Diego, Cambridge, pp. 73-77.

Rapor:

Makarewicz, JC., Lewis, T., Bertram, P. 1995. Epilimnetic phytoplankton and zooplankton biomass and species composition in Lake Michigan, 1983-1992. U.S. EPA Great Lakes National Program, Chicago, IL. EPA 905-R-95-009.

Kongre, Sempozyum:

Karahan, H., Çölgeçen, H. 2021. Uptake of silver nanoparticles in natural tetraploid Trifolium pratense L. calli. 10th International Molecular Biology and Biotechnology Congress, s. 56, Turkey.

Internet:

Eğer bir bilgi herhangi bir internet sayfasından alınmış ise (internetten alınan ve dergilerde yayınlanan makaleler hariç), kaynaklar bölümüne internet sitesinin ismi ve konu başlığı tam olarak yazılmalıdır.

Web sayfası:

TUİK 2023. <https://www.tuik.gov.tr/>

Yazarlı web sayfası:

Dawson, J., Smith, L. Deubert, K. 31 Ekim 2002. <http://studytrekk.lis.curtin.edu.au/> şeklinde belirtilmelidir.

Baskıda olan makale:

Evans, MA. 2023. Makale başlığı. Dergi. (DOI).

Tezler:

Duru, H. 2020. Geliştirilen cerchar aşındırıcılık deney aletiyle kayaçların spesifik çizme enerjisiniin araştırılması. Doktora Tezi, Zonguldak Bülent Ecevit Üniversitesi, 175 s.

Yazılım:

SPSS Statistics 24.0. Software, IBM, United States.

Çizelgeler ve Şekiller: Tüm şekil ve çizelgeler makale içerisinde sırayla numaralandırılmalı (Çizelge 1, Şekil 1, Çizelge 2 ve 3, Şekil 2 ve 3, Şekil 4, Çizelge 2) (şekil ve çizelgeler metin içerisinde verilmelidir.), şeklärerin sıra numaraları ve başlıkları alta, çizelgelerinki ise üstlerine iki yana yashı yazılmalıdır, metin içinde atıfları Çizelge 1, Şekil 1 şeklinde olmalıdır. Grafik ve şeklärler sayfa boyutları dikkatle alınarak çizilmelidir. Grafikler, çizimler ve fotoğraflar JPEG, PNG ya da TIFF formatında (en az 300 dpi çözünürlükte) siyah-beyaz veya renkli olarak sunulmalıdır. Fotoğraflarda büyütmeye göstermek için mutlaka bar kullanılmalıdır.

Çizelgede verilecek olan verilerde standart sapma veya standart hatalar (1.42 ± 1.36) şeklinde, istatistiksel analiz yapılmışsa (731.2ab) şeklinde, bunların başlık olarak yazılış şekilleri de ($\text{ort} \pm \text{SE}$; $\text{ort} \pm \text{SD}$, vb.) gibi olmalıdır.

Denklemler: Matematiksel ifadeler Cambria Math yazı stili ile “Equation Editör” (word ortamında) kullanılarak 12 punto ve alt ve üst indisler 12 punto yazılmalıdır. Metin içerisinde geçen eşitlikler normal parantez () içerisinde numaralandırılmalıdır. Denklem sıra numarası ile birlikte (parantez içerisinde) yazılmalıdır.

Ekler: Tüm ekler ayrı sayfaya yazılmalı ve Romen rakamları ile numaralandırılmalıdır. Matematik dalında yayın gönderecek yazarların konu sınıflandırma numarasını (AMS-Mathematical Subject Classification Number) belirtmeleri gereklidir.

Semboller ve Birimler: Metrik sistem veya SI birimleri (kPa, kN/m³, g/cm², m/sn, g/m³, vb.) kullanılmalıdır. Gerek metin içinde ve çizelgelerde, gerekse şeklärde rakamların ondalık bölgüllerinin belirtilmesi için nokta kullanılmalıdır (10.25 gibi). Yüzdelik birimler (%50) şeklinde belirtilmelidir.

Kısaltmalar: Zamanla ilgili olan kısaltmalar: sn (saniye), dkk (dakika), sa (saat), hf (hafta), y (yıl) olarak belirtilmelidir. Tarihler verilirken gün ay ve yıl kısaltma yapmadan tam olarak yazılmalıdır (19 Mayıs 2023).

Sayılar: Sayılar cümle başlarında yazı ile verilmelidir. Birden dokuza kadar olan sayılar yazı ile, 10 ve daha büyük sayılar rakamla belirtilmelidir. Birden küçük olan sayılar (0.05, 0.56, 0.50, p<0.05, vb.) olarak belirtilmelidir.

Dipnotlar: Çizelgede kullanılacak olan dipnotlar istatistiksel analiz yapıldığı durumlarda (*p<0.05; ** p<0.01; *** p<0.001; NS, istatistiksel olarak önesizdir, vb.) şeklinde olmalıdır. Derginin bir sayısında, ilk isim olarak bir yazarın üçten fazla eseri basılmalıdır. Dönemler içerisinde üçten fazla eser gönderilirse, ilk üçü dışında kalanlar daha sonraki sayılaraya aktarılır.

Makale Yazım Kontrol Listesi

Makale dergiye sunulmadan önce makalenin yazım kurallarına uygun olup olmadığından emin olmak için aşağıda belirtilen kontrolleri yapınız.

- Kapak sayfası, Tam metin sayfası, Telif hakkı bildirim formu ve İntihal raporu eklendi mi?
- İmla ve dilbilgisi kontrolü yapıldı mı?
- Tüm sayfa düzeni 1.5 satır aralıklı yazıldı mı?
- Köşelerden 2.5 cm boşluk bırakıldı mı?
- Yazı tipi Times New Roman ve büyülüğu 12 punto mu?
- Metin içerisindeki başlıklar sola hizalı, 12 punto ve koyu renkli yazıldı mı?
- Tüm yazarların adları ve soyadları kısaltma yapılmadan belirtildi mi?
- Adresler belirtildi mi?
- Başlık 12 punto koyu yazı karakteri ile ortalanarak yazıldı mı?
- Öz (Abstract) ve Anahtar kelimeler (Keywords) yazıldı mı?
- Kaynaklar yazım kurallarına göre ve alfabetik sırayla yazıldı mı?
- Ondalık dilimler nokta ile belirtildi mi? (10.25 gibi)
- Yüzdelik gösterimler (%63, %10 gibi) şeklinde yapıldı mı?
- Çizelgelerin maksimum boyutu 16x20 cm; minimum 8 cm mi?
- Çizelgelerin numaraları (Çizelge 1, Çizelge 2, Çizelge 3 vs.) makale içerisinde sırayla verildi mi?
- Orijinal şeklärler eklendi mi?
- Şeklärler yazım kurallarına uygun olarak düzenlenendi mi?
- Şeklärlerin maksimum boyutu 16x20 cm; minimum 8 cm, minimum 300 dpi mi?
- Şeklärlerin numaraları (Şekil 1, Şekil 2, Şekil 3 vs.) makale içerisinde sırayla verildi mi?
- Tüm sayfa ve satırlara numara verildi mi?



ETİK KURALLAR

Zonguldak Bülent Ecevit Üniversitesinin yayın organı olan Karaelmas Fen ve Mühendislik Dergisi ulusal ve uluslararası tüm kurum ve kişilere ücretsiz olarak ulaşmayı hedefleyen hakemli bir dergidir.

Dergimize gönderilen bilimsel yazınlarda, ICMJE (International Committee of Medical Journal Editors) tavsiyeleri ile COPE (Committee on Publication Ethics)'un Editör ve Yazarlar için Uluslararası Standartları dikkate alınmaktadır.

Yazarlarımızın etik ihlalleri ile ilgili tüm iddia ve kesinleşmiş süreçler kendi sorumluluklarında olup, kesinleşen etik ihlalleri durumunda makale otomatik iptal edilir.

Hakemler İçin Etik Kurallar

Hakemler;

- Değerlendirdiği yazıların gizliliğine saygı gösterir ve makaleyi tartışmaz veya yazı hakkında başka herhangi bir kişiyle iletişim kurmaz.
- Olası bir çıkar çatışması olduğunda editörü konu hakkında bilgilendirir.
- Önerileri için nesnel ve yapıcı bir açıklama sağlar.
- Makaleye ilişkin kararlarının konudan veya yazarlık biçiminden etkilenmesine izin vermez.
- Güçlü bir bilimsel gerekçe olmadıkça yazarın kendi makalelerini belirtmesini istemez.
- Yazarlar tarafından yayınlanmadan önce kendi çalışmalarının hiçbirinde incelenen makalenin herhangi bir bölümünü veya bilgiyi çoğaltmaz.
- Hakem değerlendirmelerini sadece uzmanlıkları dahilinde ve makul bir süre içinde kabul eder.
- Yazının yayına çıkışmasını geciktirecek ertelemleri yapmaz.
- Hakaret, düşmanca veya küçük düşürücü bir dil kullanmaz.
- Gönderilen makaleleri ve ilgili tüm materyalleri inceledikten sonra imha eder.

https://publicationethics.org/files/Ethical_guidelines_for_peer_reviewers_0.pdf

Yazarlar İçin Etik Kurallar

Yazarlar ve yardımcı yazarlar;

- International Committee of Medical Journal Editors (ICMJE) tarafından belirtilen yazar kriterlerine uygunluk sağlanır;
 - a. Eserin tasarımasına veya tasarımasına önemli katkılar sağlayan verilerin elde edilmesi, analizi veya yorumlanması
 - b. Çalışmanın hazırlanması veya literatürün içerik için eleştirel olarak gözden geçirilmesi
 - c. Yayınlanacak versiyonun nihai onayı
 - d. Çalışmanın herhangi bir bölümünün doğruluğu veya bütünlüğü ile ilgili soruların uygun şekilde soruşturulup çözülmemesini sağlamada, çalışmanın tüm yönlerinden sorumlu olacak anlaşma.
- Gönderilen makaleler yazar(lar)ın özgün çalışması olmalıdır ve eşzamanlı olarak farklı yayıncılara gönderilmemelidir

- Yazar(lar) araştırma önerisinde, icrasında ya da araştırma sonuçlarını raporlarken araştırma suistimalı olarak tanımlanan uydurma, tahrifat ya da intihalden sorumludur.
- Gönderilen makalelerde çıkar çatışması varsa editöre bilgi verilmelidir
- Gönderilen makalelerde ön kontrol, değerlendirme süreci ya da yayınlanmış olan sürümünde yazar veya yardımcı yazarlar tarafından hata fark edilirse bilgi vermek, düzeltmek ya da geri çekmek için editörü bilgilendirmelidir.
- Makale gönderildikten sonra yazar sıralamaları ve yazar eklemeye çikartmaları önerilmemelidir
- Yazar(lar), etik kurul kararı gerektiren araştırmalar için etik kurul onayı aldığı; etik kurul adı, karar tarihi ve sayısı aday makalenin ilk-son sayfasında ve yöntem bölümünde belirtmeli, etik kurul kararını gösteren belgeyi makalenin başvurusuya birlikte sisteme yüklemelidir.
- Yazarlar olgu sunumlarında olur/onam formunun alındığına ilişkin bilgiye makalede yer vermelidir.
- Kullanılan fikir ve sanat eserleri için telif hakları düzenlemelerine riayet edilmesi gerekmektedir.
- Makale sonunda; Araştırmacıların Katkı Oranı beyanı, varsa Destek ve Teşekkür Beyanı, Çalışma Beyanı verilmelidir.

<http://www.icmje.org/icmje-recommendations.pdf>

https://www.ease.org.uk/wp-content/uploads/2018/11/doi.10.20316_ESE_2018.44.e1.tr_.pdf

Editörler İçin Etik Kurallar

Editörler:

- Okuyucular, araştırmayı veya diğer bilimsel çalışmaları kimin finanse ettiği ve fon verenlerin araştırmada ve yayınlanmasında herhangi bir rolü olup olmadığı ve eğer öyleyse bunun ne olduğu konusunda bilgilendirilmelidir.
- Editörlerin yayın için bir makaleyi kabul etme veya reddetme kararları, makalenin önemi, özgürlüğü ve netliği ile çalışmanın geçerliliği ve derginin görev alanına uygunluğuna dayanmalıdır.
- Editörler, gönderimle ilgili ciddi sorunlar tespit edilmedikçe, gönderimleri kabul etme kararlarını tersine çevirmemelidir.
- Ciddi sorunlar tespit edilmedikçe yeni editörler, bir önceki editör tarafından yapılan başvuruları yayılama kararlarını bozmamalıdır.
- Hakem değerlendirmesi süreçlerinin bir açıklaması yapılmalı ve editörler açıklanan süreçlerden önemli sapmaları ortaya çıkarmalıdır.
- Yazarların editorial kararlara itiraz edebilmeleri için beyan edilmiş bir mekanizmaya sahiptir.
- Editörler, kendilerinden beklenen her şey hakkında yazarlara rehberlik etmelidir. Bu rehberlik düzenli olarak güncellenmeli ve bu koda atıfta bulunulmalı veya bu koda bağlantı vermelidir.
- Editörler, International Committee of Medical Journal Editors (ICMJE) önerdiği yazarlık kriterlerini belirtmelidir.
- Editörler, kabul etmeden önce gözden geçirilenlerin rekabet edebilecek potansiyel çıkarları ifşa etmelerini istemelidir bir sunumu gözden geçirin.



- Editörler, hakemlerin kimliklerinin korunmasını sağlayacak sistemlere sahip olmalıdır. Yazarlara ve hakemlere bildirilen açık bir inceleme sistemi kullanır.
- Editörler, yeni yayın kurulu üyelerine kendilerinden beklenen her şey hakkında kılavuzlar sunmalı ve mevcut üyeleri yeni politikalar ve gelişmeler hakkında güncel tutmalıdır.
- Editörler, derginin kalitesine ve uygunluğuna göre ve dergi sahibinin / yayınının müdafahesi olmadan hangi makalelerin yayınlanacağına karar vermelidir.
- Editörlerin derginin sahibi ve / veya yayını ile ilişkilerini belirleyen yazılı bir sözleşmesi olmalıdır. Bu sözleşmenin şartları Dergi Editörleri için COPE Davranış Kuralları ile uyumlu olmalıdır.
- Editörler dergilerindeki hakem değerlendirmelerinin adil, tarafsız ve zamanında yapılmasını sağlamak için çaba göstermelidir.
- Editörler, dergilerine gönderilen materyallerin incelenirken gizli kalmasını sağlayacak sistemlere sahip olmalıdır.
- Editörler, dergilerdeki bölümlerin farklı amaç ve standartlara sahip olacağını kabul ederek, yayınladıkları materyalin kalitesini sağlamak için tüm makul adımları atmalıdır.

<https://publicationethics.org/files/Code%20of%20Conduct.pdf>



YAYIN ETİĞİ

Karaelmas Fen ve Mühendislik Dergisinin yayın etiği beyanı, www.publicationethics.org adresinde bulunan Yayın Etiği Komitesi'nin (COPE) Davranış Kuralları kılavuzuna dayanmaktadır.

Editörlerin Görevleri

Adil ve editorial bağımsızlık

Editörler sunulan makaleleri, yazarlarınırkı, cinsiyeti, cinsel tercihi, etnik kökeni, vatandaşlığı, dini inancı, siyasi felsefesi veya kurumsal eğilimleri ne olursa olsun, sadece akademik yararları (önemi, özgünlük, çalışmanın geçerliliği, netliği) ve derginin kapsamıyla olan ilgisine göre değerlendirdirler. Düzenleme ve yayılama kararları, hükümetlerin veya derginin dışındaki diğer kurumların politikaları tarafından belirlenmez. Genel Yayın Yönetmeni, derginin tüm editorial içeriği ve bu içeriğin yayınlanması zamanlaması üzerinde tam yetkiye sahiptir.

Gizlilik

Editörler, gönderilen bir makaleyle ilgili hiçbir bilgiyi ilgili yazar, gözden geçenler, potansiyel gözden geçenler, diğer yayın danışmanları ve yayıncı dışında kimseye açıklamaz.

Açıklama ve çıkar tartışmaları

Editörler ve yayın kurulu üyeleri, gönderilen bir makalede açıklanan yayınlanmamış bilgileri, yazarların açık yazılı izni olmadan kendi araştırma amaçları doğrultusunda kullanmayacaktır. Yazının işlenmesi sonucunda editörler tarafından elde edilen ayrıcalıklı bilgi veya fikirler gizli tutulacak ve kişisel avantajları için kullanılmayacaktır. Editörler, makalelerde bağlı herhangi bir yazar, şirket veya kurumla rekabet, işbirlikçi veya diğer ilişkilerden/bağlantılardan kaynaklanan çıkar tartışmaları olan yazarını dikkate almaktan geri çekilecekler; bunun yerine, yayın kurulunun başka bir üyesinden yazımı işlemesini isteyeceler.

Yayın kararları

Editörler, yayınlanmak üzere değerlendirilen tüm makalelerin, alanında uzman en iki gözden geçenin tarafından hakem incelemesinden geçmesini sağlar. Sorumlu müdür, söz konusu çalışmanın doğrulanmasına, araştırmacılar ve okuyucular için önemine, eleştirmenlerin yorumlarına ve iftira, telif hakkı ihlali ve intihal ile ilgili su anda yürürlükte olan yasal gereklilikler dayanarak, dergiye gönderilen yazılarından hangisinin yayınlanmasına karar vermekten sorumludur. Sorumlu müdür bu kararı verirken diğer editörler veya yorumcularla görüşebilir.

Soruşturmala katılm ve işbirliği

Editörler (yayıncı ve/veya kurulla birlikte) gönderilen bir makale veya yayınlanmış makaleyle ilgili etik kaygılar ortaya çıktığında duyarlı önlemler alacaktır. Etik olmayan yayincılık davranışlarının rapor edildiği her eylem, yayımlandıktan yıllar sonra keşfedilmiş olsa bile incelenecaktır. Editörler, suistimal şüphesiyle uğraşırken COPE Akiş Şemalarını takip eder. Eğer, soruşturma üzerine, etik kaygı iyi kurulmuşsa, bir düzeltme, geri çekme, endişenin ifade edilmesi veya ilgili olabilecek diğer notlar dergide yayımlanacaktır.

Gözden Geçirenlerin Görevleri

Editorial kararlara katkı

Akran incelemesi editörlerin editorial kararlar almalarına yardımcı olur ve yazarlarla editorial iletişim yoluyla yazarların makalelerini geliştirmelerine

yardımcı olabilir. Akran incelemesi resmi bilimsel iletişimini önemli bir bileşenidir ve bilimsel çabanın merkezinde yer alır.

İstem

Bir makalede bildirilen araştırmayı gözden geçirmek için niteliksiz hissedilen veya derhal gözden geçirilmesinin imkansızlığını bilden davet edilen her hakem, editörleri derhal bilgilendirmeli ve alternatif hakemlerle iletişime geçilebilmesi için inceleme davetini reddetmelidir.

Gizlilik

İncelenmek için alınan tüm yazılar gizli belgelerdir ve bu şekilde ele alınmalıdır; Genel Yayın Yönetmeni tarafından izin verilmeyenleri surece (istisnai ve özel durumlarda bunu yapacak olanlar) başkalarıyla gösterilmemeli veya tartışılmamalıdır. Bu, inceleme davetini reddeden, davet edilen, gözden geçenler için de geçerlidir.

Nesnelliğ standartları

İncelemeler objektif olarak yapılmalı ve gözlemler, yazarların makalenin iyileştirilmesi için kullanılmamaları amacıyla destekleyici argümanlarla net bir şekilde formüle edilmelidir. Yazarların kişisel eleştirişi uygunsuzdur.

Kaynakların kabulü

Hakemler, yazarlar tarafından atıfta bulunulmamış ilgili yayımlanmış çalışmaları belirlemelidir. Önceki yıllarda rapor edilmiş bir gözlem, türetrme veya argüman olan herhangi bir ifadeye ilgili alıntı eşlik etmelidir. Bir hakem ayrıca, incelenmeye olan makale ile hakkında kişisel bilgi sahibi oldukları (yayınlanmış veya yayınlanmamış) herhangi bir diğer makale arasındaki herhangi bir önemli benzerlik veya örtüşmeyi editörlere bildirmelidir.

Açıklama ve çıkar tartışmaları

Makaleye bağlı yazarlar, şirketler veya kurumlarla rekabet, işbirlikçi veya diğer ilişkilerden kaynaklanan çıkar tartışmaları olan davet edilen hakemler, editörleri derhal çıkar tartışmalarını beyan etmeleri ve alternatif hakemlerle iletişime geçebilmeleri için inceleme davetini reddetmeleri konusunda bilgilendirmelidir.

Gönderilen bir yazida açıklanan yayınlanmamış materyaller, yazarların açık yazılı izni olmadan bir eleştirmenin kendi araştırmasında kullanılmamalıdır. Akran incelemesi yoluyla elde edilen ayrıcalıklı bilgiler veya fikirler gizli tutulmalı ve gözden geçenin kişisel avantajı için kullanılmamalıdır. Bu, inceleme davetini reddeden, davet edilen, gözden geçenler için de geçerlidir.

Yazarların Görevleri

Raporlama standartları

Orjinal araştırmaların yazarları, yapılan eserin ve sonuçların doğru bir açıklamasını sunmalı ve ardından çalışmanın önemini objektif bir tartışmasını sunmalıdır. Yazı, başkalarının eseri çoğaltmasına izin verecek yeterli ayrıntı ve referanslar içermelidir. İnceleme makaleleri doğru, objektif ve kapsamlı olmalı, editorial 'görüş' veya perspektif parçaları açıkça bu şekilde tanımlanmalıdır. Hileli veya bilerek yanlış ifadeler etik olmayan davranışlar teşkil eder ve kabul edilemez.

Veri erişimi ve saklama

Yazarlardan, çalışmalarının ham verilerini editorial inceleme için yazı ile birlikte sağlamaları istenebilir ve uygulanabilirse verileri kamuya açık



hale getirmeye hazır olmalıdır. Her halükarda, yazarlar, katılımcıların gizliliğinin korunması ve özel verilerle ilgili yasal hakların serbest bırakılmasını engellememesi koşuluyla, bu verilerin yayıldıktan sonra en az 10 yıl süreyle (tercihen kurumsal veya konu tabanlı veri deposu veya diğer veri merkezi aracılığıyla) diğer yetkili profesyonellere erişilebilirliğini sağlamalıdır.

Özgünlük ve intihal

Yazarlar sadece tamamen orijinal eserler yazdıklarından ve sunduklarından ve başkalarının çalışmalarını ve/veya sözlerini kullanmışlarsa, bunun uygun şekilde atıfta bulunulduğunu sağlamalıdır. Yazında bildirilen eserin niteliğinin belirlenmesinde etkili olan yayınlar da belirtilmelidir. İntihal, başka bir makalenin "yazarın kendi makalesi" olarak "aktarılmasından", başka bir makalenin önemli bölümlerini kopyalamaya veya paraphrasinge (atıf yapmadan), başkaları tarafından yapılan araştırmadan elde edilen sonuçların iddiasına kadar pek çok biçim alır. Tüm biçimlerinde intihal etik olmayan yayıncılık davranışını teşkil eder ve kabul edilemez.

Cöktü, yineleñen, gereksiz veya eşzamanlı gönderim/yayın

Temelde aynı araştırmayı açıklayan bildiriler birden fazla dergide veya birincil yanında yayınlanmamalıdır. Bu nedenle, yazarlar daha önce başka bir dergide yayınlanmış bir makaleyi değerlendirmek üzere göndermemelidir. Bir makalenin aynı anda birden fazla dergiye gönderilmesi etik dışı bir yayın davranışıdır ve kabul edilemez.

Bazı makale türlerinin (klinik kılavuzlar, çeviriler gibi) birden fazla dergide yapılması, belirli şartların karşılanması koşuluyla bazen haklı görülebilir. İlgili dergilerin yazarları ve editörleri, birincil belgenin aynı verilerini ve yorumunu yansıtması gereken ikincil yayını kabul etmelidir. Birincil referans, ikincil yayında belirtilmelidir.

Makalenin yazarlığı

Sadece bu yazarlık kriterlerini karşılayan kişiler, içeriğin kamuya açık sorumluluğunu üstlenebilmeleri için makalede yazar olarak listelenmelidir: (i) çalışmanın anlaşılmamasına, tasarımasına, yürütülmesine, veri edinilmesine veya analizine/yorumlamasına önemli katkılarda bulunmuştur; ve (ii) yazının hazırlanması veya önemli entelektüel içerik için eleştirel olarak revize edilmesi; ve (iii) gazetenin son halini görmüş ve onaylamış ve yayımlanmak üzere sunulmasını kabul etmiş ve kabul etmiş. Yazında bildirilen eserin önemli katkıları olan (teknik yardım, yazma ve düzeneleme yardımı, genel destek gibi) ancak yazarlık kriterlerini karşılamayan kişilerein yazar olarak listelenmemesi, yazılı izin alınmadan sonra "Bildirimler" bölümünde kabul edilmesi gerekmektedir. İlgili yazar, tüm uygun ortak yazarların (yukarıdaki tanıma göre) ve uygunsuz ortak yazarların yazar listesine dahil edilmemesini sağlamalı ve tüm ortak yazarların makalenin son halini görüp onayladığını ve yayına sunulmasını kabul ettiğini doğrulamalıdır.

Açıklama ve çıkar tartışmaları

Yazarlar mümkün olan en erken aşamada (genellikle gönderim sırasında bir açıklama formu göndererek ve makaleye bir ifade de dahil olmak üzere), sonuçları veya makaledeki yorumlarını etkilemek için yorumlanabilecek çıkar tartışmalarını ifşa etmelidir. Açıklanması gereken potansiyel çıkar tartışmalarına örnek olarak, fahri, eğitim hibeleri veya diğer finansman, konuşmacı bürolarına katılım, üyelik, istihdam, danışmanlık, hisse senedi sahipliği veya diğer hisse senedi çıkarları ile ücretli uzman ifadeleri veya patent lisanslama düzenlemeleri ile kişisel veya mesleki ilişkiler, ilgili kişiler, bilgi veya inançlar gibi finansal olmayan konular veya makalede tartışılan materyaller verilebilir. Çalışma için tüm finansal destek kaynakları açıklanmalıdır (hibe numarası veya varsa diğer referans numarası da dahil olmak üzere).

Kaynakların kabulü

Yazarlar, başkalarının çalışmalarını doğru bir şekilde kabul ettiklerinden emin olmalı ve bildirilen eserin niteliğini belirlemeye etkili olan yayınlara da atıfta bulunulmalıdır. Özel olarak elde edilen bilgiler (üçüncü şahıslarla konuşma, yazışma veya tartışma) kaynaktan açık, yazılı izin alınmadan kullanılmamalı veya rapor edilmemelidir. Yazarlar, bu hizmetlerde yer alan eserin yazarının açık yazılı iznini almamışsa, yazılara hakemlik veya hibe başvuruları gibi gizli hizmetlerin sağlanmasında elde edilen bilgileri kullanmamalıdır.

Tehlikeler ve insan veya hayvan denekleri

Çalışma, kullanımlarında olağandışı tehlikeler etüt eden kimyasallar, prosedürler veya ekipmanlar içeriyorsa, yazarlar bunları yazıda açıkça tanımlamalıdır. Eğer çalışma hayvanların veya insan katılımcıları kullanımını içeriyorsa, yazarlar tüm prosedürlerin ilgili yasalara ve kurumsal yönelerde uygun olarak gerçekleştirildiğinden ve ilgili kurumsal komitenin bunları onayladığından emin olmalıdır; yazı bu yönde bir ifade içermelidir. Yazarlar ayrıca, insan katılımcılarla deneyler için bilgilendirilmiş onam aldığına dair bir ifadeyi de makaleye eklemelidir. İnsan katılımcılarının gizlilik haklarına her zaman uyulmalıdır.

Akran incelemesi

Yazarlar, editörlerin ham veri, açıklama ve etik onayı, hasta onayları ve telif hakkı izinleri için isteklerine derhal yanıt vererek akran değerlendirme sürecine katılmak ve tam işbirliği yapmak zorundadırlar. İlk olarak "revizyon gerekliliği" kararı verilmesi durumunda yazarlar, hakemlerin yorumlarına sistematik olarak, her noktasına zamanında yanıt vererek, makalelerini verilen son tarihe kadar gözden geçirip dergiye yeniden göndermelidir.

Yayınlanan çalışmalarındaki temel hatalar

Yazarlar kendi yayınlanmış çalışmalarında önemli hatalar veya yanlışlıklar bulduklarında, derginin editörlerini veya yayınımcısını derhal bilgilendirmek ve çalışmaya bir hata biçiminde düzeltmek veya geri çekmek için onlarla işbirliği yapmak onların yükümlülüğüdür. Editörler veya yayıncı, yayınlanmış bir çalışmanın önemli bir hata veya yanlışlık içerdiğini üçüncü bir taraftan öğrenirse, makalenin doğruluğunu dergi editörlerine derhal düzeltmek veya geri çekmek veya dergi editörlerine kanıt sunmak yazarların yükümlülüğüdür.



INSTRUCTIONS to AUTHORS

Karaelmas Science and Engineering Journal is the international scientific journal publishing original papers in English or Turkish, reviews, short communications, technical notes and scientific editorial letters of science in the following areas: basic sciences, basic medicine science and engineering fields. This journal publishes three times a year (April, July and November). Manuscripts should be submitted online by a website: <https://dergipark.org.tr/en/pub/karaelmasfen>

Manuscript Categories:

Research articles: Manuscripts should report original information which have not been published or submitted previously. Full text should not exceed 30 pages including references.

Review articles: Reviews of recent developments in a research fields and ideas will be accepted. Manuscripts should not exceed 15 papers of printed text. The use of tables and figures to summarize critical points is encouraged.

Short communications: These include small-scale investigations, innovative methods, perspectives on existing laboratory techniques and new methodologies, clinical trials and epidemiological studies. It should no exceed 5 printed pages.

Technical notes or Case Reports: Scientific reports providing important contributions their area will be considered in this category. It should not be exceed 3 pages.

Letters to editor: These include opinions, news and suggestions. Letters should not exceed 2 pages.

Book/Software Reviews: Short but concise description of the book/software, not exceeding a page. These types are not peer reviewed.

CONDITIONS FOR PUBLICATION

Journal articles are published in Turkish or English. Manuscript should be suitable to the formal criteria of Instructions to Authors, otherwise, the manuscript will be sent back to the authors. Manuscripts should not exceed 20 papers of printed text, including tables, figures and references. Manuscripts that are found suitable for peer review will be assigned to two expert reviewers. The final decision to accept or reject a manuscript will be made by the Editor-in-Chief. After review process, the Editor-in-Chief will inform the authors of acceptance, rejection or necessity of revision of the manuscript. The paper has not already been published elsewhere and it is not currently being considered for publication elsewhere. If accepted, Karaelmas Science and Engineering Journal have exclusive license to publish. Review process is three months.

THE REFEREE PROCESS

Manuscripts that do not comply with the journal's guidelines will be returned to the authors without scientific evaluation. Articles submitted in accordance with the journal's guidelines are reviewed by the Editor-in-Chief or Assistant Editor, who will appoint them to referees. The review process is one-blind. The Editor writes the decision letter in line with the recommendations of the referees, the opinions of the field editors and the contribution of the publication to the literature. All unexamined manuscripts are returned within 10 days, and the decision letters of the manuscripts are sent within 3-6 months.

PRESENTATION

Papers should be submitted online.

The submitted articles should consist of four separate files: "**Cover Page**", "**Blind Article-Full Text**", "**Plagiarism Report**" and "**Copyright Transfer**

Form". Articles should be sent to Karaelmas Science and Engineering Journal via <https://dergipark.org.tr/tr/login>

WRITING RULES

Manuscripts should be written double space on A4 sized typing paper with 2.5 cm all margins, with 1.5 line spacing and justified on both sides. Please click on the link to access the writing rules of our journal.

<https://dergipark.org.tr/tr/pub/karaelmasfen/writing-rules>

- Text should be prepared using Microsoft Word with Times New Roman font and 12 point size. All text should be in black and white.
- All lines should be numbered continuously (including figures, tables and references). Page numbers should be placed in the bottom middle of the pages.
- The author's information should not be given due to blind refereeing, in the Full Text. Author's information should be on the Cover Page.
- Full text should be consist of Turkish Abstract, English Abstract, Introduction, Materials and method(s) (Area descriptions, Study materials, e.g. should be cited as subheadings), Results and Discussion, Conclusion and Suggestions, and References.
- Latin expression should be typed in italics.
- Full text should not exceed 30 pages including references.

Cover Page

The Cover Page should be a separate Microsoft Word file. Title, full name of all author, institutions and ORCIDs on Cover Page; Contact address and e-mail address of the responsible author should be given.

The Plan of Cover Page

- The article type should be write (Research article, review article, technical note, etc.). The article type should be centered at the top of the page.
- Turkish and English title
- Author's names and addresses: All Authors full names must be written as lower case with bold 12 font size in the middle. After authors name and surnames, authors addresses should be stated with superscript numbers (e.g. 1 2 3). Corresponding author's full name should be marked with an asterisks (*). All authors addresses must be typed with lower case 12 font in the center. The corresponding author's contact address and e-mail address should be given, and University, Faculty, Department, City and Country should be specified, respectively. Names of institutions and cities each authors also must be stated.
- Corresponding author's name, address and e-mail address
- Short title
- ORCIDs of all authors (Authors' ORCIDs should be added as footnotes.)
- Ethics Committee Decision should be attached to all studies that require ethics.

https://trdizin.gov.tr/wp-content/uploads/2022/04/TRDizin_etik_ilkeleri_akis_semasi.pdf

The Plan of the Full Text Page

The first page is the Summary Page. The plan of the Summary Page should be as follows (Table 1):



Table 1: The Plan of Full Text Page

The Plan of the Full Text Page	
English Title (12 punto)	<i>Turkish Title (İtalik 12 punto)</i>
Abstract (12 punto)	Öz (12 punto)
Keywords (12 punto)*	Anahtar Kelimeler (12 punto)

*Of the keywords, only the first letter of the first keyword should be capitalized and the first letters of the others should be lowercase.

The title: The title should be as short as possible, but give adequate information regarding the contents. Title must be written on the center with bold 12 font size. The first letter must be capital and the others must be written as lower case.

Abstract and Keywords: A brief, informative English and Turkish abstract, not exceeding 250 words, should be typed in 12 font size. Immediately following the abstract, authors should provide 3-5 English and Turkish keywords or phrases that reflect content of the article. Keywords should be given in alphabetical order. Only the first letter of the first keyword should be capitalized, the first letters of the others should be lowercase. Keywords must be separated by commas and followed by a space of one character.

The Introduction section should be started by leaving a line in between after the keywords. In full texts, the main headings in the article and subheadings, if any, should be understandable. Main text headings should be left aligned, only the first letter of the first word should be capitalized and bold. Subheadings should be written in 12 points and italic. Main and sub-headings should be numbered.

Introduction: This section should include the topic and importance of the article and prior works.

Material and Methods: The methods and techniques applied should be understandable. It should be supported by previous references. Statistical models and methods of analysis should be clearly stated.

Results and Discussion: The results contain only findings, no writing comment, and the results should be supported by figures and tables if necessary. The results should be compared with the relevant literature, and compare with other studies and discuss similarity and distinction.

Conclusion and Suggestions: Results should be summarized and recommendations made.

Acknowledgments: It should include thanks to the people and organizations supported the research.

Any conflict of interest, financial support, author's statement of contribution, donation and other editorial (statistical analysis, English/Turkish evaluation) and/or technical assistance should be presented at the end of the text.

Author contribution: Author A: Planned and designed the study, Author B: Gathered and analyzed data about the study, Author C: Wrote the article by analyzing the study.

Ethics committee approval: If available, ethics committee approval should be added. The institution giving the ethics committee approval, approval number and date should be written on it.

References: Unpublished information should not be given as a source. However, the theses that have been completed and passed the jury can be given as a source. References should be given at the end of the article in alphabetical order (according to the surnames of the authors), author's names and surnames, and the publication date of the article should be written in bold.

Plagiarism report: The general similarity rate of the submitted articles **should not exceed 20%**, excluding the bibliography. Any plagiarizing article will be automatically rejected.

Copyright transfer agreement: The form opened by clicking on the "Copyright Transfer Form" link on the page should be filled, signed and uploaded. Please click on the link to access the copyright transfer agreement of our journal.

<https://dergipark.org.tr/tr/pub/karaelmasfen/page/10931>

The use of sources in the text is given below:

1. In Turkish Paper:

- One author (Alışkan 2021). Two authors (Yıldırım ve Topaloğlu 2018).
- In the case of multiple authors they should be cited as (Yılmaz vd. 2007, Erdem vd. 2022), multiple publications by same author(s) should be written as (Erdem vd. 2022a, 2022b).
- If any source is cited: According to Karahan and Çölgeçen (2021), it was as....; according to Yılmaz et al. (2007); it should be written.

2. In English Paper:

- One author (Alışkan 2021). Two authors (Yıldırım and Topaloğlu 2018). If any source is cited: According to Ünlü and Gerçek (2023), it should be written.
- In the case of multiple authors they should be cited as (Evans et al. 2023, Landen et al. 2021). If any source is cited: According to Landen et al. (2021)... it should be written.
- References should be given at the end of the text according to alphabetical order of the first authors surname.
- In Turkish and English articles, software programs should be given as (IBM SPSS Statistics 2016) by specifying the name and year in the text.

The references at the end of the text are as follows:

References should be given at the end of the text according to alphabetical order.

Article:

One author

- Eker Şanlı, G., Tasdemir, Y. 2022. Accumulations and temporal trends of polychlorinated biphenyls (PCBs) in olive tree components. Environ. Geochem. Health., 44(8): 2577-2594. Doi:10.1007/s10653-021-01046-2
- Yaralı, O., Duru, H. 2016. Investigation into effect of scratch length and surface condition on Cerchar abrasivity index. Tunn. Undergr. Space Technol., 60: 111-120. Doi: 10.1016/j.tust.2016.08.005

Multiple authors

- Erdem, S., Gonca, E., Başoğlu, G., Aydemir, E. 2022. İskemi sonrası verilen kannabidiol reperfüzyon ile uyarılan aritmilere karşı koruyucu etkilidir. Med. J. West Black Sea, 6(1): 16-23. Doi: 10.29058/mjwbs.1016783
- Erkaymaz, O., Yapıcı, İS., Uzun Arslan, R. 2021. Effects of obesity on time-frequency components of electroretinogram signal using continuous wavelet transform. Biomed. Signal Process Control, 66: 102398. Doi: 10.1016/j.bspc.2020.102398
- Öztürk, Ş., Hazer Y., Kaşkatepe, B., Çölgeçen, H., Kulak, M. 2023. Kırmızı kantaron (*Hypericum capitatum*) bitkisi: fenolik içeriklerinin, antioksidan aktivitesinin belirlenmesi ve klinik izolatlar üzerinde antimikrobiyal etkinliğinin araştırılması. Batı Karadeniz Tıp Dergisi, 7(1): 57-65. Doi: 10.29058/mjwbs.1251370

If two or more works by the same author are used, references should be listed in chronological order.

- Berndt, T.J. (2022).
- Berndt, T.J. (2023).

If there are more than seven authors, the names of the first six authors are listed, followed by three dots and the name of the last author is added. No more than seven names should be included.

- Miller, FH., Choi, MJ., Angeli, LL., Harland, AA., Stamos, JA., Thomas,



ST, . . . Rubin, LH. 2009. Web site usability for the blind and low-vision user. *Technical Communication*, 57: 323-335.

Book:

- Reşat, U. 2001. *Uygulamalı jeoteknik bilgiler*. 4. Basım, TMMOB Jeoloji Mühendisleri Odası Yayınları, Nitelik Matbaacılık, Ankara, 385 s. Sanford, RJ. 2003.
- Principles of fracture mechanics, Prentice Hall, Pearson Education, Inc. Upper Saddle River, USA, 404 pp.

Chapter:

- Atar, H., Çölgeçen, H. 2020. Bioactive compounds of oregano seeds. Victor R. Preedy, Ronald Ross Watson [eds.], *Nuts & Seeds in Health and Disease Prevention* (2nd ed.). Oxford: Academic Press is an imprint of Elsevier, London, San Diego, Cambridge, pp. 73-77.

Report:

- Makarewicz, JC., Lewis, T., Bertram, P. 1995. Epilimnetic phytoplankton and zooplankton biomass and species composition in Lake Michigan, 1983-1992. U.S. EPA Great Lakes National Program, Chicago, IL. EPA 905-R-95-009.

Conference, Symposium:

- Karahan, H., Çölgeçen, H. 2021. Uptake of silver nanoparticles in natural tetraploid *Trifolium pratense* L. calli. 10th International Molecular Biology and Biotechnology Congress, s. 56, Turkey.

Internet:

If any information is taken from any website (except for articles taken from the internet and published in journals), the name of the website and the title of the website should be written in the references section.

Web page:

- TUİK 2023. <https://www.tuik.gov.tr/>

Web document with author:

- Dawson, J., Smith, L. Deubert, K. 31 Ekim 2002. <http://studytrekk.lis.curtin.edu.au/> şeklinde belirtilmelidir.

In press:

- Evans, MA. 2023. Article Title. Journal. (DOI).

A Thesis:

- Duru, H. 2020. Geliştirilen cerchar aşındırıcılık deney aletiyle kayaçların spesifik çizme enerjisinin araştırılması. Doktora Tezi, Zonguldak Bülent Ecevit Üniversitesi, 175 s.

Software:

- SPSS Statistics 24.0. Software, IBM, United States.

Tables and Figures:

All tables and figures should be embedded in the text and must be numbered consecutively throughout the paper (Table 1, Table 2 and 3, Figure 1, Figure 2 and 3, Figure 4). The numbers and headings of figures must be written below the figure. The numbers and headings of tables should be written at the top of the table. References in the text should be in Table 1, Figure 1. Graphs, Figures and photos must be given in the text as JPEG, PNG or TIFF(min. 300 dpi). Bars must be used to show magnification in photos.

Standart errors or deviations should be cited as (e.g., 1.42 ± 1.36), statistically data should be given as (e.g., 731.2ab) in the table. The column title of standart errors or deviations must be cited as (means \pm SD, or means \pm SE).

Equations:

Mathematical expressions should be written by an "Equation Editör" (Word format) in 12 point size, and Cambria Math. Indices font should be 12 point

size. Each equation in text should be numbered in parenthesis ().

Mathematical equations should be cited as below:

$$V_i = \frac{d_p^2(\rho_p - \rho_z)V_i^2}{18\mu R} \quad (1)$$

Attachments:

All appendices should be written on a separate page and numbered with Roman numerals. Authors who will submit publications in the area of mathematics should specify the subject classification number (AMS-Mathematical Subject Classification Number).

Symbols and Units:

Metric systems or SI units should be used (kPa, kN/m³, g/cm², m/sn, g/m³, e.g.). Current abbreviations can be used without explanation, others must be explained. Use " %" only with numerals and in tables and figures. Close up space to numerals (e.g. 60%). Use the dot for decimal units (e.g. 10.26).

Abbreviations:

Use the following abbreviations for time: s (second), min (minute), h (hour), wk (week), yr (year), mo (month), add "s" to create plurals (e.g. wks). The day, month and year should be written in full without any abbreviations (19 May 2023).

Numbers:

Spell out numbers at the beginning of sentence. Spell out the numbers one through nine. 10 and up are always cited as arabic numerals. All numbers <1 must be preceded by a zero (e.g. P<0.05).

Footnotes:

In case of statistical data in tables, use footnotes to define or clarify column headings or specific datum with in data field (*P<0.05; ** P<0.01; *** P<0.001; NS, not significant). For submitting first namely author's manuscripts should not exceed three folds in the same issue. Authors when submit the four folds manuscripts, they will be publish in another issues.

CHECKLIST OF THE MANUSCRIPT

Before submitting of your paper (and other writings as applicable), please make sure that the following requirements have all been made:

- "Cover Page", "Blind Article-Full Text", "Plagiarism Report" and "Copyright Transfer Form" are enclosed
- Spell check and grammar check have been performed
- Entire paper is 1.5-spaced including abstract, tables, captions, references
- Margins are 2.5 cm each margin
- Font type is Times new roman and Font size is 12 point
- The headings in the text is left aligned, 12 point and bold
- Names of all authors are written in full (not abbreviated)
- Address is given
- Title is in title case 12 point and bold
- Abstract and keywords are given
- References are typed according to the instructions, and listed alphabetically
- Decimals are shown by a full stop (e.g., 10.25)
- Percent signs appear without a space after the number (e.g., 63%, %10)
- Figures are maximum 16x20 cm; minimum 8 cm wide
- The numbers of the tables (Table 1, Table 2, Table 3 etc.) are given in order in the text.
- Original figures are enclosed
- Figures are prepared according to the instructions
- Figures are maximum 16x20 cm; minimum 8 cm wide, min 300 dpi
- The numbers of the tables (Figure 1, Figure 2, Figure 3 etc.) are given in order in the text.
- All pages and line are numbered

Please [click](#) on the link to access a sample of the article written according to the spelling rules of our journal.



ETHICAL PRINCIPLES

Official journal of Zonguldak Bülent Ecevit University, Karaelmas Science and Engineering Journal is a peer-reviewed journal which aims to reach all national and international institutions and individuals free of charge.

In the scientific articles sent to our journal, the recommendations of ICMJE (International Committee of Medical Journal Editors) and the International Standards of COPE (Committee on Publication Ethics) for Editors and Authors are taken into consideration.

All claims and finalized processes regarding ethical violations of our authors are under their own responsibility, and in case of ethical violations, the article is automatically canceled.

Ethical Guidelines for Peer Reviewers

Peer Reviewers,

- respect the confidentiality of the manuscript, do not discuss it and do not reveal any details of it.
- inform the editor about any conflict of interest.
- provide objective and constructive explanations for their suggestions.
- do not allow the decisions related to the article to be influenced by the subject of the manuscript or the way of writing.
- do not contact the authors directly and request their previous articles unless there is a strong scientific reason.
- do not duplicate any part of the article or information reviewed in any of their own work before it is published by the authors.
- agree to accept the reviews only within their expertise and finish the review process within a reasonable time.
- do not intentionally prolong the review process which leads to a delay for the publication of the article.
- use a language refrained from being hostile and avoids making derogatory personal comments.
- destroy the manuscript and associated material after reviewing.

https://publicationethics.org/files/Ethical_guidelines_for_peer_reviewers_0.pdf

Ethical Guidelines for Authors

Authors and co-authors,

- meet the following criteria for authorship defined by International Committee of Medical Journal Editors (ICMJE);
 - a. Substantial contributions to the conception or design of the work; or the acquisition, analysis, or interpretation of data for the work;
 - b. Drafting the work or revising it critically for important intellectual content;
 - c. Final approval of the version to be published;
 - d. Agreement to be accountable for all aspects of the work in ensuring that questions related to the accuracy or integrity of any part of the work are appropriately investigated and resolved.
- ensure that submitted articles are original and are not sent to different publishers.

- are responsible for any falsification, alteration or plagiarism which are defined as abusing research before or during the research or while reporting the findings of it.
- inform the editor if there is any conflict of interest in the submitted articles.
- inform the editor for correction or withdrawal if any mistake is noticed after publication or during the process of pre-control or evaluation.
- do not suggest reordering, adding or dropping author names after article submission.
- state, if the research requires the decision of the ethics committee, that they have the ethics committee approval with the name of the ethics committee and the date and number of the decision in the first and last page of the article and the methods section, also upload the ethics committee approval document to the system along with the application of the article.
- state in the article that they have the consent form for the case reports.
- comply with the copyright regulations for the ideas and works of art used in the article.
- provide statements for Author Contribution, Conflict of Interest, Disclosure and if necessary, Acknowledgements.

<http://www.icmje.org/icmje-recommendations.pdf>

https://www.ease.org.uk/wp-content/uploads/2018/11/doi.10.20316.ESE_2018.44.e1.tr_.pdf

Ethical Guidelines for Editors

Editors:

- The readers should be informed about who provides financial support to the study or other scientific studies and whether there is any role of sponsors in the study or publication, and if there is any, what the contribution is.
- Editors should base their decisions of acceptance or rejection on the importance, originality and clarity of the article, validity of study and its relevance to the remit of the journal.
- Editors should not reverse decisions to accept submissions unless serious problems are identified with the submission.
- New editors should not overturn decisions to publish submissions made by the previous editor unless serious problems are identified.
- A description of peer review processes should be published, and editors should be ready to justify any important deviation from the described processes.
- Journals should have a declared mechanism for authors to appeal against editorial decisions.
- Editors should publish guidance to authors on everything that is expected of them. This guidance should be regularly updated and should refer or link to this code.
- Editors should state the authorship criteria suggested by International Committee of Medical Journal Editors (ICMJE).



- Editors should provide guidance to reviewers on everything that is expected of them including the need to handle submitted material in confidence. This guidance should be regularly updated and should refer or link to this code
- Editors should require reviewers to disclose any potential competing interests before agreeing to review a submission.
- Editors should have systems to ensure that peer reviewers' identities are protected unless they use an open review system that is declared to authors and reviewers.
- Editors should provide new editorial board members with guidelines on everything that is expected of them and should keep existing members updated on new policies and developments.
- Editors should make decisions on which articles to publish based on quality and suitability for the journal and without interference from the journal owner/publisher.
- Editors should have a written contract(s) setting out their relationship with the journal's owner and/or publisher. The terms of this contract should be in line with the COPE Code of Conduct for Journal Editors.
- Editors should strive to ensure that peer review at their journal is fair, unbiased and timely.
- Editors should have systems to ensure that material submitted to their journal remains confidential while under review.
- Editors should take all reasonable steps to ensure the quality of the material they publish, recognizing that journals and sections within journals will have different aims and standards.

<https://publicationethics.org/files/Code%20of%20Conduct.pdf>



PUBLICATION ETHICS

The ethics statement of the Karaelmas Science and Engineering Journal is based on the Code of Conduct guidelines of the Committee on Publication Ethics (COPE), available at www.publicationethics.org.

This journal follows the COPE Code of Conduct and Best Practice Guidelines for Journal Editors and the Code of Conduct for Journal Publishers.

Duties of Editors

Fair play and editorial independence

Editors evaluate submitted manuscripts exclusively on the basis of their academic merit (importance, originality, study's validity, clarity) and its relevance to the journal's scope, without regard to the authors' race, gender, sexual orientation, ethnic origin, citizenship, religious belief, political philosophy or institutional affiliation. Decisions to edit and publish are not determined by the policies of governments or any other agencies outside of the journal itself. The Editor-in-Chief has full authority over the entire editorial content of the journal and the timing of publication of that content.

Confidentiality

Editors and editorial staff will not disclose any information about a submitted manuscript to anyone other than the corresponding author, reviewers, potential reviewers, other editorial advisers, and the publisher, as appropriate.

Disclosure and conflicts of interest

Editors and editorial board members will not use unpublished information disclosed in a submitted manuscript for their own research purposes without the authors' explicit written consent. Privileged information or ideas obtained by editors as a result of handling the manuscript will be kept confidential and not used for their personal advantage. Editors will recuse themselves from considering manuscripts in which they have conflicts of interest resulting from competitive, collaborative, or other relationships/connections with any of the authors, companies or institutions connected to the papers; instead, they will ask another member of the editorial board to handle the manuscript.

Publication decisions

The editors ensure that all submitted manuscripts being considered for publication undergo peer-review by at least two reviewers who are expert in the field. The Editor-in-Chief is responsible for deciding which of the manuscripts submitted to the journal will be published, based on the validation of the work in question, its importance to researchers and readers, the reviewers' comments, and such legal requirements as are currently in force regarding libel, copyright infringement and plagiarism. The Editor-in-Chief may confer with other editors or reviewers in making this decision.

Involvement and cooperation in investigations

Editors (in conjunction with the publisher and/or society) will take responsive measures when ethical concerns are raised with regard to a submitted manuscript or published paper. Every reported act of unethical publishing behaviour will be looked into, even if it is discovered years after publication. Editors follow the COPE Flowcharts when dealing with cases of suspected misconduct. If, on investigation, the ethical concern is

well-founded, a correction, retraction, expression of concern or other note as may be relevant, will be published in the journal.

Duties of Reviewers

Contribution to editorial decisions

Peer review assists editors in making editorial decisions and, through editorial communications with authors, may assist authors in improving their manuscripts. Peer review is an essential component of formal scholarly communication and lies at the heart of scientific endeavour.

Promptness

Any invited referee who feels unqualified to review the research reported in a manuscript or knows that its prompt review will be impossible should immediately notify the editors and decline the invitation to review so that alternative reviewers can be contacted.

Confidentiality

Any manuscripts received for review are confidential documents and must be treated as such; they must not be shown to or discussed with others except if authorized by the Editor-in-Chief (who would only do so under exceptional and specific circumstances). This applies also to invited reviewers who decline the review invitation.

Standards of objectivity

Reviews should be conducted objectively and observations formulated clearly with supporting arguments so that authors can use them for improving the manuscript. Personal criticism of the authors is inappropriate.

Acknowledgement of sources

Reviewers should identify relevant published work that has not been cited by the authors. Any statement that is an observation, derivation or argument that has been reported in previous publications should be accompanied by the relevant citation. A reviewer should also notify the editors of any substantial similarity or overlap between the manuscript under consideration and any other manuscript (published or unpublished) of which they have personal knowledge.

Disclosure and conflicts of interest

Any invited referee who has conflicts of interest resulting from competitive, collaborative, or other relationships or connections with any of the authors, companies or institutions connected to the manuscript and the work described therein should immediately notify the editors to declare their conflicts of interest and decline the invitation to review so that alternative reviewers can be contacted.

Unpublished material disclosed in a submitted manuscript must not be used in a reviewer's own research without the express written consent of the authors. Privileged information or ideas obtained through peer review must be kept confidential and not used for the reviewer's personal advantage. This applies also to invited reviewers who decline the review invitation.

Duties of Authors

Reporting standards

Authors of original research should present an accurate account of the



work performed and the results, followed by an objective discussion of the significance of the work. The manuscript should contain sufficient detail and references to permit others to replicate the work. Review articles should be accurate, objective and comprehensive, while editorial ‘opinion’ or perspective pieces should be clearly identified as such. Fraudulent or knowingly inaccurate statements constitute unethical behaviour and are unacceptable.

Data access and retention

Authors may be asked to provide the raw data of their study together with the manuscript for editorial review and should be prepared to make the data publicly available if practicable. In any event, authors should ensure accessibility of such data to other competent professionals for at least 10 years after publication (preferably via an institutional or subject-based data repository or other data centre), provided that the confidentiality of the participants can be protected and legal rights concerning proprietary data do not preclude their release.

Originality and plagiarism

Authors should ensure that they have written and submit only entirely original works, and if they have used the work and/or words of others, that this has been appropriately cited. Publications that have been influential in determining the nature of the work reported in the manuscript should also be cited. Plagiarism takes many forms, from “passing off” another’s paper as the author’s own, to copying or paraphrasing substantial parts of another’s paper (without attribution), to claiming results from research conducted by others. Plagiarism in all its forms constitutes unethical publishing behaviour and is unacceptable.

Multiple, duplicate, redundant or concurrent submission/publication

Papers describing essentially the same research should not be published in more than one journal or primary publication. Hence, authors should not submit for consideration a manuscript that has already been published in another journal. Submission of a manuscript concurrently to more than one journal is unethical publishing behaviour and unacceptable.

The publication of some kinds of articles (such as clinical guidelines, translations) in more than one journal is sometimes justifiable, provided that certain conditions are met. The authors and editors of the journals concerned must agree to the secondary publication, which must reflect the same data and interpretation of the primary document. The primary reference must be cited in the secondary publication.

Authorship of the manuscript

Only persons who meet these authorship criteria should be listed as authors in the manuscript as they must be able to take public responsibility for the content: (i) made significant contributions to the conception, design, execution, data acquisition, or analysis/interpretation of the study; and (ii) drafted the manuscript or revised it critically for important intellectual content; and (iii) have seen and approved the final version of the paper and agreed to its submission for publication. All persons who made substantial contributions to the work reported in the manuscript (such as technical help, writing and editing assistance, general support) but who do not meet the criteria for authorship must not be listed as an author, but should be acknowledged in the “Acknowledgements” section after their written permission to be named as been obtained. The corresponding author should ensure that all appropriate coauthors (according to the above definition) and no inappropriate coauthors are included in the author list and verify that all coauthors have seen and approved the final version of the manuscript and agreed to its submission for publication.

Disclosure and conflicts of interest

Authors should—at the earliest stage possible (generally by submitting a disclosure form at the time of submission and including a statement in the manuscript)—disclose any conflicts of interest that might be construed to influence the results or their interpretation in the manuscript. Examples of potential conflicts of interest that should be disclosed include financial ones such as honoraria, educational grants or other funding, participation in speakers’ bureaus, membership, employment, consultancies, stock ownership, or other equity interest, and paid expert testimony or patent-licensing arrangements, as well as non-financial ones such as personal or professional relationships, affiliations, knowledge or beliefs in the subject matter or materials discussed in the manuscript. All sources of financial support for the work should be disclosed (including the grant number or other reference number if any).

Acknowledgement of sources

Authors should ensure that they have properly acknowledged the work of others, and should also cite publications that have been influential in determining the nature of the reported work. Information obtained privately (from conversation, correspondence or discussion with third parties) must not be used or reported without explicit, written permission from the source. Authors should not use information obtained in the course of providing confidential services, such as refereeing manuscripts or grant applications, unless they have obtained the explicit written permission of the author(s) of the work involved in these services.

Hazards and human or animal subjects

If the work involves chemicals, procedures or equipment that have any unusual hazards inherent in their use, the authors must clearly identify these in the manuscript. If the work involves the use of animals or human participants, the authors should ensure that all procedures were performed in compliance with relevant laws and institutional guidelines and that the appropriate institutional committee(s) has approved them; the manuscript should contain a statement to this effect. Authors should also include a statement in the manuscript that informed consent was obtained for experimentation with human participants. The privacy rights of human participants must always be observed.

Peer review

Authors are obliged to participate in the peer review process and cooperate fully by responding promptly to editors’ requests for raw data, clarifications, and proof of ethics approval, patient consents and copyright permissions. In the case of a first decision of “revisions necessary”, authors should respond to the reviewers’ comments systematically, point by point, and in a timely manner, revising and re-submitting their manuscript to the journal by the deadline given.

Fundamental errors in published works

When authors discover significant errors or inaccuracies in their own published work, it is their obligation to promptly notify the journal’s editors or publisher and cooperate with them to either correct the paper in the form of an erratum or to retract the paper. If the editors or publisher learns from a third party that a published work contains a significant error or inaccuracy, then it is the authors’ obligation to promptly correct or retract the paper or provide evidence to the journal editors of the correctness of the paper.



İÇİNDEKİLER

Araştırma Makaleleri

Yeni Bir Schiff Bazı ve Platin Kompleksi: Amiloid Agregasyonunun İnhibisyonu.....	1
Özge Özcan, Salih Gündüz, Sevil İrişli	
Üç Aşamalı Derin Öğrenme Tabanlı Otomatik Araç Plakası Algılama ve Tanıma Sistemi.....	12
Emre Yücel, Yalçın İşler, Yakup Kutlu	
Ceşitli Asidik Ajanlar ile Fonksiyonelleştirilmiş Biyokütlenin Özellikleri ve Sorpsiyon Performansının Kinetik Analizi....	21
Sahra Dandil	
Kaya Parçalanma Modellerini Kullanarak Hedeflenen Ortalama Parça Boyutuna Dayalı Yük Tahminine Alternatif	36
Bir Yaklaşım	
Ozgur Yilmaz	
Edirne'deki Alışveriş Merkezi İçin Hibrit Yenilenebilir Enerji ile Çalışan Elektrikli Araç Şarj İstasyonunun.....	44
Tekno-Ekonomin Değerlendirmesi	
Hacer Akhan	
Yapım İşlerinde İhale Parametreleri Kullanılarak Makine Öğrenmesi ile Sözleşme Bedeli Tahmini.....	64
Semi Emrah Aslay	
Meme Kanseri Veri Seti Kullanılarak Sentetik Veri Üretilmesi ve Resnet18 ile Sınıflandırılması	74
Dilşat Berin Aytar, Semra Gündüz	
Su Dağıtım Şebekelerinde Bakıye Kloru Azaltan Boruların Cidar Reaksiyon Katsayısına Bağlı Olarak Tespit Edilmesi.....	86
Miraç Eryiğit	
İstanbul'daki Deprem Etki Senaryolarının Makine Öğrenmesi Algoritmaları ile Tahmin Edilmesi.....	95
Remzi Gürfidan, Mehmet Ali Yalçınkaya	
Kuaterniyon Değerli g-Metrik Uzayda Yakınsaklık Üzerine.....	106
Saime Kolancı, Mehmet Gürdal, Ömer Kişi	
Tire (İzmir) İlçesinin Atmosferik Polenleri	115
Nur Ceyhan Güvensen, Ulaş Uğuz, Aykut Güvensen, Ahmet Kaya	
Prosiulfokarbin Gaz Kromatografisi-Kütle Spektrometrisi ile Patates Unu Örneklerinde Tayini.....	129
Sezin Erarpat Bodur	
Çeşitli Tekrarlayan Sinir Ağları Kullanarak Siber Saldırı Tespiti.....	136
Nesibe Yalçın, Semih Çakır, Sibel Ünalı	
Bir Yeraltı Madeninde Kullanılan Eksenel Fanın Verimliliğini Artırmak İçin Yeni Bir Kanat Tasarımının Araştırılması ..	144
Güneyhan Taşkaya, Beytullah Erdoğan	
Kestel Bölgesinde (Kadınhanı-Konya) Yetişen Bazı Makromantarların Antimikrobiyal Aktivitelerinin Araştırılması	163
Ayşegül Yaprak, Sinan Alkan, Erdoğan Güneş, Giyasettin Kaşık	



CONTENTS

Research Articles

New Schiff Base and Its Platinum Complex: Inhibition of Amyloid Aggregation.....	1
Özge Özcan, Salih Günnaz, Sevil İrişli	
Autonomous Vehicle License Plate Detection and Identification System Based on Three-Stage Deep Learning.....	12
Emre Yücel, Yalçın İşler, Yakup Kutlu	
Characteristics and Kinetic Analysis of Sorption Performance of Functionalised Biomass by Various Acidic Agents	21
Sahra Dandil	
An Alternative Approach to Burden Estimation Based on Targeted Mean Fragment Size Using Rock.....	36
Fragmentation Models	
Ozgur Yilmaz	
Techno-Economic Assessment of a Hybrid Renewable Energy Powered Electric Vehicle Charging Station for	44
Shopping Mall in Edirne, Turkey	
Hacer Akhan	
Construction Contract Price Prediction Using Machine Learning with Bidding Parameters	44
Semi Emrah Aslay	
Generation of Synthetic Data Using Breast Cancer Dataset and Classification with Resnet18.....	74
Dilşat Berin Aytar, Semra Gündüz	
Detection of Pipes Decreasing Residual Chlorine Via Wall Reaction Coefficient in Water Distribution Networks	86
Miraç Eryiğit	
Forecasting Earthquake Impact Scenarios in Istanbul with Machine Learning Algorithms	95
Remzi Gürfidan, Mehmet Ali Yalçınkaya	
On Convergence in Quaternion-Valued g-Metric Space.....	106
Saime Kolancı, Mehmet Gürdal, Ömer Kişi	
Atmospheric Pollen Grains in Tire (İzmir) District	115
Nur Ceyhan Güvensen, Ulaş Uğuz, Aykut Güvensen, Ahmet Kaya	
Determination of Prosulfocarb in Potato Flour Samples by Gas Chromatography-Mass Spectrometry	129
Sezin Erarpat Bodur	
Cyber-Attack Detection Using Various Recurrent Neural Networks	136
Nesibe Yalçın, Semih Çakır, Sibel Ünalı	
Investigation of a New Blade Design to Improve the Efficiency of an Axial Fan Used in an Underground Mine	144
Güneyhan Taşkaya, Beytullah Erdoğan	
Investigation of the Antimicrobial Activities of Some Macrofungi Growing in the Kestel Region (Kadınhanı-Konya).....	163
Ayşegül Yaprak, Sinan Alkan, Erdoğan Güneş, Giyasettin Kaşik	



New Schiff Base and Its Platinum Complex: Inhibition of Amyloid Aggregation

Yeni Bir Schiff Bazı ve Platin Kompleksi: Amiloid Agregasyonunun İnhibisyonu

Özge Özcan , Salih Günnaz , Sevil İrişli*

Ege University, Faculty of Science, İzmir, Türkiye

Abstract

This study investigates the synthesis and characterization of a Schiff base (L) comprising amine and imine donor atoms, specifically N1-(4-(benzyloxy)benzylidene)-N2-phenylethane-1,2-diamine, along with its Platinum(II) complex (Pt-L). The structural elucidation of both the ligand and complex is accomplished through various spectroscopic techniques including Fourier-transform infrared spectroscopy (FT-IR), proton nuclear magnetic resonance (¹H-NMR), carbon-13 nuclear magnetic resonance (¹³C-NMR), and elemental analysis. Furthermore, the potential inhibitory effects of the Pt-L complex on A β ₁₋₄₂ aggregation are explored using the human neuroblastoma cell line (SH-SY5Y) as a model system. The cytotoxicity of the Pt-L complex on SH-SY5Y neuroblastoma cells is examined, revealing an IC₅₀ value of 19.22 μ M. The inhibition kinetics of A β aggregation are also investigated fluorometrically using Thioflavine-T. By analyzing the area under the curve, it is calculated that the complex (1.0:1.0 molar ratio) interacts with amyloid at a rate of 65%. These results obtained in our study show that the complex is promising in terms of inhibition of A β ₁₋₄₂.

Keywords: Anti-Alzheimer activity, cytotoxicity, schiff base, platinum-schiff base complexes.

Öz

Bu çalışma, amine ve imin donör atomlarını içeren bir Schiff bazı (L) bileşığının sentezini ve karakterizasyonunu incelemektedir. Özellikle, N1-(4-(benziloski)benziliden)-N2-feniletan-1,2-diamin bileşiği ve onun Platin(II) kompleksi (Pt-L) üzerinde durulmaktadır. Hem ligandin hem de kompleksin yapısal aydınlatılması, Fourier-dönüştürümlü kızılıötesi spektroskopisi (FT-IR), proton nükleer manyetik rezonans (¹H-NMR), karbon-13 nükleer manyetik rezonans (¹³C-NMR) ve elementel analiz gibi çeşitli spektroskopik teknikler kullanılarak gerçekleştirılmıştır. Ayrıca, Pt-L kompleksinin A β ₁₋₄₂ agregasyonu üzerindeki potansiyel inhibisyon etkileri, insan nöroblastoma hücre hattı (SH-SY5Y) kullanılarak bir model sistem olarak araştırılmıştır. Pt-L kompleksinin SH-SY5Y nöroblastoma hücreleri üzerindeki sitotoksitesi de incelenmiş ve IC₅₀ değeri 19.22 μ M olarak belirlenmiştir. A β agregasyonunun inhibisyon kinetiği ayrıca Thioflavin-T kullanılarak florometrik olarak incelenmiştir. Eğrinin altında kalan alanın değerlendirilmesi ile kompleksin 1.0:1.0 mol oranında amyloid ile %65 oranında etkileşliğini göstermiştir. Çalışmamızda elde edilen bu sonuçlar, kompleksin A β ₁₋₄₂ inhibitörü olarak umut verici bir bileşik olduğunu göstermektedir.

Anahtar Kelimeler: Anti-Alzheimer aktivitesi, sitotoksite, schiff bazları, platin-schiff bazı kompleksleri.

1. Introduction

Schiff bases are considered one of the most versatile classes of bioactive compounds due to their capacity to interact with various elements (Garai et al. 2018, Pal et al. 2020). Schiff bases and their metal complexes are widely used in

many biological fields such as anticancer, antiviral, anti-inflammatory, antifungal, etc. (Liu et al. 2014, Rao et al. 2013, Mohammed et al. 2022).

Neurodegenerative diseases (ND) are chronic and progressive disorders that share many common features. The accumulation of death-causing protein aggregates (Especially A β ₁₋₄₂, amyloid beta(1-42)) in certain areas of the brain causes damage and results in memory loss (Ross and Poirier 2004, Soto and Prizkow 2018). In Alzheimer's disease (AD), the alteration in the nerve transmission with nerve cell death is recorded by the presence of neurofibrillary tangles with phosphorylated forms of the tau protein as a microtubule protein. Studies have been carried out for the future of

*Corresponding author: sevil.irisli@ege.edu.tr

Özge Özcan orcid.org/0009-0008-1243-2552

Salih Günnaz orcid.org/0000-0002-7422-6593

Sevil İrişli orcid.org/0000-0002-3727-2216



This work is licensed by "Creative Commons Attribution-NonCommercial 4.0 International (CC)".

Alzheimer's disease, which is based on the assumption of metal ions in the treatment of Alzheimer's disease (Kepp 2017). In this context, metal ions, especially copper, play an important role. It should be noted that copper, iron and zinc ions also participate in various essential components in the functions of the body. When copper accumulates as a toxic cation, it also contributes significantly to Alzheimer's disease by increasing the aggregation of A β_{1-42} (Gaetke et al. 2014). For this reason, diamine-based pharmacophore chelators have been synthesized using aromatic or alkyl amine/imine groups (Santos et al. 2016). It is important to synthesize ligands by taking into account some pharmacophore groups of pro-drug chemicals that can be used in the treatment of AD (Palanimuthu et al. 2017). Studies on the inclusion of two nitrogen-containing compounds as chelating groups in molecules for the removal of metal ions that play a role in aggregation such as Cu and Zn have gained importance.

Another approach is the use of metal complexes that can remove metal from A β_{1-42} in case of disease or modulate A β aggregation to prevent disease (Rowinska-Zyrek et al. 2015). Based on this idea, Pt-based metal complexes were synthesized and their inhibition activities on A β_{1-42} were investigated (Liu et al. 2018). In the metal complexes formed with these ligands, the metal mostly interacts with the histidine nitrogens of amyloid, and the pharmacophore groups of the ligand can also contribute to this interaction (Valensin et al. 2012). Although Pt has generally been used in studies on this subject, especially in recent years, there have been studies including Ru, Ir and Pd complexes (Khan et al. 2024). There are limited studies on Schiff base-metal complexes (Heffern et al. 2014, Roberts et al. 2020, Iscen et al. 2019).

In the study, new platinum(II)-schiff base complex (Pt-L) which has new Schiff base (L) containing amine/imine groups was synthesized. The structures of the synthesized compounds were determined by spectroscopic methods. Ligand synthesis was planned by taking into account the groups (pharmacophores) in some drugs used in the treatment of AD (Palanimuthu et al. 2017). We aimed to prevent aggregation by binding studies of these synthesized substances. In vitro study of the complex was performed on the human neuroblastoma cell line (SH-SY5Y), and cytotoxicity tests were performed beforehand. The inhibition kinetic of Thioflavin T fluorescent aggregation of complex was measured by the method.

2. Material and Methods

2.1. Chemicals

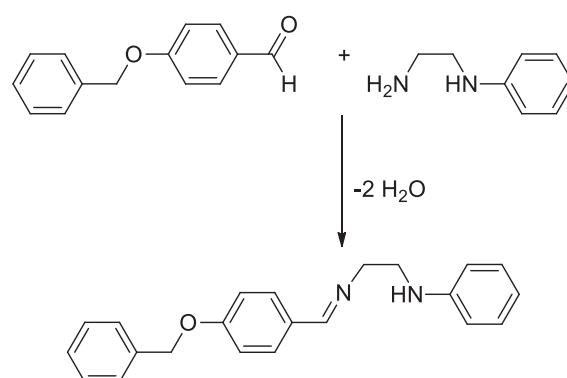
The reagents K₂PtCl₄, 4-Benzylxybenzaldehyde, methanol, chloroform, dichloromethane, and diethyl ether used in the synthesis were commercially purchased from Sigma Aldrich, and solvents were purified according to standard methods (Haas 1971). Pt(DMSO)₂Cl₂, used as the starting complex, was synthesized according to the literature (Price et al. 1972). The A β_{1-42} Aggregation Kit for fluorescence studies was purchased from Anaspec. A β_{1-42} (human) for cell studies and AFM were purchased from Bachem.

2.2. Instrumentations

Melting points were obtained using an Electrothermal Melting Point detection apparatus. Elemental analyzes were performed Ege University. Infrared spectra were recorded on a Perkin Elmer Spectrum 100 FT-IR spectrophotometer in the range of 4000- 400 cm⁻¹ for ligands, 4000- 200 cm⁻¹ for complexes. ¹H and ¹³C NMR spectra were measured at Varian AS 400 MHz spectrometer. CDCl₃ and DMSO-d₆ were used as the solvents and TMS was used as the internal standard. ThT measurements were made using Thermo Fisher Scientific, Varioskan Flash microplate reader device (Temperature 37°C) with 480 nm excitation and 484 nm emission wavelengths.

2.3. Synthesis

2.3.1. Synthesis of (N1-(4-(benzyloxy)benzylidene)-N2-phenylethane-1,2-diamine)(L)

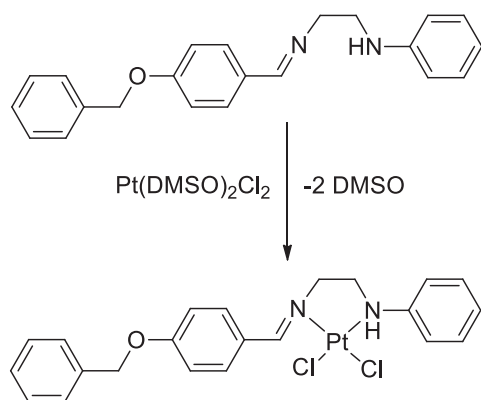


Scheme 1. Synthesis pathway for the L.

A solution of 4-Benzylxybenzaldehyde (15.5 mg, 0.079 mmol) in 2 mL methanol was prepared in a schlenk. Then, N-phenylethylenediamine (0.01 mL 0.079 mmol) solution in 1 mL methanol medium was added dropwise and stirred for 24 hours at room conditions. After 24 hours

in the reaction, a precipitate was formed. The precipitate and filtrate were separated. The precipitate was dried in the vacuum line. Yield: 87.5%, FT-IR (KBr disk, cm^{-1}) $\nu_{\text{C}=\text{N}} = 1642$. ^1H NMR (400 MHz, DMSO-d₆) δ (ppm): 8.25 (s, 1H, CH=N), 7.69 (d, 2H, $J=8.4$ Hz, Ar-H), 7.46 (d, 2H, $J=7.2$ Hz, Ar-H), 7.39 (t, 1H, $J=7.4$ Hz, Ar-H), 7.09-7.05 (m, 4H, Ar-H), 6.62 (d, 2H, $J=8.0$ Hz, Ar-H), 6.53 (t, 1H, $J=7.2$ Hz, Ar-H), 5.57 (t, 1H, $J=6.0$ Hz, N-H), 5.15 (s, 2H, O-CH₂), 3.71 (t, 2H, $J=6.2$ Hz, N-CH₂), 3.32-3.28 (m, 2H, N-CH₂). ^{13}C NMR (100 MHz, DMSO-d₆) δ (ppm): 161.5, 160.7, 149.2, 137.2, 129.9, 129.6, 129.3, 128.9, 128.4, 128.2, 116.1, 115.3, 112.6, 69.8, 60.0, 44.3. Elemental analysis (%): Calculated (C₂₂H₂₂N₂O) (330.42) C, 77.97; H, 6.71; N, 8.48; Found, C, 77.10; H, 6.64; N, 8.39.

2.3.2 Synthesis of Pt(L)Cl₂(Pt-L)



Scheme 2. Synthesis pathway for the Pt-L complex.

Ligand (L) (38.5 mg, 0.137 mmol) was dissolved in 2 mL of chloroform medium in a schlenk. Then, in a beaker, Pt(DMSO)₂Cl₂ (58 mg, 0.137 mmol) was prepared as a suspension in 3 mL chloroform medium and added dropwise onto Ligand L. The mixture was then stirred at reflux temperature for 72 hours. As a result of the reaction, the solvent volume was reduced until 1 mL of solution volume remained in the vacuum line and the solid was obtained by precipitation with 5 mL of diethyl ether. The light-yellow substance was dried under vacuum. Yield: 61%, Melting Point: 197 °C. FT-IR (KBr disk, cm^{-1}) $\nu_{\text{C}=\text{N}} = 1599$, $\nu_{\text{Pt}-\text{Cl}} = 328$ (with shoulder). ^1H NMR (400 MHz, DMSO-d₆) δ (ppm): 9.14 (s, 1H, CH=N), 7.79-7.15 (m, 14H, Ar-H), 5.51(d, 1H, -NH), 5.20 (s, 2H, -CH₂), 4.09 (bs, 1H, N-CH₂), 3.92 (bs, 1H, N-CH₂), 3.03 (bs, 1H, N-CH₂), 2.77 (bs, 1H, N-CH₂). ^{13}C NMR (100 MHz, DMSO-d₆) δ (ppm): 165.8, 161.5, 146.5, 133.1, 129.4, 129.0, 128.3, 124.5, 124.3, 124.0, 115.8, 115.3, 112.5, 70.0, 61.1, 60.1, 46.0. Elemental analysis (%): Calculated (C₂₂H₂₂Cl₂N₂OPT) (596.41) C, 44.30; H, 3.72; N, 4.70; Found, C, 43.81; H, 4.18; N, 4.08.

2.4. Thioflavin T Assay

Concentrations of the A β ₁₋₄₂ Aggregation Kit, purchased from AnaSpec, were prepared according to the kit procedure. For this purpose, stock solutions of complexes and A β ₁₋₄₂ prepared as specified in the biological measurements above were diluted with buffer containing 50 mM Tris / 150 mM NaCl, 20 mM HEPES (4-(2-hydroxyethyl)-1-piperazinepropanesulfonic acid) / 150 mM NaCl, 10 mM Phosphate / 150 mM NaCl and final concentrations 10 μM for A β ₁₋₄₂ and 10 μM for the complexes (corresponding to an interaction ratio of 1:1) were prepared. The final DMSO concentration does not exceed 1 %. ThT solution prepared with buffer was adjusted to the final concentration of 42.6 μM . It was determined by the literature data that an effective signal was obtained at this concentration (Xue et al. 2017).

Negative controls consisting of ThT and assay buffer and consisting of ThT-complex (Pt-L) was run to ensure that complex does not alter ThT fluorescence. Samples were plated in a black 96-well plate. The plate was sealed with aluminum sheets to prevent samples from light and kept in the dark. Fluorescence was measured through the plate bottom every 5 min for 165 min. at excitation 440 nm and emission 484 nm on a Thermo Fisher Scientific, Varioskan Flash microplate reader. Samples were kept at 37 °C under orbital agitation (550 rpm) in the plate reader between reads. Kinetic was plotted using GraphPad Prism.

2.5. Biological Activity

2.5.1. Preparation of monomeric A β ₁₋₄₂ and complexes stock solutions

Commercially purchased A β ₁₋₄₂ first interacted with HFIP, resolved, and published in accordance with the literature. This method primarily aimed to remove oligomers that may be present in commercial amyloid. Insoluble parts were separated by adding HFIP and the resulting solution was concentrated in a vacuum concentrator. Again, the literature was used to determine the concentration according to its effects (Ryan et al. 2013). It was then brought to the concentration to be studied by diluting with 1xPBS. In all measurements, amyloid solution was freshly prepared. Due to the low water solubility of the complexes, the complexes for the prepared stock solution were dissolved in 2:1 DMSO/H₂O medium and diluted to the targeted concentrations with phenol-free DMEM (Dulbecco's Modified Eagle Medium). In all cell measurements, an application method was followed in which the DMSO rate did not exceed 1%.

2.5.2. Cell culture studies

Human neuroblastoma cancer cell (SH-SY5Y) was used in cell culture studies. After removing the frozen cell from -80°C in the cryotube. Then it was quickly thawed in a water bath and transferred to a flask and filled with DMEM medium. Phenol-red-free DMEM was selected as the medium used to determine the cytotoxicity levels of the cells, and all procedures were carried out under sterile conditions. The DMEM medium was prepared with 1% penicillin/streptomycin, 1 % L-Glutamine, 1 % non-essential amino acid, and 1 % Sodium-pyruvate added to the bottle, and it was completed to 500 mL. For an optimal environment for cell growth, the cells were kept in an incubator at 37 °C, containing 95% humidity and 5% CO₂ conditions.

2.5.3. Cytotoxicity studies

In 96-well plates, 1 x 10⁵ SH-SY5Y cells (for 72 hours) were seeded in each well. To determine the cytotoxicity of the complexes alone, master stock solutions of the complexes were diluted with DMEM to the obtained concentrations and added to the wells at (0.1;0.5;1;10;50;100) μM concentrations. After 72 hours of cell cultivation, the medium was removed from the cells and the wells were washed 2 times with 1x PBS. At the end of the relevant time, the medium was removed from the cells, 100 μL of 0.5 mg/mL MTT (3-(4,5-Dimethylthiazol-2-yl)-2,5-diphenyltetrazolium bromide) was added to each well and incubated at 37 °C for 3 hours. After the incubation was completed, the medium with MTT was removed from each well and 150 μL of DMSO (Dimethyl sulfoxide) was added to dissolve the MTT crystals in the cell. The absorbance of the wells was measured at 570 nm with a microplate reader (Thermo Scientific, Varioskan Flash). The percent viability of the control group (untreated group) was considered 100% and the ab-

sorption value of each well was calculated as a percentage relative to the control group, and the experiments were repeated three times.

As a result of this study, the inhibitory effect of the complexes on the toxicity of Aβ₁₋₄₂ in neuronal cell culture was determined by MTT measurement. Neuronal cells were incubated with Aβ₁₋₄₂ for 72h (Interaction with HFIP (Hexafluoroisopropanol) may give erroneous results for the first 24 hours with a final concentration of 10 μM in the presence of complexes at concentrations of 10 and 5 μM respectively.

After removing the medium from the installation, 0.5 mg/mL MTT was added to the wells and incubated at 37°C for 3 hours. After the incubation period was completed, the medium with MTT was removed from each well and 150 μL of DMSO was added to open the MTT crystal cells inside. The absorbance of the wells was measured at 570 nm with a microplate reader and again compared with the control group to calculate the percentage of cell viability (Mosmann 1983).

3. Results and Discussion

3.1. Synthesis Studies of Ligands and Complexes

Synthesis schemes of the ligand and complex are shown in Schemes 1 and 2, and ¹H NMR and ¹³C NMR spectra of the ligand and complex are given in Figures 1, 2, 3 and 4, respectively.

¹H NMR and ¹³C NMR spectra of L and complex Pt-L were recorded in DMSO-d₆ media according to their solubility. The imine peak seen at 8.25 ppm in the ligand shifted to 9.14 ppm with complex formation. The signal of the CH₂ group bound to oxygen in the ligand shifted from 5.15 ppm

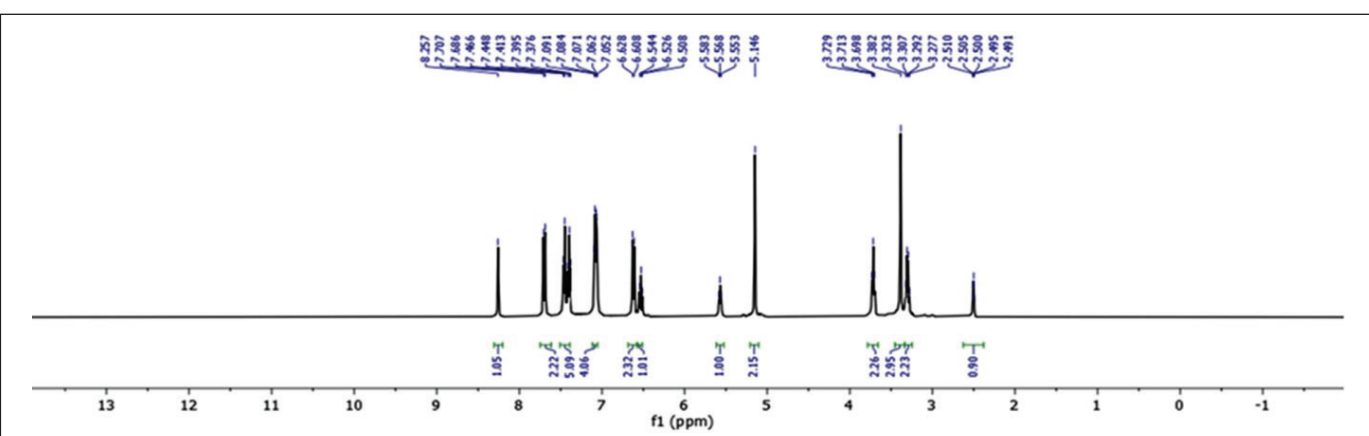


Figure 1. ¹H-NMR spectrum of Ligand (L).

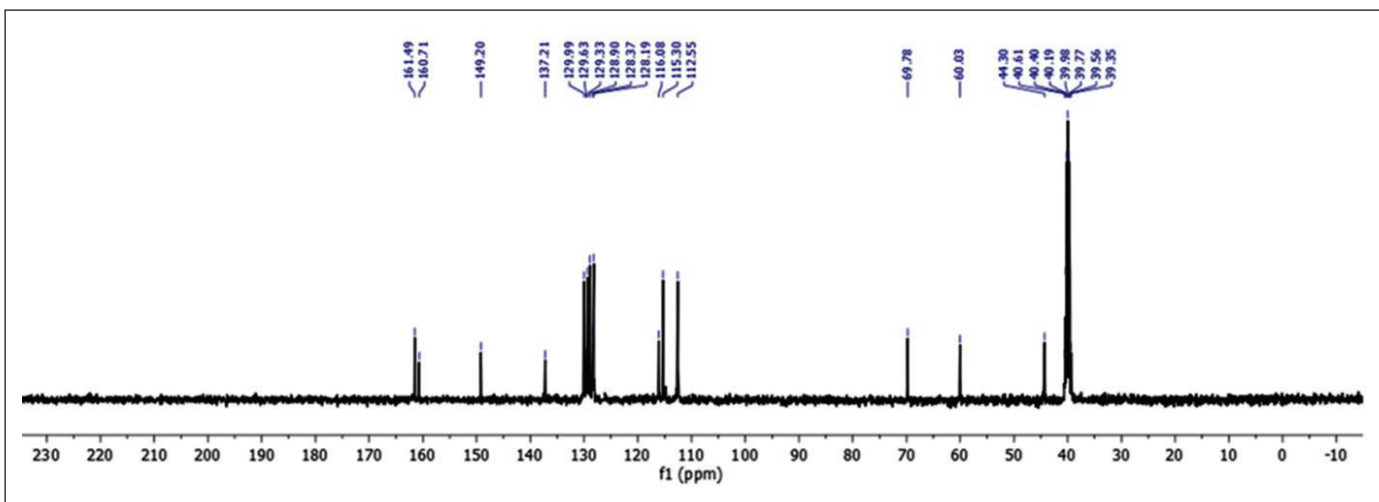


Figure 2. ^{13}C -NMR spectrum of Ligand (L).

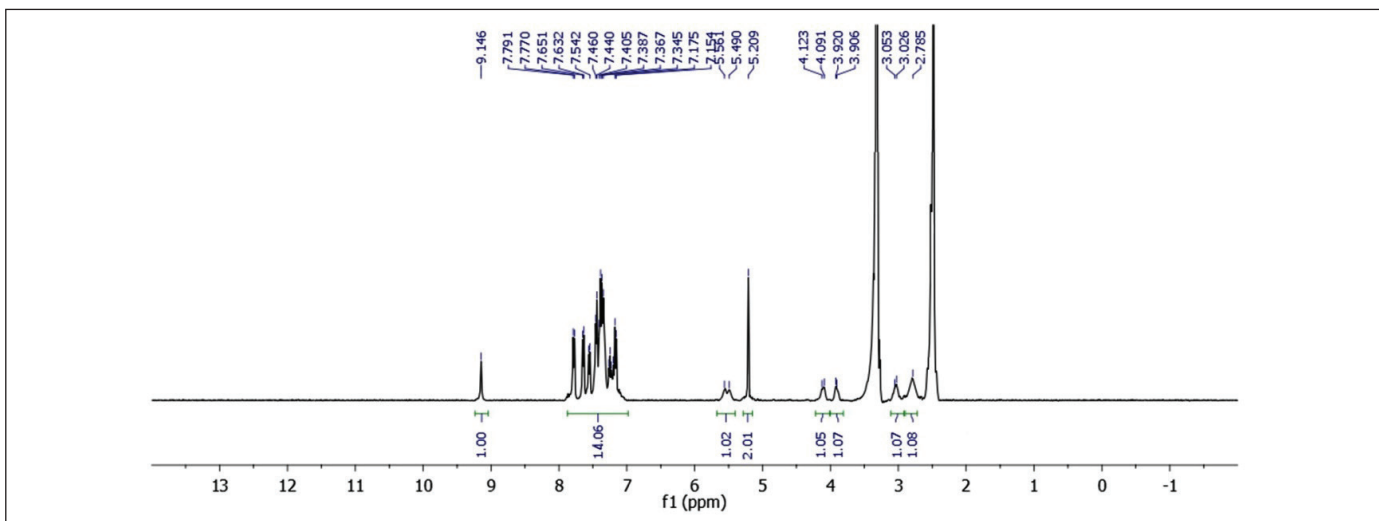


Figure 3. ^1H -NMR spectrum of complex (Pt-L).

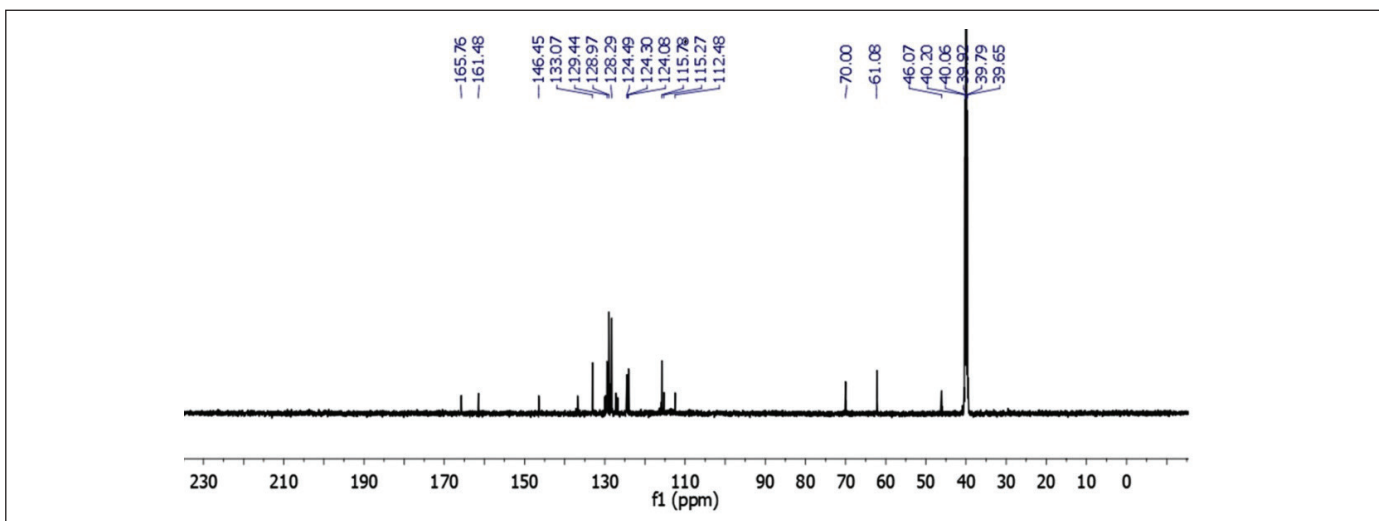


Figure 4. ^{13}C -NMR spectrum of complex (Pt-L).

to 5.20 ppm with complex formation. The proton signal of the CH_2 group bound to nitrogen is seen as a singlet at 3.71 ppm in the free ligand, while it is observed as two separate singlets at 3.92 and 4.09 ppm with complex formation. When the ^1H NMR and ^{13}C NMR spectra for L and Pt-L are examined, shifts are seen relative to the free ligand. In particular, the characteristic imine proton ($\text{N}=\text{CH}$) and imine carbon ($\text{N}=\text{CH}$) shifts to higher ppm from the free ligand indicated that the complex were imine bound (Miles et al. 2016, Patterson et al. 2014, Shiju et al. 2015). The peaks of the protons in the CH_2 group are also seen by separating them in ligand spectrum (Damoc et al. 2020). A shift in CH_2 protons was observed relative to the free ligand in the

complex spectrum. The results of the NMR assessments are presented in Table 1.

The FT-IR spectra of the complex obtained was compared with the ligand. This spectrum shows that the $\nu_{(\text{C}=\text{N})}$ modes change with complexation. While there is a clear distinction in *cis*- Pt-Cl peaks of the starting complex $[\text{PtCl}_2(\text{DMSO})_2]$, it was observed as a peak containing a shoulder in the FT-IR spectra of the Pt-L complex (Figure 6 and 7). However, when the literature data are examined, it is seen that this distinction is not fully observed in some *cis*-structured complexes (Gümüş et al. 2009).

Elemental analysis results of the ligand and complex are compatible with the suggested structure.

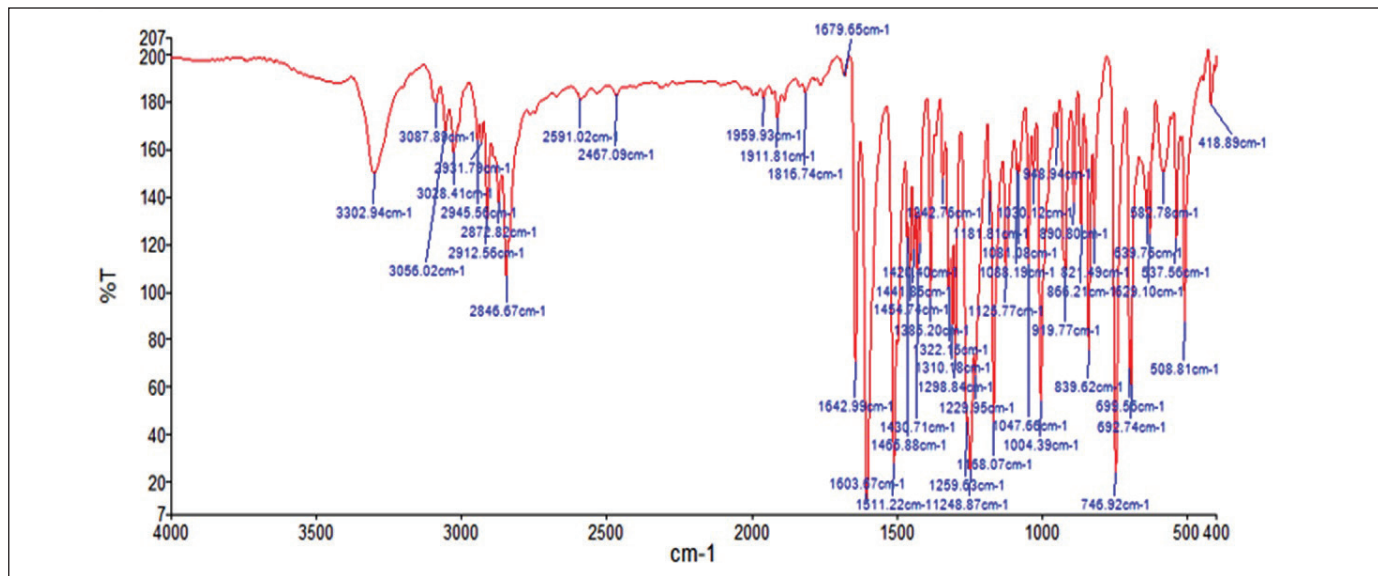


Figure 5. FT-IR spectrum of Ligand (L).

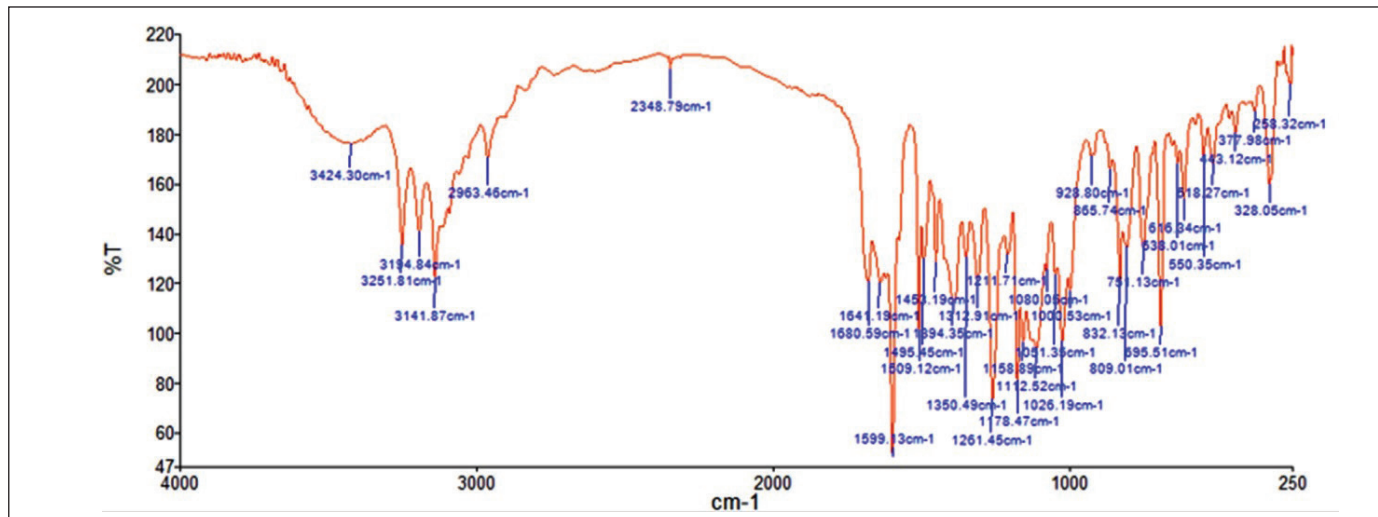
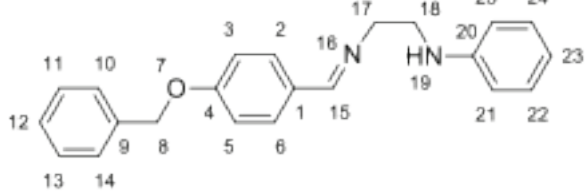
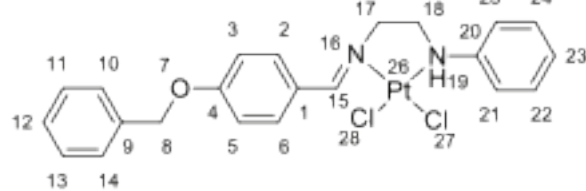


Figure 6. FT-IR spectrum of complex (Pt-L).

Table 1: ^1H - and ^{13}C -NMR peak assignments for ligand and complex.

 Ligand (L)		 complex (Pt-L)	
^1H -NMR			
Number	ppm	Number	ppm
15	8.25 (s)	15	9.14
2, 6	7.69 (d)	2, 3, 5 ,6, 10, 11, 12, 13, 14, 21, 22, 23, 24, 25	7.79-7.15 (m)
3,5	7.46 (d)		
11, 13	7.39 (t)		
10, 12, 14, 21, 25	7.09-7.05 (m)		
22, 24	6.62 (d)		
23	6.53 (t)		
19	5, 57 (bs)	19	5.51 (bs)
8	5.15 (s)	8	5.20 (s)
17	3.71 (t)	17	4.09 (bs) (1H) 3.92 (bs) (1H)
18	3.32-3.28 (m)	18	3.03 (bs) (1H) 2.77 (bs) (1H)
^{13}C -NMR			
Number	ppm	Number	ppm
4	161.5	4	165.8
15	160.7	15	161.5
20	149.2	20	146.5
9	137.2	9	133.1
2, 6	129.9	2, 6	129.4
22, 24	129.6	22, 24	129.0
1	129.3	1	128.3
11, 13	128.9	11, 13	124.5
12	128.4	12	124.3
10, 14	128.2	10, 14	124.0
23	116.1	23	115.8
21, 25	115.3	21, 25	115.3
3, 5	112.6	3, 5	112.5
8	69.8	8	70.0
17	60.0	17	61.1
18	44.3	18	46.0

*s: singlet; d: doublet; t: triplet; m: multiplet; bs: broad singlet.

3.2. Biological Assessment

3.2.1. Determination of cytotoxic activities of complex

The cytotoxicity of the complex was studied for 72 hours (Figure 7). The initial concentration was determined as 10 μM (Yello et al. 2015). The cytotoxicity of the complex for IC_{50} value over 72 hours is 19.22 μM .

After determination and evaluation of the cytotoxicity of the complex alone in the SH-SY5Y cell line, the appropriate concentration was determined for cytotoxicity studies to be measured by $\text{A}\beta_{1-42}$. The concentration of the complex was determined to correspond to the molar ratio of 1.0:1.0 and 1.0:0.5 amyloid/complex. $\text{A}\beta_{1-42}$ alone was added to the medium as a control (Figure 5).

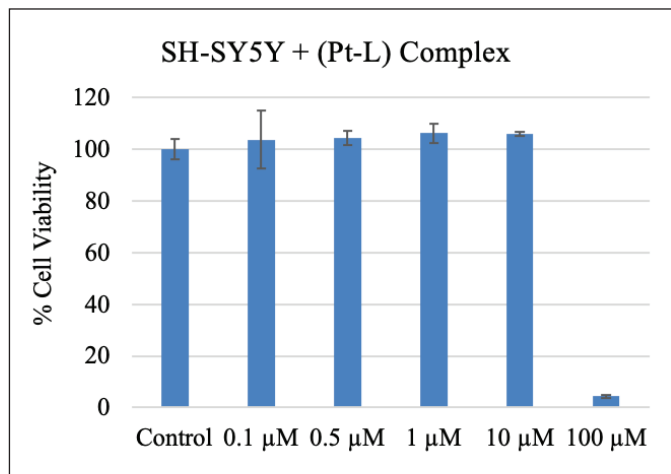


Figure 7. Cytotoxicity of the Pt-L on the cell viability

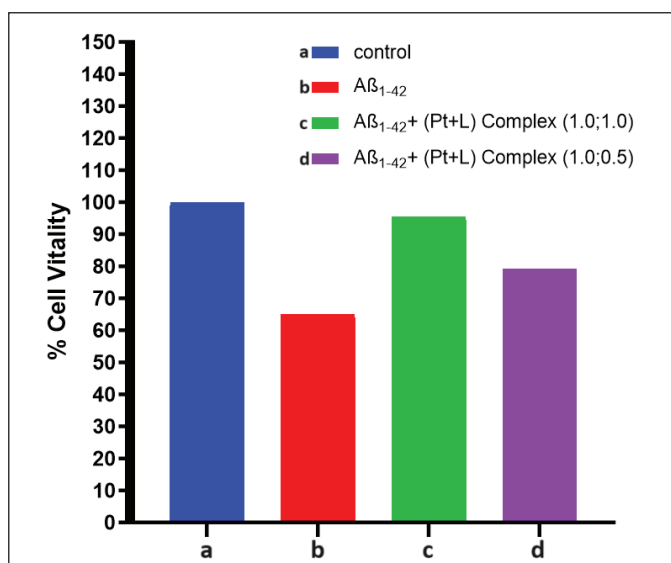


Figure 8. Inhibition of the $\text{A}\beta_{1-42}$ toxicity.

After 72 hours (Vyas et al. 2018) 10 μM . $\text{A}\beta_{1-42}$ was found to have approximately 65% cell viability by measurements, which is consistent with literature data (Kristhal et al. 2019). Interactions of the complexes with amyloid at 1:1 and 1:0.5 molar ratios were also performed over 72 hours.

As seen in the Figure 8, because of the findings, it was observed that the complex at both molar ratios inhibited the cytotoxicity caused by $\text{A}\beta_{1-42}$ aggregation.

It showed higher activity in 1.0: 1.0 molar ratio than 1.0:0.5 in 1 molar ratio. This is compatible with some literature data (Roberts et al. 2020). When the studies on Pt complexes were examined, it was observed that certain activation was obtained at 1.0:2.0 amyloid/complex ratios in general. The result determined for the complex in this study appears to be lower than the metal molar ratio found in many other studies (Messori et al. 2013).

3.3. Thioflavine-T Aggregation Inhibition Studies

One of the most common method used to determine the aggregation kinetics of $\text{A}\beta_{1-42}$ is the Thioflavine-T fluorescence measurement technique. As a control, $\text{A}\beta_{1-42}$ in the medium showed an increase in fluorescence over time. To determine the $\text{A}\beta_{1-42}$ / complex interaction ratio, measurements with $\text{A}\beta_{1-42}$ / complex molar ratios of 1.0:1.0 and 1.0: 0.5 were made. The results are given in Fig 9a and 9b. As a result of this measurement, it was observed that the interaction of 1.0:1.0 molar ratio inhibited amyloid aggregation more than other ratio. Compared with literature data, the complexes we examined show a lower molar ratio (Messori et al. 2013, Lu et al. 2015) suggesting that they are more active in amyloid aggregation. By analyzing the area under the curve, it can be calculated that complex (1.0:1.0 molar ratio) interacts with amyloide at a rate of 65%.

There are only three studies conducted with Schiff bases in the literature (Heffern et al. 2014, Roberts et al. 2020, Iscen et al. 2019), and the effect of only one Co-Schiff base complexes on the aggregation of $\text{A}\beta_{1-42}$ was examined and it was reported that the compound they synthesized interacted with amyloid at a rate of approximately 70% (Roberts et al. 2020). In studies available in the literature, the values generally found for the compounds examined in fluorescence measurement data are those with a similar effect in the molar ratio of 1.0:2.0 (amyloid/complex) (Roberts et al. 2020, Messori et al. 2013, Lu et al. 2015). In a few studies, the interaction ratio is 1.0:1.0 (Vyas et al. 2018, Florio et al. 2020). These results obtained in our study show that complex Pt-L is promising in terms of inhibition of $\text{A}\beta_{1-42}$.

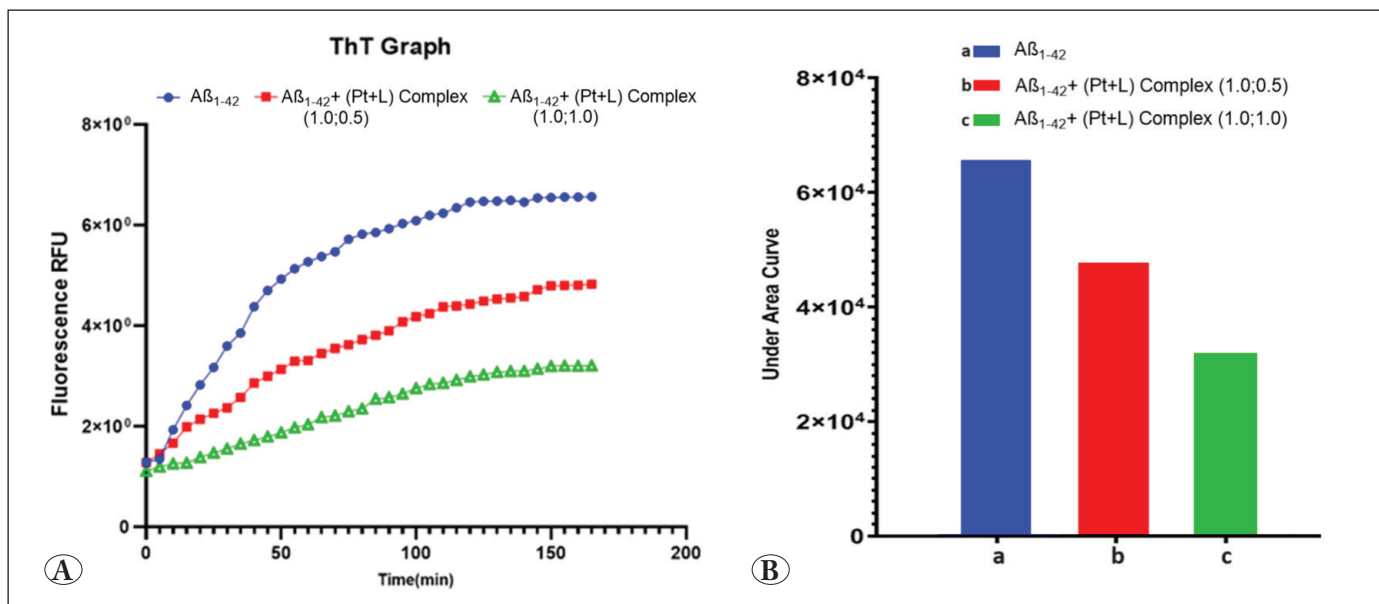


Figure 9. A) Fluorescent graphic. B) Under the curve Area.

4. Conclusion and Suggestions

In this study, the synthesis of a new amine/imine structured Schiff base and its chelated platinum complex is reported. The structures of the ligand and the complex were elucidated by spectroscopic methods. The cytotoxicity of the complex on SH-SY5Y neuroblastoma cells was examined and its IC₅₀ value was found as 19.22 µM.

The activation of the complex on the cells with amyloid was measured by determining the non-toxic concentration. It has been determined that it inhibits amyloid aggregation and increases cell viability, especially when the amyloid/complex is in a 1.0:1.0 molar ratio. Again, with the help of fluorescence measurements, it was understood that the complex interacts with 65% of the amyloid. These results obtained in our study show that the complex is promising in terms of inhibition of A_β₁₋₄₂.

5. References

- Damoc, M., Stoica, AC., Macsim, A., Dascalu, M., Zaltariov, M., Cazacu, M. 2020. Salen-type schiff bases spaced by the highly flexible and hydrophobic tetramethyldisiloxane motif. Some synthetic, structural and behavioral particularities, Journal of Molecular Liquids, 2020, 316, 113852-113863. Doi: 10.1016/j.molliq.2020.113852
- Florio, D., Cuomo, M., Iacobucci, I., Ferraro, G., Mansour, AM., Monti, M., Merlini, A., Marasco, D. 2020. Complexes modulation of amyloidogenic peptide aggregation by photoactivatable CO-releasing ruthenium(II) complexes. Pharmaceuticals, 8, 171-183. Doi: 10.3390/ph13080171
- Gaetke, LM., ChowJohnson, HS., Chow, C.K. 2014. Copper: toxicological relevance and mechanisms. Archives of Toxicology, 88, 1929-1938. Doi: 10.1007/s00204-014-1355-y
- Garai, M., Das, A., Joshi, M., Paul, S., Shit, M., Choudhury, AR., Biswas, B. 2018. Synthesis and spectroscopic characterization of a photo-stable tetrazinc (II)-Schiff base cluster: A rare case of ligand centric phenoxyazinone synthase activity. Polyhedron, 156, 223-230. Doi: 10.1016/j.poly.2018.09.044
- Gümüş, F., Eren, G., Açıkk, L., Çelebi, A., Öztürk, F., Yılmaz, Ş., Sağkan, RI., Gür, S., Özkul, A., Elmalı, A., Elerman, Y. 2009. Synthesis, cytotoxicity, and dna interactions of new cisplatin analogues containing substituted benzimidazole ligands. Journal of Medicinal Chemistry, 52, 1345-1357. Doi: 10.1021/jm8000983
- Haas, A. 1971. The synthesis and characterization of inorganic compounds. Angewandte Chemie, 83, 220-220. Doi: 10.1002/ange.19710830622.
- Heffern, MC., Velasco, PT., Matosziuk, LM., Coomes, JL., Karras, C., Ratner, MA., Klein, WI., Eckermann, AL., Meade, TJ. 2014. Modulation of amyloid-β aggregation by histidine-coordinating Cobalt(III) schiff base complexes. ChemBioChem Communications, 15, 1584-1589. Doi: 10.1002/cbic.201402201

- Iscen, A., Brue, CR., Roberts, KF., Kim, J., Schatz, GC., Meade, TJ.** 2019. Inhibition of amyloid- β aggregation by cobalt(III) schiff base complexes: A computational and experimental approach. *Journal of the American Chemical Society*, 141, 16685-16695. Doi: 10.1021/jacs.9b06388.
- Kepp, KP.** 2017. Alzheimer's disease: How metal ions define β -amyloid function. *Coordination Chemistry Reviews*, 351, 127-159. Doi: 10.1016/j.ccr.2017.05.007
- Khan, HY., Ahmad, A., Hassan, MN., Khan, YH., Arjmand, F., Khan, RH.** 2024. Advances of metallodrug-amyloid β aggregation inhibitors for therapeutic intervention in neurodegenerative diseases: Evaluation of their mechanistic insights and neurotoxicity. *Coordination Chemistry Reviews*, 501, 215580-215599. Doi: 10.1016/j.ccr.2023.215580
- Krishtal, J., Metsla, K., Bragina, O., Tougu, V., Palumaa, P.** 2019. Toxicity of amyloid- β peptides varies depending on differentiation route of SH-SY5Y cells. *Journal of Alzheimer Disease*, 71, 879-887. Doi: 10.1016/j.jipharm.2018.07.046
- Liu, HY., Li, C., Ma, JJ.** 2014. New Vanadium and Zinc Complexes with Schiff Base Ligand N,N'-bis(3-Ethoxy-2-Hydroxybenzylidene)ethylenediamine: Synthesis, Structures, and biochemical properties. *Russian journal Coordination Chemistry*, 40, 240-245. Doi: 10.1134/S1070328414040046
- Liu, H., Qu, Y., Wang, X.** 2018. Amyloid β -targeted metal complexes for potential applications in Alzheimer's disease. *Future Medicinal Chemistry*, 10, 1756-8919. Doi: 10.4155/fmc-2017-0248
- Lu, L., Zhong, HJ., Wang, M., Ho, SL., Li, HW., Leung, CH., Ma, DL.** 2015. Inhibition of beta-amyloid fibrillation by luminescent iridium (III) complex probes. *Scientific reports*, 5, 14619. Doi: 10.1038/srep14619
- Messori, L., Camarri, M., Ferraro, T., Gabbani, C., Franceschini, D.** 2013. Promising in vitro anti-alzheimer properties for a ruthenium(III) complex. *ACS Medicinal Chemistry Letters*, 4, 329-332. Doi: 10.1021/ml3003567
- Miles, BA., Patterson, AE., Vogels, CM., Decken, AJ., Waller, C., Morin, PJ., Westcott, SA.** 2016. Synthesis, characterization, and anticancer activities of lipophilic pyridinecarboxaldimine platinum(II) complexes, *Polyhedron*, 108, 23-29. Doi: 10.1016/j.poly.2015.07.039
- Mohammed, GG., Omar, MMA., Moustafa, BS., AbdEl-Halim, HF., Farag, NA.** 2022. Spectroscopic investigation, thermal, molecular structure, antimicrobial and anticancer activity with modelling studies of some metal complexes derived from isatin Schiff base ligand. *Inorganic Chemistry Communications*, 141, 109606-109619. Doi: 10.1016/j.inoche.2022.109606
- Mosmann, T.** 1983. Rapid colorimetric assay for cellular growth and survival: application to proliferation and cytotoxicity assays. *Journal of Immunological Methods*, 65, 55-63. Doi: 10.1016/0022-1759(83)90303-4.
- Pal, CK., Mahato, S., Joshi, M., Paul, S., Choudhury, AR., Biswas, B.** 2020. Transesterification activity by a zinc(II)-Schiff base complex with theoretical interpretation. *Inorganic Chimica Acta*, 506, 119541. Doi: 10.1016/j.ica.2020.119541
- Palanimuthu, D., Poon, R., Sahni, S., Anjum, R., Hibbs, D., Lin, HY., Bernhardt, PV., Kalinowski, DS., Richardson, DR.** 2017. A novel class of thiosemicarbazones show multifunctional activity for the treatment of Alzheimer's disease. *European Journal of Medicinal Chemistry*, 139, 612-632. Doi: 10.1016/j.ejmech.2017.08.021
- Patterson, AE., Miller, JJ., Miles, BA., Stewart, EL., Melanson, JM., Vogels, EJ., Cockshutt, CM., Decken, AM., Morin, A., Westcott, PJ.** 2014. Synthesis, characterization and anticancer properties of (salicylaldiminato) platinum(II) complexes, *Inorganica Chimica Acta*, 415, 88-94. Doi: 10.1016/j.ica.2014.02.028
- Price, JH., Williamson, AN., Schramm, RF., Wayland, BB.,** 1972. Palladium(II) and platinum(II) alkyl sulfoxide complexes. Examples of sulfur-bonded, mixed sulfur- and oxygen-bonded, and totally oxygen-bonded complexes. *Inorganic Chemistry*, 11, 1280-1284. Doi: 10.1021/ic50112a025
- Rao, PS., Kurumurthy, C., Veeraswamy, B., Kumar, GS., Narsaiah, B., Kumar, KP., Murthy, USN., Karnewar, S., Kotamraju, S.** 2013. Synthesis, antimicrobial and cytotoxic activities of novel 4-trifluoromethyl-(1,2,3)-thiadiazolo-5-carboxylic acid hydrazide Schiff's bases. *Medicinal Chemistry Research*, 22, 1747-1755. Doi: 10.1007/s00044-012-0168-x
- Roberts, KF., Brue, CR., Preston, A., Baxter, D., Herzog, E., Varelas, E., Meade, TJ.** 2020. Cobalt(III) Schiff base complexes stabilize non-fibrillar amyloid- β aggregates with reduced toxicity. *Journal of Inorganic Biochemistry*, 213, 111265. Doi: 10.1016/j.jinorgbio.2020.111265
- Ross, CA., Poirier, MA.** 2004. Protein aggregation and neurodegenerative disease. *Nature Medicine*, 10, 10-17. Doi: 10.1038/nm1066
- Rowinska-Zyrek, M., Salerno, M., Kozłowski, H.** 2015. Neurodegenerative diseases - Understanding their molecular bases and progress in the development of potential treatments. *Coordination Chemistry Reviews*, 284, 298-312. Doi: 10.1016/j.ccr.2014.03.026
- Ryan, TM., Caine, J., Mertens, HDT., Kirby, N., Nigro, J., Breheny, K., Waddington, LJ., Strelsov, VA., Curtain, C., Masters, CL., Robert, BR.** 2013. Ammonium hydroxide treatment of $\alpha\beta$ produces an aggregate free solution suitable for biophysical and cell culture characterization. *Peerj*, 73, 1-20. Doi: 10.7717/peerj.73

- Santos, MA., Chand, K., Chaves, S. 2016.** Recent progress in multifunctional metal chelators as potential drugs for Alzheimer's disease. *Coordination Chemistry Reviews*, 327-328, 287-303. Doi: 10.1016/j.ccr.2016.04.013
- Shiju, C., Arish, D., Bhuvanesh, N. Kumaresan, S. 2015.** Synthesis characterization and biological evaluation of schiff base-platinum(II) complexes. *Spectrochimica Acta, Part A: Molecular and Biomolecular Spectroscopy*, 145, 213-222. Doi: 10.1016/j.saa.2015.02.030
- Soto, C., Pritzkow, S. 2018.** Protein misfolding, aggregation, and conformational strains in neurodegenerative diseases. *Nature Neuroscience*, 21, 1332-1340. Doi: 10.1038/s41593-0180235-9
- Valensin, D., Gabbani, C., Messori, L. 2012.** Metal compounds as inhibitors of β -amyloid aggregation. Perspectives for an innovative metallotherapeutics on Alzheimer's disease. *Coordination Chemistry Reviews*, 256, 2357-2366. Doi: 10.1016/j.ccr.2012.04.010
- Vyas, NA., Singh, SB., Kumbhar, AS., Ranade, DS., Walke, GR., Kulkarni, PP., Jani, V., Sonavane, UB., Joshi, RR., Rapole, S. 2018.** Acetylcholinesterase and A β aggregation inhibition by heterometallic ruthenium(II)-platinum(II) polypyridyl complexes. *Inorganic Chemistry*, 57, 7524-7535. Doi: 10.1021/acs.inorgchem.8b00091
- Xue, C., Lin, TY., Chang, D., Guo, Z. 2017.** Thioflavin T as an amyloid dye: fibril quantification, optimal concentration, and effect on aggregation, *Royal Society Open Science*, 4, 160696-160708. Doi: 10.1098/rsos.160696
- Yellol, GS., Yellol, JG., Kenche, VB., Liu, XM., Barnham, KJ., Donaire, A., Janiak, C., Ruiz, J. 2015.** Synthesis of 2-pyridyl-benzimidazole iridium(III), ruthenium(II), and platinum(II) complexes. study of the activity as inhibitors of amyloid- β aggregation and neurotoxicity evaluation. *Inorganic Chemistry*, 54, 470-475. Doi: 10.1021/ic502119b



Üç Aşamalı Derin Öğrenme Tabanlı Otomatik Araç Plakası Algılama ve Tanıma Sistemi

Autonomous Vehicle License Plate Detection and Identification System Based on Three-Stage Deep Learning

Emre Yücel¹ , Yalçın İşler^{1,2,*} , Yakup Kutlu³

¹İskenderun Teknik Üniversitesi, Lisansüstü Eğitim Enstitüsü, Bilgisayar Mühendisliği Anabilim Dalı, İskenderun, Hatay, Türkiye

²İzmir Katip Çelebi Üniversitesi, Mühendislik ve Mimarlık Fakültesi, Biyomedikal Mühendisliği Bölümü, Çiğli, İzmir, Türkiye

³İskenderun Teknik Üniversitesi, Mühendislik Fakültesi, Bilgisayar Mühendisliği Bölümü, İskenderun, Hatay, Türkiye

Öz

Araç plakalarının otomatik olarak algılanması ve tanımlanması sistemleri araçlarla girilebilen ve güvenlik gerektiren ücretli otopark girişleri, otoban gişeleri, mobese kameraları, site ve alış-veriş merkezi girişleri gibi yerlerde vazgeçilmez hale gelmiştir. Araç sayısının hızlı artışı nedeniyle, araç plakalarının hızlı ve doğru tespit edilmesini gerektirmektedir. Öte yandan görüntüleme cihazına araçların ve plakaların farklı açı ve boyutlarda gelmesi nedeniyle araç plakasının otomatik tanınmasında problem yaşanmaktadır. Bu çalışmada You Only Look Once (bu yaygın İngilizce tanımına uygun yaygın kısaltması olan YOLO) ve evrişimsel sinir ağları (ESA) derin öğrenme modelleri ile araç plakasının algılanması, araç plakası üzerindeki karakterlerin yerlerinin tespit edilmesi ve bu karakterlerin sınıflandırılarak plakanın tanınması için üç aşamalı bir sistem tasarlanmıştır. Plakaların bulunması ve plaka üzerindeki karakterlerin ayrıştırılması aşamalarında kullanılan iki ayrı YOLO modelinin her ikisinde de %100 başarı elde edilmiştir. Plaka üzerindeki karakterlerin sınıflandırılması ile plaka tanıma aşamasında kullanılan ayrı bir ESA modelinde ise %94.9 başarı oranı elde edilmiştir. Literatürle kıyaslandığında, ilk iki aşamada elde edilen sonuçların diğer çalışmalardan daha yüksek olduğu ve son aşamada ise yaklaşık olarak benzer başarı elde edildiği görülmüştür.

Anahtar Kelimeler: ESA, derin öğrenme, otomatik araç plakası algılama, otomatik araç plakası tanıma, YOLO.

Abstract

Autonomous detection and identification of vehicle license plates have become indispensable in places that can be entered by vehicles and require security, such as paid parking exits, highway toll kiosks, mobile security cameras, site and shopping centre entrances. Due to the rapid increase in the number of vehicles, it is necessary to detect vehicle license plates quickly and accurately. On the other hand, the main problem in automatic recognition of vehicle license plates is that vehicles and license plates come to the imaging device at different angles and sizes. In this study, a three-stage system was designed to detect the license plate using You Only Look Once (YOLO) and Convolutional Neural Network (CNN) deep learning models, to locate the characters on the license plate, and to classify these characters and identify the license plate. 100% success was achieved in both stages of finding the license plates and separating the characters on the license plate using two distinct YOLO models. A success rate of 94.9% was achieved in the license plate recognition phase by classifying the characters on the license plate using a separate CNN model. When compared with the literature, the first two stages achieved higher accuracies than the other studies and the last stage resulted in similar accuracy.

Keywords: CNN, deep learning, automatic vehicle plate detection, automatic vehicle license recognition, YOLO.

*Sorumlu yazarın e-posta adresi: islerya@yahoo.com

Emre Yücel orcid.org/0009-0009-7617-8087

Yalçın İşler orcid.org/0000-0002-2150-4756

Yakup Kutlu orcid.org/0000-0002-9853-2878



1. Giriş

Son yıllarda araç kullanım sayısı insanların ihtiyaçları ve nüfusun çoğalmasından dolayı hızla artmıştır. Türkiye İstatistik Kurumu'na göre son 20 yılda sadece ülkemizde kayıtlı araç sayısı yaklaşık dört katına çıkmıştır (TÜİK, 2024). Araç sayısındaki bu artış yarattığı trafik yoğunluğunun yanısıra park alanları, otoyol ve köprü gişeleri gibi ücret tahsilatı noktaları ile radara yakalanan ve suça karışan araçların tespit edilmesinde sorunlarına artışına sebep olmuştur (Du vd. 2017).

Bu sorunları çözmek için araç plakalarının otomatik olarak tanımlanması bir seçenek olabilir (Özbay ve Erçelebi 2005). Otomatik araç plaka sistemleri insan bir operatöre ihtiyaç duyulmadan, araç plakalarının doğru bir şekilde tanımlanmasını amaçlamaktadır (Du vd. 2017). Temelde otomatik plaka tanıma sistemi üç temel aşamadan oluşur: (1) plaka yerinin tespiti, (2) bulunan plakadaki karakterlerinin ayrıştırılması ve (3) bu ayrıstırılan karakterlerin sınıflandırılması (Du vd. 2017).

İlk yapılan araç plaka tanıma sistemlerinin çoğunlukla görüntü işleme teknikleri kullanılmıştır (Zhuang vd. 2018). Zamanla teknolojinin gelişmesiyle birlikte, makine öğrenme algoritmalarının kullanımı her alanda artmıştır (İşler 2009). Son zamanlarda görüntü tabanlı makine öğrenmesi çalışmalarında derin öğrenme (özellikle de evrişimsel sinir ağı (ESA) modellerinin kullanımı oldukça popüler hale gelmiştir (Narin ve İşler 2021). Böylece görüntü işleme algoritmalarına ve herhangi bir ön işleme gerek olmadan daha hızlı bir sonuç elde edilmesine olanak sağlanmaktadır (Sürücü vd. 2021).

Son zamanlarda yapılan araç plaka tanıma sistemi çalışmalarına bakıldığından, görüntü işleme teknikleri ile ESA sinir ağı modelleri birlikte kullanılmaya başlandığı görülmektedir (Çay vd. 2023). Örneğin, Anagnostopoulos ve arkadaşları yaptıkları çalışmada 1334 araçlık bir veri seti kullanmışlardır. Plakadaki özellik çıkarımı için kayan ortak merkezli pencereler ve bağlı bileşen analizi, karakterlerin tanınması ve sınıflandırılması için olasılıksal sinir ağları kullanarak %89.1 sınıflandırıcı doğruluğu oranı elde etmişlerdir (Anagnostopoulos vd. 2006). Zhou ve arkadaşları yaptıkları çalışmada 410 araçlık kendi oluşturdukları ve 112 araçlık Caltech Cars veri setlerini kullanmışlardır. Bu çalışmada kelime eşleme ve Scale Invariant Feature Transform (SIFT) algoritmaları kullanılarak %93.2 sınıflandırıcı doğruluğu elde edilmiştir (Zhou vd. 2012). Laroca ve arkadaşları da yaptıkları çalışmada You Only Look Once (YOLO) derin öğrenme mode-

li kullanarak %93.5 sınıflandırıcı doğruluğu elde etmişlerdir (Laroca vd. 2018). Shashidhar ve arkadaşları ise Hint Karakterli plakalarını otomatik tanımlamayı amaçlamışlardır. Bu çalışmada plakanın yeri YOLO modeli ile bulunduktan sonra karakterlerin tanınması için geliştirdikleri bir ESA modelini görüntü iyileştirme metotları ile desteklemiştir. Bu ilginç çalışmada, araç plaka yerinin tespiti için 1200 ve karakterlerin tanımlanması için 6439 farklı Hint alfabeti nümerik görüntü veri kümesi kullanılmıştır. Sonuç olarak %91.5 sınıflandırıcı doğruluğuna ulaşmayı başarmışlardır (Shashidhar vd. 2021). Guo ve Liu ise plaka yerinin tespiti ve karakterinin tanınmasını amaçladıkları çalışmada 332 farklı araç görüntüsü kullanmışlardır. Plakanın tanınması için renk özellikleri ve Hough Dönüşümü kullanılmış olup %93.6 sınıflandırıcı doğruluğunu elde edilmiştir (Guo ve Liu 2008). Yuan ve arkadaşları ise plaka tespiti için 3828 araçlık Caltech veri seti kullanmışlardır. Plakadaki özellik çıkarımı ve plaka yerinin tespiti için kenar bulma, bölütleme ve çizgi yoğunluk filtreleri kullanılmışlardır. Yazarlar sınıflandırıcı olarak destek vektör makinesi (DVM) kullandıkları çalışmada %96.6 doğruluk elde etmişlerdir (Yuan vd. 2016). Li ve arkadaşları da plaka tespiti için elde edilen görüntünün çözünürlüğe ve gece-gündüz olmasına göre dört gruba ayrılmış toplam 1418 araçlık bir veri seti kullanmışlardır. Plaka tespiti için kenar bulma, geometrik görsel öznitelik çıkarma yöntemlerini kullanılarak %97.6 başarı elde edilmiştir (Li vd. 2013). Panahi ve Gholampour tarafından gerçekleştirilen çalışmada ise plaka yerini ve numaralarını tanımak amaçlanmıştır. Bunun için kendi oluşturdukları 8000 araçlık veri seti kullanmışlardır. Plakadan öznitelik çıkarımı için bağlı bileşenler analizi ve rastgele örneklemeye yöntemlerini kullanmışlardır. Sınıflandırıcı olarak olasılıksal DVM kullandıkları çalışmada %91.4 başarı elde edilmiştir (Panahi ve Gholampour 2016). Rafique ve arkadaşları ise ESA kullanarak plaka yerini bulmayı amaçlamışlardır. Bu nedenle Pascal VOC2007 veri seti ile kendi oluşturdukları toplamda 2871 görsellik veri seti kullanmışlardır. Plakadaki yerinin tespiti için bölge tabanlı ESA (R-ESA) derin öğrenme modeli ve DVM algoritmaları kullanılan bu çalışmada %94.5 sınıflandırıcı doğruluğu elde edilmiştir (Rafique vd. 2018). Li ve arkadaşları tarafından gerçekleştirilen başka bir çalışmada plaka algılama ve tanıma amaçlamıştır. Bunun için 322000 eğitim, 138000 test için olmak üzere toplam 460000 görsellik bir veri seti kullanılmıştır. Plakayı algılamak ve tanımak için ESA ve R-ESA modelleri kullanılmış ve %96.5 sınıflandırıcı doğruluğu elde edilmiştir (Li vd. 2018). Telatar ve Çamaşırçioğlu (2007) plaka algılamayı ve tanımayı amaçlamışlardır. Bunun için 100 araçlık veri seti

kullanılmışlardır. Plaka yerinin tespiti için renk değişimi kullanılmıştır. Plakadaki karakter tespiti için yapay sinir ağları (YSA) modeli kullanılmıştır. Yapılan çalışma sonrası %98.8 başarı oranı elde edilmiştir. Zhuang ve arkadaşları yaptıkları çalışmada plaka tanıma amaçlı AOLP 1874 araçlık, Media Lab 706 araçlık, Chinece License 5057 araçlık veri setlerini kullanmışlardır. Plakayı tanıma için DeeplabV2 Resnet 101 modellerini kullanarak %99.2 başarı oranı elde edilmiştir (Zhuang vd. 2018). Plaka tanımayı amaçlayan başka bir çalışmada, plaka tespiti için 300 eğitim ve 130 test verisinden oluşan araç veri seti ve karakter tanımak için 2165 eğitim verisinden ve 975 test verisinden oluşan karakter veri seti kullanılmışlardır. Bu çalışmada plakalar manuel olarak etiketlenmiştir. Sınıflandırma için Resnet-101 modeli kullanarak %98.4 sınıflandırıcı doğruluğu elde edilmiştir (Bayram 2020). Bingöl ve Kuşçu (2008) yaptıkları çalışmada plaka tanımayı amaçlamışlardır. Bunun için 100 görüntüden oluşan veri seti kullanılmışlardır. Plakadan öznitelik çıkarımı ve yer tespiti için görüntü işleme algoritmaları kullanılmışlardır. Karakter tespiti için ise karakter bulup veri tabanı ile karşılaştırılmıştır. Yapılan çalışma sonrası %87.0 başarı oranı elde edilmiştir. Çelik ve Oral (2003) yaptıkları çalışmada plaka tanımayı amaçlamışlardır. Bunun için 105 görsellik veri seti üzerinden görüntü işleme algoritmaları ile plaka yeri tespiti yapılmıştır. Plakadaki karakter tespiti için YSA modeli kullanılmış olup %89.0 sınıflandırıcı doğruluğu elde edilmiştir.

Araç sayısının ve trafik yoğunluğun hızlı artışı nedeniyle, araç plakalarının hızlı ve doğru tespit edilebilmesi için yukarıda açıklandığı gibi birçok çalışma yapılmıştır. Öte yan- dan görüntüleme cihazına araçların farklı açılarda girmesi ve plakaların farklı boyutlarda ve yerlerde olması nedeniyle araç plakasının otomatik tanınmasında problem yaşanmaktadır. Bu problemleri aşmak için, bu çalışmada hem görüntü kalitesini artırmak için görüntü işleme yöntemlerini hem son yıllarda umut eden başarılı sonuçları nedeniyle YOLO ve ESA tabanlı derin öğrenme modelleri kullanılarak otomatik bir plaka tanıma sistemi geliştirilmesi hedeflenmiştir. Bu hedefe ulaşmak için plaka yerinin bulunması, plaka üzerindeki karakterlerin belirlenmesi ve bu karakterlerin tanınması şeklinde üç aşamalı bir sistem önerilmiştir. Problemin tanımlanlığı ve literatürde verilen çözüm önerilerinin özetlendiği bu giriş bölümünden sonra makalenin akışı şu şekilde olacaktır. Önce çalışmada kullanılan veri setinin de açıklandığı *Gereç ve Yöntemler* bölümü, sonra çalışmanın nasıl gerçekleştirildiğinin verildiği *Uygulama* bölümü, son olarak ise elde edilen sonuçlar ve bu sonuçların literatürdeki yerleinin yorumlandığı *Sonuçlar ve Tartışma* bölümü verilecektir.

2. Gereç ve Yöntemler

2.1. Veri Setleri

Plaka yerinin tespiti, karakterlerin ayırtılması ve karakterlerin sınıflandırılması olacak şekilde üç aşamalı bir sistem geliştirilecek olması sebebiyle modellerin eğitilmesi için üç farklı veri seti kullanılmıştır. İlk aşama olan araç görseli üzerindeki plaka yerinin tespiti için internet üzerinden kolayca erişilebilen Kaggle Car License Plate Detection Dataset veri seti kullanılmıştır. Bu veri seti içerisinde, farklı ülkelerdeki farklı marka, model ve renklerde toplanmış toplam 433 araç fotoğrafı bulunmaktadır. Bu araçlara ait plakaların konumları eğitim için ayrı ayrı belirlenmiş ve bu konumlar veri setine ait XML dosyası içerisinde kaydedilmiştir. Bu veri setinden örnek araç görüntüleri Şekil 1'de gösterilmiştir (Larxel 2020).

İkinci aşama olan plakada yer alan karakterlerin konumlarının belirlenmesi için farklı bir veri seti oluşturulmuştur. Bu veri seti internet üzerinden görsel arama motorları ile araştırma yapılarak uygun olanların toplandığı farklı plakalardan oluşan yeni bir veri setidir. Bu veri seti içerisinde toplamda 451 araç plaka görseli ve her görselde 6 karakter bulunmaktadır. Bu plakalara ait karakterlerin konumları eğitim için ayrı ayrı belirlenmiş ve bu konumlar veri setine ait XML dosyası içerisinde kaydedilmiştir.

Son aşama olan plakada yer alan karakterleri sınıflandırmak için, yine internet üzerinden kolayca erişilebilen Kaggle License Plate Digits Classification Dataset veri seti kullanılmıştır (Jelal 2021). Toplamda 35 kategoride 35500 karakter görseli yer almaktadır. Her karakter için kullanılan görsellerin örnek görüntüsü Şekil 2'de gösterilmiştir.



Şekil 1. Plaka yerinin tespiti için eğitimde kullanılan örnek araç görselleri (Larxel 2020).



Şekil 2. Karakter tanıma için eğitimde kullanılan örnek karakter görselleri (Jelal 2021).

Çalışmanın test edilebilmesi için eğitimde kullanılmamış veriler olması gerektiğinden, sadece test aşaması için yeni bir veri seti oluşturulmuştur. Bu veri seti internet üzerinden görsel arama motorları kullanılarak birbirinden farklı renk, ortam, model, marka ve açılarda konumlanmış toplam 125 araç ile oluşturulmuştur. Bu araçların plakalarında bulunan toplam karakter sayısı ise 922'dir.

2.2. YOLO Algoritması

YOLO (You Look Only Once) "sadece bir kere bak" demektir ve son zamanlarda ortaya çıkan, nesne tespitinde kullanılan bir algoritma olup gerçek zamanlı görüntü işleme için kullanılan bir nesne algılama sistemidir. YOLO algoritması görselleri öncelikle bölgelere ayırır ve her bir bölgede nesne olup olmadığını incelemektedir. Algoritma bunu yaparken bölgelerdeki nesnelere güven oranı tayin ederek bu güven oranına göre nesnenin ne olduğuna karar vermektedir. YOLO giriş görüntülerini SxS ızgara hücresına bölmektedir (Redmon vd. 2016). Her bir ızgara hücresi yalnızca bir nesneyi ve sabit sayıda sınır kutusu tahmin etmektedir (Çağrı ve Yıldırım 2020). YOLO algoritması görüntüleri yaklaşık 40-90 fps (saniye başına kare) hızında işleyebildiğiinden diğer yöntemlere göre oldukça hızlıdır. Böylece bir videonun gerçek zamanlı olarak (sadece birkaç milisaniye gecikme ile) işlenebilmesini mümkün kılmaktadır (Shinde vd. 2018).

R-ESA gibi yöntemler de görüntüleri bölgelere ayırıyor olmasına rağmen, YOLO bu bölgeleri tek nöral ağdan geçirirken diğerleri her blok için ayrı nöral ağlar kullandıkları için, YOLO daha hızlı ve etkili çalışabilmektedir (Bilgin 2021). YOLO algoritması da zaman içerisinde güncellenerek geliştirilmeye devam etmekte ve sürüm olarak (YOLOv3, YOLO algoritması sürüm 3 gibi) yayınlanmaktadır. Bu çalışmada YOLOv3 sürümü kullanılmıştır. Bu sürümünde 53

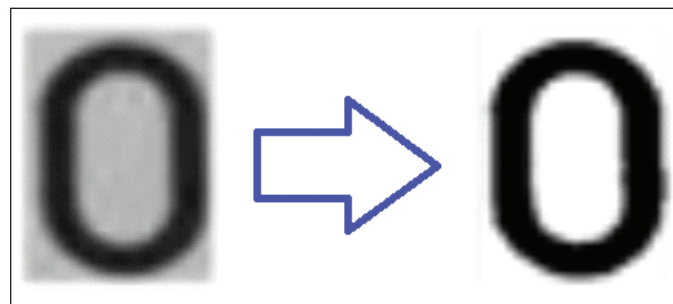
katmanlı ESA yapısı kullanan DarkNet-53 mimarisine 53 katman daha ilave edilerek toplam 106 katmanlı ESA derin öğrenme yapısına ulaşılmıştır. YOLOv3 bir önceki sürümüne göre daha yavaş çalışsa da, artı bloklar, bağlantı atlama ve yukarı örneklemeye gibi özellikler de bu yapıya eklenmiştir.

2.3. Resim İyileştirme Ön İşlemleri

Plaka üzerindeki karakterler ayırtırıldıktan sonra hem ESA eğitim aşamasında hem de karakterlerin sınıflandırılması işleminde daha doğru sonuç elde edebilmek için karakter görsellerine görüntü iyileştirme yöntemlerinden sırasıyla eşikleme ve histogram eşitleme uygulanmıştır.

Eşikleme

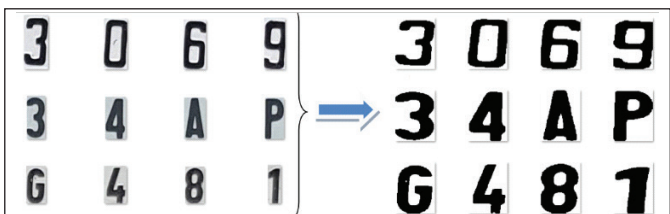
Eşikleme, bir görüntüdeki her bir piksel renk değerinin belirlenmiş olan eşik değerine göre değiştirilme işlemidir. Yani eğer piksel renk değeri belirlenen eşik değerinden küçükse o piksel renk değerine siyah atanır. Bu çalışmada görüntüdeki piksellerin ortalama değeri eşik değer olarak alınmıştır. Örnek bir araç plakasından alınan karakter görseline eşikleme uygulanması sonucu oluşan yeni görüntü Şekil 3'de gösterilmiştir.



Şekil 3. Orijinal görüntüye eşikleme uygulanması.

Histogram Eşitleme

Görüntüde histogram, bir resimdeki renk değerlerinin sayılarını gösteren grafiktir (Gonzalez ve Woods 2007). Histogram eşitleme ise bir görüntüdeki renk değerlerinin belirli bir değer aralığı içerisinde kümelenmesinden kaynaklı renk bozukluğunu gidermek için kullanılan bir yöntemdir. Hesaplama zamanı düşük ve oldukça etkili sonuçlar üretebilen bir yöntemdir (Arişoy ve Dikmen 2014). Bu yöntem sayesinde görüntüdeki renk değerleri belirli bir aralığa dağıtıldığından dolayı görüntüdeki ayrıntılara ve özniteliklere daha kolay erişilebilmektedir. Plakalardan elde edilen karakter görüntülerinin, eşikleme ve histogram eşitleme sonrası oluşan yeni görüntüleri Şekil 4'de örnek olarak gösterilmiştir.



Şekil 4. Orijinal karakter ve görüntüsünün, görüntü iyileştirme sonrası çıktıları.

2.4. ESA Modeli

ESA, genellikle görüntü işlemde kullanılan, girdi olarak görselleri alan ve otomatik olarak görüntülerini işleyen bir derin öğrenme algoritmasıdır (Sürücü 2022a, Sürücü 2022b, Narin ve İşler 2021). Farklı işlemler ile görsellerdeki özellikleri bulan ve bulduğu özellikler sayesinde görselleri sınıflandıran ESA algoritması farklı katmanlardan oluşmaktadır: Konvolüsyon katmanı, Havuzlama katmanı ve Tam Bağlantılı Sınıflandırma katmanı. ESA modeli yaygın kullanılan bir derin öğrenme modeli olup ayrıntılı bilgiye kitaplardan erişilebilir (Chollet 2018).

2.5. Metodoloji

İlk aşama olan araç üzerindeki plaka yerlerinin tespiti için YOLO ile eğitilmiş model kullanılarak araç üzerindeki plakanın konumu belirlenmiştir. Daha sonra resim kesme yöntemi ile plaka araç görselinden ayrıstırılmıştır. Şekil 5'de plakası bulunmuş ve işaretlenmiş araç görseli gösterilmiştir.

Daha sonra, plaka üzerindeki karakterlerin yerlerinin tespiti için YOLO ile eğitilmiş model kullanılmıştır. Böylece plaka üzerindeki karakterlerin konumları belirlenmiş ve karakterler resim kesme yöntemi plaka görselinden ayrıstırılmıştır.

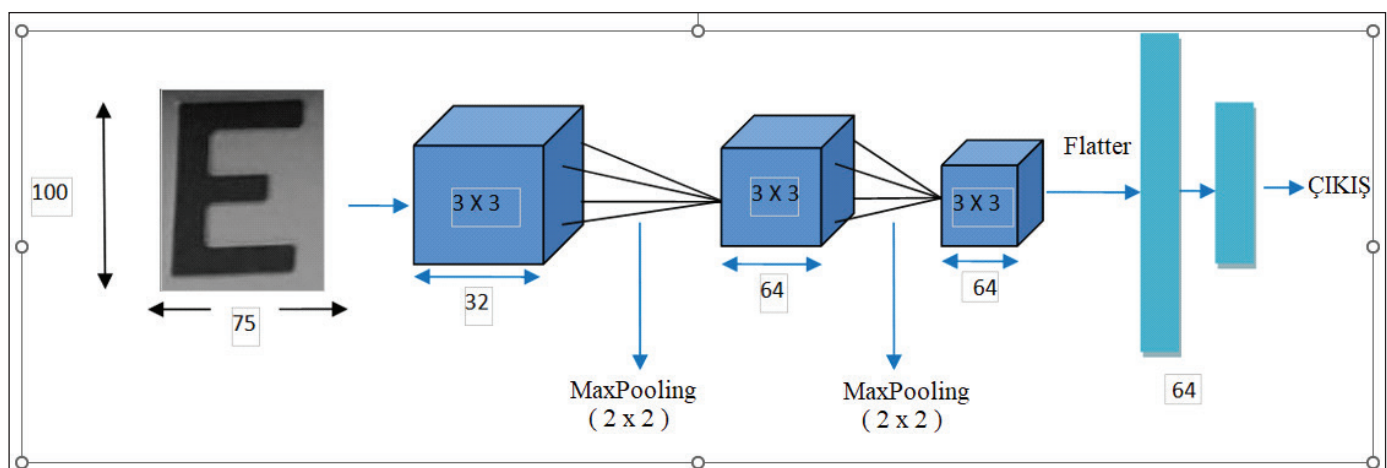


Şekil 5. YOLO algoritması ile plakası bulunmuş ve işaretlenmiş araç görseli.



Şekil 6. YOLO algoritması ile karakterleri işaretlenmiş plaka görseli.

Karakterin sınıflandırılması için ESA modeli kullanılmıştır. Eğitim için eğitim görselleri 75×100 boyutlarına getirilmiştir. Modelimizin konvolüsyon katmanları sırasıyla, 3×3 'luk 32filtreden, ardından 2×2 'lik MaxPooling katmanından, 3×3 'luk 64filtreden, ardından 2×2 'lik MaxPooling katmanından ve 3×3 'luk 64filtreden oluşmakta, fully connected katmani ise 64 nörondan oluşan tek gizli katmanından oluşmaktadır. Epoch değeri 10, batch_size değeri ise 64'tür. Eğitilen ESA modeli ile ayrıstırılan karakter görsellerin üzerinde yer alan karakterlerin sınıflandırılması sağlanmıştır. Oluşturulan ESA modeli katmanlarının ve parametrelerinin de yer aldığı hali ile Şekil 7'de görselleştirilmiştir.



Şekil 7. Oluşturulan ESA modelinin şeiksel gösterimi.

Geliştirilen ESA ve YOLO modellerinin değerlendirilmesinde iki farklı doğruluk ölçütü kullanılmıştır. Plaka veya karakterin yerinin doğru olarak sınıflandırılmasında kullanılan doğruluk ölçütünün hesaplanması için formülü kullanılmaktadır (İşler 2009). Bu formülde verilen DP, DN, YP ve YN kısaltmaları bu çalışmada kullanılan ilk iki sınıflandırıcıda farklı anımlara gelmektedir. Plaka yerinin tespiti olan birinci aşamada DP: plakayı içerecek şekilde doğru olarak işaretlenen görüntü parçası sayısını, DN: plaka içermeyen görüntü parçalarının doğru olarak işaretlendiği görüntü parçası sayısını, YP: plaka içermediği halde yanlışlıkla plaka varmış gibi işaretlenen görüntü parçası sayısını, YN: plaka içerdiği halde plaka yokmuş gibi işaretlenen görüntü parçası sayısını vermektedir. Plakadaki karakterlerin yerlerinin tespit edildiği ikinci aşamada DP: harf veya rakam içerecek şekilde doğru olarak işaretlenen görüntü parçası sayısını, DN: harf veya rakam içermeyen görüntü parçalarının doğru olarak işaretlendiği görüntü parçası sayısını, YP: harf veya rakam içermediği halde yanlışlıkla rakam veya harf varmış gibi işaretlenen görüntü parçası sayısını, YN: harf veya rakam içerdiği halde harf veya rakam yokmuş gibi işaretlenen görüntü parçası sayısını vermektedir.

Öte yandan, bu çalışmanın önceki aşamalarında yerleri zaten tespit edilmiş harf veya rakamların doğru olarak sınıflandırılmasında kullanılan doğruluk ölçütünün hesaplanması için formülü kullanılmaktadır (İşler 2009). Burada DP_i, i. harf veya rakamın doğru olarak sınıflandırılma sayısını ve N ise toplam harf ve rakam sayısını göstermektedir.

3. Sonuçlar ve Tartışma

Bu çalışmada araç plakalarının yerinin bulunması, plakalar üzerindeki karakterlerin belirlenmesi ve karakterlerin tanımlanması olmak üzere her aşaması için ayrı modelden oluşan üç aşamalı bir araç plaka tespit ve tanıma sistemi geliştirilmiş ve test edilmiştir. Bu kapsamında çevrimiçi paylaşılan iki veri seti kullanılırken karakter yeri belirlenmesi ve tüm sistemin test edilmesi için yeni veri seti daha oluşturulmuş ve sistemin geliştirilmesinde kullanılmıştır. Bu amaçla iki ayrı YOLO modeli ve bir ESA modeli oluşturulmuştur. İlk YOLO modeli araç plakasının yerini bulmak için, ikinci YOLO modeli ise araç plakası üzerindeki karakterlerin yeri bulmak için kullanılmıştır. Son aşamada ise karakterlerin sınıflandırılması için bir ESA modeli oluşturulmuştur.

YOLO ve ESA modelleri Python programlama dilinde Tensorflow ve Keras kütüphaneleri kullanılarak oluşturulmuştur. Bu derin öğrenme modellerinin eğitiminde yüksek işlem kapasiteleri bilgisayarlar kullanılması gerektiğinden,

geliştirme için Google Colab ortamı kullanılmıştır. Google Colab kısmen ücretsiz bir geliştirme ortamı olup <https://colab.research.google.com/> internet adresinden erişebilir.

Bu eğitilmiş modeller, test verileri üzerinde sırasıyla plakanın bulunması, karakterlerin bulunması ve karakterlerin sınıflandırılması olacak şekilde test edilmiş ve sonuçları alınmıştır. Araç üzerindeki plaka yerinin bulunmasında ve plaka üzerindeki karakterlerin bulunmasında %100 başarım oranı elde edilmiştir. Plaka yeri doğru tahmin edilmiş plaka üzerindeki karakterlerin sınıflandırılmasında görüntü iyileştirme işlemi kullanılmadan %85.0 ve görüntü iyileştirme işlemi yapıldıktan sonra %94.9 sınıflandırıcı doğruluğu elde edilmiştir. 125 araçlık test verileri kullanılarak plaka yerinin bulunması, karakterlerin ayırtılması ve karakterlerin sınıflandırılması şeklindeki üç aşama birlikte değerlendirildiğinde %94.9 başarım oranına ulaşılmıştır. Literatürdeki benzer çalışmalarında elde edilen sonuçlar ile bu çalışmanın ilk aşamasında elde edilen sonuçlar bir tabloda özetlenmiştir (Çizelge 1). Bu çalışmalarla kullanılan yöntemler, veri setleri ve elde edilen sınıflandırıcı doğruluk değerleri bu çizelgede karşılaştırılmıştır. Buna göre bu çalışma ile elde edilen sonuçların tatmin edici olduğu görülmektedir.

Literatürdeki benzer çalışmalarla elde edilen sonuçlar ile bu çalışmanın son aşamasında elde edilen sonuçlar bir tabloda özetlenmiştir (Çizelge 2). Diğer çalışmalarla plaka üzerindeki karakterlerin yerlerin tespit edilmesi ayrı olarak verilmemişten ikinci aşamaya ait sınıflandırıcı değerleri ayrıca karşılaştırılamamış ve tabloya karakter sınıflandırıcı sonuçları aktarılmıştır. Bu çalışmalarla hem karakter tespitinde hem de karakter sınıflandırmasında kullanılan yöntemler, veri setleri ve üçüncü aşama için elde edilen sınıflandırıcı doğruluk değerleri bu çizelgede karşılaştırılmıştır. Buna göre diğer çalışmaların ayrı bir test veri seti kullanıp kullanmadığı bilinmemekle birlikte, bu çalışmanın test verisi sınıflandırıcı doğruluk değeri çizelgeye aktarılmıştır. Bu nedenle elde edilen plaka tanıma sınıflandırıcı başarısının tatmin edici düzeyde olduğu görülmektedir.

Sonuç olarak, literatürdeki çalışmalarla farklı çevre ve boyutlardaki veri setleri kullanıldığı için objektif bir karşılaştırma olanağı mümkün değildir. Bununla birlikte, bu çalışmada önerilen üç aşamalı sistem ile elde edilen sonuçların diğer çalışmalar kadar iyi olduğu görülmektedir. Çalışmanın ilk iki aşamasında görüntü iyileştirme gerek kalmadan mükemmel başarı elde edilebilmiştir. Bununla birlikte görüntü iyileştirme yöntemi kullanılmadan ve kullanılarak elde edilen sonuçlara bakıldığından, sistemin son aşamasında görüntü iyileştirme yöntemlerinin sisteme eklenmesiyle daha başarılı

Çizelge 1. Araç plaka yerinin tespiti çalışmalarının karşılaştırılması. Çalışmalarda plaka yerinin tespiti için kullanılan yöntem(ler), kullanılan veri set(ler)i ve çalışma sonucunda ulaşılan sınıflandırıcı doğruluk değerleri yüzde (%) olarak verilmiştir.

Çalışma	Yöntem	Veri seti	Doğruluk (%)
(Guo ve Liu 2008)	Renk özellikleri Hough dönüşümü	332 araç	93.6
(Li vd. 2013)	Kenar bulma Geometrik yöntemler	1418 araç	97.6
(Rafique vd. 2018)	R-ESA DVM	Pascal Voc2007 2871 araç	94.5
(Li vd. 2018)	YOLO	-	93.5
(Zhuang vd. 2018)	DeepLab V2 Resnet 101	AOLP 1874 araç Media Lab 706 araç Chineese Lic. 5057 araç	99.2
Bu çalışma	YOLO	433 araç	100

Çizelge 2. Araç plakasının tespiti sonrası plaka üzerindeki karakterlerin sınıflandırılması çalışmalarının karşılaştırılması. Çalışmalarda karakterlerin yerinin tespiti için kullanılan yöntem(ler), karakterlerin sınıflandırılması için kullanılan yöntem(ler), kullanılan veri set(ler)i ve çalışma sonucunda ulaşılan sınıflandırıcı doğruluk değerleri yüzde (%) olarak verilmiştir.

Çalışma	Karakter tespiti	Karakter sınıflandırma	Veri seti	Doğruluk (%)
(Anagnostopoulos vd. 2006)	Bağılı bileşen analizi	Olasılıksal sinir ağı	1334 araç	89.1
(Zhou vd. 2012)	SIFT	Kelime eşleme	Caltech Cars 522 araç	93.2
(Yuan vd. 2016)	Kenar bulma Bölütleme Çizgi yoğunluğu	DVM	Caltech Cars 3828 araç	96.6
(Rafique vd. 2018)	Bağılı bileşen analizi Rastgele örneklemme	DVM	8000 araç	91.4
(Li vd. 2018)	ESA R-ESA	DVM	460000 araç	91.4
(Shashidhar vd. 2021)	YOLO	YSA	Hint RTO 1500 görüntü	91.5
(Bayram 2020)	Elle tespit	Resnet 101	430 araç	98.4
(Bingöl ve Kuşçu 2008)	Görüntü işleme	-	100 araç	97.0
(Telatar ve Caasircioglu 2007)	Görüntü işleme	YSA	100 araç	98.8
(Çelik ve Oral 2021)	Görüntü işleme	YSA	105 araç	89.0
Bu çalışma	YOLO	Resim iyileştirme ESA	451 araç 48321 karakter	94.9

sonuçlar elde edilebileceği görülmektedir. Bu durum derin öğrenme modellerinin görüntüden doğrudan öznitelik çi-karabildiği ayrıca başka bir işleme gerek kalmadığı (Chollet 2018, Sürücü 2021a, Sürücü 2021b) inanışına ters düşmekte birlikte aynı kanya ulaşan başka çalışmalar (Sürücü vd. 2021) da mevcuttur. Gelecek çalışmalarda iyi bilinen diğer görüntü işleme yöntemlerinin de eklenmesiyle daha başarılı bir sonuç elde edilmesi planlanmaktadır.

Yazar katkıları

Emre Yücel: Çalışma hakkında verileri toplamış ve analiz etmiştir, Yalçın İşler: Çalışmanın analizlerini yaparak makaleyi yazmıştır, Yakup Kutlu: çalışmayı planlamış ve tasarlamış olup diğer iki yazarın tez danışmanıdır.

4. Kaynaklar

- Anagnostopoulos, CNE., Anagnostopoulos, IE., Loumos, V., Kayafas, E.** 2006. A license plate-recognition algorithm for intelligent transportation system applications. *IEEE Trans. Intell. Transp. Syst.*, 7(3):377-392. Doi: 10.1109/TITS.2006.880641
- Arisoy, MÖ., Dikmen, Ü.** 2014. Manyetik belirti haritalarının histogram eşitleme yöntemi kullanılarak iyileştirilmesi. *Yerbilimleri*, 35(2):141-168. Doi: <https://doi.org/10.17824/huyuam.23614>
- Bayram, F.** 2020. Derin öğrenme tabanlı otomatik plaka tanıma. *Politeknik Dergisi*, 23(4):955-960. Doi: 10.2339/politeknik.515830
- Bilgin, A.** 2021. YOLO (You Only Look Once) mimarisini nedir? <https://aylablgn.medium.com/yolo-you-only-look-once-mimarisini-nedir-754d0bc6a6ba>. Yayın tarihi 30 Nisan 2021. Son erişim tarihi 16 Mayıs 2024.
- Bingöl, O., Kuşcu, Ö.** 2008. Bilgisayar tabanlı araç plaka tanıma sistemi. *Bilişim Teknolojileri Dergisi*, 1(3): 1-5. Url: <https://dergipark.org.tr/tr/pub/gazibtd/issue/6614/87879>
- Chollet, F.** 2018. Deep Learning with Python. 2. baskı, Manning Yayınevi.
- Çağıl, G., Yıldırım, B.** 2020. Bir montaj parçasının derin öğrenme ve görüntü işleme ile tespiti. *Zeki Sistemler Teori ve Uygulamaları Dergisi*, 3(2):31-37. Doi: 10.38016/jista.710144
- Çay, T., Ölmez, E., Er, O.** 2023. Bölgesel tabanlı evrişimsel sinir ağları ile araç plaka tanıma. *Düzce Üniversitesi Bilim ve Teknoloji Dergisi*, 11(1):10-20. Doi: 10.29130/dubited.1058850
- Çelik, U., Oral, M.** 2003. Motorlu araçlar için plaka tanıma sistemi. *Elektrik Elektronik- Bilgisayar Mühendisliği* 10. Ulusal Kongre ve Fuarı, İstanbul, 17-21 Eylül, s. 499-502.
- Du, S., Ibrahim, M., Shehata, M., Badawy, W.** 2017. Automatic license plate recognition (ALPR): A state-of-the-art review. *IEEE Trans. Circuits Syst. Video Technol.*, 23(2):311-325. Doi: 10.1109/TCST.2012.2203741
- Gonzalez, RC., Woods, RE.** 2007. Digital Image Processing. 3. baskı, ISBN: 978-0131687288, Prentice Hall International.
- Guo, JM., Liu, YF.** 2008. License plate localization and character segmentation with feedback self-learning and hybrid binarization techniques. *IEEE Trans. Veh. Technol.*, 57(3):1417-1424. Doi: 10.1109/TVT.2007.909284
- İşler, Y.** 2009. A detailed analysis of the effects of various combinations of heart rate variability indices in congestive heart failure. Doktora tezi, Dokuz Eylül Üniversitesi, Fen Bilimleri Enstitüsü, Elektrik-Elektronik Mühendisliği Anabilim Dalı, İzmir, s. 166.
- Jelal.** 2021. License plate digits classification dataset. <https://www.kaggle.com/aladdins/l-license-plate-digits-classification-dataset> Yayın tarihi 5 Haziran 2021. Erişim tarihi 29 Aralık 2023.
- Laroca, R., Severo, E., Zanlorensi, LA., Oliveira, LS., Gonçalves, GR., Schwartz, WR., Menotti, D.** 2018. A robust real-time automatic license plate recognition based on the YOLO detector. *International Joint Conference on Neural Networks (IJCNN)*, Rio de Janeiro, Brazil, 1-10. Doi: 10.1109/IJCNN.2018.8489629.
- Larxel.** 2020. Car license plate detection dataset. <https://www.kaggle.com/andrewmvrd/car-plate-detection>. Yayın tarihi 1 Haziran 2020. Son erişim tarihi 29 Aralık 2023.
- Li, B., Tian, B., Li, Y., Wen, D.** 2013. Component-based license plate detection using conditional random field model. *IEEE Trans. Intell. Transp. Syst.*, 14(4):1690-1699. Doi: 10.1109/TITS.2013.2267054
- Li, H., Wang, P., Shen, C.** 2018. Toward end-to-end car license plate detection and recognition with deep neural networks. *IEEE Trans. Intell. Transp. Syst.*, 20(3):1126-1136. Doi: 10.1109/TITS.2018.2847291
- Narin, A., İşler, Y.** 2021. Detection of new coronavirus disease from chest x-ray images using pre-trained convolutional neural networks. *Journal of the Faculty of Engineering and Architecture of Gazi University*, 36(4):2095-2107. Doi: 10.17341/gazimmfd.827921
- Özbay, S., Erçelebi, E.** 2005. Automatic vehicle identification by plate recognition. *World Acad. Eng. Technol.*, 9(41):222-225. Doi: 10.5281/zenodo.1331865
- Panahi, R., Gholampour, I.** 2016. Accurate detection and recognition of dirty vehicle plate numbers for high-speed applications. *IEEE Trans. Intell. Transp. Syst.*, 18(4):767-779. Doi: 10.1109/TITS.2016.2586520
- Rafique, MA., Pedrycz, W., Jeon, M.** 2018. Vehicle license plate detection using region-based convolutional neural networks. *Soft Comput.*, 22(19):6429-6440. Doi: 10.1007/s00500-017-2696-2
- Redmon, J., Divvala, S., Girshick, R., Farhadi, A.** 2016. You only look once: Unified, real-time object detection. *IEEE Conference on Computer Vision and Pattern Recognition (CVPR)*, Las Vegas, NV, USA, 779-788. Doi: 10.1109/CVPR.2016.91
- Shashidhar, R., Manjunath, AS., Kumar, RS., Roopa, M., Puneeth, SB.** 2021. Vehicle number plate detection and recognition using YOLO-V3 and OCR method. *2021 IEEE International Conference on Mobile Networks and Wireless Communications (ICMNWC)*, 1-5, Tumkur, Karnataka, India. Doi: 10.1109/ICMNWC52512.2021.9688407

- Shinde, S., Kothari, A., Gupta, V.** 2018. YOLO based human action recognition and localization. *Procedia Comput. Sci.*, 133:831-838. Doi: 10.1016/j.procs.2018.07.112
- Sürütü, M., İşler, Y., Perc, M., Kara, R.** 2021. Convolutional neural networks predict the onset of paroxysmal atrial fibrillation: Theory and applications. *Chaos*, 31(11):34881615. Doi: 10.1063/5.0069272
- Sürütü, M.** 2022a. Predicting capacity change in li-ion batteries using regression models. *J. Intell. Syst. Appl.*, 5(2):120-125. Doi: 10.54856/jiswa.202212229
- Sürütü, M.** 2022b. Improvement of CNN network parameters in turkish music emotion recognition. *J. Intell. Syst. Appl.*, 5(2):126-131. Doi: 10.54856/jiswa.202212230
- Telatar, Z., Çamaşırçioğlu, E.** 2007. Plate detection and recognition by using colour information and ANN. 2007 IEEE 15th Signal Processing and Communications Applications, Eskisehir, Turkey, 1-4. Doi: 10.1109/SIU.2007.4298583.
- TÜİK.** 2024. Motorlu Kara Taşıtları (Nisan 2024). 53456 nolu yayın. <https://data.tuik.gov.tr/Bulton/Index?p=Motorlu-Kara-Tasitlari-Nisan-2024-53456> Yayın tarihi 1 Mayıs 2024. Son erişim tarihi 27 Temmuz 2024.
- Yuan, Y., Zou, W., Zhao, Y., Wang, X., Hu, X., Komodakis, N.** 2016. A robust and efficient approach to license plate detection. *IEEE Trans. Image Process.*, 26(3):1102-1114. Doi: 10.1109/TIP.2016.2631901
- Zhou, W., Li, H., Lu, Y., Tian, Q.** 2012. Principal visual word discovery for automatic license plate detection. *IEEE Trans. Image Process.*, 21(9):4269-4279. Doi: 10.1109/TIP.2012.2199506
- Zhuang, J., Hou, S., Wang, Z., Zha, ZJ.** 2018. Towards human-level license plate recognition. *Proceedings of the European Conference on Computer Vision (ECCV)*, 306-321. Doi: 10.1007/978-3-030-01219-9_19



Characteristics and Kinetic Analysis of Sorption Performance of Functionalised Biomass by Various Acidic Agents

Çeşitli Asidik Ajanlar ile Fonksiyonelleştirilmiş Biyokütlenin Özellikleri ve Sorpsiyon Performansının Kinetik Analizi

Sahra Dandil*

Bilecik Şeyh Edebali University, Faculty of Engineering, Department of Chemical Engineering, Bilecik, Türkiye

Abstract

In this study, kiwi fruit peels were functionalized using hydrochloric acid (HCl), sulfuric acid (H_2SO_4) and phosphoric acid (H_3PO_4). The properties of the functionalized materials were determined. Fourier transform infrared spectrometer (FTIR) used to show functional groups caused by the agents. Crystalline or amorphous structure clarified by X-ray diffraction (XRD) analysis. Scanning electron microscope (SEM) revealed the changes by acidic agents on the surface of kiwi peel. The elemental composition was examined using energy-dispersive X-ray spectroscopy (EDX) analysis. The performance of kiwi peels functionalized with different acidic agents in sorption experiments were investigated. Kiwi peel functionalized with hydrochloric acid (HAFKP), kiwi peel functionalized with sulphuric acid (SAFKP), and kiwi peel functionalized with phosphoric acid (PAFKP) exhibited 94.53, 98.62, and 96.76% sorption, respectively, from 50 mL of 10 mg/L dye solution for 0.1 g after 24 h. The data obtained for the sorption of the materials were evaluated with kinetic models. Pseudo-first order, pseudo-second order, Elovich and Bangham models considered the processes as time-dependent. The processes carried out with HAFKP and PAFKP were fit the pseudo-second order kinetic model and determined to interact strongly with dye via chemical bonds. SAFKP, on the other hand, interacts physically with dye according to the pseudo-first order kinetic model.

Keywords: Characterization, functionalization, kinetics, kiwi.

Öz

Bu çalışmada kivi kabukları hidroklorik asit (HCl), sülfürk asit (H_2SO_4) ve fosforik asit (H_3PO_4) kullanılarak fonksiyonelleştirildi. Fonksiyonelleştirilmiş malzemelerin özellikleri belirlendi. Ajanların neden olduğu fonksiyonel grupları göstermek için Fourier dönüşümlü kızılötesi spektrometresi (FTIR) kullanıldı. X-ışını kirinimi (XRD) analiziyle kristal veya amorf yapı açıklandı. Taramalı elektron mikroskopu (SEM), kivi kabuğunun yüzeyinde asidik ajanların neden olduğu değişiklikleri ortaya koydu. Elementel bileşim, enerji dağılımlı X-ışını spektroskopisi (EDX) analizi kullanılarak incelendi. Farklı asidik ajanlarla fonksiyonelleştirilen kivi kabuklarının sorpsiyon deneylerindeki performansı araştırıldı. Hidroklorik asit ile fonksiyonelleştirilmiş kivi kabuğu (HAFKP), sülfürk asit ile fonksiyonelleştirilmiş kivi kabuğu (SAFKP) ve fosforik asit ile fonksiyonelleştirilmiş kivi kabuğu (PAFKP) 0.1 g için 24 saat sonra 50 mL'lik 10 mg/L boyalı çözeltisinden sırasıyla % 94.53, 98.62 ve 96.76 sorpsiyon sergiledi. Malzemelerin sorpsiyonu için elde edilen veriler kinetik modellerle değerlendirildi. Yalancı birinci derece, yalancı ikinci derece, Elovich ve Bangham modelleri prosesleri zamana bağlı olarak ele aldı. HAFKP ve PAFKP ile gerçekleştirilen proseslerin yalancı ikinci derece kinetik modele uydugu ve boyalı kimyasal bağlar yoluyla kuvvetli etkileşime girdikleri belirlendi. SAFKP ise yalancı birinci dereceden kinetik modele göre boyalı fiziksel olarak etkileşime girdi.

Anahtar Kelimeler: Karakterizasyon, fonksiyonelleştirme, kinetikler, kivi.

*Corresponding author: sahra.ugur@bilecik.edu.tr

Sahra Dandil orcid.org/0000-0001-9724-5597



This work is licensed by "Creative Commons Attribution-NonCommercial 4.0 International (CC)".

1. Introduction

Biomass is agricultural and industrial materials such as wood, annual crops, and agricultural and forestry residues that are rich in fixed carbon (Panichkittkul et al. 2024). Materials obtained from agricultural wastes, industrial by-products and typical wastes can be used to remove impurities in sorption processes (Araujo et al. 2021). In addition to their low cost, carbonaceous materials exhibit high surface area and porosity and superior stability properties (Taylor et al. 2024). One way to best utilize biomass is to apply it as a precursor to the production of bio-based carbon porous materials (dos Reis et al. 2022).

Materials can be activated by applying physical and chemical processes (Tang et al. 2023). The chemical method involves treating the material with chemicals (Pereira et al. 2014). Although chemicals are used for this method, physical activation requires a long time and high temperature and energy needs (Yossa et al. 2020). Functional groups can be introduced by chemical treatment to ensure the affinity of materials to impurities in the aqueous environment (Gita et al. 2023). Moreover, chemical activation results in high carbon yield, large surface area and well-developed porous structure (Kılıç et al. 2012). Different reactions occur for different agents, as explained by Xing et al (Xing et al. 2019). Chemical agents cause strong cross-links through dehydration and elimination reactions, prevent volume shrinkage, provide high porosity and add functional groups to the material (Guo and Lua 2003). Chemical treatment agents can be acidic, alkaline and oxidizing agents, metal salts and a combination thereof (Zhang et al. 2023). Commonly used acidic activating agents are nitric acid, hydrochloric acid, sulfuric acid, and phosphoric acid (España et al. 2019).

Dyes are difficult to remove from wastewater because they are resistant to biological degradation (Zhu et al. 2014). The elimination of crystal violet, an alkaline dye, from industrial wastewater attracts attention in terms of water improvement (Gupta et al. 2023). It is used in many areas such as fabric dyeing, adhesive tapes, ink production, leather processing, food industry, fingerprint detection and veterinary medicine (Abd El-Hamid et al. 2022, Kumbhar et al. 2022). Since crystal violet is widely used as a dye with high economic value, it is mixed in effluents and therefore poses a health risk (Huang et al. 2023). It can be more toxic than many other types of dyes due to the production of dangerous aromatic amino products (Benhalima et al. 2023). Its complex structure makes it more toxic and dangerous than anionic dyes (Tan et al. 2023). Even very low concentrations

(1 mg/L) threaten living life by negatively affecting light transmission to aquatic environments (Loganathan et al. 2022). Therefore, its effective removal from water is of great necessity (Wu et al. 2021).

In this study, it is aimed to determine the changes caused by different acidic agents in the properties of kiwi peels, to evaluate the effects of each acidic agent individually and to compare them with each other. In addition, the sorption performances provided by the properties that each acidic agent brings to the kiwi peels and the kinetics of the sorptions were investigated. In the literature, many different biomass such as algae (Kumar et al. 2016), green seaweed (Bertoni et al. 2015), soy hull (Blanes et al. 2016), flower (Lingamdinne et al. 2016), hickory chips, cotton stalks and peanut hulls (Ding et al. 2014), exhausted coffee (Liu et al. 2016), reed (Rawajfih and Nsour 2008) and hazelnut and almond shell (Pehlivan et al. 2009) have been used for sorption purposes. There have been studies involving kiwi peels in sorption processes, and it is noteworthy that these studies are current. Gubitosa et al. (2022) used kiwi peels as adsorbent for Ciprofloxacin removal. A Zn–Fe biochar (KB/Zn–Fe) was designed from a kiwi branch and used in Pb (II) removal from an aqueous solution by Tan et al. (2022a). There is a study in which chitosan-modified kiwi branch biochar was prepared for Cd (II) removal (Tan et al. 2022b). Gong et al. (2024) produced manganese dioxide-decorated kiwi peel powder for the removal of Pb²⁺. Unlike previous studies, this study revealed the changes in the properties of kiwi peels with hydrochloric acid (HCl), sulfuric acid (H₂SO₄) and phosphoric acid (H₃PO₄). In addition, the effect of each agent on the crystal violet sorption performance of kiwi peels was investigated. In this way, the preparation of kiwi peels with a different method and the use of a different material for sorption than the studies on kiwi mentioned above demonstrates the innovative aspect of the study. The important points of the study that contribute to the studies in this field are that a detailed study is carried out by determining the effects of different agents for both characterization and sorption, that a wide scope is provided for the study by comparing various functionalizations, and that the study includes an easy process with common chemicals as a preparation method. In addition, according to the literature reviews above, the fact that the studies on kiwi are from recent years shows that studies on kiwi have intensified, and it is seen that this study carried out in this direction is currently remarkable.

2. Materials and Methods

2.1. Functionalization of Biomass

Kiwi fruits were purchased from a market in Bilecik. They were peeled and the peels were collected. It was left to dry for approximately 2 months in the presence of sunlight. The dried peels were broken and ground. It was then functionalized by HCl ($\geq 37\%$, Honeywell Fluka), H_2SO_4 (95–97%, Honeywell Riedel-de Haen) and H_3PO_4 (orthophosphoric acid, 85%, Carlo Erba). Acidic agents were used without any treatment or dilution. Material preparation was carried out by chemical treatment similar to previous studies (Van Veenhuyzen et al. 2021, Almeida et al. 2021). 8 g of ground kiwi peel was placed in 60 mL of acid and stirred slowly for 2 h at $90^\circ C$ for effective contact. Then, it was kept at $90^\circ C$ for 2 h without mixing. Kiwi peels functionalized with acidic agents were washed several times with 0.5M sodium hydroxide (NaOH, Carlo Erba) solution. It was washed with distilled water and the pH was ensured to reach between 6–7. Kiwi peels were dried in an oven at $105^\circ C$. Raw kiwi peels were named KP, and kiwi peels prepared by functionalizing using HCl, H_2SO_4 and H_3PO_4 were called HAFKP, SAFKP and PAFKP, respectively.

2.2. Sorption

Sorption studies were carried out with kiwi peels prepared by functionalizing them with acidic agents. The sorption efficiency of HAFKP, SAFKP and PAFKP was investigated by preparing simulated wastewater containing crystal violet (Fluka) dye. Simulated wastewater was prepared at its own pH value and in a volume of 50 mL, containing dye at an initial concentration of 10 mg/L. A shaking water bath was used for the experiments. The experiments were repeated twice. Absorbance values of aqueous solutions including the dye were determined by Ultraviolet-Visible region (UV-Vis) spectroscopy at 590 nm wavelength and recorded. These values were converted to concentration values using the absorbance versus concentration curve prepared at different concentrations of the dye. The concentration values were used to calculate the sorption percentage and capacity given in Equations (1) and (2), respectively (Manzar et al. 2023):

$$\text{sorption \%} = \frac{(C_0 - C_e)}{C_0} \times 100 \quad (1)$$

$$q_t = \frac{(C_0 - C_t) V}{m} \quad (2)$$

C_0 , C_e and C_t represent the initial, equilibrium and concentration values at any time t (mg L^{-1}), q_t indicates the

sorption capacity (mg g^{-1}), V represents the solution volume (L), and m indicates the mass of the material (g), respectively (Manzar et al. 2023).

2.2.1. Kinetics

Kinetic studies were carried out to evaluate the processes in which HAFKP, SAFKP and PAFKP were used in sorption processes. The equations used are listed below (Cui et al. 2015, Berhane et al. 2017, Veneu et al. 2019):

Pseudo-first order kinetic model:

$$q_t = q_e (1 - e^{-k_1 t}) \quad (3)$$

Pseudo-second order kinetic model:

$$q_t = \frac{q_e^2 k_2 t}{1 + q_e k_2 t} \quad (4)$$

$$\text{Elovich model: } q_t = \frac{1}{\beta} \ln(\beta \alpha t + 1) \quad (5)$$

$$\text{Bangham model: } q_t = k_3 t^{\alpha B} \quad (6)$$

q_e indicates the amount retained in the solid at equilibrium (mg g^{-1}), and k_1 is the pseudo-first order reaction velocity constant ($\text{g mg}^{-1} \text{ min}^{-1}$), t represents time (min), k_2 is the pseudo-second order reaction velocity constant ($\text{g mg}^{-1} \text{ min}^{-1}$), α indicates the initial sorption rate constant ($\text{mg kg}^{-1} \text{ min}^{-1}$), β indicates a sorption constant (kg mg^{-1}) and α β and k_3 are related constants for Bangham isotherm (Cui et al. 2015, Berhane et al. 2017, Veneu et al. 2019).

2.3. Apparatus

For KP, HAFKP, SAKKP and PAFKP, functional groups of raw kiwi peels and materials prepared depending on the changing agent were detected using Fourier transform infrared spectroscopy (FTIR). The X-ray diffraction (XRD) method was applied to investigate the amorphous or crystalline structure of functionalized kiwi peels. The surface morphologies of the materials were investigated and elemental composition of the surfaces was exhibited using scanning electron microscopy-energy dispersive X-ray spectroscopy (SEM-EDX).

3. Results and Discussion

3.1. Characteristics

The functional groups of KP, HAFKP, SAFKP and PAFKP were determined and the effective groups for dye sorption were analyzed. Figure 1(a), (b), (c) and (d) show the FTIR spectra of KP, HAFKP, SAFKP and PAFKP, respectively. The broad and distinct peak seen at 3293 cm^{-1} for KP in Figure 1(a) belongs to the vibrations of O-H groups,

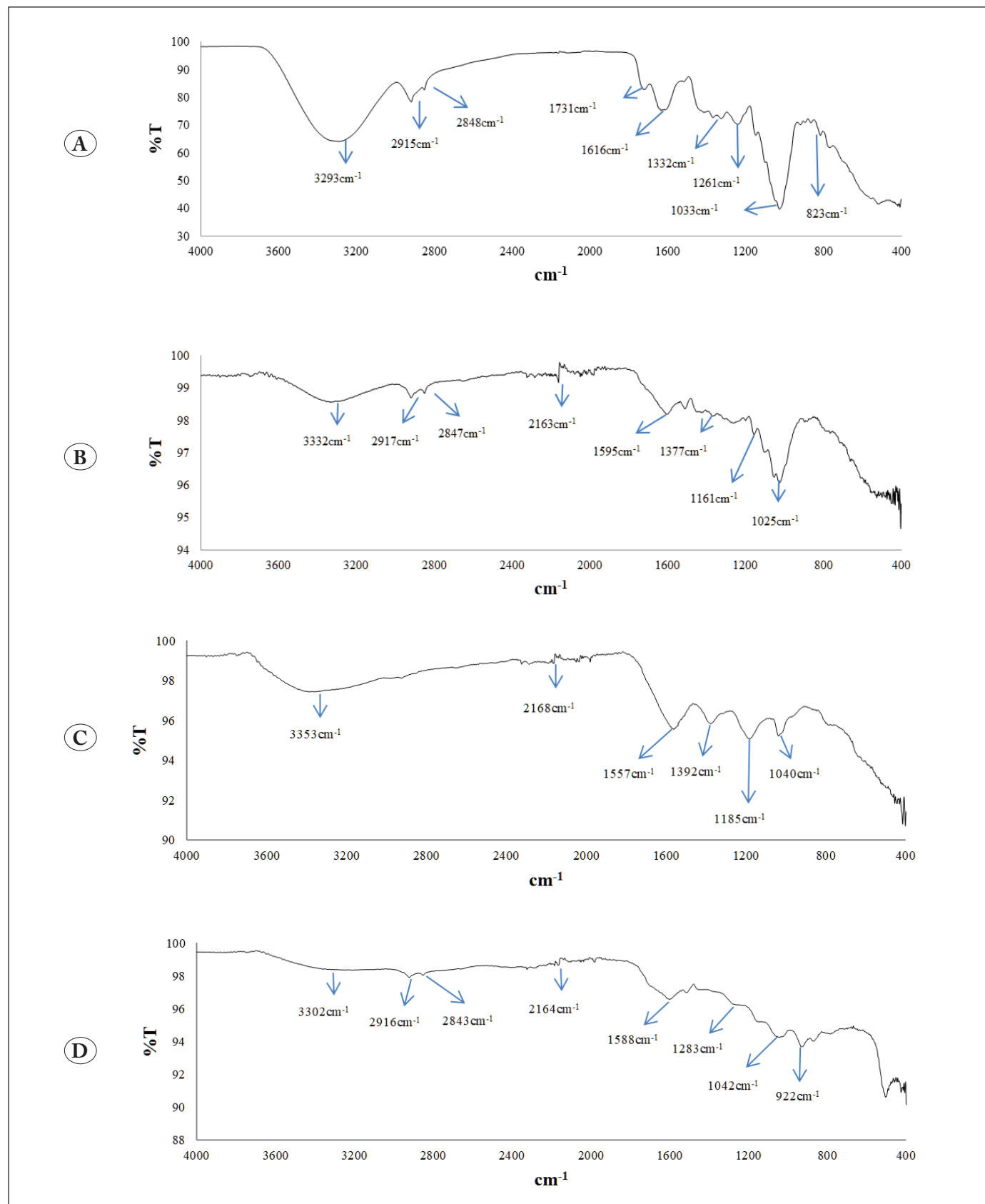


Figure 1. FTIR spectra of (A) KP, (B) HAFKP, (C) SAFKP, and (D) PAFKP.

however, its effect seems to have decreased, which may be due to the thermal treatment along with the functionalization at 3332, 3353 and 3302 cm^{-1} for HAFKP, SAFKP and PAFKP, respectively (Zbair et al. 2020, Adnan and Moses 2020, Hao et al. 2023, Tirkey and Babu 2024). The peaks that lose their effect for SAFKP and in the range of 2915–2917 and 2843–2848 cm^{-1} for other samples indicate CH_2 stretching vibrations (Kuracina et al. 2023, Stelescu et al. 2022). CO stretching peaks appeared in the range of 2163–2168 cm^{-1} in the materials prepared by functionalization of KP (Yang and Wöll 2017). KP has a C=O band according to 1731 and 1616 cm^{-1} (Phothong et al. 2024, B.Aziz et al. 2019). The peaks seen at 1595, 1557 and 1588 cm^{-1} for HAFKP, SAFKP and PAFKP may belong to C-H, C-N and -COOH vibrations, respectively (Gan and Tan 2001, Dutta et al. 2019, Yamada and Mizuno 2021). While the CH_3 bending peak was observed at 1377 cm^{-1} for HAFKP, C-O peaks were observed at 1332, 1392 and 1283 cm^{-1} for KP, SAFKP and PAFKP, respectively (Gupta et al. 2017, Jung et al. 2018, Rani et al. 2016, Rajaniverma et al. 2022).

In Figure 1(a), a CH_3 bending peak was detected at 1261 cm^{-1} in KP (Guo et al. 2012). The peaks at 1185 (Figure 1(c)), 1161 (Figure 1(b)) and 1033 (Figure 1(a)) cm^{-1} indicate C-O vibrations (Nikafshar et al. 2017, Karabiyik et al. 2023, Bandyopadhyay et al. 2021). The 1042 cm^{-1} peak in Figure 1(d) may belong to P=O and P-O-P vibrations of PAFKP (Tang et al. 2019, Silva et al. 2021, Wu et al. 2023). For SAFKP, the peak at 1040 cm^{-1} may belong to the $-\text{SO}_2$ group (Figure 1(c)) (Wu et al. 2017). The 1025 cm^{-1} peak in Figure 1(b) indicates C-OH stretching vibrations (Zhang et al. 2022). The 922 cm^{-1} peak seen for PAFKP may belong to the presence of P (Mustafa et al. 2023). For KP, there is a C—O—C stretching vibration peak at 823 cm^{-1} (Abolins et al. 2020). Interactions of different elements may take place in the region below 800 cm^{-1} (Peng et al. 2023, Isaac et al. 2023, Jin et al. 2023).

XRD analysis was performed to determine whether HAFKP, SAFKP and PAFKP were amorphous or crystalline. Figure 2(a), (b) and (c) are the XRD diffractograms of HAFKP,

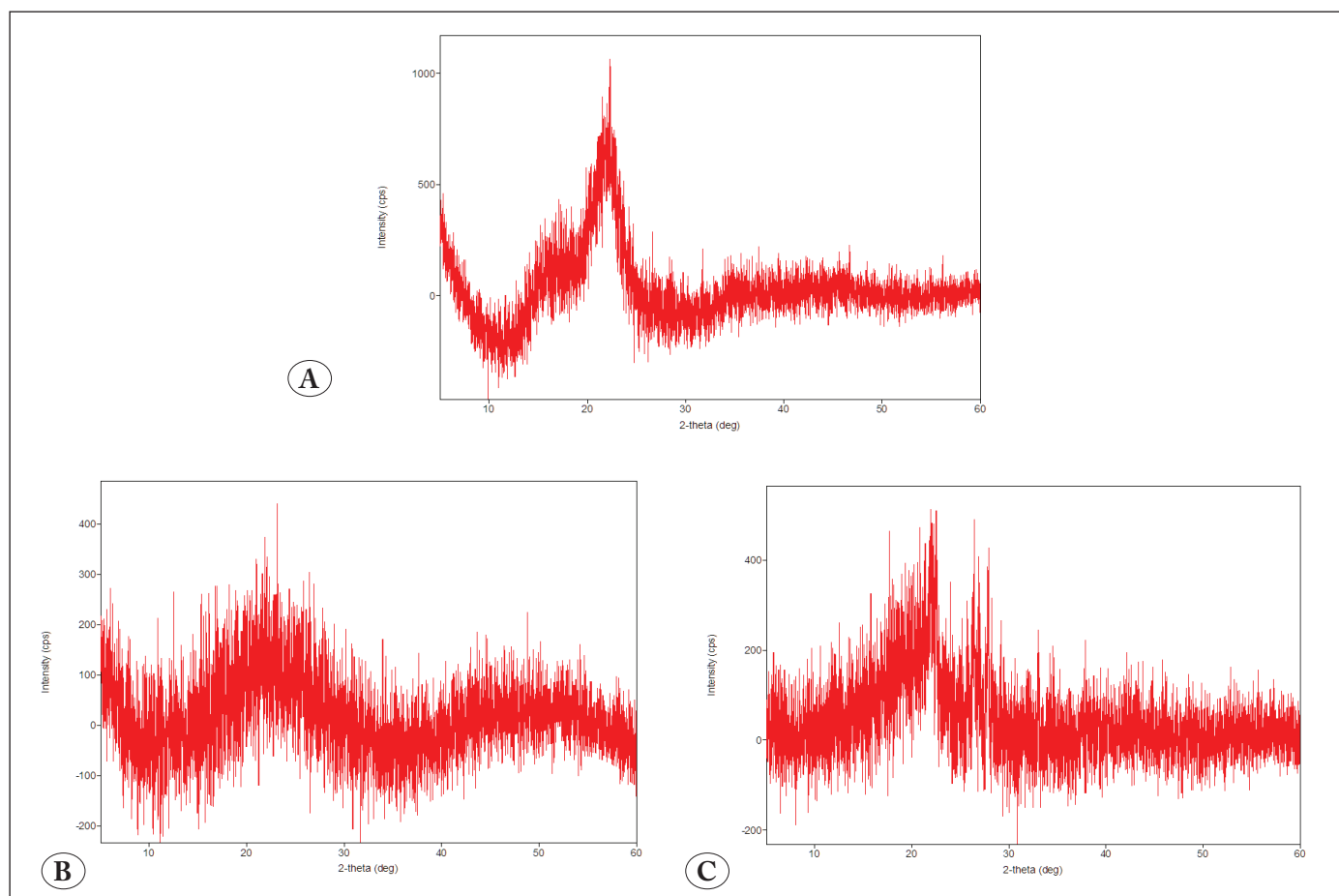
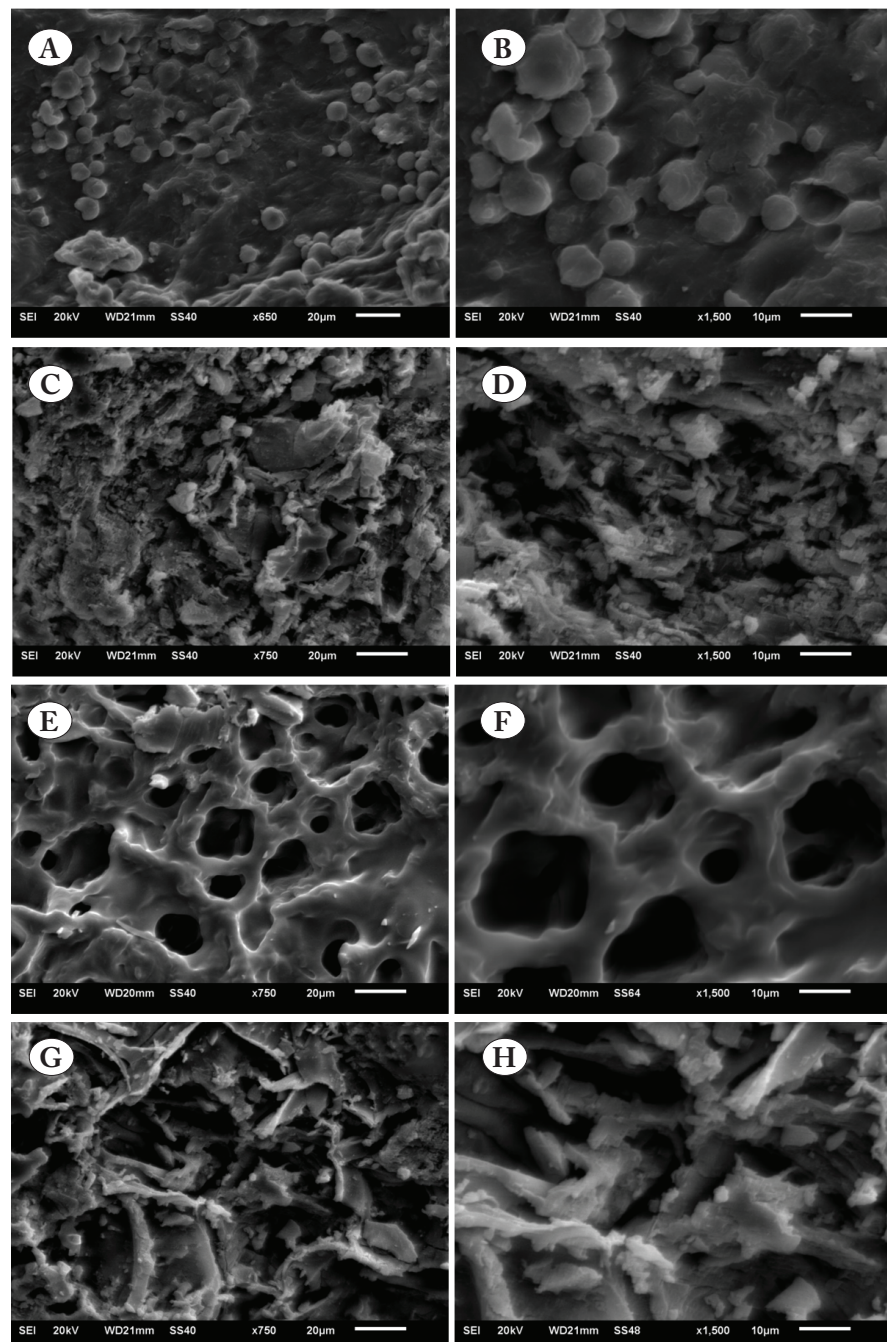


Figure 2. X-ray diffractograms of (A) HAFKP, (B) SAFKP, and (C) PAFKP.

SAFKP and PAFKP, respectively. According to Figure 2, peaks at similar 2θ values were observed for HAFKP, SAFKP and PAFKP. Similar to the study by Santos et al., HAFKP, SAFKP and PAFKP exhibited an amorphous structure with a small number of crystal patterns (Santos et al. 2023).

To monitor the changes in the surface structure of KP with functionalization, SEM analyzes were performed for HAFKP, SAFKP and PAFKP and these analyzes were



compared with the SEM analyzes of KP. In the SEM images of KP at different magnifications in Figures 3(a) and (b), a non-porous, irregular and lumpy surface structure is seen, as in the study by Gubitosa et al. in which they examined the external and internal structure of the kiwi peel (Gubitosa et al. 2022). In the SEM images of HAFKP in Figure 3(c) and (d), it is clear that HCl causes the formation of irregular and crevice-shaped regions on the surface of KP. Similar to the previous study presented by Xing et al., it

Figure 3. SEM images of KP (A and B), HAFKP (C and D), SAFKP (E and F), and PAFKP (G and H).

resulted in a corrugated and layered surface structure on the KP surface with agglomerations with HCl (Xing et al. 2016). In Figure 3(e) and (f) of SAFKP, it is seen that H_2SO_4 causes the formation of a highly porous structure containing open pores of different sizes, as shown by Guo et al (Guo et al. 2023). In Figure 3(g) and (h) of PAFKP, an irregular surface with wide cracks is seen. Accordingly, it is seen that the surface structures change as a result of the functionalization of the raw material with acidic agents. In addition, it is clear in the SEM images in Figure 3 that different acidic agents change the surface structure of the raw material and cause surface structures of different shapes, sizes and distributions. These surface structures show that changes have been created on the surface of the non-porous KP by acidic functionalizations and that these structures of the newly prepared HAFKP, SAFKP and PAFKP may be suitable areas for sorption.

EDX analyzes were performed to examine the effect of different acids used for functionalization on the elemental composition on the surfaces of the materials. Figure 4(a), (b), (c) and (d) are EDX analyzes for KP, HAFKP, SAFKP and PAFKP, respectively. According to Figure 4(a), KP is a material with 21.5% O, 21.3% K, 16.1% Mg, 12.9% Zn and 11.6% Cu content by mass. For HCl applied HAFKP, 71.0% C, 11.4% O, 8.5% Cl and 5.5% Na content were determined (Figure 4(b)). SAFKP exhibited 57.9% C, 24.0% Na and 11.4% O content in Figure 4(c). The major elements for PAFKP were 47.1% C, 10.8% O and 10.5% Na (Figure 4(d)). According to EDX results, it was determined that the functionalization of kiwi peels with acidic chemical agents provided C content for HAFKP, SAFKP and PAFKP.

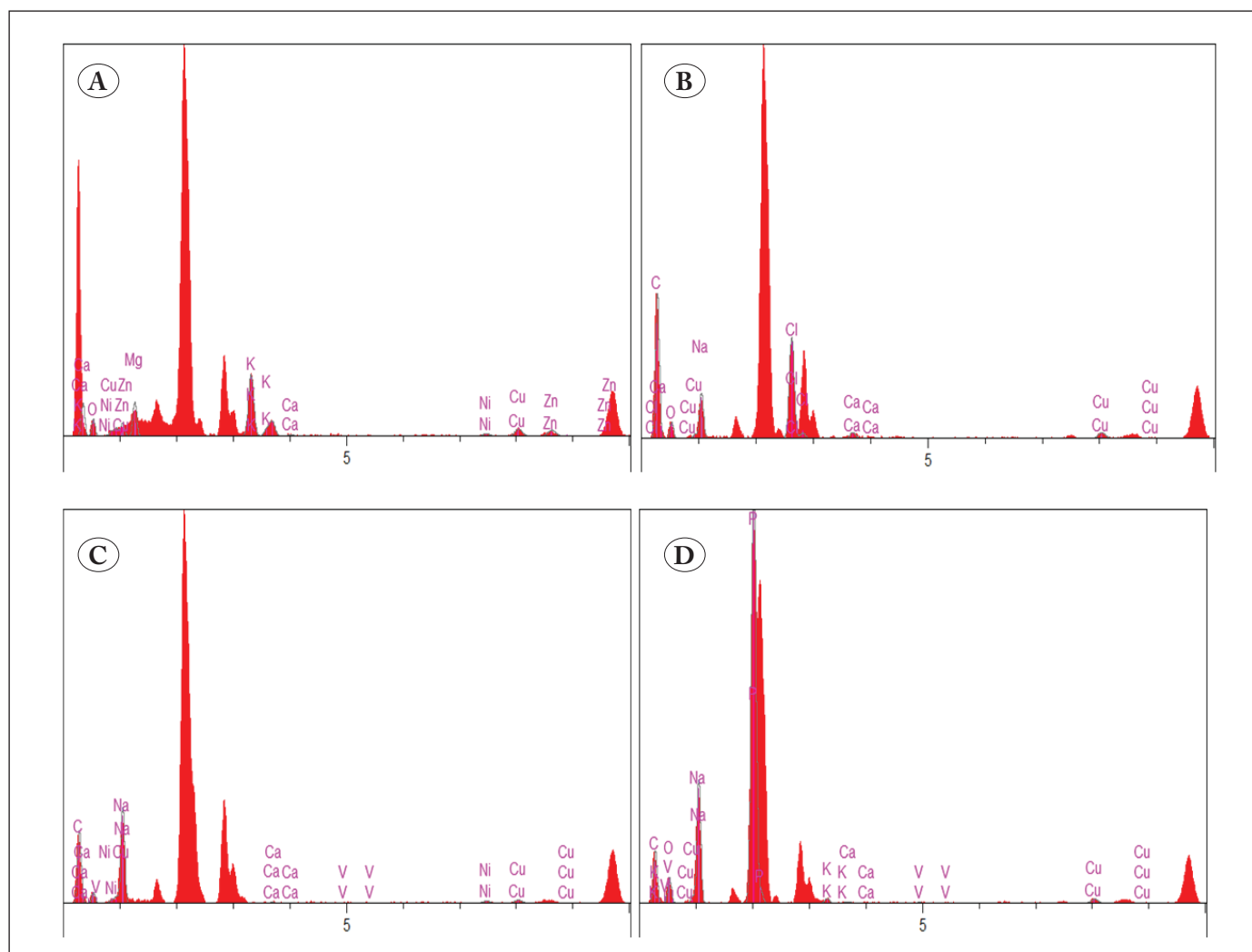


Figure 4. EDX analysis of (A) KP, (B) HAFKP, (C) SAFKP, and (D) PAFKP.

3.2. Sorption Analysis

3.2.1. Determination of sorption performance

The sorption performance of HAFKP, SAFKP and PAFKP over time is given in Figure 5(a), (b) and (c), respectively. For the experiments, the amount of material was determined as

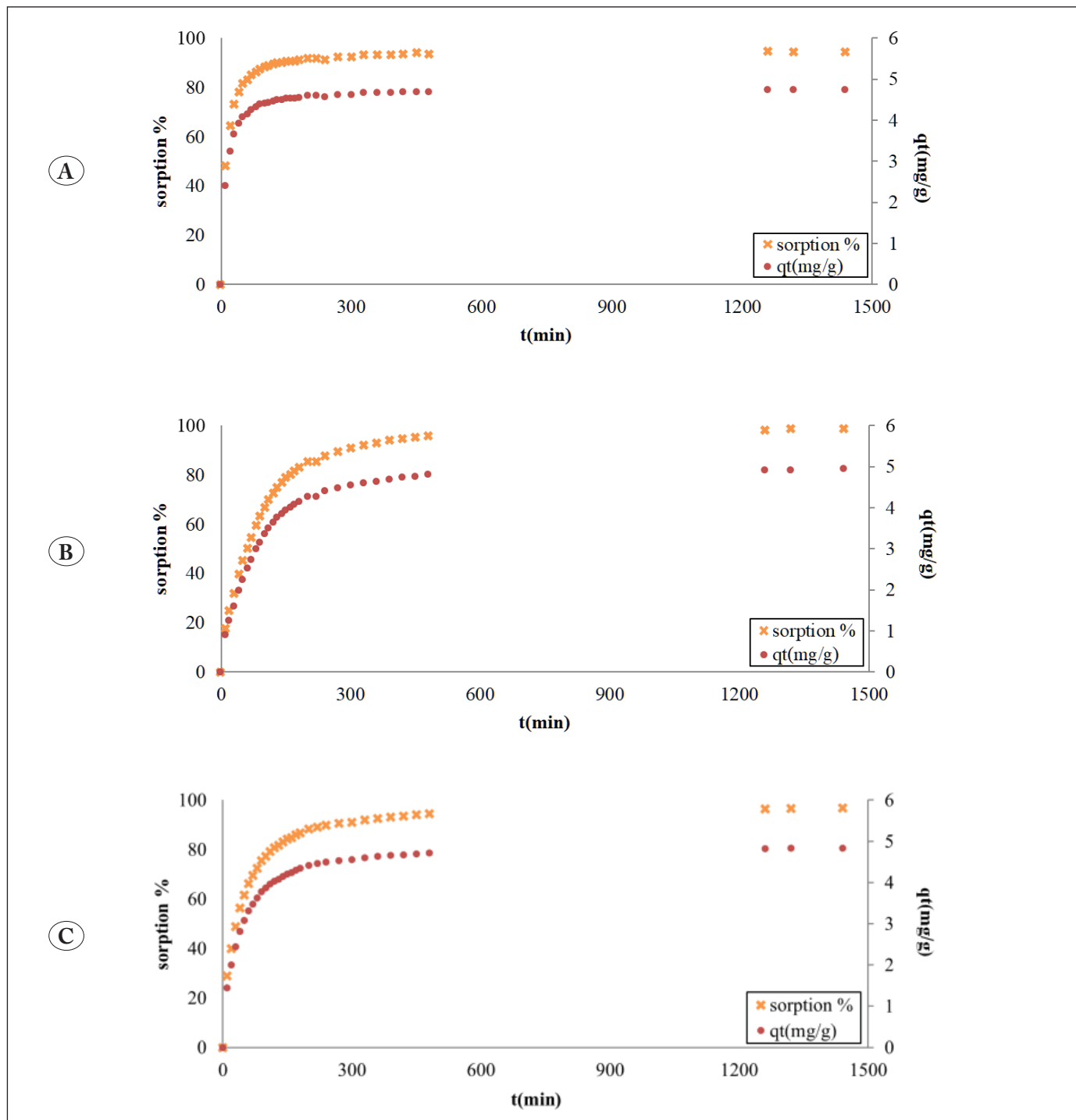


Figure 5. Sorption performance of (A) HAFKP, (B) SAFKP, and (C) PAFKP.

0.1 g, the volume of the dye solution was 50 mL, the initial concentration of the dye solution was 10 mg/L, the pH value of the dye solution itself, the temperature was 24 °C and the shaking speed was 190 rpm. Under these conditions, concentration changes were monitored to determine the equilibrium times of the processes.

In the graph of HAFKP given in Figure 5(a), it is seen that high sorption is achieved (~50%) as soon as the experiment starts and this situation continues to increase rapidly until approximately 120 min. According to the figure, the increase continues after 120 min, but the rate of increase gradually decreases. A similar situation was observed for capacity values. When concentration changes were continued to be monitored to determine the equilibrium time, it was observed that the sorption performance increased with very small increases after 120 min. It was determined that the sorption performance of the process did not change due to the concentration value remaining constant at the end of 1440 min and therefore 1440 min was determined as the equilibrium time. When the performance of SAFKP was followed over time, Figure 5(b) was obtained. As seen in the figure, process performance increased over time at lower rates than HAFKP. The increasing trend, which started in the first moments of the experiment, continued for 480 min. Although the increases continued after 480 min, they remained at very low rates. 1440 min was chosen as the equilibrium time due to negligible increases at the end of 1440 min. This behavior caused the formation of the curve in Figure 5(b). However, similar to HAFKP, SAFKP also showed high performance at the end of 1440 min. Figure 5(c) shows the performance of PAFKP. PAFKP provided lower percent sorption values than HAFKP but higher than SAFKP in the first moments of the experiment. Although the stable sorption rates, which continued for 360 min, decreased after 360 min, PAFKP continued to perform. Similar to SAFKP,

increases at the end of 1440 min were neglected and 1440 min was determined as the equilibrium time. Similar to HAFKP and SAFKP, PAFKP also exhibited high sorption performance at equilibrium time. At the end of 1440 min, HAFKP, SAFKP and PAFKP exhibited 94.53, 98.62 and 96.76% sorption and 4.73, 4.93 and 4.84 mg/g capacity, respectively. Although the sorption percentage and capacity values are very close to each other, the highest values were obtained for SAFKP.

3.2.2. Application of kinetic models to sorption

Kinetic studies were conducted to explain the performance of HAFKP, SAFKP and PAFKP. Kinetic studies for HAFKP, SAFKP and PAFKP using pseudo-first order, pseudo-second order, Elovich and Bangham models are plotted in Figure 6(a), (b) and (c), respectively.

The variables of the kinetic models are given in Table 1. According to the magnitude of the correlation coefficients (R^2) of the kinetic models in Table 1, pseudo-second order>pseudo-first order>Elovich>Bangham order was determined for HAFKP. For SAFKP, R^2 values increased in the order pseudo-first order>pseudo-second order>Elovich>Bangham. According to R^2 values, PAFKP showed a fit as pseudo-second order>pseudo-first order>Elovich>Bangham. The largest R^2 value for HAFKP and PAFKP was determined for the pseudo-second order kinetic model. Supporting this situation, the experimental q_e values were found to be close to the q_e values of the pseudo-second order

Table 1. Variables of kinetic models.

Model	Parameter	HAFKP	SAFKP	PAFKP
	experimental q_e	4.73	4.93	4.84
PFO	q_e	4.55	4.74	4.55
	k_1	0.058	0.012	0.022
	R^2	0.9129	0.9901	0.9481
PSO	q_e	4.79	5.38	5.00
	k_2	11.75	2.56	4.24
	R^2	0.9976	0.9891	0.9966
Elovich	α	349.19	0.28	1.41
	β	2.73	1.053	1.45
	R^2	0.7381	0.8922	0.8684
Bangham	αB	0.091	0.22	0.15
	k_3	2.73	1.18	1.80
	R^2	0.6651	0.7898	0.7793

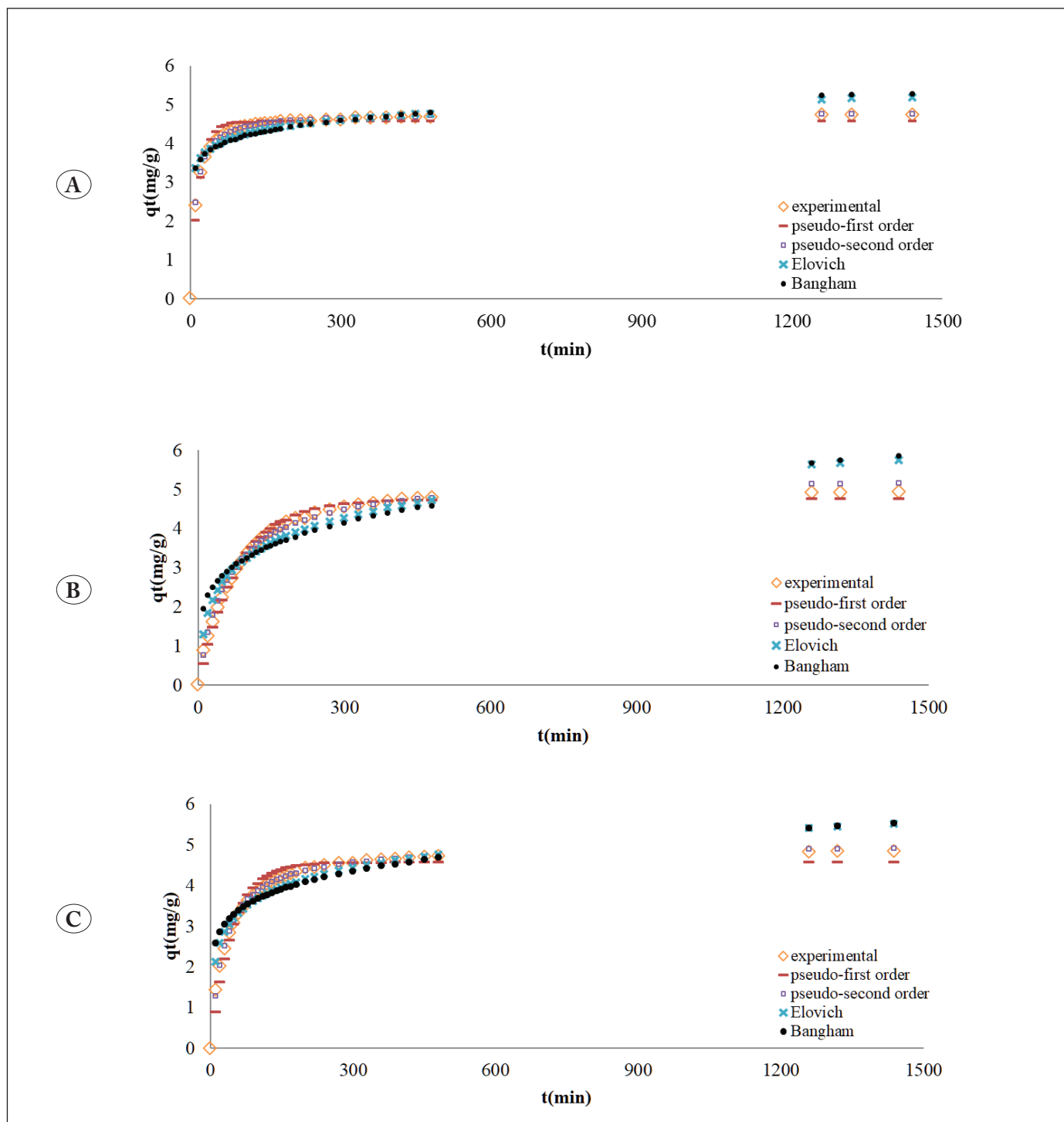


Figure 6. Experimental and kinetic model graphs of (A) HAFKP, (B) SAFKP and (C) PAFKP.

kinetic model for HAFKP and PAFKP. This model explains that chemisorption is the rate-determining step (Lammini et al. 2022). The fact that the processes for HAFKP and PAFKP are chemical sorption indicates that a chemical reaction occurs between the dye molecules and HAFKP and

PAFKP, thus a strong bonding occurs through covalent bonds (Sasamoto et al. 2022). For SAFKP, although high and close R^2 values were obtained for both the pseudo-first order and pseudo-second order models, the R^2 value of the pseudo-first order was found to be higher with a very slight

difference. In addition, when the q_e values of the experimental and models are compared, the experimental q_e value for SAFKP was found to be closer to the q_e value for pseudo-first order. Therefore, it was determined that SAFKP and pseudo-first order kinetic model are compatible. Physical sorption is effective in processes suitable for the pseudo-first order kinetic model (Yin et al. 2023). Therefore, in the process involving SAFKP, sorption occurs physically. Physical sorption refers to processes that involve a reversible interaction through weak van der Waals forces (Atif et al. 2022). Therefore, it can be explained that SAFKP has a physical interaction with dye molecules. The Elovich model refers to the heterogeneous material surface when it comes to chemical sorption (Dinh et al. 2023). Bangham model describes diffusion into pores (Rojas et al. 2019). According to R^2 values, the processes carried out with HAFKP, SAFKP and PAFKP were not found to be compatible with the Elovich and Bangham model.

4. Conclusion

In this study, kiwi fruit peels were functionalized with different acidic agents and the properties of the resulting materials were determined. FTIR analysis showed that different acidic agents impart different functional groups to kiwi peel. The amorphous structure of the functionalized materials was revealed by XRD analysis. SEM analysis revealed that KP, which has a non-porous and non-homogeneous surface, exhibited open, large and circular pores when functionalized with H_2SO_4 , while pores in the form of slits were formed for HAFKP and PAFKP. EDX analysis detected that acidic agents increase the C content in the elemental composition of the materials. Additionally, sorption performances of HAFKP, SAFKP and PAFKP were investigated. HAFKP, SAFKP and PAFKP exhibited crystal violet sorption performance of 94.53, 98.62 and 96.76%, respectively. In the kinetic analyzes applied for the processes, it was determined that the R^2 and q_e values of the processes in which HAFKP and PAFKP were used were compatible with the pseudo-second order kinetic model, and therefore, a strong bonding occurred between HAFKP and PAFKP and the dye molecules through covalent bonds. On the other hand, SAFKP was suitable for the pseudo-first order kinetic model and it was explained that sorption occurred with weaker binding.

5. Acknowledgements

The author received no funding for the research.

Conflict of Interest

The author declares that no conflict of interest.

6. References

- Abd El-Hamid, HT., AlProl, AE., Hafiz, MA.** 2022. The efficiency of adsorption modelling and Plackett-Burman design for remediation of crystal violet by *Sargassum latifolium*. Biocatalysis and Agricultural Biotechnology, 44: 102459. Doi: 10.1016/j.bcab.2022.102459
- Abolins, A., Kirpluks, M., Vanags, E., Fridrihsone, A., Cabulis, U.** 2020. Tall oil fatty acid epoxidation using homogenous and heterogeneous phase catalysts. Journal of Polymers and the Environment, 28: 1822-1831. Doi: 10.1007/s10924-020-01724-9
- Adnan, M., Moses, J.** 2020. A study on the thermophysiological and tactile comfort properties of silk/lyocell blended fabrics. Matéria (Rio de Janeiro), 25: e-12796. Doi: 10.1590/S1517-707620200003.1096
- Almeida, ACM., do Nascimento, RA., Amador, ICB., de Sousa Santos, TC., Martelli, MC., de Faria, L.J.G., da Paixão Ribeiro, NF.** 2021. Chemically activated red mud: assessing structural modifications and optimizing adsorption properties for hexavalent chromium. Colloids and Surfaces A: Physicochemical and Engineering Aspects, 628: 127325. Doi: 10.1016/j.colsurfa.2021.127325
- Araujo, LA., Bezerra, CO., Cusiolli, LF., Rodríguez, MT., Gomes, RG., Bergamasco, R.** 2021. Diclofenac adsorption using a low-cost adsorbent derived from Guazuma ulmifolia Lam. fruit via chemical and thermal treatment. Journal of Environmental Chemical Engineering, 9(6): 106629. Doi: 10.1016/j.jece.2021.106629
- Atif, M., Haider, HZ., Bongiovanni, R., Fayyaz, M., Razzaq, T., Gul, S.** 2022. Physisorption and chemisorption trends in surface modification of carbon black. Surfaces and Interfaces, 31: 102080. Doi: 10.1016/j.surfin.2022.102080
- Aziz, BS., Hussein, G., Brza, MA., Mohammed, JS., Abdulwahid, TR., Raza Saeed, S., Hassanzadeh, A.** 2019. Fabrication of interconnected plasmonic spherical silver nanoparticles with enhanced localized surface plasmon resonance (LSPR) peaks using quince leaf extract solution. Nanomaterials, 9(11): 1557. Doi: 10.3390/nano9111557
- Bandyopadhyay, S., Sáha, T., Sanétrník, D., Saha, N., Sáha, P.** 2021. Thermo compression of thermoplastic Agar-Xanthan gum-carboxymethyl cellulose blend. Polymers, 13(20): 3472. Doi: 10.3390/polym13203472

- Benhalima, T., Chicha, W., Ferfara-Harrar, H.** 2023. Sponge-like biodegradable polypyrrole-modified biopolymers for selective adsorption of basic red 46 and crystal violet dyes from single and binary component systems. *International Journal of Biological Macromolecules*, 253: 127532. Doi: 10.1016/j.ijbiomac.2023.127532
- Berhane, TM., Levy, J., Krekeler, MP., Danielson, ND.** 2017. Kinetic sorption of contaminants of emerging concern by a palygorskite-montmorillonite filter medium. *Chemosphere*, 176: 231-242. Doi: 10.1016/j.chemosphere.2017.02.068
- Bertoni, FA., Medeot, AC., González, JC., Sala, LF., Bellú, SE.** 2015. Application of green seaweed biomass for MoVI sorption from contaminated waters. Kinetic, thermodynamic and continuous sorption studies. *Journal of colloid and interface science*, 446: 122-132. Doi: 10.1016/j.jcis.2015.01.033
- Blanes, PS., Bordoni, ME., González, JC., García, SI., Atria, AM., Sala, LF., Bellú, SE.** 2016. Application of soy hull biomass in removal of Cr (VI) from contaminated waters. Kinetic, thermodynamic and continuous sorption studies. *Journal of environmental chemical engineering*, 4(1): 516-526. Doi: 10.1016/j.jece.2015.12.008
- Cui, L., Guo, X., Wei, Q., Wang, Y., Gao, L., Yan, L., Yan, T., Du, B.** 2015. Removal of mercury and methylene blue from aqueous solution by xanthate functionalized magnetic graphene oxide: sorption kinetic and uptake mechanism. *Journal of colloid and interface science*, 439: 112-120. Doi: 10.1016/j.jcis.2014.10.019
- Ding, Z., Hu, X., Zimmerman, AR., Gao, B.** 2014. Sorption and cosorption of lead (II) and methylene blue on chemically modified biomass. *Bioresource technology*, 167: 569-573. Doi: 10.1016/j.biortech.2014.06.043
- Dinh, LX., Van Tung, N., Lien, NT., Minh, PT., Le, TH.** 2023. The Adsorption Kinetic and Isotherm Studies of Metal Ions (Co^{2+} , Sr^{2+} , Cs^+) on Fe_3O_4 Nanoparticle of Radioactive Importance. *Results in Chemistry*, 6: 101095. Doi: 10.1016/j.rechem.2023.101095
- dos Reis, GS., Guy, M., Mathieu, M., Jebrane, M., Lima, EC., Thyrel, M., Dotto, GL., Larsson, SH.** 2022. A comparative study of chemical treatment by MgCl_2 , ZnSO_4 , ZnCl_2 , and KOH on physicochemical properties and acetaminophen adsorption performance of biobased porous materials from tree bark residues. *Colloids and Surfaces A: Physicochemical and Engineering Aspects*, 642: 128626. Doi: 10.1016/j.colsurfa.2022.128626
- Dutta, R., Rao, MN., Kumar, A.** 2019. Investigation of ionic liquid interaction with ZnBDC-metal organic framework through scanning EXAFS and inelastic neutron scattering. *Scientific Reports*, 9(1): 14741. Doi: 10.1038/s41598-019-51344-0
- España, VAA., Sarkar, B., Biswas, B., Rusmin, R., Naidu, R.** 2019. Environmental applications of thermally modified and acid activated clay minerals: Current status of the art. *Environmental Technology & Innovation*, 13: 383-397. Doi: 10.1016/j.eti.2016.11.005
- Gan, SN., Tan, BY.** 2001. FTIR studies of the curing reactions of palm oil alkyd-melamine enamels. *Journal of Applied Polymer Science*, 80(12): 2309-2315. Doi: 10.1002/app.1336
- Gita, S., Shukla, SP., Deshmukhe, G., Singh, AR., Choudhury, TG.** 2023. Adsorption linked fungal degradation process for complete removal of Lanasyne olive dye using chemically valorized sugarcane bagasse. *Waste Management Bulletin*, 1(1): 29-38. Doi: 10.1016/j.wmb.2023.04.002
- Gong, H., Cao, Y., Zeng, W., Sun, C., Wang, Y., Su, J., Ren, H., Wang, P., Zhou, L., Kai, G., Qian, J.** 2024. Manganese dioxide decorated kiwi peel powder for efficient removal of lead from aqueous solutions, blood and Traditional Chinese Medicine extracts. *Environmental Research*, 249: 118360. Doi: 10.1016/j.envres.2024.118360
- Gubitoso, J., Rizzi, V., Cignolo, D., Fini, P., Fanelli, F., Cosma, P.** 2022. From agricultural wastes to a resource: Kiwi Peels, as long-lasting, recyclable adsorbent, to remove emerging pollutants from water. The case of Ciprofloxacin removal. *Sustainable Chemistry and Pharmacy*, 29: 100749. Doi: 10.1016/j.scp.2022.100749
- Guo, J., Lua, AC.** 2003. Surface functional groups on oil-palm-shell adsorbents prepared by H_3PO_4 and KOH activation and their effects on adsorptive capacity. *Chemical Engineering Research and Design*, 81(5): 585-590. Doi: 10.1205/026387603765444537
- Guo, F., Schulte, L., Vigild, ME., Ndoni, S.** 2012. Load-release of small and macromolecules from elastomers with reversible gyroid mesoporosity. *Soft Matter*, 8(45): 11499-11507. Doi: 10.1039/C2SM26480C
- Guo, Z., Fan, Y., Liu, T., Zhang, Y., Wan, Q.** 2023. Adsorption and enrichment of Ag (I) from industrial wastewater using woody biomass-based biosorbent. *Hydrometallurgy*, 219: 106083. Doi: 10.1016/j.hydromet.2023.106083
- Gupta, A., Lakshmp, YN., Manivannan, R., Victoria, SN.** 2017. Visible range photocatalysts for solid phase photocatalytic degradation of polyethylene and polyvinyl chloride. *Journal of the Chilean Chemical Society*, 62(1): 3393-3398. Doi: 10.4067/S0717-97072017000100018
- Gupta, S., Prajapati, A., Kumar, A., Acharya, S.** 2023. Synthesis of silica aerogel and its application for removal of crystal violet dye by adsorption. *Watershed Ecology and the Environment*, 5: 241-254. Doi: 10.1016/j.wsee.2023.10.003

- Hao, J., Chen, Y., Zhu, M., Zhao, Y., Zhang, K., Xu, X. 2023.** Spatial-Temporal Heterogeneity in Large Three-Dimensional Nanofibrillar Cellulose Hydrogel for Human Pluripotent Stem Cell Culture. *Gels*, 9(4): 324. Doi: 10.3390/gels9040324
- Huang, YP., Niu, HB., Jin, L., Jiao, L., Johnson, D., Tian, HL., Sarina, S., Zhu, HY., Fang, YF. 2023.** Selective adsorption of Crystal Violet via hydrogen bonded water bridges by InVO4. *Chemical Engineering Journal Advances*, 15: 100508. Doi: 10.1016/j.ceja.2023.100508
- Isaac, R., Siddiqui, S., Aldosari, OF., Uddin, MK. 2023.** Magnetic biochar derived from *Juglans regia* for the adsorption of Cu²⁺ and Ni²⁺: Characterization, modelling, optimization, and cost analysis. *Journal of Saudi Chemical Society*, 27(6): 101749. Doi: 10.1016/j.jscs.2023.101749
- Jin, Y., Liu, F., Li, Y., Du, Q., Song, F., Chen, B., Chen, K., Zhang, Y., Wang, M., Sun, Y., Zhao, S., Jing, Z., Pi, X., Wang, Y., Wang, D. 2023.** Efficient adsorption of azo anionic dye Congo Red by micro-nano metal-organic framework MIL-68 (Fe) and MIL-68 (Fe)/chitosan composite sponge: preparation, characterization and adsorption performance. *International Journal of Biological Macromolecules*, 252: 126198. Doi: 10.1016/j.ijbiomac.2023.126198
- Jung, MR., Horgen, FD., Orski, SV., Rodriguez, V., Beers, KL., Balazs, GH., Jones, TT., Work, TM., Brignac, KC., Royer, SJ., Hyrenbach, KD., Jensen, BA., Lynch, JM. 2018.** Validation of ATR FT-IR to identify polymers of plastic marine debris, including those ingested by marine organisms. *Marine pollution bulletin*, 127: 704-716. Doi: 10.1016/j.marpolbul.2017.12.061
- Karabiyik, M., Cihanoğlu, G., Ebil, Ö. 2023.** CVD deposited epoxy copolymers as protective coatings for optical surfaces. *Polymers*, 15(3): 652. Doi: 10.3390/polym15030652
- Kılıç, M., Apaydın-Varol, E., Pütün, AE. 2012.** Preparation and surface characterization of activated carbons from *Euphorbia rigida* by chemical activation with ZnCl₂, K₂CO₃, NaOH and H₃PO₄. *Applied surface science*, 261: 247-254. Doi: 10.1016/j.apsusc.2012.07.155
- Kumar, D., Pandey, LK., Gaur, JP. 2016.** Metal sorption by algal biomass: From batch to continuous system. *Algal research*, 18: 95-109. Doi: 10.1016/j.algal.2016.05.026
- Kumbhar, P., Narale, D., Bhosale, R., Jambhale, C., Kim, JH., Kolekar, S. 2022.** Synthesis of tea waste/Fe₃O₄ magnetic composite (TWMC) for efficient adsorption of crystal violet dye: Isotherm, kinetic and thermodynamic studies. *Journal of Environmental Chemical Engineering*, 10(3): 107893. Doi: 10.1016/j.jece.2022.107893
- Kuracina, R., Szabová, Z., Buranská, E., Kosár, L., Rantuch, P., Blinová, L., Měřínská, D., Gogola, P., Jurina, F. 2023.** Study into the fire and explosion characteristics of polymer powders used in engineering production technologies. *Polymers*, 15(21): 4203. Doi: 10.3390/polym15214203
- Lammini, A., Dehbi, A., Omari, H., ELazhari, K., Mehanned, S., Bengamra, Y., Dehmani, Y., Rachid, O., Alrashdi, AA., Gotore, O., Abdellaoui, A., Lgaz, H. 2022.** Experimental and theoretical evaluation of synthetized cobalt oxide for phenol adsorption: Adsorption isotherms, kinetics, and thermodynamic studies. *Arabian Journal of Chemistry*, 15(12): 104364. Doi: 10.1016/j.arabjc.2022.104364
- Lingamdinne, LP., Yang, JK., Chang, YY., Koduru, JR. 2016.** Low-cost magnetized *Lonicera japonica* flower biomass for the sorption removal of heavy metals. *Hydrometallurgy*, 165: 81-89. Doi: 10.1016/j.hydromet.2015.10.022
- Liu, C., Fiol, N., Villaescusa, I., Poch, J. 2016.** New approach in modeling Cr (VI) sorption onto biomass from metal binary mixtures solutions. *Science of The Total Environment*, 541: 101-108. Doi: 10.1016/j.scitotenv.2015.09.020
- Loganathan, M., Raj, AS., Murugesan, A., Kumar, PS. 2022.** Effective adsorption of crystal violet onto aromatic polyimides: Kinetics and isotherm studies. *Chemosphere*, 304: 135332. Doi: 10.1016/j.chemosphere.2022.135332
- Manzar, MS., Aziz, HA., Meili, L., Ihsanullah, I., Palaniandy, P., Al-Harthi, MA. 2023.** Insights into the adsorption of tetracycline onto cellulose nanocrystal structured MgAl/LDH composite. *Materials Chemistry and Physics*, 299: 127247. Doi: 10.1016/j.matchemphys.2022.127247
- Mustafa, MN., Abdah, MAAM., Numan, A., Sulaiman, Y., Walvekar, R., Khalid, M. 2023.** Development of high-performance MXene/nickel cobalt phosphate nanocomposite for electrochromic energy storage system using response surface methodology. *Journal of Energy Storage*, 68: 107880. Doi: 10.1016/j.est.2023.107880
- Nikafshar, S., Zabihi, O., Hamidi, S., Moradi, Y., Barzegar, S., Ahmadi, M., Naebe, M. 2017.** A renewable bio-based epoxy resin with improved mechanical performance that can compete with DGEBA. *RSC advances*, 7(14): 8694-8701. Doi: 10.1039/C6RA27283E
- Panichkittikul, N., Mariyappan, V., Wu, W., Patcharavorachot, Y. 2024.** Improvement of biohydrogen production from biomass using supercritical water gasification and CaO adsorption. *Fuel*, 361: 130724. Doi: 10.1016/j.fuel.2023.130724
- Pehlivan, E., Altun, T., Cetin, S., Bhanger, MI. 2009.** Lead sorption by waste biomass of hazelnut and almond shell. *Journal of hazardous materials*, 167(1-3): 1203-1208. Doi: 10.1016/j.jhazmat.2009.01.126

- Peng, SY., Lin, YW., Lin, YY., Lin, KL.** 2023. Hydrothermal synthesis of hydroxyapatite nanocrystals from calcium-rich limestone sludge waste: Preparation, characterization, and application for Pb²⁺ adsorption in aqueous solution. *Inorganic Chemistry Communications*, 160: 111943. Doi: 10.1016/j.inoche.2023.111943
- Pereira, RG., Veloso, CM., da Silva, NM., de Sousa, LF., Bonomo, RCF., de Souza, AO., da Guarda Souza, MO., Fontan, RDCI.** 2014. Preparation of activated carbons from cocoa shells and siriguela seeds using H₃PO₄ and ZnCl₂ as activating agents for BSA and α -lactalbumin adsorption. *Fuel Processing Technology*, 126: 476-486. Doi: 10.1016/j.fuproc.2014.06.001
- Phothong, N., Boontip, T., Chouwatat, P., Aht-Ong, D., Napaphorn, SC.** 2024. Preparation and characterization of astaxanthin-loaded biodegradable polyhydroxybutyrate (PHB) microbeads for personal care and cosmetic applications. *International Journal of Biological Macromolecules*, 257: 128709. Doi: 10.1016/j.ijbiomac.2023.128709
- Rajaniverma, D., Rao, DJ., Prasanna Kumar, PV., Seetaramaiah, V., Ramakrishna, Y.** 2022. Characterization of Structure-Property Relations and Second Harmonic Generation of 6-Methoxy-2-Naphthaldehyde. *Polycyclic Aromatic Compounds*, 42(8): 5796-5808. Doi: 10.1080/10406638.2021.1956553
- Rani, S., Kumar, M., Garg, R., Sharma, S., Kumar, D.** 2016. Amide functionalized graphene oxide thin films for hydrogen sulfide gas sensing applications. *IEEE Sensors Journal*, 16(9): 2929-2934. Doi: 10.1109/JSEN.2016.2524204
- Rawajfih, Z., Nsour, N.** 2008. Thermodynamic analysis of sorption isotherms of chromium (VI) anionic species on reed biomass. *The Journal of Chemical Thermodynamics*, 40(5): 846-851. Doi: 10.1016/j.jct.2008.01.005
- Rojas, J., Suarez, D., Moreno, A., Silva-Agredo, J., Torres-Palma, RA.** 2019. Kinetics, isotherms and thermodynamic modeling of liquid phase adsorption of crystal violet dye onto shrimp-waste in its raw, pyrolyzed material and activated charcoals. *Applied Sciences*, 9(24): 5337. Doi: 10.3390/app9245337
- Santos, NC., Almeida, RLJ., Saraiva, MMT., de Alcântara Ribeiro, VH., De Sousa, FM., De Lima, TLB., de Alcântara Silva, VM., André, AMMCN., Leite Filho, MT., de Almeida Mota, MM.** 2023. Application of microwave-assisted freeze-thaw pretreatment in kiwi drying: mass transfer, X-ray diffraction and bioaccessibility of phenolic compounds. *Journal of Food Measurement and Characterization*, 17(4): 3523-3533. Doi: 10.1007/s11694-023-01895-8
- Sasamoto, R., Kanda, Y., Yamanaka, S.** 2022. Difference in cadmium chemisorption on calcite and vaterite porous particles. *Chemosphere*, 297: 134057. Doi: 10.1016/j.chemosphere.2022.134057
- Silva, MC., Spessato, L., Silva, TL., Lopes, GK., Zanella, HG., Yokoyama, JT., Cazetta, AL., Almeida, VC.** 2021. H₃PO₄-activated carbon fibers of high surface area from banana tree pseudo-stem fibers: adsorption studies of methylene blue dye in batch and fixed bed systems. *Journal of Molecular Liquids*, 324: 114771. Doi: 10.1016/j.molliq.2020.114771
- Stelescu, MD., Sonmez, M., Alexandrescu, L., Nituica, M., Gurau, DF., Georgescu, M.** 2022. Structure and properties of blends based on vulcanized rubber waste and styrene-butadiene-styrene thermoplastic elastomer. *Journal of Rubber Research*, 25(5): 421-434. Doi: 10.1007/s42464-022-00187-y
- Tan, Q., Jia, X., Dai, R., Chang, H., Woo, MW., Chen, H.** 2023. Synthesis of a novel magnetically recyclable starch-based adsorbent for efficient adsorption of crystal violet dye. *Separation and Purification Technology*, 320: 124157. Doi: 10.1016/j.seppur.2023.124157
- Tan, Y., Wan, X., Zhou, T., Wang, L., Yin, X., Ma, A., Wang, N.** 2022a. Novel Zn-Fe engineered kiwi branch biochar for the removal of Pb (II) from aqueous solution. *Journal of Hazardous Materials*, 424: 127349. Doi: 10.1016/j.jhazmat.2021.127349
- Tan, Y., Wan, X., Ni, X., Wang, L., Zhou, T., Sun, H., Wang, N., Yin, X.** 2022b. Efficient removal of Cd (II) from aqueous solution by chitosan modified kiwi branch biochar. *Chemosphere*, 289: 133251. Doi: 10.1016/j.chemosphere.2021.133251
- Tang, Y., Zhao, Y., Lin, T., Li, Y., Zhou, R., Peng, Y.** 2019. Adsorption performance and mechanism of methylene blue by H₃PO₄-modified corn stalks. *Journal of Environmental Chemical Engineering*, 7(6): 103398. Doi: 10.1016/j.jece.2019.103398
- Tang, Z., Gao, J., Zhang, Y., Du, Q., Feng, D., Dong, H., Peng, Y., Zhang, T., Xie, M.** 2023. Ultra-microporous biochar-based carbon adsorbents by a facile chemical activation strategy for high-performance CO₂ adsorption. *Fuel Processing Technology*, 241: 107613. Doi: 10.1016/j.fuproc.2022.107613
- Taylor, JH., Troisi, G., Soltani, SM.** 2024. Application of chemically-activated recycled carbon fibres for aqueous-phase adsorptions-part I: Optimisation of activation process. *Chemical Engineering Journal Advances*, 18: 100591. Doi: 10.1016/j.ceja.2024.100591
- Tirkey, A., Babu, PJ.** 2024. Synthesis and characterization of citrate-capped gold nanoparticles and their application in selective detection of creatinine (A kidney biomarker). *Sensors International*, 5: 100252. Doi: 10.1016/j.sintl.2023.100252
- Van Veenhuyzen, B., Tichapondwa, S., Hörstmann, C., Chirawa, E., Brink, HG.** 2021. High capacity Pb (II) adsorption characteristics onto raw-and chemically activated waste activated sludge. *Journal of Hazardous Materials*, 416: 125943. Doi: 10.1016/j.jhazmat.2021.125943

- Veneu, DM., Yokoyama, L., Cunha, OGC., Schneider, CL., de Mello Monte, MB.** 2019. Nickel sorption using Bioclastic Granules as a sorbent material: equilibrium, kinetic and characterization studies. *Journal of Materials Research and Technology*, 8(1): 840-852. Doi: 10.1016/j.jmrt.2018.05.020
- Wu, Q., Wei, J., Xu, B., Liu, X., Wang, H., Wang, W., Wang, Q., Liu, W.** 2017. A robust, highly stretchable supramolecular polymer conductive hydrogel with self-healability and thermo-processability. *Scientific reports*, 7(1): 41566. Doi: 10.1038/srep41566
- Wu, Z., Deng, W., Tang, S., Ruiz-Hitzky, E., Luo, J., Wang, X.** 2021. Pod-inspired MXene/porous carbon microspheres with ultrahigh adsorption capacity towards crystal violet. *Chemical Engineering Journal*, 426: 130776. Doi: 10.1016/j.cej.2021.130776
- Wu, Z., Chen, Z., Tang, J., Zhou, Z., Chen, L., Fang, Y., Hu, X., Lv, J.** 2023. Efficient adsorption and reduction of Cr (VI) in water using one-step H₃PO₄-assisted prepared Leersia hexandra Swartz hydrochar. *Materials Today Sustainability*, 21: 100260. Doi: 10.1016/j.mtsust.2022.100260
- Xing, Z., Ju, Z., Zhao, Y., Wan, J., Zhu, Y., Qiang, Y., Qian, Y.** 2016. One-pot hydrothermal synthesis of Nitrogen-doped graphene as high-performance anode materials for lithium ion batteries. *Scientific reports*, 6(1): 26146. Doi: 10.1038/srep26146
- Xing, X., Jiang, W., Li, S., Zhang, X., Wang, W.** 2019. Preparation and analysis of straw activated carbon synergistic catalyzed by ZnCl₂-H₃PO₄ through hydrothermal carbonization combined with ultrasonic assisted immersion pyrolysis. *Waste Management*, 89: 64-72. Doi: 10.1016/j.wasman.2019.04.002
- Yamada, T., Mizuno, M.** 2021. Infrared Spectroscopy in the Middle Frequency Range for Various Imidazolium Ionic Liquids—Common Spectroscopic Characteristics of Vibrational Modes with In-Plane+ C (2)-H and+ C (4, 5)-H Bending Motions and Peak Splitting Behavior Due to Local Symmetry Breaking of Vibrational Modes of the Tetrafluoroborate Anion. *ACS omega*, 6(2): 1709-1717. Doi: 10.1021/acsomega.0c05769
- Yang, C., Wöll, C.** 2017. IR spectroscopy applied to metal oxide surfaces: adsorbate vibrations and beyond. *Advances in Physics*: X, 2(2): 373-408. Doi: 10.1080/23746149.2017.1296372
- Yin, H., Xiong, Q., Zhang, M., Wang, B., Zhang, F.** 2023. Multi-principles analysis of Cu (II) adsorption in water on magnetic microspheres and modified Chitosan. *Journal of Environmental Chemical Engineering*, 11(6): 111285. Doi: 10.1016/j.jece.2023.111285
- Yossa, LN., Ouimbinga, SK., Sidibe, SS., Ouedraogo, IWK.** 2020. Synthesis of a cleaner potassium hydroxide-activated carbon from baobab seeds hulls and investigation of adsorption mechanisms for diuron: Chemical activation as alternative route for preparation of activated carbon from baobab seeds hulls and adsorption of diuron. *Scientific African*, 9: e00476. Doi: 10.1016/j.sciaf.2020.e00476
- Zbair, M., Bottlinger, M., Ainassaari, K., Ojala, S., Stein, O., Keiski, RL., Bensitel, M., Brahmi, R.** 2020. Hydrothermal carbonization of argan nut shell: functional mesoporous carbon with excellent performance in the adsorption of bisphenol A and diuron. *Waste and biomass valorization*, 11: 1565-1584. Doi: 10.1007/s12649-018-00554-0
- Zhang, M., Ding, R., Hu, F.** 2022. Comparison on FTIR spectrum and thermal analysis for four types of Rehamnnia glutinosa and their extracts. Doi: 10.21203/rs.3.rs-1319441/v1
- Zhang, Y., Zhang, J., Chen, K., Shen, S., Hu, H., Chang, M., Chen, D., Wu, Y., Yuan, H., Wang, Y.** 2023. Engineering banana-peel-derived biochar for the rapid adsorption of tetracycline based on double chemical activation. *Resources, Conservation and Recycling*, 190: 106821. Doi: 10.1016/j.resconrec.2022.106821
- Zhu, S., Jiao, S., Liu, Z., Pang, G., Feng, S.** 2014. High adsorption capacity for dye removal by CuZn hydroxyl double salts. *Environmental science: nano*, 1(2): 172-180. Doi: 10.1039/C3EN00078H



An Alternative Approach to Burden Estimation Based on Targeted Mean Fragment Size Using Rock Fragmentation Models

Kaya Parçalanma Modellerini Kullanarak Hedeflenen Ortalama Parça Boyutuna Dayalı Yük Tahminine Alternatif Bir Yaklaşım

Ozgur Yilmaz*

Zonguldak Bülent Ecevit University, Zonguldak Vocational School, Department of Mining and Mineral Extraction, Zonguldak, Türkiye

Abstract

In the mining industry, bench blasting efficiency is determined by rock fragmentation. Therefore, it is crucial to predict the result of rock fragmentation before blasting. It is widely accepted that empirical fragmentation models like Kuz-Ram and Chung and Katsabanis (C&K) are the most reliable tools for predicting the size distribution of rock fragments following blasting. The main aim of this study is to provide an approach to estimating the optimal burden according to the intended mean fragment size using rock fragmentation models. It is necessary to determine or know the rock factor used in the mentioned models in attempting to apply the method proposed in this study. Initially, studies were conducted to determine the most appropriate burden according to the intended mean fragment for a quarry where the rock factor is known. After this, simplified equations were derived for the optimal burden depending on the rock factor, the intended mean fragment size, the bench height and the density of the explosive.

Keywords: Burden, fragmentation size, kuz-ram model, rock factor.

Öz

Madencilik sektöründe, basamak patlatmalarının verimliliği kaya parçalanma derecesine göre belirlenmektedir. Bu nedenle, patlatma öncesinde kaya parçalanma derecesinin tahmin edilmesi oldukça önem taşımaktadır. Kuz-Ram ve Chung ve Katsabanis (C&K) gibi görgül parçalanma modellerinin, patlatma sonrası kaya parçalarının boyut dağılımının tahmin edilmesinde en güvenilir yöntemler olduğu yaygın olarak kabul edilmektedir. Bu çalışmanın temel amacı, kaya parçalanma modellerini kullanarak istenilen ortalama parça boyutuna göre en uygun yük mesafesinin tahmin edilmesine yönelik bir yaklaşım sağlamaktır. Bu çalışmada önerilen yöntemin uygulanabilmesi için söz konusu modellerde kullanılan kaya faktörünün belirlenmesi veya bilinmesi gerekmektedir. İlk olarak, kaya faktörünün bilindiği bir ocase için istenilen ortalama parça boyutuna göre en uygun yük mesafesinin belirlenmesine yönelik çalışmalar yapılmıştır. Bundan sonra ise, kaya faktörüne, amaçlanan ortalama parça boyutuna, basamak yüksekliğine ve patlayıcının yoğunluğuna bağlı olarak en uygun yük mesafesinin belirlenmesine yönelik basitleştirilmiş denklemler türetilmiştir.

Anahtar Kelimeler: Yük mesafesi, parçalanma boyutu, kuz-ram modeli, kaya faktörü.

1. Introduction

The use of explosives is probably the most common and cost-effective method of excavating rock on mining, quarrying, and construction sites (Hu et al. 2020, Li et al. 2021). Several reasons may have contributed to this, including efficiency, economy, and the ability to break even the hardest rocks.

Explosive energy is used in blast design to break rock masses into smaller, more manageable sizes and shapes that are easier to excavate, load, transport, crush and grind in the future (Ouchterlony 2003, Sanchidrian and Ouchterlony 2017). The first step in size reduction in quarries is blasting, followed by crushing and grinding. One of the most important parameters for determining yield is the fragment size distribution of blasted rock fed to the crusher, since oversize blocks cannot be loaded into the crusher bins (Cunningham 2005). During loading and transportation, smaller or finer fragments cause ore loss, while larger or coarser fragments require further processing, thereby increasing production

*Corresponding author: oyilmaz@beun.edu.tr

Ozgur Yilmaz orcid.org/0000-0002-4706-6723



This work is licensed by "Creative Commons Attribution-NonCommercial 4.0 International (CC BY NC)".

costs. Therefore, bench blasting effectiveness is measured by rock fragmentation in the mining industry. Prediction of rock fragmentation is therefore essential before blasting (Li et al. 2021, Cho et al. 2003).

The size distribution resulting from a particular blast design has been predicted by different models over the years (Ouchterlony 2003). Indirect and direct methods are used to measure fragmented rock's size distribution after blasting. Despite its accuracy, the sieving analysis method, a typical technique in the direct method, is not practical due to time and cost constraints. To address these limitations, indirect methods have emerged, including observational, empirical, and digital methods (Esen and Bilgin 2000). In practice, the empirical models are the ones that are used for daily blast designs.

Engineering fragmentation models can be defined as equations which define the position and shape of the fragment size distribution and how these properties are influenced by factors such as explosive strength, blasting geometry, and rock properties, as well as the amount of explosives used (Ouchterlony and Sanchidrian 2019). Several fragmentation models have been developed in response to the need to provide engineering solutions to full scale blasting problems such as optimisation of run of mine fragmentation (Ouchterlony 2003, Cunningham, 2005, Chung and Katsabanis 2000, Gheibie et al. 2009) Based on Kuznetsov's mean fragment size equation as well as Rosin-Rammler's fragment size distribution equations, Cunningham introduced a model for estimating fragmentation in the early 1980's called the Kuz-Ram model (Cunningham 1983, Cunningham 1987). For predicting rock fragmentation size distribution after blasting, the Kuz-Ram model is the most commonly used model in the industry (Gheibie et al. 2009). Due to the ease of parameterizing the model for blast layout spreadsheets, it has become widely used, but has not been seriously updated since 1987 (Cunningham 2005). After that, in the early 2000's, Chung and Katsabanis (2000) verified the accuracy of the Kuz-Ram model by using other researchers' data. They proposed that the RR function describes fragment size distribution data well enough used (Ouchterlony and Sanchidrian 2019). Chung and Katsabanis (C&K) model (2000) is a modification of original Kuz-Ram model.

This study includes studies on estimating the optimal burden according to the intended mean fragment size using empirical fragmentation models such as Kuz-Ram and Chung and Katsabanis models. It is necessary to determine or know the rock factor used in the mentioned models in

attempting to apply the method proposed in this study. This rock factor is in fact the most crucial parameter for fragmentation models to function correctly.

Despite the fact that this method might seem complicated at first glance to calculate the burden, it should be remembered that it is based on fragmentation theories. Nevertheless, this study derived simplified equations from the complex relations, resulting in practical solutions for the researchers. Finally, generalized equations were derived for the optimal burden depending on the rock factor, the intended mean fragment size, the bench height and the density of the explosive.

2. Kuz-Ram Model

The estimation of fragmentation before blasting has been the subject of some modelling research from past to present. It is often the first target of a blast fragmentation model to predict the mean fragment size (50% passing size). An empirical fragmentation model, Kuz-Ram fragmentation model, is presented by Cunningham (1983). The Kuznetsov equation, which forms the basis of the Kuz-Ram fragmentation model, was first introduced in an article published by Kuznetsov in 1973. Kuznetsov (1973) developed an empirical equation to predict, as a function of rock type, the mean fragment size and blast energy applied per unit volume. Based on the mass percentage passing through versus fragment size, the model predicts fragmentation from blasting. The equation of Kuznetsov is

$$X_m = A \left(\frac{V_0}{Q_e} \right)^{0.8} Q_e^{1/6} \quad (1)$$

where X_m is the mean fragment size (cm), Q_e is the mass of explosive per blasthole (kg), V_0 is the rock volume broken per blasthole (m^3) and A is the rock factor (Kuznetsov 1973). The rock factor here represents the blastability of the rock mass. This equation was originally been prepared according to TNT. Since the strength of TNT compared to ANFO ($ANFO=100$) is 115, Cunningham (1983) rearranged this equation based upon ANFO instead of TNT. The adapted Kuznetsov equation is

$$X_m = A \left(\frac{V_0}{Q_e} \right)^{0.8} Q_e^{1/6} \left(\frac{Sanfo}{115} \right)^{-19/30} \quad (2)$$

where all symbols are as given before and S_{anfo} is the relative weight strength of the explosive to ANFO ($ANFO = 100$). Since

$$\frac{V_0}{Q_e} = \frac{1}{K} \quad (3)$$

where K is the powder factor (kg/m^3), Equation (2) can be rewritten as

$$X_m = A(K)^{-0.8} Q_e^{1/6} \left(\frac{115}{\text{Sanfo}} \right)^{19/30} \quad (4)$$

The fragment size distribution is then predicted using the Rosin-Rammler equation. According to this model, fragmentation in blasted rocks can be reasonably described. The equation is as follows (Rosin and Rammler 1933).

$$R_x = e^{-(X/X_c)^n} \quad (5)$$

where R_x is the mass fraction retained on screen opening X (%), X is the fragment size (cm), X_c is the characteristic size (cm) and n is the index of uniformity. The characteristic size X_c is one through which 63.2% of the particles pass. A typical fragmentation curve can be plotted if the characteristic size X_c and the index of uniformity n are known. Rearranging Equation (5) yields the following expression for characteristic size:

$$X_c = \sqrt[n]{-In R_x} \quad (6)$$

According to the Kuznetsov formula, 50% of material passes through a screen size X_m . Therefore, substituting X = X_m and R = 0.5 into Equation (6) yields

$$X_c = \sqrt[n]{\frac{X_m}{0.693}} \quad (7)$$

($-ln 0.5=0.693$). Calculating the index of uniformity is the most important step in this equation. The value of n determines the shape of the Rosin-Rammler curve. Uniform sizing is indicated by high values. Conversely, low values suggest a wide range of sizes, including both oversize and fines (Gheibie et al. 2009). By considering the effects of blast geometry, hole diameter, burden, spacing, hole length and drilling accuracy, Cunningham (1987) established the applicability of index of uniformity. The index of uniformity, n, is estimated by

$$n = \left(2.2 - 14 \frac{B}{D} \right) \left(\frac{1}{2} + \frac{S}{2B} \right)^{0.5} \left(1 - \frac{W}{B} \right) \left(\frac{L}{H} \right) \quad (8)$$

where B is the burden (m), S is the spacing (m), D is the borehole diameter (mm), W is the standard deviation of drilling accuracy (m), L is the total charge length (m) and H is the bench height (m). When there is more than one

explosive in the hole (bottom charge and column charge), Equation (8) is modified as follows:

$$n = \left(2.2 - 14 \frac{B}{D} \right) \left(1 - \frac{W}{B} \right) \left(\frac{1}{2} + \frac{S}{2B} \right)^{0.5} \left(0.1 + abs \left(\frac{BCL - CCL}{L} \right) \right)^{0.1} \left(\frac{L}{H} \right) \quad (9)$$

where BCL is the bottom charge length (m) and CCL is the column charge length (m). It is necessary to multiply this equation by 1.1 if you are using a staggered pattern. Besides, Gustafsson (1973) suggested the following relation for standard deviation of drilling accuracy.

$$W = 0.1 + (0.03 \times H) \quad (10)$$

where all symbols are as given before in meters. It has been referred to as the Kuz-Ram fragmentation model after combining the Kuznetsov and Rosin-Rammler equations. Using the Kuznetsov and Rosin-Rammler equations and an algorithm, it derives the exponent of uniformity in the Rosin-Rammler equation from blasting parameters.

3. Chung and Katsabanis (C&K) Model

A number of papers were published on rock blasting by the US Bureau of Mines (USBM) until the mid-1990s (Ouchterlony and Sanchidrian 2019). Using data from the literature, Chung and Katsabanis (2000) introduced new relations that can be interpreted as a modification of the Kuz-Ram model.

The Kuz-Ram model calculates the mean fragment size for a given rock type and explosive, using the specific charge and the amount of explosive per blasthole. Chung and Katsabanis (2000) suggested that delay time and distribution of explosive in rock mass should be considered when calculating the mean fragment size. However, they later concluded that delay time has a critical effect but after a certain point there is no remarkable change in the fragmentation. Therefore they removed the delay time parameters from the model. They presented the following equations with the Kuz-Ram a value as an improvement:

$$X_{50} = A Q_e^{-1.193} B^{2.461} (S/B)^{1.254} H^{1.266} \quad (11)$$

$$X_{80} = 3 A Q_e^{-1.073} B^{2.43} (S/B)^{1.013} H^{1.111} \quad (12)$$

$$n = 0.842 (\ln x_{80} - \ln x_{50}) \quad (13)$$

where all symbols are as given before and X_{50} and X_{80} are the 50% and 80% passing size respectively. As the definition of specific charge is $q = Q_e / (\text{BSH})$, Equation (11) may be rewritten as

$$X_{50} = A (B^{0.005} S^{0.009} H^{0.003}) Q_e^{0.07} q^{-1.263} \quad (14)$$

4. Determination of Rock Factor A

The rock factor represents the blastability of the rock mass, which quantifies the compound effect of the geological and geotechnical site factors on fragmentation (Salmi and Sellers 2021). It is therefore essential to correctly determine the rock factor A so that the Kuz-Ram model can be used effectively. Due to the complex parameters involved, determining this factor that defines the rock is difficult. Cunningham (1987) adapted Lilly's (1986) Blastability Index for Kuznetsov's model in an attempt to better quantify the selection of rock factor A, which made determining rock factor A easier. Cunningham (1987) stated that every assessment of rock for blasting should at least take into account the density, mechanical strength, elastic properties and fractures. A single rock factor A can be calculated by addressing some of the key issues despite the difficulty of estimating individual geological effects:

$$A = 0.006 (RMD + JF + RDI + HF) \quad (15)$$

where RMD is the rock mass description, JF is the joint factor, RDI is the rock density influence and HF is the hardness factor. Generally rock factor is 7 for medium hard rocks, 10 for hard highly fissured Rocks, 13 for hard, weakly fissured rocks (Cunningham 2005). The description of the rock factor parameters and rates are given in Table 1.

As can be seen in Table 1, rock factor A, which represents the structural geology of rock mass, is influenced by several factors including joint factors such as vertical joint plane spacing, joint plane angle and joint condition, rock density, and hardness factor, which is determined by the young's modulus or the uniaxial compressive strength of intact rock.

The vertical joint plane spacing depends partly on the absolute joint spacing, and partly on the spacing to drilling pattern ratio. In addition vertical joint plane angle is related to dip, which is steeper than 30 degrees (Cunningham 2005).

5. Estimation of Burden Based on Mean Fragment Size

If the rock factor A in the Kuz-Ram and C&K models is known or predefined, it can be used to determine the most appropriate blast pattern for future blasts. The Kuz-Ram and C&K models will be used to calculate the burden according to the intended mean fragment size in this part of the study.

In the Kuz-Ram model, the mean fragment size is obtained as a function of the explosive charge in each blasthole and the rock volume broken per blasthole. The rock volume broken per blasthole (V_0) can calculated as

$$V_0 = BSH \quad (16)$$

where B is the burden (m), S is the spacing (m) and H is the bench height (m). Spacing is the distance between adjacent blastholes and is measured perpendicular to the burden. According to Swedish researchers (Gustafsson 1973, Olofsson 1988) the relation between burden and spacing is

$$S = 1.25 B \quad (17)$$

Substituting the values $S = 1.25 B$ into Equation (16) and rearranging to yield the following expression for the burden gives

Table 1. Rock factor parameters and rates (Ouchterlony 2003).

RMD		Rock Mass Description
Powdery/friable		10
Vertically jointed		JF
Massive		50
JF		Joint Factor
		$JF = (JCF JPS) + JPA$
JPS		Joint Plane Spacing
<0.1 m		10
0.1–0.3 m		20
0.3 m–95% of P		80
> P		50
JPA		Joint Plane Angle
Horizontal		10
Dip into face		20
Strike out of face		30
Dip out of face		40
JCF		Joint Condition Factor
Tight joints		1
Relaxed joints		1.5
Gouge-filled joints		2
RDI		Rock Density Influence
		$RDI = (0.025 RD - 50)$
HF		Hardness Factor (GPa)
Young's modulus (E)<50 GPa		$HF = E / 3$
E>50 GPa		$HF = UCS / 5$
$P = \sqrt{Burden \cdot Spacing}$		
RD: Rock Density (kg/m ³)		
UCS = Uniaxial Compressive Strength (MPa)		

$$B = \sqrt{\frac{V_0}{1.25H}} \quad (18)$$

For the Kuz-Ram model, Equation (2) can be rearranged to yield the following expression for the rock volume broken per blasthole (m^3):

$$V_0 = Q_e (X_m / (AQ_e^{1/6} (S_{anfo}/115)^{-19/30}))^{1.25} \quad (19)$$

Equation (18) and Equation (19) can be combined to give the burden (B) as follows:

$$B = \sqrt{\frac{Q_e (X_m / (AQ_e^{1/6} (S_{anfo}/115)^{-19/30}))^{1.25}}{1.25H}} \text{ for Kuz-Ram model} \quad (20)$$

As far as the C&K model is concerned, Equation (11) can be directly rearranged to yield the following expression for burden (B) by substituting the values S/B = 1.25:

$$B = \left(\frac{X_{50}}{AQ_e^{-1.193} 1.25^{1.254} H^{1.266}} \right)^{1/2.461} \text{ for C&K model} \quad (21)$$

Thus, the burden can be estimated by using Equation 20 or Equation 21 depending on the intended mean fragment size and bench height for a certain site whose rock factor has been determined beforehand. The mass of explosive in the hole here can be calculated depending on the blasthole diameter, the charge height and the density of the explosive used. The unloaded part of the blasthole is defined as the stemming. There are different approaches in the literature to calculate the stemming according to the burden or blasthole diameter. In accordance with Swedish researchers the stemming is equal to the burden $H_s = B$ (Langefors and Kihlsröm 1963, Olofsson 1988). Konya and Walter (1990), on the other hand, suggested the stemming as a function of blasthole diameter as $H_s = 0.7d$. These approaches will give a constant value for the stemming height according to the varying bench height. However, it is a very common practice in quarrying to leave 1/3 of the blasthole height as the stemming length in general. Therefore, it would be more accurate to calculate the stemming height as a function of the bench height to calculate the specific charge density. In this study, the ratio S/B = 1.25 which was observed to give the best results in terms of fragmentation was used.

6. Simplified Equations

In first part of this section, since the mass of explosive per blasthole (Q_e) varies according to the density of the explosive (ρ_e), multiple regression analyses were performed using Equation (20) and Equation (21) for a certain type of explosive. In this context, ANFO with a density of 800

kg/m^3 was taken as a reference explosive. In other words, the linear charge concentration of the referenced explosive is 5 kg/m in the blasthole for a blasthole diameter of 89 mm. It is also critical to note that the mass of explosive per blasthole changes as a function of the bench height, as previously discussed.

In the work done here, regression analysis is not used to estimate the relationship between the dependent variable and independent variables. Instead it is used to reduce the number of independent variables given in Equation (20) and Equation (21) rearrange the equation. In the regression analyses using Equation (20) and Equation (21), a burden value (B) was obtained by randomly assigning different values for the rock factor (A), the mean fragment size (X_m) and the bench height (H). In the regression analyses, B is the dependent variable, while A, X_m and H are independent. For those analyses values from 0.8 to 22 were assigned for the rock factor, values of 30, 40, 50, 60, 80 and 100 cm were assigned for the mean fragment size, and values ranging from 5 to 30 m were assigned for the bench height (H). A total of 1800 calculations were made for each equation. If the results obtained by Equation (20) and Equation (21) are rearranged by regression analysis, it can be re-written as follows according to the rock factor, the mean fragment size and the bench height as

$$B = 1.36 \left(\frac{X_m}{A} \right)^{5/8} H^{-0.104} \text{ for Kuz-Ram model using ANFO} \quad (22)$$

$$B = 1.60 \left(\frac{X_c}{A} \right)^{2/5} H^{-0.030} \text{ for C&K model using ANFO} \quad (23)$$

where all the symbols and units are as given before. With this equation, the burden can be calculated according to the intended mean fragment size for different sites by using standard ANFO for 89 mm blasthole.

In addition to the above mentioned equations, in the second part of the study different explosive densities were also considered in a more general form. The mass of explosive in the blasthole Q_e , which is the independent variable in Equation (20) and Equation (21), is actually a variable depending on the blasthole diameter, the charge length and the density of the explosive. In order to generalize the obtained relations for any field, regression analyses were performed by taking the explosive density as an independent variable. Rearranging the results obtained by Equation (20) and Equation (21) by regression analysis, it is possible to write it according to the density of the explosive as

$$B = 0.097 \left(\frac{X_m}{A} \right)^{5/8} H^{-0.104} \rho_e^{79/200} \text{ for Kuz-Ram model} \quad (24)$$

$$B = 0.114 \left(\frac{X_c}{A} \right)^{2/5} H^{-0.030} \rho_e^{79/200} \text{ for C&K model} \quad (25)$$

where ρ_e is the density of the explosive (kg/m^3). Thus, using Equation (24) and Equation (25), the burden B (m) can be determined depending on the rock constant A, the intended mean fragment size X_m (cm), the bench height H (m) and the density of the explosive ρ_e (kg/m^3).

7. Results and Discussion

As a result of the variety of factors involved in blasting operations as well as the unpredictable response of rock masses to excavation, correlations between blasting quality parameters and rock mass quality have not always been clear (Costamagna et al. 2021). Inevitably, blasting loads have some negative effects, such as damage and vibration. To reduce and minimise these problems, blasting design has incorporated a variety of control techniques. By controlling blasting, rocks beyond the contour of the excavation are minimized from being damaged (over-broken) (Cardu et al. 2022). This study focused on calculating the burden according to rock fragmentation size distribution after production blasting in quarries. Since slopes or blasted surfaces are beyond the

scope of this study, only fragmentation of rock is addressed. Keeping open pit excavation damage to a minimum can also provide satisfactory results in terms of stability conditions and control over block size distribution in quarry aggregates.

As much as both models are concerned separately, Figure 1 shows the relationship between the burden and the bench height for the reference explosive ANFO according to considered four different mean fragment sizes (30, 50, 80 and 100) using Equation 22 and Equation 23. Three different rock factor values were considered here: 7 for medium hard rock, 10 for hard, highly fissured rocks and 13 for very hard, weakly fissured rock. As can be seen from Figure 1, unlike the Kuz-Ram model, which varies significantly with bench height, the C&K model is not significantly affected. Besides, according to the C&K model, burden varies within a narrow range when the rock factor changes, but in the Kuz-Ram model, burden varies quite a bit when the rock factor changes.

With respect to three different rock factor values ($A= 7, 10$ and 13), Figure 2 illustrates the relationship between the burden and the density of the explosive for both models taken into consideration using Equation 24 and Equation 25. For better understanding, in this figure, bench height

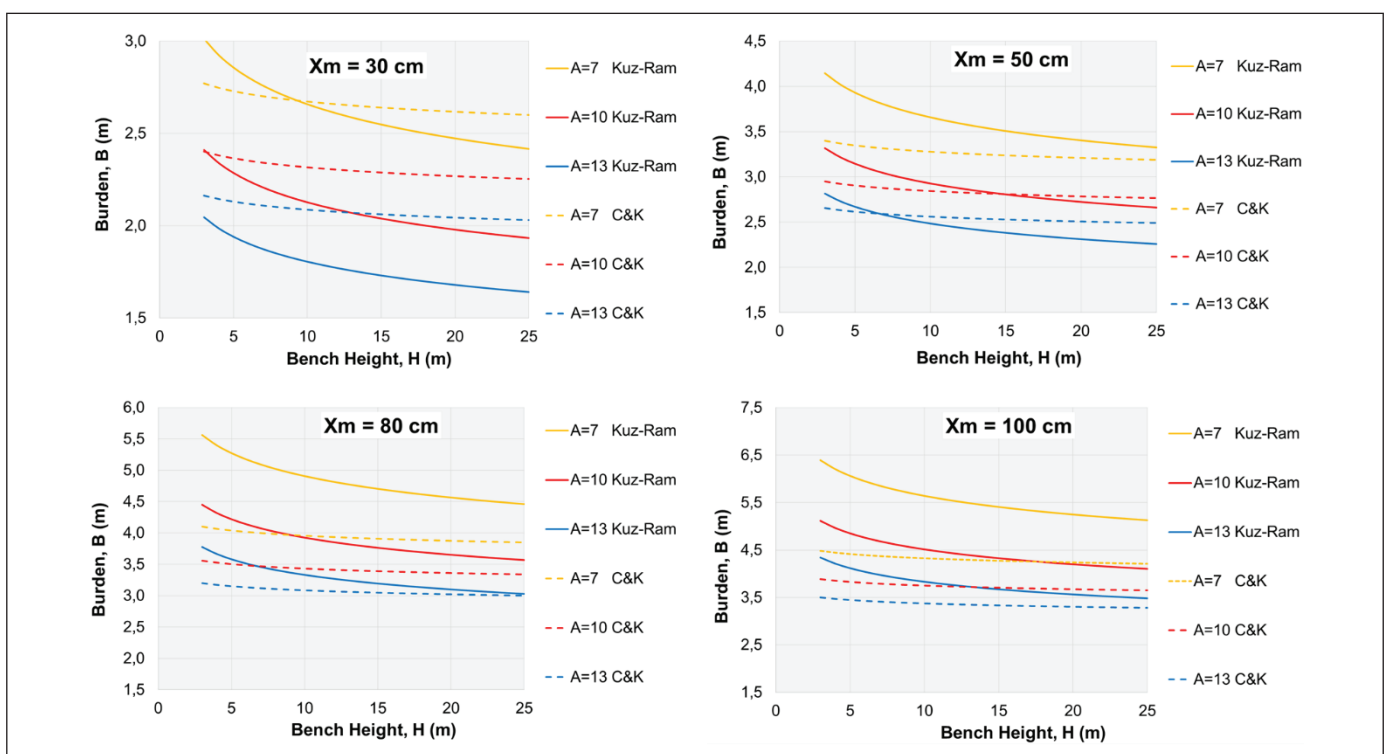


Figure 1. The relationship between the burden and the bench height for the reference explosive ANFO according to four different mean fragment sizes for both models.

was chosen as 15 m and the mean fragment size was chosen as 80 cm. As shown in Figure 2, for both models, the burden increases in direct proportion to explosive density as expected. It is important to note here that the Kuz-Ram model gives wider burden values than the C&K model. While this chart demonstrates the consistency of the proposed equations, it also shows how practical they can be for calculating the burden for a given site.

For three different explosive densities (800, 1200 and 1800 kg/cm³), Figure 3 shows the relationship between burden

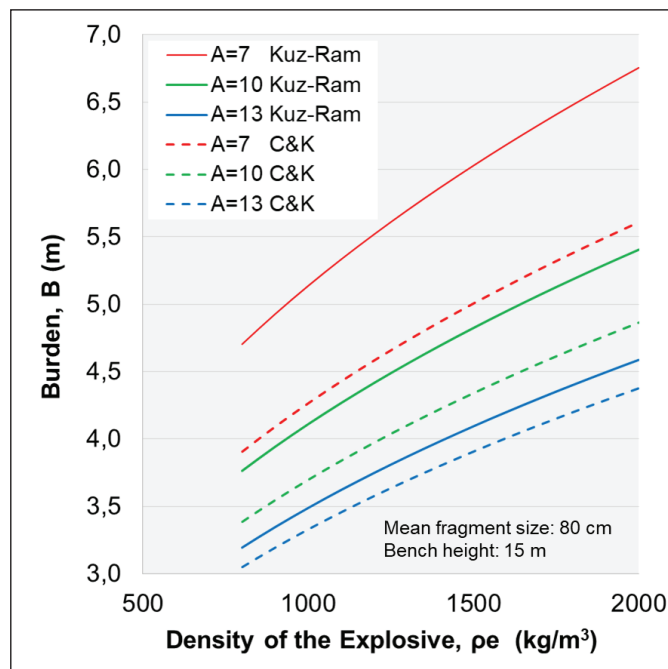


Figure 2. The relationship between the burden and the density of the explosive for both fragmentation models.

and rock factor representing the blastability of the rock mass is given separately for two fragmentation models considered using Equation 24 and Equation 25. Similar to Figure 2, in this Figure 3 bench height was chosen as 10 m and the mean fragment size was chosen as 50 cm. As can be seen from Figure 3, for the rock factor between 10 and 20, which represents hard rocks, the burden varies between 2 and 3 m, which is what is commonly used in practice.

7. Conclusions

The objective of this study is to recommend alternative approaches to design quarry blast rounds according to intended fragmentation size. The interrelated Kuz-Ram and C&K fragmentation models that are widely used in the literature were considered in this context. Kuznetsov's model is derived from geomechanical and geometrical parameters as well as explosive properties. Therefore, in order to apply this proposed method correctly, the rock factor reflecting the geomechanical properties of blasted rock masses needs to be well defined.

In this study, the approach of calculating the burden according to the intended mean fragment size based on the aforementioned fragmentation models was introduced. Based on this, the Equation 20 and Equation 21 were first obtained mathematically using Kuz-Ram and C&K fragmentation models, then four simplified equations were proposed based on these equations. Two of these are in their simplest form for ANFO (Equation 22 and Equation 23), while the other two include explosive density in a more general form (Equation 24 and Equation 25). Afterwards, charts that provide guidance in practical applications were

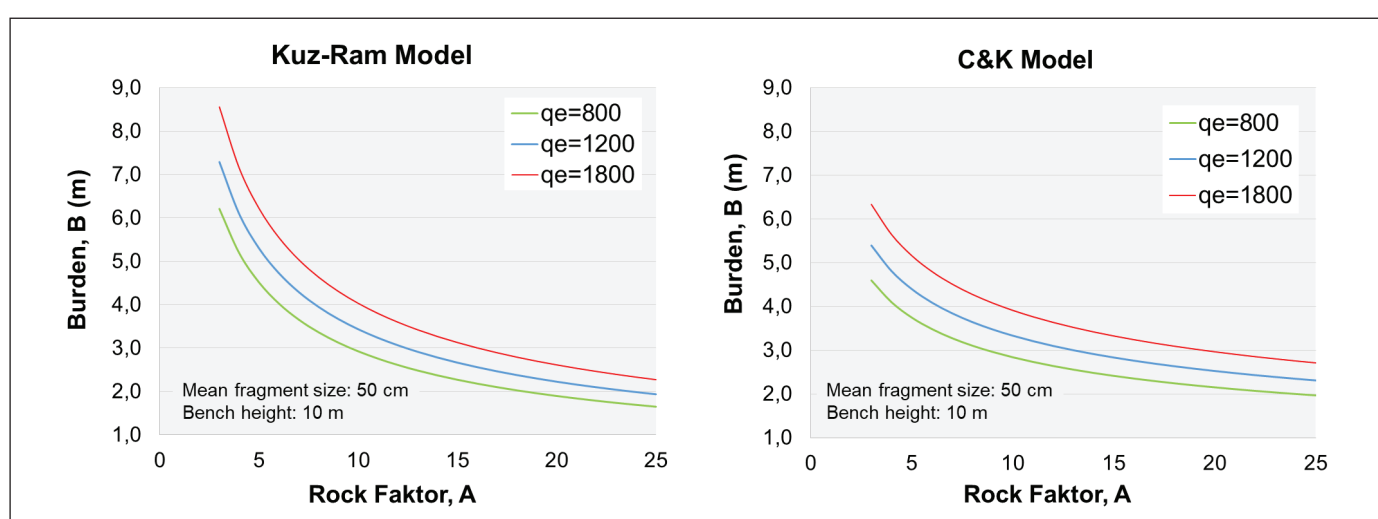


Figure 3. The relationship between the burden and the rock factor according to three different explosive densities.

created using Equations 22–25 for certain conditions. These site-specific diagrams demonstrate not only the consistency of the proposed equations, but also show how practical they can be for calculating the burden for a given site. Hereby, each quarry can prepare practical charts according to its own conditions and design blasting accordingly. As a result, the proposed method for calculating the burden yields results consistent with the intended mean fragment size.

8. References

- Cardu, M., Godio, A., Oggeri, C., Seccatore, J. 2022.** The influence of rock mass fracturing on splitting and contour blasts. *Geomechanics and Geoengineering*, 17:3, 822–833, <https://doi.org/10.1080/17486025.2021.1890234>
- Cho, HS., Nishi, M., Yamamoto, M., Kaneko, K. 2003.** Fragment Size Distribution in Blasting. *Materials Transactions*, Vol. 44, No. 5, pp. 951–956.
- Chung, SH., Katsabanis, PD. 2000.** Fragmentation prediction using improved engineering formulae. *Fragblast* 4 (3-4) 198–207.
- Costamagna, E., Oggeri, C., Vinai, R. 2021.** Damage and contour quality in rock excavations for quarrying and tunnelling: Assessment for properties and solutions for stability. *IOP Conference Series: Earth and Environmental Science*, 833(1), 012137. <https://doi.org/10.1088/1755-1315/833/1/012137>
- Cunningham, CVB. 1983.** The Kuz–Ram model for prediction of fragmentation from blasting. In: Holmberg R & Rustan A (eds) *Proceedings of First International Symposium on Rock Fragmentation by Blasting*, Luleå, pp 439–454.
- Cunningham, CVB. 1987.** Fragmentation estimations and the Kuz–Ram model—four years on. In: Fourney W (ed) *Proceedings of Second International Symposium on Rock Fragmentation by Blasting*, Keystone, Colorado, pp 475–487.
- Cunningham, CVB. 2005.** The Kuz–Ram Fragmentation Model – 20 Years On. In: *Proceedings of the EFEE 5th World Conference on Explosives and Blasting*, European Federation of Explosives Engineers, Brighton, pp 201–210.
- Esen, S., Bilgin, HA. 2000.** Effect of explosive on fragmentation. In: *The 4th Drilling and Blasting Symposium*. Ankara, Turkey.
- Gheibie, S., Aghababaei, H., Hoseinie, SH., Pourrahimian, Y. 2009.** Modified Kuz–Ram fragmentation model and its use at the Sungun Copper Mine. *Int J Rock Mech Min Sci* 46, 967–973. <https://doi.org/10.1016/j.ijrmms.2009.05.003>
- Gustafsson, R. 1973.** Swedish Blasting Technique. Published by SPI, Gothenburg, Sweden.
- Hu, H., Lu, W., Yan, P., Chen, M., Gao, Q., Yang, Z. 2020.** A new horizontal rock dam foundation blasting technique with a shock-reflection device arranged at the bottom of vertical borehole. *Eur. J. Environ. Civ. Eng.* 24 (4), pp. 481–499.
- Konya, CJ., Walter, EJ. 1990.** Controlled Blasting. *Surface Blast Design*, Prentice-Hall, USA.
- Kuznetsov, VM. 1973.** The mean diameter of fragments formed by blasting rock. *Sov. Min. Sci.* 9. 144–148.
- Langefors, V., Kihlsröm, B. 1963.** *The Modern Technique of Rock Blasting*. Halsted press, Wiles and Sons.
- Li, E., Yang, F., Ren, M., Zhang, X., Zhou, J., Khandelwal, M. 2021.** Prediction of blasting mean fragment size using support vector regression combined with five optimization algorithms. *Journal of Rock Mechanics and Geotechnical Engineering* 13, 1380–1397.
- Lilly, PA. 1986.** An empirical method of assessing rock mass blastability. In: Davidson JR (ed) *Proceedings of the Large Open Pit Mining Conference*, The Aus IMM, Parkville, Victoria. pp 89–92.
- Olofsson, OS. 1988.** *Applied Explosives Technology for Construction and Mining*. Sweden.
- Ouchterlony, F. 2003.** Influence of Blasting on the Size Distribution and Properties of Muckpile Fragments. A State-of-the-art Review. Luelia University of Technology.
- Ouchterlony, F. and Sanchidrian, J.A. 2019.** A review of development of better prediction equations for blast fragmentation. *J Rock Mech Geotech Eng* 11. 1094–1109. <https://doi.org/10.1016/j.jrmge.2019.03.001>
- Rosin, R., Rammler, E. 1933.** Laws governing the fineness of coal. *J Inst Fuels* 7:29–36.
- Salmi, EF., Sellers, EJ. 2021.** A review of the methods to incorporate the geological and geotechnical characteristics of rock masses in blastability assessments for selective blast design. *Engineering Geology* 281. 2021: 105970. <https://doi.org/10.1016/j.enggeo.2020.105970>
- Sanchidrian, JA, Ouchterlony, FA. 2017.** A Distribution-Free description of fragmentation by blasting based on dimensional analysis. *Rock Mech Rock Eng* (2017) 50:781–806. <https://doi.org/10.1007/s00603-016-1131-9>



Techno-Economic Assessment of a Hybrid Renewable Energy Powered Electric Vehicle Charging Station For Shopping Mall in Edirne, Turkey

Edirne'deki Alışveriş Merkezi İçin Hibrit Yenilenebilir Enerji ile Çalışan Elektrikli Araç Şarj İstasyonunun Tekno-Ekonominik Değerlendirmesi

Hacer Akhan*

Trakya University, Engineering Faculty, Mechanical Engineering Department, Edirne, Türkiye

Abstract

24% of global greenhouse gas emissions originate from the transport vehicles, with the use of fossil fuels in vehicles. If electric vehicles are charged with renewable energy, there is an 80–95% reduction in carbon dioxide emissions compared to electricity produced by conventional methods. In this study, the technical and economic evaluation of a photovoltaic (PV)-wind hybrid energy system for two electric vehicle charging stations for a shopping mall in Edirne was investigated. Optimization of the hybrid renewable energy powered charging station was made using HOMER software. The optimal system types, cash flows, impact analyse, and energy production analyse were discussed. The results show that the most suitable wind-PV hybrid system for the EVS station includes vertical axis wind turbines with 50 kW rated power, 50 kW PV system and 52.1 kW power converters. The wind-PV hybrid system has a total net present cost of \$145,961, the net present cost of \$145,961, an annual operating cost of \$1,881/year and the levelized cost of energy of \$0.0193/kWh. The renewable energy powered hybrid electric vehicle charging station for shopping mall is engineering solutions that can be applied universally.

Keywords: Charging station, electric vehicle, greenhouse gas reduction, renewable energy.

Öz

Küresel sera gazı emisyonlarının %24'ü ulaşım araçlarından, araçlarda fosil yakıtların kullanılmasından kaynaklanmaktadır. Elektrikli araçların yenilenebilir enerji ile şarj edilmesi durumunda, geleneksel yöntemlerle üretilen elektriğe kıyasla karbondioksit emisyonlarında %80-95 oranında azalma olmaktadır. Bu çalışmada, Edirne'deki bir alışveriş merkezi için iki elektrikli araç şarj istasyonu için fotovoltaik (PV)-rüzgar hibrit enerji sisteminin teknik ve ekonomik değerlendirmesi incelenmiştir. Hibrit yenilenebilir enerji ile çalışan şarj istasyonunun optimizasyonu HOMER yazılımı kullanılarak yapılmıştır. Optimum sistem tipleri, nakit akışları, etki analizleri ve enerji üretim analizleri tartışılmıştır. Sonuçlar, EVS istasyonu için en uygun rüzgar-PV hibrit sisteminin 50 kW nominal gücü sahip dikey eksenli rüzgar türbinleri, 50 kW PV sistemi ve 52.1 kW güç dönüştürücülerini içerdigini göstermektedir. Rüzgar-FV hibrit sisteminin toplam net bugünkü maliyeti 145.961 \$, yıllık işletme maliyeti 1.881 \$/yıl ve seviyelendirilmiş enerji maliyeti 0,0193 \$/kWh'dır. Alışveriş merkezi için yenilenebilir enerji ile çalışan hibrit elektrikli araç şarj istasyonu, evrensel olarak uygulanabilecek mühendislik çözümleridir.

Anahtar Kelimeler: Şarj istasyonu, elektrikli araç, sera gazı azaltımı, yenilenebilir enerji.

1. Introduction

Transportation networks, which are part of the modern world, use vehicles that are heavily dependent on fossil

fuels. Transport emissions from fossil fuels alone cause 24% of energy sector emissions. 74.5% of transport emissions come from road vehicles. The disruption of transportation in the COVID-19 crisis reduced global fossil oil demand by 57% in 2020 and a decrease in transportation emissions was observed. Global CO₂ emissions from the transport sector rose 8% to around 7.7 Gt CO₂ in 2021, as pandemic restrictions were lifted, and passenger and transportation increased after the decline in 2020. Transport emissions

*Corresponding author: hacera@trakya.edu.tr

Hacer Akhan orcid.org/0000-0002-7896-6441



This work is licensed by "Creative Commons Attribution-NonCommercial 4.0 International (CC)".

increased by an average of 1.7% annually from 1990 to 2021; this was faster than any other sectors (www.iea.org/reports).

Annual emissions caused by the transport vehicles in Turkey decreased by 1.8 million tons of CO₂ equivalent (2.18%) in 2020 compared to the previous year and decreased to 80.68 million tons of CO₂ equivalent. Figure 1 shows the annual greenhouse gas emissions caused by transportation in Turkey from 2011 to 2020 (www.eurostat.ec.europa.eu).

There are about 16 million electric cars on the roads around the world, and around 30 TWh of electricity is consumed annually. Figure 2. Shows the global EV sales by scenario from 2020 to 2030. Electric cars have helped reduce fossil fuel consumption and CO₂ emissions in 2021 (www.iea.org/commentaries).

Hybrid electric car sales in Türkiye continued to rise steadily. Figure 3 shows the electric car sales in Turkey from 2015 to 2022. The number of electric cars sold in the first 6 months of 2022 reached 2413 with a 3-fold increase compared to the same period of 2021. According to the data, hybrid car sales figures declined for the first time in the first 6 months of 2022. Despite the addition of new models this year to the hybrid car market, which breaks records every year, the total figure amounted to 9,731 units. In the first 6 months of 2021, 11 thousand 851 hybrid cars were sold (www.tehad.org/2022). With the increasing interest in electric vehicles in Turkey, there has been a great increase in charging stations. Currently, there are a total of 2981 (2714 AC, 267 DC) charging stations throughout Turkey (www.tehad.org/2021). There are 9 charging stations in Edirne. 2 of the 9

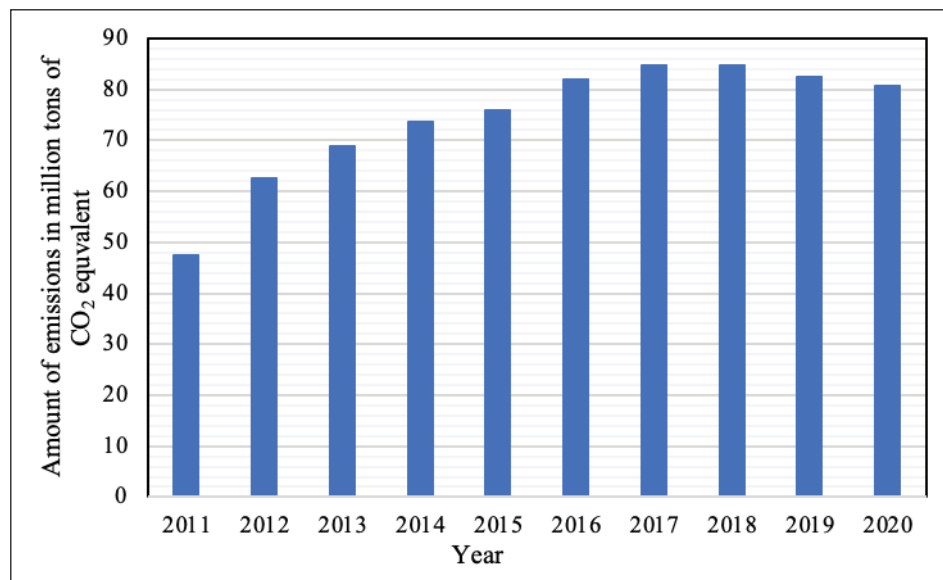


Figure 1. Greenhouse gas emissions in the transport vehicles in Turkey.

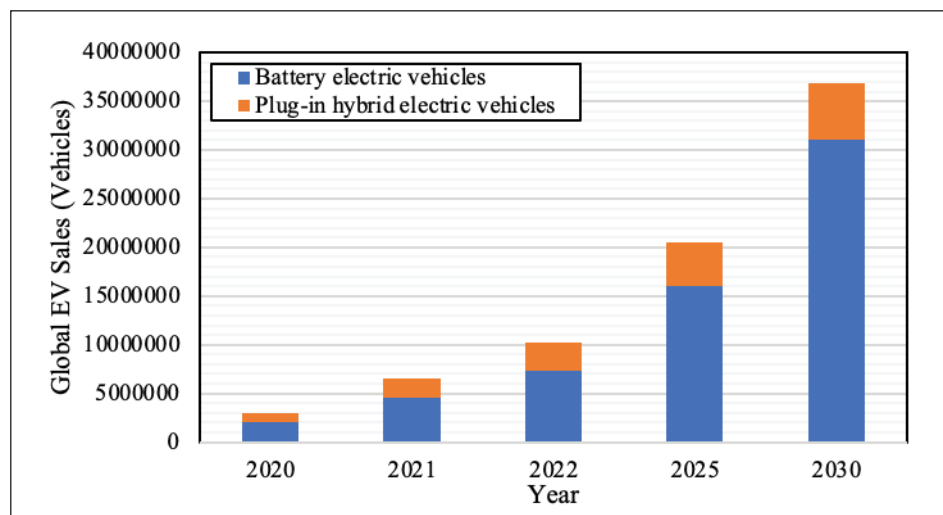


Figure 2. Global EV sales by scenario from 2020 to 2030 (www.iea.org/data).

charging stations are in the shopping mall (www.elektrikli.com.tr). Figure 4 shows the main EV charging stations in Turkey.

Electric vehicles drawing high amounts of energy from the grid will lead to an increase in energy demand, albeit indirectly, through tourism. Especially in the tourism season, with the increase in the visitors' number, there is an increase in the number of charged electric vehicles in shopping malls. Depending on the charging habits of the users, simultaneous charging of many vehicles will cause problems in seasonal demand variability in the load and energy supply security in the grid (Moslehi and Kumar 2010). Existing power system components are not designed to handle the extra loads for long periods. This can cause overloading of components or damage existing transformers. In addition, phase and voltage imbalance in the energy grid is one of the

important problems encountered. If many electric vehicles are charged using the same phase, a phase imbalance may occur in the grid. Unplanned charging of electric vehicles causes serious problems in distribution networks (Geth et al. 2012). Simultaneous charging of many EVs may cause voltage drops and deviations at the connection points of the chargers (Singh et al. 2010, Ma et al. 2017, Ucer et al. 2018). During charging, electric vehicles cause active power consumption with high power demand from the grid, which leads to power loss in the distribution system. Positioning the charging stations at the most suitable points and choosing the right power capacity can minimize the power loss in the network (Nurmuhammed and Karadağ 2021). Excessive harmonics that will occur during the charging of electric vehicles pose a potential problem in power systems (Staats et al. 1997). Charging systems with excessive harmonic

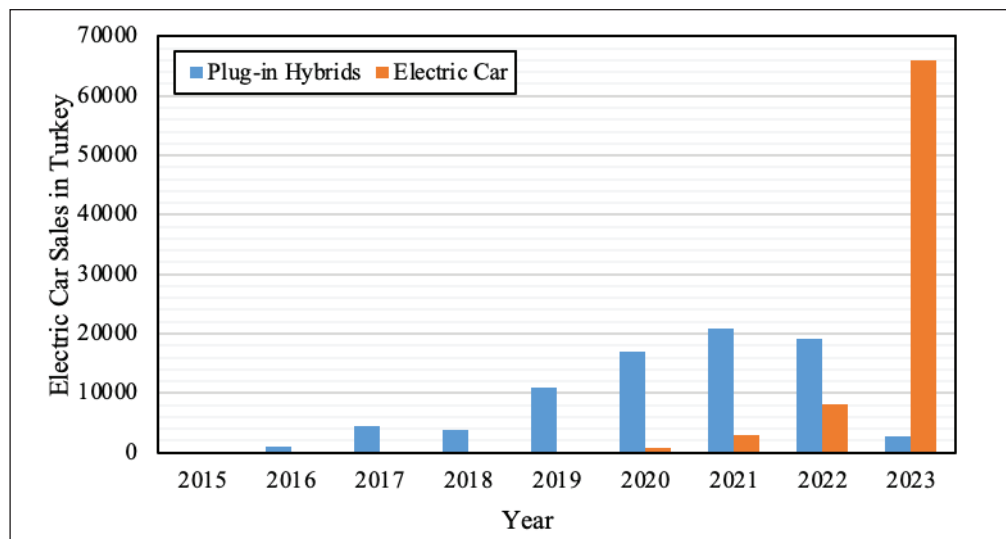


Figure 3. Electric car sales in Turkey from 2015 to 2023 (www.statista.com/chart).

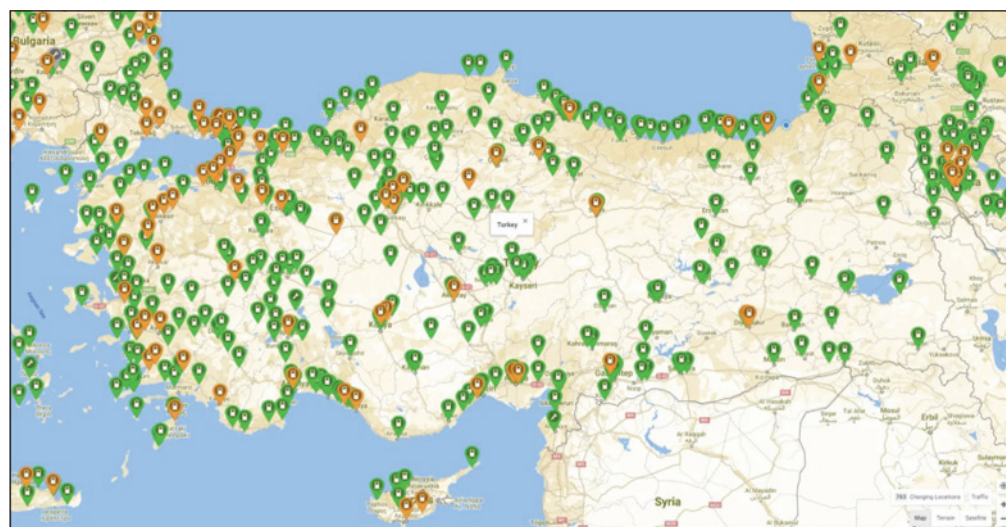


Figure 4. Main EV charging stations in Turkey (www.google.com/maps).

current distortion may cause secondary distribution line and transformer value reductions or quality of service problems (Bass et al. 2001).

The simultaneous or unpredictable charging of many electric vehicles causes large differences in electricity supply and demand drawn from the grid. In addition, vehicles charging at high speeds can cause the power losses and the voltage imbalance in the grid, thus negatively affecting the electricity grid. It is important that the charging stations are in the right place and that the electrical energy is supported by renewable energy systems or that they are fed with RES independently from the grid. In addition to planning, operation and control in the grid, renewable energy provides solutions to the problems of providing environmentally energy production.

Since electric vehicles do not emit carbon, they provide 100% nature-friendly transportation. Greenhouse gas emissions in transportation are prevented with electric vehicles that are charged at charging stations that work with grid electricity. However, if the grid electricity is not produced with environmentally friendly energy production systems, greenhouse gas emissions are released for the operation of the electric vehicle in general. At this stage, it would be appropriate for the charging stations to be independent from the grid or connected to the grid, to be fed with a minimum level of grid electricity and to be operated with mostly or completely renewable energy sources. In addition, if electric vehicles are charged with renewable energy, 80-95% more reduction is achieved in carbon dioxide emissions compared to electricity produced by conventional methods (www.eea.europa.eu/highlights).

In the literature, many studies have been carried out on the hybrid electric vehicle charging station. Li et al. conducted a technical and economic feasibility study of a hybrid wind turbine/ PV/battery power system in Urumqi, China using HOMER (Li et al. 2013). Hiendro et al. analysed the potential use of wind turbine and PV for a hybrid system at a remote location using HOMER software (Hiendro et al. 2013). Mouli et al. In the Netherlands, they studied the possibility of charging battery electric vehicles by using solar energy at work. A 10kW PV array was considered and modelled in MATLAB with data from the Netherlands Meteorological Institute. Considering the air temperature, they concluded that the angle at which the maximum efficiency is achieved is 28°C (Mouli et al. 2016). Das et al. realized the hybrid charge station in Bangladesh, a combination of an off-grid biogas generator, PV modules,

diesel generators and wind turbines by using Homer (Das et al. 2017). Çiçek and Erdinç designed a PV battery hybrid system with the aim of reducing the total energy cost of the electric vehicle parking lot. They have created a charge management model to reduce the total cost by charging the batteries both with increased energy from PV and during tariff periods when electricity is cheap, and by using them during periods when electricity is expensive (Çiçek and Erdinç 2019). Bansal et al. investigated the technical and economic analysis of the charging station for electric vehicles and fuel cell electric vehicles (Bansal et al. 2020). Li investigated the technical and economic evaluation of a off-grid wind fuel cell (FC)-battery hybrid power system for a residence in Xining-China by using HOMER (Li 2021). Early et al. designed and optimized a wind solar hybrid charging station via HOMER software (Early et al. 2021). Sun reviewed the optimal design for fast EV charging stations with wind turbine, PV, and energy storage system. An EV charge load simulation model has been created that dynamically changes the charge expectation according to the electricity price for the duration of use and considers the demand response (Sun 2021). Agustin and Lopez described the design and control strategies for diesel hybrid systems containing wind and/or PV and/or batteries or fuel cells as energy storage components (Agustin and Lopez 2009). Calise et al. proposed a new approach to the problems due to the high density of vehicular traffic in the shopping malls by incorporating PV panels into the energy system by considering a shopping mall in Italy (Calise et al. 2021). Jain and Bhullar studied the operating modes of an electric vehicle charging station powered by a grid-connected solar PV system (Jain and Bhullar 2024). Nandini et al used hybrid optimization approach to study power quality and grid dependency in electric vehicle charging station with photovoltaic system (Nandini et al. 2023). Ulah et al. worked on the optimal scheduling and techno-economic analysis of a grid-connected charging station powered by a PV system (Ullah et al. 2023). Topuz et al. investigated the design parameters of the photovoltaic system and modelled it in computer environment (Topuz et al. 2017).

There are several studies in the literature outlining methods that attempt the control, optimization, and analysis of a PV power system with an EV charging station. Muhammed et al. presented an optimization algorithm for an EV charging station with a PV power system (Mohamed et al. 2020). Islam et al. proposed a new correlated probabilistic model for EV charge loads in coordination with a PV system (Islam et al. 2021). Fadaee and Radzi investigated optimization

methods for a off-grid hybrid renewable energy system with evolutionary methods (Fadee and Radzi 2012). Engin examined the suitability of a wind turbine and PV hybrid system. The system was designed in the HOMER. As a result of the analyses made by introducing the wind speed, solar radiation values and temperature values of the selected region to the program, it was stated that the PV-wind system is unsuitable for energy production (Engin 2010). Veliz et al. developed a new model for optimal programming of PV assisted charging stations (Veliz et al. 2022). Engelhardt et al. proposed an energy management system for interfacing power converters (Engelhardt 2022). Chang et al. Evaluated the performance of rooftop PV and EVs for different building types in Seoul, Korea (Chang et al. 2022). Wali et al. investigated the techno-economic evaluation of an off-grid hybrid system in a rural community in Bangladesh (Wali et al. 2023). Shad Abid et al. undertook a techno-economic and environmental assessment of electric vehicle charging stations powered by renewable energy sources (Shadman Abid et al. 2024). Lee et al. conducted a techno-economic assessment of hybrid PV/wind-powered EV charging stations with integrated hydrogen production in Kentucky (Lee et al. 2024). Karthikeyan and Thomas studied optimisation strategies for EV charging and routing (Karthikeyan and Thomas 2024).

This research aims to perform an analysis of a hybrid electric vehicle charging station for shopping mall in Edirne, Turkey. The contribution of this paper is to present a comprehensive hybrid electric vehicle charging station model for shopping malls that will reduce the possible interference between the electric grid and EVs and CO₂ emissions. A solar and wind energy hybrid system has been investigated to provide electricity to electric vehicle charging stations in a shopping centre independent from the main electricity grid in Turkey. The renewable energy powered hybrid electric vehicle charging station for shopping mall is engineering solutions that can be applied universally.

In this study, a techno-economic analysis has been made on the support of the EV charging station in a shopping mall located in Edirne, Turkey with renewable energy sources. The designed hybrid charging station consists of PV – Wind Turbine components. In the hybrid system where wind energy is used, a horizontal axis air guided wind turbine is selected. The selected horizontal axis wind turbine is suitable for high building roof applications. Since shopping malls are in residential areas, the use of horizontal axis turbines with the same power will have disadvantages

and application difficulties. With the increase in the number of visitors in shopping mall, especially in the tourism season, the number of charged vehicles increases. In this case, the fact that the charging station is supported by renewable energy prevents possible overloading of components, phase and voltage imbalance in the energy grid, and greenhouse gas emissions. In the analyses made, the status of the hybrid charging station being connected to the grid and being independent from the grid was also examined. The hybrid charging station has been conducted by employing HOMER software. The optimal system types, power generation, cash flows, sensitivity analysis and operating conditions have been discussed. This article aims to optimize an electric vehicle charging station powered by renewable energy sources for a shopping mall and provide a general guideline for future studies. The main purpose of the article is to provide useful information for electric vehicle charging station power supply design.

2. Material and Methods

2.1. Simulation Tool Description

Homer Pro is used for power generation systems analysis and optimization. HOMER allows the modeler to provide a method for finding and comparing several different design options, considering the technical and economic characteristics of the system components. It performs the lowest cost system analysis based on energy source data and a specific load size (www.homerenergy.org/ chapter3_HOMERMODELING).

2.2. Site Description

The case study under review represents a typical example of Turkey's shopping mall buildings. The land area is 20.500 m² and the total construction area is 96.000 m². It has been accepted that the shopping mall operates 12 hours a day, the working hours range is 10.00-22.00 and the average number of people is 5500. In the design, a rather wide gallery is left in the middle of the main mass, which is placed in a linear manner. The gallery space is shaped to provide maximum visual connection between the floors by continuing across 4 floors. Above the gallery, a roof structure made of steel and glass was designed on the roof. There is an area of 5.000 m² on the roof for system installation. The shopping mall building's height is 20 m, and the building roof is suitable for vertical axis wind turbine installation. Figure 5 shows the shopping mall building. Table 1 summarises the shopping mall building's location and heating characteristics in Edirne.

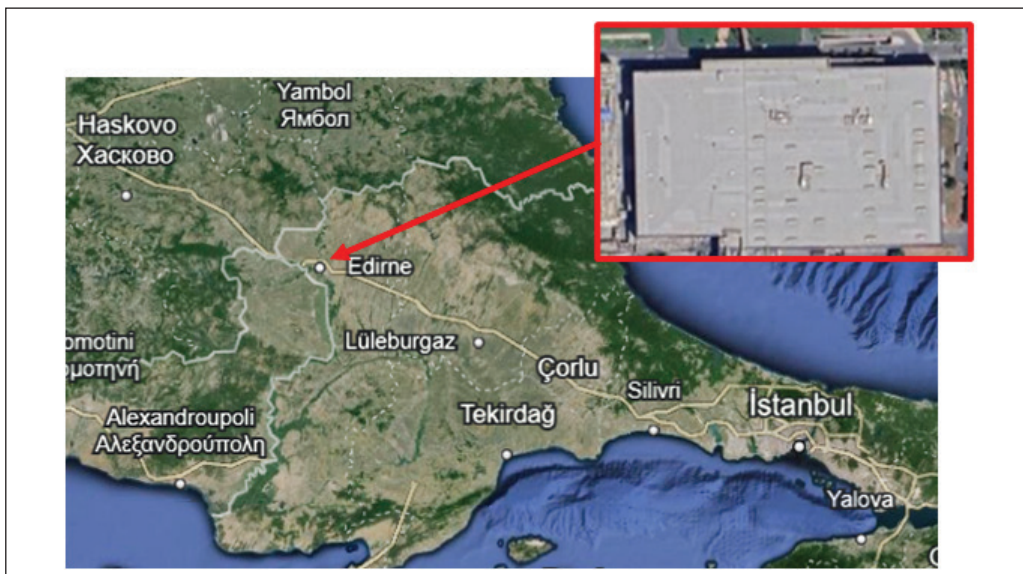


Figure 5. Shopping mall building.

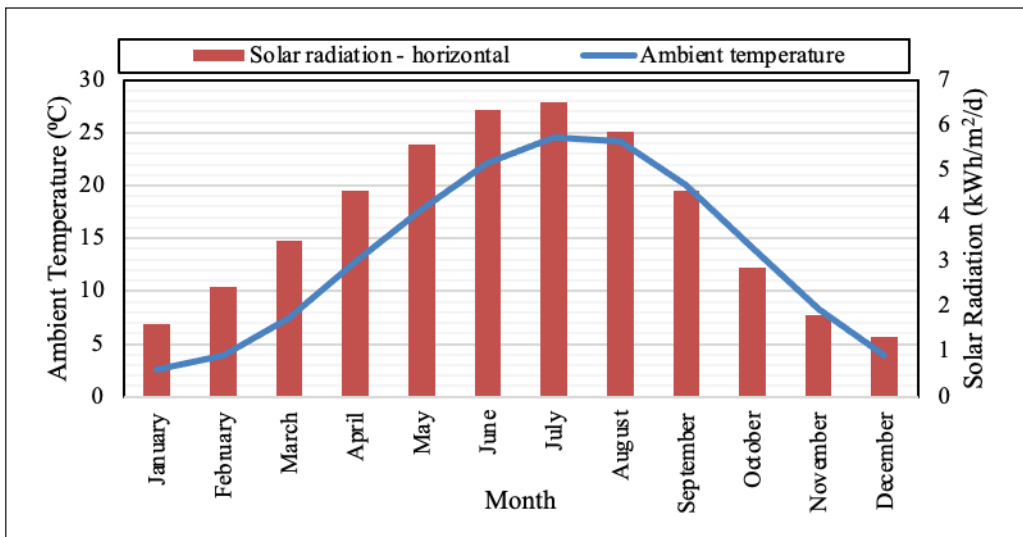


Figure 6. Monthly average ambient temperature and solar radiation in Edirne, Turkey (www.RETScreen-NRCan).

Table 1. Shopping mall location's climate data (www.RETScreen-NRCan).

Parameter	Unit	Edirne
Latitude	°N	41.7
Longitude	°E	26.6
Elevation	m	51
Earth temperature amplitude	°C	21.8
Average annual air temperature	°C	13.5
Annual relative humidity	%	69.5
Annual average of horizontal solar radiation	kWh/m²/d	3.91
Annual atmospheric pressure	kPa	99.3
Annual average of wind speed	m/s	1.9

- Solar energy potential

A detailed analysis of the solar source, meteorological, geographic data and PV power potential helps to identify the most suitable locations for a full understanding of the climate of a region and the installation of solar power plants (www.solargis.com/products/regional-solar-study). The monthly average ambient temperature and solar radiation of the shopping mall location in Edirne are seen Figure 6.

- Wind energy potential

The monthly average wind speed in Edirne is seen Figure 7. The wind speed ($V_{(Hr)}$) measured at a height of 10 meters is taken as reference (www.RETScreen-NRCan). The hub height of the wind turbines discussed in this study is 20 m.

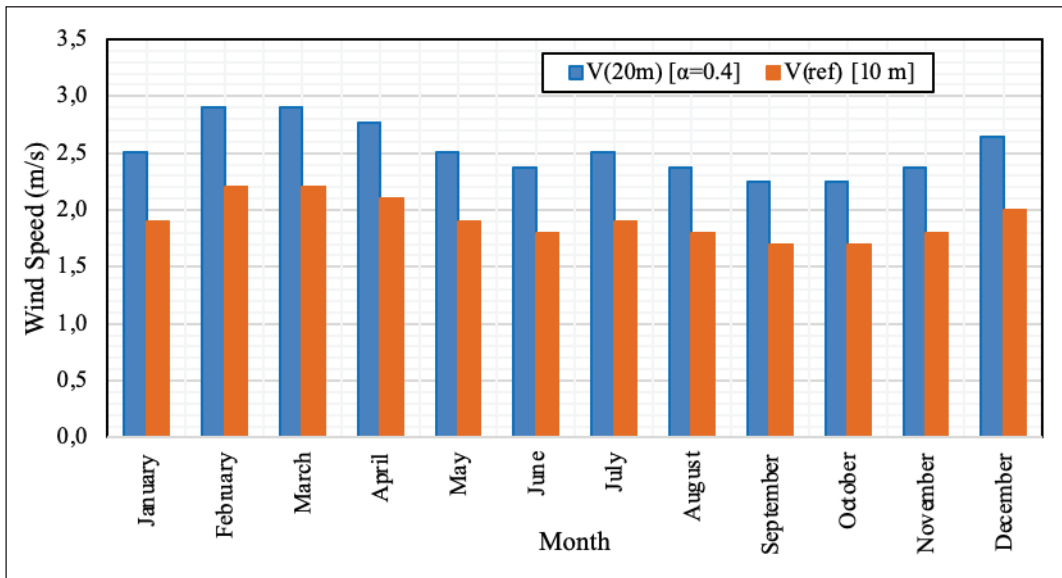


Figure 7. Monthly average wind speed in for 10 m and 20 m in Edirne.

The wind power profile law is used to find the value at the desired height by using the wind data measured at a certain height (Patel 2006). The following equation is calculated using the wind speed power law for different heights.

$$\frac{V_{(H)}}{V_{(H_r)}} = \left(\frac{H}{H_r}\right)^\alpha \quad (1)$$

In the Equation 1, $V_{(H_r)}$ is the measured wind speed, $V_{(H)}$ is the wind speed to be determined, the height at which $V_{(H_r)}$ is measured is $H(r)$, the height at which $V_{(H)}$ is to be determined is H , α is the Hellmann coefficient and the wind speed is the measurement location. depends on its features. Figure 10 shows the monthly average wind speed for 10 m and 20 m in Edirne. When calculating the wind speed at 20 m, the Hellmann coefficient was taken as 0.4, considering the characteristics of the region where the installation was made.

The turbine power curve of this function was found by using the wind energy potential analysis, Weibull probability density function for Edirne. With the help of wind speed averages, the wind energy potential of the site can be found (Manwell et al. 2009). Weibull distribution function can be represented as:

$$f(v) = \left(\frac{k}{c}\right)\left(\frac{v}{c}\right)^{k-1} \exp\left(-\left(\frac{v}{c}\right)^k\right) \quad (2)$$

where $P(v)$ is the probability density function, k is the shape factor, c is the scale parameter, v is the wind speed. The shape parameter is calculated with the following equation.

$$k = \left[\frac{\sum_{i=1}^n v_i^k \ln(v_i)}{\sum_{i=1}^n v_i^k} - \frac{\sum_{i=1}^n \ln(v_i)}{n} \right]^{-1} \quad (3)$$

$$k = \left(\frac{\sigma}{V_{ort}} \right)^{-1.086} \quad (4)$$

where σ is the standard deviation. Weibull scale parameter can be expressed as follows:

$$C = \frac{V_{ort}}{\Gamma\left(1 + \frac{1}{k}\right)} \quad (5)$$

where Γ represents a gamma function, which can be represented as:

$$\Gamma(X) = \int_0^\infty e^{-t} t^{x-1} dt \quad (6)$$

The above equation can be expanded as:

$$\Gamma(x) = (\sqrt{2\pi x})(x^{x-1})(e^{-x}) \left(1 + \frac{1}{12x} + \frac{1}{288x^2} - \frac{139}{51840x^3} + \dots\right) \quad (7)$$

In energy potential analysis with Weibull distribution, Weibull probability density function was calculated with the help of average wind speeds. In Figure 8, the probability density function based on annual average wind speeds for Edirne is plotted. The shape parameter (k) for Edirne is taken as 1.5.

Based on the Weibull distribution, the wind speed with the greatest frequency is calculated with the following equation.

$$v_{mod} = c \left(1 - \frac{1}{k}\right)^{1/k} \quad (8)$$

Deaves and Lines also determined the maximum wind speed with Equation 9 (Deaves and Lines 1997).

$$v_{max} = c \left(\frac{k+2}{k}\right)^{1/k} \quad (9)$$

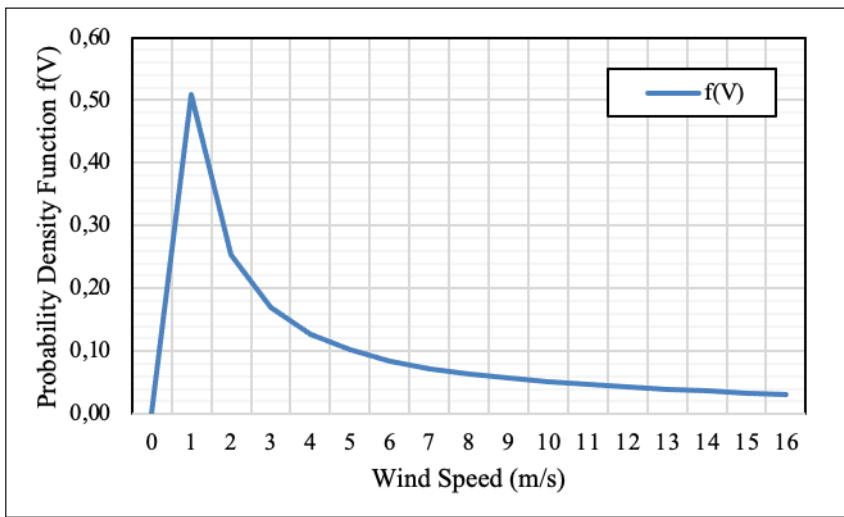


Figure 8. Probability density function $f(V)$ based on annual average wind speeds for Edirne.

Table 2. Weibull parameters, speed, and power estimates for all months for Edirne.

	$V_{(20m)}$ (m/s)	k	c (m/s)	$f(V)$	$V(\text{mod})$ (m/s)	V_{\max} (m/s)	P_w (W/m ²)
January	2.5071	1.5	3.342753	0.202971	1.607028	5.880607	45.44
February	2.9029	1.5	3.870557	0.175294	1.86077	6.809124	70.54
March	2.9029	1.5	3.870557	0.175294	1.86077	6.809124	70.54
April	2.7710	1.5	3.694622	0.183641	1.776189	6.499619	61.35
May	2.5071	1.5	3.342753	0.202971	1.607028	5.880607	45.44
June	2.3751	1.5	3.166819	0.214248	1.522448	5.571102	38.64
July	2.5071	1.5	3.342753	0.202971	1.607028	5.880607	45.44
August	2.3751	1.5	3.166819	0.214248	1.522448	5.571102	38.64
September	2.2432	1.5	2.990885	0.22685	1.437867	5.261596	32.55
October	2.2432	1.5	2.990885	0.22685	1.437867	5.261596	32.55
November	2.3751	1.5	3.166819	0.214248	1.522448	5.571102	38.64
December	2.6390	1.5	3.518688	0.192823	1.691609	6.190113	53.00

Considering that the wind turbine power shaft is a rotating machine with the exchange of momentum of the air mass particles flowing through the blade swept area, the wind power in the swept area is proportional to the size of this area, the density of the air and the cube of its speed. Accordingly, the power that can be obtained from the wind can be written as (Simmons 1975):

$$P = \frac{1}{2} \rho A v^3 \quad (10)$$

Where, P is the power output of the wind turbine as a function of wind speed. However, it should be noted that with the Equation 10, power is estimated for wind speeds lower than 15 m/s (Deaves and Lines 1997).

Considering the density of air at sea level at 15.6 °C and 1

atmosphere pressure as $\rho_0 = 1.225 \text{ kg/m}^3$ and height above sea level (H_m) as 71 m, the corrected air density (1.2165226 kg/m^3) for other location information is found as follows (Patel 1999):

$$\rho = \rho_0 - 0.0001194 H_m \quad (11)$$

where, A (m²) is the swept area, ρ (kg/m³) is the air density calculated depending on the location, pressure, and temperature of the region. Average power density (P_w) for the Weibull distribution can be expressed as:

$$P_w = \frac{1}{2} \rho c^3 \Gamma \left(1 + \frac{3}{k} \right) \quad (12)$$

Table 2 shows the Weibull parameters, speed, and power estimates of the wind turbines for all months. The Weibull power density is shown in Figure 9.

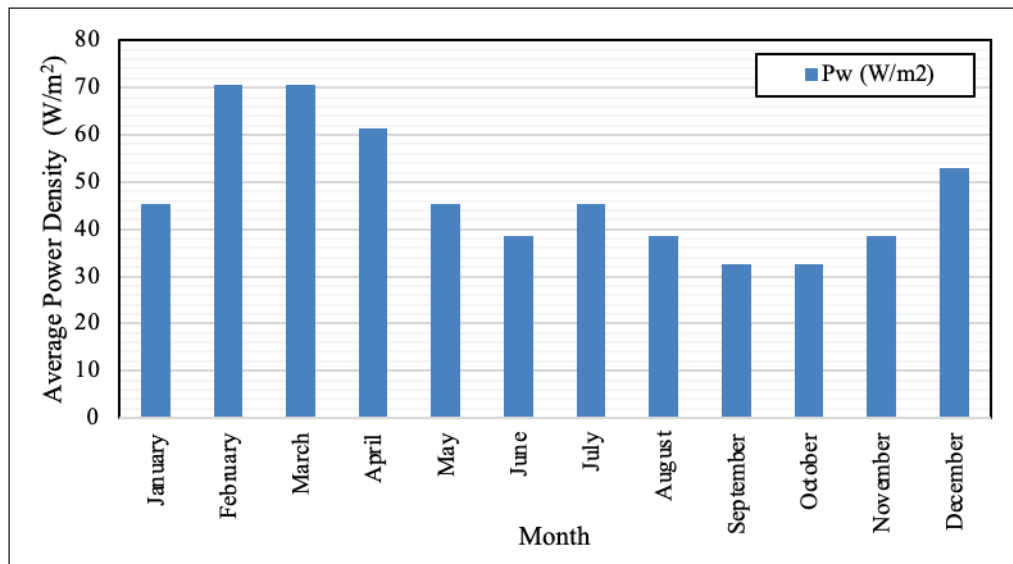


Figure 9. Average monthly Weibull power density for Edirne.

Table 3. EV Charging stations technical specifications.

Technical Specifications	
Type	EVC04-AC22 (Type 2)
Power	22 kW max AC
Voltage	400 V AC, 50/60 Hz, 3-Phase
Current	3x32 A
Power level control	10-13-16-20-25-30-32 A
Socket type	IEC 62196 Type 2 EU
Protection	DC 6mA RCD function
Material	PC plastic, 5VA Flame retardant
Dimensions	460x315x135
IP rating	IP 54
IK rating	IK08

There are 2 electric vehicle charging stations in the shopping mall. Table 3 shows the technical specifications of the electric vehicle charging station. Two charging stations consume an average of 3500 kWh and 4000 kWh of energy per month. On weekends, when tourism increases, there is a daily energy consumption of 190-210 kWh (shopping mall technical office manager's report).

2.3. The Developed Interface

- Electrical load

The number of vehicles charged at the charging stations in shopping malls is proportional to the number of visitors, especially during the tourism season. While making the technical and economic evaluation of a hybrid charging

station for shopping mall by using HOMER software, the average monthly energy consumption of the charging station in the shopping mall and the tourism statistics data (data.tuik.gov.tr) for the province of Edirne are ., and total electrical load of the charging station is predicted as shown in Figure 10. Two charging stations consume an average of 3500 kWh and 4000 kWh of energy per month.

- PV module

PV panels are monocrystalline type. PV panels' lifetime is 25 years. The capital cost is 900 \$/kW, the replacement cost is 900 \$/kW and the maintenance cost is 1.55 \$/kW/year (yenitrakyaenerji.com). The technical properties of monocrystalline PV module are shown at Table 4.

- Wind turbine

Table 5 shows the technical properties of two wind turbines selected for system analysis. The lifetime for wind turbines was 15 years. The wind turbines' capital cost is \$1,600 per kW, the replacement cost is \$1,600 per kW and the operational and maintenance cost is \$30 per kW (hi-techsolution.eu).

The wind turbines system can be combined with solar PV modules and function as a hybrid system. Vertical axis wind turbine has 11 moving blades and 11 wind booster driving blades. The wind booster driving blades increase the wind speed reaching the moving blades approximately 2.5 times (Moreno et al. 2021).

The wind turbine capacity factor CF is calculated as follows (Li and Priddy 1985):

$$CF = \left(\frac{E_c}{WTC h_y} \right) 100 \quad (13)$$

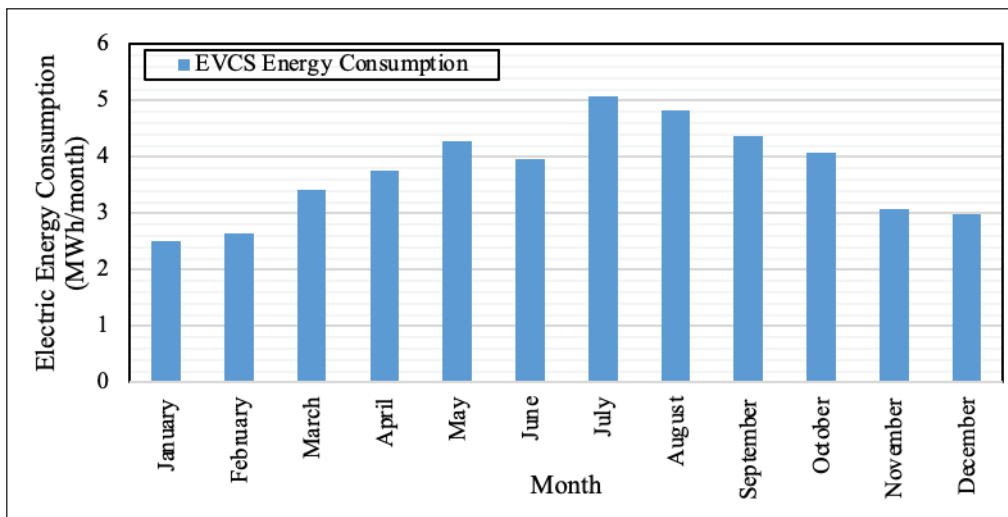


Figure 10. Total EVCS electrical load used in Homer software's analysis.

Table 4. Technical properties of PV module (www.anerngroup.com).

Properties	
Power	400W
Voltage (Maximum Power)	41.70 V
Current (Maximum Power)	9.60 A
Voltage (Open Circuit)	49.80 V
Current (Short Circuit)	10.36 A
PV module efficiency	20.14 %
Number of cells	72
Cell type	Monocrystalline
Power rating	0 W / 5 W
Working range	-40°C ~ +85°C
Dimensions	1989 x 1005 x 40 mm
Area	2 m ²
Warranty	25 Years
Weight	20,0 kg
Front surface	Low iron tempered glass
Certificate	IP67

where E_C is the renewable energy collected, expressed in kWh, WTC is the wind turbine capacity, expressed in kW, and b_y is the number of hours in a year. Figure 11 shows the wind turbine power curve and energy curve.

-Storage battery

The capacity of the Li-ion battery chosen for electricity storage is 100 kWh, its nominal capacity is 167 Ampere-hour (Ah), and its efficiency is 90%. The battery's capital

Table 5. Technical properties of wind turbine (<https://hi-techsolution.eu/products>).

Properties	
Power	10.5 kW
Nominal Power	12 kW
Voltage	AC, 110/220 V, Three phase
Blades	22 (11 driving blades + 11 moving blades)
Startup wind speed	2,5 m/s
Dimensions	D:350cm, H:450 cm
Swept area	15.75 m ²
Noise levels	<40 dB
Wind turbine type	Vertical axis
Generator type	Tree-Phase Permanent Magnet
Lifetime	15 Years
Weight	435 kg
Certificate	IP54

cost per quantity was \$15,000, the replacement cost was \$15,000, and the operating and maintenance cost was \$1,000 per battery per year.

-Converter

The selected converter has a capacity of 150 kW, a life of 25 years and an efficiency of 95%. The capital cost of the converter is \$300 per kW, the replacement cost is \$300 per kW, and the operating and maintenance cost is \$5 per kW.

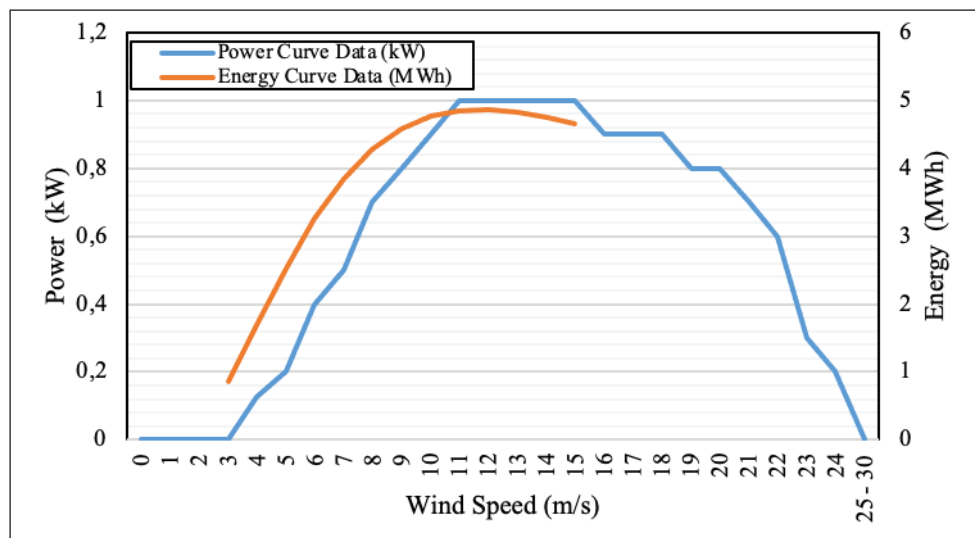


Figure 11. Wind turbine power curve and energy curve.

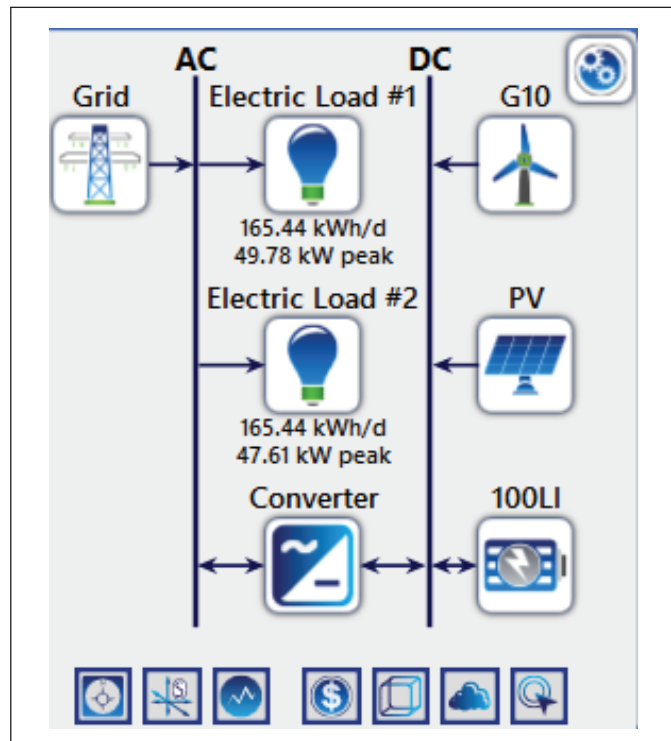


Figure 12. Hybrid system configuration for EV charge station in Homer.

Table 6. Hybrid system optimization inputs in HOMER analysis.

Components	Optimization inputs
PV size (kW)	0 – 10 – 20 – 30 – 40 – 50
WT size (kW)	0 – 10 – 20 – 30 – 40 – 50
Converter capacity (kW)	0 – 7.2 – 14.4 – 21.6 – 28.8 – 36.0 – 43.2 – 50.4 – 57.6 – 64.8 – 72.0
Battery strings	0 – 3 – 6 – 9 – 12 – 15 – 18 – 21 – 24 – 27 – 30
Grid (kW)	999,999

-Grid

Grid power price is \$0.089 per kWh, grid sellback price is \$0.05 per kWh. Carbon Dioxide emission is 632 g/kWh, Sulphur Dioxide emission is 2.74 g/kWh and Nitrogen Oxides emission is 1.34 g/kWh.

3. Results and Discussion

The Electricity production, economic gain, and emission analysis calculations of the hybrid system with Homer software are included.

Homer hybrid system analysis

After entering the data of the hybrid system elements into the HOMER software, the system diagram was created. Figure 12 shows the hybrid system configuration for EVS station in Homer. Table 6 shows the hybrid system optimization inputs in HOMER analysis. There are two electrical vehicle charging stations with a power of 22 kW in the shopping mall. Two charging stations consume an average of 3500 kWh and 4000 kWh of energy per month. Figure 13 shows the hybrid system's electric load (one EVS station's load) specifications in HOMER simulation.

3.1. Energy Production

Figure 14 shows the daily electricity produced by the PV system and Figure 15 shows the daily electricity produced by the wind turbines in Homer simulation.

3.2. Economic Analysis Results

Table 7 shows the cost of EV charging station components. Table 8 shows the renewable energy powered hybrid system cost summary of HOMER analysis. Figure 16 shows the hybrid system cumulative nominal cash flow. Discount rate

is 10%, inflation rate is 14% and project life is 25 years in the HOMER analysis.

3.3. Optimization Results

In this study, 6,334 solutions were simulated: 6,334 were feasible. 4001 optimization results were obtained with Homer analysis, only 8 of them were presented. Table 9 shows the Homer optimization's hybrid system's architecture results.

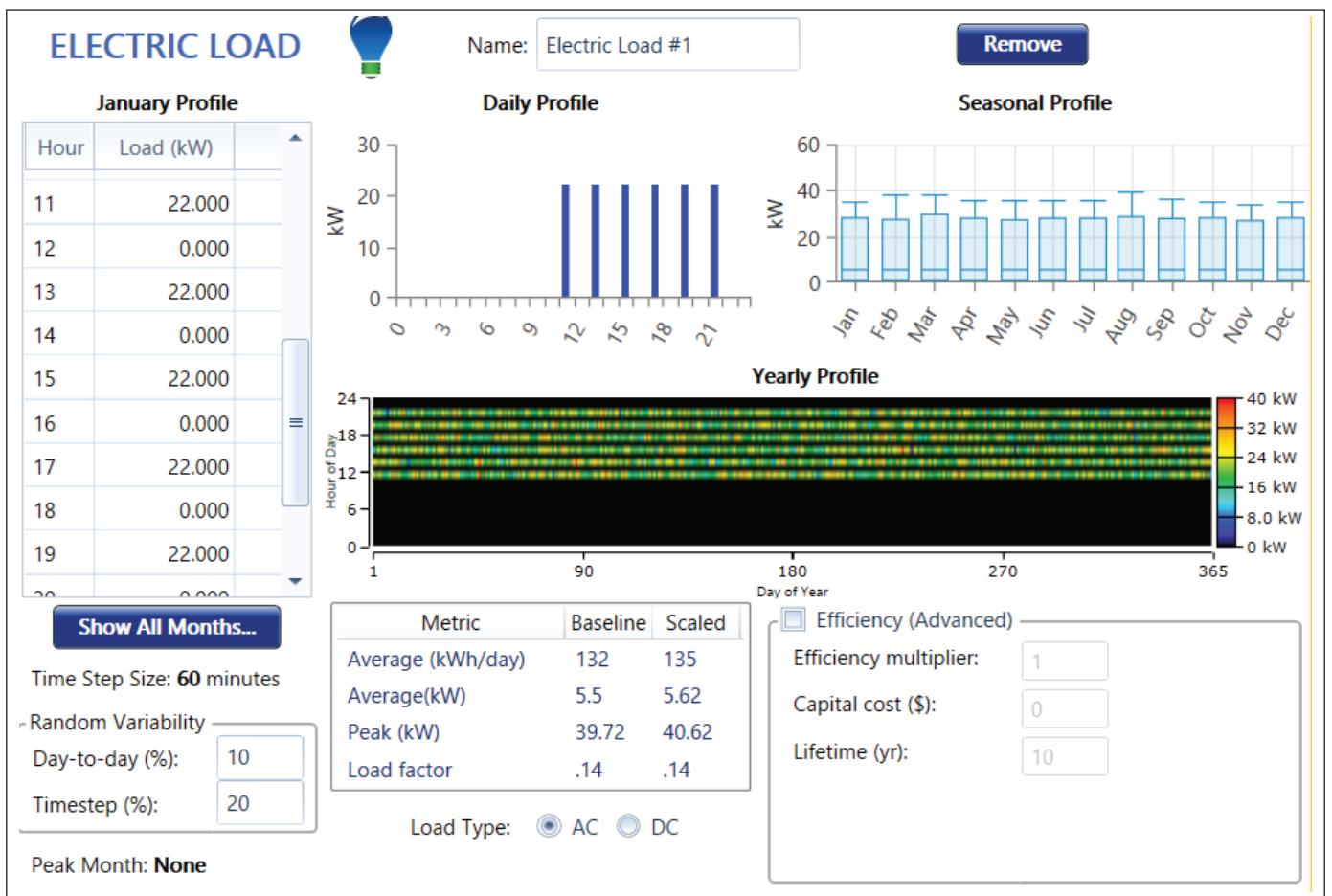


Figure 13. Hybrid system's electric load (one EVS station's load) specifications in HOMER simulation.

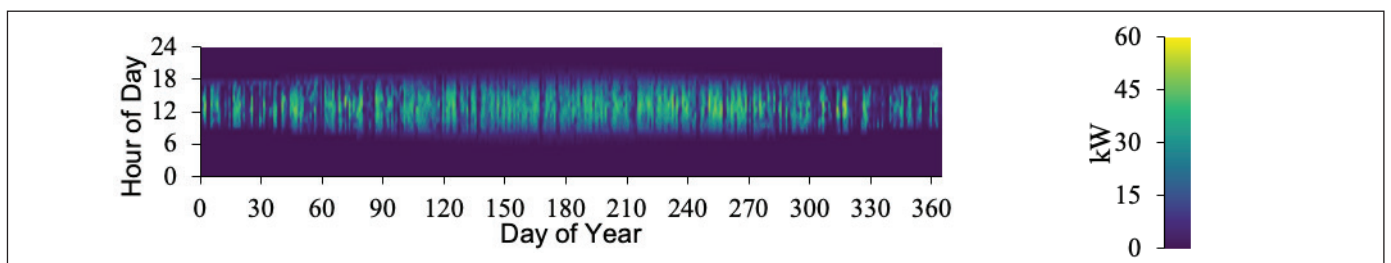


Figure 14. Daily electricity produced by the PV system in Homer simulation.

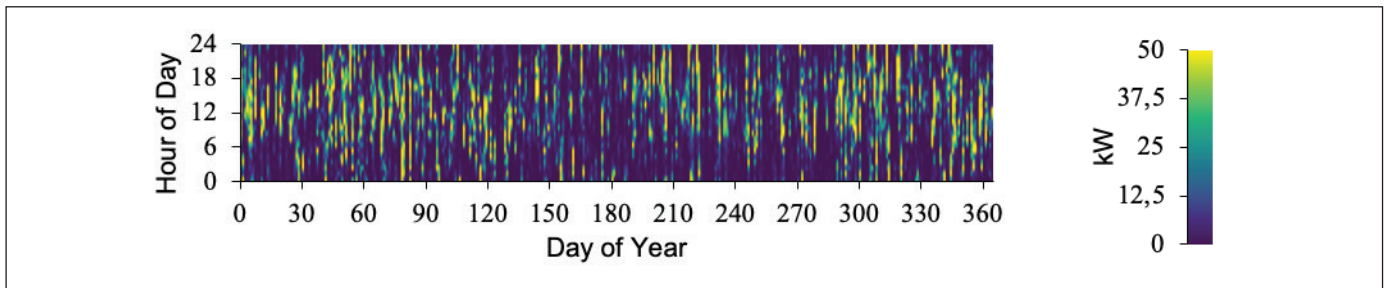


Figure 15. Daily electricity produced by the wind turbines in Homer simulation.

Table 7. The components' cost.

	Capital Cost (\$)	Replacement Cost (\$)	O & M Cost (\$)
Converter (per kW)	300	300	10
Battery (per quantity)	15,000	15,000	1000
Wind Turbine (\$/kW)	1,600	1,600	30
PV Module (\$/kW)	900	900	5

Table 8. Renewable energy powered hybrid system cost summary of HOMER analysis.

Economic Metrics		
IRR		11%
ROI		7.4%
Simple Payback		8.4 yr
Cost Summary		
	Base Case	Lowest Cost System
NPC	\$401,191	\$145,961
Initial Capital	\$0	\$68,638
O&M	\$9,760/yr	\$1,881/yr
LCOE	\$0.0890/kWh	\$0.0193/kWh

PV capacity factor is 14.6%, PV total production is 64,131 kWh/yr, PV hours of operation is 4,386 hrs/yr. Wind turbines' capacity factor is 19.3%, wind turbines total production is 84,391 kWh/yr, wind turbines' hours of operation is 6,122 hrs/yr. Converter capacity factor is 29.5%, converter operation hours are 7,141 hrs/yr and converter energy out is 142,748 kWh/yr. The electricity storage system's nominal capacity is 100 kWh. The annual throughput is 24,657 kWh/yr.

Table 10 shows the Homer optimization's electrical results. The annual energy purchased from the grid and the annual energy sold to the grid for eight cases are seen Table 14.

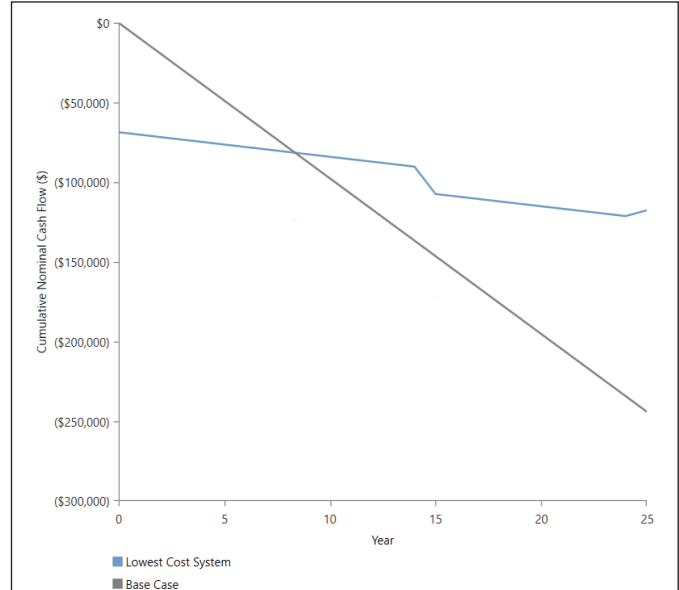


Figure 16. Hybrid system cumulative nominal cash flow.

Figure 17 shows the monthly energy purchased and energy sold for the case 1, 2, 3, 4, 5, 6, 7 and 8.

Table 11 shows the Homer optimization's cost, renewable energy fraction and grid results. Table 12 shows the Homer optimization's economics results.

Figure 18 shows the annual savings of optimization's cases. Figure 19 shows the cumulative cash flow over project lifetime for case 1, 2, 3, 4, 5, 6, 7 and 8.

3.4. Impact Analysis Results

The effects of the proposed application on the environment or other equipment and systems, and the CO₂ emission

reduction due to the savings to be made are given in Table 13. Net annual GHG emission reduction 29.7 tCO₂ is equivalent to 5.4 cars and light trucks not used.

Table 9. Homer optimization results: Hybrid system's architecture.

Case	Architecture										
	PV	WT	B	G	C	PV (kW)	WT (kW)	Battery	Grid (kW)	Converter (kW)	Dispatch
1			-			50	50	-	999,999	52.5	CC
2						50	50	1	999,999	51.0	LF
3	-		-			-	50	-	999,999	43.9	CC
4	-					-	50	1	999,999	40.5	LF
5		-	-			50	-	-	999,999	32.1	CC
6		-				50	-	1	999,999	27.0	LF
7	-	-	-		-	-	-	-	999,999	-	CC
8	-	-				-	-	1	999,999	1.50	LF

Table 10. Homer optimization results: Electrical.

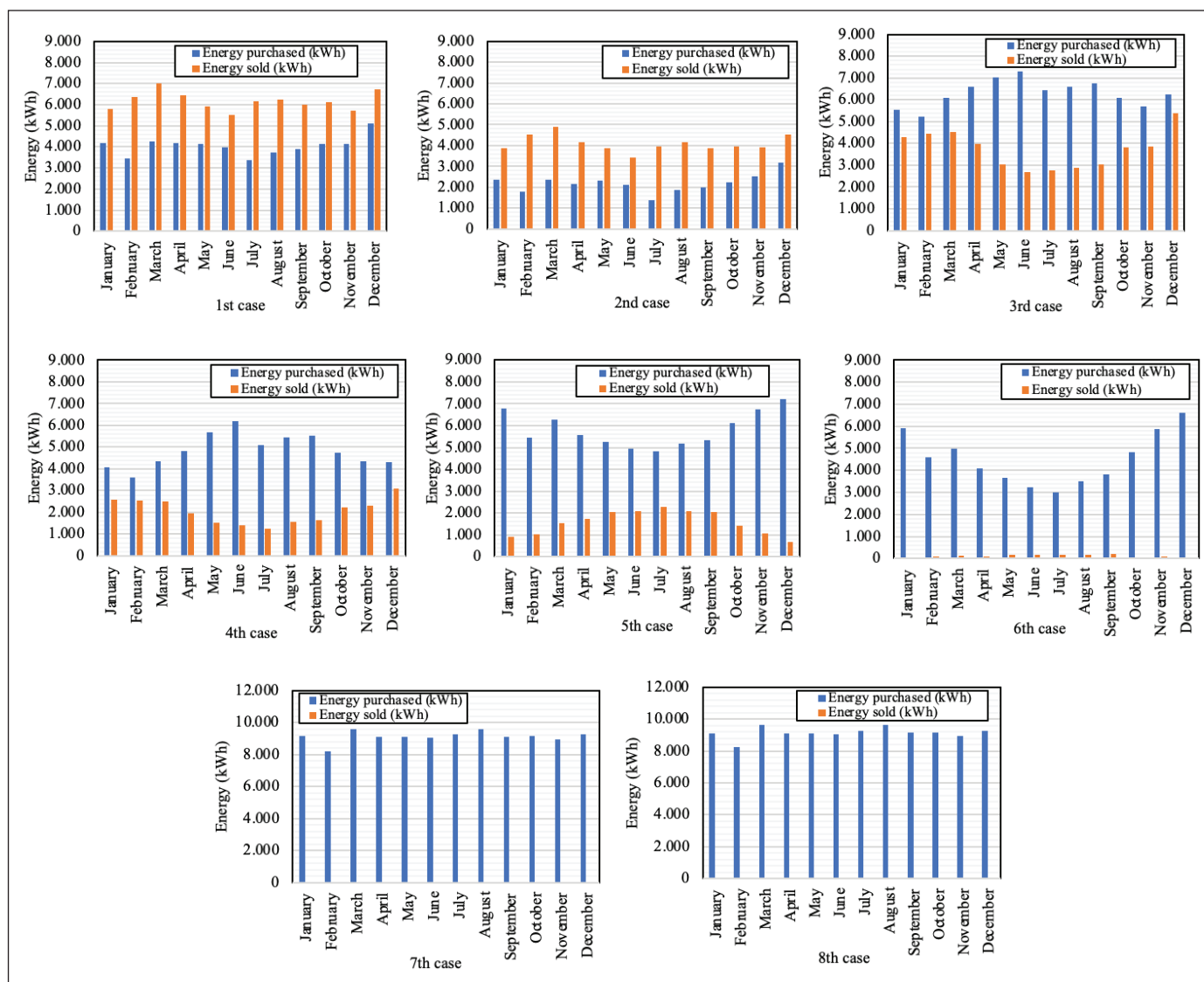
Case	Production (kWh/yr)				Consumption (kWh/yr)		
	PV	WT	Grid purchases	Total	AC load	Grid sales	Total
1	64,131	83,978	48,539	196,648	109,661	74,010	183,671
2	64,131	83,978	26,317	174,426	109,661	49,132	158,793
3	-	83,978	75,599	159,578	109,661	44,684	154,345
4	-	83,978	58,181	142,159	109,661	24,509	134,170
5	64,131	-	69,685	133,816	109,661	18,913	128,574
6	64,131	-	54,115	118,246	109,661	1,421	111,082
7	-	-	109,661	109,661	109,661	-	109,661
8	-	-	109,589	109,589	109,661	-	109,661

Table 11. Homer optimization results: Cost, renewable energy fraction and grid.

Case	Cost				CAPEX Capital Investment (\$)	Renewable Fraction	Grid	
	NPC (\$)	LCOE (\$/kWh)	Operating Cost (\$/yr)	Energy Purchased (kWh)			Energy Sold (kWh)	
1	145,961	0.0193	1,881	68,638	73.6	48,539	74,010	
2	195,107	0.0299	2,720	83,300	83.4	26,317	49,132	
3	241,877	0.0381	5,369	21,163	51.0	75,599	44,684	
4	285,840	0.0518	6,099	35,150	56.6	58,181	24,509	
5	302,786	0.0573	6,037	54,631	56.9	69,685	18,913	
6	346,307	0.0758	6,768	68,100	45.8	54,115	1,421	
7	401,191	0.0890	9,760	0.00	0	109,661	0	
8	471,923	0.1050	11,105	15,450	0.0657	109,589	0	

Table 12.Homer optimization results: Compare economics.

Case	Net Present Value (\$)	Annual worth (\$/yr)	Return of investment (%)	Internal rate of return (%)	Simple payback (yr)	Discounted payback (yr)
1	255,230	6,209	7.4	10.5	8.35	7.19
2	226,085	5,013	4.3	6.8	10.46	8.75
3	159,314	3,876	16.4	21.2	4.52	4.12
4	115,352	2,806	6.0	9.1	8.27	7.13
5	98,405	2,394	2.7	8.9	8.39	7.22
6	54,884	1,335	0.2	0.4	24.65	20.50
7	-	-	-	-	-	-
8	70,732	1,721	-13.2	-	-	-

**Figure 17.** Monthly energy purchased, and energy sold for the case 1, 2, 3, 4, 5, 6, 7 and 8.

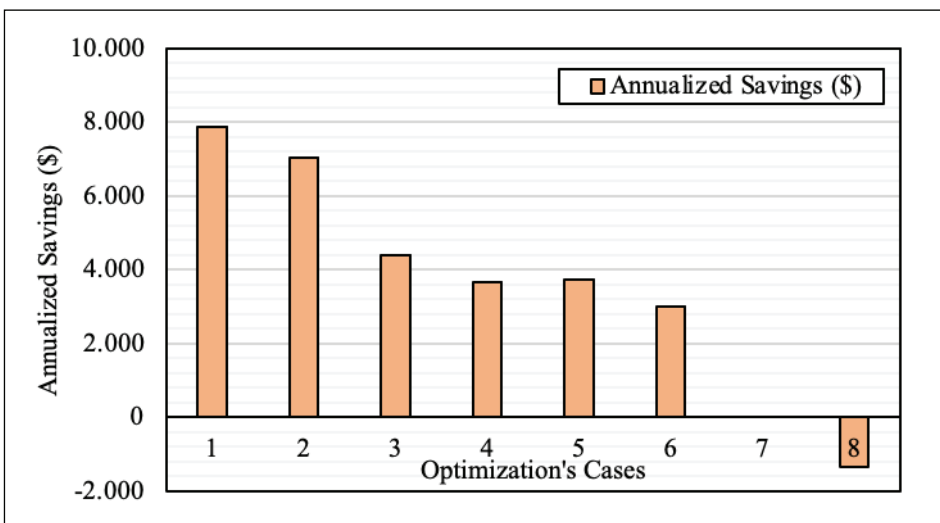


Figure 18. Annual savings of optimization's cases.

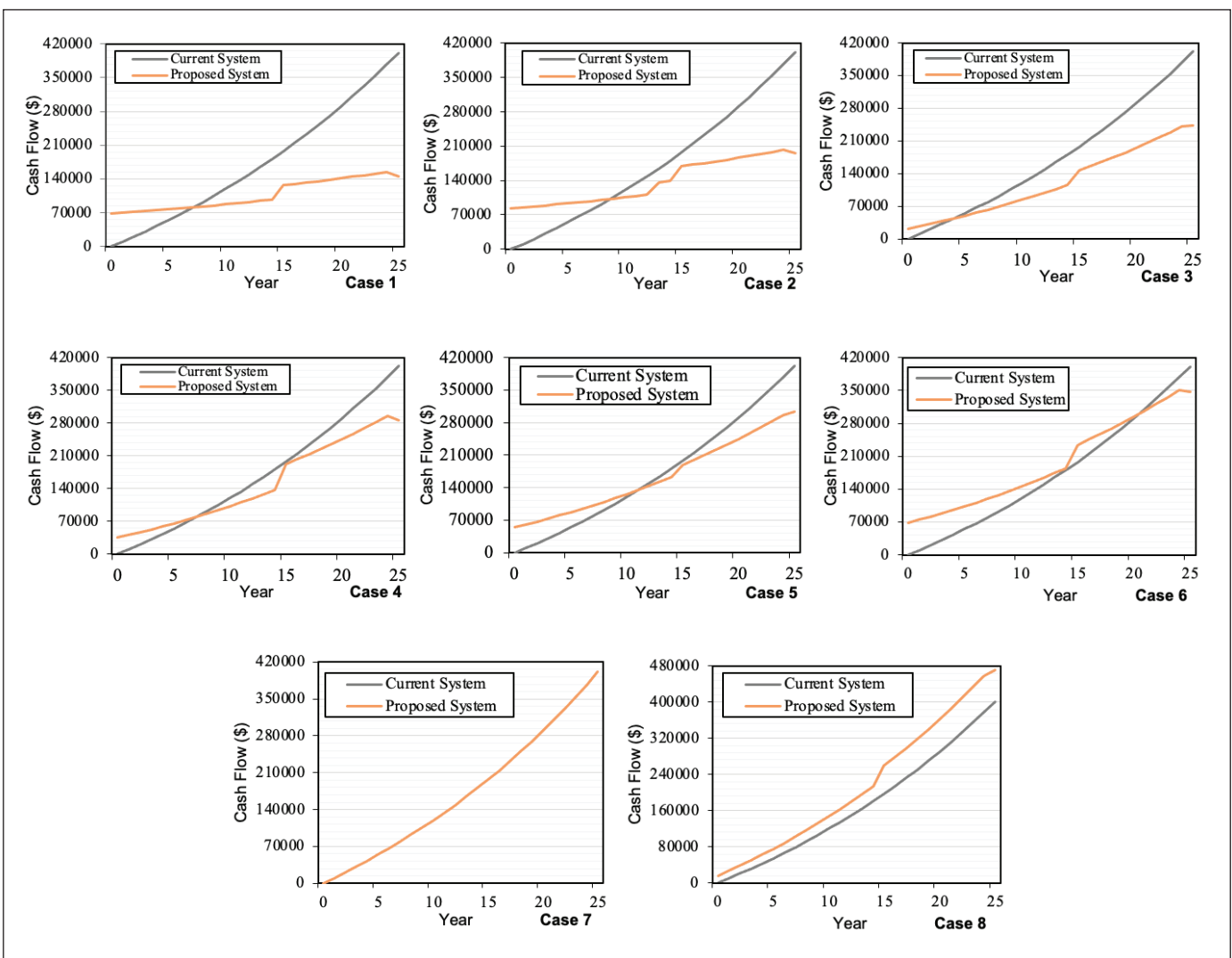


Figure 19. Cumulative cash flow over project lifetime for case 1, 2, 3, 4, 5, 6, 7 and 8.

Table 13. Impact analysis of the PV system.

Emission Analysis		
Country - region	-	Turkey
GHG emission factor	tCO ₂ /MWh	0.460
Produced electricity	MWh	64,513
Net annual GHG emission reduction	tCO ₂	29.7

The effects of the proposed application on the environment or other equipment and systems, and the CO₂ emission reduction due to the savings to be made are given in Table 14. Net annual GHG emission reduction 38.2 tCO₂ is equivalent to 7 cars and light trucks not used.

Table 14. Impact analysis of the wind turbines.

Emission Analysis		
Country - region	-	Turkey
GHG emission factor	tCO ₂ /MWh	0.4596
Produced Electricity	MWh	83,145
Net annual GHG emission reduction	tCO ₂	38.2

The effects of the proposed application on the environment and the Homer optimization's emissions results for cases are shown in Table 15.

Table 15. Homer optimization results: Emissions.

Case	Carbon Dioxide (kg/yr)	Sulphur Dioxide (kg/yr)	Nitrogen Oxides (kg/yr)
1	30,677	133	65
2	16,632	72.1	35.3
3	47,779	207	101
4	36,770	159	78.0
5	44,041	191	93.4
6	34,201	148	72.5
7	69,306	300	147
8	69,260	300	147

4. Conclusion and Suggestions

As a result of generating electricity with renewable energy in the shopping mall, greenhouse gas emissions will decrease, and the effects of global warming caused by carbon emissions will decrease. At this point, it becomes important that the charging stations in shopping malls work with renewable

energy support. However, the fact that many electric vehicles are charged at the same time or in unpredictable time periods causes huge differences in electricity supply and demand. This situation causes voltage imbalance and power losses in the network with the effect of charging stations fed to the grid and may adversely affect the energy grid. At this stage, the importance of a battery hybrid EV charging stations working with renewable energy sources is increasing day by day.

This research investigates the techno-economic feasibility of a renewable energy powered hybrid electric vehicle charging station for shopping mall by using HOMER software. The contribution of this paper is to present a comprehensive hybrid electric vehicle charging station model for shopping malls that will reduce the possible interference between the electric grid and EVs and CO₂ emissions. The results indicate that the optimal wind-PV hybrid system for the EVS station contains the wind turbines with rated power of 50 kW, PV system of 50 kW, and 52.1 kW power converters. This wind-PV hybris system is found to have the net present cost NPC of \$145,961, an annual operating cost OC of \$1,881/year, a total net present cost NPC of \$145,961 and the leveled cost of energy LCOE of \$0.0193/kWh.

The following is the study's main conclusion:

- By installing a renewable energy system with a capacity of 100 kW on the roof of the shopping mall in Edirne, Turkey. 148.52 MWh/yr electrical energy can be produced annually.
- PV capacity factor is 14.6%, PV total production is 64,131 kWh/yr, PV hours of operation is 4,386 hrs/yr.
- Wind turbines' capacity factor is 19.3%, wind turbines total production is 84,391 kWh/yr, wind turbines' hours of operation is 6,122 hrs/yr.
- Converter capacity factor is 29.5%, converter operation hours are 7,141 hrs/yr and converter energy out is 142,748 kWh/yr.
- The electricity storage system's nominal capacity is 100 kWh. The annual throughput is 24,657 kWh/yr.
- Thus, the electricity needs of the electric vehicle charging station will be produced using renewable energy sources and the emission of 67.9 tCO₂ to the atmosphere will be prevented. Net annual GHG emission reduction 67.9 tCO₂ is equivalent to 12.4 cars and light trucks not used.

- The payback period of the renewable energy powered hybrid electric vehicle charging station for shopping mall is 8.35 years.
- The annualized saving of the hybrid system is \$7,879/yr and the capital investment is \$68,638.

The hybrid system is engineering solutions that can be applied universally. This study provides methodology to improve energy efficiency not only for electric vehicle charging station in Turkey but also for the other electric vehicle charging station in shopping mall worldwide. Although the hybrid system has been studied for a case study in Edirne, the analysis can be applied anywhere in the world by modifying solar and wind energy data.

5. Acknowledgment

No conflict of interest is declared by the authors. There are no individuals or organizations supporting the research.

Author contribution:

Hacer Akhan: Planned, designed, gathered and analyzed data about the study, wrote the article by analyzing the study.

Ethics committee approval: There is no need for ethics committee approval.

6. References

- Agustin, JLB., Lopez, RD. 2009.** Simulation and Optimization of Independent Hybrid Renewable Energy Systems. *Renewable and Sustainable Energy Reviews*, 13: 2111-2118. <https://doi.org/10.1016/j.rser.2009.01.010>
- Bansal, S., Zong, Y., You, S., Popa, LM., Xiao, J. 2020.** Technical and Economic Analysis of One-Stop Charging Stations for Battery and Fuel Cell EV with Renewable Energy Sources. *Energies*, 13: 2855. doi:10.3390/en13112855
- Bass, R., Harley, R., Lambert, F., Rajasekaran, V., Pierce, J. 2001.** Residential harmonic loads and EV charging. In: Proceedings of the 2001 IEEE Power Engineering Society Winter Meeting, 3: 803-808. doi:10.1109/PESW.2001.916965
- Calise, F., Fabozzi, S., Vanoli, L., Vicedomini, M. 2021.** A sustainable mobility strategy based on electric vehicles and photovoltaic panels for shopping malls. *Sustainable Cities and Society*, 70: 102891. <https://doi.org/10.1016/j.scs.2021.102891>
- Chang, S., Cho, J., Heo, J., Kang, J., Kobashi, T. 2022.** Energy infrastructure transitions with PV and EV combined systems using techno-economic analyses for decarbonization in cities. *Applied Energy*, 319: 119254. <https://doi.org/10.1016/j.apenergy.2022.119254>
- Cicek, A., Erdinc, O. 2019.** PV-Batarya Hibrit Sistemi İçeren Elektrikli Araç Otoparkının Şarj Yönetimi. *Avrupa Bilim ve Teknoloji Dergisi*, (15): 466-474. <https://doi.org/10.31590/ejosat.527350>
- Das, BK., Hoque N., Mandal, S., Pal, TK., Raihan, MA. 2017.** A techno-economic feasibility of a stand-alone hybrid power generation for remote area application in Bangladesh. *Energy*, 134: 775-788. <https://doi.org/10.1016/j.energy.2017.06.024>
- Deaves, DM., Lines, IG. 1997.** On the Fitting of Low Mean Wind Speed Data to the Weibull Distribution. *Journal of wind engineering and industrial*, 66: 169-78.
- Ekren, O., Canbaz, CH., Guvel, CB. 2021.** Sizing of a solar-wind hybrid electric vehicle charging station by using HOMER software. *Journal of Cleaner Production*, 279: 123615. DOI:10.1016/j.jclepro.2020.123615
- Engin, M. 2010.** Solar-Wind Hybrid Energy Generation System Design for Bornova, Celal Bayar University Soma Vocational School. *Journal of Technical Sciences*, 2(13): 11-20.
- Engelhardt, J., Zepter, JM., Gabderakhmanova, T., Marinelli, M. 2022.** Energy management of a multi-battery system for renewable-based high power EV charging. *Transportation*, 14: 100198. DOI:10.48550/arXiv.2112.00351
- Fadee, M., Radzi, MA. 2012.** Multi-objective optimization of a stand-alone hybrid renewable energy system by using evolutionary algorithms: A review. *Renewable and Sustainable Energy Reviews*, 16: 3364-3369. <https://doi.org/10.1016/j.rser.2012.02.071>
- Geth, F., Leemput, N., Van Roy, J., Buscher, J., Ponnette, R., Driesen, J. 2012.** Voltage droop charging of electric vehicles in a residential distribution feeder. In: *Proceedings of the 3rd IEEE PES Innovative Smart Grid Technologies Europe (ISGT Europe)*, 1-8. doi:10.1109/ISGTEurope.2012.6465692
- Hiendro, A., Kurnianto, R., Rajagukguk, M., Simanjuntak, YM., Junaidi. 2013.** Techno-economic analysis of photovoltaic/wind hybrid system for onshore/remote area in Indonesia. *Energy*, Elsevier, 59(C): 652-657. DOI: 10.1016/j.energy.2013.06.005
- Islam, MS., Mithulananthana, N., Hung, DQ. 2021.** Coordinated EV charging for correlated EV and grid loads and PV output using a novel, correlated, probabilistic model. *Journal of Cleaner Production*, 279: 123615. <https://doi.org/10.1016/j.jclepro.2020.123615>
- Jain, A., Bhullar, S. 2024.** Operating modes of grid integrated PV-solar based electric vehicle charging system- a comprehensive review. *e-Prime - Advances in Electrical Engineering, Electronics and Energy*, 8: 100519. <https://doi.org/10.1016/j.prime.2024.100519>

- Karthikeyan, SP., Thomas, P. 2024.** Optimization Strategies for Electric Vehicle Charging and Routing: A Comprehensive Review. GU J Sci. 37(3): 1256-1285. DOI: 10.35378/gujs.1321572
- Lee S., Al-Ghussain L., Alrbai M., Al-Dahidi S. 2024.** Integrating hybrid PV/wind-based electric vehicles charging stations with green hydrogen production in Kentucky through techno-economic assessment. International Journal of Hydrogen Energy, 71: 345–356. <https://doi.org/10.1016/j.ijhydene.2024.05.053>
- Li, KW., Priddy, AP. 1985.** Power Plant System Design, John Wiley & Sons, Inc., New York, NY USA.
- Li, CC., Ge, X., Zheng, Y., Xu, C., Ren, Y., Song, C., Yang, C. 2013.** Techno-economic feasibility study of autonomous hybrid wind/PV/ battery power system for a household in Urumqi. Energy, 55: 263-272. DOI: 10.1016/j.energy.2013.03.084
- Li, C. 2021.** Technical and economic potential evaluation of an off-grid hybrid wind-fuel cell-battery energy system in Xining, China. International Journal Of Green Energy, 18(3): 258-270. <https://doi.org/10.1080/15435075.2020.1854267>
- Ma, H., Balthasar, F., Tait, N., Riera-Palou, XA. 2012.** Harrison, A new comparison between the life cycle greenhouse gas emissions of battery electric vehicles and internal combustion vehicles. Energy Policy, 44: 160-173. DOI: 10.1016/j.enpol.2012.01.034
- Ma, G., Jiang, L., Chen, Y., Dai, C., Ju, R. 2017.** Study on the impact of electric vehicle charging load on nodal voltage deviation. Archives of Electrical Engineering, 66(3): 495-505. doi:10.1515/ae-2017-0037
- Manwell, JF., McGowan, JG., Rogers, AL. 2009.** Wind Energy Explained: Theory, Design and Application, Wiley, 2nd edition.
- Mohamed,AAS.,El-Sayedc,A.,Metwallya,H.,Selem,SI.2020.** Grid integration of a PV system supporting an EV charging station using Salp Swarm Optimization. Solar Energy, 205: 170-182. <https://doi.org/10.1016/j.solener.2020.05.013>
- Moreno-Armendariz, MA., Duchanoy, CA., Calvo, H., Ibarra-Ontiveros, E., Salcedo-Castaneda, J., Ayala-Canseco, M., Garcia, D. 2021.** Wind Booster Optimization for On-Site Energy Generation Using Vertical-Axis Wind Turbines. 21(14): 4775 <https://doi.org/10.3390/s21144775>
- Moslehi, K., Kumar, R. 2010.** A reliability perspective of the smart grid. IEEE Transactions on Smart Grid, 1(1): 57-64. doi:10.1109/TSG.2010.2046346
- Mouli, GC., Bauer, P., Zeman, M. 2016.** System design for a solar powered electric vehicle charging station for workplaces. Applied Energy, 168, 434-443. <https://doi.org/10.1016/j.apenergy.2016.01.110>
- Nandini, KK., Jayalakshmi, NS., Vinay, KJ., Dattatraya, NG., Ashish, S., Vidya, SR., Ganesh, K. 2023.** Optimal Placement and Sizing of Electric Vehicle Charging Infrastructure in a Grid-Tied DC Microgrid Using Modified TLBO Method. Energies, MDPI, 16(4): 1-27. DOI:10.3390/en16041781
- Nurmuhammed, M., Karadağ, T. 2021.** A review on locating the electric vehicle charging stations and their effect on the energy network. Journal of Science, PART A: Engineering and Innovation, 8(2): 218-233. DOI:10.35833/MPCE.2018.000374
- Patel, MP. 1999.** Wind and Solar Power Systems, CRC Press LLC, New York.
- Patel, MR. 2006.** Wind and Solar Power System Design Analysis and Operation, Taylor & Francis, Raton. http://uk.farnell.com/images/en_UK/design_findings8pt2.pdf
- Shadman Abid, M., Ahshan R., Al Abri R., Al-Badi A., Albadi M. 2024.** Techno-economic and environmental assessment of renewable energy sources, virtual synchronous generators, and electric vehicle charging stations in microgrids. Applied Energy, 353: 122028. DOI:10.1016/j.apenergy.2023.122028
- Simmons, DM. 1975.** Wind Power, Noyes Data Corporation, Park Ridge, California, 1975.
- Singh, M., Kar, I., Kumar, P. 2010.** Influence of EV on grid power quality and optimizing the charging schedule to mitigate voltage imbalance and reduce power loss. In: Proceedings of the 14th International Power Electronics and Motion Control Conference (EPE-PEMC), 196-203. doi:10.1109/EPEPEMC.2010.5606657
- Staats, PT., Grady, WM. 1997.** A. Arapostathis, R.S. Thallam, A statistical method for predicting the net harmonic currents generated by a concentration of electric vehicle battery chargers. IEEE Transactions on Power Delivery, 12(3): 1258-1266. doi:10.1109/61.637002
- Sun, B. 2021.** A multi-objective optimization model for fast electric vehicle charging stations with wind, PV power and energy storage. Journal of Cleaner Production, 288: 125564. <https://doi.org/10.1016/j.jclepro.2020.125564>
- Topuz, A., Erdoğan, B., Taşkaya G. 2017.** Modeling of the Solar Irrigation System Using Photovoltaic Effect. Karaelmas Fen ve Müh. Derg. 7(2): 356-363.
- Ucer, E., Kisacikoglu, MC., Gurbuz, AC. 2018.** Learning EV Integration Impact on a Low Voltage Distribution Grid. In: Proceedings of the 2018 IEEE Power and Energy Society General Meeting (PESGM), 1-5. doi:10.1109/PESGM.2018.8586208
- Ullah, H., Czapp, S., Szultka, S., Tariq, H., Qasim, UB., Imran, H. 2023.** Crystalline silicon (c-Si)-based tunnel oxide passivated contact (topcon) solar cells: A review. Energies, 16 (2): 715. <https://doi.org/10.3390/en16020715>

- Veliz, MT., Kamel, S., Hasanien, HM., Arevalo, P., Turky, RA., Jurado, F. 2022.** A stochastic-interval model for optimal scheduling of PV-assisted multi-mode charging stations. *Energy*, 253: 124219. DOI: 10.1016/j.energy.2022.124219
- Wali, SB., Hannan, MA., Pin Jern Ker, Abd., Rahman, MS., Tiong, SK., Begum, RA., Indra Mahlia, TM. 2023.** Techno-economic assessment of a hybrid renewable energy storage system for rural community towards achieving sustainable development goals. *Energy Strategy Reviews*, 50: 101217. <https://doi.org/10.1016/j.esr.2023.101217>
- EEA 2024.** <https://www.eea.europa.eu/highlights/electric-vehicles-will-help-the>
- IEA 2024.** <https://www.iea.org/reports/electric-vehicles>
- IEA 2024.** <https://www.eurostat.ec.europa.eu>; EEA
- IEA 2023.** <https://www.iea.org/topics/transport>
- IEA 2023.** [\(Paoli\)](https://www.iea.org/commentaries/electric-cars-fend-off-supply-challenges-to-more-than-double-global-sales)
- SATATISTA 2024.** <https://www.statista.com/chart/26845/global-electric-car-sales/>
- IEA 2023.** https://www.iea.org/data-and-statistics/data-tools/global-ev-data-explorer?gclid=Cj0KCQjwwISIBhD6ARIaAESAm5pa6qp5XiiqW5tOuchBIscktxrk04oiSV3l70xuEDgHCzyOgID_0aAqAXEALw_wcB
- IEA 2024.** [\(Paoli\)](https://www.iea.org/commentaries/electric-cars-fend-off-supply-challenges-to-more-than-double-global-sales)
- TEHAD 2024.** <https://www.tehad.org/2022/07/08/2022-yili-ilk-6-ayinda-satilan-elektrikli-ve-hibrid-otomobil-satis-rakamlari/>
- TEHAD 2024.** <https://www.tehad.org/2021/04/07/2021-yili-ilk-ceyreginde-elektrikli-ve-hibrid-arac-satislari-artti/>
- Elektrikli-sarj-istasyonları 2024.** [>elektrikli-sarj-istasyonları](https://www.elektrikli.com.tr)
- Googlemaps 2023.** <https://www.google.com/maps/search/turkiye+sarj+istasyonları/@41.2651324,26.3597646,8z/data=!3m1!4b1>
- HOMER 2023.** https://www.file:///chapter3_HOMERMOD-ELING.pdf
- RETScreen 2023.** <https://www.RETScreen-NRCan/Canmet-ENERGY>
- SOLARGIS 2024.** <https://solargis.com/products/regional-solar-study>
- Shopping mall 2023.** <http://shopping mall technical office manager's report>
- TUİK 2023.** <https://data.tuik.gov.tr/Bulten/Index?p=Tourism-Statistics-Quarter-IV:-October-December-and-Annual,-2020-37438>
- Anerngroup 2024.** <https://www.anerngroup.com/products/solar-panel/>
- Yeni Trakya Enerji 2024.** <http://www.yenitrakyaenerji.com>
- Hi-techsolution 2024.** <https://hi-tchsolution.eu/products/vertical-axis-wind-turbine/vertical-axis-wind-turbine-aeolos-wv-09/>



Yapım İşlerinde İhale Parametreleri Kullanılarak Makine Öğrenmesi ile Sözleşme Bedeli Tahmini

Construction Contract Price Prediction Using Machine Learning with Bidding Parameters

Semi Emrah Aslay*

Erzincan Binali Yıldırım Üniversitesi, Mühendislik Mimarlık Fakültesi, İnşaat Mühendisliği Bölümü, Erzincan, Türkiye

Öz

Kamu ihalelerinde sözleşme bedelleri, temel olarak metraj ve birim fiyatlardan oluşmaktadır ve dolayısıyla bu parametrelerle yakından ilişkilidir. Bu parametrelerden başka, daha sade sayısal ifadeler üretebilen ve parasal anlaşma bedelleri hakkında önemli ipuçları veren ihale verileriyle de anlamlı ilişkilere sahiptir. Dolayısıyla ihale verileri ile sözleşme bedeli arasındaki anlamlı ilişkinin değerlendirilmesi önem kazanmaktadır. Bu çalışmada inşaat işlerinde ihale değişkenleri kullanılarak makine öğrenmesi yöntemleri ile sözleşme bedelleri tahmin edilmeye çalışılmıştır. Bunun için temel ve popüler algoritmalarдан yararlanılmıştır. Tahmin modellerini geliştirmek amacıyla bir dizi hiper parametre optimizasyonu yapılarak olumlu sonuçlar alınmıştır. Özellikle çalışmada en iyi sonuçlara sahip olan XGBoost ve ANN algoritmalarında uygulanan parametrik optimizasyonlar, mevcut modelin daha iyi bir performansı göstermesini sağlamıştır. XGBoost 0.9435, MAE 1.2988, RMSE 2.0621 en iyi genelleme yeteneğine sahip algoritma olmuştur. Çalışma hem kullandığı parametrelerin özgünlüğü hem de makine öğrenmesi modelinde uygulanan hiper parametre optimizasyonları ile literatüre katkı sunmaktadır.

Anahtar Kelimeler: ANN, kamu ihaleleri, makine öğrenmesi, sözleşme bedeli, XGBoost.

Abstract

In public tenders, contract values are primarily composed of quantities and unit prices, and therefore are closely related to these parameters. Besides these parameters, contract values are also meaningfully associated with procurement data that can produce more straightforward numerical expressions and provide significant insights into monetary agreement values. Therefore, evaluating the meaningful relationship between procurement data and contract value becomes crucial. This study aims to predict contract amounts in construction works using machine learning methods with bidding variables. Basic and popular algorithms were employed for this purpose. A series of hyperparameter optimizations were conducted to enhance prediction models, yielding positive results. Particularly, the parametric optimizations applied to XGBoost and ANN algorithms, which demonstrated the best results in the study, improved the performance of the existing model. XGBoost achieved the best generalization ability with an of 0.9435, MAE of 1.2988, and RMSE of 2.0621. The study contributes to the literature by introducing novel parameters and implementing hyperparameter optimizations in the machine learning model.

Keywords: ANN, public tenders, machine learning, contract price, XGBoost.

1. Giriş

Yapım işlerinde kamu kurumlarına ait binalar, yüklenici firmalara ihale edilerek yapılmaktadır.

İhale süreçleri rekabetçilik ve eşitlik ilkelerine dayanarak en uygun fiyatla, istenilen yapıların inşa edilmesini kapsar. Ku-

rumalar veya harcama yetkilileri farklı kullanım amacı için, insanların ihtiyaçlarını karşılayacak yapıların tanımını, târifini belirler, yasalara ve yönetmeliklere göre süreci yönetir. Bu süreç açık bir şekilde duyurulur ve yüklenici firmalar kâr-zarar oranlarını gözeterek ihale teklif sürecine girer. İhalelere katılan inşaat firmaları, istekli veya teklif verenler olarak adlandırılırlar. Teklif verenlere ait bilgiler ihale süreçlerinde önemli göstergelerden biridir. Toplam tekliflerin sayısal ifadeleri inşaat işlerine olan ilgiyi, yoğunluğu, maliyet ve bütçe planlamasına ait bilgiler sunabilir. Bu bilgilerin sözleşme bedeli arasındaki ilişki araştırılması, önemli noktalara

*Sorumlu yazarın e-posta adresi: seaslay@erzincan.edu.tr

Semi Emrah Aslay orcid.org/0000-0002-0127-5474



Bu eser "Creative Commons Ahıntı-GayriTicari-4.0 Uluslararası Lisansı" ile lisanslanmıştır.

vurgulanarak ihtiyaç duyulan tahmin yöntemi belirlenmesi önemlidir.

Son yıllarda birçok bilim dallarında tahmin yöntemleri araştırmalarda yer almaktadır. Bu alanda makine öğrenmesi literatürdeki popüler konulardan biridir. Metinsel dil modellerinin baskınlığı son zamanlarda sıkılıkla kullanılmasına karşılık (Yazgılı ve Baykara 2022), dijital alanlardaki araştırmalar her geçen gün artmaktadır (İlgün vd. 2023). Makine öğrenmesi yöntem ve konuları diğer farklı disiplinlerde de sıkılıkla kullanılmaktadır (Zeynep ve Erdal 2019). Farklı disiplinlerde yer alan bu yöntem ve konular inşaat mühendisliğinde de sıkılıkla kullanılmaktadır. İnşaat mühendisliğinin tüm alt dallarında bu çalışmaları görmek mümkündür (Thai 2022). İnşaat malzeme fiyatlarının tahmini için sinir ağı tabanlı modelin kullanılması (Mir vd. 2021), makroekonomik göstergelerle yapı malzemesi tahminin yapılması (Shihab vd. 2020), kuraklık analizleri (Başakın vd. 2019), ve konut tahmin taleplerinin tahminleri (Emeç ve Tekin 2022) örnek olarak verilebilir.

1.1. Literatür Taraması

Yapım işlerinde maliyeti temel almak suretiyle yapılan çalışmaların günden güne artmaktadır (Aslay ve Dede 2022). Çalışmalarda inşaat maliyetlerinin birçok alt kümesi olarak değerlendirilebilen kavramlar yer alır (Aslay ve Dede 2023). Bu kavumlardan biri de sözleşme bedelidir. Ancak sözleşme bedelleri ile ilgili çalışmaların daha çok maliyet odaklı olduğu söylenebilmektedir. Skitmore vd. (2003), 93 adet inşaat projesi ele alarak, sözleşme bedelini makine öğrenmesi ile tahmin etmeye çalışmıştır. Bunun için farklı modeller geliştirmiştir. Yüklenici seçim yöntemi, sözleşme düzenlemesi, proje türü gibi kriterleri kullanmıştır. Parasal tutarın yanında sözleşme türü ve inşaat süresi de analize dahil etmiştir. Ancak çalışmada sözleşme tutarı tahmininde elde edilen performans metrikleri oldukça düşüktür ve bu durum modelin genel tahmin yeteneğinin iyi olmadığını göstermektedir. Elhag vd. (2005) sözleşme bedeli tahmini için 67 farklı değişken üzerinde seçim yapmaya çalışmışlardır. Sözleşme bedeli aynı zamanda ihale öncesi maliyet tahmini olarak değerlendirilmişlerdir. Yapılan bu çalışmada parametrelerin belirlenmesi anket yoluyla yapılmıştır ve sonuçlar tahmin modeli olarak değerlendirilmemiştir. Aziz vd. (2014) sözleşme bedeli maliyet azaltma metotları ile kullanmaya çalışmışlardır. Sözleşmede bedelinin azaltılmasından ziyade optimum değerlere ulaşmaya çalışmışlardır. Pusic vd. (2020) maliyet tahminin inşaat sisteminin bir parçası olarak değerlendirerek, sözleşme bedelin olarak ön finans tahminini sinir ağı tabanlı model ile uygulamışlardır. Bunun için tarihsel veriler

ve bazı bina teknik verilerinden yararlanılmışlardır. Kovacevic vd. (2021) 181 adet betonarme köprü projesi incelemiştir. Farklı makine öğrenmesi modellerinden yaralanmışlardır. Girdi parametreleri olarak yapısal elemanlardan faydalananarak, inşaat maliyetini tahmin etmeye çalışmışlardır. Gurmu ve Miri (2023) bina maliyetini bulmak için çeşitli girdi parametreleri değerlendirmiştir. Bunlardan bazıları brüt zemin alanı, kullanılan malzemeler ve mimari iş kalemleridir. Farklı algoritmalar sunan çalışmada birçok parametre değeri denemiş olsa da verimlilik ölçütlerinin yeterli olmadığı söylenebilmektedir. Dang-Trinh vd. (2022), fabrika inşaat maliyeti tahmini için farklı makine öğrenmesi yöntemlerini kullandılar. Çalışma maliyet tahmincileri için çeşitli tahmin metodolojilerine erişim sağlamıştır ve bir fabrikanın ön maliyetinin tahmininde en iyi modelin belirlenmesini dair çıktılar elde etmiştir. Rafiee and Adeli (2018), bina özelliklerinin yanı sıra, işçilik-malzeme endekslerini kullanarak, sinir ağları ve destek vektör makinelere dayanan maliyet modeli geliştirdiler. Sanni-Anibire vd. (2021) yüksek binaların ön maliyeti için tahmin modelleri oluşturmuştur. Çalışmada makine öğrenmesi gibi modern dijital teknolojilerin inşaat endüstrisinin sorunlarını çözme potansiyeli ve tanımlanan prosedür, maliyet tahmin modellerinin geliştirilmesine katkı sunulmuştur.

İnşaat maliyetinin tahmin modeli ile ilgili geliştirilen çalışmalarda, özellikle girdi parametreleri statik veya mimari projeden elde edilen verilerle yapılmaktadır (Kovacevic vd. 2021, Gurmu ve Miri 2023). Bu durum hem uygulama süreçlerini zorlaştırmaktadır hem de zaman kaybına neden olmaktadır. Literatürdeki çalışmalarla kullanılan proje sayıları da oldukça azdır (Elhag vd. 2005, Kovacevic vd. 2021). Makine öğrenmesi modellerinde, örnek sayısı olarak net ifade söylenemez ancak veri noktalarının, tahmin modelleri üzerinde homojen bir dağılım elde edilebilmesi için örnekler analiz sonucu çıktılarında tatmin edici olmalıdır. Aynı zamanda sözleşme bedeli ile ilgili yapılan bu çalışmalarla hiper parametre optimizasyonun yapılmaması önemli bir eksikliktir (Skitmore vd. 2003). Araştırmalarda sözleşme bedeli tahmini için makine öğrenmesi modellerinin daha fazla geliştirilmesi ve farklı parametrelerin çalışmalarla yer verilmesi ihtiyaç duyulmaktadır. Her ne kadar maliyet analizlerinde makine öğrenmesi yöntemleri sıkılıkla kullanılsa da sözleşme bedeli olarak değerlendirilmesi ve yeni değişkenlerin ışığında modellerin geliştirilmesi önemlidir. Son araştırmalarda optimum parametrelerle öğrenme algoritma tabanlı modellerin gelişimi hızla ilerlemektedir (Takçı 2023). Kamu ihalelerinde sözleşme bedelleri tahmin yaklaşımının ihale parametrelerini kullanarak ve yeni model geliştiriciler ile

desteklenerek analizlerine yer verilmesi beklenen araştırma konularından biridir.

Bu çalışmada, yapım işleri kamu ihalelerinde, yeni yapım işlerinde, ihale parametresi olarak değerlendirilen toplam teklif sayıları, toplam geçerli teklif sayıları, doküman satın alma sayıları gibi değişkenlerle yüklenici firmalar ile kamu idareleri arasında imzalanan parasal karşılık olan sözleşme bedeli tahmin edilmeye çalışılmıştır. Bunun için 397 adet Açık İhale usulü ve Anahtar Teslim Götürü Bedel sözleşme türüne ait yapı projeleri ele alınmıştır. Makine öğrenmesi metotları uygulanmıştır. Analizlerde klasik makine öğrenmesi metotlarının dışına çıkılarak son zamanlarda kullanılan popüler tahmin metotları çalışılmıştır. Modeller ait parametrelerin optimizasyonlar yapılarak, her bir modele özel olarak hiper parametrik model geliştirici yöntemler denemiştir. Hiper parametre optimizasyonları ile modellerin genel tahmin yeteneklerinin artırılması başarılı bir şekilde gerçekleştirilmiştir. Yapılan çalışmanın optimum değişken türleri ve mümkün olan model geliştirici yöntemlerle, literatüre katkı sunmaktadır.

1.2. Kamu İhaleleri ile İnşaat İşlerin Yapılması

Bu çalışmada Türkiye'de yapım işlerinde betonarme yapıların inşası ve tanzimi için harcama yetkilisi idareler tarafından gerçekleştirilen kamu ihalelerindeki verilerden yararlanılmaktadır. Kamu binaları, ilgili idarelerin ihale yapmak suretiyle gerçekleştirdiği süreçlerle mümkün olmaktadır. Bunun için 4734 ve 4735 sayılı kanunlar kullanılmaktadır. Genellikle ihale usulü olarak; açık ihale usulü, belli istekliler arasında ihale usulü ve pazarlık ihale usulü ve sözleşme türü olarak; birim fiyat, anahtar teslim götürü bedel ve karma sözleşme türleri kullanılmaktadır (Kocaman vd. 2020). Bu araştırmada kullanılan veri setlerinin tümü açık ihale usulü ve anahtar teslim götürü bedel sözleşme türüne sahip ihalelerden elde edilmiştir. Çalışmada kullanılan ihale usulü ve sözleşme türü Çizelge 1'de verilmektedir. Açık ihale usulünde ihalesi yapılacak olan yapım işinin duyurusu tüm isteklilere yapılır. Herhangi özel çağrı veya teklif yapılmaz. İnşaat işi ile ilgili gerekli şartlara sahip olan herhangi bir yüklenici firma, ilgili harcama yetkilisinin belirttiği koşullara uygun

şekilde teklif verebilir. Teklifler ihale şartnamesinde belirtilir ve işin durumuna bağlı olarak uygun standartlarda değerlendirilerek sonuçlanır. Sözleşme türü olan ve çalışmada da kullanılan anahtar teslim götürü bedel sıklıkla ihalelerde tercih edilir. Bu ifade, yüklenici inşaat firmalarının taahhüt etmiş oldukları parasal bedel karşılığında, bir inşaat projesinin baştan sona tüm aşamaları ile insanların kullanımına hazır olacak şekilde tamamlanmasını belirtir. Bunun için söz konusu iş, işverene teslim edilir ve ilgili idare fen-sanat noktasından belirli aralıklarla kontrolleri yapar. Bu tür ihalelerde proje bütçesi değişmez veya çok az değişir ve tüm riskleri müteahhit firma üstlenir. İnşaat işi anlaşmaya varılan gün ve sözleşme bedeli ile tamamlanır.

2. Gereç ve Yöntem

2.1. Veri Setinin Tanımı

Bu çalışmada Türkiye'de kamu ihalelerinde ihalesi yapılmış olan 397 adet, yeni yapım işlerinden oluşan ve betonarme yapılardan alınan veriler kullanılmıştır. Bu veriler elektronik kamu alım platformundan 'ekap' elde edilmiştir. Bunun için konusunda uzman inşaat mühendis tarafından gereklili inşaat taban alanı hesabı ve ihale parametre bilgilerine ait okumalar yapılmıştır. Projeler sadece yeni yapım işlerini kapsamaktadır, tadilat işleri, onarım-güçlendirme işleri yer almamaktadır. Projelerin tamamı temelden başlamak üzere, inşaata ait tüm imalatların sonlandırılmasını kapsamaktadır. Aynı zamanda bu durum Kamu İhale Mevzuatında 'Anahtar teslim götürü bedel' olarak adlandırılan ihale yöntemi ile yapımı tamamlanan işleri kapsamaktadır. Yapıların tamamı betonarme olarak inşa edilmiştir. Farklı kat sayıları ve farklı kullanım amacı olan bina verilerinden yararlanılmıştır. Çalışma kapsamında oluşturulan modelde 5 farklı bağımsız değişken ve 1 adet bağımlı değişken yer almaktadır. Toplam 6 adet olan özniteliklerin açıklamaları Çizelge 2'de verilmektedir.

Bağımsız değişkenler seçilirken temel amaçlardan biri statik proje değişkenleri (Kovacevic vd. 2021) ve mimari projelerdeki değişken (Gurmuz ve Miri 2023) bilgileri tam olarak bilinmeden ihale aşamasında sözleşme bedeli hakkında tahmin modeli oluşturmaktır. Çalışmanın özgün yanlarından

Çizelge 1. İhale Usulleri ve Sözleşme Türleri (4734 Sayılı Kamu İhale Kanunu).

İhale Usulleri	Sözleşme Türleri	Bu Çalışmada Kullanılan Sözleşme Türleri ve İhale Usulleri
* Açık ihale usulü	* Anahtar Teslim Götürü bedel	* Açık ihale usulü
* Belli istekliler arasında ihale usulü	* Birim fiyat	* Anahtar Teslim Götürü bedel
* Pazarlık ihale usulü	* Karma	

Çizelge 2. Özniteliklere ait açıklamalar (4734, Sayılı Kamu İhale Kanunu).

Tanım	Değişken Türü	Açıklama	Kısaltma
Sözleşme Bedeli	Bağımlı Deḡ.	Yüklenici firma ile işin idaresi arasında anlaşmaya varılan parasal tutar	sb
Doküman Satın Alan Sayısı	Bağımsız Deḡ.	İsteklilerin işin idaresine gelerek para karşılığı yapım işi hakkında belge olarak aldığı doküman sayısı	dsas
Dokümanı EKAP üzerinden e-imza kullanarak indiren sayısı	Bağımsız Deḡ.	İsteklilerin internet üzerinden talep ettikleri ihale dokümanı sayısı	deis
Toplam Teklif Sayısı	Bağımsız Deḡ.	İsteklilerin yapım işini taahhüt ettikleri parasal karşılık ile yapacaklarına dair verdikleri beyan sayısı	tts
Toplam Geçerli Teklif Sayısı	Bağımsız Deḡ.	İsteklilerin taahhüt etmiş oldukları beyanlarından herhangi eksiklik olmaksızın idarenin yapabilir onayı verme sayısı	tgts
İnşaat Taban Alanı	Bağımsız Deḡ.	İlgili yapım işine ait binanın sahip olduğu taban alanı. M2 olarak değerlendirilmeye alınmıştır.	tabal

bir tanesi de budur. Bunun için sözleşme bedeli ile ilişkili olan ve analizlerde olumlu sonuçlar veren, satın alan sayıları, isteklilerin internet üzerinden talep ettikleri ihale doküman sayıları, toplam teklif sayıları, geçerli teklif sayıları girdi parametreleri kullanılmıştır. Bununla birlikte mevcut girdileri destekleyen ve bina karakteristiğini yansitan inşaat taban alanı kullanılmıştır. Bu alan, maliyet tahmininde regresyon analizi gibi istatistiksel modellerde yaygın olarak kullanılan bir değişkendir ve maliyet ile doğrudan ilişkisi bulunur (Ali ve Burhan 2023, Wang vd. 2022). Aynı zamanda hedef verisi olarak da adlandırılan bağımsız değişken ise sözleşme bedelidir. Sözleşme bedeli müteahhit firmaların herhangi bir iş için ilgili idareye verdikleri taahhüt bedelini ve bu bedele karşılık da harcama yetkilisinin onayını ifade eder. Harcama yetkilisi ihale isteklileri arasından en avantajlı teklifi değerlendirek uygun gördüğü fiyat üzerinden yüklenici ile anlaşır. Bu anlaşma koşul ve detayları 4734 ve 4735 sayılı kanunlarda yer almaktadır. Veri setlerinde bağımlı öznitelik olarak teklif sayıları ve bina karakteristik özelliklerini değerlendirilmektedir. Teklif sayıları kendi aralarında farklı kategoriler içermektedir. İhale büyülüğu veya avantaj durumunu göre bu kategoriler farklı anlamlar ifade etmektedir. Hem korelasyon matrislerinde hem de veri analizlerinde bu durum detaylı olarak değerlendirilmiştir.

2.2. Makine Öğrenmesi Yöntemleri

2.2.1. Gradyan Artırıcı Karar Ağacı (Extreme Gradient Boosting)

Literatürde 'XGBoost' olarak adlandırılan yöntem, karar ağacı temellidir. Topluluk öğrenme prensibine dayanır ve parametrelere farklı ağırlıklar vererek tahminlerde bulunur.

Veri setlerine ait değişkenlerdeki ağırlıklar ağaç topluluğu büyündükçe güncellenir (Ay ve Ekinci 2022). Bu yöntem gradyan artırma makinesi algoritmasını daha hızlı yapmak için geliştirilmiştir. Bunun için bir modelin eğitim verisi üzerinde çok iyi performans göstermesine rağmen, yeni veriler üzerinde yetersiz performans sergilemesi olan aşırı öğrenmeye azaltmak ve eğitim hızını artırmak için rasgele örnek alma tekniği kullanır. Aynı zamanda sütn tabanlı bir yapısı vardır ve büyük veri kümelerinde doğru sonuca ulaşır. Tüm bu nedenlerden dolayı son dönemler sıklıklar kullanılan popular bir algoritmadır (Thai 2022). Bu yönteme ait denklem eşitlik 1'de verilmektedir. Buradaki amaç daha küçük parçalarla başarının daha fazla arttırılmasıdır. Bu denkleme göre, $\sum_{i=1}^n L(x_i, y_i)$ indisine bağlı olarak 1'den 'ne' kadar toplamı, $L(x_i, y_i)$ modelin verimliliğini ve hatasını ölçen fonksiyondur, $\frac{1}{2}\alpha$ modele ait düzenleme parametresidir, $O^2 v$ modelin ikinci derece türevini temsil eder.

$$\sum_{i=1}^n L(x_i, y_i) + \frac{1}{2}\alpha O^2 v \quad (1)$$

2.2.2. Yapay Sinir Ağları (Artificial Neural Network)

İnsan beyninden esinlenerek oluşturulan model, makine öğrenmesi yöntemlerinde sıkılıkla başvurulmaktadır. Temelinde katmanlar ve ağırlıklandırmalar bulunur (Emeç ve Tekin 2022). Katmanlar genellikler 3 tiptedir. Her katman birbirlerine nöronlarla bağlıdır. Nöronların girişlerinde ağırlıklandırmalar bulunur ve işleyişi etkileyen ana unsurdur. Ağırlıklandırmalar, öğrenme, genelleme, hesaplama maliyeti ve performans doğrulukları ile belirlenir. Bu şekilde modelin genelleme yeteneği performans kabiliyeti problem üzerinde önemli bir rol oynar. Yöntemde kullanılan girdi ve

çıktı nöronlarının nasıl işleyeceğini gösteren matematiksel ifade aynı zamanda temel fonksiyondur (Eşitlik 2). Burada ‘y’ nöronun çıktısı, ‘f’ aktivasyon fonksiyonu, ‘n’ girdi sayısı, ‘i. Girdinin ağırlık değeri, “i. Girdi ve ‘b’ bias terimidir (Li, Zhang ve Liu 2017).

$$y = f(\sum_{i=1}^n w_i x_i + b) \quad (2)$$

2.2.3. Destek Vektör Makinesi (Support Vector Machine)

Bağımsız değişkenlerin sayısı kadar boyutu olan bir uzayda, en uygun hiper düzlem oluşturulmaya çalışılır. Hiper düzlem herhangi bir x-y doğrusunda verileri bağlı oluşturulan paralel çizgilerdir (Sinap 2023). Bu çizgiler en iyi tahminin yapılması amacıyla geniş tutulmaya çalışılır. Bunlar aynı zamanda karar sınırları olarak da adlandırılırlar. Karar sınırları olarak belirlenen alan veri gruplarında tahminlerin en iyi şekilde temsil edilmesi beklenir. Gerçek değerler ile tahmin değerler ilişkili için genel bir çözüm sunar (Şahin vd. 2023). Yönteme ait denklem eşitlik 3'te verilmektedir. Burada çekirdek parametreleri olarak γ , r ve d kullanılmıştır ve fonksiyon radyal tabanlıdır. Denklemde, $K(x_i, y_i)$ kernel (çekirdek) fonksiyondur, exp üstel fonksiyondur, $-\gamma$ üstel fonksiyonun içerisinde yer alan negatif bir katsayıyı ifade eder, $\|x_i, y_i\|^2$ x ve y arasındaki öklid mesafenin karesini ifade eder.

$$K(x_i, y_i) = \exp(-\gamma \|x_i, y_i\|^2) \quad \gamma > 0 \quad (3)$$

2.2.4 Bayes Regresyonu (Bayesian Regression)

Bayes yaklaşımı veri analizlerinde olasılıksal dağılım kullanır. Veri setlerindeki uyumsuzlukları, başlangıç tahmini ve veriye dayalı olasılık fonksiyonu kullanarak gidermeye çalışır. Geleneksel makine öğrenimi yöntemlerinin aksine, nokta tahminlerine odaklanmak yerine, model parametreleri ve tahminler üzerinde olasılık dağılımlarını içerir ve bu da belirsizliğin daha kapsamlı çözümünü ortaya çıkarır (Bhadradiya 2023). Yönteme ait örneğin deneme ile elde edilen olasılığını hesaplayan denklem eşitlik 4'te verilmektedir. Burada, ‘X’ bağımsız değişkenler matrisini, ‘β’ ağırlıklar matrisi ve biası temsil etmektedir (Özçift vd. 2019).

$$P(y = 1 | X, \beta) = \frac{1}{(1 + \exp(-(X \beta)))} \quad (4)$$

2.2.5 K-En Yakın Komşu (K-Nearest Neighbour)

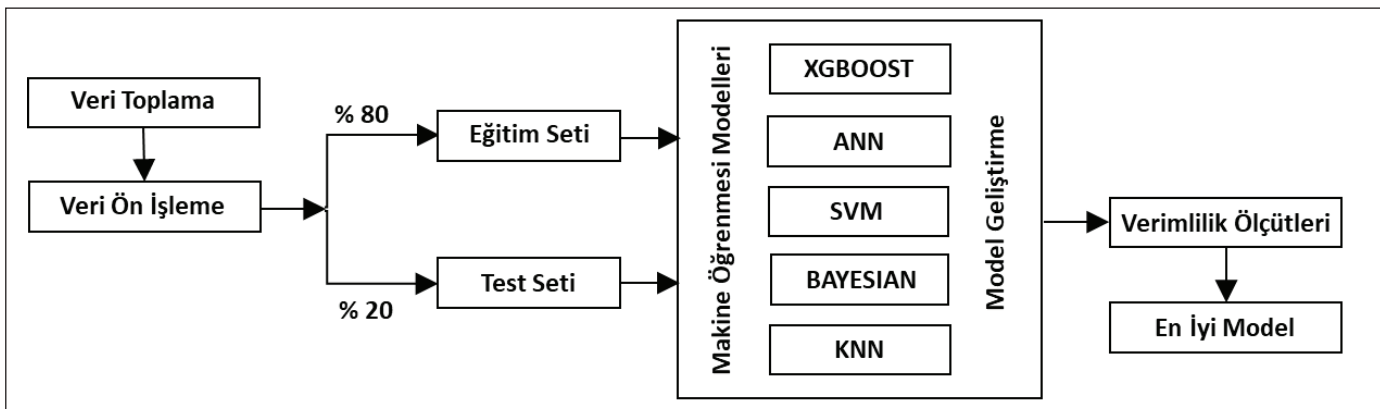
Bu yöntem uygulama kolaylığı ve işlem süresinin az olması nedeniyle araştırmalarda sıkılıkla kullanılmaktadır. Parametrik olmayan bir modeldir. ‘K’ harfi komşu sayısını ifade eder ve verilerin oluşturduğu kümelerin adetidir. Eğitim kümesi içerisinde k adet oluşan sınıfların ortalaması ‘K’ sayısı ile

hesaplanır. Mesafe fonksiyonu oluşturularak, bağımsız değişkenlerin yakınlıklarını ve tahmin değerlerinin ortalaması alınarak en iyi sonuca ulaşımaya çalışılır (Başakın vd. 2019, Sonuç ve Özcan 2022). KNN yöntemi temel olarak metrik mesafe değerine dayanır ve eşitlik 5'de verilmektedir.

$$d(x, y) = \sqrt{\sum_{i=1}^n \sqrt{(y_i - x_i)^2}} \quad (5)$$

2.3. Tahmin Modelinin Oluşturulması

Bu çalışmada 5 farklı makine öğrenmesi algoritmasından yararlanılmaktadır. Bunlar; gradyan Artırıcı karar ağacı (XGBoost), yapay sinir ağları (ANN), destek vektör makinesi (SVM), bayes regresyonu (Bayesian Regression), K-en yakın komşu (KNN) algoritmalarıdır. Kullanılan algoritmalar farklı avantajlar sunarak çeşitli veri setleri ve problemler için etkili çözümler sağlar. XGBoost, yüksek doğruluk oranı elde eder, karmaşık problemlerde etkilidir ve esneklik sunar. ANN karmaşık desenleri öğrenme yeteneği iyidir büyük verilerde etkili çözüm sunar. SVM, kategorik özelliğe sahiptir ve yüksek boyutlu veri setlerinde margin farkını maksimize eder. Bayes regresyonu, güven aralıklarını hesaplar ve veri setlerindeki belirsizliği yönetebilir. KNN temel bir öğrenim algoritmadır, yöntem olarak mesafeleri kullanarak hızlı ve etkili tahminlerde bulunur. Bu algoritmaların kullanımı, veri setinin özelliklerine ve problem gereksinimlerine bağlı olarak model performansını karşılaştırarak en uygun çözümün seçimine olanak tanır. Bu algoritmalar seçilirken tüm bu özellikleri ve veri setlerinin yapısı, problem türü göz önüne alınmıştır. Eğitimi ve test verileri için kaynak havuzundan alınan örneklerde %50-%50, %60-%40, %70-%30 ve %80-%20 oranlarının tümü değerlendirilerek analiz yapılmıştır. Tüm karşılaştırmalı analiz sonuçların içerisinde eğitim-test verisi olarak en iyi sonuç veren oranı %80-%20'dir. Bu nedenle, literatürde de kullanılabilen (Kilinc, Haznedar, Ozkan ve Katipoğlu, 2024) %80-%20 oranı bu çalışmada da kullanılmıştır. Hazırlanan veriler eğitim ve test verileri %80-%20 olarak bölünmüştür. Veri ön işleme adımları standart olarak kontrol edilmiştir. Veri setindeki değerleri belirli bir standart formata dönüştürme işlemi olan standardizasyon işlemleri gerçekleştirilmiştir. Veri setindeki değerlerin belirli bir ortalamaya ve varyansa sahip olmasını sağlanmıştır, böylece farklı özellikler arasındaki ölçek farklılıklarını gidererek işlemlere devam edilmiştir. Analiz işlemleri yapılarak etkinlik metrikleri ayrı ayrı incelenmiştir. Etkinlik değerlerinin arttırılabilmesi için çapraz doğrulama sayısını değiştirerek farklı kombinasyonlar elde edilmiştir. Çapraz doğrulama işlemi makine öğrenimi ve istatistiksel işlemlerde doğrulama tekniklerindendir. K-katman veya araştırmalardaki bilinen



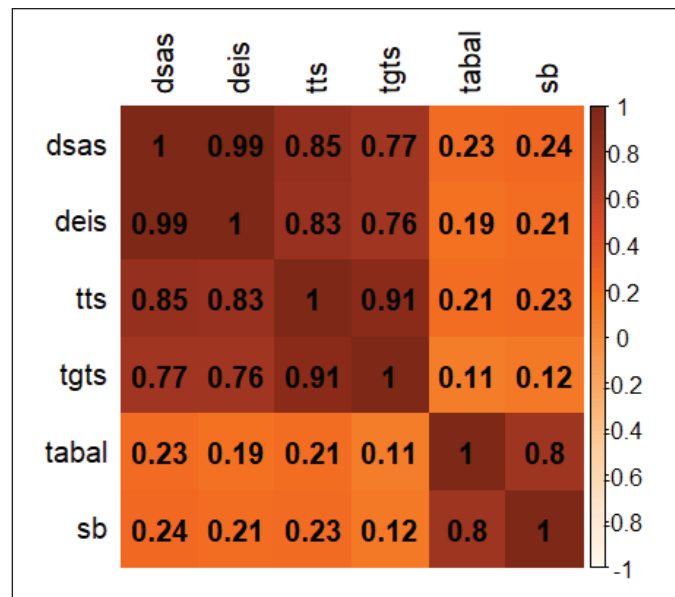
Şekil 1. İş akış diyagramı.

diğer adıyla K-fold değeri veri kümelerini alt kümelere ayıra-
rak farklı ihtimalleri kullanıcı sunmaktadır. Bu çalışmada
k-katman değeri 5-10 arasında denemiştir. En iyi sonucu 5
katmana bölünmesi ile elde edilmiştir. Hiper parametre op-
timizasyon işlemi çalışmada başvurulan diğer aşamadır. Bu
surette modele ait algoritmaların parametre değerleri, mo-
del verimliğini artırmak için optimize edilir. Bu çalışmada
artırıcı karar ağacı ve yapay sinir ağlarında model per-
formansına katkıda bulunduğu söyleyenilmektedir. Değerlen-
dirme ölçüyü olarak, ortalama mutlak hata (MAE), karekök
ortalama kare hatası (RMSE) ve R-kare (R^2) metrikleri kul-
lanılarak karşılaştırılmıştır. En verimli modeller bu metrik-
ler üzerinden değerlendirilmiştir. Çalışma aşamalarına ait iş
akış şeması Şekil 1'de verilmektedir.

3. Bulgular

Bu çalışmada 5 farklı öznitelikten yararlanılmıştır. Bunlar özellikle ihale istekli teklifleri ve inşaat özelliklerini barındırmaktadır. Bunlar doküman satın alan sayıları, isteklilerin internet üzerinden talep ettikleri ihale doküman sayıları, toplam teklif sayıları, geçerli teklif sayıları ve inşaat taban alanları olarak belirlenmiştir. Değişkenlerin etki değerleri göz önünde bulundurulmuştur. Bu özelliklerin hem kendi aralarında hem de hedef öznitelik arasındaki ilişkileri korela-
syon matrisi ile anlatılmıştır. Şekil 2'de değişkenlere ait ilişki sayıları verilmektedir. Buna göre inşaatın taban alanının sahip olduğu etki puanı fazla olmasına karşılık, diğer değişkenlerde anlamlı değerlere sahiptir. Ayrıca öznitelikler ayrı analize dahil edilmiştir. Etki puanı fazla olan değişkenler ayrı analizlerle birlikte değerlendirildiğinde tek başına olmasından ziyade birlikte değerlendirilerek daha performanslı metriklerin elde edildiği görülmektedir.

Bu çalışmada gradyan artırıcı karar ağacı, yapay sinir ağları, destek vektör makinesi, bayes regresyonu, K-en yakın komşu



Şekil 2. Korelasyon matrisi.

algoritmaları ile veri analizleri gerçekleştirilmektedir. Bu al-
goritmalara ait etkinlik kriterleri Çizelge 3'te verilmektedir.
Buna göre en iyi sonuçlar R-kare değeri 0,9435 olan grad-
yan artırıcı karar ağacından ve R-kare değeri 0,9215 olan
yapay sinir ağlarından elde edilmektedir. Bu 2 modelin yine
metrikleri olan ortalama mutlak hata ve karekök ortalama
kare hatası uyumlu seviyelerdedir. Destek vektör makinesi
ve bayes regresyonu verimlilik ölçütleri her ne kadar 3. ve 4.
sırada bulunsa da elde edilen metriklerin tümüne bakıldı-
ğında kabul edilebilir seviyelerde olduğu söyleyenilmekte-
dir. Etkinlik seviyesinde en alta yer alan K-en yakın komşu
yönteminin R-kare değeri 0,7768 olarak elde edilmiştir. Bu
sonuçla verimlilik değeri olumsuz algoritma olarak test edil-
miştir. Şekil 3'te kullanılan yöntemlerin saçılım grafikleri
verilmektedir. Buna göre modellere ait gerçek değerler ve

Çizelge 3. Makine öğrenmesi modellerine ait performans metriklerinin karşılaştırılması.

Method	R ²	MAE	RMSE
Gradyan artırıcı karar ağacı (XGBOOST)	0.9435	1.2988	2.0621
Yapay sinir ağları (ANN)	0.9215	1.3939	2.5762
Destek vektör makinesi (SVM)	0.8735	1.6265	5.3335
Bayes regresyonu (BAYESIAN REG)	0.8632	1.8288	4.6595
K-en yakın komşu (KNN)	0.7768	2.0097	6.0291

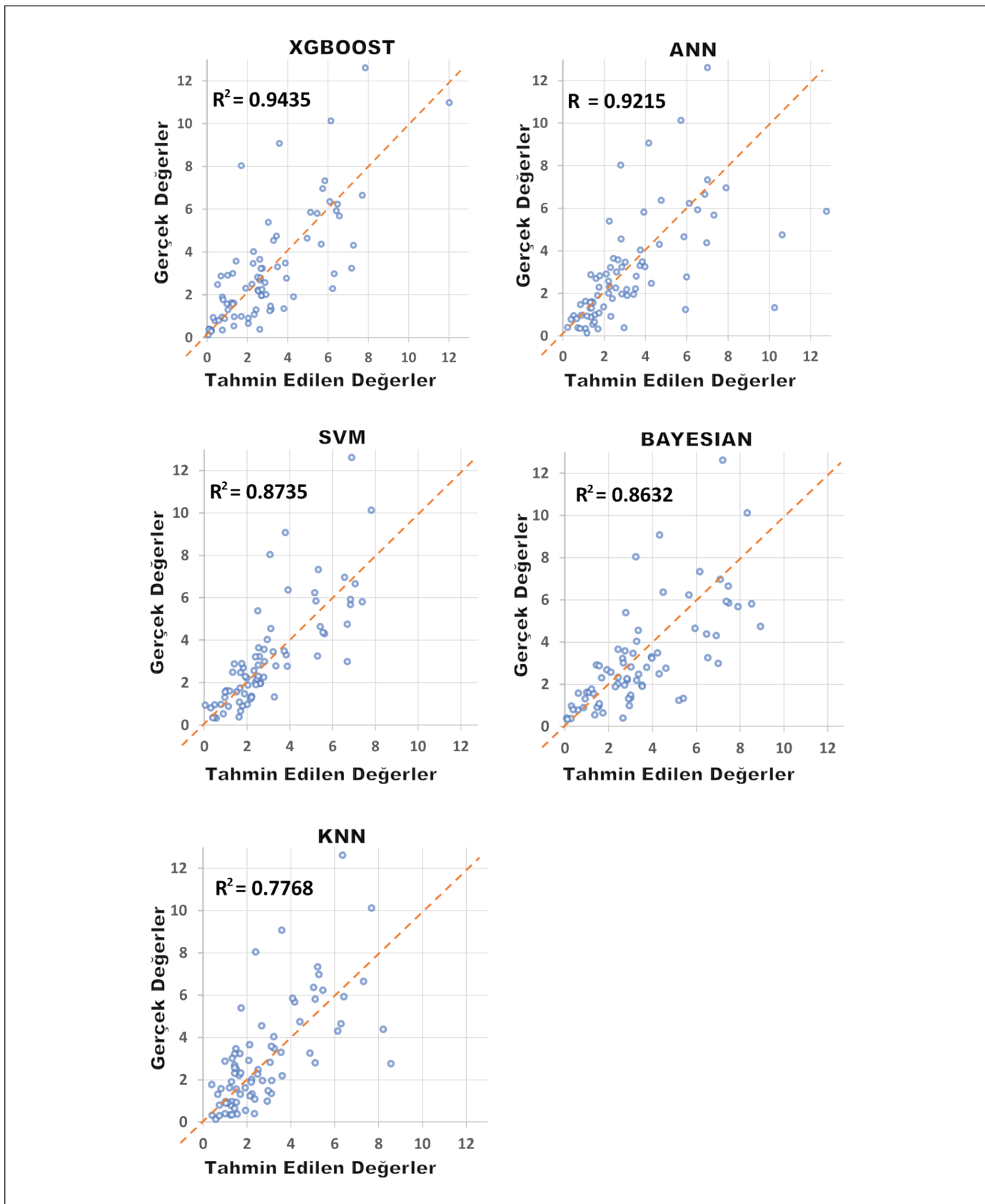
tahmini değerler arasındaki ilişki kolayca anlaşılabilir. Veri nokta dağılımları olarak bakılabilen grafiklerde, bu dağılımların XGBoost'da ve ANNde diğer modellere göre daha homojen olduğu görülmektedir. Ancak diğer modellerde de noktasal dağılımin çok kötü olduğu söylenemez. Tüm grafiklerde rasgele dağılmış olan verilerin varlığı olsa da belirli bir desen görünümü vardır ve görünüm kabul edilebilir seviyededir. Araştırmada kullanılan yapım işleri ihalelerindeki parametrelerin kullanıldığı çalışmalara literatürde pek rastlanmadığı söylenebilmektedir. İnşaat maliyetleri ile ilgili makine öğrenmesi araştırmalar bulunmakla birlikte veri setlerine ve değişken tiplerini göre performans metrikleri çok farklılık göstermektedir. Bununla birlikte regresyon analizlerinde R-kare değeri veri analizlerinde sıklıkla başvurulan sayısal ifadelerdir. Bu çalışmada bina özelliği olarak sadece taban inşaat alanı kullanılmaktadır. Bu parametre ihale teklif verileri ile uyumlu olduğu gözlenmiştir. Aynı zamanda parametreler birbirinin performanslarını artırıcı rol oynamıştır. Bunun için farklı veri analizleri kullanılmıştır. Çalışmada model etkinliği artırmaya yönelik olarak hiper parametre optimizasyonu kullanılmıştır. Yapılan parametre optimizasyonu ile özellikle gradyan artırıcı karar ağacı ve yapay sinir ağları yöntemlerinde başarılı sonuçlar elde edilmiştir. Tüm veri önişleme ve model geliştirme bölümleri rutin bir şekilde denenerek mümkün olan en iyi sonuçlarında elde edilmesinden sonra yapılan hiper parametre optimizasyonu modelin performans metriklerini artırmıştır. Yapılan optimizasyon işlemi ile algoritmaların farklı kombinasyon seçenekleri hızlı bir şekilde denenmiştir ve mümkün olan en iyi sonuçlara ulaşımaya çalışılmıştır. Yönetilen tüm süreçlerle modelin daha iyi bir genelleme yapılması sağlanmıştır.

4. Tartışma

İnşaat projelerinin maliyetine yönelik çalışmalarında girdi parametreleri çok farklılık gösterebilmektedir. Kamu ihalelerinde yüklenici firmalar için inşaat maliyetlerinin karşılığı olarak, sözleşme bedelinin hızlı bir şekilde tahmin edilmesi

önemlidir. İnşaat maliyetine yönelik olarak yapılan birçok çalışmada farklı mimari (Gurmuz ve Miri 2023), statik (Kovacevic vd. 2021) veya projeye özgü parametreleri (Skitmore vd. 2003), kullandıkları söylenebilir.

Rafiee and Adeli (2018), inşaat-arsa alanları, inşaat süresi, işçilik-malzeme endekslerini, Dang-Trinh vd. (2022), bina katsayıları, kolon aks mesafelerini, duvar -çatı tiplerini, Gurmuz and Miri (2023), bina tipleri, çatı-duvar-çerçeve malzeme özelliklerini girdi parametreleri olarak kullanmışlardır. Bu çalışmada ise kamu ihalelerindeki proje parametreleri kullanılmıştır. Bu parametrelere bina karakteristik özelliklerinden sadece 1 tanesi eklenmiştir. Girdi parametrelerinin ihaleye ait verilerden seçilme nedeni ise, yüklenici firmaların ve ilgili idarelerin projedeki verileri tam olarak bilmeden dahi sözleşme bedeli için bir hızlı öngörü kazanmalarını sağlamaktır. Literatürdeki benzer çalışmalarda Skitmore vd. (2003) 93 adet inşaat projesi, Kovacevic vd. (2021) 181 adet betonarme köprü projesinden faydalılmıştır. Mevcut proje sayılarının makine öğrenmesi yöntemleri için fazla olduğu söylenemez, zira bu veri adeti grafiksel yorumlarda yeterli seviyede olamamaktadır. Özellikle saçılım grafiklerinde verilerin homojen dağılımına bakılmak için fazla veriye ihtiyaç vardır. Bu çalışmada 397 adet veri kullanılmıştır. Grafik ve tabloların yorumlanması diğer çalışmalara göre daha net ifade edilmiştir. Aynı zamanda ihale parametrelerinin kullanılması daha fazla projeden hızlı veri elde etme imkanı sunmuştur. Literatürdeki çalışmaların performans metriklerine bakıldığından yönteminin R-kare değerlerinin çok iyi olmadığı görülmektedir. Gurmuz and Miri (2023) ve Skitmore vd. (2003) R-kare değerleri 0,50-0,66 arasında değişirken, Kovacevic vd. (2021) 0,89, Dang-Trinh vd. (2022) 0,91, Sanni-Anibire vd. (2021) 0,81 olarak elde etmiştir. Bu çalışmada en iyi R-kare değeri 0,94 olarak elde edilmiştir. Bu araştırma girdi parametrelerinin zenginliği, proje sayıları, kullandığı yöntemler ve elde ettiği başarılı verimlilik ölçüt sonuçlarıyla sözleşme bedeli tahmini konusunda literatüre katkı sunmaktadır.



Şekil 3. Saçılım grafiği.

5. Sonuç ve Öneriler

Bu çalışmada yapım işlerinde kamu ihalelerinde, yüklenici firmalara ait farklı teklif parametreleri kullanılarak, makine öğrenmesi yöntemi ile sözleşme bedeli tahmini yapılmaya çalışılmıştır. Bunun için elektronik kamu alım platformundan, 397 adet yapı projelerine ait veriler toplanmıştır. Bu verilerden bağımsız değişkenler olarak; müteahhit firmaların ilgili projeleri anahtar teslim götürü bedel olarak yapmayı planlayarak verdikleri toplam teklif sayıları, toplam geçerli teklif sayıları, doküman satın alma sayıları ve dokümanı e-imza ile indirme sayılarını kapsamaktadır. Ayrıca bina karakteristiği için yapı taban alanları da bağımsız değişkenlere dahil edilerek, netice de yüklenici firma ile işin idaresi arasında anlaşmaya varılan parasal tutar, yani sözleşme bedeli tahmin edilmeye amaçlanmıştır. Esasen ihale parametrelerinin sözleşme bedeli tahmini olan katkısı ve ilişkisi yapay zekâ alt dallarından olan makine öğrenmesi ile gerçekleşmiştir.

Makine öğrenmesi algoritmalarında farklı seçenekler çalışmada değerlendirilmiştir ve 5 farklı algoritmanın veri setleri için uyumlu olduğuna karar verilmiştir. Bunlar; gradyan artırıcı karar ağacı (XGBoost), yapay sinir ağları (ANN), destek vektör makinesi (SVM), bayes regresyonu (BAYESIAN REG), K-en yakın komşu (KNN) algoritmalarıdır. Bunlar hem temel algoritmalar hem de son yıllarda literatürde sıkılıkla kullanılan algoritmalarıdır.

Makine öğrenmesi yöntemlerindeki aşamalar özenle değerlendirilmiştir. Veri ön işleme aşamaları makale içerisinde detaylı olarak anlatılmıştır ve modellerin genelleme yeteneğine katkıda bulunmuştur. Model geliştirme teknikleri de her aşamada analize dahil edilmiştir. Veri analizlerinde hiper parametre optimizasyonu da uygulanmıştır. Özellikle gradyan artırıcı karar ağacı ve yapay sinir ağlarında hiper parametre optimizasyonu model tahminine katkıda bulunarak performans metriklerinde değerlendirilmiştir. Tüm algoritmalar göz önüne alındığında hem metriklerde hem saçılım grafiklerinin uyumlu ve kabul edilebilir seviyelerde olmasına karşılık, K-en yakın komşu algoritması en zayıf tahmin değerini elde etmiştir. Bundan sonra, bayes regresyonu ve destek vektör makenesi bu veri setlerinde daha iyi sonuç vermiştir. En iyi sonuçlar R-kare değerleri 0,90 üzerinde olan gradyan artırıcı karar ağacı ve yapay sinir ağlarından elde edilmiştir. Gradyan artırıcı karar ağacı (XGBoost), 0,9435 R-kare katsayısi ve 2,0621 karekök ortalaması kare hatası ile en gerçekçi sonuçları vermiştir. Buna göre makine öğrenmesi algoritmalarından başarılı sonuçlar elde edilerek uygun genellemelerde bulunulmuştur. Kamu ihalelerinde inşaat

karakteristiği ile ihale parametrelerinin yüklenicilerin taahhüt ettiği değer üzerinde anlamlı ilişkisi vardır. Bununla birlikte ihale isteklilerin hem gerçek teklifleri hem de projeleri değerlendirmek için dokümana olan talep ve yoğunlukları inşaatın parasal değeri üzerindeki etkisi anlaşılmıştır. Bu çalışma ile proje verilerine ihtiyaç olmaksızın ihale parametreleri kullanılarak, ilgili idare ve yüklenici firma için hızlı öngörülebilir bir maliyet sunmaktadır. İhaleyi yapan idareler elde ettikleri maliyet tahminiyle ihale sonucunda yapılabilecek herhangi bir teknik-parasal hatanın veya olağandışı sözleşme bedelinin fark edilmesi durumunda, yükleniciler ise ihale sonucunda yapılabilecek herhangi bir hatanın veya olağandışı fiyatların fark edilmesi, kar analizinin yapılması, hızlı finansal değerlendirme sonucunda aksi bir durumla karşılaşılması halinde, her iki taraf da itiraz süreçlerinin veya hukuksal başvuruların zamanında başlatılabileceklerdir. Bu çalışma İdare ve yüklenici arasında parasal problemlerin yaşanmaması ve yapım ihalelerinin uygulama süreçlerindeki hata-aksaklılıkların oluşmaması için çözüm sunmaktadır.

Gelecekteki çalışmalarında, bu çalışmanın kısıtları olarak da değerlendirilebilecek noktalar arasında, performans metriklerinin geliştirilmesi, veri setinin genişletilmesi ve açıklanabilir makine öğrenmesi yöntemlerinin uygulanması yer almaktadır.

6. Kaynaklar

- 4734 Sayılı Kamu İhale Kanunu. (t.y.).**
- Ali, ZH., Burhan, AM. 2023.** Hybrid machine learning approach for construction cost estimation: an evaluation of extreme gradient boosting model. *Asian Journal of Civil Engineering*, 24(7): 2427-2442. doi:10.1007/s42107-023-00651-z
- Aslay, SE., Dede, T. 2022.** 3D cost optimization of 3 story RC constructional building using Jaya algorithm. *Structures*, 40: 803-811. doi:10.1016/j.istruc.2022.04.055
- Aslay, SE., Dede, T. 2023.** Reduce the construction cost of a 7-story RC public building with metaheuristic algorithms. *Architectural Engineering and Design Management*, doi:10.1080/17452007.2023.2195612
- Ay, Ş., Ekinci, E. 2022.** Comparison of Machine Learning and Deep Learning Methods for Modeling Ozone Concentrations. *Journal of Intelligent Systems: Theory and Applications*, 5(2): 106-118. doi:10.38016/jista.1054331
- Aziz, RF., Hafez, SM., Abuel-Magd, YR. 2014.** Smart optimization for mega construction projects using artificial intelligence. *Alexandria Engineering Journal*, 53(3): 591-606. doi:10.1016/j.aej.2014.05.003
- Başakın, EE., Ekmekcioğlu, Ö., Ozger, M. 2019.** Drought Analysis with Machine Learning Methods. *Pamukkale University Journal of Engineering Sciences*, 25(8): 985-991. doi:10.5505/pajes.2019.34392

- Bharadiya, JP.** 2023. A Review of Bayesian Machine Learning Principles, Methods, and Applications. International Journal of Innovative Science and Research Technology (C. 8). www.ijisrt.com adresinden erişildi.
- Car-Pusic, D., Petrusheva, S., Zileska Pancovska, V., Zafirovski, Z.** 2020. Neural Network-Based Model for Predicting Preliminary Construction Cost as Part of Cost Predicting System. Advances in Civil Engineering. doi:10.1155/2020/8886170
- Dang-Trinh, N., Duc-Thang, P., Nguyen-Ngoc Cuong, T., Duc-Hoc, T.** 2022. Machine learning models for estimating preliminary factory construction cost: case study in Southern Vietnam. International Journal of Construction Management, doi:10.1080/15623599.2022.2106043
- Elhag, TMS., Boussabaine, AH., Ballal, TMA.** 2005. Critical determinants of construction tendering costs: Quantity surveyors' standpoint. International Journal of Project Management, 23(7): 538-545. doi:10.1016/j.ijproman.2005.04.002
- Emeç, Ş., Tekin, D.** 2022. Housing Demand Forecasting with Machine Learning Methods. Erzincan Üniversitesi Fen Bilimleri Enstitüsü Dergisi, 15(Special Issue I): 36-52. doi:10.18185/erzifbed.1199535
- Gurmu, A., Miri, MP.** 2023. Machine learning regression for estimating the cost range of building projects. Construction Innovation. doi:10.1108/CI-08-2022-0197
- İlgün, EG., Sönmez, Y., Dener, M.** 2023. Makine Öğrenme Yöntemi Kullanılarak DarkWEB Trafiği Tespiti ve Sınıflandırılması. Gazi Journal of Engineering Sciences, 9(4): 126-140. doi:10.30855/gmbd.0705s13
- Kilinc, HC., Haznedar, B., Ozkan, F., Katipoğlu, OM.** 2024. An evolutionary hybrid method based on particle swarm optimization algorithm and extreme gradient boosting for short-term streamflow forecasting. Acta Geophysica. doi:10.1007/s11600-024-01307-5
- Kocaman, E., Kuru, M., Çalış, G.** 2020. Investigating the effect of tendering procedure and contract type on the construction contract price. Teknik Dergi/Technical Journal of Turkish Chamber of Civil Engineers, 31(1): 9789-9812. doi:10.18400/TEKDERG.458054
- Kovacevic, M., Ivaniševic, N., Petronijevic, P., Despotovic, V.** 2021. Construction cost estimation of reinforced and pre-stressed concrete bridges using machine learning. Gradjevinar, 73(1): 1-13. doi:10.14256/JCE.2738.2019
- Li, H., Zhang, Z., Liu, Z.** 2017. Application of artificial neural networks for catalysis: A review. Catalysts. MDPI. doi:10.3390/catal7100306
- Mir, M., Kabir, HM. D., Nasirzadeh, F., Khosravi, A.** 2021. Neural network-based interval forecasting of construction material prices. Journal of Building Engineering, 39. doi:10.1016/j.jobe.2021.102288
- Özçift, A., Klinc, D., Bozyigit, F.** 2019. Grid Aramayla Optimize Edilmiş Bayes Lojistik Regresyon Algoritmasının Türkçe Mikro Blog Verilerinde Sanal Zorbalık Tespitinde Kullanılması. Academic Platform Journal of Engineering and Science, 7(3): 355-361. doi:10.21541/apjes.496018
- Rafiei, MH., Adeli, H.** 2018. Novel Machine-Learning Model for Estimating Construction Costs Considering Economic Variables and Indexes. Journal of Construction Engineering and Management, 144(12). doi:10.1061/(asce)co.1943-7862.0001570
- Sanni-Anibire, MO., Mohamad Zin, R., Olatunji, SO.** 2021. Developing a preliminary cost estimation model for tall buildings based on machine learning. International Journal of Management Science and Engineering Management, 16(2): 134-142. doi:10.1080/17509653.2021.1905568
- Shiha, A., Dorra, EM., Nassar, K.** 2020. Neural Networks Model for Prediction of Construction Material Prices in Egypt Using Macroeconomic Indicators. Journal of Construction Engineering and Management, 146(3). doi:10.1061/(asce)co.1943-7862.0001785
- Sinap, V.** 2023. Makine Öğrenmesi Teknikleri ile Counter-Strike: Global Offensive Raunt Sonuçlarının Tahminlenmesi. Journal of Intelligent Systems: Theory and Applications, 6(2): 119-129. doi:10.38016/jista.1235031
- Skitmore, RM., Ng, ST., Ng, T.** 2003. Building and Environment Forecast Models for Actual Construction Time and Cost. Building and Environment, 38(8): 1075-1083.
- Sonuç, E., Özcan, E.** 2022. Makine Öğrenme Teknikleri Kullanılarak Küükürt Giderme İşleminde Kullanılan Malzeme Miktarının Tahmini. Journal of Intelligent Systems: Theory and Applications, 5(1): 57-63. doi:10.38016/jista.993853
- Şahin, F., Tulum, G., Karaca, Ş.** 2023. Anne Sağlığı Riski İçin Makine Öğrenmesi Modellerinin Performans Karşılaştırması. DÜMF Mühendislik Dergisi. doi:10.24012/dumf.1325431
- Takci, H.** 2023. Performance-enhanced KNN algorithm-based heart disease prediction with the help of optimum parameters. Journal of the Faculty of Engineering and Architecture of Gazi University, 38(1): 451-460. doi:10.17341/gazimmfd.977127
- Thai, HT.** 2022. Machine learning for structural engineering: A state-of-the-art review. Structures. Elsevier Ltd. doi:10.1016/j.istruc.2022.02.003
- Wang, R., Asghari, V., Cheung, CM., Hsu, SC., Lee, CJ.** 2022. Assessing effects of economic factors on construction cost estimation using deep neural networks. Automation in Construction, 134. doi:10.1016/j.autcon.2021.104080
- Yazgılı, E., Baykara, M.** 2022. Türkçe metinlerde makine öğrenmesi yöntemleri ile siber zorbalık tespiti. Gümüşhane Üniversitesi Fen Bilimleri Enstitüsü Dergisi. doi:10.17714/gumusfenbil.935448
- Zeynep, AD., Kılıç, E.** 2019. Prediction of Bank Stocks Price with Machine Learning Techniques. TBV-BBMD, 12(2): 30-39.



Generation of Synthetic Data Using Breast Cancer Dataset and Classification with Resnet18

Meme Kanseri Veri Seti Kullanılarak Sentez Veri Üretilmesi ve Resnet18 ile Siniflandırılması

Dilşat Berin Aytar* , Semra Gündüz

Ankara University, Department of Computer Engineering, Ankara, Türkiye

Abstract

Since technology is advancing so quickly in the modern era of information, data is becoming an essential resource in many fields. Correct data collection, organization, and analysis make it a potent tool for successful decision-making, process improvement, and success across a wide range of sectors. Synthetic data is required for a number of reasons, including the constraints of real data, the expense of collecting labeled data, and privacy and security problems in specific situations and domains. For a variety of reasons, including security, ethics, legal restrictions, sensitivity and privacy issues, and ethics, synthetic data is a valuable tool, particularly in the health sector. A Deep Learning (DL) model called GAN (Generative Adversarial Networks) has been developed with the intention of generating synthetic data. In this study, the Breast Histopathology dataset was used to generate malignant and benign labeled synthetic patch images using MSG-GAN (Multi-Scale Gradients for Generative Adversarial Networks), a form of GAN, to aid in cancer identification. After that, real and synthetic data were classified in four different ways with Transfer Learning (TL) using the ResNet18 model. In the first classification, real data is used as training and test data and an accuracy rate of 84%, in the second classification, synthetic data is used as training and test data and the accuracy rate is 99%, in the third classification, real data is used as training and synthetic data is used as test data and an accuracy rate of 81%, in the fourth classification, synthetic data is used as training and real data is used as test data and an accuracy rate of 76%. As a result of the study, four different classifications were associated and it was tried to determine whether the synthetic images are similar to the original data and whether they behave like real data.

Keywords: Generative adversarial networks, histopathology, MSG-GAN, ResNet18, synthetic data.

Öz

Bilgi çağı olan günümüzde veri, özellikle teknolojinin hızla ilerlemesiyle birçok alanda kritik bir kaynak hâline gelmiştir. Veri doğru bir şekilde toplandığında, düzenlenliğinde ve analiz edildiğinde birçok sektörde etkili kararlar almak, süreçleri iyileştirmek ve başarı elde etmek için güçlü bir araç hâline gelir. Gerçek verinin kısıtlılığı, etiketlenmiş verinin elde edilmesinin maliyetli olması, bazı durumlarda ve alanlarda gizlilik ve güvenlik endişeleri gibi sebepler sentetik verilere ihtiyaç duyulmasına sebep olmuştur. Sentez veriler, özellikle sağlık alanında hassaslık ve gizlilik endişeleri, yasal düzenlemeler, etik ve güvenliğin sağlanmasına gibi nedenlerden dolayı önemli bir araçtır. Sentez veri üretme amacıyla Derin Öğrenme (DÖ) modeli olan ÇÜA (Çekişmeli Üretici Ağlar) ortaya çıkmıştır. Bu çalışmada Meme Histopatoloji veri seti kullanılarak bir ÇÜA çeşidi olan ÇÖD-ÇÜA (Üretken Rekabetçi Ağlar için Çok Ölçekli Değişimler) ile kanser tespitinde yarar sağlamak amacıyla kötü huylu ve iyi huylu etiketli sentetik yama görselleri oluşturulmuştur. Sonrasında gerçek ve sentetik veriler ResNet18 modeli kullanılarak Aktarımlı Öğrenme ile dört farklı şekilde sınıflandırılmıştır. İlk sınıflandırmada gerçek veriler eğitim ve test verisi olarak kullanılıp %84 doğruluk oranı, ikinci sınıflandırmada sentetik veriler eğitim ve test verisi olarak kullanılıp %99 doğruluk oranı, üçüncü sınıflandırmada gerçek veriler eğitim, sentetik veriler test verisi olarak kullanılıp %81 doğruluk oranı, dördüncü sınıflandırmada sentetik veriler eğitim, gerçek veriler test verisi olarak kullanılıp %76 doğruluk oranı elde edilmiştir. Çalışma sonucunda dört farklı sınıflandırma ilişkilendirilerek sentetik görüntülerin orijinal verilere olan benzerliği ve gerçek veri gibi davranışını tespit edilmeye çalışılmıştır.

Anahtar Kelimeler: Çekişmeli üretici ağlar, histopatoloji, ÇÖD-ÇÜA, ResNet18, sentetik veri.

*Corresponding author: aytar.berin@gmail.com

Dilşat Berin Aytar orcid.org/0009-0006-9984-241X

Semra Gündüz orcid.org/0000-0002-3811-9547



This work is licensed by "Creative Commons Attribution-NonCommercial 4.0 International (CC BY NC)".

1. Introduction

In today's world, data has become an extremely important resource in many fields, akin to a valuable commodity. The usability of data in numerous areas has led to the emergence of new data and an increased need for more data. Fields such as scientific research, decision-making processes, strategic planning, performance monitoring, Artificial Intelligence (AI) and Machine Learning (ML), customer experience and personalization, scientific research and innovation, healthcare services and medicine, security and risk management, solving societal issues, and marketing demonstrate the significance of data.

Data plays many important roles in the field of healthcare and medicine, contributing significantly to the development of healthcare services, patient treatment, and the formation of health policies. However, there are limitations to accessing real data in healthcare. Health data often contains sensitive and confidential information. The sharing and access of medical data are subject to strict regulations and can be limited due to privacy concerns, ethics, and security. Examples of legal regulations governing health data include HIPAA (Health Insurance Portability and Accountability Act) in the United States, GDPR (General Data Protection Regulation) in the European Union, and various other regulations in different countries related to the protection and processing of health data. Furthermore, health data is protected under medical ethical rules and standards. These principles address issues such as data confidentiality, patient privacy, and patient rights, guiding healthcare providers. Therefore, healthcare institutions and providers must strictly adhere to these regulations and take various measures to ensure the confidentiality and security of health data, ensuring patient safety and preventing data misuse. Overcoming limitations in accessing data is crucial for health research and innovations.

Overcoming limitations and addressing data scarcity, synthetic data generated by AI presents a significant solution. Synthetic data, created artificially by a computer program, is designed to mimic the characteristics of real-world data while preserving individual privacy and avoiding data breaches. Organizations can generate nearly unlimited amounts of data for testing, research, and analysis using synthetic data without worrying about ethical and legal issues associated with real-world data. Synthetic data, generated through advanced algorithms and models, offers a viable solution to these challenges by creating artificial datasets that mimic the statistical properties of real-world data. This enables researchers to augment existing datasets,

perform robust experiments, and train ML models more effectively (Goodfellow et al. 2014).

Generative Adversarial Networks (GANs) have emerged for the purpose of synthetic data generation. GANs, introduced by Goodfellow et al. in 2014, consist of two neural networks—a generator and a discriminator—that compete against each other to produce realistic data samples. This adversarial training process results in highly realistic synthetic data that can be used in various applications, including image classification, natural language processing, and anomaly detection (Goodfellow et al. 2014). Recent advancements in GANs have led to the development of more sophisticated models, such as StyleGAN and CycleGAN, which further enhance the quality and diversity of synthetic data (Karras et al. 2019, Zhu et al. 2017).

GANs are a significant and innovative modeling approach in the field of DL. They consist of two networks, a generator and a discriminator, which compete with each other. These networks compete to ultimately produce realistic images. For example, GAN-generated medical images have been used to improve the accuracy of diagnostic models and to train models on rare diseases where real data is scarce (Frid-Adar et al. 2018, Salehinejad et al. 2018). Various types of GAN model variants have been developed to meet different needs. This article will describe Multi-Scale Gradients for Generative Adversarial Networks (MSG-GAN), a type of GAN model.

In MSG-GAN, the generator and discriminator networks compete at a single resolution and improve together. The MSG technique utilizes different resolution levels to stabilize this competition. This approach gradually increases operations starting from lower resolutions and scales up to real dimensions. This innovation addresses common issues in GAN training, such as mode collapse and training instability, leading to more robust synthetic data generation (Karnewar et al. 2019). As a result, a faster, more stable, and improved training process is provided, contributing to more realistic, consistent, and high-quality results by better utilizing information at different scales. MSG-GAN introduces a multi-scale gradient approach that enables the generator to produce high-resolution images with finer details by receiving gradients at multiple scales during the training process. MSG-GAN is particularly successful in tasks such as image generation and synthesis involving visual datasets. It has a wide range of applications in data augmentation, AI studies, art, computing, medicine, automotive, finance, and many other fields.

After synthetic data generation with MSG-GAN, the generated synthetic data will be classified using TL techniques such as ResNet18 (Residual Neural Network). ResNet18 is a DL model commonly used for visual recognition and classification problems. The term “ResNet” stands for “Residual Networks,” and “18” denotes the number of layers in the model.

ResNet represents an architecture that includes residual blocks developed to facilitate the training of deep neural networks and reduce overfitting. The residual block passes the input data through an activation function and several convolutional and summation layers. An important feature of ResNet is the presence of “residual connections” in these blocks.

TL refers to the reuse of features learned by a pre-trained model to solve a different task. If necessary, weights are adjusted and new layers are added based on the new task and dataset. For example, a pre-trained ResNet18 model may have been trained for many image classification tasks. In a new image classification task, the pre-trained ResNet18 model can be taken and retrained on the new dataset.

Breast cancer is the second most common cancer type globally after lung cancer (Teh et al. 2015). Invasive Ductal Carcinoma (IDC) is the most common subtype among all breast cancers. The aim is to reduce reliance on pathologists and thereby reduce errors and human-related biases during disease detection, as well as minimize the high economic cost and time loss associated with it. In this study, IDC+ and IDC- histopathological images will be generated using MSG-GAN for disease detection, and the images will be classified using ResNet18.

2. Material and Methods

In the two-stage study, in the first stage, synthetic images were produced using MSG-GAN, and in the second stage, classification was made using ResNet18, one of the TL techniques. Finally, the classification results were evaluated with metrics.

2.1. MSG-GAN (Multi-Scale Gradients Generative Adversarial Network)

MSG-GAN (Karnewar et al. 2019), is a technique used to enhance the performance of traditional GANs (Goodfellow et al. 2014) by stabilizing their training process and achieving high-quality results.

The MSG technique uses different resolution levels (starting from lower to higher resolutions) to stabilize this competition. This approach begins with lower resolutions and gradually scales up operations to the actual size. This ensures a faster, more stable, and improved training process, leveraging information at different scales to produce more realistic, consistent, and high-quality results.

The process generally involves the following steps:

- **Start at Low Resolution:** Initially, the generator network operates at a lower resolution, learning simpler patterns.
- **Increase Resolution:** As the generated images are scaled to higher resolutions, the complexity of the network increases, adding more detail and realism.
- **Finalize at Real Size:** The process continues until the target resolution is reached, allowing the network to learn more complex patterns and details.

This technique is considered a significant advancement in the evolution of GANs, often leading to better performance on high-resolution images or other complex data types. MSG-GAN is utilized in various image synthesis and other application areas.

Figure 1 shows the basic MSG-GAN architecture used in the study. The architecture includes connections from the intermediate layers of the generator to the intermediate layers of the discriminator. The multi-scale images sent to the discriminator are combined with activation volumes obtained from the main path of the convolutional layers using a “Combine Function” (shown in yellow) (Karnewar et al. 2019).

2.1.1. MSG-GAN Generator Architecture and Function

The generator architecture used to produce a 64x64x3 image with MSG-GAN typically consists of 5 blocks. While Table 1, illustrates the entire generator architecture, the 5 blocks used to generate 64x64x3 images in the study are highlighted in bold.

The generator architecture generally involves upsampling and convolutional operations. Upsampling refers to transforming images into higher resolutions. After each upsampling step, two convolution operations are usually performed. The generator processes input noise to generate realistic images with dimensions of 64x64x3.

The generator typically takes random noise vectors as input. This noise is processed and transformed into a feature map containing pixel values. After upsampling the images, the

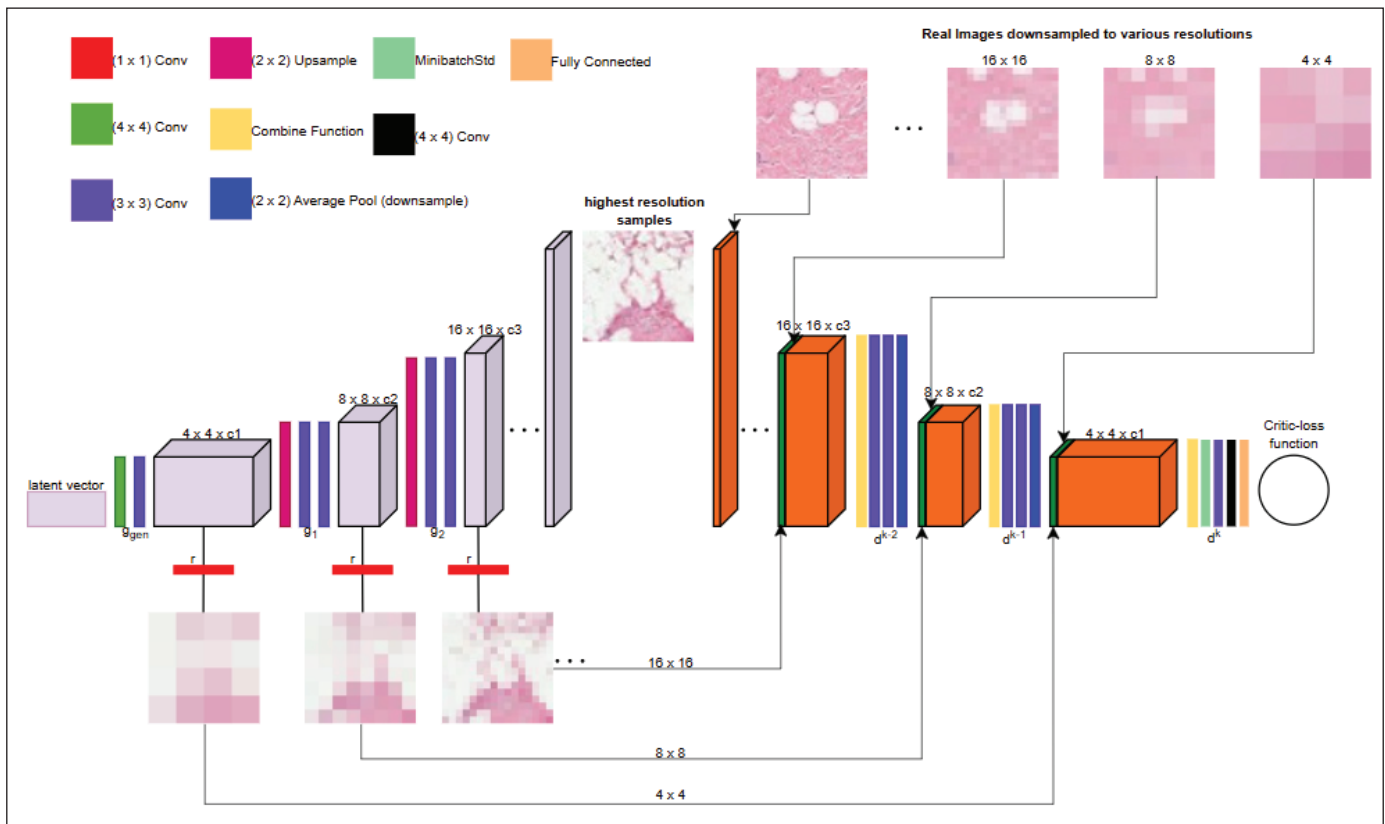


Figure 1. MSG-GAN architecture.

generator typically learns features using convolutional layers with 3x3 filters. Higher-level features are learned at each layer. Initially, these features may represent simple patterns and shapes, which later evolve into more complex objects and structures. The LeakyReLU activation function (Xu et al. 2015) is used in each block.

The generator performs two transmission operations in each block:

- Firstly, after every second convolution operation, the generator passes its output to the next block until reaching the final block. The output size, for example, is 512x16x16.
- Secondly, in addition to Table 1, a 1x1 convolution operation is applied to the output of the respective block before transitioning to the next block. This ensures that the block output has 3 channels (RGB features). This output is transmitted as input to the discriminator. The output size, for example, is 3x16x16.

By following the specified steps and performing the 1x1 convolution operation, the generator produces high-quality

images of size 64x64x3 in five blocks and transmits them to the discriminator.

The generator is trained using feedback from the discriminator. The discriminator evaluates the realism of the generated images and provides feedback. The generator learns to make the generated images increasingly realistic based on this feedback. During the training process, the generated images are optimized to resemble real images as closely as possible. This helps prevent issues such as mode collapse and training instability.

2.1.2. MSG-GAN Discriminator Architecture and Function

The discriminator architecture used to generate a 64x64x3 image with MSG-GAN typically consists of 5 blocks. Table 2 displays the entire discriminator architecture, with the 5 blocks highlighted in bold for generating the 64x64x3 images in the study. The 5 blocks used in the discriminator architecture are the last 5 blocks compared to the first 5 blocks used in the generator architecture. This is because, as described below, the output of each block from the generator will be the input to the corresponding blocks of the discriminator from end to start.

The discriminator model is structured to handle images of different sizes in each block. Each block in Table 2 represents a different scale level. Block operations typically involve taking the raw RGB image, concatenating it with feature maps from previous blocks (Concat/φ_simple), adding minibatch standard deviation (MiniBatchStd) to the feature maps, applying a 3x3 convolution operation (a 3x4 convolution operation is applied in the last block), and performing average pooling (Avg Pooling). Each convolution layer uses a certain number of filters, and the LeakyReLU activation function (Xu et al. 2015) is used.

Table 1. Generator architecture.

Block	Operation	Activation Function	Output Shape
1.	Latent vector	Norm	512x1x1
	Conv 4x4	LReLU	512x4x4
	Conv 3x3	LReLU	512x4x4
2.	Upsample	-	512x8x8
	Conv 3x3	LReLU	512x8x8
	Conv 3x3	LReLU	512x8x8
3.	Upsample	-	512x16x16
	Conv 3x3	LReLU	512x16x16
	Conv 3x3	LReLU	512x16x16
4.	Upsample	-	512x32x32
	Conv 3x3	LReLU	512x32x32
	Conv 3x3	LReLU	512x32x32
Model 1 ↑			
5.	Upsample	-	512x64x64
	Conv 3x3	LReLU	256x64x64
	Conv 3x3	LReLU	256x64x64
6.	Upsample	-	256x128x128
	Conv 3x3	LReLU	128x128x128
	Conv 3x3	LReLU	128x128x128
Model 2 ↑			
7.	Upsample	-	128x256x256
	Conv 3x3	LReLU	64x256x256
	Conv 3x3	LReLU	64x256x256
Model 3 ↑			
8.	Upsample	-	64x512x512
	Conv 3x3	LReLU	32x512x512
	Conv 3x3	LReLU	32x512x512
9.	Upsample	-	32x1024x1024
	Conv 3x3	LReLU	16x1024x1024
	Conv 3x3	LReLU	16x1024x1024
Model full ↑			

In the last block, average pooling is not performed. Instead, there is a fully connected layer. The fully connected layer produces an output to determine whether an input image of size 64x64x3 is real or fake. During training, it attempts to produce high output values for real images and low output values for generated images as much as possible.

2.2. ResNet18

ResNet (He et al. 2015) is a neural network model introduced to facilitate the training of deep networks and

Table 2. Discriminator architecture.

Block	Operation	Activation Function	Output Shape
Model full ↓			
1.	Raw RGB images 0 FromRGB 0 MiniBatchStd Conv 3x3 Conv 3x3 AvgPool	- - - LReLU LReLU -	3x1024x1024 16x1024x1024 17x1024x1024 16x1024x1024 32x1024x1024 32x512x512
	Raw RGB images 1 Concat/ MiniBatchStd Conv 3x3 Conv 3x3 AvgPool	- - - LReLU LReLU -	3x512x512 35x512x512 36x512x512 32x512x512 64x512x512 64x256x256
	Raw RGB images 2 Concat/ MiniBatchStd Conv 3x3 Conv 3x3 AvgPool	- - - LReLU LReLU -	3x256x256 67x256x256 68x256x256 64x256x256 128x256x256 128x128x128
	Raw RGB images 3 Concat/ MiniBatchStd Conv 3x3 Conv 3x3 AvgPool	- - - LReLU LReLU -	3x128x128 131x128x128 132x128x128 128x128x128 256x128x128 256x64x64
	Raw RGB images 4 Concat/ MiniBatchStd Conv 3x3 Conv 3x3 AvgPool	- - - LReLU LReLU -	3x64x64 259x64x64 260x64x64 256x64x64 512x64x64 512x32x32

Table 2. Cont.

Block	Operation	Activation Function	Output Shape
Model 1 ↓			
6.	Raw RGB images 5	-	3x32x32
	Concat/	-	515x32x32
	MiniBatchStd	-	516x32x32
	Conv 3x3	LReLU	512x32x32
	Conv 3x3	LReLU	512x32x32
	AvgPool	-	512x16x16
7.	Raw RGB images 6	-	3x16x16
	Concat/	-	515x16x16
	MiniBatchStd	-	516x16x16
	Conv 3x3	LReLU	512x16x16
	Conv 3x3	LReLU	512x16x16
	AvgPool	-	512x8x8
8.	Raw RGB images 7	-	3x8x8
	Concat/	-	515x8x8
	MiniBatchStd	-	516x8x8
	Conv 3x3	LReLU	512x8x8
	Conv 3x3	LReLU	512x8x8
	AvgPool	-	512x4x4
9.	Raw RGB images 8	-	3x4x4
	Concat/	-	515x4x4
	MiniBatchStd	-	516x4x4
	Conv 3x3	LReLU	512x4x4
	Conv 3x4	LReLU	512x1x1
	Fully Connected	Linear	1x1x1

increase performance in the field of visual processing. The main purpose of ResNet is to reduce training difficulties that may occur by making the network deeper.

ResNet uses the concept of residual learning. In this approach, the network tries to learn the difference between the input data and the output, instead of just predicting the outputs of the layers. The basic structural unit of ResNet is the Residual Block. This block is slightly different from a traditional neural network layer. A Residual Block consists of convolution, activation, normalization layers and Residual Connection (Shortcut). Residual connections, which ease the training of deep neural networks, enhance their performance, and enable deeper networks.

ResNet is named according to the number of layers used. In this study, the ResNet18 model with 18 layers was used. ResNet18, a pre-trained TL model, is used to perform binary classification in this study.

ResNet18 comprises convolutional layers, batch normalization, and ReLU activation functions (Liu 2020), Residual connections involve adding the output of the previous layer to the next layer. This technique mitigates the vanishing gradient problem and allows the training of very deep networks possible.

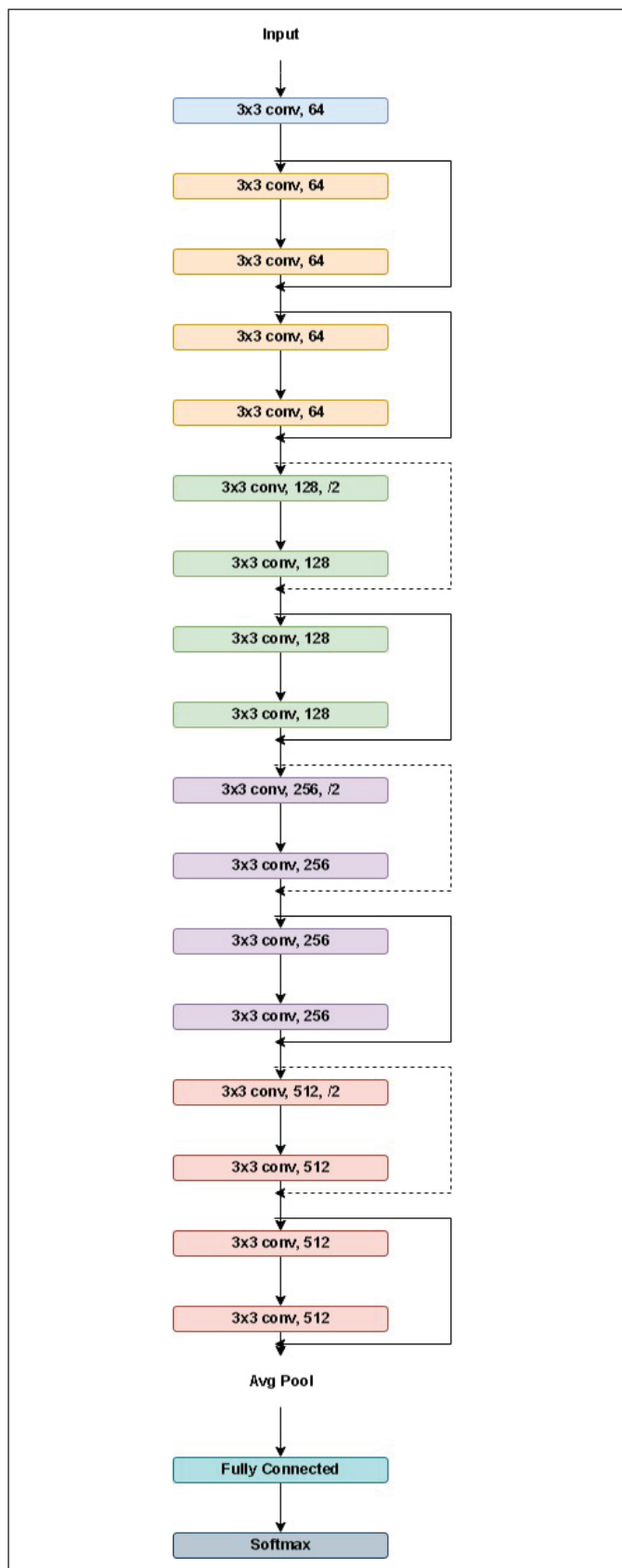
ResNet18 and other ResNet architectures are applied in many areas such as image processing, object recognition, face recognition and medical image analysis. In particular, TL techniques and pre-trained networks such as ResNet18 are used to achieve high success rates in various tasks.

The reasons for choosing the ResNet18 model in this project are based on various factors. First, the large dataset size supports the use of a medium-scale model such as ResNet18. While this model can provide sufficient performance on a data set of 160,000 samples, it can optimize training times and memory usage by having a lighter structure than deeper networks. Moreover, thanks to its ability to capture general data patterns, it can be used effectively in various scenarios of the project (e.g. combinations of real and synthetic data). As a result, the ResNet18 model was evaluated as a suitable choice to achieve the balance of scale and performance required by working with large data sets.

In the study, all layers of the pre-trained model except the last layer are frozen and will not be updated during training. Only the last Full Connection layer of the model was changed and the output was arranged to be two classes (positive or negative). The parameters (weights and bias) of the last added Full Connectivity layer are set to be open to training. Figure 2 shows the ResNet18 architecture used in the study.

2.3. Dataset and Summary of Work

Firstly, the training dataset was downloaded from <https://www.kaggle.com/datasets/paultimothymooney/breast-histopathology-images>. Janowczyk et al. 2016, Cruz-Roa et al. 2014). Patches of IDC, the most prevalent subtype of breast cancer, are seen in the dataset. Of all breast cancers, invasive ductal carcinoma (IDC) is the most prevalent subtype. Pathologists normally concentrate on areas with IDC when determining the aggressiveness levels of each assembly sample. Thus, locating the precise IDC zones across the entire assembly slide is a typical preprocessing step for automatic aggressiveness rating. There are 156,000 patches in all, consisting of 78,000 IDC negative and 78,000 IDC positive patches. The pictures have three channels and a 50x50 dimension. Data that is IDC negative is labeled 0, whereas data that is IDC positive is labeled 1.

**Figure 2.** ResNet18 architecture.

The dataset was divided into two parts for synthetic data generation (40,000 x 2) and classification (38,000 x 2). The reason for this is to ensure that the test data consists of previously unseen data during the training phase when performing classification.

The study consists of two parts.

- Firstly, synthetic data generation was performed using MSG-GAN with 80,000 images. As a result of this study, 38,000 synthetic IDC negative and 38,000 synthetic IDC positive data were generated.
- Secondly, four different classifications were performed using ResNet18, which is one of the TL models.

2.4. Environmental Variables Used

All models used in this study were compiled with GPU/CPU support. All codes are implemented with the PyTorch 2.0 framework, an open-source deep neural network library written in Python.

3. Results and Discussion

A certain number of datasets were divided into two parts, one used to generate breast cancer negative and positive labeled images using MSG-GAN. The generated images and the unused portion of the real data were used as training and test data, and four different classification processes were performed using ResNet18. The model was evaluated based on the results obtained.

3.1. Synthetic Data Generation with MSG-GAN

As explained in section 2.1.1 and section 2.1.2, a 5-block generator and discriminator architecture was used with MSG-GAN. In the study, WGAN-GP (Gulrajani et al. 2017) was determined as the loss function for both the generator and discriminator models. As a result, 38,000 synthetic IDC- and 38,000 synthetic IDC+ data of size 64x64x3 were produced by using 40,000 IDC+ and 40,000 IDC- data from the real data set. The hyperparameters used in each of the classifications are as follows: Batch size is 16, learning rate is 0.0001, and optimizer is RMSprop (Graves 2013).

Figure 3 shows examples of synthetic IDC+ data produced using MSG-GAN, and Figure 4 shows examples of synthetic IDC- data produced using MSG-GAN.

38,000 synthetic IDC+ and 38,000 synthetic IDC- data produced using MSG-GAN were used in the next stage of the study, namely classification.

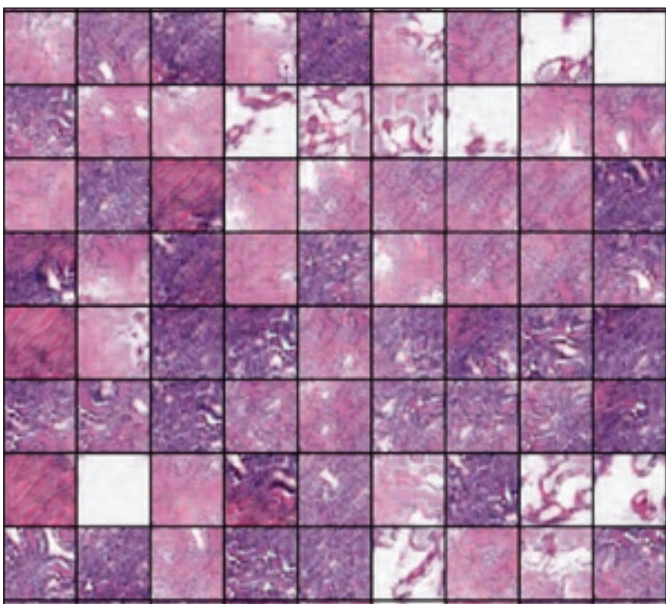


Figure 3. Synthetic IDC+ data examples.

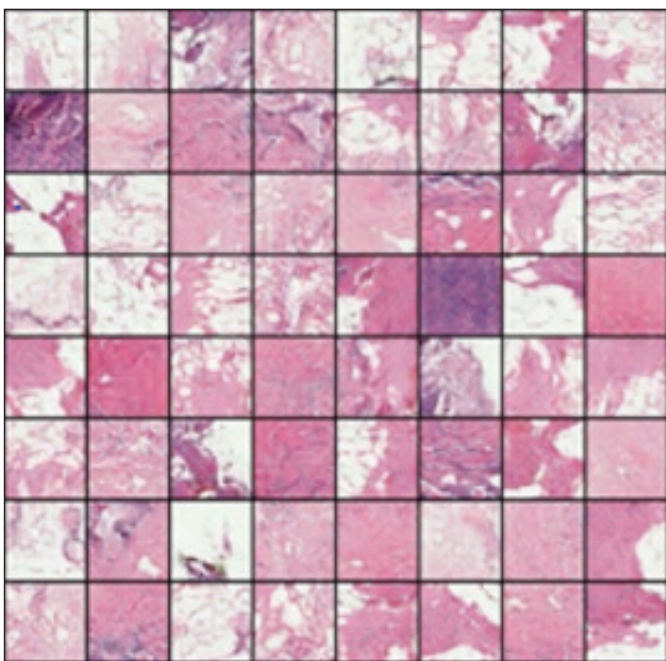


Figure 4. Synthetic IDC- data examples.

3.2. Classification of Real and Synthetic Data with ResNet18

In this stage, classification was performed using the unused 76,000 portion of the real dataset and the generated 76,000 synthetic data with the pre-trained ResNet18 model.

The purpose of this section was to determine how similar synthetic data was generated to the real data and to classify images. This section was divided into four sub-sections. The

same model was used in each subsection. The subsections are as follows:

- Training and classification of real data: 70% (53,200 patches) of the real data was used as training and 30% (22,800 patches) as testing. (Even though the data set was divided into training and test data in the ratios of 80:20, 60:40, 50:50, the result did not change. For this reason, the division is shown as 70:30.)
- Training and classification of synthetic data: 70% (53,200 patches) of the synthetic data was used as training and 30% (22,800 patches) as testing. (Even though the data set was divided into training and test data in the ratios of 80:20, 60:40, 50:50, the result did not change. For this reason, the division is shown as 70:30.)
- Training with real data and classification of synthetic data: All real data (76,000 patches) was used as training and all synthetic data (76,000 patches) was used as test data.
- Training with synthetic data and classification of real data: All synthetic data (76,000 patches) was used as training data and all real data (76,000 patches) was used as test data.

The purpose of the four different classifications is to establish a relationship between the classification results, examine the ability of synthetic data to reflect real data, and determine whether synthetic data behaves like real data.

A DL model like ResNet18 generally expects an input size of 224x224x3. Therefore, in the study, real and synthetic data were resized to 224x224x3 dimensions before the classification process. The ResNet18 model architecture described in Section 2.2 was implemented.

CrossEntropyLoss (LeCun et al. 1998) was used as the loss function. The hyperparameters used in each of the classifications are as follows: Batch size is 32, learning rate is 0.001, and optimizer is Adam (Kingma and Ba, 2015).

Training lasted for 150 epochs for each classification. Loss was calculated for each batch, gradients were propagated backward, and model parameters were updated using the optimizer.

3.3. Evaluation of The Classification Results

To evaluate the system's performance, accuracy, precision, recall, and F1 score metrics were used. Table 3 shows the metrics obtained from four different classifications conducted in the study.

Table 3. Metrics obtained as a result of classification of real and synthetic data.

Train/Test Data	Accuracy	Precision	Recall	F1 Score
Real/Real	0.84	0.84	0.84	0.84
Synthetic /Synthetic	0.99	0.98	0.98	0.98
Real / Synthetic	0.81	0.82	0.78	0.78
Synthetic / Real	0.76	0.77	0.76	0.76

Firstly, achieving high accuracy, precision, recall, and F1 score values when using real data as both training and test data (Real/Real) for classification indicates that the pre-trained ResNet18 model can be considered as a baseline model for this study. These results reflect the model's ability to classify real-world data accurately. Figure 5 shows the ROC curve of the classification and Table 4 shows the confusion matrix of the classification.

Table 4. Confusion matrix (Percentage).

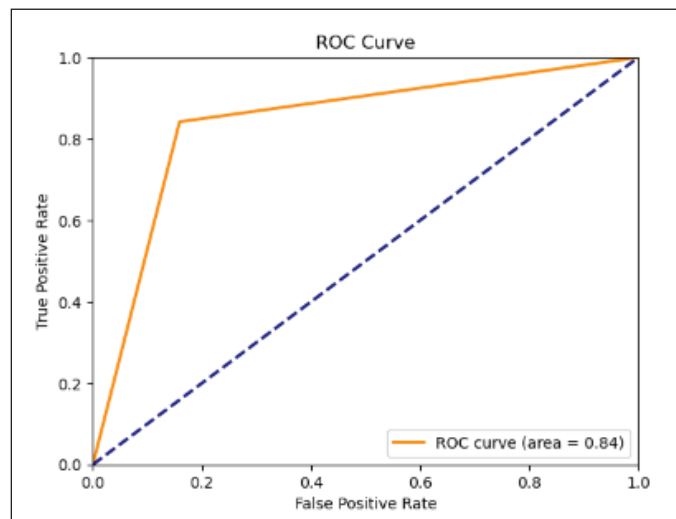
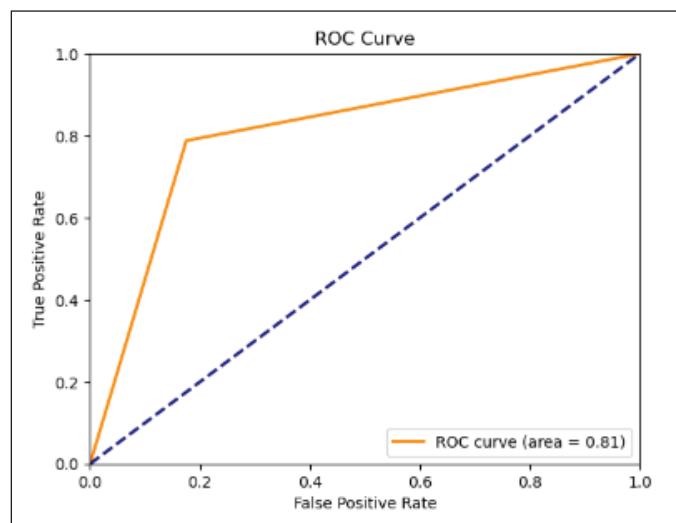
		Actual	
		IDC+	IDC-
Predicted	IDC+	84.1	15.9
	IDC-	15.8	84.2

The lower accuracy, precision, recall, and F1 score values obtained when using real data for training and synthetic data for testing (Real/Synthetic) compared to Real/Real results can be attributed to the fact that the distribution conformity in synthetic data does not perfectly match that of real data, leading to out of distribution data samples in the generated data. These data samples decrease the accuracy rate of the respective classification. However, the similarity between the metric values obtained from Real/Real and Real/Synthetic classifications indicates that synthetic data closely resemble real data. Figure 6 shows the ROC curve of the classification and Table 5 shows the confusion matrix of the classification.

Table 5. Confusion matrix (Percentage).

		Actual	
		IDC+	IDC-
Predicted	IDC+	82.5	17.5
	IDC-	21.2	78.8

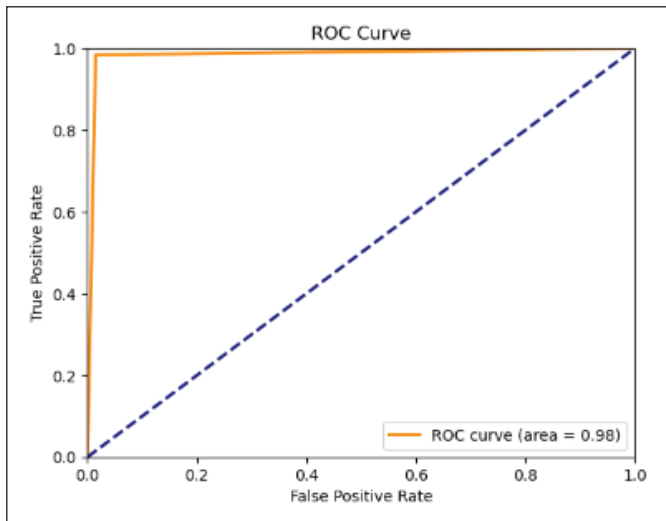
Achieving nearly 100% accuracy, precision, recall, and F1 score values when using synthetic data as both training and test data (Synthetic/Synthetic) suggests that the model's

**Figure 5.** ROC curve.**Figure 6.** ROC curve.

capacity is sufficient to learn the distribution of the data. These high rates indicate that synthetic data can be easily learned by the model. Figure 7 shows the ROC curve of the classification and Table 6 shows the confusion matrix of the classification.

Table 6. Confusion matrix (Percentage).

		Actual	
		IDC+	IDC-
Predicted	IDC+	98.5	1.5
	IDC-	1.6	98.4

**Figure 7.** ROC curve.

The lower metric results obtained from Real/Real classifications compared to Synthetic/Synthetic classifications in both cases of ResNet18 classification can be explained as follows: The real dataset contains out of distribution examples within itself, which negatively affect synthetic data generation and classification results. Upon examination of the dataset, many out of distribution data points were found.

The lower accuracy, precision, recall, and F1 score values obtained when using synthetic data for training and real data for testing (Synthetic/Real) compared to Real/Real classifications by 8% can be interpreted as follows:

- As mentioned earlier, the presence of out of distribution examples within the real dataset and the use of real data as test data affect the classification results. The model could not find correlation for out of distribution data.
- The lesser diversity of synthetic data compared to real data might imply that synthetic data have less diversity than real data (since the area learned from the real data distribution during synthetic data generation is small compared to the total distribution of real data, the diversity within synthetic data is low). When synthetic data is tested with real data, low metric values are obtained due to the low diversity of the training data.

Table 7. Confusion matrix (Percentage).

		Actual	
		IDC+	IDC-
Predicted	IDC+	72.6	22.4
	IDC-	23.4	76.6

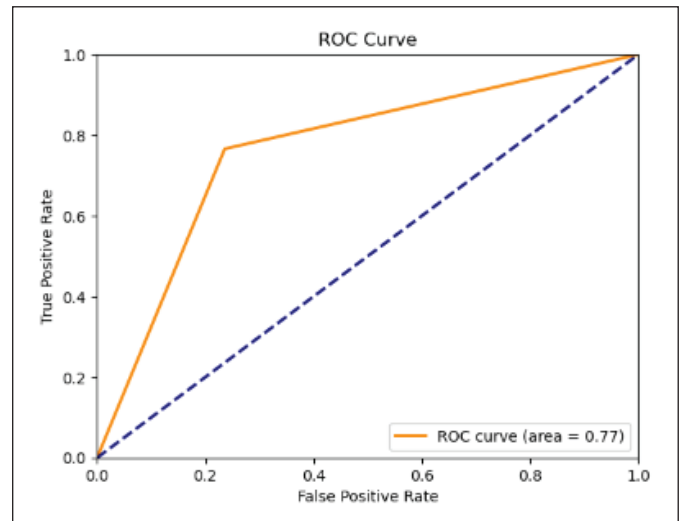
**Figure 8.** ROC curve.

Figure 8 shows the ROC curve of the classification and Table 7 shows the confusion matrix of the classification.

The similar metric values obtained from Synthetic/Real and Real/Synthetic classifications using the ResNet18 model highlight the similarity between real and synthetic data. Furthermore, achieving high results using a dataset containing out of distribution data demonstrates the success of the model.

The MSG-GAN model used in the study was successful in the production of synthetic data and high accuracy rates were achieved in the classification of these data.

In this study, unlike other studies in the literature, four different classification results that were expected to be related and close to each other were found. In this way, it was tried to determine whether synthetic data could be used instead of real data.

In summary, the results of the classification in four different scenarios were examined to see whether the synthetic data reflected the real world data, and the classification results were found to be related and close to each other. In this case, it has been determined that high quality and similar to reality synthetic data is produced.

Moreover, to evaluate the similarities between synthetic and real image data generated by GANs, various criteria are used. Statistical metrics (mean, variance, distribution, and correlation), machine learning model performance comparisons, visualization techniques (PCA and t-SNE), and feature maps are among these evaluation methods. Ensuring the reliability of these evaluations involves using multiple criteria together, having sufficient data size, ensuring the repeatability of the methods, and performing independent validations. These approaches are crucial for determining how closely GAN-generated synthetic data resembles real data and its reliability in specific applications.

4. Conclusion and Suggestions

This article discusses the increasing importance of data in today's world and the growing need for more data in the technological age, despite the current insufficiency of data in certain areas, particularly in healthcare, due to limitations such as data scarcity, data imbalance, data accessibility, and privacy. Therefore, synthetic data is required. Synthetic data can enrich and diversify real datasets. This enables the model to be trained from a broader perspective and adapt to various conditions. As a solution to the problem, this article proposes generating highly realistic synthetic data from breast cancer histopathology images using MSG-GAN and then classifying both real and synthetic data using the pre-trained ResNet18 model to determine the similarity of synthetic data to real data. Additionally, the article discusses algorithms and architectures from Convolutional Neural Network (CNN) and DL.

This research presents the results of experiments conducted on four different classification tasks to evaluate how close synthetic data is to real data. The results show that synthetic data can perform similarly to real data but must be carefully evaluated. Successful outcomes include the generation of realistic synthetic images, eliminating the need for manual visual breast cancer detection. It is predicted that the production of synthetic data in healthcare will reduce the need for human intervention in the disease detection and diagnosis process and accelerate research in the healthcare field. Therefore, it is concluded that the use of GANs in healthcare for purposes such as data augmentation, dataset enrichment, and balancing is highly beneficial and reliable.

In future studies, the focus should be on improving the process of synthetic data generation using datasets with less skewed distributions and enhancing the quality of synthetic data. Additionally, it is recommended to employ different

metrics to further measure the similarity of synthetic data to real data.

5. References

- Cruz-Roa, A., Basavanhally, A., González, FA., Gilmore, H., Feldman, MD., Ganeshan, S., Shih, N., Tomaszewski, JE., Madabhushi, A. 2014.** Automatic detection of invasive ductal carcinoma in whole slide images with convolutional neural networks. *Medical Imaging*, Doi: 10.1117/12.2043872
- Frid-Adar, M., Klang, E., Amitai, M., Goldberger, J., Greenspan, H. 2018.** Synthetic data augmentation using GAN for improved liver lesion classification. *IEEE 15th International Symposium on Biomedical Imaging (ISBI)*, pp. 289-293. Doi: 10.1109/ISBI.2018.8363576
- Goodfellow, IJ., Pouget-Abadie, J., Mirza, M., Xu, B., Warde-Farley, D., Ozair, S., Courville, AC., Bengio, Y. 2014.** Generative adversarial networks. *Communications of the ACM*, 63(10): 139-144. Doi: 10.1145/3422622
- Graves, A. 2013.** Generating sequences with recurrent neural networks. *ArXiv preprint*, abs/1308.0850.
- Gulrajani, I., Ahmed, F., Arjovsky, M., Dumoulin, V., Courville, A. 2017.** Improved training of wasserstein gans. *arXiv preprint*, arXiv:1704.00028.
- He, K., Zhang, X., Ren, S., Sun, J. 2015.** Deep residual learning for image recognition. *2016 IEEE Conference on Computer Vision and Pattern Recognition (CVPR)*, pp. 770-778. Doi: 10.1109/CVPR.2016.90
- Janowczyk, A., Madabhushi, A. 2016.** Deep learning for digital pathology image analysis: A comprehensive tutorial with selected use cases. *J Pathol Inform.*, 7(29). Doi: 10.4103/2153-3539.186902
- Karnewar, A., Wang, O. 2019.** MSG-GAN: Multi-scale gradients for generative adversarial networks. *2020 IEEE/CVF Conference on Computer Vision and Pattern Recognition (CVPR)*, pp. 7796-7805. Doi: 10.1109/CVPR42600.2020.00778
- Karras, T., Laine, S., Aila, T. 2019.** A style-based generator architecture for generative adversarial networks. *IEEE/CVF Conference on Computer Vision and Pattern Recognition (CVPR)*, pp. 4401-4410. Doi: 10.1109/CVPR.2019.00453
- Kingma, DP., Ba, J. 2015.** Adam: A method for stochastic optimization. *CoRR*, abs/1412.6980.
- LeCun, Y., Bottou, L., Bengio, Y., Haffner, P. 1998.** Gradient-based learning applied to document recognition. *Proceedings of the IEEE*, 86(11): 2278-2324. Doi: 10.1109/5.726791
- Liu, S., Setio, AAA., Ghesu, FC., Gibson, E., Grbic, S., Georgescu, B., Comaniciu, D. 2020.** No surprises: Training robust lung nodule detection for low-dose CT scans by augmenting with adversarial attacks. *IEEE Trans. Med. Imaging*, 40(1): 335-345. Doi: 10.1109/TMI.2020.3028311

- Salehinejad, H., Colak, E., Dowdell, T., Barfett, J., Valaei, S.** 2018. Synthesizing chest X-ray pathology for training deep convolutional neural networks. IEEE International Conference on Acoustics, Speech and Signal Processing (ICASSP), pp. 990-994. Doi: 10.1109/ICASSP.2018.8461382
- Teh, Y., Tan, GH., Taib, NA., Rahmat, K., Westerhout, CJ., Fadzli, F., See, MH., Jamaris, S., Yip, CH.** 2015. Opportunistic mammography screening provides effective detection rates in a limited resource healthcare system. BMC Cancer, 15: 405. Doi: 10.1186/s12885-015-1420-4
- Xu, B., Wang, N., Chen, T., Li, M.** 2015. Empirical evaluation of rectified activations in convolutional networks. ArXiv preprint, abs/1505.00853.
- Zhu, JY., Park, T., Isola, P., Efros, AA.** 2017. Unpaired image-to-image translation using cycle-consistent adversarial networks. IEEE International Conference on Computer Vision (ICCV), pp. 2242-2251. Doi: 10.1109/ICCV.2017.244



Detection of Pipes Decreasing Residual Chlorine Via Wall Reaction Coefficient in Water Distribution Networks

Su Dağıtım Şebekelerinde Bakiye Kloru Azaltan Boruların Cidar Reaksiyon Katsayısına Bağlı Olarak Tespit Edilmesi

Miraç Eryiğit

Bolu Abant Izzet Baysal University, Faculty of Engineering, Department of Environmental Engineering, Bolu, Türkiye

Abstract

This paper intended to build an optimization model utilizing the modified clonal selection algorithm (one of the famous heuristic optimization techniques) to detect pipes which reduces a residual chlorine in the water distribution networks (WDNs). MATLAB programming language was used to code the model linked with EPANET. The model performance was evaluated in a two-loop hypothetical WDN under steady-state flow conditions. In nodes of this hypothetical WDN, free chlorine concentrations were assumed to be measured since an objective function depends on model calibration. Pipes decreasing residual chlorine concentrations were determined by running the model which minimizes a total of concentration differences between estimated and measured free chlorine in each node. In order to find these pipes, pipe wall reaction rate coefficients were utilized. The model was run 10 times to obtain average reaction rate coefficient of each pipe in the WDN. After 10 runs, mean estimated and actual/real reaction rate coefficient values were almost equal ($R^2=0.99$). The optimization model appeared to be viable for detecting pipes causing a residual chlorine loss in the WDN.

Keywords: Artificial immune systems, model calibration, pipe wall reaction coefficient, residual chlorine, water distribution network.

Öz

Bu çalışmada, su dağıtım şebekelerindeki bakiye kloru azaltan boruların tespit edilmesi için modifiye klonal seçim algoritması (çoğul bilinen sezgisel optimizasyon tekniklerinden biri) kullanan bir optimizasyon modeli inşa edilmesi amaçlanmıştır. Model, EPANET ile bağlı olarak MATLAB yazılım dilinde kodlanmıştır. Modelin performansı, kararlı/sabit akım koşulları altında iki gözlü farazi bir su dağıtım şebekesinde değerlendirilmiştir. Amaç fonksiyonu, model kalibrasyonuna dayalı olduğu için şebekenin düğüm noktalarında serbest klor konsantrasyonlarının ölçüldüğü kabul edilmiştir. Bakiye klor konsantrasyonlarını azaltan borular, her bir düğüm noktasındaki ölçülen ve tahmin edilen serbest klor konsantrasyonları arasındaki farkların toplamının minimize edilmesine bağlı olarak model tarafından belirlenmiştir. Boruların belirlenmesi için boru cidarı reaksiyon hız katsayılarından yararlanılmıştır. Model 10 kez çalıştırılarak su dağıtım şebekesindeki her bir borunun ortalama reaksiyon hız katsayıları elde edilmiştir. Model 10 kez çalıştırıldıkten sonra, ortalama tahmin ve gerçek reaksiyon hız katsayı değerlerinin hemen hemen aynı olduğu sonucuna varılmıştır ($R^2=0.99$). Su dağıtım şebekesindeki bakiye klor kaybına neden olan boruların tespit edilmesi için optimizasyon modelinin uygulanabilir olduğu görülmüştür.

Anahtar Kelimeler: Yapay bağıışıklık sistemleri, model kalibrasyonu, boru cidar reaksiyon katsayısı, bakiye klor, su dağıtım şebekesi.

1. Introduction

The chlorine used to disinfect drinking and domestic water is a vital and critical chemical in terms of the public health.

Water should be supplied and distributed as disinfected from water tanks/reservoirs to settlements/residences/cities by water distribution networks (WDN). But the chlorination should be appropriately applied to avoid toxic effects of the chlorine. The total residual chlorine consists of free chlorine (hypochlorite ion/ OCl^- and hypochlorous acid/ $HOCl$) (more oxidizing/more powerful disinfectant) and chloramines (more stable and long-lived/durable) remained after a certain residence time of water, and it should be

*Corresponding author: miracyigit@hotmail.com

Miraç Eryiğit orcid.org/0000-0002-7035-7078



This work is licensed by "Creative Commons Attribution-NonCommercial 4.0 International (CC)".

provided as desired concentrations (e.g., 0.3–0.5 mg/l free chlorine) in the nodes of the WDNs (see Askenaizer 2003, Oğur et al. 2004 for the chemical reactions). The guidelines of World Health Organization (WHO) on water quality suggests limit concentrations of residual chlorine (as free chlorine) in the drinking water to the range 0.2–5 mg/l (WHO 2022). As well as free chlorine decay due to reactions with natural organic matters in the bulk flow over time, the metal pipes of the WDNs are corroded over time and cause to reduce the concentration of the residual chlorine since free chlorine oxidizes iron (Fe) released from pipe wall corrosion or pipe wall reactions/decay with biofilm (Rossman 2000, Han et al. 2017, Fisher et al. 2017a, Xu et al. 2018). Therefore, both health risk occurs and costs increase due to extreme chlorine consumption.

In the literature, there are many studies regarding residual chlorine modelling in the WDNs (Onyutha and Kwio-Tamale 2022, Elsherif et al. 2023, Hossain et al. 2022, Ardila et al. 2023). Rossman et al. (1994) improved a mass-transfer-based model which considers first-order reactions of chlorine to occur both in the bulk flow and at the pipe wall for predicting chlorine decay in the WDNs. Islam et al. (1997) proposed a new computer model using an inverse method to model chlorine concentration in the pipe networks. Rodriguez and Sérodes (1998) applied two empirical models to simulate and predict residual chlorine concentrations in the urban water systems. Li et al. (2003) built a model of residual chlorine decay in the WDN considering a chlorine consumption in reactions with chemicals in a bulk water, in corrosion process, bio-films occurring on a pipe wall, and the chlorine mass transport from a bulk water to a pipe wall. Gibbs et al. (2006) used different data-driven techniques (artificial neural networks and linear regression model) to predict concentrations of chlorine in the Hope Valley WDN (South Australia). Helbling and VanBriesen (2009) performed modeling residual chlorine related to a microbial contamination in the WDNs. Monteiro et al. (2014) carried out a chlorine decay modelling in drinking water supply systems by using EPANET MSX. Kim et al. (2014) investigated the relationship between a temporal variation in a chlorine concentration and hydraulic conditions for a pilot scale WDN (Similarly, Kim et al., 2015). Blokker et al. (2014) predicted residual chlorine concentrations in WDN under the effect of stochastic water demands. Chelsea (2016) modelled residual chlorine and trihalomethanes using EPANET for the City of Akron's WDN (Ohio, US). Fisher et al. (2017b) implemented a bulk chlorine decay model (the augmented two-reactant (2RA) model) for

simulating residuals in the WDNs. Monteiro et al. (2020) modelled pipe wall decay of chlorine residuals in a full-scale water supply system using the traditional first-order and EXPBIO models. García-Ávila et al. (2021) proposed a model of residual chlorine decay to forecast chlorine concentration levels in a real WDN during the COVID-19 pandemic. Fisher et al. (2021) modelled residual chlorine and trihalomethane profiles in the WDNs after pre-chlorination of the water treatment plant. Absalan et al. (2022) performed predictions of chlorine and trihalomethanes in the WDN in southern Quebec (Canada). Abhijith and Ostfeld (2022) developed a novel computer-based tool (EPANET-C) to simulate variations in residual chlorine concentrations in the WDNs. Wu and Dorea (2022) applied basic chlorine decay kinetic models in the literature for humanitarian emergency water supply. Yimer et al. (2022) conducted modelling of residual chlorine in the Arada sub-city supply system (Addis Ababa water supply distribution systems, Ethiopia) by using Water CAD. Onyutha (2022) predicted residual chlorine concentrations in drinking water using machine and deep learning techniques. Wang (2022) optimized the chlorine injection mass to maintain chlorine in the WDN by using a fuzzy chance-constrained optimization model. Huang and Wang (2023) developed a double-sided fuzziness chance-constrained programming model to cut down costs of the disinfectant booster under uncertainty. Kyritsakas et al. (2023) designed a data-driven model that uses different machine learning algorithms for the prediction of chlorine losses in water distribution trunk mains. Wang et al. (2023) proposed an improved VRC-3R- residual chlorine decay model in the UV/Cl₂ process in the WDN. Wongpeerak et al. (2023) applied a novel method based on a simple theoretical analysis (theoretical disinfectant mass loss models) to simulate residual chlorine concentrations in the real WDNs in Thailand. Enriquez et al. (2023) estimated chlorine and trihalomethanes concentrations in the trunk network of Bogota's WDN (Colombia) by using evolutionary polynomial regression models and artificial neural networks. Belcaid et al. (2023) presented a new methodology for chlorine decay modeling in the WDN of Mohammedia City (Morocco). Helm et al. (2024) implemented machine learning models by developing a gradient-boosting method to forecast a free chlorine residual in a drinking water treatment plant (Georgia, U.S.). Li et al. (2024) improved a novel gated graph neural network model/approach for a chlorine prediction in nodes of a real WDN (Yantian WDN, China).

These studies generally focused on modelling of residual chlorine concentrations (not detecting pipes which decrease the concentrations). By considering this gap in this broad literature, this study aimed to develop a heuristic optimization model based on model calibration to detect pipes which reduce residual chlorine concentrations (as free chlorine) in nodes of the WDNs (considering pipe wall reaction coefficients).

2. Material and Methods

2.1. Algorithm

The heuristic optimization model was coded by linking with EPANET software in MATLAB programming language. EPANET, a commonly known WDN simulation software, was chosen for the hydraulic calculations since it is simple and efficient (also, it can be linked with MATLAB). It was developed as a tool for understanding the movement and fate of drinking water constituents within WDNs and can be used for many different applications in distribution systems analysis (Rossman 2000). As for MATLAB, it is a programming and numeric computing platform used by engineers and scientists to analyze data, develop/improve algorithms, and build models.

The model uses the modified clonal selection algorithm (modified Clonalg) (one of the artificial immune systems) developed by Eryiğit (2015) as a heuristic optimization method. (See Figure 1). This algorithm mimics the clonal selection theory of the natural immune system. In Figure 1, Ab is the antibody population randomly created, f is the antibody's antigenic affinity (representing an objective function), C is the cloned antibody population, C^* is the mutated antibody population. The algorithm process can be briefly defined as follows (Eryiğit 2015, Eryiğit and Sulaiman 2022):

- 1) An antibody set/population (Ab) is randomly generated.
- 2) An objective function (f) is computed to be minimized or maximized (optimization) for each individual in Ab.
- 3) All individuals are cloned/copied.
- 4) All antibody clones (C) are exposed to the maturation (mutation) process which is inversely proportional to their antigenic affinities. Besides, new antibody genes are generated for the clones in this step.
- 5) An objective function (f) is recalculated for each matured clone in C^* .

- 6) The matured/mutated clones owning the highest affinity (best individuals) are chosen to replace the antibodies which own the lowest affinity in Ab.

This loop goes on until the iteration reaches a maximum number (or a certain error/difference between worst and best individuals in Ab). Hence, the optimum result can be obtained.

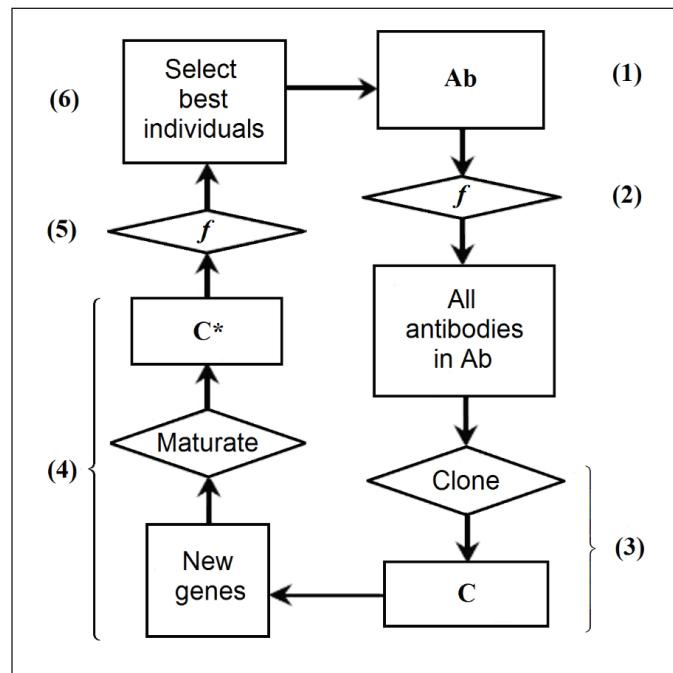


Figure 1. The flow diagram of the modified Clonalg (Eryiğit 2015).

In the modified Clonalg (step 4), new genes are produced for each antibody clone by taking in consideration a certain probability which is referred to “probability rate” (PR) depending on an optimization problem. The antibody clone number can be computed as below (De Castro and Von Zubén 2002):

$$N_c = \sum_{i=1}^{N_{Ab}} \text{round}(\beta \cdot N_{Ab}) \quad i = 1, \dots, N_{Ab} \quad (1)$$

where N_c is the total clone number, β is the coefficient of multiplying, and “round” is a rounding operator for the integer.

A mutation rate can be obtained as the following (De Castro and Von Zubén 2002):

$$\alpha_i = \exp(-\rho \cdot f_i) \quad (2)$$

where α_i is the mutation rate, ρ is the coefficient of decay,

and f_i is a value of the antigenic affinity (value of the objective function) normalized between 0 and 1.

Population Ab is defined as shown below:

$$\begin{bmatrix} Ab_1 = x_{11} \dots & x_{1j} & \dots x_{1nd} \\ \vdots & \ddots & \vdots \\ Ab_i = x_{i1} & \dots & x_{ind} \\ \vdots & \ddots & \vdots \\ Ab_{N_{Ab}} = x_{N_{Ab}1} \dots & x_{N_{Ab}nd} & \dots x_{N_{Ab}nd} \end{bmatrix} \rightarrow \begin{bmatrix} f_1 \\ \vdots \\ f_i \\ \vdots \\ f_{N_{Ab}} \end{bmatrix} \quad (3)$$

$$i = 1, \dots, N_{Ab} \quad j = 1, \dots, nd$$

where N_{Ab} is the total antibody number (population Ab), x_{ij} is the gene of Ab_i (decision variable of f_i), nd is the gene number of Ab_i . In this study, x_{ij} corresponds to the wall reaction rate coefficient (K_w) of each pipe in the WDN. f was minimized depending on pipe wall reaction coefficients (genes) produced and mutated/matured through the algorithm processes. The objective function (f) is based on model calibration in the study:

$$\text{minimize} \sum_{i=1}^{NRC} 10^3 | RC_{ipred} - RC_{iobs} | \quad (4)$$

where RC_{ipred} is the i -th predicted residual chlorine, RC_{iobs} is the i -th observed residual chlorine, NRC is the number of observed residual chlorine values in nodes of the WDN.

2.2. Implementation

The optimization model was applied to a two-loop hypothetical WDN consisting of 6 nodes (junctions), 8 pipes and one reservoir under steady-state gravity flow conditions in EPANET (See Figure 2). The data of the WDN was given in Table 1. This scenario includes some assumptions as follows:

- 1) Free chlorine concentrations are assumed to be measured in the WDN nodes in each hour for 24 hours.
- 2) Bulk reaction coefficient (K_b) in the WDN is assumed as $-0.01/\text{day}$ (most of the chlorine decay in the network is occurring in the reservoir and residual chlorine concentration is 1 mg/l).
- 3) Pipe corrosion and biofilm are dominant in the system because of pipe age and material.
- 4) All pipe wall reaction coefficients in the WDN are unknown.

The residual chlorine concentrations (as free chlorine) measured in the nodes after 24 hours and pipe wall reaction coefficients (K_w) are shown in Figure 2. First-order ($n=1$) re-

actions/decay kinetics ($R = K_b \cdot C^n$ and $R = (A/V) \cdot K_w \cdot C^n$ for bulk and wall reactions (R), respectively. A/V : The surface area per unit volume within a pipe, C : The reactant concentration) were used for the chlorine, and lower and upper limits for pipe wall reaction coefficient were assigned as -1.5 and 0 m/day , respectively (Rossman 2000, Rossman et al. 2020). The optimization model reaches a global minimum (f) by assigning coefficient values in this range $[-1.5, 0]$ to the pipes of the WDN during the iteration.

The analyses were carried out by using a computer with Intel Core I5-8300H CPU 2.3 GHz, and the model was run 10 times with maximum iteration number (I_{\max}) of 1000 for examining a model stability. In this study, N_{Ab} , β , ρ , and PR were assigned as 30, 1, 0.5, and 0.2, respectively.

3. Results and Discussion

There are 8 pipes in the WDN. Their wall reaction coefficients are assumed to be unknown. As it is seen in Figure 2, Pipe 1, 3, 5 and 8 (red lines with -1.5 m/day) cause a higher loss of residual chlorine concentration while

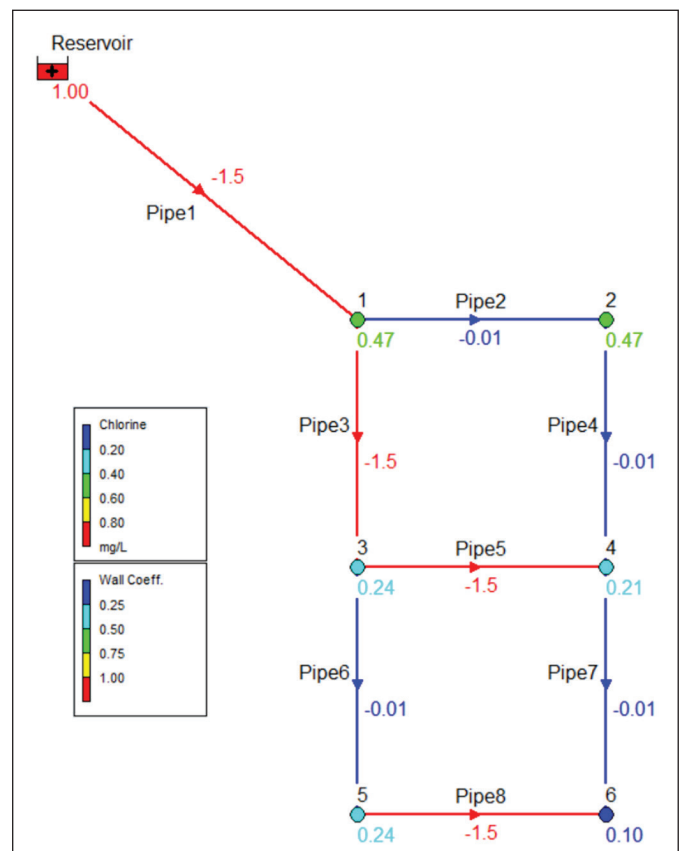


Figure 2. Layout and operational data of the two-loop hypothetical WDN.

Table 1. The main characteristics of the two-loop hypothetical WDN.

Node	Elevation (m)	Base Demand (l/s)	Pipe	Length (m)	Diameter (mm)	C_p
Reservoir	150	-	1	5000	450	130
1	80	20	2	3000	250	140
2	70	20	3	3000	300	130
3	70	20	4	3000	150	140
4	60	20	5	3000	200	130
5	60	20	6	3000	250	140
6	60	20	7	3000	150	140
			8	3000	150	130

Table 2. Results of predicted wall reaction coefficient for each pipe in the WDN after 10 runs.

Run No	f	Pipe 1 (m/day)	Pipe 2 (m/day)	Pipe 3 (m/day)	Pipe 4 (m/day)	Pipe 5 (m/day)	Pipe 6 (m/day)	Pipe 7 (m/day)	Pipe 8 (m/day)	Run Time (min)
1	0.34	-1.5	-0.01	-1.5	-0.01	-1.5	-0.01	-0.02	-1.5	38.3
2	0.21	-1.5	-0.01	-1.5	-0.01	-1.5	-0.01	-0.02	-1.5	38.7
3	0.30	-1.5	-0.01	-1.5	-0.01	-1.5	-0.01	-0.02	-1.5	39.0
4	0.27	-1.5	-0.01	-1.5	-0.01	-1.5	-0.01	-0.01	-1.5	38.8
5	0.27	-1.5	-0.01	-1.5	-0.01	-1.5	-0.01	-0.01	-1.5	38.4
6	0.80	-1.5	-0.01	-1.5	-0.01	-1.5	-0.01	-0.13	-1.01	38.4
7	0.15	-1.5	-0.01	-1.5	-0.01	-1.5	-0.01	-0.01	-1.5	38.5
8	0.37	-1.5	-0.01	-1.5	-0.01	-1.5	-0.01	-0.01	-1.5	38.5
9	0.24	-1.5	-0.01	-1.5	-0.01	-1.5	-0.01	-0.01	-1.5	38.4
10	0.31	-1.5	-0.01	-1.5	-0.01	-1.5	-0.01	-0.01	-1.5	38.3
Mean	0.32	-1.5	-0.01	-1.5	-0.01	-1.5	-0.01	-0.02	-1.45	38.5
Std	0.180	0	0.0004	0	0.001	0	0.0004	0.037	0.154	0.23
Min	0.15	-1.5	-0.01	-1.5	-0.01	-1.5	-0.01	-0.13	-1.5	38.3
Max	0.80	-1.5	-0.01	-1.5	-0.01	-1.5	-0.01	-0.01	-1.01	39.0

Pipe 2, 4, 6 and 7 (blue lines with -0.01 m/day) cause a lower loss in the WDN. After the model was run 10 times, results obtained in each run were given in Table 2. Also, the comparison of mean predicted coefficients and actual pipe wall coefficients was shown in Table 3 and Figure 3. As it is seen in Table 2, the model was able to determine accurately wall reaction coefficients of all pipes in all runs except run 6 (ratio of 9/10 runs). This demonstrates that the optimization model is stable. Mean predicted and actual values are almost equal each other ($R^2=0.99$) (See Table 3 and Figure 3). Consequently, the pipes reducing residual chlorine concentrations in the WDN were successfully detected by the model (Pipe corrosion and biofilm are assumed to be dominant in the network). By detecting these pipes, it can be said that we also specify the old/worn

Table 3. A comparison of mean predicted and actual pipe wall reaction coefficients.

Pipe	*Mean Predicted Coefficient (m/day)	Actual Coefficient (m/day)
1	-1.5	-1.5
2	-0.01	-0.01
3	-1.5	-1.5
4	-0.01	-0.01
5	-1.5	-1.5
6	-0.01	-0.01
7	-0.02	-0.01
8	-1.45	-1.5

*Average of 10 runs

out pipes (especially corroded metal pipes) which may cause pressure losses in the WDN because a higher Darcy-Weisbach roughness coefficient or a lower Hazen-Williams C-factor results in a greater frictional head loss in a flow along the pipe (Rossman 2000). The pipe wall reaction coefficient (K_w) can be assigned as the function of the roughness coefficient for each pipe in EPANET. For this, site-specific field measurements should be performed. In this study, Hazen-Williams C-factors (C_p) for the frictional head loss were selected independently from the pipe wall reaction coefficients (K_w) because the hypothetical WDN was applied.

On the other hand, the optimization model can detect the pipes which decrease residual chlorine with mean run time of 38.5 minutes. Run time depends on iteration number (or error/difference between minimum and maximum affinity values of antibodies in the population) and population number as well as the algorithm structure. Better results (ratio of 10/10 runs) might be obtained by increasing population and iteration numbers (or assigning lower error

value). But, this makes the run time longer. So, N_{ab} of 30 and I_{max} of 1000 were enough to obtain acceptable/satisfying results during the analyses.

The optimization model obtained good results under steady-state flow conditions. Of course, flows are not steady/constant in real WDNs. However, dynamic flow conditions could be neglectable for this study because the bulk flow reaction was assumed to be too low (-0.01/day) in the WDN (most of the chlorine decay is occurring in the reservoir) according to the scenario.

In the related literature, mostly residual chlorine concentrations have been modeled in the WDNs. The present study differs from the others because pipes reducing the chlorine concentrations were detected instead of modelling the concentrations in the WDNs. Thus, it can be said the paper is the first optimization study based on K_w in terms of the detection of the pipes decreasing the residual concentrations. While reviewing the literature, it is seen that average K_w value of -0.066 m/day was (coincides with the range [-1.5, 0]) experimentally determined by García-Ávila et al. (2021). But experimental methods could be expensive and time-consuming. Zaghini et. al. (2024) assumed an overall rate coefficient K (1/time) combining K_b and K_w due to the difficulties of the accurate estimation of individual K_b and K_w decay contributions. They obtained K values between -0.4 and -1.1 (1/day) for the multiple-source WDNs. But K_w values were uncertain since they were included in the overall rate coefficients. Therefore, the pipes reducing the chlorine concentrations were unknown.

4. Conclusion and Suggestions

The worn-out pipes in the water supply have a risk to the public health due to corrosion and biofilm (pathogens etc.) and increase the costs of the chlorination. These pipes should be detected and renewed as quickly as possible. For this problem, the optimization model could be utilized. In this study, wall reaction coefficients (K_w) of the pipes in the WDN were determined by utilizing the model calibration. Thus, the pipes reducing residual chlorine concentrations were able to be detected by the optimization model considering their reaction coefficients (since pipe corrosion and biofilm are dominant in the present WDN). This also indicates that these pipes are old (especially corroded pipes) and decrease pressure heads desired in the nodes of the WDN. Consequently, the model is useful to detect pipes which decrease both residual chlorine concentrations and pressures by measuring only free chlorine in the nodes of the

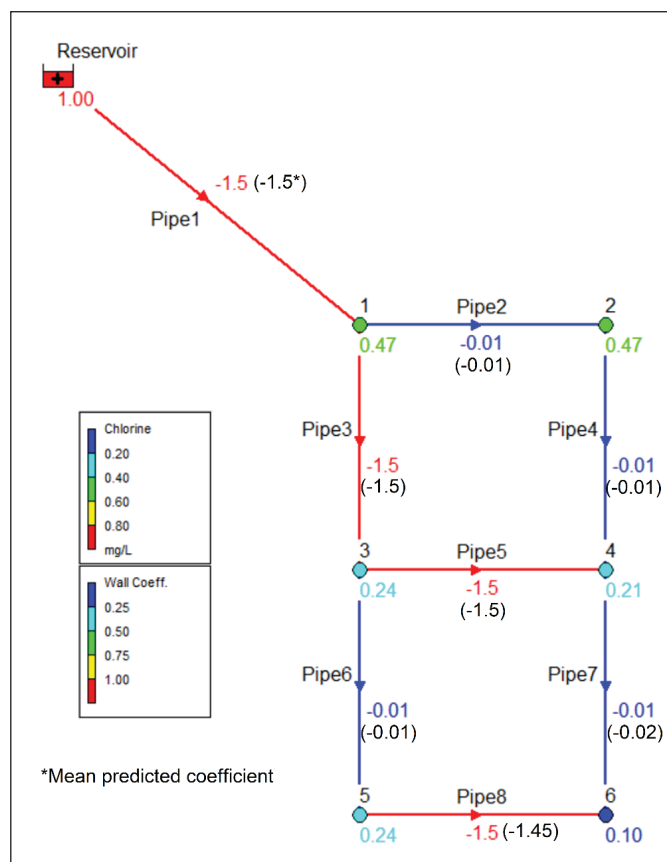


Figure 3. Mean predicted and actual pipe wall reaction coefficients (m/day).

WDN in case of domination/dominance of corrosion and biofilm. K_w coefficients could be assigned as the function of the roughness coefficient/C-factors (C_p) for each pipe of the real WDN to show relationship between the pipes causing the frictional head losses and chlorine losses in the future studies.

The optimization model was run under steady-state flow conditions. Therefore, it might need to be tested under non-steady state flow conditions in real WDNs in the future studies. However, this study is a pioneer in terms of detection of pipes resulting in chlorine losses in the WDN and inspires the researchers about this subject.

Author contribution: The entire study was performed by the author.

5. References

- Abhijith, GR., Ostfeld, A. 2022.** Contaminant Fate and Transport Modeling in Distribution Systems: EPANET-C. Water, 14: 1665.
- Absalan, F., Hatam, F., Barbeau, B., Prévost, M., Bichai, F. 2022.** Predicting Chlorine and Trihalomethanes in a Full-Scale Water Distribution System under Changing Operating Conditions. Water, 14(22): 3685. <https://doi.org/10.3390/w14223685>.
- Ardila, A., Rodriguez, MJ., Pelletier, G. 2023.** Spatiotemporal optimization of water quality degradation monitoring in water distribution systems supplied by surface sources: A chronological and critical review. Journal of Environmental Management, 337: 117734. Doi: 10.1016/j.jenvman.2023.117734.
- Askenaizer, D. 2003.** Drinking Water Quality and Treatment, Editor(s): Robert A. Meyers, Encyclopedia of Physical Science and Technology (Third Edition), Academic Press, 651-671, <https://doi.org/10.1016/B0-12-227410-5/00186-1>.
- Belcaid, A., Faycal, T., Tounssi, TA. 2023.** Chlorine Decay Modeling in a Water Distribution Network in Mohammedia City, Morocco. Ecological Engineering and Environmental Technology, 24(2): 269-278. Doi: <https://doi.org/10.12912/27197050/157538>.
- Blokker, M., Vreeburg, J., Speight, V. 2014.** Residual Chlorine in the Extremities of the Drinking Water Distribution System: The Influence of Stochastic Water Demands. Procedia Engineering, 70: 172-180. Doi: 10.1016/j.proeng.2014.02.020.
- Chelsea, J. 2016.** Operational and Water Quality Analysis for the City of Akron's Water Treatment Plant and Distribution System. Honors Research Projects, 369.
- De Castro LN., Von Zuben FJ. 2002.** Learning and optimization using the clonal selection principle. IEEE Transactions on Evolutionary Computation, 6(3): 239-251. Doi: 10.1109/TEVC.2002.1011539.
- Enriquez, L., Saldarriaga, J., Berardi, L., Laucelli, D., Giustolisi, O. 2023.** Using artificial intelligence models to support water quality prediction in water distribution networks. IOP Conference Series: Earth and Environmental Science, 1136: 012009. Doi: 10.1088/1755-1315/1136/1/012009.
- Elsherif, SM., Wang, S., Taha, AF., Sela, L., Giacomon, MH., Abokifa, AA. 2023.** Control-theoretic modeling of multi-species water quality dynamics in drinking water networks: Survey, methods, and test cases. Annual Reviews in Control, 55: 466-485, doi.org/10.1016/j.arcontrol.2022.08.003.
- Eryiğit M. 2015.** Cost optimization of water distribution networks by using artificial immune systems. Journal of Water Supply: Research and Technology-AQUA, 64(1): 47-63. <https://doi.org/10.2166/aqua.2014.031>.
- Eryiğit, M., Sulaiman, SO. 2022.** Specifying optimum water resources based on cost-benefit relationship for settlements by artificial immune systems: Case study of Rutba City, Iraq. Water Supply, 22(6): 5873-5881. <https://doi.org/10.2166/ws.2022.227>.
- García-Ávila, F., Avilés-Añazco, A., Ordoñez-Jara, J., Guanuchi-Quezada, C., Pino, LF., Ramos-Fernández, L. 2021.** Modeling of residual chlorine in a drinking water network in times of pandemic of the SARS-CoV-2 (COVID-19). Sustainable Environment Research, 31(12). <https://doi.org/10.1186/s42834-021-00084-w>.
- Gibbs, MS., Morgan, N., Maier, HR., Dandy, GC., Nixon, JB., Holmes, M. 2006.** Investigation into the relationship between chlorine decay and water distribution parameters using data driven methods. Mathematical and Computer Modelling, 44(5-6): 485-498. Doi: 10.1016/j.mcm.2006.01.007.
- Han, KS., Park, JH., Park, YB., Kim, SJ., Kim, HD., Choi, YJ., Choi, IC., Hong, SH. 2017.** Effect of Residual Chlorine Concentration on Water Pipe Corrosion. ECS Meeting Abstracts, MA2017-02, 687. Doi: 10.1149/MA2017-02/9/687.
- Helbling, DE., VanBriesen, JM. 2009.** Modeling Residual Chlorine Response to a Microbial Contamination Event in Drinking Water Distribution Systems. Journal of Environmental Engineering, 135(10): 918-927. [https://doi.org/10.1061/\(ASCE\)EE.1943-7870.0000080](https://doi.org/10.1061/(ASCE)EE.1943-7870.0000080).
- Helm, W., Zhong, S., Reid, E., Igou, T., Chen, Y. 2024.** Development of gradient boosting-assisted machine learning data-driven model for free chlorine residual prediction. Frontiers of Environmental Science and Engineering, 18(17). <https://doi.org/10.1007/s11783-024-1777-6>.

- Hossain, S., Chow, CWK., Cook, D., Sawade, E., Hewa, GA. 2022.** Review of chloramine decay models in drinking water system. *Environmental Science: Water Research and Technology*, 8(5): 926-948. <https://doi.org/10.1039/D1EW00640A>.
- Huang, X., Wang, Y. 2023.** Optimization of injection costs for water distribution systems under double-sided fuzziness. *Urban Water Journal*, 20(5): 513-520. Doi: 10.1080/1573062X.2023.2184702.
- Fisher, I., Kastl, G., Sathasivan, A. 2017a.** New model of chlorine-wall reaction for simulating chlorine concentration in drinking water distribution systems. *Water Research*, 125: 427-437. <https://doi.org/10.1016/j.watres.2017.08.066>.
- Fisher, I., Kastl, G., Sathasivan, A. 2017b.** A comprehensive bulk chlorine decay model for simulating residuals in water distribution systems. *Urban Water Journal*, 14(4): 361-368. <https://doi.org/10.1080/1573062X.2016.1148180>.
- Fisher, I., Kastl, G., Sathasivan, A., Catling, R. 2021.** Modelling chlorine residual and trihalomethane profiles in water distribution systems after treatment including pre-chlorination. *Journal of Environmental Chemical Engineering*, 9(4): 105686. <https://doi.org/10.1016/j.jece.2021.105686>.
- Islam, MR., Chaudhry, MH., Clark, RM. 1997.** Inverse Modeling of Chlorine Concentration in Pipe Networks under Dynamic Condition. *Journal of Environmental Engineering*, 123(10): 1033-1040. [https://doi.org/10.1061/\(ASCE\)0733-9372\(1997\)123:10\(1033\)](https://doi.org/10.1061/(ASCE)0733-9372(1997)123:10(1033)).
- Kim, H., Kim, S., Koo, J. 2014.** Prediction of Chlorine Concentration in Various Hydraulic Conditions for a Pilot Scale Water Distribution System. *Procedia Engineering*, 70: 934-942. <https://doi.org/10.1016/j.proeng.2014.02.104>.
- Kim, H., Kim, S., Koo, J. 2015.** Modelling Chlorine Decay in a Pilot Scale Water Distribution System Subjected to Transient. *Procedia Engineering*, 119: 370-378. <https://doi.org/10.1016/j.proeng.2015.08.897>.
- Kyritsakas, G., Speight, V., Boxall, J. 2023.** A data driven model for the prediction of chlorine losses in water distribution trunk mains. *IOP Conference Series: Earth and Environmental Science*, 1136: 012048. Doi:10.1088/1755-1315/1136/1/012048.
- Li, X., Gu, DM., Qi, JY., M, U., Zhao, HB. 2003.** Modeling of residual chlorine in water distribution system. *Journal of Environmental Sciences*, 15(1): 136-144.
- Li, Z., Liu, H., Zhang, C., Fu, G. 2024.** Real-time water quality prediction in water distribution networks using graph neural networks with sparse monitoring data. *Water Research*, 250: 121018. <https://doi.org/10.1016/j.watres.2023.121018>.
- Monteiro, L., Carneiro, J., Covas, DIC. 2020.** Modelling chlorine wall decay in a full-scale water supply system. *Urban Water Journal*, 17(8): 754-762. <https://doi.org/10.1080/1573062X.2020.1804595>.
- Monteiro, L., Figueiredo, D., Dias, S., Freitas, R., Covas, D., Menaia, J., Coelho, ST. 2014.** Modeling of Chlorine Decay in Drinking Water Supply Systems Using EPANET MSX. *Procedia Engineering*, 70: 1192-1200. <https://doi.org/10.1016/j.proeng.2014.02.132>.
- Öğur, R., Tekbaş, ÖF., Hasde, M. 2004.** Klorlama Rehberi (İçme ve Kullanma Sularının Klorlanması). *Gülhane Askeri Tip Akademisi*, Ankara.
- Onyutha, C. 2022.** Multiple Statistical Model Ensemble Predictions of Residual Chlorine in Drinking Water: Applications of Various Deep Learning and Machine Learning Algorithms. *Journal of Environmental and Public Health*, 7104752. <https://doi.org/10.1155/2022/7104752>.
- Onyutha, C., Kwio-Tamale, JC. 2022.** Modelling chlorine residuals in drinking water: a review. *International Journal of Environmental Science and Technology*, 19: 11613-11630. <https://doi.org/10.1007/s13762-022-03924-3>.
- Rodriguez, MJ., Sérodes, JB. 1998.** Assessing empirical linear and non-linear modelling of residual chlorine in urban drinking water systems. *Environmental Modelling and Software*, 14(1): 93-102. [https://doi.org/10.1016/S1364-8152\(98\)00061-9](https://doi.org/10.1016/S1364-8152(98)00061-9).
- Rossmann, L. 2000.** EPANET 2 Users Manual, Technical Report EPA/600/R-00/057. Water Supply and Water Resources Division, National Risk Management Research Laboratory, U.S., Environmental Protection Agency, Cincinnati, OH.
- Rossmann, L., Woo, H., Tryby, M., Shang, F., Janke, R., Haxton, T. 2020.** EPANET 2.2 User Manual. U.S. Environmental Protection Agency, Washington, DC, EPA/600/R-20/133.
- Rossmann, LA., Clark, RM., Grayman, WM. 1994.** Modeling Chlorine Residuals in Drinking-Water Distribution Systems. *Journal of Environmental Engineering*, 120(4): 803-820. [https://doi.org/10.1061/\(ASCE\)0733-9372\(1994\)120:4\(803\)](https://doi.org/10.1061/(ASCE)0733-9372(1994)120:4(803)).
- Wang, H., Wang, B., Peng, Y., Crittenden, JC., Pan, H., Wang, L. 2023.** Improved VRC-3R- model for bulk water residual chlorine decay in the UV/Cl₂ process for a water distribution network. *Environmental Science: Water Research and Technology*, 9: 308-330. <https://doi.org/10.1039/D2EW00647B>.
- Wang, Y. 2022.** Optimization of booster chlorination for water distribution system under dual uncertainties. *Urban Water Journal*, 19(4): 363-373. <https://doi.org/10.1080/1573062X.2021.2016868>.

- Wongpeerak, K., Charuwimolkul, N., Changklom, J., Lipiwattanakarn, S., Pornprommin, A.** 2023. Theoretical Estimation of Disinfectant Mass Balance Components in Drinking Water Distribution Systems. *Water*, 15(2): 368. <https://doi.org/10.3390/w15020368>.
- World Health Organization** 2022. Guidelines for drinking-water quality: fourth edition incorporating the first and second addenda. Geneva, Licence: CC BY-NC-SA 3.0 IGO.
- Wu, H., Dorea, CC.** 2022. Evaluation and application of chlorine decay models for humanitarian emergency water supply contexts. *Environmental Technology*, 43(21): 3221-3230. <https://doi.org/10.1080/09593330.2021.1920626>.
- Xu, J., Huang, C., Shi, X., Dong, S., Yuan, B., Nguyen, TH.** 2018. Role of drinking water biofilms on residual chlorine decay and trihalomethane formation: An experimental and modeling study. *Science of The Total Environment*, 642: 516-525. <https://doi.org/10.1016/j.scitotenv.2018.05.363>.
- Yimer, T., Desale, T., Asmare, M., Endris, S., Ali, A., Metaferia, G.** 2022. Modeling of Residual Chlorine on Addis Ababa Water Supply Distribution Systems. *Water Conservation Science and Engineering*, 7: 443-452. <https://doi.org/10.1007/s41101-022-00153-0>.
- Zaghini, A., Gagliardi, F., Marsili, V., Mazzoni, F., Tirello, L., Alvisi, S., Franchini, M.** 2024. A Pragmatic Approach for Chlorine Decay Modeling in Multiple-Source Water Distribution Networks Based on Trace Analysis. *Water*, 16, 345. <https://doi.org/10.3390/w16020345>.



Forecasting Earthquake Impact Scenarios in Istanbul with Machine Learning Algorithms

İstanbul'daki Deprem Etki Senaryolarının Makine Öğrenmesi Algoritmaları ile Tahmin Edilmesi

Remzi Gürfidan¹ , Mehmet Ali Yalçınkaya^{2*}

¹Isparta University of Applied Sciences, Yalvaç Technical Sciences Vocational School, Department of Computer Technologies, Isparta, Türkiye

²Kırşehir Ahi Evran University, Faculty of Engineering and Architecture, Department of Computer Engineering, Kırşehir, Türkiye

Abstract

This study employs machine learning algorithms to forecast the impacts of a potential magnitude 7.5 earthquake in Istanbul, focusing on casualty rates, hospitalization needs, and temporary shelter requirements. Using a dataset compiled from the Istanbul Metropolitan Municipality Open Data Portal and the Turkish Statistical Institute, the research assesses Gradient Boosting, AdaBoost, Random Forest, and ExtraTrees algorithms. Gradient Boosting emerged as the most effective model, exhibiting high accuracy and low prediction errors in determining disaster impacts. This approach underscores the critical role of advanced analytics in enhancing urban disaster preparedness and management, providing valuable insights for policymaking and infrastructure development in earthquake-prone areas.

Keywords: Earthquake impact forecasting, disaster preparedness, machine learning, urban risk management.

Öz

Bu çalışmada, İstanbul'da olası bir 7.5 büyüklüğündeki depremin etkilerini, özellikle de can kaybı sayısı, hastaneye ihtiyaç duyacak kişi sayısı ve geçici barınma ihtiyacı duyan kişi sayısını tahmin etmek için makine öğrenmesi algoritmaları kullanılmaktadır. İstanbul Büyükşehir Belediyesi Açık Veri Portalı ve Türkiye İstatistik Kurumu'ndan derlenen bir veri seti kullanılarak Gradyan Artırma (Gradient Boosting), Uyarlanabilir Artırma (AdaBoost), Rastgele Orman (Random Forest) ve Ekstra Ağaçlar (ExtraTrees) algoritmaları değerlendirilmiştir. Gradient Boosting modeli, yüksek doğruluk ve düşük tahmin hataları ile en etkili model olarak öne çıkmıştır. Bu yaklaşım, gelişmiş analitiklerin kentsel afet hazırlığı ve yönetimini geliştirmeye konusundaki kritik rolünü vurgulamakta ve depreme eğilimli bölgelerdeki alınacak önlemler ve altyapı gelişimi için değerli öngörüler sağlamaktadır.

Anahtar Kelimeler: Deprem etki tahmini, afet hazırlığı, makine öğrenmesi, kentsel risk yönetimi.

1. Introduction

Earthquakes rank among the most devastating natural disasters globally, causing significant destruction and loss of life. Turkey, due to its geological location, is situated in one of the most active earthquake zones in the world. The North Anatolian Fault Line (NAF) runs through the northern part of the country, causing significant seismic

activity. Historically, this fault line has been responsible for most of the devastating earthquakes in Turkey. Notably, the major tremor on August 17, 1999, known as the Marmara Earthquake, occurred along this fault line. This earthquake caused extensive destruction, particularly in Kocaeli and its surroundings, leading to over 17,000 deaths and injuring tens of thousands, according to official reports (Erdik 2001). The scale of the destruction was recorded as one of the most severe disasters in Turkey's modern history.

The economic impact of the Marmara Earthquake was also severe. The direct damage and subsequent economic losses amounted to over 25 billion dollars, constituting approximately 2-3% of Turkey's gross domestic product (GDP) (Ambraseys 2001). Workplaces were destroyed,

*Corresponding author: mehmetyalcinkaya@ahievran.edu.tr

Remzi Gürfidan orcid.org/0000-0002-4899-2219

Mehmet Ali Yalçınkaya orcid.org/0000-0002-7320-5643



This work is licensed by "Creative Commons Attribution-NonCommercial 4.0 International (CC)".

infrastructure was damaged, and many industrial facilities had to cease operations. This situation created long-term negative effects on both local and national economies. Moreover, with thousands left homeless, the state faced significant responsibilities for housing and reconstruction. The economic recovery took years and was significantly supported by international aid. This heavy burden led to major changes in Turkey's urban transformation and disaster management policies, promoting the development of stronger building standards and effective disaster management strategies (Stein 2000).

The earthquakes centered in Kahramanmaraş last year, particularly the main shock of magnitude 7.8 on February 6, 2023, caused serious destruction in Southern and Central Turkey. This disaster resulted in the loss of thousands of lives and left hundreds of thousands homeless. The provinces of Hatay, Kahramanmaraş, Gaziantep, Malatya, and Adiyaman saw the most severe damage, accounting for 81% of the estimated total damage. This calamity is recorded as the largest natural disaster Turkey has faced in the last 80 years. Furthermore, these provinces house approximately 7.4% of Turkey's population, significantly impacting the region's socio-economic structure (World Bank 2023). Economically, the cost of the earthquake to Turkey is estimated at 34.2 billion dollars in direct physical damages, equating to about 4% of the country's GDP in 2021 (Korkut et al. 2023).

Minimizing losses caused by earthquakes is possible through preventative measures and preparations. Earthquake scenario analysis allows for the anticipation of potential earthquake effects and the planning of necessary precautions based on this information. Particularly in major urban areas, the preparation of such scenarios can significantly reduce the loss of life and property (Jaiswal and Wald 2010).

Istanbul, as Turkey's largest metropolis, is distinguished by its dense population and cosmopolitan structure. The city harbors a serious risk of a major earthquake due to sporadic urbanization and a high proportion of structurally unsound buildings. The potential devastation of an earthquake in Istanbul is feared due to the concentration of the nation's population and industrial density in this region (Parsons 2000).

The literature contains various studies on estimating potential fatalities and other damages prior to earthquakes. In China, data from 84 earthquakes occurring between 1970 and 2017 were tested using methods such as elaboration likelihood model (ELM), artificial neural networks, support vector machine (SVM), and Gaussian curves. The study

achieved an r squared (R^2) value of 96% (Xing et al. 2020). Another study analyzed 30 historical earthquakes in China, comparing the performance of the support vector regression (SVR) model with other machine learning (ML) methods. The comparisons concluded that the SVR model produced more successful outcomes than other models (Li et al. 2021). Additionally, another study attempted to estimate the number of potential fatalities in a severe earthquake using logistic regression on a dataset containing four attributes (age, gender, physical disability, and socioeconomic status). In one of the studies on earthquakes in Turkey, data collected from buildings damaged after three major earthquakes were used to predict structural damage and mitigate potential harms. This process demonstrated that the SVR model yielded better results than other models (Arslan et al. 2017). Corbi et al. (2019) discuss how machine learning can predict the timing and size of earthquakes by reconstructing complex system dynamics in subduction zones. Rouet-Leduc et al. (2017) show how machine learning can predict laboratory earthquakes based on acoustic signals previously thought to be noise, potentially improving earthquake forecasting. Ahamed and Daub (2019) present a machine learning model for predicting whether an earthquake rupture will propagate, using neural networks and random forest algorithms.

This study predicted the number of loss of lifes, the number of people needing hospital treatment, and the number of people requiring temporary shelter that a potential 7.5 magnitude earthquake could cause during night hours in Istanbul. The data used for this analysis were obtained from the Istanbul Metropolitan Municipality (IMM) Open Data Portal and the Turkish Statistical Institute (TUIK). Initially, the "Earthquake Scenario Analysis Results" and "Neighborhood-Based Building Counts" datasets from the Istanbul Metropolitan Municipality Open Data Portal were merged. Subsequently, population and area data for each neighborhood in Istanbul were obtained from TUIK and added to the dataset. This merger produced a comprehensive and original dataset. Various ML techniques and algorithms were used on the collected dataset to perform detailed analyses. These analyses are critical for better understanding the potential effects of earthquakes and planning necessary precautions in advance.

2. Material and Methods

This section describes the dataset used in the study, the algorithms applied, and the metrics employed to evaluate the data derived from these algorithms.

2.1. Dataset

In this study, a hybrid dataset was constructed. The attributes included in this dataset were obtained from various sources. There are 12 different attributes within this dataset. These attributes and their value ranges are shown in Table 1. The first attribute in the dataset, "Population Density," was calculated using the population and area information for each neighborhood in Istanbul, as published by the TUIK. The attributes related to the total number of buildings, the rate of buildings built before 1980, the rate for buildings constructed between 1980-2000, the rate for buildings constructed after 2000, and the rates for building intervals of 1-4 floors, 5-9 floors, and 9-19 floors were sourced from the "Neighborhood-Based Building Counts" dataset created by the IMM (IMM Open Data Portal 2017). The last four attributes (Number of Too Severely Damaged Buildings Rate, Number of Severely Damaged Buildings Rate, Number of Moderately Damaged Buildings Rate, Number of Lightly Damaged Buildings Rate) along with three dependent variables used for model predictions (Number of Casualties, Number of People in Need of Shelter, Number of People in Need of Hospital Treatment) were also derived from the "Earthquake Scenario Analysis Results" dataset produced by the IMM (IMM Open Data Portal 2021). This dataset contains a simulation of the potential outcomes of a 7.5 magnitude earthquake occurring at night in Istanbul. The rationale behind our study's focus on predicting the

effects of a nighttime earthquake is precisely this. Following these processes, a unique dataset containing data from three different sources was established. For the hybrid dataset obtained by combining different datasets, the input values are similar for all datasets. Instead of forcing the algorithms to predict multiple outcomes, they are designed to predict each outcome independently. The absence of null values and outliers in the dataset eliminated the need for cleaning the dataset before the process. Techniques such as Principal Component Analysis (PCA) were not used for feature selection. The dataset used does not contain a large number of input parameters that would need to be eliminated.

The dataset underwent several preprocessing steps to ensure its quality and suitability for the analysis. These steps included:

- **Data Cleaning:** Removal of any duplicate records and handling of missing values. Missing values were addressed using mean imputation for continuous variables and mode imputation for categorical variables.
- **Normalization:** Scaling of numerical features to a standard range using min-max normalization, ensuring that all features contribute equally to the model training process.
- **Outlier Detection:** Identification and treatment of outliers to prevent them from skewing the model results.

Table 1. The features within the dataset and their value ranges.

Variables Type	Features	Min – Max Range
Independent Variables	Population Density	0.10992953-726.5714286
	Total number of buildings	95-8118
	Before 1980 Rate	0-0.958970793
	1980-2000_Between Rate	0.01122449-0.930743243
	2000_After Rate	0-0.986734694
	1-4 Floor Interval Rate	0.045566502-0.997938144
	5-9 Floor Interval Rate	0.002061856-0.951970443
	9-19 Floor Interval Rate	0-0.844036697
	Number of Too Severely Damaged Buildings Rate	0-0.095384615
	Number of Severely Damaged Buildings Rate	0.002132196-0.143076923
	Number of Moderately Damaged Buildings Rate	0.026448363-0.327443401
	Number of Lightly Damaged Buildings Rate	0.099461049-0.508196721
Dependent Variables	Number of Casualties	0-0.01563
	Number of People in Need of Shelter	0-0.460440986
	Number of People in Need of Hospital Treatment	0-0.071428571

2.2. Models Used

2.2.1. Gradient Boosting (GB)

GB is a method that sequentially enhances weak learners (typically decision trees) to form a strong predictive model. Each new learner focuses on minimizing the errors made by its predecessors. This process continues by assigning increasing weight to successive learners to reduce error terms. Mathematically, the model $F(x)$ is shown at Equation 1. In this equation, (x) is the prediction of the t -th learner and λ is the learning rate (Friedman 2001).

$$F_{t+1}(x) = F_t(x) + \lambda h_t \quad (1)$$

2.2.2. Adaptive Boosting (Adaboost)

AdaBoost combines a series of weak classifiers to create a strong classifier. In each learning iteration, higher weight is given to observations that were incorrectly classified, thus the next classifier focuses on better predicting these observations. The fundamental update equation of AdaBoost is shown at Equation 2.

$$D_{t+1}(i) = \frac{D_t(i) \cdot \exp(-\alpha_t y_i h_t(x_i))}{Z_t} \quad (2)$$

In Equation 2, $D_t(i)$ is the weight of the i -th sample, α_t is the weight of the t -th learner, y_i is the actual class label, $h_t(x_i)$ is the predicted class, and Z_t is the normalization factor (Freund and Schapire 1997).

2.2.3. Random Forest (RF)

RF operates by aggregating the predictions of multiple decision trees and presenting the most frequent outcome as the final prediction. Each tree is constructed independently using randomly selected subsets of data. This method reduces both variance and bias, generally yielding more stable and reliable predictions. Mathematically, the RF prediction is calculated as follows:

$$f(x) = \frac{1}{B} \sum_{b=1}^B T_b(x) \quad (3)$$

In this formula, $T_b(x)$ represents the prediction of the b -th tree at point x (Breiman 2001).

2.2.4. Extremely Randomized Trees (ExtraTrees)

ExtraTrees method is an ensemble learning technique akin to RF, but it incorporates greater randomization at each node during splits. In this model, the optimal splitting point at each node is determined based on features chosen at random. This approach can further reduce the model's variance while decreasing computational time. ExtraTrees

is particularly effective for high-dimensional datasets as it minimizes unnecessary computations and reduces the risk of overfitting. Mathematically, the ExtraTrees model can be expressed as shown at Equation 4.

$$f(x) = \frac{1}{B} \sum_{b=1}^B T_b(x, \theta_b) \quad (4)$$

In Equation 4, θ_b denotes the random parameters used in the construction of the b -th tree (Geurts et al. 2006)

2.2.5. Evaluation of the Models

Error metrics used to evaluate the success of ML algorithms are used to measure how well the model performs. These metrics help to assess how well a model's predictions match the true values and the generalization ability of the model.

The symbols P , r , m , c , and d commonly used in performance evaluation metrics are key terms frequently employed in modeling studies. P refers to the predicted values generated by the model, while r represents each observation or data point. m signifies the predicted values produced by the model, and c denotes the actual or observed values. Finally, d typically reflects the difference between the predicted and observed values, which is used to calculate error or deviation. These symbols form the foundation for measuring model performance and evaluating the accuracy of predictions.

Mean absolute error (MAE) is a metric that shows how close the predicted values are to the true values. This metric is calculated by Equation 5 (Hammid et al. 2018, Mishra et al. 2017, AlOmar et al. 2020).

$$MAE = \frac{1}{n} \sum_{r=1}^n |P_d^{r,m} - P_d^{r,c}| \quad (5)$$

Root mean square error (RMSE) was chosen to compare the prediction errors of different trained models. The closer the RMSE value is to 0, the better the predictive ability of the model in terms of its absolute deviation. The RMSE value is calculated by Equation 6 (Hammid et al. 2018, Mishra et al. 2017, AlOmar et al. 2020, Willmott and Matsuura 2005).

$$RMSE = \sqrt{\frac{1}{n} \sum_{r=1}^n (P_d^{r,m} - P_d^{r,c})^2} \quad (6)$$

The coefficient of determination (R^2) is used to estimate model efficiency and is calculated by Equation 7 (Hammid et al. 2018).

$$R^2 = 1 - \frac{\sum_{r=1}^n (P_d^{r,m} - P_d^{r,c})^2}{\sum_{r=1}^n (P_d^{r,m} - P_d^{r,m})^2} \quad (7)$$

MSE either assesses the quality of an estimator. The MSE metric is calculated by Equation 8.

$$MSE = \frac{1}{n} \sum_{i=1}^n (P_i - P'_i)^2 \quad (8)$$

Accuracy is one of the fundamental metrics used to evaluate the performance of a classification model. It represents the ratio of correctly classified samples to the total number of samples. Mathematically, accuracy is defined as follows:

$$Accuracy = \frac{\text{Number of Correct Predictions}}{\text{Total Number of Samples}} \quad (9)$$

This formula shows the percentage of correct predictions made by the model. For example, a model that makes 90 correct predictions out of 100 total samples would have an accuracy of 90% (James et al. 2013).

3. Results

3.1. Model Fine-Tuning Process and Results

Different algorithms are used to model data sets and provide predictions in the fields of ML and data analytics. Hyperparameters must be adjusted to boost these algorithms' efficiency and produce more accurate results. This work involves fine-tuning well-known algorithms including GB, AdaBoost, RF, and ExtraTrees using the datasets used for training. The hyperparameters were fine-tuned to maximize the performance of every algorithm. The most successful hyperparameter values obtained are presented in Table 2.

3.2. Selection Criteria for Hyperparameter Settings

In this study, the optimal hyperparameters obtained because of the experiments on the specified data sets were tested to improve the performance of each algorithm and improve the accuracy of the model. The process of hyperparameter tuning involved extensive experimentation to identify the optimal settings for each ML algorithm. The following criteria were used to select the final hyperparameters:

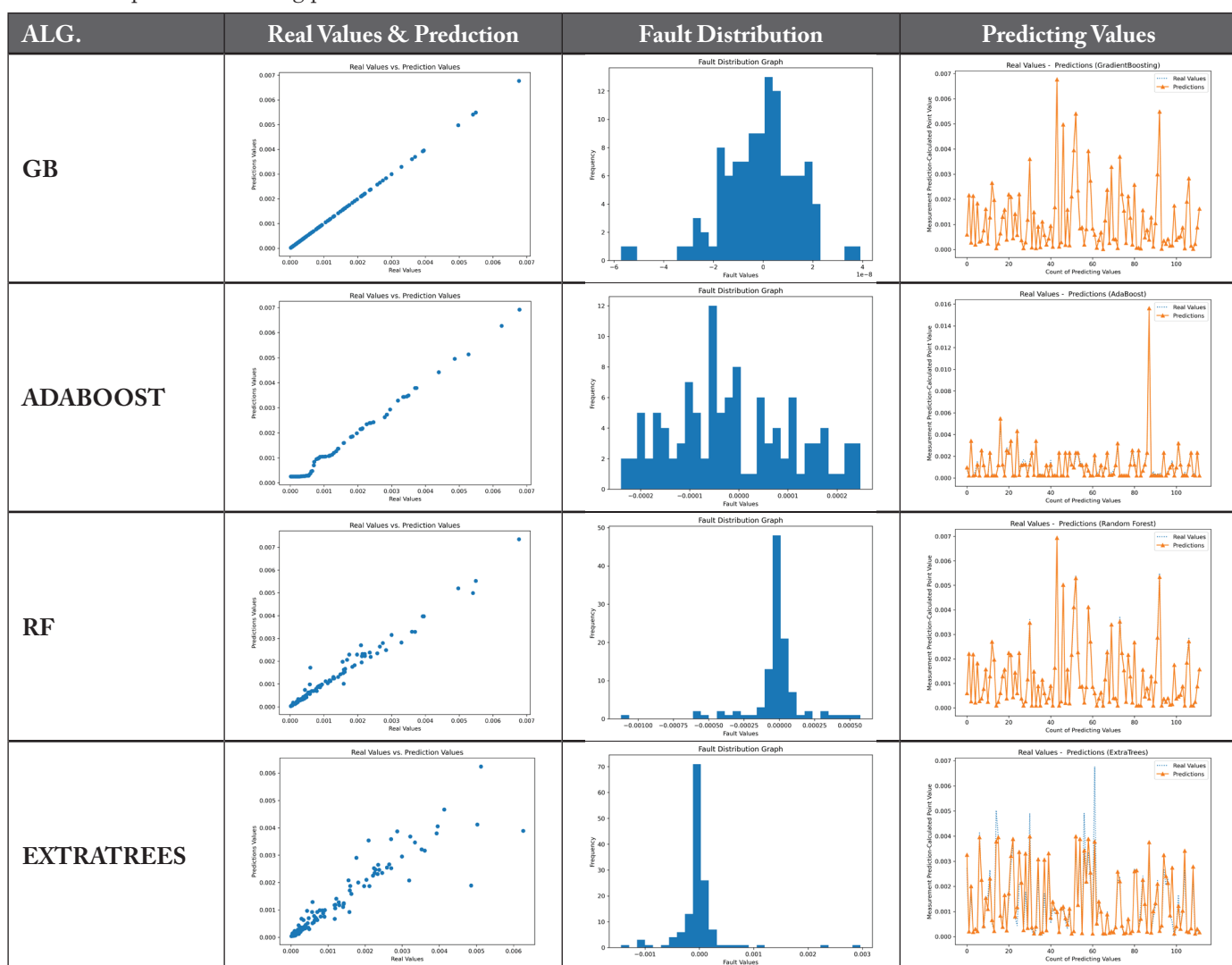
- Performance Metrics: MAE, RMSE, and R² were the primary metrics used to evaluate model performance.
- Cross-Validation: A k-fold cross-validation (with k=5) approach was employed to ensure that the models were robust and generalizable. This method helps in mitigating overfitting by training and validating the model on different subsets of the data.
- Grid Search: A grid search strategy was used to explore a predefined set of hyperparameters systematically. The grid search covered a range of values for each hyperparameter to identify the combination that yielded the best performance.

3.3. Trainings Conducted for Loss of Lifes Data and Results

Table 3 presents the training and test graphs, prediction error distributions, prediction and accuracy graphs, and validation graphs for the most and least successful

Table 2. The best values of the hyperparameter values of the ML models tried and obtained for the best result.

Algorithms	Trained Hypermeters	Best Hypermeters Values
GB	‘n_estimators’: [50, 75, 100], ‘max_depth’: [2, 4, 8], ‘min_samples_split’: [1,2,4], ‘min_samples_leaf’: [1,2 ,8], ‘learning_rate’: [0.05, 0.1 ,0.5, 1]	‘learning_rate’: 1, ‘max_depth’: 8, ‘min_samples_leaf’: 1, ‘min_samples_split’: 4, ‘n_estimators’: 50
ADABOOST	‘n_estimators’: [30, 50, 75, 100,200], ‘learning_rate’: [0.05, 0.1 ,0.5 ,1, 2]	‘learning_rate’: 0.1, ‘n_estimators’: 100
RF	‘n_estimators’: [50,100,200], ‘max_depth’: [2, 4, 8, 16], ‘min_samples_split’: [2,3,4], ‘min_samples_leaf’ : [2,3,4,8]	‘max_depth’: 16, ‘min_samples_leaf’: 2, ‘min_samples_split’: 3, ‘n_estimators’: 50
EXTRATREES	‘n_estimators’: [50, 100, 200], ‘max_depth’: [None, 10, 20, 30], ‘min_samples_split’: [2, 5, 10], ‘min_samples_leaf’: [1, 2, 4]	‘max_depth’: 10, ‘min_samples_leaf’: 1, ‘min_samples_split’: 2, ‘n_estimators’: 100

Table 3. Graphs for estimating possible casualties.

algorithms used in predicting the loss of life in the Istanbul earthquake scenario using ML. Table 3 shows the training and test graphs, prediction error distributions, prediction and accuracy graphs and validation graphs of the most successful and least successful algorithms of the models trained to predict the loss of life in the earthquake scenario for Istanbul with ML. In the training and test graph, a linear line graph is expected for successful training. In the test and training graphs of the ExtraTrees Regressor algorithm, there are some values that break the linear line. However, in the GB Regressor algorithm, it is seen that this graph forms a linear line graph. In the error distributions graph, it is expected to see distributions that do not differ as much as possible. In the ExtraTrees Regressor algorithm, the error distribution graph of the GB Regressor algorithm concentrates almost all of them at the 0 point with a

tolerance of 1e-8, while the false predictions of 0.003 are seen at different frequencies. This clearly demonstrates the prediction success. In the prediction and accuracy graph, the blue lines show the actual values, and the orange lines show the values predicted by the model. What we want to see in this graph is the overlap of these two different colored lines. In the ExtraTrees Regressor algorithm, the blue and orange lines overlap, but not perfectly. On the other hand, in the GB Regressor algorithm, only orange colors are seen in the graph with two different colors. This proves the high accuracy of the prediction.

According to Table 4, the performance of the models trained using four different algorithms (GB, AdaBoost, RF and ExtraTrees) is evaluated. MSE, MAE, RMSE, R² and Accuracy metrics were commonly used. The GB model performed the best, achieving very low error rates in MSE,

MAE and RMSE values. The r^2 value of 0.99 indicates a very high explanation rate. Moreover, the accuracy rate is also very high at 99.99%. Although the AdaBoost model has slightly higher error rates in the other metrics, it still has a very high R^2 value and an acceptable accuracy rate. The RF and ExtraTrees models have higher error rates and lower R^2 values. These models were less successful compared to GB and AdaBoost.

Table 4. Metrics for estimating possible casualties.

Algorithm	MSE	MAE	RMSE	R^2	Accuracy
GB	2.366194013919057e-16	1.1559507427903762e-08	1.538243808347382e-08	0.99	99.99
AdaBoost	1.561541483737388e-08	0.0001048052560926842	0.00012496165346766937	0.99	86.54
RF	3.99632097624034e-08	0.00010438015990870665	0.00019990800324750234	0.97	86.41
ExtraTrees	1.9283873995273218e-07	0.0001937100020273874	0.0004391340796985952	0.87	71.82

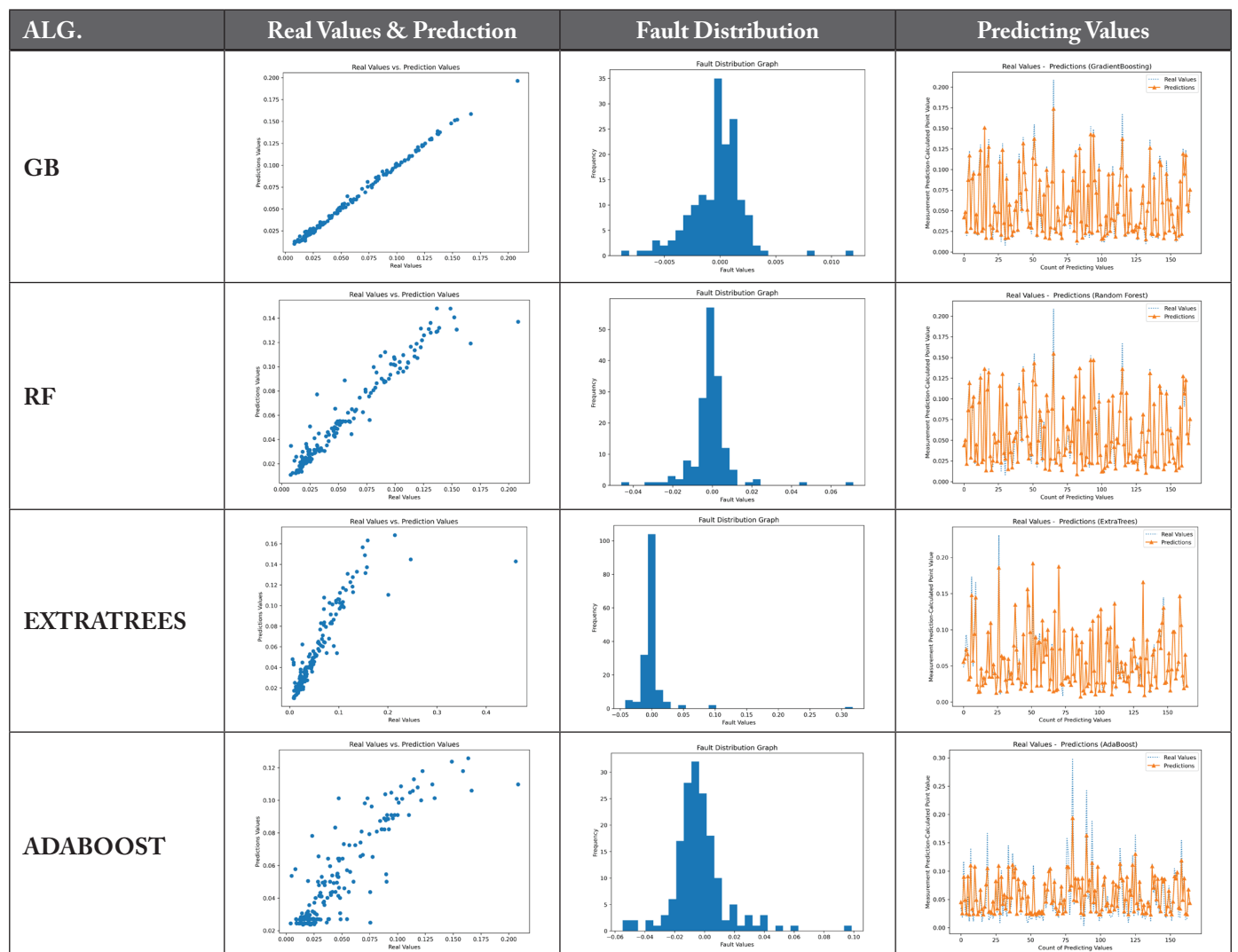
Table 5. Graphs for estimating the number of people who will potentially need shelter.

Table 6 evaluates the performance of models trained with four different algorithms (GB, RF, ExtraTrees and AdaBoost). Again, various metrics such as MSE, MAE, RMSE, R² and Accuracy are used. The GB model has very low error rates and shows high performance in other metrics. In particular, the R² value of 0.99 represents a very high explanation rate. The accuracy rate is also quite high at 95.03%. RF and ExtraTrees models show increased error rates and decreased R² values. They perform slightly lower

compared to the GB model. The AdaBoost model has higher error rates and lower R² values compared to the other algorithms, and its accuracy is significantly lower than the other models.

3.5. Trainings Conducted for the Number of Treatment Needs in the Hospital and Results

As can be seen from Table 7, the ExtraTrees Regressor algorithm is quite successful in the Real Values and

Table 6. Metrics for estimating the number of people who will potentially need shelter.

Algorithm	MSE	MAE	RMSE	R ²	Accuracy
GB	5.907810132908763e-06	0.0016719927767314552	0.0024305987190214604	0.99	95.03
RF	0.00011401742245214174	0.005899589280678199	0.010677894101935164	0.93	84.83
ExtraTrees	0.0008459893248166345	0.00980782252598891	0.029085895633736886	0.70	74.49
AdaBoost	0.00035198198721687386	0.012938087377026323	0.01876118299086904	0.75	50.22

Table 7: Graphs for estimating the number of people who will potentially require hospital treatment

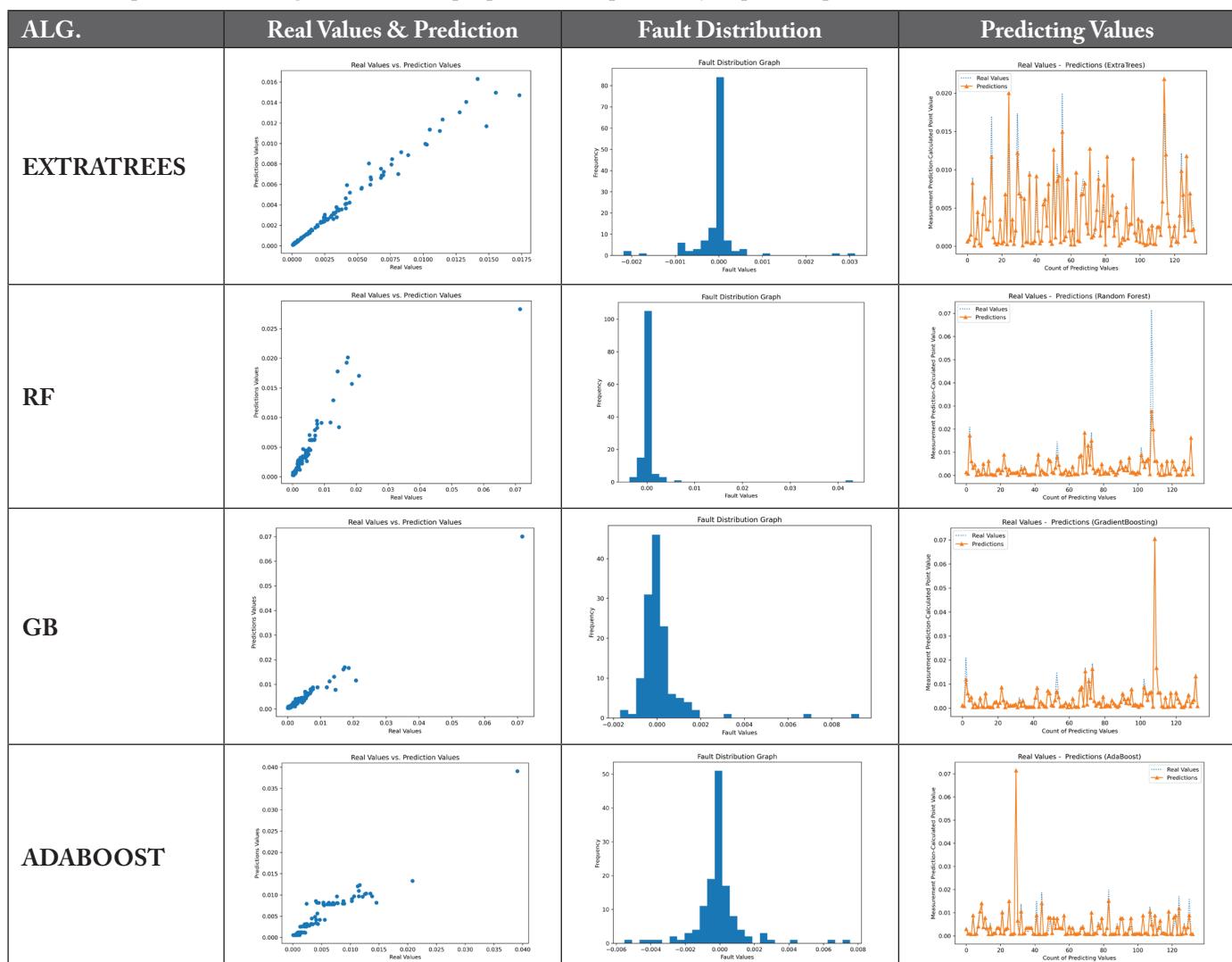


Table 8. Metrics for estimating the number of people who will potentially require hospital treatment.

Algorithm	MSE	MAE	RMSE	R ²	Accuracy
ExtraTrees	2.917018737514533e-07	0.00022766724876766196	0.0005400943193104823	0.97	92.57
RF	1.4933443438588122e-05	0.0008048125853343117	0.0038643813785117173	0.70	72.05
GB	1.3869019221264514e-06	0.0005328583098645869	0.0011776680016568554	0.97	55.25
AdaBoost	2.221970996035838e-06	0.0008394849115527844	0.0014906277187936086	0.91	51.80

Prediction Values graph. In addition, although it looks like a scattered column graph in the error distribution graph, the tolerance multiplier value is quite low compared to other algorithms.

Table 8 shows the performance of the models trained with four different algorithms (ExtraTrees, RF, GB and AdaBoost). Again, various metrics such as MSE, MAE, RMSE, R² and Accuracy are used. The ExtraTrees model has very low error rates and a high R² value. The RMSE value is also quite low. This indicates that the model explains the dataset well and makes accurate predictions. The accuracy rate is also high at 92.57%. The RF model has higher error rates and lower R² value compared to the other models. However, its accuracy is still acceptable (72.05%). The GB and AdaBoost models perform moderately in terms of error rates and R² values. However, their accuracy rates are lower than the other models (55.25% and 51.80%).

According to the performance metrics given in the tables, the GB algorithm is superior to the other algorithms. This superiority is especially evident in metrics such as MSE, MAE, RMSE, R² and Accuracy.

One of the main reasons behind the success of the GB algorithm is that this algorithm has a structure that iteratively corrects errors. By correcting the errors at each step, GB improves model performance and can produce more accurate and generalized results. This iterative learning process allows the model to better learn the complexities in the dataset, resulting in lower error rates and higher accuracy rates. In terms of practical applications, a model with low MSE and RMSE values can make more accurate predictions, which can reduce the cost of error. A high R² value indicates that the model is better able to explain the variability of the data set, which increases model reliability. In line with this analysis, it is clear why the GB algorithm is more successful especially in our dataset. Therefore, it is recommended to prefer the GB algorithm for similar problems.

4. Discussion and Conclusion

Istanbul, as Turkey's largest metropolis, is notable for its dense population and cosmopolitan structure, yet it faces significant earthquake risks due to unplanned urbanization and a high proportion of structurally unsound buildings. This study utilized various ML techniques to predict potential casualties, the number of people requiring hospital treatment, and the number of people needing temporary shelter in the event of a potential magnitude 7.5 earthquake occurring during nighttime in Istanbul. The dataset used in this analysis was a composite set enriched with data obtained from the Istanbul Metropolitan Municipality Open Data Portal and the TUIK.

The dataset includes diverse features such as neighborhood-based building counts, distribution of buildings according to their construction years, and structural damage rates. These features are critical for understanding the potential outcomes of earthquake scenarios and planning necessary measures during model training.

The modeling process employed algorithms like GB, AdaBoost, RF, and ExtraTrees, evaluating each algorithm's performance using metrics such as MAE, RMSE, and the R². Results indicate that the GB algorithm outperformed others by achieving lower error rates and a high determination coefficient, signifying its ability to model the dataset with high accuracy and close proximity to true values.

When compared to the literature, similar studies also demonstrate the potential of ML approaches to successfully predict earthquake outcomes. While these studies provide significant insights, our study contributes uniquely by utilizing a hybrid dataset specific to Istanbul, which integrates neighborhood-based building counts, construction year distributions, and structural damage rates. Unlike the aforementioned studies that primarily focus on broad regional datasets or specific technical methods, our research emphasizes the application of multiple ML algorithms (GB, AdaBoost, RF, and ExtraTrees) on a localized and context-specific dataset. This allows for a more nuanced understanding

of earthquake impacts in an urban setting like Istanbul. Furthermore, our approach highlights the practical implications for urban disaster preparedness and management, providing actionable insights for policymakers. Compared to previous studies, our work stands out in the following ways:

- **Localized Dataset:** The use of a hybrid dataset specific to Istanbul, incorporating detailed local attributes not commonly found in broader datasets.
- **Algorithm Comparison:** A comprehensive comparison of multiple ML algorithms on the same dataset, providing a clear evaluation of their relative performance.
- **Practical Implications:** Direct applicability to urban disaster management and preparedness in Istanbul, offering specific recommendations based on the findings.

These aspects of our study offer a valuable contribution to the existing body of literature, addressing the need for localized analysis and practical applications in disaster management.

This study utilizes a dataset specific to the Istanbul province. Future studies aim to conduct similar analyses in other regions of Turkey or in other earthquake-prone areas around the world. This will help assess how the proposed models perform under different geographical and demographic conditions. Additionally, it is intended to test new and emerging ML and deep learning techniques on the current topic, alongside the existing algorithms.

In conclusion, this study contributes to understanding the possible damages a major earthquake could cause in Istanbul and assists in planning to mitigate these impacts. The findings provide valuable insights for policymakers in enhancing urban transformation and disaster management strategies. Future research could extend similar modeling to different regions, further improving earthquake risk management and emergency preparedness.

5. Acknowledgment

The authors have not received any financial support for the research, authorship, or publication of this study. No conflict of interest or common interest has been declared by the authors.

Author contribution: The authors contributed equally to the study.

Ethics committee approval: This study does not require ethics committee permission or any special permission.

6. References

- AlOmar, MK., Hameed, MM., AlSaadi MA. 2020.** Multi hours ahead prediction of surface ozone gas concentration. Robust artificial intelligence approach Atmospheric Pollution Research, 11(9): 1572–1587. Doi: 10.1016/j.apr.2020.06.024
- Ahamed, S., Daub, E. 2019.** Machine learning approach to earthquake rupture dynamics. ArXiv, Doi:10.48550/arXiv.1906.06250
- Ambraseys, N. 2001.** The earthquake of 10 July 1894 in the Gulf of Izmit (Turkey) and its relation to the earthquake of 17 August 1999. Journal of Seismology, 5(1): 117–128. Doi: 10.1023/A:1009871605267
- Arslan, G., Fawzy, D., Coskun, A. 2017.** On the prediction of structural reactions to big earthquakes in Turkey. PressAcademia Procedia. 5(1): 335–340. Doi: 10.17261/Pressacademia.2017.608
- Breiman, L., 2001.** Random forests. Machine learning. 45(1): 5–32. Doi: 10.1023/A:1010933404324
- Corbi, F., Sandri, L., Bedford, J., Funiciello, F., Brizzi, S., Rosenau, M., Lallemand, S. 2019.** Machine learning can predict the timing and size of analog earthquakes. Geophysical Research Letters, 46: 1303 - 1311. Doi:10.1029/2018GL081251.
- Erdik, M. 2001.** Report on 1999 Kocaeli and Düzce (Turkey) earthquakes. Structural Control For Civil And Infrastructure Engineering. p. 149–186. Paris. France.
- Freund, Y., Schapire, RE. 1997.** A decision-theoretic generalization of on-line learning and an application to boosting. Journal of Computer and System Sciences. 55(1): 119–139. Doi: 10.1006/jcss.1997.1504
- Friedman, JH. 2001.** Greedy function approximation: A gradient boosting machine. Annals of Statistics. 29(5):1189–1232. Doi: 10.1214/aos/1013203451
- Geurts, P., Ernst, D., Wehenkel, L. 2006.** Extremely randomized trees. Machine Learning. 63(1): 3–42. Doi: 10.1007/s10994-006-6226-1.
- Hammid, AT., Sulaiman, MH, Abdalla, AN. 2018.** Prediction of small hydropower plant power production in Himreen Lake dam (HLD) using artificial neural network. Alexandria Engineering Journal. 57(1): 211–221. Doi: 10.1016/j.aej.2016.12.011.
- IMM Open Data Portal 2017.** Neighborhood based building numbers. <https://data.ibb.gov.tr/dataset/mahalle-bazili-bina-analiz-verisi/resource/cef193d5-0bd2-4e8d-8a69-275c50288875>
- IMM Open Data Portal 2021.** Earthquake scenario analysis results. <https://data.ibb.gov.tr/dataset/deprem-senaryo-su-analiz-sonuclari/resource/9c3ac492-de4b-4245-b418-7ad3df67a193>

- James, G., Witten, D., Hastie, T., Tibshirani, R.** 2013. An introduction to statistical learning. Springer. New York, USA, 607 pp.
- Jaiswal, K., Wald, DJ.** 2010. An empirical model for global earthquake fatality estimation. *Earthquake Spectra*, 26(4): 1017-1037. Doi: 10.1193/1.3480331
- Korkut, U., Basbugoglu, T., Sahin, O.** 2023. Turkey's 2023 elections: another victory for Erdogan. *Political Insight*, 14(3): 16-19. Doi: 10.1177/20419058231198579
- Li, B., Gong, A., Zeng, T., Bao, W., Xu, C., Huang, Z.** 2021. A zoning earthquake casualty prediction model based on machine learning. *Remote Sensing*, 14(1): 30. Doi: 10.3390/rs14010030
- Mishra, G., Sehgal, D., Valadi, JK.** 2017. Quantitative structure activity relationship study of the antihepatitis peptides employing random forests and extra-trees regressors. *Bioinformation*, 13(3): 60, Doi: 10.6026/97320630013060.
- Parsons, T.** 2000. Heightened odds of large earthquakes near Istanbul: An interaction-based probability calculation. *Science*, 288(5466): 661-665, Doi: 10.1126/science.288.5466.661
- Rouet-Leduc, B., Hulbert, C., Lubbers, N., Barros, K., Humphreys, C., Johnson, P.** 2017. Machine learning predicts laboratory earthquakes. *Geophysical Research Letters*. 44: 9276 - 9282. Doi:10.1002/2017GL074677.
- Stein, RS.** 2000. Earthquake conversations. *Scientific American*, 282(1): 68-75. Doi:10.1038/scientificamerican012003-DipeiQnMaPMOL1RMjOPhi
- Willmott, CJ., Matsuura, K.** 2005. Advantages of the mean absolute error (MAE) over the root mean square error (RMSE) in assessing average model performance. *Climate Research*. 30(1): 79–82, Doi: 10.3354/cr030079.
- World Bank** 2023. Earthquake damage in Türkiye estimated to exceed \$34 billion: World bank disaster assessment report. <https://www.worldbank.org>
- Xing, H., Junyi, S., Jin, H.** 2020. The casualty prediction of earthquake disaster based on Extreme Learning Machine method. *Natural Hazards*, 102(3): 873-886, Doi: 10.1007/s11069-020-03937-6



On Convergence in Quaternion-Valued g-Metric Space

Kuaterniyon Değerli g-Metrik Uzayda Yakınsaklık Üzerine

Saime Kolancı¹ , Mehmet Gürdal¹ , Ömer Kişi^{2*}

¹Süleyman Demirel University, Faculty of Science, Department of Mathematics, Isparta, Türkiye

²Bartın University, Faculty of Science, Department of Mathematics, Bartın, Türkiye

Abstract

This study presents and investigates the notion of convergence for double sequences in the quaternion-valued g-metric space, as well as a review of certain fundamental features. Moreover, statistical convergence in this context is examined and defined in detail. The final section, focusing on the relationship between the statistical convergence of quaternion-valued g-metric spaces and strong summability, delves into this connection and discusses its implications.

Keywords: Generalized metric spaces, quaternion space, statistical convergence, strong summability.

Öz

Bu makalede, kuaterniyon değerli g-metrik uzayda çift dizilerin yakınsama kavramı tanıtılpı incelenmekte, bazı temel özellikler de ele alınmaktadır. Ayrıca, bu bağlamda istatistiksel yakınsama ayrıntılı olarak incelenip tanımlanmaktadır. Son bölümde ise, kuaterniyon değerli g-metrik uzayların istatistiksel yakınsaması ile güçlü toplanabilirlik arasındaki ilişkiye odaklanılmakta ve bu bağlantının sonuçları tartışılmaktadır.

Anahtar Kelimeler: Genelleştirilmiş metrik uzaylar, kuaterniyon uzayı, istatistiksel yakınsaklık, güçlü toplanabilirlik.

1. Introduction

Fast (1951) conducted the first study on statistical convergence. Three individuals, Tripathy (2003), Mursaleen and Edely (2003), and Moricz (2003), each separately pioneered this field of study on statistical convergence in double sequences.

A distance function or metric expands on the concept of physical distance in mathematical analysis. Large and complex datasets provide a number of issues, hence Khamsi (2015) suggested a number of methods to expand this idea. A 2-metric, as proposed by Gähler (1966), is a more general version of the standard metric, although further studies have not found a connection between these functions. Ha et al.

(1988), for example, showed that a 2-metric does not always show continuity with regard to its variables. These results led to Bapure Dhage's (1992) doctoral research on a new class of generalized metric spaces known as D-metric spaces. Determining these spaces' topological characteristics was the goal of Dhage (1992), and it proved essential for later studies in this area. However, studies by Mustafa and Sims (2003) and Naidu et al. (2005) have pointed out inaccuracies in many foundational claims regarding the basic topological characteristics of D-metric spaces, thereby undermining the validity of numerous results obtained in this area.

Mustafa and Sims (2006) pioneered the concept of G-metric space, whereas Choi et al. (2018) generalized this concept to degree l .

Let's review some basic symbols used in quaternion spaces. The quaternion space, denoted as \mathbf{H} , consists of four-dimensional real algebra with unity. The zero element of \mathbf{H} is represented as $0_{\mathbf{H}}$, and the multiplicative identity is denoted as $1_{\mathbf{H}}$. Within \mathbf{H} , there are three specific imaginary units referred to as i, j, k . These units are defined by the following relationships:

*Corresponding author: okisi@bartin.edu.tr

Saime Kolancı orcid.org/0000-0001-8056-0072

Mehmet Gürdal orcid.org/0000-0003-0866-1869

Ömer Kişi orcid.org/0000-0001-6844-3092



This work is licensed by "Creative Commons Attribution-NonCommercial 4.0 International (CC BY NC)".

$$i^2 = j^2 = k^2 = -1, ij = -ji = k, jk = -kj = i \text{ and } ki = -ik = j.$$

For each quaternion $\rho = y_0 + y_1i + y_2j + y_3k$; where y_0, y_1, y_2 and y_3 are real numbers, the elements $1, i, j, k$ are considered as a basis for the real vector space \mathbf{H} . Given $\rho = y_0 + y_1i + y_2j + y_3k \in \mathbf{H}$, we recall that:

- (i) $\overline{\rho} = y_0 - y_1i - y_2j - y_3k$ is the conjugate quaternion of ρ ,
- (ii) $|\rho| = \sqrt{\rho\overline{\rho}} = \sqrt{y_0^2 + y_1^2 + y_2^2 + y_3^2} \in \mathbb{R}$

$$(iii) \operatorname{Re}(\rho) = \frac{1}{2}(\rho + \overline{\rho}) = y_0 \in \mathbb{R}$$

$$(iv) \operatorname{Im}(\rho) = \frac{1}{2}(\rho - \overline{\rho}) = y_1i + y_2j + y_3k \text{ is the imaginary part of } \rho.$$

When $\rho = \operatorname{Re}(\rho)$, the element $\rho \in \mathbf{H}$ is termed as real. It is evident that ρ is real only if and only if $\rho = \overline{\rho}$. If $\overline{\rho} = -\rho$ or $\rho = \operatorname{Im}(\rho)$, ρ is considered imaginary.

The idea of a complex metric space was introduced by Azam et al. (2011) in the following way.

Definition 1.1. Assume that X is a nonempty set and that $d_c: X \times X \rightarrow \mathbb{C}$ is a mapping satisfying the following criteria:

- (i) $0 < d_c(t_1, t_2)$, for all $t_1, t_2 \in X$ and $d_c(t_1, t_2) = 0$ if and only if $t_1 = t_2$,

$$(ii) d_c(t_1, t_2) = d_c(t_2, t_1) \text{ for all } t_1, t_2 \in X,$$

$$(iii) d_c(t_1, t_2) \leq d_c(t_1, t_3) + d_c(t_3, t_2) \text{ for all } t_1, t_2, t_3 \in X.$$

As a result, we refer to the pair (X, d_c) as a complex metric space.

Ahmed et al. (2014) broadened the preceding definition to encompass Clifford analysis in the subsequent manner:

Definition 1.2. Assume that X is a nonempty set and that $d_H: X \times X \rightarrow \mathbf{H}$ is a mapping satisfying the following criteria:

- (i) $0 < d_H(t_1, t_2)$, for all $t_1, t_2 \in X$ and $d_H(t_1, t_2) = 0$ if and only if $t_1 = t_2$,

$$(ii) d_H(t_1, t_2) = d_H(t_2, t_1) \text{ for all } t_1, t_2 \in X,$$

$$(iii) d_H(t_1, t_2) \leq d_H(t_1, t_3) + d_H(t_3, t_2) \text{ for all } t_1, t_2, t_3 \in X.$$

Therefore, the pair (X, d_c) is termed a quaternion-valued metric space.

Ahmed et al. (2014) defined a partial order \preceq on the space \mathbf{H} (set of all quaternions).

Let $\rho_1, \rho_2 \in \mathbf{H}$, then $\rho_1 \preceq \rho_2$ if and only if $\operatorname{Re}(\rho_1) \leq \operatorname{Re}(\rho_2)$ and $\operatorname{Im}_s(\rho_1) \leq \operatorname{Im}_s(\rho_2), \rho_1, \rho_2 \in \mathbf{H}, s = i, j, k$ where $\operatorname{Im} m_i = b, \operatorname{Im} m_j = c, \operatorname{Im} m_k = d$. It was noted that $\rho_1 \preceq \rho_2$, if any of the following conditions hold:

$$(i) \operatorname{Re}(\rho_1) = \operatorname{Re}(\rho_2), \operatorname{Im}_{s_1}(\rho_1) = \operatorname{Im}_{s_1}(\rho_2) \text{ where } s_1 = j, k, \operatorname{Im}_i(\rho_1) < \operatorname{Im}_i(\rho_2);$$

$$(ii) \operatorname{Re}(\rho_1) = \operatorname{Re}(\rho_2), \operatorname{Im}_{s_2}(\rho_1) = \operatorname{Im}_{s_2}(\rho_2) \text{ where } s_2 = j, k, \operatorname{Im}_j(\rho_1) < \operatorname{Im}_j(\rho_2);$$

$$(iii) \operatorname{Re}(\rho_1) = \operatorname{Re}(\rho_2), \operatorname{Im}_{s_3}(\rho_1) = \operatorname{Im}_{s_3}(\rho_2) \text{ where } s_3 = j, k, \operatorname{Im}_k(\rho_1) < \operatorname{Im}_k(\rho_2);$$

$$(iv) \operatorname{Re}(\rho_1) = \operatorname{Re}(\rho_2), \operatorname{Im}_{s_1}(\rho_1) = \operatorname{Im}_{s_1}(\rho_2), \\ \operatorname{Im} m_i(\rho_1) = \operatorname{Im}_i(\rho_2);$$

$$(v) \operatorname{Re}(\rho_1) = \operatorname{Re}(\rho_2), \operatorname{Im}_{s_2}(\rho_1) = \operatorname{Im}_{s_2}(\rho_2), \\ \operatorname{Im} m_j(\rho_1) = \operatorname{Im}_j(\rho_2);$$

$$(vi) \operatorname{Re}(\rho_1) = \operatorname{Re}(\rho_2), \operatorname{Im}_{s_3}(\rho_1) = \operatorname{Im}_{s_3}(\rho_2), \\ \operatorname{Im} m_k(\rho_1) = \operatorname{Im}_k(\rho_2);$$

$$(vii) \operatorname{Re}(\rho_1) = \operatorname{Re}(\rho_2), \operatorname{Im}_s(\rho_1) < \operatorname{Im}_s(\rho_2);$$

$$(viii) \operatorname{Re}(\rho_1) < \operatorname{Re}(\rho_2), \operatorname{Im}_s(\rho_1) = \operatorname{Im}_s(\rho_2);$$

$$(ix) \operatorname{Re}(\rho_1) < \operatorname{Re}(\rho_2), \operatorname{Im}_{s_1}(\rho_1) = \operatorname{Im}_{s_1}(\rho_2), \\ \operatorname{Im}_i(\rho_1) < \operatorname{Im}_i(\rho_2);$$

$$(x) \operatorname{Re}(\rho_1) < \operatorname{Re}(\rho_2), \operatorname{Im}_{s_2}(\rho_1) = \operatorname{Im}_{s_2}(\rho_2), \\ \operatorname{Im} m_j(\rho_1) < \operatorname{Im} m_j(\rho_2);$$

$$(xi) \operatorname{Re}(\rho_1) < \operatorname{Re}(\rho_2), \operatorname{Im}_{s_3}(\rho_1) = \operatorname{Im}_{s_3}(\rho_2), \\ \operatorname{Im}_k(\rho_1) < \operatorname{Im}_k(\rho_2);$$

$$(xii) \operatorname{Re}(\rho_1) < \operatorname{Re}(\rho_2), \operatorname{Im}_{s_1}(\rho_1) < \operatorname{Im}_{s_1}(\rho_2), \\ \operatorname{Im}_i(\rho_1) = \operatorname{Im} m_i(\rho_2);$$

$$(xiii) \operatorname{Re}(\rho_1) < \operatorname{Re}(\rho_2), \operatorname{Im}_{s_2}(\rho_1) < \operatorname{Im}_{s_2}(\rho_2), \\ \operatorname{Im} m_j(\rho_1) = \operatorname{Im} m_j(\rho_2);$$

$$(xiv) \operatorname{Re}(\rho_1) = \operatorname{Re}(\rho_2), \operatorname{Im}_{s_3}(\rho_1) = \operatorname{Im}_{s_3}(\rho_2), \\ \operatorname{Im}_k(\rho_1) = \operatorname{Im}(m_k);$$

$$(xv) \operatorname{Re}(\rho_1) < \operatorname{Re}(\rho_2), \operatorname{Im}_s(\rho_1) < \operatorname{Im}_s(\rho_2);$$

$$(xvi) \operatorname{Re}(\rho_1) = \operatorname{Re}(\rho_2), \operatorname{Im}_s(\rho_1) = \operatorname{Im}_s(m_s).$$

Specifically, we denote $\rho_1 \preccurlyeq \rho_2$ if $\rho_1 \neq \rho_2$ and any one of conditions (i) to (xvi) is satisfied, and $\rho_1 \prec \rho_2$ if only condition (xv) is satisfied.

Remark 1.1. It is important to emphasize that $\rho_1 \preceq \rho_2 \Rightarrow |\rho_1| \leq |\rho_2|$.

Inspired by the research of Ahmed et al. (2014), Adewale et al. (2019) proposed the following definition.

Definition 1.3. Let $G^g: X \times X \times X \rightarrow \mathbf{H}$ be a function that meets the following conditions, and let X be a nonempty set, \mathbf{H} a collection of quaternions:

- (i) $G^g(\alpha, \beta, \gamma) = 0$ if and only if $\alpha = \beta = \gamma$,

- (ii) $0 < G^{\varrho}(\alpha, \alpha, \beta), \forall \alpha, \beta \in X$, with $\alpha \neq \beta$,
- (iii) $G^{\varrho}(\alpha, \alpha, \beta) \leq G^{\varrho}(\alpha, \beta, \varrho), \forall \alpha, \beta, \varrho \in X$, with $\varrho \neq \beta$,
- (iv) $G^{\varrho}(\alpha, \beta, \varrho) = G^{\varrho}(\beta, \varrho, \alpha) = G^{\varrho}(\alpha, \varrho, \beta) = \dots$ (symmetry),

(v) A real number $m \geq 1$ exists such that

$$G^{\varrho}(\alpha, \beta, \varrho) \leq m[G^{\varrho}(\alpha, y, y) + G^{\varrho}(y, \beta, \varrho)],$$

$$\forall y, \alpha, \beta, \varrho \in X$$

The G^{ϱ} -metric space is therefore represented as (X, G^{ϱ}) , and the function G^{ϱ} is referred to as a quaternion G -metric. When each Cauchy sequence in a G^{ϱ} -metric space converges under G^{ϱ} , the space is said to be complete. The following extends the concept of G -metric space to degree l .

Definition 1.4. Assume that X is a non-empty set. If a function $g: X^{l+1} \rightarrow \mathbb{R}^+$ satisfies the following requirements, it is defined as a g -metric space with order l on:

- (i) $g(t_0, t_1, t_2, \dots, t_l) = 0$ iff $t_0 = t_1 = \dots = t_l$,
- (ii) $g(t_0, t_1, t_2, \dots, t_l) = g(t_{\sigma(0)}, t_{\sigma(1)}, t_{\sigma(2)}, \dots, t_{\sigma(l)})$ for permutation σ on $\{0, 1, 2, \dots, l\}$,
- (iii) $g(t_0, t_1, t_2, \dots, t_l) \leq g(v_0, v_1, v_2, \dots, v_l)$ for each $(t_0, t_1, t_2, \dots, t_l), (v_0, v_1, v_2, \dots, v_l) \in X^{l+1}$ with $\{t_i: i = 0, 1, \dots, l\} \subseteq \{v_j: j = 0, 1, \dots, l\}$,
- (iv) For each $t_0, t_1, \dots, t_{\eta}, v_0, v_1, \dots, v_{\delta}, u \in X$ with $\eta + \delta + 1 = l$

$$g(t_0, t_1, t_2, \dots, t_{\eta}, v_0, v_1, v_2, \dots, v_{\delta}) \leq g(t_0, t_1, t_2, \dots, t_{\eta}, u, u, \dots, u) + g(v_0, v_1, v_2, \dots, v_{\eta}, u, u, \dots, u).$$

A g -metric space of degree l is designated for the pair (X, g) . When $l = 1, 2$ it corresponds to a metric space and a G -metric space, respectively.

Recall that a subset T of the set of natural numbers, \mathbb{N} possesses a “natural density” $\delta(T)$ if it fulfills the subsequent conditions:

$$\delta(T) = \lim_{V \rightarrow \infty} \frac{1}{V} |\{n \leq V: n \in T\}|.$$

The sequence $t = (t_n)$ considered statistically convergent to number L if, for every $\varrho > 0$

$$\lim_{V \rightarrow \infty} \frac{1}{V} |\{n \leq V: |t_n - L| \geq \varrho\}| = 0,$$

and x is termed a statistically Cauchy sequence if, for all $\varrho > 0$ there exists a number $Q = Q(\varrho)$ so that

$$\lim_{V \rightarrow \infty} \frac{1}{V} |\{n \leq V: |t_n - t_Q| \geq \varrho\}| = 0.$$

Abazari (2021) provided the following definition.

Definition 1.5. Let $p \in \mathbb{N}$ and define

$$T(\alpha) = \{(r_0, r_1, r_2, \dots, r_p) \leq \alpha (\alpha \in \mathbb{N}): (r_0, r_1, r_2, \dots, r_p) \in T\}.$$

Then, the p -dimensional asymptotic (or natural) density of the set T denoted by $\delta_{(p)}(T)$ is defined as:

$$\delta_{(p)}(T) = \lim_{\alpha \rightarrow \infty} \frac{p!}{\alpha^p} |T(\alpha)|.$$

Now, we recall the definition of quaternion-valued g -metric space in this section, along with some fundamental characteristics (see, Jan and Jalal (2023)).

Definition 1.6. Assume that X is a non-empty set. A function $g_H: X^{p+1} \rightarrow H$ (where H is the space of quaternions) is called quaternion valued g -metric space with order p on X if it satisfies the following criterias :

- (i) $g_H(t_0, t_1, t_2, \dots, t_p) = 0$ if and only if $t_0 = t_1 = \dots = t_p$,
 - (ii) $g_H(t_0, t_1, t_2, \dots, t_p) = g_H(t_{\sigma(0)}, t_{\sigma(1)}, t_{\sigma(2)}, \dots, t_{\sigma(p)})$ for permutation σ on $\{0, 1, 2, \dots, p\}$,
 - (iii) $g_H(t_0, t_1, t_2, \dots, t_p) \leq g_H(v_0, v_1, v_2, \dots, v_p)$ for all $(t_0, t_1, t_2, \dots, t_p), (v_0, v_1, v_2, \dots, v_p) \in X^{p+1}$ with $\{t_i: i = 0, 1, \dots, p\} \subseteq \{v_j: j = 0, 1, \dots, p\}$,
 - (iv) For all $t_0, t_1, \dots, t_{\eta}, v_0, v_1, \dots, v_{\delta}, v \in X$ with $\eta + \delta + 1 = p$
- $$g_H(t_0, t_1, \dots, t_{\eta}, v_0, v_1, \dots, v_{\delta}) \leq g_H(t_0, t_1, \dots, t_{\eta}, v, v, \dots, v) + g_H(v_0, v_1, \dots, v_{\eta}, v, v, \dots, v)$$

We call the pair (X, g_H) a quaternion-valued g_H -metric space of degree p . When $p = 1$ and $p = 2$, respectively, it corresponds to quaternion-valued metric space and quaternion-valued G -metric space.

The following theorem demonstrates that quaternion-valued g -metrics extend the concepts of quaternion-valued metric and quaternion-valued G -metric.

Theorem 1.1. Assume X is a given, non-empty set. The following claims are true:

- (a) d_H is a quaternion valued g -metric of order 1 on X iff d_H is a quaternion valued metric on X .
- (b) G_H is a quaternion valued g -metric of order 2 on X iff G_H is a G -metric on X with quaternion values.

These criteria are equivalent to those of metric spaces with quaternion values and G -metric spaces with quaternion values. As a result, quaternion-valued metric and quaternion-valued G -metric spaces are equivalent to quaternion-valued g -metrics of order 1 and 2, respectively.

Proposition 1.1. Consider (X, g_H) and (X, \bar{g}_H) as quaternion g-metric spaces. Quaternion-valued g-metrics on X are the functions indicated by d_H , are.

$$(1) d_H(t_0, t_1, \dots, t_p) = g_H(t_0, t_1, \dots, t_p) + \bar{g}_H(t_0, t_1, \dots, t_p)$$

(2) $d_H(t_0, t_1, \dots, t_p) = \Phi(d_H(t_0, t_1, \dots, t_p))$ where Φ is a function on H

(i) Φ is increasing on H ;

(ii) $\Phi(0) = 0$;

(iii) $\Phi(t+v) \leq \Phi(t) + \Phi(v)$ for all $t, v \in H$

Example 1.1. (Discrete quaternion valued g-metric space) Consider a nonempty set X . Define $d_H: X^{p+1} \rightarrow H$ as follows:

$$d_H(t_0, t_1, \dots, t_p) = \begin{cases} 0, & \text{if } t_0 = t_1 = \dots = t_p \\ 1, & \text{otherwise.} \end{cases}$$

for all $t_0, t_1, \dots, t_p \in X$. This function d_H represents a quaternion-valued g-metric on X .

Theorem 1.2. On a nonempty set X , let (X, g_H) represent a quaternion-valued g-metric of order n . The following claims are accurate:

$$1. g_H\left(\underbrace{t, \dots, t}_{\eta \text{ times}}, y, \dots, y\right) \leq g_H\left(\underbrace{t, \dots, t}_{\eta \text{ times}}, v, \dots, v\right) + g_H\left(\underbrace{t, \dots, t}_{\eta \text{ times}}, y, \dots, y\right),$$

$$2. g_H\left(\underbrace{t, \dots, t}_{\eta \text{ times}}, v, \dots, v\right) \leq \eta g_H(t, v, \dots, v) \text{ and}$$

$$g_H\left(\underbrace{t, \dots, t}_{\eta \text{ times}}, v, \dots, v\right) \leq (n+1-\eta) g_H(v, t, \dots, t),$$

$$3. g_H(t_0, t_1, \dots, t_n) \leq \sum_{i=0}^n g_H(t_i, v, \dots, v),$$

$$4. g_H(t, v, \dots, v) \leq (1 + (\eta - 1)(n+1-\eta)) g_H\left(\underbrace{t, \dots, t}_{\eta \text{ times}}, v, \dots, v\right).$$

Definition 1.7. Let (X, g_H) be a g-metric space with quaternion values.

(i) Any point $t_0 \in X$ is said to be the interior of a set $A \subset X$, if there exists $q \in H: 0 \prec q$ such that

$$B_{g_H}(t_0, q) := \{y \in X \mid g_H(t_0, y, \dots, y) \prec q\} \subset A.$$

(ii) When every point in subset A is an interior point in subset A , then A is said to be open in subset X .

Here, we investigate the notion of convergence for double sequences in the context of g-metric spaces with quaternion values and discuss some of their basic characteristics. This study is significant as it extends the traditional framework of metric spaces by incorporating quaternion values, which are essential in various applications such as signal processing, control theory, and three-dimensional computer graphics. We meticulously examine statistical convergence within this

context, providing a detailed definition and analysis. By doing so, we contribute to the mathematical foundation necessary for advanced theoretical research and practical applications in areas where quaternion-valued functions are prevalent. Furthermore, our investigation culminates in the final section, where we explore the intricate relationship between statistical convergence in quaternion-valued g-metric spaces and the concept of strong summability. This exploration not only connects theoretical concepts but also sheds light on their practical implications, offering new insights and tools for researchers and practitioners working with complex multidimensional data structures. The results of this study can potentially lead to new methodologies and algorithms that improve the efficiency and accuracy of computational processes in various scientific and engineering fields.

2. New Concepts

This section defines quaternion valued g-metric space and goes over some of its fundamental properties.

Definition 2.1. Assume that (X, g_H) is a quaternion valued g-metric space, $t \in X$ is a point and $\{t_{r_1 u_1}, t_{r_2 u_2}, \dots, t_{r_p u_p}\} \subseteq X$ is a sequence. $\{t_{r_1 u_1}, t_{r_2 u_2}, \dots, t_{r_p u_p}\} g_H$ -converges to t denoted by $\{t_{r_1 u_1}, t_{r_2 u_2}, \dots, t_{r_p u_p}\} \xrightarrow{g_H} t$ if for every $0 \prec q \in H$ there exists $N \in \mathbb{N}$ such that

$$r_1, r_2, \dots, r_p \geq N, u_1, u_2, \dots, u_p \geq N \Rightarrow g_H(t, t_{r_1 u_1}, t_{r_2 u_2}, \dots, t_{r_p u_p}) \prec q$$

In such a situation, $\{t_{r_1 u_1}, t_{r_2 u_2}, \dots, t_{r_p u_p}\}$ is called g_H -convergent in X and t is said to be g_H -limit of $\{t_{r_1 u_1}, t_{r_2 u_2}, \dots, t_{r_p u_p}\}$.

Definition 2.2. Let (X, g_H) be a quaternion valued g-metric space. Let $t \in X$ be a point and $\{t_{r_1 u_1}, t_{r_2 u_2}, \dots, t_{r_p u_p}\} \subseteq X$ be a sequence. $\{t_{r_1 u_1}, t_{r_2 u_2}, \dots, t_{r_p u_p}\}$ is called g_H -Cauchy if for all $q \in H, 0 \prec q$, there exists $N \in \mathbb{N}$ such that $r_0, r_1, r_2, \dots, r_p \geq N, u_0, u_1, u_2, \dots, u_p \geq N$

$$\Rightarrow g_H(t_{r_0 u_0}, t_{r_1 u_1}, t_{r_2 u_2}, \dots, t_{r_p u_p}) \prec q.$$

Definition 2.3. Assume that (X, g_H) is a g-metric space with quaternion values. If all g_H -Cauchy sequence in (X, g_H) is g_H -convergent in (X, g_H) , then (X, g_H) is complete.

Proposition 2.1. The following claims are accurate:

(a) In a quaternion valued g-metric space, the limit of a g_H -convergent sequence is unique.

(b) In a quaternion valued g-metric space, every convergent sequence is a g_H Cauchy sequence.

Proof. (a) Assume that (X, g_H) is a quaternion valued g-metric space and $\{t_{r_1 u_1}, t_{r_2 u_2}, \dots, t_{r_p u_p}\} \subseteq X$. By Definition 2.1 for $0 \prec q \in H$, there exists N_1 and N_2 such that

$g_{\mathbb{H}}(\alpha, \mathbf{t}_{r_1 u_1}, \mathbf{t}_{r_2 u_2}, \dots, \mathbf{t}_{r_p u_p}) \prec \frac{q}{w+1}$ for all

$r_1, r_2, \dots, r_p > N_1, u_1, u_2, \dots, u_p > N_1,$

$g_{\mathbb{H}}(\beta, \mathbf{t}_{r_1 u_1}, \mathbf{t}_{r_2 u_2}, \dots, \mathbf{t}_{r_p u_p}) \prec \frac{q}{w+1}$ for all

$r_1, r_2, \dots, r_p > N_2, u_1, u_2, \dots, u_p > N_2.$

Set $N = \max\{N_1, N_2\}$. If $m, n \geq N$, then by the condition (iv) of definition 1.6 and Theorem 1.1, it follows that

$$\begin{aligned} |g_{\mathbb{H}}(\alpha, \beta, \beta, \dots, \beta)| &\leq |g_{\mathbb{H}}(\alpha, \mathbf{t}_{mn}, \mathbf{t}_{mn}, \dots, \mathbf{t}_{mn})| \\ + |g_{\mathbb{H}}(\mathbf{t}_{mn}, \beta, \beta, \dots, \beta)| &\leq |g_{\mathbb{H}}(\alpha, \mathbf{t}_{mn}, \mathbf{t}_{mn}, \dots, \mathbf{t}_{mn})| \\ + w |g_{\mathbb{H}}(\beta, \mathbf{t}_{mn}, \mathbf{t}_{mn}, \dots, \mathbf{t}_{mn})| &< \frac{q}{w+1} + \frac{wq}{w+1} = q. \end{aligned}$$

Since $0 \prec q \in \mathbb{H}$ is arbitrary, $g_{\mathbb{H}}(\alpha, \beta, \beta, \dots, \beta) = 0$. Hence $\alpha = \beta$.

(b) Assume that $(X, g_{\mathbb{H}})$ is a quaternion valued g -metric space and $\{\mathbf{t}_{r_1 u_1}, \mathbf{t}_{r_2 u_2}, \dots, \mathbf{t}_{r_p u_p}\} \subseteq X$ is a sequence that

$g_{\mathbb{H}}(\mathbf{t}, \mathbf{t}_{r_1 u_1}, \mathbf{t}_{r_2 u_2}, \dots, \mathbf{t}_{r_p u_p}) \prec \frac{q}{w+1}$ for all $\{r_1, r_2, \dots, r_p\} > N$ and $\{u_1, u_2, \dots, u_p\} > N$.

Following from Theorem 1.2 and quaternion valued g -metric space's monotonicity requirement,

$$g_{\mathbb{H}}(\mathbf{t}_{r_0 u_0}, \mathbf{t}_{r_1 u_1}, \mathbf{t}_{r_2 u_2}, \dots, \mathbf{t}_{r_p u_p}) \preceq \sum_{k=0}^w g_{\mathbb{H}}(\mathbf{t}_{r_k u_k}, \mathbf{t}, \dots, \mathbf{t}) \preceq \sum_{k=0}^w \frac{q}{w+1} = q.$$

Thus, $\{\mathbf{t}_{r_1 u_1}, \mathbf{t}_{r_2 u_2}, \dots, \mathbf{t}_{r_p u_p}\}$ is $g_{\mathbb{H}}$ -Cauchy in $(X, g_{\mathbb{H}})$.

Proposition 2.2. Assume that $(X, g_{\mathbb{H}})$ is a quaternion valued g -metric space and $\{\mathbf{t}_{r_1 u_1}, \mathbf{t}_{r_2 u_2}, \dots, \mathbf{t}_{r_p u_p}\}$ is a sequence in X . Then $\{\mathbf{t}_{r_1 u_1}, \mathbf{t}_{r_2 u_2}, \dots, \mathbf{t}_{r_p u_p}\}$ converges to \mathbf{t} iff

$|g_{\mathbb{H}}(\mathbf{t}, \mathbf{t}_{r_1 u_1}, \mathbf{t}_{r_2 u_2}, \dots, \mathbf{t}_{r_p u_p})| \rightarrow 0$ as $\{r_1, r_2, \dots, r_p\} \rightarrow \infty$ and $\{u_1, u_2, \dots, u_p\} \rightarrow \infty$.

Proof. Suppose that $\{\mathbf{t}_{r_1 u_1}, \mathbf{t}_{r_2 u_2}, \dots, \mathbf{t}_{r_p u_p}\}$ converges to \mathbf{t} . Assume $q = \frac{\varrho}{2} + i \frac{\varrho}{2} + j \frac{\varrho}{2} + k \frac{\varrho}{2}$ and a real number $\varrho > 0$.

. Thus, $0 \prec q \in \mathbb{H}$ and there is natural number N such that $|g_{\mathbb{H}}(\mathbf{t}, \mathbf{t}_{r_1 u_1}, \mathbf{t}_{r_2 u_2}, \dots, \mathbf{t}_{r_p u_p})| < |q| = \varrho$ for all $\{r_1, r_2, \dots, r_p\} > N$ and $\{u_1, u_2, \dots, u_p\} > N$. Hence $|g_{\mathbb{H}}(\mathbf{t}, \mathbf{t}_{r_1 u_1}, \mathbf{t}_{r_2 u_2}, \dots, \mathbf{t}_{r_p u_p})| \rightarrow 0$ as $\{r_1, r_2, \dots, r_p\} \rightarrow \infty$ and $\{u_1, u_2, \dots, u_p\} \rightarrow \infty$.

Conversely, suppose that $|g_{\mathbb{H}}(\mathbf{t}, \mathbf{t}_{r_1 u_1}, \mathbf{t}_{r_2 u_2}, \dots, \mathbf{t}_{r_p u_p})| \rightarrow 0$ as $\{r_1, r_2, \dots, r_p\} \rightarrow \infty$ and $\{u_1, u_2, \dots, u_p\} \rightarrow \infty$. Then, given $q \in \mathbb{H}$ with $0 \prec q$, there is a real number $\delta > 0$, such that, for $h \in \mathbb{H}$,

$$|h| < \delta \Rightarrow h \prec q.$$

For this δ , there is a natural number N such that $|g_{\mathbb{H}}(\mathbf{t}, \mathbf{t}_{r_1 u_1}, \mathbf{t}_{r_2 u_2}, \dots, \mathbf{t}_{r_p u_p})| < \delta$ for all $\{r_1, r_2, \dots, r_p\} > N$ and $\{u_1, u_2, \dots, u_p\} > N$. Implying that $g_{\mathbb{H}}(\mathbf{t}, \mathbf{t}_{r_1 u_1}, \mathbf{t}_{r_2 u_2}, \dots, \mathbf{t}_{r_p u_p}) \prec q$ for all $\{r_1, r_2, \dots, r_p\} > N$ and $\{u_1, u_2, \dots, u_p\} > N$, hence $\{\mathbf{t}_{r_1 u_1}, \mathbf{t}_{r_2 u_2}, \dots, \mathbf{t}_{r_p u_p}\}$ converges to \mathbf{t} .

Proposition 2.3. Assume that $(X, g_{\mathbb{H}})$ is a quaternion valued g -metric space and $\{\mathbf{t}_{r_1 u_1}, \mathbf{t}_{r_2 u_2}, \dots, \mathbf{t}_{r_p u_p}\}$ is a sequence in X . Then $\{\mathbf{t}_{r_1 u_1}, \mathbf{t}_{r_2 u_2}, \dots, \mathbf{t}_{r_p u_p}\}$ is a Cauchy sequence if and only if

$$|g_{\mathbb{H}}(\mathbf{t}, \mathbf{t}_{r_1 u_1}, \mathbf{t}_{r_2 u_2}, \dots, \mathbf{t}_{r_p u_p})| \rightarrow 0 \text{ as } r_1, u_1, r_2, u_2, \dots, r_p, u_p \rightarrow \infty.$$

Proof. Suppose that $\{\mathbf{t}_{r_1 u_1}, \mathbf{t}_{r_2 u_2}, \dots, \mathbf{t}_{r_p u_p}\}$ converges to \mathbf{t} . Assume $q = \frac{\varrho}{2} + i \frac{\varrho}{2} + j \frac{\varrho}{2} + k \frac{\varrho}{2}$ and a real number $\varrho > 0$. Thus, $0 \prec q \in \mathbb{H}$ and there is natural number N such that $g_{\mathbb{H}}(\mathbf{t}_{r_0 u_0}, \mathbf{t}_{r_1 u_1}, \mathbf{t}_{r_2 u_2}, \dots, \mathbf{t}_{r_p u_p}) \prec q$ for all $\{r_1, r_2, \dots, r_p\} > N$ and $\{u_1, u_2, \dots, u_p\} > N$. Therefore, $|g_{\mathbb{H}}(\mathbf{t}_{r_0 u_0}, \mathbf{t}_{r_1 u_1}, \mathbf{t}_{r_2 u_2}, \dots, \mathbf{t}_{r_p u_p})| < |q| = \varrho$ for all $\{r_1, r_2, \dots, r_p\} > N$ and $\{u_1, u_2, \dots, u_p\} > N$. Hence $|g_{\mathbb{H}}(\mathbf{t}_{r_0 u_0}, \mathbf{t}_{r_1 u_1}, \mathbf{t}_{r_2 u_2}, \dots, \mathbf{t}_{r_p u_p})| \rightarrow 0$ as $\{r_1, r_2, \dots, r_p\} \rightarrow \infty$ and $\{u_1, u_2, \dots, u_p\} \rightarrow \infty$.

Conversely, suppose that $|g_{\mathbb{H}}(\mathbf{t}_{r_0 u_0}, \mathbf{t}_{r_1 u_1}, \mathbf{t}_{r_2 u_2}, \dots, \mathbf{t}_{r_p u_p})| \rightarrow 0$ as $\{r_1, r_2, \dots, r_p\} \rightarrow \infty$ and $\{u_1, u_2, \dots, u_p\} \rightarrow \infty$. Then, given $q \in \mathbb{H}$ with $0 \prec q$, there is a real number $\delta > 0$, such that, for $h \in \mathbb{H}$,

$$|h| < \delta \Rightarrow h \prec q.$$

For this δ , there is a natural number N such that $|g_{\mathbb{H}}(\mathbf{t}_{r_0 u_0}, \mathbf{t}_{r_1 u_1}, \mathbf{t}_{r_2 u_2}, \dots, \mathbf{t}_{r_p u_p})| < \delta$ for all $\{r_1, r_2, \dots, r_p\} > N$ and $\{u_1, u_2, \dots, u_p\} > N$. Implying that $g_{\mathbb{H}}(\mathbf{t}_{r_0 u_0}, \mathbf{t}_{r_1 u_1}, \mathbf{t}_{r_2 u_2}, \dots, \mathbf{t}_{r_p u_p}) \prec q$ for all $\{r_1, r_2, \dots, r_p\} > N$ and $\{u_1, u_2, \dots, u_p\} > N$, hence $\{\mathbf{t}_{r_1 u_1}, \mathbf{t}_{r_2 u_2}, \dots, \mathbf{t}_{r_p u_p}\}$ is a Cauchy sequence to \mathbf{t} .

Definition 2.4. Assume that $(X, g_{\mathbb{H}})$ is a quaternion valued g -metric space and $0 \prec q \in \mathbb{H}$ is given.

(i) A set $A \subset X$ is said to be $q, g_{\mathbb{H}}$ -net of $(X, g_{\mathbb{H}})$ if for $\mathbf{t} \in X$, there exists $a \in A$ such that $\mathbf{t} \in B_{g_{\mathbb{H}}}(a, q)$. A set is referred to as finite $q, g_{\mathbb{H}}$ -net of $(X, g_{\mathbb{H}})$ if it is finite.

(ii) A quaternion valued g -metric space $(X, g_{\mathbb{H}})$ is called totally $g\mathbb{H}$ -bounded if for all $0 \prec q \in \mathbb{H}$ there exists a finite $q, g_{\mathbb{H}}$ -net.

(iii) If a quaternion valued g -metric space $(X, g_{\mathbb{H}})$ is complete and totally $g_{\mathbb{H}}$ -bounded, it is referred to as $g_{\mathbb{H}}$ -compact.

Definition 2.5. Let $(X, g_{\mathbb{H}_1})$ and $(X, g_{\mathbb{H}_2})$ be quaternion valued g -metric spaces. A mapping $T: X_1 \rightarrow X_2$ is said to be $g_{\mathbb{H}}$ -continuous at point $\mathbf{t} \in X_1$ provided that for each open ball $B_{g_{\mathbb{H}_2}}(T(\mathbf{t}), q)$ there exists an open ball $B_{g_{\mathbb{H}_1}}(\mathbf{t}, \delta) \subseteq B_{g_{\mathbb{H}_2}}(T(\mathbf{t}), q)$.

3. Statistical Convergence of Double Sequences in Quaternion Valued g -metric Space

In this section, we introduce statistical convergence for double sequences in quaternion-valued g -metric space and give several key characteristics.

Definition 3.1. Let $(X, g\mathbf{H})$ be a quaternion valued g-metric space, $\mathbf{t} \in X$ be a point, and $\{\mathbf{t}_{\alpha\beta}\} \subseteq X$ be a sequence.

(i) $\{\mathbf{t}_{\alpha\beta}\}$ statistically converges to \mathbf{t} if for each $q \prec \mathbf{H}$ with $0 \prec q$ such that

$$\lim_{\alpha, \beta \rightarrow \infty} \frac{p!}{(\alpha\beta)^p} |\{(r_1, r_2, \dots, r_p), (u_1, u_2, \dots, u_p)\} \in \mathbb{N}^p \times \mathbb{N}^p, \\ r_1, r_2, \dots, r_p \leq \alpha, u_1, u_2, \dots, u_p \\ \leq \beta (\alpha, \beta \in \mathbb{N}): |g_{\mathbf{H}}(\mathbf{t}, \mathbf{t}_{r_1u_1}, \mathbf{t}_{r_2u_2}, \dots, \mathbf{t}_{r_pu_p})| \geq |q|\}| = 0.$$

and denoted by $g_{\mathbf{H}}(\eta\mathbf{t}) - \lim_{\alpha, \beta \rightarrow \infty} \{\mathbf{t}_{r_1u_1}, \mathbf{t}_{r_2u_2}, \dots, \mathbf{t}_{r_pu_p}\} = \mathbf{t}$ or $\{\mathbf{t}_{\alpha\beta}\} \xrightarrow{g_{\mathbf{H}}(\eta\mathbf{t})} \mathbf{t}$.

(ii) $\{\mathbf{t}_{\alpha\beta}\}$ is said to be statistically $g_{\mathbf{H}}$ -Cauchy if for every $q \in \mathbf{H}$ with $0 \prec q$, there exists $r_m, u_n \prec \mathbf{H}$ such that

$$\lim_{\alpha, \beta \rightarrow \infty} \frac{p!}{(\alpha\beta)^p} |\{(r_1, r_2, \dots, r_p), (u_1, u_2, \dots, u_p)\} \in \mathbb{N}^p \times \mathbb{N}^p, \\ r_1, r_2, \dots, r_p \leq \alpha, u_1, u_2, \dots, u_p \\ \leq \beta (\alpha, \beta \in \mathbb{N}): |g_{\mathbf{H}}(x_{r_mu_n}, \mathbf{t}_{r_1u_1}, \mathbf{t}_{r_2u_2}, \dots, \mathbf{t}_{r_pu_p})| \geq |q|\}| = 0.$$

$(X, g\mathbf{H})$ is called a complete quaternion valued -metric space.

(iii) $\{\mathbf{t}_{\alpha\beta}\}$ is bounded if there exists a positive number M such that $|\{\mathbf{t}_{r_1u_1}, \mathbf{t}_{r_2u_2}, \dots, \mathbf{t}_{r_pu_p}\}| \leq M$ for all $\{(r_1, r_2, \dots, r_p), (u_1, u_2, \dots, u_p)\}$.

The set of all bounded sequences will be represented by ℓ_∞ .

Theorem 3.1. If a sequence $\{\mathbf{t}_{\alpha\beta}\}$ is statistically convergent in $(X, g\mathbf{H})$ then $g_{\mathbf{H}}(\eta\mathbf{t}) - \lim(\mathbf{t}_{\alpha\beta})$ is unique.

Proof. Suppose that $\{\mathbf{t}_{\alpha\beta}\}$ statistically converges in $(X, g\mathbf{H})$. Let $g_{\mathbf{H}}(\eta\mathbf{t}) - \lim(\mathbf{t}_{\alpha\beta}) = \gamma_1$ and $g_{\mathbf{H}}(\eta\mathbf{t}) - \lim(\mathbf{t}_{\alpha\beta}) = \gamma_2$.

Given $\varepsilon > 0$ and $0 \prec q \in \mathbf{H}$, let

$$q = \frac{\varrho}{4p} + i \frac{\varrho}{4p} + j \frac{\varrho}{4p} + k \frac{\varrho}{4p}.$$

Define the following sets as:

$$K_1(\varrho) = \{(r_1, r_2, \dots, r_p), (u_1, u_2, \dots, u_p)\} \in \mathbb{N}^p \times \mathbb{N}^p, \\ r_1, r_2, \dots, r_p \leq \alpha, u_1, u_2, \dots, u_p \leq \\ \beta (\alpha, \beta \in \mathbb{N}): |g_{\mathbf{H}}(\gamma_1, \mathbf{t}_{r_1u_1}, \mathbf{t}_{r_2u_2}, \dots, \mathbf{t}_{r_pu_p})| \geq |q| = \frac{\varrho}{2p}\},$$

$$K_2(\varrho) = \{(r_1, r_2, \dots, r_p), (u_1, u_2, \dots, u_p)\} \in \mathbb{N}^p \times \mathbb{N}^p, \\ r_1, r_2, \dots, r_p \leq \alpha, u_1, u_2, \dots, u_p \leq \\ \beta (\alpha, \beta \in \mathbb{N}): |g_{\mathbf{H}}(\gamma_2, \mathbf{t}_{r_1u_1}, \mathbf{t}_{r_2u_2}, \dots, \mathbf{t}_{r_pu_p})| \geq |q| = \frac{\varrho}{2p}\}.$$

Since $g_{\mathbf{H}}(\eta\mathbf{t}) - \lim(\mathbf{t}_{r_1u_1}, \mathbf{t}_{r_2u_2}, \dots, \mathbf{t}_{r_pu_p}) = \gamma_1$, we have $\delta(K_1(\varrho)) = 0$.

Similarly $g_{\mathbf{H}}(\eta\mathbf{t}) - \lim(\mathbf{t}_{r_1u_1}, \mathbf{t}_{r_2u_2}, \dots, \mathbf{t}_{r_pu_p}) = \gamma_2$, implies $\delta(K_2(\varrho)) = 0$.

Let $K(\varrho) = K_1(\varrho) \cup K_2(\varrho)$. Then $\delta(K(\varrho)) = 0$ and we have $K^c(\varrho)$ is non-empty and $\delta(K^c(\varrho)) = 1$. Suppose $\{r_1, r_2, \dots, r_p\}, \{u_1, u_2, \dots, u_p\} \in K^c(\varrho)$, then by Theorem 1.2, we have:

$$|g_{\mathbf{H}}(\gamma_1, \gamma_2, \gamma_2, \dots, \gamma_2)| \leq |g_{\mathbf{H}}(\gamma_1, \mathbf{t}_{mn}, \mathbf{t}_{mn}, \dots, \mathbf{t}_{mn})| \\ + |g_{\mathbf{H}}(\mathbf{t}_{mn}, \gamma_2, \gamma_2, \dots, \gamma_2)| \leq |g_{\mathbf{H}}(\gamma_1, \mathbf{t}_{mn}, \mathbf{t}_{mn}, \dots, \mathbf{t}_{mn})| \\ + p|g_{\mathbf{H}}(\gamma_2, \mathbf{t}_{mn}, \mathbf{t}_{mn}, \dots, \mathbf{t}_{mn})| \leq |g_{\mathbf{H}}(\gamma_1, \mathbf{t}_{r_1u_1}, \mathbf{t}_{r_2u_2}, \dots, \mathbf{t}_{r_pu_p})| \\ + p|g_{\mathbf{H}}(\gamma_2, \mathbf{t}_{r_1u_1}, \mathbf{t}_{r_2u_2}, \dots, \mathbf{t}_{r_pu_p})| \leq p|g_{\mathbf{H}}(\gamma_1, \mathbf{t}_{r_1u_1}, \mathbf{t}_{r_2u_2}, \dots, \mathbf{t}_{r_pu_p})| \\ + p|g_{\mathbf{H}}(\gamma_2, \mathbf{t}_{r_1u_1}, \mathbf{t}_{r_2u_2}, \dots, \mathbf{t}_{r_pu_p})| \leq p\left(\frac{\varrho}{2p} + \frac{\varrho}{2p}\right) = \varrho.$$

Since $\varrho > 0$ was arbitrary, we get $g_{\mathbf{H}}(\gamma_1, \gamma_2, \gamma_2, \dots, \gamma_2) = 0$, therefore $\gamma_1 = \gamma_2$.

Theorem 3.2. If $g_{\mathbf{H}} - \lim(\mathbf{t}_{\alpha\beta}) = \mathbf{t}$, then $g_{\mathbf{H}}(\eta\mathbf{t}) - \lim(\mathbf{t}_{\alpha\beta}) = \mathbf{t}$ the opposite need not always hold.

Proof. Assume that $g_{\mathbf{H}} - \lim(\mathbf{t}_{\alpha\beta}) = \mathbf{t}$. Thus for all $0 \prec q \in \mathbf{H}$ there exists $N \in \mathbb{N}$ such that

$$r_1, r_2, \dots, r_p \geq N, u_1, u_2, \dots, u_p \geq N \Rightarrow g_{\mathbf{H}}(\mathbf{t}, \mathbf{t}_{r_1u_1}, \mathbf{t}_{r_2u_2}, \dots, \mathbf{t}_{r_pu_p}) \prec q.$$

The set

$$A(\varrho) = \{(r_1, r_2, \dots, r_p), (u_1, u_2, \dots, u_p)\} \in \mathbb{N}^p \times \mathbb{N}^p, \\ r_1, r_2, \dots, r_p \leq \alpha, u_1, u_2, \dots, u_p \\ \leq \beta (\alpha, \beta \in \mathbb{N}): |g_{\mathbf{H}}(\mathbf{t}, \mathbf{t}_{r_1u_1}, \mathbf{t}_{r_2u_2}, \dots, \mathbf{t}_{r_pu_p})| \geq |q| = \varrho\} \\ \subset \{(1, 1), (2, 2), (3, 3), \dots\}, \\ \text{where } q = \frac{\varrho}{2} + i \frac{\varrho}{2} + j \frac{\varrho}{2} + k \frac{\varrho}{2}, \delta(A(\varrho)) = 0. \text{ Hence} \\ g_{\mathbf{H}}(\eta\mathbf{t}) - \lim(\mathbf{t}_{\alpha\beta}) = \mathbf{t}.$$

The following example demonstrates that the reverse does not have to be true.

Example 3.1. Let $X = \mathbb{R}$ and $G_{\mathbf{H}}: \mathbb{R} \times \mathbb{R} \times \mathbb{R} \rightarrow \mathbf{H}$ be a quaternion valued G-metric space defined by

$$G_{\mathbf{H}}(p_1, p_2, p_3) = |z_0^1 - z_0^2| + |z_0^1 - z_0^3| \\ + i(|z_1^1 - z_1^2| + |z_1^1 - z_1^3| + |z_1^2 - z_1^3|) \\ + j(|z_2^1 - z_2^2| + |z_2^1 - z_2^3| + |z_2^2 - z_2^3|) \\ + k(|z_3^1 - z_3^2| + |z_3^1 - z_3^3| + |z_3^2 - z_3^3|)$$

where $y_r = y_0' + y_0^r i + y_0^r j + y_0^r k$ for $r = 1, 2, 3$. Let

$\mathbf{t}_{mn} = \{\mathbf{t}_{r_1u_1}, \mathbf{t}_{r_2u_2}, \dots, \mathbf{t}_{r_pu_p}\}$ be a sequence defined as

$$\mathbf{t}_{mn} = \begin{cases} mn, & \text{if } m, n \text{ is a square} \\ 1, & \text{if not.} \end{cases}$$

It is easy to see that $g_{\mathbf{H}}(\eta\mathbf{t}) - \lim(\mathbf{t}_{mn}) = 1$, since

$$|(m, n) \in \mathbb{N}^p, m \leq \alpha, n \leq \beta (\alpha, \beta \in \mathbb{N}): |g_{\mathbf{H}}(1, \mathbf{t}_{mn})| > |q| \\ = \varrho| \leq \sqrt{mn}$$

for every $\varrho > 0$ and $q = \frac{\varrho}{2} + i \frac{\varrho}{2} + j \frac{\varrho}{2} + k \frac{\varrho}{2}$. But $\{\mathbf{t}_{mn}\}$ is neither convergent nor bounded.

Theorem 3.3. Allow $(X, g_{\mathbb{H}})$ to be the complete g-metric space with quaternion values. A sequence $\{\mathbf{t}_{\alpha\beta}\}$ of points in $(X, g_{\mathbb{H}})$ is considered statistically g-convergent iff it is statistically $g_{\mathbb{H}}$ -Cauchy.

Proof. Assume $g_{\mathbb{H}} - \lim(\mathbf{t}_{\alpha\beta}) = \mathbf{t}$. So, we have

$$\delta(A(\varrho)) = 0, \text{ where}$$

$$A(\varrho) = \{((r_1, r_2, \dots, r_p), (u_1, u_2, \dots, u_p)) \in \mathbb{N}^p \times \mathbb{N}^p,$$

$$r_1, r_2, \dots, r_p \leq \alpha, u_1, u_2, \dots, u_p$$

$$\leq \beta(\alpha, \beta \in \mathbb{N}): |g_{\mathbb{H}}(\mathbf{t}, \mathbf{t}_{r_1 u_1}, \mathbf{t}_{r_2 u_2}, \dots, \mathbf{t}_{r_p u_p})| \geq |q| = \frac{\varrho}{2}\},$$

$$\text{where } q = \frac{\varrho}{4} + i \frac{\varrho}{4} + j \frac{\varrho}{4} + k \frac{\varrho}{4}.$$

This implies that

$$\delta(A^c(\varrho)) = \{((r_1, r_2, \dots, r_p), (u_1, u_2, \dots, u_p)) \in \mathbb{N}^p \times \mathbb{N}^p,$$

$$r_1, r_2, \dots, r_p \leq \alpha, u_1, u_2, \dots, u_p$$

$$\leq \beta(\alpha, \beta \in \mathbb{N}): |g_{\mathbb{H}}(\mathbf{t}, \mathbf{t}_{r_1 u_1}, \mathbf{t}_{r_2 u_2}, \dots, \mathbf{t}_{r_p u_p})| < |q| = \frac{\varrho}{2}\} = 1.$$

Let $(j_1, j_2, \dots, j_n), (k_1, k_2, \dots, k_n) \in A^c(\varrho)$. Then

$$|g_{\mathbb{H}}(\mathbf{t}, \mathbf{t}_{j_1 k_1}, \mathbf{t}_{j_2 k_2}, \dots, \mathbf{t}_{j_n k_n})| < |q| = \frac{\varrho}{2}.$$

Let

$$B(\varrho) = \{((r_1, r_2, \dots, r_p), (u_1, u_2, \dots, u_p)) \in \mathbb{N}^p \times \mathbb{N}^p,$$

$$r_1, r_2, \dots, r_p \leq \alpha, u_1, u_2, \dots, u_p$$

$$\leq \beta(\alpha, \beta \in \mathbb{N}): |g_{\mathbb{H}}(\mathbf{t}_{j_1 k_1}, \mathbf{t}_{j_2 k_2}, \dots, \mathbf{t}_{j_n k_n}, \mathbf{t}_{r_1 u_1}, \mathbf{t}_{r_2 u_2}, \dots, \mathbf{t}_{r_p u_p})| \geq \varrho\},$$

we need to show that $B(\varrho) \subset A(\varrho)$. Let $\alpha, \beta \in B(\varrho)$. Then

$$|g_{\mathbb{H}}(\mathbf{t}_{j_1 k_1}, \mathbf{t}_{j_2 k_2}, \dots, \mathbf{t}_{j_n k_n}, \mathbf{t}_{r_1 u_1}, \mathbf{t}_{r_2 u_2}, \dots, \mathbf{t}_{r_p u_p})| \geq \varrho$$

$$\text{and hence } |g_{\mathbb{H}}(\mathbf{t}, \mathbf{t}_{r_1 u_1}, \mathbf{t}_{r_2 u_2}, \dots, \mathbf{t}_{r_p u_p})| \geq \frac{\varrho}{2}.$$

That is $r_1, r_2, \dots, r_p \leq \alpha, u_1, u_2, \dots, u_p \leq \beta(\alpha, \beta \in \mathbb{N}) \in A(\varrho)$.

Otherwise if $|g_{\mathbb{H}}(\mathbf{t}, \mathbf{t}_{r_1 u_1}, \mathbf{t}_{r_2 u_2}, \dots, \mathbf{t}_{r_p u_p})| \leq \varrho$ then

$$\begin{aligned} \varrho &\leq |g_{\mathbb{H}}(\mathbf{t}_{j_1 k_1}, \mathbf{t}_{j_2 k_2}, \dots, \mathbf{t}_{j_n k_n}, \mathbf{t}_{r_1 u_1}, \mathbf{t}_{r_2 u_2}, \dots, \mathbf{t}_{r_p u_p})| \\ &\leq g_{\mathbb{H}}(\mathbf{t}, \mathbf{t}_{r_1 u_1}, \mathbf{t}_{r_2 u_2}, \dots, \mathbf{t}_{r_p u_p}) + (\mathbf{t}, \mathbf{t}_{j_1 k_1}, \mathbf{t}_{j_2 k_2}, \dots, \mathbf{t}_{j_n k_n}) \\ &< \frac{\varrho}{2} + \frac{\varrho}{2} = \varrho \end{aligned}$$

which is not possible. Hence $B(\varrho) \subset A(\varrho)$, which implies that $\{\mathbf{t}_{r_1 u_1}, \mathbf{t}_{r_2 u_2}, \dots, \mathbf{t}_{r_p u_p}\}$ is $g_{\mathbb{H}}(\eta\mathbf{t})$ -Cauchy.

Conversely, suppose that $\{\mathbf{t}_{\alpha\beta}\}$ is $g_{\mathbb{H}}(\eta\mathbf{t})$ -Cauchy but not $g_{\mathbb{H}}(\eta\mathbf{t})$ -convergent. So, there exists $(j_1, j_2, \dots, j_n), (k_1, k_2, \dots, k_n) \in \mathbb{N}^p \times \mathbb{N}^p$ such that $\delta(G(\varrho)) = 0$ where

$$G(\varrho) = \{((r_1, r_2, \dots, r_p), (u_1, u_2, \dots, u_p)) \in \mathbb{N}^p \times \mathbb{N}^p,$$

$$r_1, r_2, \dots, r_p \leq \alpha, u_1, u_2, \dots, u_p$$

$$\leq \beta(\alpha, \beta \in \mathbb{N}): |g_{\mathbb{H}}(\mathbf{t}_{j_1 k_1}, \mathbf{t}_{j_2 k_2}, \dots, \mathbf{t}_{j_n k_n}, \mathbf{t}_{r_1 u_1}, \mathbf{t}_{r_2 u_2}, \dots, \mathbf{t}_{r_p u_p})| \geq \varrho\}$$

and $\delta(D(\varrho)) = 0$, where

$$D(\varrho) = \{((r_1, r_2, \dots, r_p), (u_1, u_2, \dots, u_p)) \in \mathbb{N}^p \times \mathbb{N}^p,$$

$$r_1, r_2, \dots, r_p \leq \alpha, u_1, u_2, \dots, u_p$$

$$\leq \beta(\alpha, \beta \in \mathbb{N}): |g_{\mathbb{H}}(\mathbf{t}, \mathbf{t}_{r_1 u_1}, \mathbf{t}_{r_2 u_2}, \dots, \mathbf{t}_{r_p u_p})| < \frac{\varrho}{2}\},$$

that is, $\delta(D^c(\varrho)) = 1$.

Since

$$|g_{\mathbb{H}}(\mathbf{t}_{j_1 k_1}, \mathbf{t}_{j_2 k_2}, \dots, \mathbf{t}_{j_n k_n}, \mathbf{t}_{r_1 u_1}, \mathbf{t}_{r_2 u_2}, \dots, \mathbf{t}_{r_p u_p})|$$

$$\leq 2|g_{\mathbb{H}}(\mathbf{t}, \mathbf{t}_{r_1 u_1}, \mathbf{t}_{r_2 u_2}, \dots, \mathbf{t}_{r_p u_p})| \leq \varrho$$

$$\text{if } |g_{\mathbb{H}}(\mathbf{t}, \mathbf{t}_{r_1 u_1}, \mathbf{t}_{r_2 u_2}, \dots, \mathbf{t}_{r_p u_p})| \leq \frac{\varrho}{2}.$$

Therefore $\delta(G^c(\varrho)) = 0$ that is $\delta(G(\varrho)) = 1$, which leads the contradiction, since $\{\mathbf{t}_{r_1 u_1}, \mathbf{t}_{r_2 u_2}, \dots, \mathbf{t}_{r_p u_p}\}$ was $g_{\mathbb{H}}(\eta\mathbf{t})$ -Cauchy. Hence $\{\mathbf{t}_{\alpha\beta}\}$ is $g_{\mathbb{H}}(\eta\mathbf{t})$ -convergent.

4. Strong Summability

The relationship between $g_{\mathbb{H}}$ -statistical convergence and strong summability in quaternion valued g-metric space is established in this section.

Definition 4.1. A sequence $\{\mathbf{t}_{\alpha\beta}\}$ is called strongly p -Cesàro summable ($0 < p < \infty$) to limit \mathbf{t} in $(X, g_{\mathbb{H}})$ if

$$\lim_{\alpha, \beta \rightarrow \infty} \frac{p!}{(\alpha\beta)^p} \sum_{r_1, r_2, \dots, r_p=1}^{\alpha} \sum_{u_1, u_2, \dots, u_p=1}^{\beta} (g_{\mathbb{H}}(\mathbf{t}_{r_1 u_1}, \mathbf{t}_{r_2 u_2}, \dots, \mathbf{t}_{r_p u_p}, \mathbf{t}))^p = 0.$$

and we write it as $\mathbf{t}_{\alpha\beta} \rightarrow \mathbf{t}[C_1, g_{\mathbb{H}}]_p$. Here, I represents the $[C_1, g_{\mathbb{H}}]$ -limit of $\{\mathbf{t}_{\alpha\beta}\}$.

Theorem 4.1. (a). If $0 < p < \infty$ and $\mathbf{t}_{\alpha\beta} \rightarrow \mathbf{t}[C_1, g_{\mathbb{H}}]_p$, then $\{\mathbf{t}_{\alpha\beta}\}$ is statistically $g_{\mathbb{H}}$ -convergent to \mathbf{t} in $(X, g_{\mathbb{H}})$.

(b). If $g_{\mathbb{H}}$ -statistically convergent to \mathbf{t} in $(X, g_{\mathbb{H}})$ and $\{\mathbf{t}_{\alpha\beta}\}$ is bounded, then $\mathbf{t}_{\alpha\beta} \rightarrow \mathbf{t}[C_1, g_{\mathbb{H}}]_p$.

Proof. (a) Let

$$K_\varrho(p) = \{((r_1, r_2, \dots, r_p), (u_1, u_2, \dots, u_p)) \in \mathbb{N}^p \times \mathbb{N}^p,$$

$$r_1, r_2, \dots, r_p \leq \alpha, u_1, u_2, \dots, u_p$$

$$\leq \beta(\alpha, \beta \in \mathbb{N}): |g_{\mathbb{H}}(\mathbf{t}_{r_1 u_1}, \mathbf{t}_{r_2 u_2}, \dots, \mathbf{t}_{r_p u_p}, \mathbf{t})|^p \geq \varrho\}.$$

Now since $\mathbf{t}_{r_1 u_1}, \mathbf{t}_{r_2 u_2}, \dots, \mathbf{t}_{r_p u_p} \rightarrow \mathbf{t}[C_1, g_{\mathbb{H}}]$, then

$$\begin{aligned} 0 &\leftarrow \frac{p!}{(\alpha\beta)^p} \sum_{r_1, r_2, \dots, r_p=1}^{\alpha} \sum_{u_1, u_2, \dots, u_p=1}^{\beta} (g_{\mathbb{H}}(\mathbf{t}_{r_1 u_1}, \mathbf{t}_{r_2 u_2}, \dots, \mathbf{t}_{r_p u_p}, \mathbf{t}))^p \\ &= \frac{p!}{(\alpha\beta)^p} \left(\sum_{r_1, r_2, \dots, r_p=1, r_i \notin K_\varrho(p)}^{\alpha} \sum_{u_1, u_2, \dots, u_p=1, u_i \notin K_\varrho(p)}^{\beta} (g_{\mathbb{H}}(\mathbf{t}_{r_1 u_1}, \mathbf{t}_{r_2 u_2}, \dots, \mathbf{t}_{r_p u_p}, \mathbf{t}))^p \right) \\ &\quad + \sum_{r_1, r_2, \dots, r_p=1, r_i \in K_\varrho(p)}^{\alpha} \sum_{u_1, u_2, \dots, u_p=1, u_i \in K_\varrho(p)}^{\beta} (g_{\mathbb{H}}(\mathbf{t}_{r_1 u_1}, \mathbf{t}_{r_2 u_2}, \dots, \mathbf{t}_{r_p u_p}, \mathbf{t}))^p \Big) \\ &\geq \frac{p!}{(\alpha\beta)^p} |K_\varrho(p)| \varrho^p, \text{ as } \alpha, \beta \rightarrow \infty. \end{aligned}$$

That is, $\lim_{\alpha, \beta \rightarrow \infty} \frac{p!}{(\alpha\beta)^p} |K_\varrho(p)| = 0$ and $\delta(K_\varrho(p)) = 0$.

(b) Suppose that $\{\mathbf{t}_{r_1 u_1}, \mathbf{t}_{r_2 u_2}, \dots, \mathbf{t}_{r_p u_p}\}$ is bounded and statistically g_H -convergent to \mathbf{t} in (X, g_H) . So, for $\varrho > 0$, we have $\delta(K_\varrho(p)) = 0$. Since $\{\mathbf{t}_{r_1 u_1}, \mathbf{t}_{r_2 u_2}, \dots, \mathbf{t}_{r_p u_p}\} \in \ell_\infty$, there exists $M > 0$ such that $|g_H(\mathbf{t}_{r_1 u_1}, \mathbf{t}_{r_2 u_2}, \dots, \mathbf{t}_{r_p u_p}, \mathbf{t})|^p \leq M$. We have

$$\begin{aligned} & \frac{p!}{(\alpha\beta)^p} \sum_{r_1, r_2, \dots, r_p=1}^{\alpha, \beta} \sum_{u_1, u_2, \dots, u_p=1}^{\alpha, \beta} (g_H(\mathbf{t}_{r_1 u_1}, \mathbf{t}_{r_2 u_2}, \dots, \mathbf{t}_{r_p u_p}, \mathbf{S})^p) \\ &= \frac{p!}{(\alpha\beta)^p} \sum_{r_1, r_2, \dots, r_p=1, r_i \notin K_\varrho(p)}^{\alpha} \sum_{u_1, u_2, \dots, u_p=1, u_i \notin K_\varrho(p)}^{\beta} (g_H(\mathbf{t}_{r_1 u_1}, \mathbf{t}_{r_2 u_2}, \dots, \mathbf{t}_{r_p u_p}, \mathbf{S})^p) \\ &+ \frac{p!}{(\alpha\beta)^p} \sum_{r_1, r_2, \dots, r_p=1, r_i \in K_\varrho(p)}^{\alpha} \sum_{u_1, u_2, \dots, u_p=1, u_i \in K_\varrho(p)}^{\beta} (g_H(\mathbf{t}_{r_1 u_1}, \mathbf{t}_{r_2 u_2}, \dots, \mathbf{t}_{r_p u_p}, \mathbf{S})^p) \\ &= U_1(\varrho) + U_2(\varrho), \end{aligned}$$

where

$$U_1(\varrho) = \frac{p!}{(\alpha\beta)^p} \sum_{\substack{r_1, r_2, \dots, r_p=1, r_i \notin K_\varrho(p) \\ u_1, u_2, \dots, u_p=1, u_i \notin K_\varrho(p)}}^{\alpha, \beta} (g_H(\mathbf{t}_{r_1 u_1}, \mathbf{t}_{r_2 u_2}, \dots, \mathbf{t}_{r_p u_p}, \mathbf{S})^p)$$

and

$$U_2(\varrho) = \frac{p!}{(\alpha\beta)^p} \sum_{\substack{r_1, r_2, \dots, r_p=1, r_i \in K_\varrho(p) \\ u_1, u_2, \dots, u_p=1, u_i \in K_\varrho(p)}}^{\alpha, \beta} (g_H(\mathbf{t}_{r_1 u_1}, \mathbf{t}_{r_2 u_2}, \dots, \mathbf{t}_{r_p u_p}, \mathbf{S})^p).$$

Now if $\{r_1, r_2, \dots, r_p\}, \{u_1, u_2, \dots, u_p\} \notin K_\varrho(\varrho)$ then $U_1(\varrho) < \varrho^p$. For $\{r_1, r_2, \dots, r_p\}, \{u_1, u_2, \dots, u_p\} \in K_\varrho(\varrho)$,

we deduce that

$$\begin{aligned} U_2(\varrho) &\leq \sup |g_H(\mathbf{t}_{r_1 u_1}, \mathbf{t}_{r_2 u_2}, \dots, \mathbf{t}_{r_p u_p}, \mathbf{t})| \left(\frac{p! |K_\varrho(p)|}{(\alpha\beta)^p} \right) \\ &\leq M \frac{p! |K_\varrho(p)|}{(\alpha\beta)^p} \rightarrow 0 \end{aligned}$$

as $\alpha, \beta \rightarrow \infty$, since $\delta(K_\varrho(p)) = 0$. Hence $\mathbf{t}_{r_1 u_1}, \mathbf{t}_{r_2 u_2}, \dots, \mathbf{t}_{r_p u_p} \rightarrow [\mathbf{C}_1, g_H]$.

5. Conclusion and Suggestions

In this manuscript, we have introduced and explored the concept of convergence for double sequences within the quaternion-valued g-metric space, examining several foundational properties. Furthermore, we have conducted a detailed analysis of statistical convergence in this context, aiming to provide a comprehensive understanding of sequence behavior in this specialized metric environment.

The final part of our investigation has focused on the relationship between statistical convergence in quaternion-valued g-metric spaces and the concept of strong summability. This exploration has not only deepened our understanding

of how sequences behave under statistical measures but has also shed light on their summation properties within this unique framework. These findings underscore the intricate connections between statistical convergence and summability, offering valuable insights into the nature of convergence in quaternion-valued g-metric spaces.

Acknowledgment: This study was supported by Süleyman Demirel University Scientific Research Projects Coordination Unit. Project Number: FYL-2024-9258. The authors declare that there is no conflict of interest. This research received no external funding.

Author contribution: Author Kolancı, Author Gürdal and Author Kişi: Planned and designed the study, gathered and analyzed data about the study, and wrote the article by analyzing the study.

6. References

- Abazari, R.** 2021. Statistical convergence in probabilistic generalized metric spaces wrt strong topology. *J. Inequal Appl.*, 2021(134): 1-11. Doi: 10.1186/s13660-021-02669-w
- Adewale, OK., Olaleru, J., Akewe, H.** 2019. Fixed point theorems on a quaternion-valued G metric spaces. *Commun. Nonlinear Sci.*, 7(1): 73-81.
- Azam, A., Fisher, B., Khan, M.** 2011. Common fixed point theorems in complex valued metric spaces. *Numer. Funct. Anal. Optim.*, 32(3): 243-253. Doi:10.1080/01630563.2011.533046
- Choi, H., Kim, S., Yang, SY.** 2018. Structure for g-metric spaces and related fixed point theorems. arXiv preprint arXiv:1804.03651.
- Dhage, BC.** 1992. Generalized metric space and mapping with fixed point. *Bull. Calcutta Math. Soc.*, 84(1): 329-336.
- Fast, H.** 1951. Sur la convergence statistique. *Colloq. Math.*, 2: 241-244.
- Gähler, S.** 1966. Zur geometric 2-metrische raume. *Rev. Roumaine Math. Pures Appl.*, 11: 664-669.
- Ha, KS., Cho, YJ., White, A.** 1988. Strictly convex and strictly 2-convex linear 2-normed spaces. *Math. Japon.*, 33: 375-384.
- Jan, AH., Jalal, T.** 2023. On the structure and statistical convergence of quaternion valued g-metric space: *Bol. Soc. Paran Mat.*, to appear (2023)
- Khamsi, MA.** 2015. Generalized metric spaces: A survey. *J. Fixed Point Theory Appl.*, 17, (2015), 455-475. Doi: 10.1007/s11784-015-0232-5
- Moricz, F.** 2003. Statistical convergence of multiple sequences. *Arch. Math.*, 81: 82-89. Doi: 10.1007/s00013-003-0506-9

- Mursaleen, M., Edely, OHH.** 2003. Statistical convergence of double sequences. *J. Math. Anal. Appl.*, 288(1): 223-231. Doi: 10.1016/j.jmaa.2003.08.004
- Mustafa, Z., Sims, B.** 2003. Concerning D-metric spaces. Proceedings of the International Conferences on Fixed Point Theory and Applications, Valencia (Spain), 189-198.
- Mustafa, Z., Sims, B.** 2006. A new approach to generalized metric spaces. *J. Nonlinear Convex Anal.*, 7(2): 289-297.
- Naidu, SVR., Rao, KPR., Rao, NS.** 2005. On the concepts of balls in a D-metric space. *Int.J. Math. Math. Sci.*, 1: 133-141.
- Tripathy, BC.** 2003. Statistically convergent double sequences. *Tamkang J. Math.*, 34(3): 231-237. Doi: 10.5556/j.tkjm.34.2003.314



Tire (İzmir) İlçesinin Atmosferik Polenleri

Atmospheric Pollen Grains in Tire (İzmir) District

Nur Ceyhan Güvensen¹ , Ulaş Uğuz² , Aykut Güvensen^{2*} , Ahmet Kaya³

¹Ege Üniversitesi Tire Kutsan Meslek Yüksekokulu Gıda Teknolojisi Programı, İzmir, Türkiye

²Ege Üniversitesi Fen Fakültesi Biyoloji Bölümü, Botanik Anabilim Dalı, İzmir, Türkiye

³Ege Üniversitesi Tire Kutsan Meslek Yüksekokulu Bilgisayar Teknolojisi Programı, İzmir, Türkiye

Öz

Bu çalışmada, 01 Kasım 2021 ile 31 Ekim 2022 tarihleri arasında volumetrik yöntem uyarınca “Lanzoni VPPS 2010” marka polen yakalama aracı kullanılarak Tire ilçesinin atmosferik polen konsantrasyonlarındaki aylık değişimler ortaya konulmuştur. Atmosferde 27 odunsu ve 15 otsu olmak üzere toplam 42 taksona ait polene rastlanmıştır. En yüksek polen konsantrasyonları Pinaceae %29.6 (6.969 polen/m³), Cupressaceae/Taxaceae %25.8 (6.079 polen/m³), Quercus %11.2 (2.636 polen/m³), Olea europaea %10.7 (2.520 polen/m³), Morus %5.69 (1.332 polen/m³), Poaceae %4.43 (1.043 polen/m³), Urticaceae %1.45 (350 polen/m³) ve Plantago %1.31 (304 polen/m³) taksonlarına aittir. Havada toplam polen miktarları en fazla olan ayların sırasıyla Nisan %28.8 (6.775 polen/m³), Mayıs %26.55 (6.254 polen/m³) ve Mart %26.22 (6.176 polen/m³) olduğu tespit edilmiştir. Havadaki polen konsantrasyonları ile yağış miktarı, sıcaklık, rüzgar hızı ve nisbi nem gibi atmosferik parametreler arasındaki ilişkiler istatistiksel olarak ortaya konulmuştur. Tüm bitki gruplarına ait toplam polen miktarlarının sıcaklık ve yağış parametrelerinden istatistiksel olarak önemli düzeyde etkilendiği belirlenmiştir ($p<0.001$).

Anahtar Kelimeler: Alerji, İzmir, polen, sıcaklık, yağış.

Abstract

In this study, between 01 November 2021 and 31 October 2022, weekly and monthly changes in atmospheric pollen concentrations of the Tire district were revealed using the “Lanzoni VPPS 2010” brand pollen capture tool according to the volumetric method. Pollen belonging to a total of 42 taxa, 27 woody, and 15 herbaceous, was found in the atmosphere. The highest pollen concentrations were in Pinaceae 29.61% (6.969 pollen/m³), Cupressaceae/Taxaceae 25.8% (6.079 pollen/m³), Quercus 11.2% (2.636 pollen/m³), Olea europaea 10.7% (2.520 pollen/m³), Morus 5.69% (1.332 pollen/m³), Poaceae 4.43% (1.043 pollen/m³), Urticaceae 1.45% (350 pollen/m³) and Plantago 1.31% (304 pollen/m³) taxa. It has been determined that the months with the highest total pollen amounts in the air are April 28.8% (6.775 pollen/m³), May 26.55% (6.254 pollen/m³) and March 26.22% (6.176 pollen/m³), respectively. The relationships between pollen concentrations in the air and atmospheric parameters such as precipitation amount, temperature, wind speed and relative humidity have been revealed statistically. It was determined that the total pollen amounts of all plant groups were statistically significantly affected by temperature and precipitation parameters ($p<0.001$).

Keywords: Allergy, İzmir, pollen, temperature, precipitation.

*Sorumlu yazarın e-posta adresi: aykut.guvensen@ege.edu.tr

Nur Ceyhan Güvensen orcid.org/0000-0001-8753-2664

Ulaş Uğuz orcid.org/0000-0002-0808-0151

Aykut Güvensen orcid.org/0000-0002-6384-3668

Ahmet Kaya orcid.org/0000-0001-5109-8130



Bu eser “Creative Commons Alıntı-GayriTicari-4.0 Uluslararası Lisansı” ile lisanslanmıştır.

1. Giriş

Alerji; tıbbi anlamda insan vücutuna normalde zararsız olan maddelere karşı başka insanların göstermediği şekilde immun sistemin farklı ve aşırı tepki göstermesi olarak tanımlanmaktadır. Ev tozu, akarlar, hayvan kılı, kuş tüyü, rüzgâr, güneş, bazı meyve ve sebzeler, penisilin, polen ve fungal sporları gibi canlı ve canlı olmayan partiküller atopik bün-yeli kişilerde ani aşırı duyarlılık gösterebilir. İnsan vücutuna solunum yolu, sindirim ve deri yollarıyla girebilen fungal sporları ve polen insanlar için antijendir. Polenlere karşı olan alerji, alerjik rinit, alerjik konjunktivit, alerjik astım ve akut ürtiker şeklindeki semptomlara sebep olmaktadır. Polenler mevsimsel alerjenler olarak bilinirler ve semptomları atmosferik yoğunlukları ile yüksek bir korelasyon göstermektedir (Samolinski vd. 1996). Havada uzun süre kalabilme yetenekleri ve çapraz reaksiyonlardan dolayı tüm yıl boyunca etkili olabilmektedirler. Semptomların şiddetli olduğu hastalarda psikolojik sorunlar ortaya çıkabilir (Baybek vd., 2002). Ayrıca, alerjik rinitin önemli sayılabilcek bir sosyo-ekonomik yükü vardır (Malone vd. 1997). Her polenin alerjik hastalıklara neden olma potansiyeli birbirinden farklılık göstermektedir. Bir polen ne kadar çok IgE proteini yapımına yol açıysa alerjenitesi o kadar yüksek demektir. Alerjenin immün duyarlanmaya neden olan yanı antikorlarla bağlanan, özel bir aminoasit dizilimi gösteren bölümünü epitop denir. Duyarlı kişilerde aynı alerjen molekülünün farklı epitoplara yanıt oluşturabilmektedir.

Polen proteinlerinin aminoasit dizilimlerinde familya, cins ve tür kategorilerinde %80-90 benzerlik söz konusu olabilmekte ve bu benzerlikten dolayı da aynı epitoplara birçok farklı polen bağlanabilmektedir. Bu nedenle, epitoplara farklı alerjenlerin bağlanabilmesi de "çapraz reaksiyon" olarak tanımlanmaktadır. Havada uzun süre kalabilme yetenekleri ve çapraz reaksiyonlardan dolayı tüm yıl boyunca etkili olabilmektedirler. Avrupa'da ve Kuzey Amerika'da insanlar üzerindeki alerjik hastalıkların oranının %5-7 olduğu rapor edilmiştir (Weiss 1993). Diğer bazı ülkelerde ise bu oranın; Finlandiya'da %14, Fransa'da %6-18.5, Hollanda'da %6.6, İtalya'da %13, Japonya'da %12.9-32.7, Norveç'te %10-20, İspanya'da %10, İsviçre'de %4.4-14.2, İsveç'te %13, İngiltere'de %11-24, Amerika'da %10-42, Almanya'da %9.5-22.7, Danimarka'da %3.2, Hırvatistan'da %15-20, Yeni Zelanda'da %15-20 (Bousquet 2001) olduğu rapor edilmiştir. Yapılan çalışmalar aeroalerjenlerden kaynaklanan hastalıklara sahip olan bireylerin sayısında bir artış olduğunu ortaya koymaktadır. Türkiye'de ise alerjik hastalıklar toplumumuzun %15-18 kadarını etkilemeye olup, yarattığı

ışgücü kaybı ve maddi kayıplar nedeniyle önemli bir hastalık grubunu oluşturmaktır ve yayılım hızı her geçen gün artmaktadır.

Ülkemizde gerçekleştirilen aeropalinojik araştırmalarda, alerjen polenlerin konsantrasyonları da ortaya konulmuştur. Bu çalışmalar genel olarak verilecek olursa: Alerjen polenler ve bu polenleri üreten taksonların tozlaşma dönemleri ile ilgili ya da meteorolojik faktörlerle ilişkilendirilmiştir (Pınar vd. 1999, Biçakçı vd. 2000, Güvensen ve Öztürk 2003, İnce vd. 2004, Kaplan 2004, Potoğlu Erkara 2007, Çelenk vd. 2010, Çeter vd. 2012, Tosunoğlu vd. 2013, Acar Şahin vd. 2017, Alan ve Kaplan 2018, Uğuz vd. 2018, Güvensen vd. 2020, Uğuz 2023). Ülkemizde olduğu gibi, yurt dışında da birçok aeropalinojik çalışmalar yapılmıştır (Galán vd. 2007, Medek vd. 2016, Majeed vd. 2018, Charalampopoulos vd. 2018, Gross vd. 2019, Camachoa vd. 2020, Frisk vd. 2024).

Bu araştırma projesi, nüfusu 2021 yılı itibarıyla 86.758 olan Tire ilçesinde gerçekleştirilmiştir. Nüfusun yaklaşık 45.000'i merkezde, 38.000'i ise belde ve köylerde yaşamaktadır. İlçe-de tarım ve hayvancılık ürünlerine dayanan önemli sanayi ve ticaret faaliyetleri gerçekleştirmektedir. Akdeniz ikliminin hüküm sürdüğü ve zengin bitki örtüsüne sahip olan ilçede volumetrik yöntem uyarınca çalışan "Lanzoni VPPS 2010" marka polen yakalama aracı kullanılarak 01 Kasım 2021- 31 Ekim 2022 tarihleri arasında metreküp teki polen konsantrasyonlarının aylık değişimleri ilk kez saptanmıştır. Diğer taraftan havadaki polen konsantrasyonlarının değişimi ile yağış miktarı, sıcaklık, rüzgar hızı ve yönü, nisbi nem gibi atmosferik parametreler arasındaki ilişkiler istatistiksel olarak ortaya konulmuştur. Elde edilen Tire ilçesinde bulunan atopik kişilerin gündelik hayatlarını daha verimli bir şekilde planlayarak, yaşam kalitelerinin arttırılması için elde edilecek olan veriler doğrultusunda, alerjik hastalıkların tedavisinde bölgedeki sağlık kuruluşlarının önceden tedbir alabilmesine katkı sağlanmış olacaktır.

1.1. Coğrafik Konum

Tire, Türkiye'nin İzmir ilinin bir ilçesidir. İlçenin doğusunda Ödemiş, kuzeyinde Bayındır, batısında Torbalı ve Selçuk ilçeleri, güneyinde Aydın ili bulunmaktadır. Tire'nin yüzölçümü 802 km² dir. Deniz seviyesinden yüksekliği 92 m. olan Tire ilçenin; kuzeyindeki Küçük Menderes Ovası ve akarsuyu ile güneyindeki Aydın Dağları'nın bir uzantısı olan Güme (Küme) Dağları en önemli yer şekillerini oluşturmaktadır. Küçük Menderes Ovası tektonik hareketler sonucunda oluşmuş bir çöküntü ovasıdır (Graben). Ova boyunca

akan Küçük Menderes Nehri taşıdığı alüvyonları biriktirek tarımsal anlamda oldukça verimli arazilerin oluşmasını sağlamış, bu özelliği ile ilk çağlardan bu yana insanların başlıca yerleşim alanını teşkil etmiştir. Küçük Menderes Nehri 175 km uzunluğunda olup, Selçuk ilçesi yakınlarından Ege Denizine dökülmektedir (Ersoy, 1999).

1.2. İklim Özellikleri

Akdeniz ikliminin hüküm sürdüğü Tire, yazları sıcak ve kurak kışları ise ılık ve yağışlıdır. Kırk yıllık atmosferik ortalamalara göre ilçede sıcaklık yazın $+40^{\circ}\text{C}$ ye kadar yükselirken kışları en düşük sıcaklık $+3^{\circ}\text{C}$ civarında olmaktadır. Her yıl ortalama yağış miktarı 600-650 mm olarak gerçekleşmekte, en fazla yağış sırasıyla Aralık, Ocak, Şubat ve Mart aylarında görülmektedir. Baskın rüzgar yönü kuzey yönlü olup çevre ilçelere oranla Tire'nin bol yağış olmasını sağlamaktadır. Ege Bölgesinde dağların denize dik uzanmasından dolayı denizel etkiler iç kışılarda kadar girebilmektedir. Bu yönyle Tire'de denizin ılıman etkisi altındadır. Bu durum tarımsal ürün çeşitliliğini ve verimliliğini olumlu yönde etkilemektedir (Ersoy, 1999).

1.3. Bitki Örtüsü

Doğal bitki örtüsünü karakteristik Akdeniz iklimine ait bozulmuş ormanlıklar ve makiler oluşturmaktadır. Güme Dağı'nda başlıca yayılış gösteren bitki türlerinden ağaçlar; *Pinus brutia* Ten., *Pistacia terebinthus* L., *Quercus coccifera* L., *Quercus infectoria* Olivier, *Q. cerris* L., *Celtis australis* L., *Cupressus sempervirens* L., *Fraxinus angustifolia* Vahl., *F. ornus* L., *Juniperus oxycedrus* L. subsp. *oxycedrus*, *Castanea sativa* Miller, *Ficus carica* L., *Juglans regia* L., *Laurus nobilis* L., *Morus alba* L., *M. nigra* L., *Olea europaea* L. ve *Platanus orientalis* L.'tir. Başlıca çalı ve frigana türleri arasında ise; *Arbutus andrachne* L., *A. unedo* L., *Asparagus acutifolius* L., *Astragalus tmoleus* Boiss., *Arundo donax* L., *Avena barbata* L., *Aegilops triuncialis* L., *Briza humilis* Bieb., *B. maxima* L., *Chronanthus orientalis* (Lois.) Heywood et Frodin, *Cistus creticus* L., *C. salviifolius* L., *C. laurifolius* L., *Chenopodium botrys* L., *Crataagus monogyna* Jacq., *Dactylis glomerata* L., *Eryngium campestre* L., *Ferula anatolica* Boiss., *Ferulago humilis* Boiss., *Genista lydia* Boiss., *Gonocytisus angulatus* (L.) Spach, *Hypéricum perforatum* L., *Lavandula stoechas* L., *Myrtus communis* L., *Paliurus spina-christii* Mill., *Phillyrea latifolia* L., *Spartium junceum* L., *Rosa canina* L., *Lagurus ovatus* L., *Olea europaea* L., *Origanum onites* L., *Papaver rhoeas* L., *Plantago lanceolata* L., *P. lagopus* L., *Poa bulbosa* L., *Polypogon monspeliensis* (L.) Desf., *Populus alba* L., *Pyrus amygdaliformis* Vill., *Rubus cabescens* DC., *Salix alba* L., *Sanguisorba minor*

Scop., *Sarcopoterium spinosum* (L.) Spach., *Spartium junceum* L., *Styrax officinalis* L., *Cyperus longus* L., *Juncus acutus* L., *Carex muricata* L., *C. pendula* Hudson, *Rumex acetosella* L., *R. crispus* L., *R. patientia* L., *R. pulcher* L., *R. tuberosus* L., *Ruscus aculeatus* L., *Vitex agnus-castus* L. ve *Vitis vinifera* L. gibi bitkilerin yayılış gösterdiği kaydedilmiştir. Güme Dağı'nda gerçekleştirilen floristik çalışmalarla takson sayısı en fazla olan ilk 5 familyanın sırasıyla Fabaceae, Asteraceae, Poaceae, Lamiaceae ve Caryophyllaceae olduğu; ilk 3 cinsin ise *Bromus*, *Rumex* ve *Anthemis*'e ait oldukları rapor edilmişdir (Seçmen vd. 2015).

Diğer taraftan Kent içinde yol kenarları, park ve bahçelerde yayılış gösteren bitkilerin başlıcaları ise; *Acacia cyanophylla* Lindl., *Acer negundo* L., *Ailanthus altissima* (Miller) Swingle, *Alnus glutinosa* (L.), *Amaranthus retroflexus* L., *Amygdalus communis* L., *Casuarina equisetifolia* L., *Cedrus libani* A. Rich., *Cercis siliquastrum* L., *Citrus aurantium* L., *Chenopodium album* L., *Cupressus sempervirens* L., *C. arizonica* Greene, *Elaeagnus angustifolia* L., *Eucalyptus camaldulensis* Dehnh., *Ficus carica* L., *Hedera helix* L., *Inula viscosa*, *Juniperus oxycedrus* L. subsp. *oxycedrus*, *Laurus nobilis* L., *Lonicera etrusca* Santi, *Ligustrum vulgare* L., *Liquidambar orientalis* Miller., *Malva sylvestris* L., *Melia azedarach* L., *Mercurialis annua* L., *Morus alba* L., *M. nigra* L., *Nerium oleander* L., *Olea europaea* L., *Parietaria judaica* L., *Pinus brutia* Ten., *P. pinea* L., *Platanus orientalis* L., *Plantago lanceolata* L., *Populus alba* L., *Robinia pseudoacacia* L., *Rosmarinus officinalis* L., *Salix babylonica* L., *Rumex acetosella* L., *Sophora japonica* L., *Thuja orientalis* L., *Tilia argentea* Desf. Ex Dc., *Tribulus terrestris* L., *Ulmus minor* Miller, *Urtica dioica* L., *U. urens* L. ve *Xanthium strumarium* L.'dur.

Yörenin toprak yapısı kumlu, killi ve kır taban bir görüntüye vermesine rağmen oldukça verimli ve çok çeşitli kültür bitkilerinin yetiştirilmesine elverişlidir. Tarım ürünleri olarak başta pamuk olmak üzere arpa, buğday, yulaf, silajlık mısır, arpa, tütün, susam, domates, biber, lahana, brokoli, enginar ile karpuz, kavun, incir, zeytin, kestane, nar, ceviz, kiraz, kardut ve her türlü meyve sebzeleridir (Ersoy 1999, Seçmen vd. 2015).

2. Gereç ve Yöntem

Bu çalışmada, 1 yıl boyunca Tire (İzmir) ilçesinin baskın atmosferik polen konsantrasyonlarındaki değişimler ortaya konulmuştur. Çalışmada kullanılan polen tuzaklama cihazı, ilçe merkezinde bulunan Ege Üniversitesi Tire Kutsan Meslek Yüksekokulu'nun çatısına (yaklaşık 15 m) her yanı açık olacak şekilde yerleştirilmiştir. Volumetrik yöntem vakum-

lama (emme) etkisine bağlı olarak havadaki birim hacime düşen (polen/m³) polen miktarını belirlemeye yarayan bir yöntemdir. Cihaz, yaklaşık 24 saatte 14,4 m³ (1 saatte 0,6 m³, dakikada 10 litre) hava emme kapasitesine sahiptir. Bir haftada devrini tamamlayan disk 1 saatte 2mm, 1 günde 48 mm yol kat etmektedir. Bir hafta sonunda diskten alınan bantlar, "Biyoloji Bölümü Palinoloji Laboratuvarına" getirilip safranlı gliserin-jelatin ile boyanarak preparatlar hazırlanmıştır (Wodehouse 1965). Bu preparatlardaki polen teşhis ve sayımları Olympus CX 21 marka ışık mikroskopunda 10x oküler ve 40x objektif kullanılarak gerçekleştirilmiştir. Atmosferik örneklerin alınması ve teşhisinde, İspanyol Aerobiyojoloji Ağı tarafından açıklanan yöntemden yararlanılmıştır (Galan vd. 2007).

Tire ilçesine ait günlük ortalama sıcaklık (°C), nispi nem (%), ortalama rüzgar hızı (m/sn) ve ortalama yağış (mm) gibi meteorolojik faktörler Devlet Meteoroloji İşleri Genel Müdürlüğü'nden temin edilmiştir. Polen konsantrasyonları ile meteorolojik faktörler arasındaki istatistiksel işlemler ise çoklu regresyon analizleri ile ortaya konulmuştur.

Bu çalışmada inceleme konusu olan odunsu ve otsu taksonlara ait aylık toplam polen değişimleri incelenmiştir. İlgili verilerin istatistiksel analizlerden önce normal dağılıma uygunluk testi yapılarak aşırı gözlemler olup olmadığı araştırılmıştır. Çalışma alanı olan Tire ilçesine ait sayılan baskın spor ve polenlerin aylık ortalama sıcaklık (°C), nispi nem (%), ortalama rüzgar hızı (mm) ve ortalama yağış (mm) gibi meteorolojik faktörler arasındaki ilişkilerin değişimleri incelenmiştir. Bu amaçla odunsu, otsu polenler ve bu iki taksonun polen toplamları ile atmosferik parametreler arasındaki ilişkiler çoklu regresyon analizi ile incelenmiştir (Ljung ve Box 1979, Kaya 2010). Çalışmadaki tüm analizlerde IBM SPSS v20 istatistik programı kullanılmıştır.

3. Bulgular ve Tartışma

Tire ilçesinde gerçekleştirilen 1 yıllık (01 Kasım 2021- 31 Ekim 2022) çalışma sonucunda; atmosferde 27'si odunsu ve 15'i otsu olmak üzere toplam 42 taksona ait 23.527 polen/m³ adet polen saptanmıştır. Bunun %89.54'ü odunsulara, %10.46'sı otsulara aittir (Çizelge 1 ve 2). Atmosferde polenlerine en fazla rastlanan odunsu taksonlar sırasıyla; Pinaceae, Cupressaceae/Taxaceae, *Quercus*, *Olea europaea* ve *Morus* olup odunsu taksonların %71'ini temsil etmektedirler. Otsu bitkilere ait polenler ise en fazla sırasıyla; Poaceae, Urticaceae, *Plantago* ve Amaranthaceae'ye ait olup, bu gruba ait bitkilerin yaklaşık %8.77'sini temsil etmektedirler (Çizelge 1 ve 2). Diğer taraftan otsulara ait polenlerin toplam mik-

tarları, sadece temmuz (%0.75), ağustos (%0.38) ve eylül (%0.47) aylarında odunsulardan daha fazladır. Atmosferde toplam polen miktarları ise en fazla sırasıyla nisan (6.775 polen/m³), mayıs (6.254 polen/m³) ve mart (6.176 polen/m³) aylarında tespit edilmiştir (Şekil 1 ve 2).

Kasım (2021) ayında gözlemlenen polenlerin 4'ü odunsu ve 3'ü otsu taksonlara aittir. Odunsulara ait toplam polen sayısı 42 (%0.18) iken, otsuların toplamı 12 (%0.05) dir. Cupressaceae/Taxaceae (%0.081; 19 polen/m³) polenleri en fazladır. Aralık 2021'de, 2'si odunsu ve 2'si otsu olmak üzere toplam 4 taksona ait polene rastlanmıştır. Odunsulara ait polenlerin toplamı 28 (%0.12), otsulara ait polenlerin toplamı ise 10 (%0.05)'dir. Toplam 38 polen/m³ (%0.17) tespit edilmiştir. Yine Cupressaceae/Taxaceae (%0.11; 25 polen/m³) baskındır (Çizelge 1 ve 2, Şekil 1 ve 2). Ocak 2022'de, 3 odunsu ve 2 otsu taksona ait polene rastlanmıştır. Odunsulara ait polenlerin toplamı 34 (%0.15), otsulara ait polenlerin toplamı ise 16 (%0.06)'dır. Toplam polen miktarı ise 50 (%0.21)'dir. Şubat 2022'de, 4 odunsu ve 3 otsu taksona ait polene rastlanmıştır. Odunsulara ait polenlerin toplamı 2463 polen/m³ (%10.47), bu değerinde çok büyük bir kısmını Cupressaceae/Taxaceae (2428 polen/m³) (%10.32) polenleri temsil etmekte olup, bu taksonun polenleri en yüksek değerlerine ulaşmıştır. Otsu polenlerinin toplamı yine çok düşük değerlerdedir (%0.1; 23 polen/m³). Toplam polen miktarı ise 2486 polen/m³ (%10.57) olarak hesaplanmıştır (Çizelge 1 ve 2, Şekil 1 ve 2). Mart 2022'de, 20 odunsu ve 10 otsu taksona ait polene rastlanmıştır. Birçok odunsu bitkinin tozlaşma süreçlerinin başladığı bu ay içerisinde odunsulara ait polenlerin toplamı (%22.8; 5169 polen/m³), otsulara ait polenlerin toplamı ise (%3.42; 807 polen/m³ tür. En fazla sırasıyla; Cupressaceae/Taxaceae (%9.15; 2.153 polen/m³), Pinaceae (%7.59; 1.785 polen/m³), Poaceae (%1.78; 420 polen/m³), *Quercus* (%2.36; 353 polen/m³), *Morus* (%1.43; 335 polen/m³) ve *P. orientalis* (%1.02; 240 polen/m³) polenleri temsil etmiştir (Çizelge 1 ve 2, Şekil 1). Nisan 2022 ayında 19 odunsu ve 10 otsu olmak üzere toplam 19 taksonun poleni görülmüştür. Odunsulara ait polenlerin toplamı 5.169 polen/m³ (%27.68), otsulara ait polenlerin toplamı ise 281 polen/m³ (%1.2) olarak hesaplanmıştır. Toplam polen miktarının en fazla nisan ayında olduğu hesaplanmıştır (%28.88; 6.775 polen/m³). Baskın taksonlar Pinaceae (%13.04; 3.068 polen/m³), Cupressaceae/Taxaceae (%5.8; 1.355 polen/m³), *Quercus* (%3.45; 811 polen/m³) ve *Morus* (%3.2; 748 polen/m³) polenlerine aittir. Mayıs 2022'de, 15 odunsu ve 11 otsu taksona ait polene rastlanmış olup, odunsu polenlerinin toplamı 5.699 polen/m³ (%24.2), otsu polenlerinin toplamı ise

Çizelge 1. Tire atmosferinde odunsu taksonlara ait polenlerin aylık % dağılımları (01 Kasım 2021- 31 Ekim 2022).

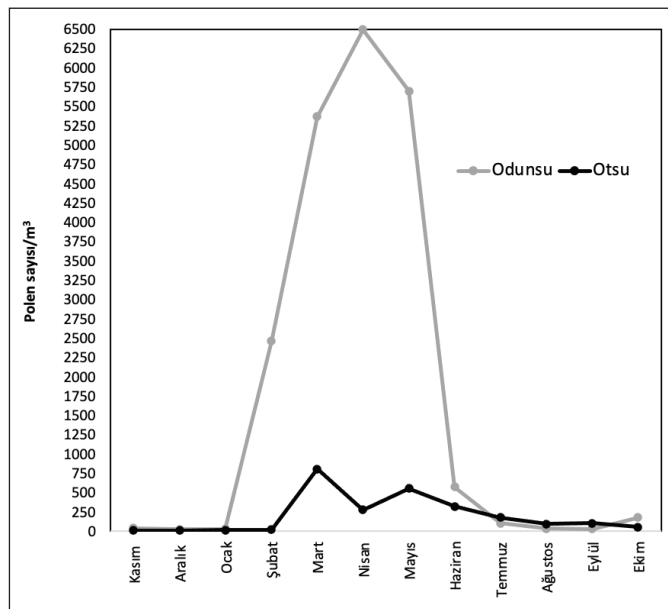
Taksonlar	Kasım	Aralık	Ocak	Şubat	Mart	Nisan	Mayıs	Haziran	Temmuz	Augustos	Eylül	Ekim	%
<i>Acer</i>					0.081	0.12							0.2
<i>Ailanthus altissima</i>		0.013		0.06	0.05	0.12							0.24
<i>Alnus glutinosa</i>			0.013		0.15								0.16
<i>Castanea sativa</i>								0.07	0.09	0.022			0.18
<i>Casuarina equisetifolia</i>	0.043										0.039	0.67	0.75
Cupressaceae/ Taxaceae	0.081	0.11	0.11	10.32	9.15	5.8	0.2	0.08				0.043	25.8
Cistaceae					0.2	0.15	0.11	0.05					0.51
Ericaceae					0.02	0.03	0.02	0.03				0.02	0.12
<i>E. camaldulensis</i>	0.008				0.043	0.056	0.081	0.17	0.05	0.05	0.03		0.49
<i>Fraxinus</i>					0.18	0.073							0.25
<i>Juglans regia</i>					0.025	0.081	0.022						0.13
<i>Ligustrum vulgare</i>							0.022	0.11	0.12	0.03			0.28
<i>Liquidambar orientalis</i>					0.064	0.064							0.13
<i>Morus</i>					1,43	3.2	1.06						5.69
<i>Olea europaea</i>						0.63	9.52	0.56					10.7
<i>Paliurus spina-christii</i>							0.05	0.07					0.12
<i>Phillyrea latifolia</i>					0.05								0.05
Pinaceae	0.047		0.026	0.06	7.59	13.04	7.85	0.75	0.08	0.055	0.07	0.04	29.61
<i>Pistacia</i>					0.055	0.12	0.04						0.21
<i>P. orientalis</i>					1.02	0.36	0.04						1.42
<i>Populus</i>					0.06	0.008							0.06
Rosaceae						0.03	0.05	0.026	0.013				0.12
<i>Quercus</i>					2.36	3.45	4.87	0.47	0.055				11.21
<i>Salix</i>					0.19	0.03							0.22
<i>Sarcopoterium spinosum</i>					0.08	0.32	0.29	0.069	0.008				0.77
<i>Tilia argentea</i>									0.03				0.03
<i>Ulmus</i>				0.03	0.06								0.09
Odunsu Toplam	0,18	0.12	0.15	10.47	22.8	27.68	24.2	2.45	0.44	0.15	0.13	0.77	89.54

555 polen/m³ (%2.35) olarak hesaplanmıştır. Mayıs ayında toplam polen miktarı 6.254 polen/m³ (%26.55) olup en fazla polenin hesaplandığı ikinci ay konumundadır. Bu ay içinde polenleri yoğun olarak saptanan taksonlar; *O. europaea* (%9.52; 2.240 polen/m³), Pinaceae (%7.85; 1847 polen/m³), *Quercus* (%4.87; 1.148 polen/m³) ve *Morus* (%1.06; 249 polen/m³)tur. Haziran 2022'de birçok bitki tozlaşma süreçlerini tamamlamıştır (%3.85; 901 polen/m³). Odunsuların top-

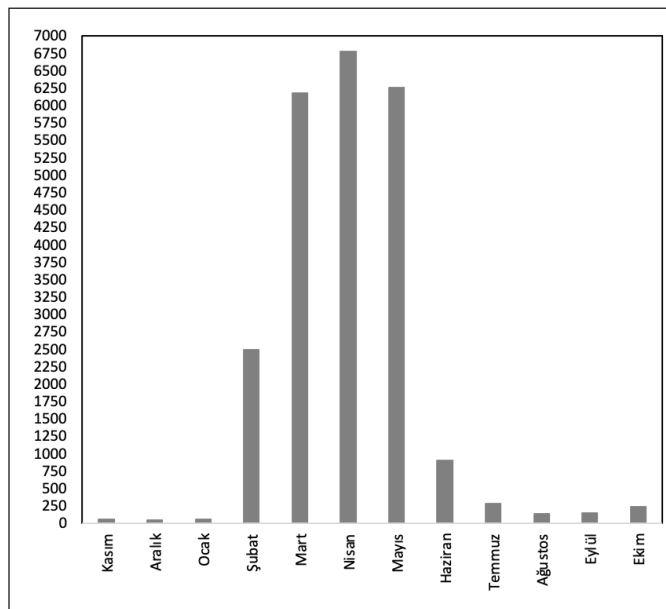
lamı 577 polen/m³ (%2.45), otsuların toplamı ise 324 polen/m³ (%1.4) olup, Pinaceae (%0.75; 178 polen/m³), *O. europaea* (%0.56; 132 polen/m³) ve *Quercus* (%0.47; 111 polen/m³) polenleri daha fazladır. Temmuz 2022'de 8'i odunsu ve 12'si otsu olmak üzere toplam 20 taksona ait polene rastlanmıştır. Toplam polen miktarı 283 polen/m³ (%1.19) olarak hesaplanmıştır. Odunsulara ait polenlerin toplamı %0.44 olup, bu değer otsuların toplamından (%0.75) daha düşüktür. Poa-

Çizelge 2. Tire atmosferinde otsu taksonlara ait polenlerin aylık % dağılımları (01 Kasım 2021- 31 Ekim 2022).

Taksonlar	Kasım	Aralık	Ocak	Şubat	Mart	Nisan	Mayıs	Haziran	Temmuz	Augustos	Eyli	Ekim	%
Amaranthaceae	0.02				0.06	0.08	0.14	0.11	0.08	0.09	0.17	0.08	0.83
Apiaceae					0.03	0,04	0.03	0.04	0.04	0.03			0.21
Asteraceae					0.08	0.03	0.03	0.05	0.02	0.03	0.02	0.01	0.27
Brassicaceae					0.05	0.03	0.03	0.04	0,02				0.17
<i>Centaurea</i>								0.03	0.017	0.03			0.08
Cyperaceae							0.03	0.04	0.02	0.01	0.02		0.12
<i>M. annuua</i>				0.03	0.24	0.04	0.09	0.08					0.48
<i>Papaver</i>						0,05	0.06	0.05	0.03				0.19
<i>Plantago</i>					0.21	0.21	0.5	0.23	0,15		0.008		1.31
Poaceae	0.02	0.017	0.03	0.05	1.78	0,5	0.98	0.5	0.23	0.11	0.14	0.08	4.44
<i>Rumex</i>					0.13	0.08	0.31	0.14	0.08				0.74
<i>Taraxacum</i>										0.02			0.02
<i>Typha</i>										0.03			0.03
Urticaceae	0.013	0.03	0.03	0.02	0.81	0.13	0.15	0.09	0.04	0.05	0.04	0.05	1.45
<i>Xanthium strumarium</i>					0.03					0.01	0.07	0.008	0.12
Otsu Toplam	0.05	0.05	0.06	0.1	3.42	1.2	2.35	1.4	0.75	0.38	0.47	0.23	10.46
Odunsu + Otsu Toplam	0.23	0.17	0.21	10.57	26.22	28.88	26.55	3.85	1.19	0.53	0.6	1	100



Şekil 1. Odunsu ve otsulara ait aylık toplam polen değişimleri.



Şekil 2. Atmosferdeki toplam polen miktarlarının aylık değişimleri (01.Kasım.2021- 31.Ekim.2022).

ceae (%0.23; 54 polen/m³), *Plantago* (%0.15; 34 polen/m³), Amaranthaceae (%0.08; 19 polen/m³) ve *Rumex* (%0.08; 19 polen/m³) polenleri otsu grubu baskın duruma getirmiştir. Ağustos 2022'de 4 odunsu ve 9 otsu taksona ait polene rastlanmıştır. Odunsulara ait polenlerin toplamı 37, otsulara ait polenlerin toplamı ise 96'dır. Toplam polen miktarı ise 133'tür. Sadece 2 gün atmosferde polene rastlanmamıştır. Odunsular arasında Pinaceae (%0.07; 13 polen/m³) polenleri en fazladır. Otsular arasında ise Poaceae (%0.11; 28 polen/m³), Amaranthaceae (%0.09; 39 polen/m³) ve Urticaceae (%0.05; 13 polen/m³) polenleri baskın durumdadır. Eylül 2022'de 3 odunsu ve 7 otsu taksona ait polene rastlanmıştır. Odunsulara ait polenlerin toplamı 34, otsulara ait polenlerin toplamı ise 106'dır. Toplam polen miktarı ise 140'tır. Her gün atmosferde polene rastlanmıştır. Odunsular arasında Pinaceae (%0.07; 18 polen/m³) polenleri baskındır. Otsular

arasında ise Amaranthaceae (%0.17; 39 polen/m³), Poaceae (%0.14; 20 polen/m³) ve *X. strumarium* (%0.07; 15 polen/m³) polenleri baskın durumdadır. Ekim 2022'de 4 odunsu ve 5 otsu taksona ait polene rastlanmıştır. Odunsulara ait polenlerin toplamı 181, otsulara ait polenlerin toplamı ise 56'dır. Toplam polen miktarı ise 237'dir. Her gün atmosferde polene rastlanmıştır. Odunsular arasında *C. equisetifolia* (%0.67; 157 polen/m³) polenleri baskındır. Otsulardan ise Poaceae (%0.08; 20 polen/m³) ve Amaranthaceae (%0.08; 19 polen/m³) polenleri baskın durumdadır (Çizelge 1 ve 2, Şekil 1 ve 2).

Ülkemizde gravimetrik (G) veya volumetrik (V) metodlar kullanılarak birçok yörede aeropalinojik araştırmalar gerçekleştirılmıştır. Bunlardan bazılarına ait veriler Tire ilçesi ile karşılaştırılmıştır (Çizelge 3). Buna göre odunsu bitkilere

Çizelge 3. Bazı yörelere ait atmosferik polen çalışmalarının karşılaştırılması.

İl/İlçe	Odunsu Takson (%)	Otsu Takson (%)	Polen Sezonu (Ay)	Baskın Taksonlar		Metot	Kaynak
				Odunsu	Otsu		
*Tire	89.54	10.46	Nisan, Mayıs, Mart	Pinaceae, Cupres./ Taxaceae, Quercus	Poaceae, Urticaceae, <i>Plantago</i>	V	
Ayvalık	81.38	17.44	Mayıs, Nisan, Mart	Pinaceae, <i>Olea europaea</i> , <i>Quercus</i>	Poaceae, Urticaceae, Amaranthaceae	V	1
Bodrum	86.99	12.82	Mart, Nisan, Mayıs	Cupres./Taxaceae, <i>Quercus</i> , <i>Pinus</i>	Poaceae, Urticaceae, <i>Plantago</i>	V	2
Çeşme	79.74	15.54	Mayıs, Mart, Nisan	Cupres./Taxaceae, <i>Olea europaea</i> , Pinaceae	Poaceae, Amaranthaceae, <i>Mercurialis</i>	V	3
Didim	89.85	9.74	Mart, Nisan, Mayıs	<i>Pinus</i> , Cupres./Taxaceae, <i>Olea europaea</i>	Poaceae, <i>Plantago</i> , Amaranthaceae	G	4
Foca	89.92	10	Mart, Nisan, Mayıs	Pinaceae, Cupres./ Taxaceae, <i>Olea europaea</i>	Poaceae, Urticaceae,	V	5
Marmaris	85.96	13.51	Nisan, Mayıs, Mart	Cupres./Taxaceae, Pinaceae, Oleaceae	Poaceae, Urticaceae, <i>Plantago</i>	G	6
İzmir	84.05	15.29	Mayıs, Nisan, Mart	<i>Pinus</i> , <i>Quercus</i> , Oleaceae	Poaceae, Amaranthaceae	G	7
Aydın	73.97	24.95	Mayıs, Nisan, Mart	<i>Olea europaea</i> , <i>Quercus</i> , Pinaceae	Poaceae, Urticaceae, <i>Plantago</i>	V	8
Denizli	79.68	19.48	Mayıs, Nisan, Mart	Pinaceae, Cupres./ Taxaceae, <i>Olea europaea</i>	Poaceae, Amaranthaceae, <i>Plantago</i>	V	9
Manisa	72.36	25.98	Mayıs, Nisan, Mart	Quercus, Pinaceae, <i>Olea europaea</i> ,	Poaceae, Urticaceae, Amaranthaceae	V	10
Muğla	84.30	14.90	Nisan, Mayıs, Mart	Pinaceae, <i>Quercus</i> , <i>Olea europaea</i>	Poaceae, <i>Plantago</i> , <i>Rumex</i>	V	11

*mevcut çalışmamız, G: gravimetrik (cm²), V: volumetrik (m³)

1. Yurtcan (2021), 2. Tosunoğlu ve Bıçakçı (2015), 3. Uğuz vd. (2017), 4. Bilişik vd. (2008), 5. Yağmur İlkerenler (2023), 6. Turfan (2010), 7. Güvensen ve Öztürk (2003), 8. Güvensen vd. (2020), 9. Güvensen vd. (2013), 10. Buluç (2016), 11. Güvensen vd. (2017).

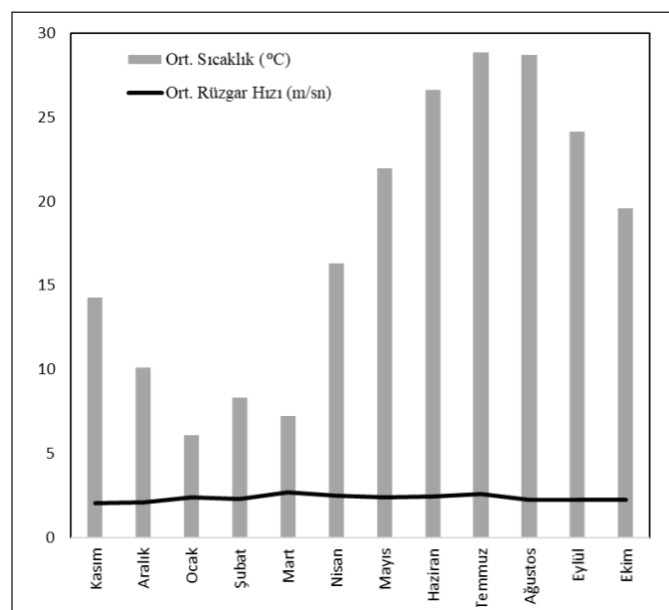
ait polenlerin otsulardan daha fazla olduğu görülmektedir. Bunun nedeni odunsu bitkilerin çok daha fazla polen üretmelerine bağlanabilir. Diğer taraftan odunsulardan Pinaceae, Cupressaceae/Taxaceae, *Quercus*, *Olea europaea*; otsulardan ise Poaceae, *Plantago*, Amaranthaceae, *Plantago*, Urticaceae gibi bitkilere ait polenlerin baskınlıklarını da benzerlik göstermektedir. Bunun nedeni araştırmaların yapıldığı bu yörenlerin iklim benzerliğinden dolayı benzer vejetasyon yapısına sahip olmalarına bağlanabilir. Akdeniz ikliminin görüldüğü ülkelerde gerçekleştirilmiş olan aeropalinojik çalışmalarla göz atacak olursak; Ürdün'ün genelinde (Al-Eisavi ve Dejani 1988) *Cupressus*, *Pinus* ve *Quercus* taksonlarına ait polenlerin; Portekiz'in Coimbra şehrinde (Paiva ve Leitao 1989) Poaceae, Cupressaceae ve Pinaceae üyelerine ait polenlerin atmosferde baskın oldukları belirtilmiştir. İtalya'nın Cagliari kentinde (Cosentino 1990) tarafından atmosferde Cupressaceae, Oleaceae, Pinaceae, Poaceae, Urticaceae polenlerinin; İtalya'nın Perugia bölgesindeki araştırmalarında ise Cupressaceae/Taxaceae, *Quercus*, Poaceae, Oleaceae ve Urticaceae üyelerine ait polenlerin havada yoğun bir şekilde bulunduğu tespit edilmiştir (Romano vd. 1995). İsrail'in kıyı kesimlerinde ise; Cupressaceae, *Pistacia*, *Olea* ve *Pinus* gibi ağaç polenleriyle; *Urtica*, *Parietaria*, *Mercurialis*, Poaceae ve Amaranthaceae gibi otsulara ait polenlerin yoğunlukları fazladır (Waisel vd. 1997).

Birçok araştırmada atmosferdeki polen konsantrasyonlarının, sıcaklık, nem, rüzgar hızı ve yağış miktarı gibi meteorolojik faktörlerden etkilendiği bildirilmektedir (Bogawska vd. 2014, Elvira-Rendueles, vd. 2019, García-Mozo vd. 2016, Pınar vd. 2004, Porsbjerg vd. 2003). Çalışmamızda da Devlet Meteoroloji İşleri Genel Müdürlüğü'nden almış olduğumuz verilere göre (MGM 2022) havadaki aylık polen değişimleri irdelenmiştir.

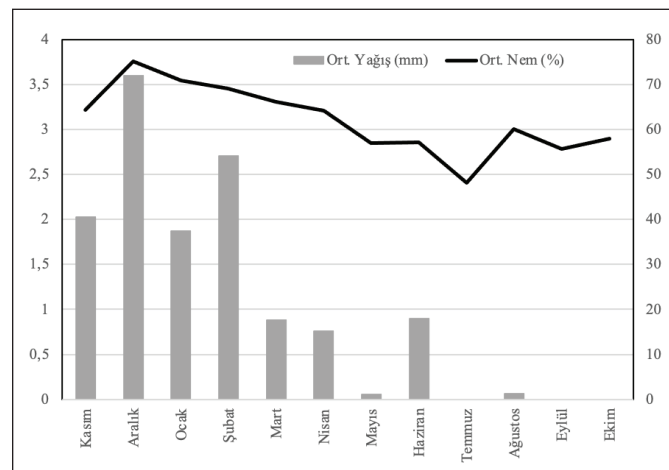
Kasım ayında sıcaklık değerleri 9.5°C ile 21°C arasında olup ortalama değeri 14.28°C 'dir. Rüzgar hızı ise 3.24 km/h (8. gün) ile 33.48 km/h (29. gün) arasında olup genelde hafif rüzgarın olduğu ayda sadece 29. gündə kuvvetli rüzgar görülmüştür. Ortalama rüzgar hızı 2.02 m/sn dir. Yağış toplam 14 gün görülmüştür ve ortalama değeri 2.01 mm dir. Birinci gün (14.7 mm) ve 24. gün (39.1 mm) dışında kalan 12 gün içerisinde yok denecek kadar azdır ($0.1\text{-}2.8 \text{ mm}$). Bu ayda ortalama nem değeri %64.3'tür. Aralık'ta sıcaklık değerleri düşmüştür (1.1°C - 18.2°C). Rüzgar hızı ise 2.8 km/h - 12.6 km/h arasında olup hafif rüzgarlı karakterdedir. Ortalama yağış miktarı 3.6 mm , nisbi nem %75.5'tir Ocak ayında ortalama sıcaklık değeri 6.08°C , ortalama rüzgar hızı 2.8 m/sn dir. Yağış ortalama değeri 1.87 mm , ortalama nem

değeri %70.9'dur (Şekil 3 ve 4). Kasım, Aralık ve ocak ayları birçok bitkinin disseminasyon süreçlerini kapsamadığı için atmosferde oldukça düşük miktarlarda polene rastlanmıştır (Çizelge 1 ve 2, Şekil 2).

Şubat'ta en fazla yağış 9. günde 31.9 mm görülmüştür, fakat yağış ortalaması düşüktür (2.81 mm) ve ortalama nisbi nem %71.62 olarak ölçülmüştür. Sıcaklık ortalaması 8.32°C ve rüzgar hızı genellikle hafif şiddettedir. Meteorolojik parametreler, tozlaşma süreci başlayan Cupressaceae/Taxaceae (%10.32)'nın polen miktarının artmasını da tetiklemiştir (Çizelge 1), bu da odunsu taksonların baskınlığına yol açmıştır. Şubatta birçok otsu bitkinin çiçeklenme dönemi henüz başlamadığı için polenlerine de çok az rastlanmıştır (Şe-



Şekil 3. Aylık ortalama sıcaklık ($^{\circ}\text{C}$) ve rüzgar hızı (m/sn) değerleri.



Şekil 4. Aylık ortalama yağış (mm) ve nem (%) değerleri.

kil 1). Mart ayında 1.2 mm -8.1 mm arasındadır. Ay içinde yağışın 24 gün görülmemesi atmosferdeki polen konsantrasyonunun artmasına yol açmıştır. Mart ayındaki toplam polen yoğunluğunun tüm yıla oranı %26.22 olup, bu oranın da %24.59'unu Cupressaceae/Taxaceae, Pinaceae, *Quercus*, *Morus*, *Platanus orientalis*, Poaceae, Urticaceae, *Mercurialis annuua* ve *Plantago* gibi baskın taksonlar temsil etmiştir (Çizelge 1 ve 2). Nisan'da, nisbi nem değerleri %40.3 ile %74.5, rüzgar hızı genellikle hafif şiddettedir. Yağış değerleri 0.1 mm ile 14 mm (11. gün) arasında olup, sadece 6 gün görülmüştür. Bu ayda odunsu bitkilerden Cupressaceae/Taxaceae (%5.8), *P. orientalis* (%0.36); otsulardan ise Poaceae (%0.5), Urticaceae (%0.13) ve *M. annuua* (%0.04) polenlerinde bir düşüş görülmüştür (Çizelge 1 ve 2). Bunun nedeni bu taksonların polen saçılımlarının azalmasına bağlanabilir. Mayıs ayında sıcaklık değerleri 16.4 °C ile 28.7°C; nisbi nem ise %42 - %78 arasında olup. Rüzgar hızı ise 2.9 - 13.32 m/sn arasında olup hafif rüzgarlıdır (Şekil 3 ve 4). Yağış miktarlarının da çok düşük olması disseminasyon süreci devam eden *O. europaea*, *Quercus*, Poaceae, Urticaceae, *M. annuua*, *Plantago*, *Rumex*, Amaranthaceae polenlerinin yoğunluğunu artırmıştır. Özellikle *Morus* ve Pinaceae taksonları hemen hemen tamamladıkları için bir önceki aya oranla toplam polen yoğunlığında ise %2.33'lük bir azalma gözlenmiştir (Çizelge 1 ve 2). Dolayısıyla, bazı taksonların tozlaşma süreçlerindeki artış ve azalışlara bağlı olmasından kaynaklanmaktadır.

Haziran ayında sıcaklık değerleri 22°C ile 29°C arasında olup. Toplam 4 gün yağış görülmüştür. Nem %45.1 - %76.9 değerlerindedir. Rüzgar hızı ise 6.12 m/sn ile 11.16 m/sn arasında olup genellikle hafif rüzgarlıdır. Atmosferik parametreler polen saçılımları için uygun olsa da, birçok odunsu ve otsu bitki taksonu polinasyon süreçlerini tamamladığı için toplam polen miktarı yaklaşık 7 kat azalmıştır. En fazla polenine rastlanan taksonlar; Pinaceae (%0.75), Poaceae (%0.5) ve *Quercus* (%0.47) olsa da disseminasyon süreçlerini tamamladıkları için havadaki yoğunlukları çok düşüktür. Temmuz, ağustos ve eylül aylarında otsularda ait toplam polen yoğunlıklarında azalma olmasına rağmen, tozlaşma süreçlerini tamamlayan odunsulara göre polen miktarları daha fazladır. Ekim ayında da birçok bitki polinasyon süreçlerini tamamlamasına rağmen temmuz, ağustos ve eylül aylarının tersine odunsu (%0.77) polenler otsulara (%0.23) göre daha fazladır. Bunun nedeni, *C. equisetifolia* (157 polen/m³) polenlerinin disseminasyon periyodunu içermesine bağlanabilir. Ayrıca, hiç yağışın olmaması bu taksona ait polenlerin havadaki saçılımını engellememiştir (Çizelge 1, Şekil 1 ve 2). Çalışma alanı olan Tire ilçesinde odunsu ve otsu tak-

sonlarına ait polenlerin havadaki yoğunluklarıyla ortalama sıcaklık (°C), nispi nem (%), ortalama rüzgar hızı (mm) ve ortalama yağış (mm) gibi meteorolojik faktörler arasındaki ilişkiler istatistiksel olarak analiz edilmiştir.

Odunsu bitki polenleri ile atmosferik parametreler arasında çoklu regresyon analizi yapılmıştır. Analiz sonucunda aşağıdaki verilen regresyon denklemi tahminlenmiştir.

$$\text{Odunsu Polenleri} = 154 - 3.12 \text{ Sıcaklık} - 4.84 \text{ Yağış} - 0.711 \text{ Nem} + 1.13 \text{ Rüzgar hızı}$$

Varyans analizi sonucunda bu denklemin istatistiksel olarak önemli olduğu görülmüştür ($F= 6.14$, $p<0.001$). Ancak, bağımsız değişken incelendiğinde bu önemliliğin sıcaklık ($t=-3.60$, $p<0.001$) ve yağıştan ($t=-3.11$, $p<0.01$) kaynaklandığı anlaşılmıştır. Nisbi nem ($t=-1.02$, $p>0.05$) ve rüzgar hızının ($t= 1.02$, $p>0.05$) istatistiksel olarak önemli olmadığı saptanmıştır (Çizelge 4).

Çizelge 4. Odunsu polenlerle atmosferik parametreler arasında regresyon analizi.

Predictor	Coef	StDev	T	P
Constant	153.59	56.82	2.70	0.007
Sıcaklık*	-3.12	0.87	-3.60	<0.001
Yağış*	-4.84	1.56	-3.11	0.002
Nisbi nem	-0.71	0.70	-1.02	0.310
Rüzgar hızı	1.13	1.12	1.02	0.311

Otsu bitki polenleri ile atmosferik parametreler arasında çoklu regresyon analizi yapılmıştır. Analiz sonucunda aşağıdaki verilen regresyon denklemi tahminlenmiştir.

$$\text{Otsu Polenleri} = 18.87 - 0.246 \text{ Sıcaklık} - 0.453 \text{ Yağış} - 0.170 \text{ Nem} + 0.387 \text{ Rüzgar hızı}$$

Varyans analizi sonucunda bu denklemin istatistiksel olarak önemli olduğu görülmüştür ($F= 11.07$, $p<0.001$). Ancak, bağımsız değişken incelendiğinde bu önemliliğin sıcaklık ($t=-3.30$, $p<0.001$), yağış ($t=-3.38$, $p<0.001$), nisbi nem ($t=-2.82$, $p<0.01$) ve rüzgar hızından ($t=4.02$, $p<0.001$) kaynaklandığı anlaşılmıştır. Bu da, tüm atmosferik parametrelerin otsu polenlerin dağılımında istatistiksel olarak önemli taşıdığını ortaya koymaktadır (Çizelge 5).

Odunsu ve otsu polenlerin toplam miktarları ile atmosferik parametreler arasında çoklu regresyon analizi yapılmıştır. Analiz sonucunda aşağıdaki verilen regresyon denklemi tahminlenmiştir.

Çizelge 5. Otsu polenlerle atmosferik parametreler arasında regresyon analizi.

Predictor	Coef	StDev	T	P
Constant	18.866	4.899	3.85	<0.001
Sıcaklık*	-0.24617	0.07470	-3.30	0.001
Yağış*	-0.4534	0.1343	-3.38	0.001
Nisbi nem	-0.16979	0.06023	-2.82	0.005
Rüzgar hızı	-0.38653	0.09616	4.02	<0.001

$$\text{Odunsu ve otsu polenler} = 172 - 3.36 \text{ Sıcaklık} - 5.29 \text{ Yağış} - 0.881 \text{ Nem} + 1.51 \text{ Rüzgar hızı}$$

Varyans analizi sonucunda bu denklemin istatistiksel olarak önemli olduğu görülmüştür ($F= 6.59$, $p<0.001$). Ancak, bağımsız değişken incelendiğinde bu önemliliğin sıcaklık ($t=-3.69$, $p<0.001$) ve yağıştan ($t=-3.23$, $p<0.001$) kaynaklandığı anlaşılmıştır. Nisbi nem ($t=-1.20$, $p>0.05$) ve rüzgar hızının ($t= 1.29$, $p>0.05$) istatistiksel olarak önemli olmadığı saptanmıştır (Çizelge 6).

Çizelge 6. Odunsu ve otsu polenler ile atmosferik parametreler arasında regresyon analizi.

Predictor	Coef	StDev	T	P
Constant	172.47	59.74	2.89	0.004
Sıcaklık*	-3.3609	0.9109	-3.69	<0.001
Yağış*	-5.291	1.637	-3.23	0.001
Nisbi nem	-0.8810	0.7345	-1.20	0.231
Rüzgar hızı	1.510	1.173	1.29	0.199

İstatistikî değerlendirme sonucunda odunsu, otsu ve odunsu-otsu bitki gruplarına ait toplam polen miktarlarının sıcaklık ve yağış parametrelerinden istatistiksel olarak önemli düzeyde etkilendiği tespit edilmiştir ($p<0.001$).

İlçe atmosferinde polenlerine yoğun olarak rastlanan bitki taksonlarına ait polenlerin yoğun olarak görüldüğü aylar ve alerjik dereceleri verilmiştir (Çizelge 7). Dominant olan bu taksonların yıllık toplam polen miktarları %1 den fazladır. Buna göre odunsulara ait polen yoğunlukları şubat, mart, nisan ve Mayıs aylarında, otsu polen yoğunlukları ise mart, nisan, Mayıs ve Haziran aylarında daha fazladır. Bununla birlikte odunsular en yüksek değerlerine şubat, nisan ve Mayıs, otsular ise mart ve Mayıs aylarında ulaşmışlardır (Çizelge 1 ve 2). *Pinus brutia* ve *P. pinea* (Pinaceae) Güme Dağı'nda yayılış göstermekle birlikte ilçedeki park-bahçelerde ve yol kenarlarında dikimleri söz konusudur. Pinaceae polenlerinin alerjik etkilerinin düşük olduğu bildirilmiştir (Grant Smith 1990).

Smith 1990). *Cupressus sempervirens* ve *Thuja* spp. (Cupressaceae/Taxaceae) gibi bitkiler ise her dem yeşil oluşu ve bakımı kolay olduğundan ilçedeki park ve bahçelerde dikimi tercih edilen başlıca bitkiler arasında yer almaktadır. Bu bitkiere ait polenlerin yoğun olarak rastlanmasıın sebebi çok fazla polen üremelerinden kaynaklanmaktadır Cupressaceae/Taxodiaceae polenlerinin Akdeniz bölgesinde ülkelerinde en önemli aeroallerjenler arasında olduğu rapor edilmiştir (Geller- Bernstein vd. 2000). *Quercus* polenlerinin orta ve yüksek alerjik reaksiyonlara yol açtığı (Aytuğ vd. 1995, Peternel vd. 2003) ve polinosisin nedenleri arasında olduğu ifade edilmiştir (Middleton vd. 1988). Yine akdeniz ikliminin tipik bitkilerinden olan *O. europaea* doğal olarak (Güme Dağı'nda) yayılış göstermekle birlikte ilçedeki park-bahçelerde ve yol kenarlarında dikimleri söz konusudur. Polenlerinin yüksek alerjik reaksiyonlara yol açtığı bildirilmektedir (Waisel vd. 1996). *Morus* polenlerinin de yoğun olarak gözlenmesinin sebebi, ilçede dikimi yapılan meyve ağaçları arasında yer almasından kaynaklanmaktadır. *Morus* polenlerinin astım, alerjik rinit, alerjik konjuktivit ve septomlarına neden oldukları İspanya'daki hastalar üzerinde ortaya konulmuştur (Papia vd. 2020). Atmosferde yoğun olarak polenleri görülen otsu bitkiler arasında; Poaceae üyelerinden *Aegilops*, *Avena*, *Bromus*, *Hordeum*, *Phleum* ve *Poa* gibi cinslerine ait çok sayıda takson doğal alanlarda, yol kenarlarında ve terk edilmiş alanlarda yayılış göstermektedir. Poaceae üyelerinin dünya vejetasyonunun yaklaşık % 20'sini oluşturduğu rapor edilmiştir (Sabariego vd. 2011). Yine bu familya üyelerinden arpa, buğday, yulaf, silajlık mısır ve arpanın tarımının yapılıyor olması da Poaceae polenlerinin atmosferdeki yoğunluğunu artırmıştır. *Cynodon dactylon*, *Dactylis glomerata*, *Poa pratensis*, *Phleum pratense*, *Agrostis* sp. ve *Lolium* sp. gibi Poaceae üyeleri yüksek alerjik reaksiyonlara sahiptir (Garty vd. 1998). Özellikle ilçede yol kenarlarında, duvarlarda ve terk edilmiş alanlarda yayılış gösteren Urticaceae üyelerinden *Parietaria* polenlerinin oldukça alerjik olduğu, fakat *Urtica* polenlerinin çok allerjenik olmadığı bildirilmesine rağmen (Bousquet vd. 1984), Amerika'daki bazı vakalarda *Urtica dioica* polenlerinin alerjik rinitin sorumlusu oldukları ifade edilmiştir (Vega-Maray vd. 2006). Yine yol kenarlarında, refüjlerde ve terk edilmiş alanlarda yayılış göstren *Plantago* polenlerinin düşük ve yüksek alerjik etkilerinin olduğu bildirilmiştir (Grant Smith 1990).

4. Sonuç ve Öneriler

Tire ilçesinde gerçekleştirilen bu çalışma; polene duyarlı olan hastalar için alerjik hastalıkların teşhis ve tedavisinde gerekli önlemlerin alınmasına, böylece tedavi ve deri testle-

Çizelge 7. Baskın taksonlara ait polenlerin yoğun olarak görüldüğü aylar ve alerjik dereceleri.

Taksonlar	Polen Yoğunluğunun Fazla Olduğu Aylar	Polen Yoğunluğunun En Fazla Olduğu Ay	Toplam (%)	Alerjik potansiyel ^a
Odunsular				
Pinaceae	Mart, Nisan, Mayıs	%13.04/Nisan	29.6	*
Cupressaceae/Taxaceae	Şubat, Mart, Nisan	%10.32/Şubat	25.89	**
<i>Quercus</i>	Mart, Nisan, Mayıs	%4.87/Mayıs	11.2	**, ***
<i>Olea europaea</i>	Mayıs	%9.52/Mayıs	10.71	***
<i>Morus</i>	Nisan	%3.2/Nisan	5.69	**
Otsular				
Poaceae	Mart, Nisan, Mayıs, Haziran	%1.78/Mart	4.43	*; **; ***
Urticaceae	Mart, Nisan, Mayıs	%0.81/Mart	1.45	*; **
<i>Plantago</i>	Mayıs	%0.5/Mayıs	1.3	*; ***

^a(Grant Smith 1990); *** yüksek, ** orta, * düşük

rinde kullanılacak ekstrelerin hazırlanması için ihtiyaç duyulan polen örneklerinin toplanmasında yararlı olacaktır. Diğer taraftan, polene bağlı alerjik hastalıklar için sık olan acil servis başvurusu, daha fazla ilaç kullanım gereksinimi, iş gücü kaybı, sosyal yaşamda sıkıntılar nedeni ile hem kendisi etkilenmekte hem de ülke ekonomisi olumsuz bir şekilde etkilenmektedir. Tire ilçesinde bu alerjen ajanlarının atmosferde çıkmadan, ya da çıkar çıkmaz hastaların uyarılması, basit korunma önlemlerinin, uygun tedavilerin düzenlenmesi hastaların sağlığı açısından hem de toplumun sosyal ve ekonomik gelişimi açısından önem taşımaktadır. Bir başka deyişle, polene duyarlı kişilerin günlük hayatlarını daha verimli bir şekilde planlayarak, yaşam kalitelerinin yükseltilmesine katkılar sağlayarak sağlık kuruluşlarına önemli bir veri kaynağı oluşturacaktır. Ayrıca park ve bahçelerde kullanılan bitkilerin, bölgede yaşayan insanlarda alerjik reaksiyonlara neden olabileceği düşünülperek, peyzaj ve ağaçlandırma çalışmalarıının bu bilgiler doğrultusunda yapılmasını sağlayacaktır. Tire (İzmir) ilçesi için ilk kez yapılan bu aeropalinojik çalışmanın, ülkemizin polen haritasının hazırlanmasına yönelik çalışmalarla ve bölgede yapılacak uzun süreli aeropalinojik çalışmalarla beraber meteorolojik parametrelerin polen dağılımları üzerindeki etkilerinin belirlenmesinde önemli katkılar sağlayacağı inancındayız.

Teşekkür: Bu çalışma, Ege Üniversitesi Rektörlüğü, Bilimsel Araştırma Projeleri (BAP) Koordinatörlüğü tarafından desteklenmiştir (Proje no: FGA-2021-22909). Bu bağlamda kurumumuzun bizlere vermiş olduğu destek için teşekkür borç biliriz.

Yazar katkısı

Nur Ceyhan Güvensen: Çalışmanın gerçekleştirilebilmesi için BAP Projesi yürütücülüğünü yapmış ve literatür taramıştır.

Ulaş Uğuz: Polen teşhislerini gerçekleştirerek veri grafiklerini oluşturmuştur

Aykut Güvensen: Polen teşhislerini gerçekleştirerek veri çizelgelerini oluşturmuştur.

Ahmet Kaya: Elde edilen verilere ait istatistiksel analizleri gerçekleştirmiştir.

5. Kaynaklar

Alan, Ş., Kaplan, A. 2018. Comparison of Two Aerobiological Stations Data in Zonguldak. Commun. Fac. Sci. Univ. Ank. Series C., 27 (2): 132-140. https://doi.org/10.1501/commuc_0000000208

Al-Eisavi, D., Dejani, B. 1988. Airborne Pollen of Jordan. Grana, 27: 219-227. <https://doi.org/10.1080/00173138809428929>

Acar Şahin, A., Kaplan, A., Özmen Baysal, E., Doğan, C., Pınar, NM. 2017. General Trends in Atmospheric Pollen Concentration in the High Populated City of Ankara Turkey. Karaelmas Fen ve Müh. Dergisi, 7 (1): 40-46. <https://doi.org/10.7212/2fzkufbd.v1i1.485>

Aytuğ B., Yalçınk F., Efe A. 1995. Allergenic Pollen Producing Plants of Turkey. Proceedings of the National Palynology Congress, İstanbul University, Forest Faculty, 201-212, İstanbul, Turkey.

Baybek, S., Kumbasar, H., Tuğcu, H., Mısırlıgil, S. 2002. Psychological Status of Patients with Seasonal and Perennial Allergic Rhinitis, J Investig Allergol Clin Immunol., 12: 204-210.

- Bıçakçı, A., Tosunoğlu, A, Altunoğlu, MK., Saatcioglu, G., Keser, AM., Özgökçe, F.** 2017. An Aeropalynological Survey in the City of Van, a High Altitudinal Region, East Anatolia-Turkey. *Aerobiologia*, 33: 93-108. <https://doi.org/10.1007/s10453-016-9453-3>
- Bıçakçı, A., Akyalçın, H.** 2000. Analysis of Airborne Pollen Fall in Balikesir, Turkey, 1996-1997. *Annals of Agricultural and Environmental Medicine*, 7(1): 5-10.
- Bilişik, A., Yenigün, A., Bıçakçı, A., Eliaçık, K., Canitez, Y., Malyer, H., Sapan, N.** 2008. An Observation Study of Airborne Pollen Fall in Didim (SW Turkey): Years 2004–2005. *Aerobiologia*, 24: 61–66. <https://doi.org/10.1007/s10453-007-9077-8>
- Bogawski, P., Grewling, Ł., Nowak, M., Smith, M., Jackowiak, B.** 2014. Trends in Atmospheric Concentrations of Weed Pollen in the Context of Recent Climate Warming in Poznań (Western Poland). *International Journal of Biometeorology*, 58(8): 1759-1768. <https://doi.org/10.1007/s00484-013-0781-5>
- Bousquet, J.** 2001. Epidemiology and genetics. Aria Workshop Report. *Journal of Allergy and Clinical Immunology*, 108: 153-161. <https://doi.org/10.1067/mai.2001.118891>
- Bousquet, J., Hewitt, B., Guérin, B., Dhivert, H., Michel, B.** 1984. Allergy in the Mediterranean Area II: Cross-allergenicity Among Urticaceae Pollens (*Parietaria* and *Urtica*). *Clinical Allergy*, 16: 57-64. <https://doi.org/10.1111/j.1365-2222.1986.tb01954.x>
- Buluç, E.** 2016. Manisa ili atmosferik polenlerin volumetrik yöntemle analizi. Ege Üniversitesi Fen Bilimleri Enstitüsü, Yüksek Lisans Tezi, 263s, İzmir.
- Camachoa, I., Caeiro, E., Nunes, C., Morais-Almeida, M.** 2020. Airborne pollen calendar of Portugal: A15-year Survey (2002-2017). *Allergologia et Immunopathologia*, 48(2): 194-201. <https://doi.org/10.1016/j.aller.2019.06.012>
- Charalampopoulos, C., Lazarina, M., Tsiripidis, I., Vokou, D.** 2018. Quantifying the Relationship Between Airborne Pollen and Vegetation in the Urban Environment. *Aerobiologia*, 34: 285–300. <https://doi.org/10.1007/s10453-018-9513-y>
- Cosentino, S., Pisano, PL., Fadda, ME., Palmas, F.** 1990. Pollen and Mold Allergy, Aerobiologic Survey in the Atmosphere of Cagliari. Italy. *Annals of Allergy*, 65(5): 393-400.
- Çelenk, S., Bıçakçı, A., Tamay, Z., Güler, N., Altunoğlu, MK., Canitez, Y., Malyer, H., Sapan, N., Ones, U.** 2010. Airborne Pollen in European and Asian Parts of Istanbul. *Environmental Monitoring and Assessment*, 164(1-4): 391-402. <https://doi.org/10.1007/s10661-009-0901-1>
- Çeter, T., Pınar, NM., Keseli, T., Aydin, F., Acar, A.** 2012. One Year Aeropalynological Analysis of Atmospheric Pollens in Çankırı, Turkey. *Japanese Journal of Palynology*, 58: 30-31. https://doi.org/10.24524/jjp.58.Special_23_2
- Elvira-Rendueles, B., Moreno, J., Costa- Gómez, I., Banon, D., Martinez-Garcia, MJ., Moreno, S.** 2019. Pollen calendars of Cartagena, Lorca, and Murcia (Region of Murcia), Southeastern Iberian Peninsula: 2010–2017. *Aerobiologia*, 35: 477- 496. <https://doi.org/10.1007/s10453-019-09578-y>
- Ersoy, C.** 1999. Güme Dağı (Tire) Florası. Ege Üniversitesi Fen Bilimleri Enstitüsü, Yüksek Lisans Tezi.
- Frisk, CA., Brobakk, TE., Ramford, H.** 2024. Allergenic Pollen Seasons and Regional Pollen Calendars for Norway. *Aerobiologia*, 40:145–159. <https://doi.org/10.1007/s10453-023-09806-6>
- Galán, C., Cariñanos, P., Alcázar, P., Dominguez-Vilches, E.** 2007. Spanish Aerobiology Network (REA): Management and Quality Manual. Córdoba, Spain: Servicio de Publicaciones Universidad de Córdoba.
- García-Mozo, H., Oteros, JA., Galán, C.** 2016. Impact of Land Cover Changes and Climate on the Main Airborne Pollen Types in Southern Spain. *Science of the Total Environment*, 548: 221–228. <https://doi.org/10.1016/j.scitotenv.2016.01.005>
- Garty, BZ., Kosman, E., Ganor, E., Berger, V., Garty, L., Weitzen, T., Waisman, Y., Mimouni, M., Waisel, Y.** 1998. Emergency Room Visits of Asthmatic Children, Relation to air Pollution. *Weather and Airborne Allergens*, 81(6): 563- 570. [https://doi.org/10.1016/S1081-1206\(10\)62707-X](https://doi.org/10.1016/S1081-1206(10)62707-X)
- Geller-Bernstein, C., Waisel, Y., Lahoz, C.** 2000. Environmental and sensitization to Cypress in Israel. *Allergie et Immunologie*, 3: 92-93.
- Grant Smith, E.** 1990. Sampling and Identifying Allergenic Pollens and Molds. Blewstone press, San Antonio, Texas, 196s.
- Gross, L., Weber, R., Wolf, M., Crooks, JL.** 2019. The Impact of Weather and Climate on Pollen Concentrations in Denver, Colorado, 2010-2018. *Annals of Allergy, Asthma & Immunology*, 123(5): 494-502. <https://doi.org/10.1016/j.anai.2019.08.002>
- Güvensen, A., Uğuz, U., Şengonca Tort, N., Eşiz Dereboylu, A., Altun, T., Buluç, E.** 2017. Aydın, Manisa, Muğla ve Uşak İllerinin Atmosferik Polenlerinin Volumetrik Yöntemle Analizi, TÜBİTAK (Proje no:113Z065).
- Güvensen, A., Çelik, A., Topuz, B., Öztürk, M.** 2013. Analysis of Airborne Pollen Grains in Denizli. *Turkish Journal of Botany*, 37(1): 74- 84. <https://doi.org/10.3906/bot-1201-4>
- Güvensen, A., Öztürk, M.** 2003. Airborne Pollen Calendar of Izmir- Turkey. *Annals of Agricultural and Environmental Medicine*, 10: 37–44.
- Güvensen, A., Uğuz, U., Altun, T., Dereboylu Eşiz, A., Tort Şengonca, N.** 2020. Aeropalynological Survey in the City Center of Aydın (Turkey). *Turkish Journal of Botany*, 44: 539- 551. <https://doi.org/10.3906/bot-1909-38>

- İnce, A., Kart, L., Demir, R., Özyurt, MS.** 2004. Allergenic Pollen in the Atmosphere of Kayseri, Turkey. Asian Pacific Journal of Allergy and Immunology, 22(2-3): 123-132.
- Kaplan, A.** 2004. Airborne Pollen Grains in Zonguldak, Turkey, 2001-2002. Acta Botanica Sinica, 46 (6): 668-674.
- Kaya, A.** 2010. AR (1) Modelinde A Tipi Sapan Etki. İstatistikçiler Dergisi, 3: 1-7.
- Ljung, GM., Box, GEP.** 1979. The Likelihood Function of Stationary Autoregressive-Moving Average Models. Biometrika, 66(2): 265-270.
- M.G.M.** 2022. Meteoroloji Genel Müdürlüğü Verileri. <https://www.turkiye.gov.tr/mevbis-meteorolojik-veri-bilgi-satis-sunum-sistemi> (Erişim Tarihi: 13.01.2024).
- Majeed, HT., Periago, C., Alarcon, M., Belmonte, J.** 2018. Airborne Pollen Parameters and their Relationship with Meteorological Variables in NE Iberian Peninsula. Aerobiologia, 34: 375-388. <https://doi.org/10.1007/s10453-018-9520-z>
- Malone, DC., Lawson, KA., Smith, DH.** 1997. A Cost of Illness Study of Allergic Rhinitis in the United States. Journal of Allergy and Clinical Immunology, 99(1): 22-27. [https://doi.org/10.1016/s0091-6749\(97\)70296-3](https://doi.org/10.1016/s0091-6749(97)70296-3)
- Medek, DE., Beggs, PJ., Erbas, B., Jaggard, AK., Campbell, BC., Vicendese, D., Johnston, FH., Godwini I., Huete, AR., Green, BJ., Burton, PK., Bowman, DMJS., Newnham, RM., Katelaris, CH., Haberle, SG., Newbigin, E., Davies, JM.** 2016. Regional and Seasonal Variation in Airborne Grass Pollen Levels Between Cities of Australia and New Zealand. Aerobiologia, 32(2): 289-302. <https://doi.org/10.1007/s10453-015-9399-x>
- Middleton, E., Reed, CE., Ellis, EF., Adkinson, NF., Yunginger, JW.** 1988. Allergy Principles and Practice. 1, Toronto, 372p.
- Paiva, J., Leitao, T.** 1989. Five Year Air Sampling Study in Coimbra, Portugal. Boletim da Sociedade Broteriana, 62(2): 131-138.
- Papia, F., Incorvaia, C., Genovese, L., Gangemi, S., Minciullo, PL.** 2020. Allergic Reactions to Genus *Morus* Plants: A Review. Clinical and Molecular Allergy, 18:1. <https://doi.org/10.1186/s12948-020-00116-7>.
- Peternel, R., Čulig, J., Mitić, B., Vukušić, I., Šostar, Z.** 2003. Analysis of Airborne Pollen Concentrations in Zagreb, Croatia, 2002. Annals of Agricultural and Environmental Medicine, 10(1): 107-122.
- Pınar, NM., Şakıyan, N., İnceoğlu, O., Kaplan, A.** 1999. A One-year Aeropalyngological Study at Ankara, Turkey. Aerobiologia, 15: 307-310. <https://doi.org/10.1023/a:1007690231345>
- Pınar, NM., Geven, F., Tuğ, GN., Ketenoglu, O.** 2004. Ankara Atmosferinde Gramineae Polen Sayılarının Meteorolojik Faktörlerle ilişkisi (1999-2002). Astım Allerji İmmünojoloji, 2(2): 65-70.
- Porsbjerg, C., Rasmussen, A., Backer, V.** 2003. Airborne Pollen in Nuuk, Greenland, and the Importance of Meteorological Parameters. Aerobiologia, 19: 29-37. <https://doi.org/10.1023/A:1022674007985>
- Potoğlu Erkara, I., Pehlivan, S., Tokur, S.** 2007. Concentrations of Airborne Pollen Grains in Eskisehir City (Turkey). Journal of Applied Biological Sciences, 1(1): 33-42.
- Romano, B., Frenguelli, G., Fornaciari, M., Bricchi, E.** 1995. Pollination Season in Perugia Area. Studio Botanica, 14: 177-188.
- Sabariego, S., Pérez-Badia, R., Bouso, V., Gutiérrez, M.** 2011. Poaceae Pollen in the Atmosphere of Aranjuez, Madrid and Toledo (central Spain). Aerobiologia, 27(3): 221-228. <https://doi.org/10.1007/s10453-010-9191-x>
- Samolinski, B., Rapiejko, P., Arcimowicz, M., Zawisza, E.** 1996. Comparison of Cumulated Pollen Count and Frequency of Positive Pollen Allergens Skin Test Reactions in Population of Warsaw, Poland. Annals of Agricultural and Environmental Medicine, 3(2): 183-87.
- Seçmen, Ö., Şenol, SG., Leblebici, E., Şentürk, O.** 2015. Tire Güme Dağı Çiçekli Bitkileri. Tire Belediye Başkanlığı Kültür Yayınları, 360s.
- Tosunoğlu, A., Bıçaklı, A.** 2015. Seasonal and Intradiurnal Variation of Airborne Pollen Concentrations in Bodrum, SW Turkey. Environmental Monitoring and Assessment, 87(4):167. <https://doi.org/10.1007/s10661-015-4384-y>.
- Tosunoğlu, A., Yenigün, A., Bıçaklı, A., Eliaçık, K.** 2013. Airborne Pollen Content of Kuşadası. Turkish Journal of Botany, 37(2): 297-305. <https://doi.org/10.3906/bot-1203-5>
- Turfan, N.** 2010. Marmaris, Milas ve Datça ilçelerinin atmosferik polen takvimi. Ege Üniversitesi Fen Bilimleri Enstitüsü, Doktora Tezi, 366 sayfa, Bornova, İzmir.
- Uğuz, U., Güvensen, A., Tort, NS.** 2017. Annual and Intradiurnal Variation of Dominant Airborne Pollen and the Effects of Meteorological Factors in Çeşme (İzmir, Turkey). Environmental Monitoring and Assessment, 189(10): 530. <https://doi.org/10.1007/s10661-017-6238-2>.
- Uğuz, U.** 2023. The Relationship Between Airborne Pollen Concentration and Wind-Related Parameters in the Atmosphere of İzmir, Turkey. Aerobiologia, 39: 441-455. <https://doi.org/10.1007/s10453-023-09802-w>
- Uğuz, U., Güvensen, A., Tort Sengonca, N., Eşiz Dereboylu, A.** 2018. Volumetric Analysis of Airborne Pollen Grains in the City of Uşak, Turkey. Turkish Journal Botany, 42(1): 57-72. <https://doi.org/10.3906/bot-1703-58>

- Vega-Maray, AM., Fernández-González, D., Valencia-Barrera, R., Suárez-Cervera, M.** 2006. Allergenic Proteins in *Urtica dioica*, a Member of the Urticaceae Allergenic Family. Annals of Allergy, Asthma & Immunology, 97(3): 343-349. [https://doi.org/10.1016/S1081-1206\(10\)60799-5](https://doi.org/10.1016/S1081-1206(10)60799-5)
- Waisel, Y., Ganor, E., Glikman, M., Epstein, V., Brenner, S.** 1997. Seasonal Distribution of Airborne Pollen in the Coastal Plain of Israel. Aerobiologia, 13:127-134. <https://doi.org/10.1007/bf02694429>
- Waisel, Y., Geller-Bernstein, C., Keynan, N., Arad, G.** 1996. Antigenicity of the Pollen Proteins of Allergens. Annals of Allergy, Asthma & Immunology, 81: 563- 570.
- Weiss, KB.** 1993. Breathing Better or Wheezing Worse? The Changing Epidemiology of Asthma Morbidity and Mortality. Annual Review of Public Health, 14: 491-513. <https://doi.org/10.1146/annurev.pu.14.050193.002423>
- Wodehouse, RP.** 1965. Pollen Grains, Hamer Press, New York, 249p.
- Yağmur İlkerenler, Y.** 2023. Foça (İzmir) İlçesinin Atmosferik Polen Analizi. Ege Üniversitesi Fen Bilimleri Enstitüsü Doktora Tezi, 383 sayfa, Bornova, İzmir.
- Yurtcan, HE.** 2021. Ayvalık (Balıkesir) Atmosferik Polenlerinin Volumetrik Analizi. Ege Üniversitesi Fen Bilimleri Enstitüsü, Yüksek Lisans Tezi, 148 s, Bornova, İzmir.



Determination of Prosulfocarb in Potato Flour Samples by Gas Chromatography-Mass Spectrometry

Proşülfokarbin Gaz Kromatografisi-Kütle Spektrometrisi ile Patates Unu Örneklerinde Tayini

Sezin Erarpas Bodur*

Yıldız Technical University, Faculty of Arts and Sciences, Department of Chemistry, İstanbul, Türkiye

Abstract

In this study, a gas chromatography-mass spectrometry (GC-MS) method was developed for the detection of prosulfocarb in potato flour matrix. GC-MS parameters were elaborately evaluated to achieve well-separated analyte signal with high signal to noise ratio. Under the optimum instrumental conditions, the limits of detection and quantification (LOD and LOQ) were found as 0.54 mg/kg and 1.80 mg/kg, respectively, which facilitates the determination of prosulfocarb at ppm levels. The established method was applied to potato flour samples spiked to six different concentration levels (2.6–101.7 mg/kg). Blank analyses were also performed for three different brand samples but prosulfocarb were found in the samples below the detection limit. Satisfactory percent recoveries between 90.9 and 105.7% with %RSD ($\leq 3.6\%$) were acquired for the selected sample matrix. High recoveries obtained with the matrix matching calibration strategy proved the accuracy and applicability of the developed method while low %RSD value showed the precision of the analytical method. It is suggested that the established method can be used to detect ppb/ppt levels of the analyte after a preconcentration method was applied to the sample solutions.

Keywords: GC-MS, matrix matching calibration method, potato flour, prosulfocarb.

Öz

Bu çalışmada, patates unu örneklerinde prosülfokarbin tayini için bir gaz kromatografisi-kütle spektrometresi (GC-MS) yöntemi geliştirilmiştir. Yüksek sinyal/gürültü oranına sahip iyi ayrılmış analit sinyali elde etmek için GC-MS parametreleri ayrıntılı bir şekilde değerlendirilmiştir. Optimum enstrümantal koşullar altında, gözlenebilme ve tayin limitleri (GL ve TL) sırasıyla 0,54 mg/kg ve 1,80 mg/kg olarak bulunmuştur, bu da prosülfokarbin ppm seviyelerinde belirlenmesine imkân tanımaktadır. Belirlenen yöntem, altı farklı konsantrasyon seviyesinde (2,6–101,7 mg/kg) standart eklenen patates unu örneklerine uygulanmıştır. Üç farklı marka örnek için kör analizler yapılmış ancak prosülfokarbin, tespit limitinin altında bulunmuştur. Seçilen örnek matriksi için %RSD ($\leq 3,6\%$) ile %90,9 ile %105,7 arasında kabul edilebilir yüzde geri kazanımlar elde edilmiştir. Matriks eşleştirme kalibrasyon stratejisi kullanılarak elde edilen yüksek geri kazanımlar, geliştirilen yöntemin doğruluğunu ve uygulanabilirliğini kanıtlarken, düşük %RSD değerleri analitik yöntemin kesinliğini göstermiştir. Örnek çözeltilerine ön deristirme yöntemi uygulandıktan sonra analitin ppb/ppt seviyelerini tespit etmek için oluşturulan yöntemin kullanılabileceği önerilmektedir.

Anahtar Kelimeler: GC-MS, matriks eşleştirme kalibrasyon yöntemi, patates unu, prosülfokarbin.

1. Introduction

Herbicides are substances applied to kill, control or prevent excessive growth of weeds or unwanted plants (Hormenoo et al. 2021). These substances are important chemicals used in agriculture, industry, domestic and commercial areas (Bo

et al. 2020). Among these chemicals, thiocarbamates have been used as herbicides (Guarda et al. 2020), insecticides (Lee et al. 2004) and fungicides (Gnatyshyna et al. 2020). These molecules with S-benzyl, S-alkyl or S-chlorobenzyl group are converted into sulfoxides in mammalian and plant bodies (Bo et al. 2020). Prosulfocarb (S-benzyl dipropylthiocarbamate) is used as herbicide for winter cereals (Nègre et al. 2006). It was discovered by Stauffer Chemical in Belgium in the late of 1980s (Shaner 2014). In European countries, prosulfocarb is used to selectively control grass and broad-leaved weeds in potatoes and winter

*Corresponding author: sezinerarpas@gmail.com

Sezin Erarpas Bodur orcid.org/0000-0002-9879-6662



This work is licensed by "Creative Commons Attribution-NonCommercial 4.0 International (CC)."

wheat (European Food Safety Authority 2007). It has low water solubility (~10 mg/L) that reduces the possibility of leaching downward (Nègre et al. 2006). It has been detected higher than 1.0 ng/m³ in atmosphere in France (Villiot et al. 2018) and detected in two different sampling location in Denmark (Ellermann et al. 2012, Muñoz et al. 2018). In literature, acceptable daily intake for human bodies is 0.005 mg/kg body weight per day (Devault et al. 2022). Although prosulfocarb effect on human health is not deeply highlighted in literature, thiocarbamate herbicides can be metabolized and reacted with biologically active compounds that impairs important cell processes. In addition, these chemicals can easily pass into cell membranes and physiological barriers like blood-brain and fetal placental barriers due to their lipophilic nature (Mathieu et al. 2015). For this reason, determination of prosulfocarb in food samples is an important issue for human health and environment.

In literature, prosulfocarb has been generally separated and detected by high performance liquid chromatography (HPLC) (Gennari et al. 2002, Marín-Benito et al. 2018). However, gas chromatography (GC) is a powerful instrumental method for volatile and semi-volatile analytes. It has many detector options to obtain sensitive, selective and specific analyte detection (Erarpat et al. 2020). Among them, mass selective detector (MS) is a prominent instrumental method as a detector for GC systems because it gives the number of analyte and their concentration in a sample and structural information of analytes as well (Stauffer 2013). LC-MS systems needs hazardous solvents as mobile phases but GC-MS has no problem about mobile phase issues (Sparkman et al. 2011). In addition, GC-MS has a great advantage of having library based-sample identification that provides compound names, molecular structure, elemental formula (Tsizin et al. 2017). Hence, GC-MS system was performed in the presented study for the quantification of prosulfocarb in potato flour samples.

Calibration is one of the most important steps in any analytical procedure. In ideal conditions, calibration standards and sample solutions have similar matrix medium. It is difficult to perform calibration process if the sample matrix is less similar to calibration standards or more complicated (Sloop et al. 2019). Matrix effects can be minimized by matrix matching calibration method meaning that the matrix of the calibration standards is adjusted to match the matrix of the sample (Vogl 2005). The matrix-matched calibration plot was constructed via the spiked sample solution. In this method, the sample solution used during the construction

of calibration plot should be analyzed and not contain target analyte (Bodur et al. 2024). Matrix matching calibration method was used during the recovery experiments of prosulfocarb in order to alleviate matrix effects.

Potato (*Solanum tuberosum L.*) ranks fourth after wheat, rice and corn in terms of production volume among various agricultural products in the world. The total potato cultivation area in Turkey is 203,000 hectares and a total of 5,250,000 tons of potatoes are produced (Ünlü et al. 2006). According to Republic of Türkiye Ministry of Agriculture and Forestry, prosulfocarb is used at high concentration levels (800 g/L with 400-500 mL/da) for barley, wheat and potato (Tarım ve Orman Bakanlığı Gıda ve Kontrol Genel Müdürlüğü 2024). In this study, different potato flour samples produced in Turkey were analyzed for their prosulfocarb concentration due to its high usage.

The objective of this study was to develop an accurate and precise analytical method for the determination of prosulfocarb in potato flour samples. GC-MS system was used to separate the analyte in GC and detect in MS system. After system analytical performance study, the developed method was implemented for the determination of prosulfocarb in the spiked potato flour samples.

2. Materials and Methods

2.1. Chemicals and Reagents

Prosulfocarb (%98) was supplied from Dr Ehrenstorfer GmbH, Germany. Gravimetric standard/sample preparation was followed during all experiments in this study. A 3110.2 mg/kg stock solution was prepared in methanol and diluted to obtain working standard solutions. Methanol was purchased from Merck, Germany. High purity helium gas was attained from a local gas supplier, Türkiye (İstanbul).

2.2. Instrumentation

An Agilent 6890 N gas chromatograph with mass selective detector was used to separate and quantify target analyte. Helium gas was used as mobile phase in GC-MS system at the flow rate of 1.8 mL/min. HP-5MS column (30 m; 250 µm; 0.25 µm) was placed into the oven compartment of GC system. Inlet temperature, injection volume, injection mode were 280 °C, 1.0 µL and splitless mode, respectively. Initial oven temperature was 100 °C. Oven temperature program had only one ramp from 100 °C to 300 °C at the rate of 20 °C/min. MS quadrupole, MS source and transfer line temperature values were 230, 150 and 280 °C, respectively. ChemStation mass spectrum database was utilized to check

and confirm fragments of the analyte obtained by MS system. Qualifier and quantifier ions for prosulfocarb were 128 and 91, respectively.

2.3. Samples

Three different brand potato flours (A, B and C) were purchased from three different sellers located in Türkiye. A clean centrifuge tube was placed into an analytical balance and 50 mg potato flour sample was weighed into the centrifuge tube. The solid sample was spiked to the desired concentration level with the analyte standard solution. The spiked flour sample was diluted to 10 g with methanol in order to extract the analyte from the sample matrix. The sample solution was vortexed for 20 s and centrifuged at 3000 rpm (3461 g) for 4.0 min. The upper liquid part was transferred into a clean glass vial and sent to GC-MS system.

Table 1. GC-MS conditions for Program I and II.

Parameter	Program I	Program II
Helium flow rate	1.80 mL/min	1.80 mL/min
Inlet temperature	280 °C	280 °C
Injection volume/mode	1.0 µL, splitless	1.0 µL, splitless
Oven temperature program	Initial oven temperature: 100 °C, one ramp from 100 °C to 300 °C at the rate of 20 °C/min.	Initial oven temperature: 100 °C, one ramp from 100 °C to 300 °C at the rate of 30 °C/min.
MS quad/ source/ transfer line temperature	230, 150 and 280 °C	230, 150 and 280 °C

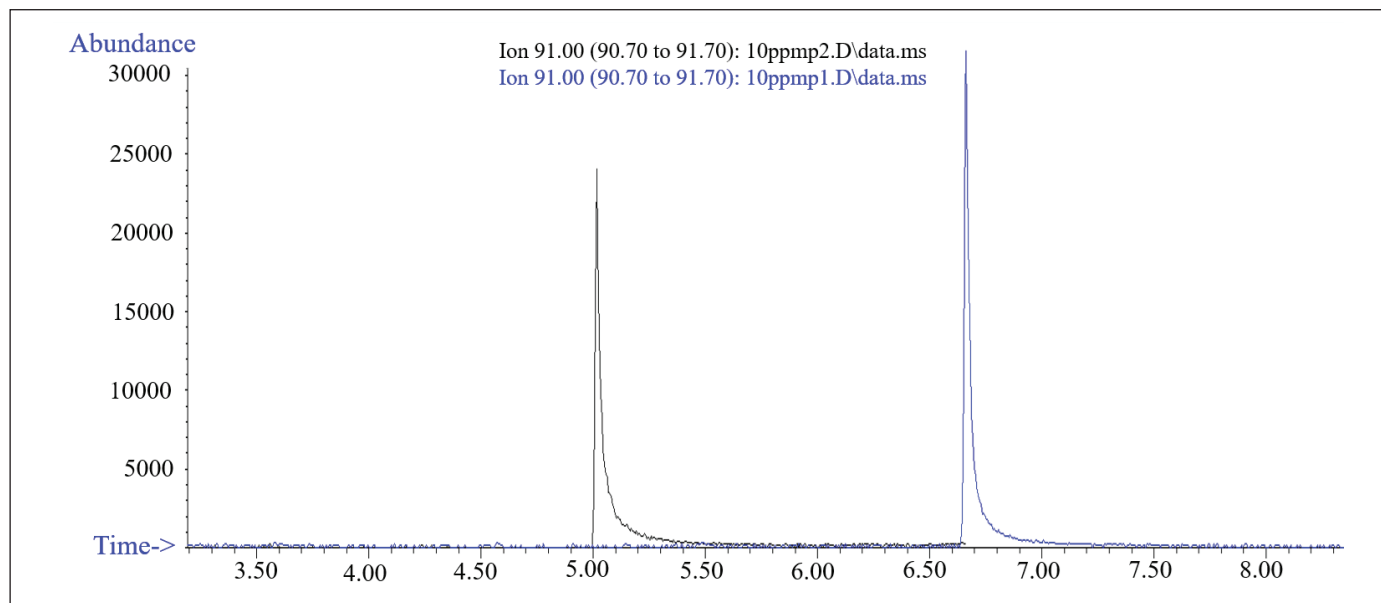


Figure 1. Chromatograms obtained by Program I (blue) and Program II (black).

3. Results and Discussion

3.1. Analytical Performance of GC-MS System

Two different oven temperature programs were tried to achieve high signal to noise ratio and good chromatographic conditions for prosulfocarb. The programs are given in Table 1. According to the chromatograms given in Figure 1, Program I gave highest signal to noise ratio than Program II. Hence, Program I was selected as optimum oven temperature program for the determination of prosulfocarb by GC-MS system.

Analytical performance of GC-MS system for the analyte was tested by calculating limit of detection (LOD), limit of quantitation (LOQ), linear working range, correlation coefficient (R^2) and percent relative standard deviation (%RSD) values. LOD and LOQ were found by mathematical for-

mulas as $3SD/m$ and $10SD/m$, respectively, where SD is standard deviation of the six repetitive measurements for the lowest concentration in the calibration plot and m is the slope of the calibration plot (Sanagi et al. 2009). LOD and LOQ are two important performance characteristics in method validation. This work compares three methods based on the International Conference on Harmonization and EURACHEM guidelines, namely, signal-to-noise, blank determination, and linear regression, to estimate the LOD and LOQ for volatile organic compounds (VOCs). For this purpose, a series of prosulfocarb standard solutions (2.4–237 mg/kg) was prepared in methanol. Under the optimum GC-MS conditions, all standard solutions were analyzed and calibration plot was drawn between 2.4 and 96.6 mg/kg. Linearity was excellent due to high R^2 value (0.9997). LOD and LOQ values were figured out to be 0.54 mg/kg and 1.80 mg/kg, respectively. %RSD value calculated by dividing standard deviation of six measurements for 2.4 mg/kg to mean of the measurements was found as 7.7%. The analytical performance of GC-MS system is summarized in Table 2. Overlay ion chromatograms belonging to the standard solutions are presented in Figure 2.

3.2. Recovery Studies by Matrix Matching Calibration Strategy

Three different potato flour samples (A, B, C) were treated with the procedure given in Samples Section. Blank analyses for the samples gave no analytical signals for the analyte.

Table 2. Analytical performance parameters for GC-MS system.

Parameter	Value
LOD, mg/kg	0.54
LOQ, mg/kg	1.80
Linear working range, mg/kg	2.4–96.6
R^2	0.9997
%RSD*	7.7
Linear equation	$y=84154x+6005$

*The %RSD value is belonging to the lowest concentration found in calibration plot.

For this reason, a calibration plot was drawn using Brand C sample which spiked to six different concentration levels (2.5–99.4 mg/kg). Brand A and Brand B sample were also spiked to different concentration levels and percent recovery results for the spiked Brand A and B samples were calculated using the linear equation ($y=100640x-37087$) obtained by Brand C sample. In addition to matrix matching calibration method, percent recovery values were calculated for Brand A and B samples via external calibration plot with the linear equation as . Table 3 gives all percent recovery and %RSD values for the spiked samples. Overlay ion chromatograms for the spiked samples and standard solution of the analyte are given in Figure 3.

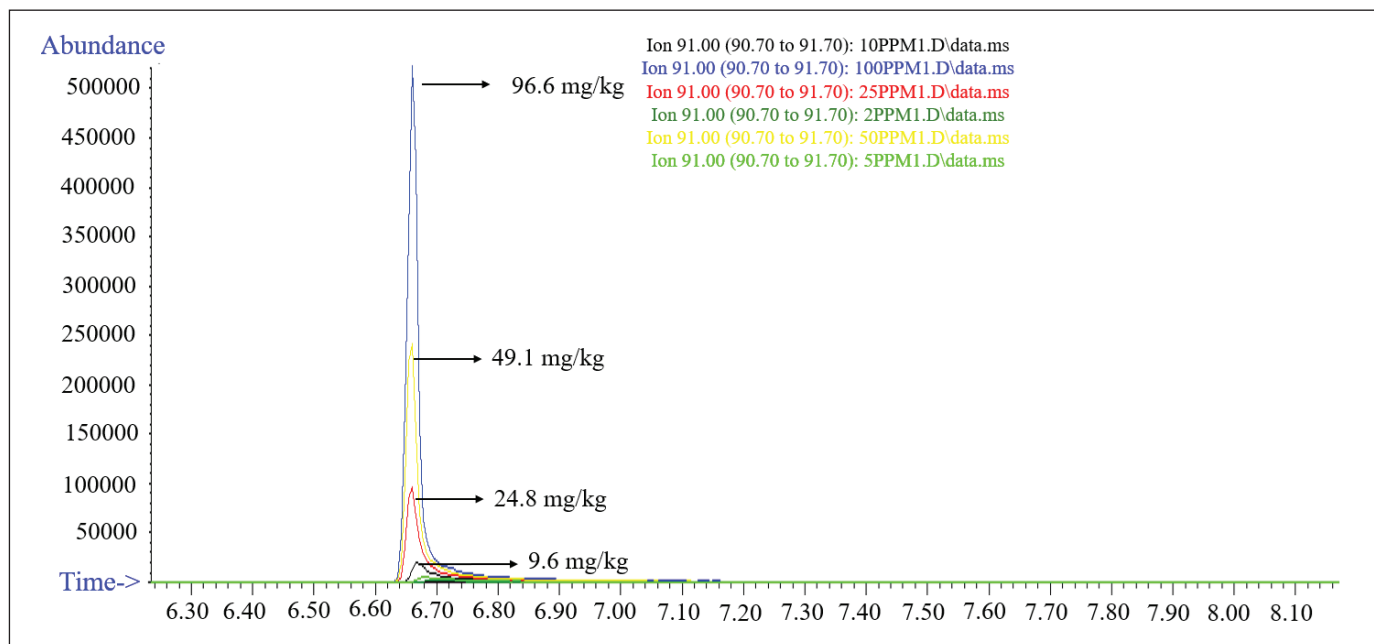


Figure 2. Overlay ion chromatograms (prosulfocarb: 91 m/z) of standard solutions in the range of 2.4–96.6 mg/kg.

According to the results given in Table 3, the developed GC-MS method can be applied to potato flour samples with matrix matching calibration method and external calibration method. High percent recovery results (90.9–105.7%) obtained by matrix matching calibration method validated the applicability and accuracy of the developed analytical method. Low \pm SD values (0.5–3.4) also proved the precision of the developed method. When compared to

external calibration method, matrix matching calibration strategy gave percent recovery results close to 100% more than external calibration method. Further, positive matrix effects were observed for Brand A (9.9–99.8 mg/kg) and B (10.2–101.7 mg/kg) samples. For these reasons, matrix matching calibration method was appropriate to achieve excellent percent recovery results for the selected sample.

Table 3. Percent recovery results for the spiked potato flour samples.

Sample code	Spiked concentration, mg/kg	%Recovery \pm SD*	%Recovery \pm SD**
Brand A	2.6	94.4 \pm 1.8	93.3 \pm 2.2
	5.0	94.6 \pm 3.4	102.9 \pm 4.0
	9.9	98.5 \pm 2.7	112.6 \pm 3.2
	24.9	104.4 \pm 1.8	122.8 \pm 2.2
	49.9	103.3 \pm 0.5	122.5 \pm 0.6
	99.8	100.2 \pm 0.9	119.3 \pm 1.1
Brand B	2.6	92.9 \pm 1.7	91.2 \pm 2.0
	5.1	90.9 \pm 2.1	98.7 \pm 2.5
	10.2	99.8 \pm 1.7	114.3 \pm 2.0
	25.8	105.7 \pm 1.8	124.4 \pm 2.1
	50.4	100.1 \pm 2.5	118.7 \pm 3.0
	101.7	97.4 \pm 1.5	115.9 \pm 1.8

*Matrix matching calibration method. **External calibration method.

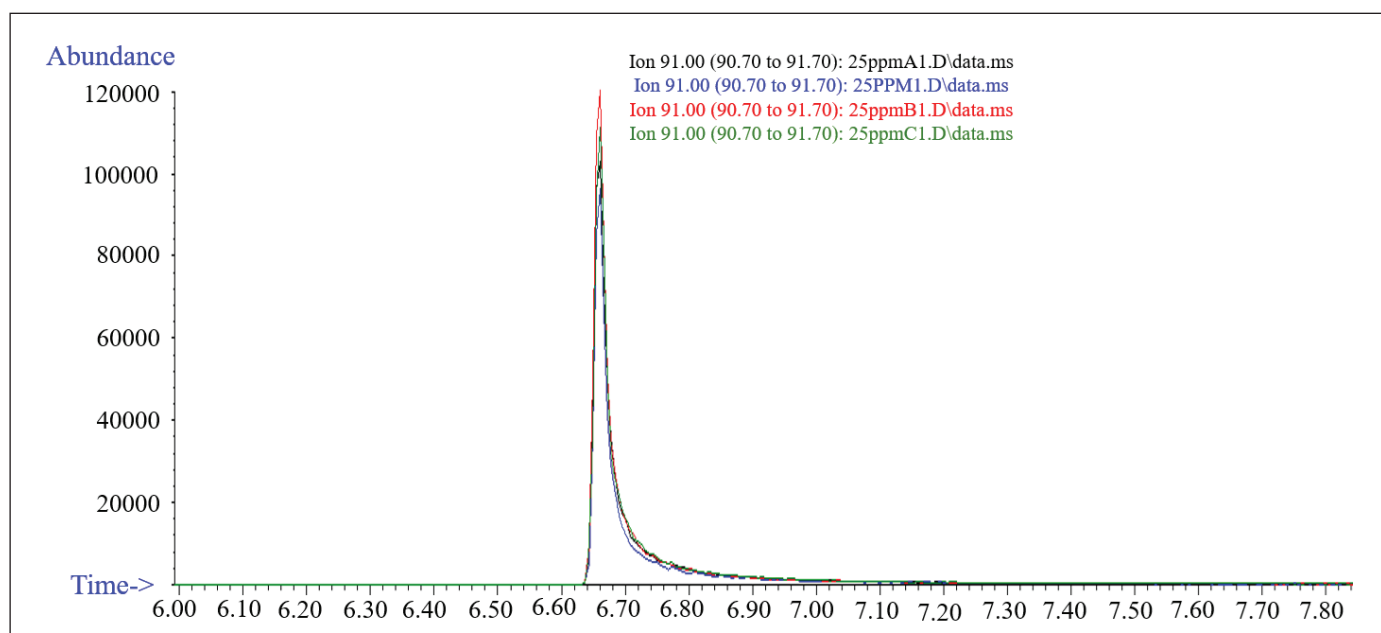


Figure 3. Overlay ion chromatogram for prosulfocarb standard solution (24.8 mg/kg) and spiked potato flour samples (24.9, 25.8 and 25.6 mg/kg spiked Brand A, B and C, respectively).

In literature, there are several analytical methods for the determination of prosulfocarb in vegetables by GC-MS system. For example, Przybylski et al. developed direct analysis method for carbamates. QuEChERS method was used to clean up and extract the analytes from green vegetables. LOD, LOQ and R² values were found as 0.50 µg/L, 1.4 µg/L and 0.9772. The method was applied to green bean, spinach, lettuce samples (Przybylski and Bonnet 2009). Another study proposed an analytical method based on QuEChERS and liquid chromatography-tandem mass spectrometry (LC-MS/MS) methods for the determination of pesticides including prosulfocarb in honey. LOQ and R² values were 0.01 mg/kg and 0.996, respectively (Gawel et al. 2019). In 2019, Fu et. al. presented an analytical method for the determination of pesticides in herbal species by gas chromatography-tandem mass spectrometry (GC-MS/MS). QuEChERS method was also used as clean up and extraction step in this study. LOQ and R² for prosulfocarb in different herb matrices were 2.0-8.0 ng/mL and 0.9946-0.9992, respectively (Fu et al. 2019). To the best our knowledge, there is no study about the determination of prosulfocarb in potato flour samples in literature. This study proposed an analytical approach for the detection of prosulfocarb in potato flour. In literature, clean up and extraction methods have been generally used to remove the matrix effects and extract the analyte. The developed GC-MS method can be also performed after a clean-up or extraction method. Hence, ppb/ppt detection limits can be obtained for the analyte in potato flour samples.

4. Conclusion and Suggestions

In the presented study, an analytical method for direct determination of prosulfocarb in potato flour by GC-MS system was proposed. Target analyte was separated on HP5MS column within 10 min. After the selection of optimum oven temperature program for the analyte, studies to figure out the system analytical performance were carried out by sending a series of analyte standard solutions to GC-MS system. LOD, LOQ, linear working range, %RSD and R² were found as 0.54 mg/kg, 1.80 mg/kg, 2.4-96.6 mg/kg, 7.7% and 0.9997, respectively. Further, applicability/accuracy of the proposed analytical method was checked by spiking potato flour samples. According to the results obtained via matrix matching calibration strategy, excellent percent recovery values (90.9-105.7%) with low SD (0.5-3.4) values verified the applicability and accuracy of the proposed method. The presented method can be used to qualify and quantify prosulfocarb in potato flour samples.

This is the first study where an analytical method for the determination of prosulfocarb in potato flour samples by GC-MS system was developed. The developed GC-MS method can be carried out after sample preparation methods like clean up and extraction are performed.

5. Acknowledgment

The authors have not received any financial support for this study. The authors have declared that there is no conflict of interest.

Author contribution

Sezin Erarpat Bodur: Conceptualization, Formal analysis, Data curation, Methodology, Investigation, Validation, Visualization, Supervision, Writing – original draft, review & editing.

Ethics committee approval: No ethical approval is required.

6. References

- Bo, X., Sun, J., Mei, Q., Wei, B., An, Z., Han, D., Li, Z., Xie, J., Zhan, J., He, M. 2020.** Degradation of prosulfocarb by hydroxyl radicals in gas and aqueous phase: Mechanisms, kinetics and toxicity. Ecotoxicol. Environ. Saf., 191: 110175. Doi: 10.1016/j.ecoenv.2020.110175
- Bodur, S., Tutar, BK., Tutar, ÖF., Bakırdere, S. 2024.** An accurate and sensitive determination of selected pesticides in mixed fruit juice samples using the combination of a simple and efficient microextraction method and GC-MS with a matrix matching calibration strategy. Anal. Methods, 16: 1363–1370. Doi: 10.1039/D3AY02327C
- Devault, DA., Guillemin, JP., Millet, M., Eymery, F., Hulin, M., Merlo, M. 2022.** Prosulfocarb at center stage! Environ. Sci. Pollut. Res., 29: 61–67. Doi: 10.1007/s11356-019-06928-8
- Ellermann, T., Andersen, HV., Bossi, R., Christensen, JH., Løfstrøm, P., Monies, C., Grundahl, L., Geels, C. 2012.** Atmosfærisk deposition., 2011. Novana. <http://www2.dmu.dk/Pub/SR30.pdf>
- Erarpat, S., Bodur, S., Ayyıldız, MF., Günkara, ÖT., Erulaş, F., Chormey, DS., Turak, F., Budak, TB., Bakırdere, S. 2020.** Accurate and simple determination of oxcarbazepine in human plasma and urine samples using switchable-hydrophilicity solvent in GC-MS. Biomed. Chromatogr., 34 (10): e4915. Doi: 10.1002/bmc.4915
- European Food Safety Authority. 2007.** Conclusion regarding the peer review of the pesticide risk assessment of the active substance prosulfocarb. EFSA J., 5(8): 111r. Doi: 10.2903/j.efsa.2007.111r

- Gennari, M., Ambrosoli, R., Nègre, M., Minati, JL.** 2002. Bioavailability and Biodegradation of Prosulfocarb in Soil. *J. Environ. Sci. Heal. Part B*, 37: 297–305. Doi: 10.1081/PFC-120004471
- Gnatyshyna, L., Falfushynska, H., Stolar, O., Dallinger, R.** 2020. Preliminary Study of Multiple Stress Response Reactions in the Pond Snail *Lymnaea stagnalis* Exposed to Trace Metals and a Thiocarbamate Fungicide at Environmentally Relevant Concentrations. *Arch. Environ. Contam. Toxicol.*, 79: 89–100. Doi: 10.1007/s00244-020-00728-9
- Guarda, PM., Pontes, AMS., de S. Domiciano, R., da S. Gualberto, L., B. Mendes, D., A. Guarda, E., da Silva, JEC.** 2020. Determination of Carbamates and Thiocarbamates in Water, Soil and Sediment of the Formoso River, TO, Brazil. *Chem. Biodivers.*, 17. Doi: <https://doi.org/10.1002/cbdv.201900717>
- Hormenoo, YA., K. Agbenorhevi, J., Ekyem, SO., Bonsu, KO., Torve, V., Voegborlo, BR.** 2021. Determination of some herbicide residues in sweet potato. *Cogent Food Agric.*, 7. Doi: 10.1080/23311932.2021.1910159
- Lee, SJ., Caboni, P., Tomizawa, M., Casida, JE.** 2004. Cartap Hydrolysis Relative to Its Action at the Insect Nicotinic Channel. *J. Agric. Food Chem.*, 52: 95–98. Doi: 10.1021/jf0306340
- Marín-Benito, JM., Barba, V., Ordax, JM., Andrades, MS., Sánchez-Martín, MJ., Rodríguez-Cruz, MS.** 2018. Application of green compost as amendment in an agricultural soil: Effect on the behaviour of triasulfuron and prosulfocarb under field conditions. *J. Environ. Manage.*, 207: 180–191. Doi: 10.1016/j.jenvman.2017.11.024
- Mathieu, C., Duval, R., Xu, X., Rodrigues-Lima, F., Dupret, JM.** 2015. Effects of pesticide chemicals on the activity of metabolic enzymes: focus on thiocarbamates. *Expert Opin. Drug Metab. Toxicol.*, 11: 81–94. Doi: 10.1517/17425255.2015.975691
- Muñoz, A., Borrás, E., Ródenas, M., Vera, T., Pedersen, HA.** 2018. Atmospheric Oxidation of a Thiocarbamate Herbicide Used in Winter Cereals. *Environ. Sci. Technol.*, 52: 9136–9144. Doi: 10.1021/acs.est.8b02157
- Nègre, M., Passarella, I., Boursier, C., Mozzetti, C., Gennari, M.** 2006. Evaluation of the bioavailability of the herbicide prosulfocarb through adsorption on soils and model soil colloids, and through a simple bioassay. *Pest Manag. Sci.*, 62: 957–964. Doi: 10.1002/ps.1264
- Przybylski, C., Bonnet, V.** 2009. Use of spermine and thiabendazole as analyte protectants to improve direct analysis of 16 carbamates by gas chromatography-mass spectrometry in green vegetable matrices. *Anal. Bioanal. Chem.*, 394: 1147–1159.
- Sanagi, MM., Ling, SL., Nasir, Z., Hermawan, D., Wan Ibrahim, WA., Naim, AA.** 2009. Comparison of signal-to-noise, blank determination, and linear regression methods for the estimation of detection and quantification limits for volatile organic compounds by gas chromatography. *J. AOAC Int.*, 92: 1833–1838. Doi: 10.1093/jaoac/92.6.1833
- Shaner, DL.** 2014. *Herbicide Handbook*, 10th Editi. ed. Weed Science Society of America, Lawrence, KS, USA. <https://wssa.net/wp-content/uploads/Christian-Willenborg-herbicide-handbook-2014.pdf>
- Sloop, JT., Bonilla, HJB., Harville, T., Jones, BT., Donati, GL.** 2019. Automated matrix-matching calibration using standard dilution analysis with two internal standards and a simple three-port mixing chamber. *Talanta* 205: 120160. Doi: 10.1016/j.talanta.2019.120160
- Sparkman, OD., Penton, ZE., Kitson, FG.** 2011. Points of Comparison of LC/MS vs GC/MS. In: *Gas Chromatography and Mass Spectrometry: A Practical Guide*. Elsevier, pp. 459–462. Doi: 10.1016/B978-0-12-373628-4.00044-7
- Stauffer, E.** 2013. *Gas Chromatography-Mass Spectrometry*. Encycl. Forensic Sci., 596–602. Doi: 10.1016/B978-0-12-382165-2.00249-X
- T.C. Tarım ve Orman Bakanlığı Gıda ve Kontrol Genel Müdürlüğü.** 2024. Bitki Koruma Ürünleri Veritabanı. <https://bku.tarimorman.gov.tr/AktifMadde/Details/667>
- Tsizin, S., Bokka, R., Keshet, U., Alon, T., Fialkov, AB., Tal, N., Amirav, A.** 2017. Comparison of electrospray LC–MS, LC–MS with Cold EI and GC–MS with Cold EI for sample identification. *Int. J. Mass Spectrom.*, 422: 119–125. Doi: 10.1016/j.ijms.2017.09.006
- Ünlü, M., Kanber, R., Şenyigit, U., Onaran, H., Diker, K.** 2006. Trickle and sprinkler irrigation of potato (*Solanum tuberosum* L.) in the Middle Anatolian Region in Turkey. *Agric. Water Manag.*, 79: 43–71. Doi: 10.1016/j.agwat.2005.02.004
- Villiot, A., Chrétien, E., Drab-Sommesous, E., Rivière, E., Chakir, A., Roth, E.** 2018. Temporal and seasonal variation of atmospheric concentrations of currently used pesticides in Champagne in the centre of Reims from 2012 to 2015. *Atmos. Environ.*, 174: 82–91. Doi: 10.1016/j.atmosenv.2017.11.046
- Vogl, J.** 2005. Calibration Strategies and Quality Assurance. In: Nelms, S. (Ed.), *Inductively Coupled Plasma Mass Spectrometry Handbook*, 1:147–181. Doi: 10.1002/9781444305463.ch4



Çeşitli Tekrarlayan Sinir Ağları Kullanarak Siber Saldırı Tespiti

Cyber-Attack Detection Using Various Recurrent Neural Networks

Nesibe Yalçın^{1*} , Semih Çakır² , Sibel Ünalı³

¹Erciyes Üniversitesi, Mühendislik Fakültesi, Bilgisayar Mühendisliği Bölümü, Kayseri, Türkiye

²Zonguldak Bülent Ecevit Üniversitesi, Kdz. Ereğli Meslek Yüksekokulu, Bilgisayar Teknolojileri Bölümü, Zonguldak, Türkiye

³Bilecik Şeyh Edebali Üniversitesi, Mühendislik Fakültesi, Elektrik-Elektronik Mühendisliği Bölümü, Bilecik, Türkiye

Bu makale, 10-11 Mayıs 2024 tarihleri arasında Karaelmas International Science and Engineering Symposium (KISES 2024) isimli sempozyumda sözlü olarak sunulan ve özet kitabındaki yayınlanan çalışmanın genişletilmiş versiyonudur (Sempozyum bildirisinin başlığı: "Cyber-Attack Detection Using Various Recurrent Neural Networks").

Öz

Siber saldırıların erken tespiti ve tanımlanması; saldırıların etkisinin doğru bir şekilde değerlendirilmesi, bunlara karşı hızlı ve etkili önlemlerin alınması, veri ve sistemlerin korunması, iş sürekliliğin sağlanması, kurumsal itibarın korunması, yasal ve düzenleyici standartlara uyumun sağlanması açısından hayatı önem taşımaktadır. Bu çalışmada, bir siber saldırı tespit sistemi önerilmiştir. Saldırı tespiti için çeşitli Tekrarlayan Sinir Ağı (Recurrent Neural Network, RNN) derin öğrenme yöntemlerinin yanı sıra K En Yakın Komşu (K Nearest Neighbour, KNN), Karar Ağacı ve Rastgele Orman makine öğrenme algoritmaları uygulanmıştır. Sistemin saygınlığı, KDD'99 veri setinin %10'u üzerinden değerlendirilmiş ve tartışılmıştır. Öğrenme modellerinin başarısını karşılaştırmak için çeşitli değerlendirme metrikleri kullanılmıştır. Aynı veri setini kullanan çalışmalarla karşılaşıldığında önerilen Çift Yönlü Uzun Kısa Süreli Bellek, daha yüksek başarıya sahip RNN modeli olarak öne çıkmaktadır. Ayrıca KNN de yüksek bir test doğruluğu (%99.92) ve duyarlılık (%99.94) sunmuştur. Önerilen modeller, siber saldırılardan erken aşamada tespit edilmesini kolaylaştırabilir.

Anahtar Kelimeler: Derin öğrenme, KDD'99, RNN, siber güvenlik, saldırı tespiti.

Abstract

Early detection and identification of cyber-attacks is vital to accurately assess their impact, take swift and effective countermeasures against them, protect data and systems, maintain operational continuity, preserve organizational reputation, and ensure compliance with legal and regulatory standards. A cyber-attack detection system was proposed in this study. K Nearest Neighbour (KNN), Decision Tree, and Random Forest machine learning algorithms, and also various Recurrent Neural Network (RNN) deep learning methods were applied for attack detection. The reputability of the system was evaluated and discussed using 10% of the publicly available KDD'99 dataset. Various evaluation metrics were used to compare the performance of these learning models. In comparison to the studies using the same dataset, the proposed Bidirectional Long Short-Term Memory stands out with its higher performance as an RNN model. KNN also presented a higher test accuracy (99.92%) and recall (99.94%). The proposed models may facilitate the detection of cyber-attacks at an early stage.

Keywords: Deep learning, KDD'99, RNN, cyber security, attack detection.

*Sorumlu yazarın e-posta adresi: nesibeyalcin@erciyes.edu.tr

Nesibe Yalçın orcid.org/0000-0003-0324-9111

Semih Çakır orcid.org/0000-0003-3072-9532

Sibel Ünalı orcid.org/0000-0001-9948-4284



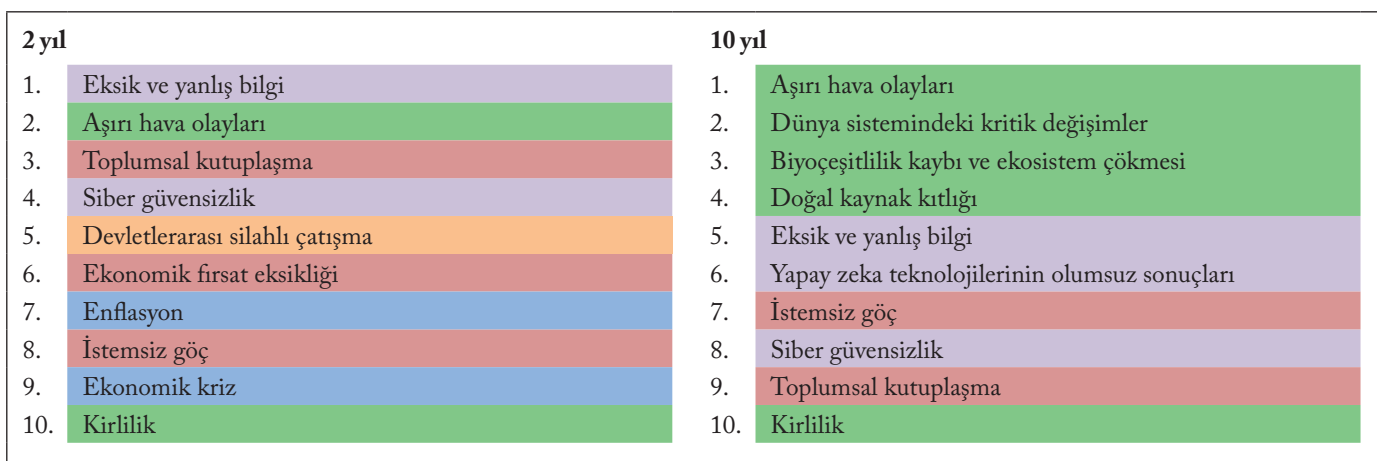
Bu eser "Creative Commons Ahılu-GayriTicari-4.0 Uluslararası Lisansı" ile lisanslanmıştır.

1. Giriş

Dünya Ekonomik Forumu (World Economic Forum, WEF)'nun 2024 Küresel Riskler Raporu'nda (WEF 2024) siber güvensizlik, en büyük 10 küresel risk arasında gösterilmiş, kısa vadeden en ciddi 4. ve uzun vadeden 8. küresel risk olarak sıralanmıştır (Şekil 1). Ayrıca siber saldırılar, küresel ölçekte maddi bir krize neden olma ihtimali en yüksek olduğuna inanılan ve en acil çözüm gerektiren 5 küresel risk arasındadır. Siber saldırıların öümüzdeki yıllarda sürekli ve önemli bir endişe kaynağı olmaya devam edecekmişdir. Bununla birlikte siber güvenlik saldırılarını tespit etmek ve etkilerini azaltmak için çok çeşitli güvenlik araçları ve sistemleri (güvenlik duvarları, saldırı tespit sistemleri, bulut güvenlik yazılımları gibi) mevcuttur.

Günümüzde büyük bir tehdit haline gelen siber saldırılarla karşı otomatik/erken tespit ve önlem alma, önemli bir savunma stratejisidir. Yapay zeka ve makine öğrenmesi gibi teknolojilerin kullanılması, anomalileri ve potansiyel saldırı işaretlerini tanımlamada yardımcı olabilmektedir. Literatürde bilgisayar ağlarında saldırının tespiti için çeşitli yapay zeka yöntemlerini kullanan birçok model önerilmiş ve yüksek başarı elde edilmiştir. 2020 yılında Iwendi ve diğerleri, yaptıkları çalışmada KDD'99 (KDD Cup 1999 Data) ve NSL-KDD veri setlerini makine öğrenmesi tabanlı saldırının tespitinde kullanılmışlardır (Iwendi vd. 2020). 5 ana saldırının türüne ait sınıfları ele alarak korelasyon tabanlı öznitelik seçimi + topluluk sınıflandırıcıları (Bagging ve Adaboost) yaklaşımını önermişler ve yüksek doğruluk ile düşük yanlış alarm oranına sahip saldırı takip sistemi geliştirmiştir. Önerdikleri yaklaşım, KDD'99 veri setinde 0 yanlış

alarm oranı ve %99.90 tespit oranı, NSL-KDD veri setinde %0.5 yanlış alarm oranı ve %98.60 tespit oranı başarımına sahiptir. Yapılan bir başka çalışmada (Gao vd. 2021) ise SCADA ağları için saldırular, ilk kez zamansal ilişkili olma ve olmama durumları için kategorize edilmiş ve derin öğrenmeye dayalı çok yönlü bir saldırı tespit sistemi üzerine çalışılmıştır. Çalışmada %10 KDD'99 veri seti; 1) normal ve ilişkisiz saldırular, 2) normal ve ilişkili saldırular ve 3) hem ilişkili hem de ilişkisiz saldıruları içeren 3 farklı veri seti şeklinde düzenlenmiştir. Çalışmadan elde edilen bulgular zamansal ilişkili saldıruları tespit etmede Uzun Kısa Süreli Bellek (Long Short-Term Memory, LSTM)'nin daha iyi performans gösterdiğini, zamansal ilişkili olmayan saldıruların tespitinde ise İleri Beslemeli Sinir Ağı (Feedforward Neural Network, FNN)'nın daha avantajlı olduğunu ortaya koymuştur. Saldırı tespitinde Zamansal Evrişimli Ağlar (Temporal Convolutional Networks, TCN)'ın başarısının incelendiği bir çalışmada (Çakır ve Angin 2021), KDD'99 veri seti kullanılmıştır. Araştırmada Tam Evrişimli Ağlar (Fully Convolutional Networks, FCN) ile LSTM ve TCN tabanlı otomatik kodlayıcılar geliştirilerek başarımları karşılaştırılmış ve ikili sınıflandırmada TCN'nin en az LSTM kadar başarılı olduğu raporlanmıştır. Laghrissi ve diğerleri (2021), siber saldırıları tespit etmek için LSTM tabanlı bir derin öğrenme yaklaşımı sunmuştur. Boyut azaltmanın uygulandığı bu yaklaşım, KDD'99 veri seti üzerinde test edilmiş ve %99.49 doğruluk - %99.15 duyarlılık sağlamıştır. LSTM Tekrarlayan Sinir Ağı (Recurrent Neural Network, RNN) uygulanan bir saldırı tespit modelinde ise değerlendirme UNSW-NB15 veri seti üzerinde yapılmış ve Basit RNN modeli ile karşılaştırıldığında %99'un üzerinde doğ-



Şekil 1. Önem derecesine göre küresel riskler (WEF 2024).

ruluk ile daha iyi başarılm göstermiştir (Thant vd. 2023). Kasongo tarafından Basit RNN, LSTM ve Geçitli Tekrarlayan Birim (Gated Recurrent Unit, GRU) yöntemlerini kullanan bir saldırı tespit sistemi önerilmiştir. Sistemin performansını değerlendirmek için UNSW-NB15 ve NSL-KDD veri setleri dikkate alınmış, ayrıca özellik seçimi yapılmıştır. LSTM, NSL-KDD veri seti üzerinde %88.13 test doğruluğu ile en iyi başarımı göstermiştir. UNSW-NB15 veri seti üzerinde Basit RNN, %87.07 doğruluk oranı ile en etkili model olmuştur (Kasongo 2023). Ağ saldırısı tespit sistemi için Çift Yönlü LSTM (Bidirectional LSTM, Bi-LSTM) kullanan sinir ağlarının değerlendirildiği bir çalışmada (Pooja ve Shrinivasacharya 2021) ise KDD'99 ve UNSW-NB15 veri setleri üzerinde deneyler gerçekleştirılmıştır. Bi-LSTM modeli, her iki veri seti için %99 doğrulukla yüksek sonuçlar vermiştir. KDD'99 veri seti üzerinde yapılan bir başka çalışmada (Liu ve Zhang 2020) ise Evrişimli Sinir Ağları kullanılarak %98.02 doğruluk elde edilmiştir. Ale-nazi ve Mishra (2024), saldırısı tespit için Ekstrem Gradyan Artırma (Extreme Gradient Boosting, XGBoost) modeli önermişler, KDD'99 veri setinde %99.98 ve NSL-KDD veri setinde %99.97 ise doğruluk elde etmişlerdir. Ayrıca çalışmalarında, Gaussian Naïve Bayes (NB) ile XGBoost modelini karşılaştırmışlar ve her iki veri setinde de XGBoost modelinin üstün yanlarını vurgulamışlardır. İlgün ve Samet, 2024 yılında yaptıkları çalışmada ise NSL-KDD veri setine ön işlem uygulanmadan ve sırasıyla kategorik veri kodlama, ölçeklendirme, hibrit öznitelik seçimi ön işlemlerini hem ayrı ayrı hem de beraber uygulayarak 5 farklı senaryo oluşturmuş ve böylelikle 5 farklı veri seti elde etmişlerdir. Çalışmanın bir sonraki adımda bu veri setleri üzerinde çeşitli makine öğrenmesi yöntemlerini kullanmışlardır. En son adımda ise en başarılı sonuçları veren yöntemler ele alınarak hiperparametre optimizasyonu ile modellerin performansları iyileştirilmiştir. Çalışmada optimizasyon uygulanmasının, genel olarak saldırısı tespit başarısını artırsa da eğitim ve test süresini uzattığı görülmüştür (İlgün ve Samet 2024).

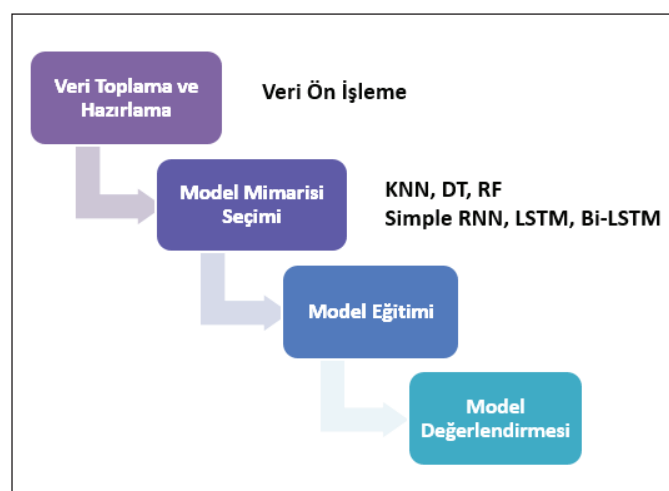
Bu çalışmada, Basit RNN, LSTM ve Bi-LSTM olmak üzere farklı türde RNN modelleri kullanılarak siber saldırısı tespiti gerçekleştirilmiştir. Ayrıca Karar Ağacı (Decision Tree, DT), Rastgele Orman (Random Forest, RF) ve K En Yakın Komşu (K Nearest Neighbour, KNN) modelleri geliştirilmiş ve karşılaştırmalı analizi yapılmıştır. Yapılan analizlere ilişkin sonuçlar incelendiğinde, bütün öğrenme modelleri için %97.76 ve üzeri sınıflandırma doğruluğu elde edilmiştir. En yüksek duyarlılığa sahip modeller ise %99.94 ile KNN ve Bi-LSTM olmuştur. Ayrıca, elde edilen sonuçlar aynı veri seti kullanılarak saldırısı tespit sistemi geliştirilmesi amaçlı

literatürdeki çalışmalar ile karşılaştırıldığında daha yüksek başarılm sağlanmıştır.

KDD'99 veri seti kullanılarak siber saldırısı tespitinin araştırıldığı bu çalışmanın geri kalan bölümleri şu şekilde organize edilmiştir: 2. Bölümde, veri seti ve çalışmada ele alınan yöntemler açıklanmıştır. Ardından, 3. Bölümde, çalışma kapsamında elde edilen bulgular sunulmuş ve tartışılmıştır. Son bölümde ise sonuçlar değerlendirilmiştir.

2. Gereç ve Yöntemler

Saldırısı tespiti için farklı yapay zeka yöntemleri kullanılarak modeller geliştirilmiş ve modellerin performansları çeşitli metrikler açısından değerlendirilmiştir. Çalışmanın ana hatları Şekil 2'de gösterilmiştir.



Şekil 2. Çalışmanın iş akışı.

2.1. Veri Seti

Çalışmada %10 KDD'99 veri seti kullanılmıştır (UCI KDD Archive 1999). Yaklaşık 25 yıllık bir veri seti olmasına rağmen, zaman yayılımı, içerdigi saldırısı çeşitliliği ve toplam veri sayısının büyülüüğü gibi nedenlerle saldırısı tespit sistemlerinin başarımının değerlendirilmesinde halen yaygın olarak kullanılmaktadır. Veri setinde, bağlantının başlangıcından bitişine kadar geçen süre (duration), bağlantının durumu (flag), kullanılan iletişim protokolü (protocol_type), ağ hizmeti (service), kaynağa/hedefe iletlenen toplam veri miktarı (src_bytes, dst_bytes), geçersiz giriş denemesi sayısı (num_failed_logins), sunucu hata oranı (dst_host_srv_error_rate) gibi 41 özellik yer almaktadır. 97,277 normal ve 396,744 saldırısı içeren trafik verisi olmak üzere toplamda 494,021 kayıt bulunmaktadır.

2.2. RNN

RNN, düğümler arasında bağlantıların yer aldığı ve yönlendirilmiş döngü oluşturduğu bir sinir ağı türüdür (Şeker vd. 2017, Mikolov vd. 2010). İleri beslemeli bir sinir ağında, tüm girdiler ile çıktıların birbirinden bağımsız olduğunu varsayılarken RNN'de, önceki adımlarda elde edilen çıktılar bir sonraki adımda girdi olarak kullanılır ve böylece zamanla (veya döngüle) geri besleme sağlanır. İleri beslemeleri ağların aksine RNN'lerin kısa süreli hafiza oluşturma olasılığı vardır (Mikolov vd. 2010) ve geçmiş girdilerden gelen bilgileri kullanarak durumu koruyan bağlantılarla sahiptir. Başka bir ifade ile sabit sayıda giriş vektörü kullanmak yerine, tahmin için mevcut bir zaman dilimine kadar tüm giriş bilgilerinden yararlanabilir. Diziye yakın veri noktaları arasındaki korelasyonları içeren (zaman) sıralı verilerle baş etmek için bir çözüm sunar (Schuster ve Paliwal 1997). Basit RNN, model olarak bir girdi katmanı (input layer), bir gizli (hidden/context) katman ve bir çıkış (output) katmanına sahiptir.

LSTM ağları, dizi verilerinin zaman adımları arasında uzun süreli bağımlılıkları öğrenebilen bir RNN türüdür (Cakır vd. 2020, Bouktif vd. 2020). Geniş bir kullanım alanına sahip olan LSTM, basit yapılı RNN'lerin eğitim zamanında meydana gelen kaybolan (vanishing) gradyan sorunuunu çözmek amaçlı Hochreiter ve Schmidhuber (1997) tarafından tasarlanmıştır. LSTM'nin temel yapısını 3 ana kapı oluşturur: 1) giriş kapısı (input gate), 2) çıkış kapısı (output gate) ve 3) unutma kapısı (forget gate). Bu üç kapı, LSTM hücresinin hücre durumunu ve gizlilik durumunu kontrol ederek elde ettiği bilginin depolanması, güncelleme zamanı ve çıkış zamanı konularında karar vermektedir.

Graves ve Schmidhuber tarafından 2005 yılında ilk kez LSTM ağına çift yönlü eğitim uygulanmış ve Bi-LSTM, LSTM'nin gelişmiş bir türü olarak önerilmiştir. Dizi içerişinde yer alan bağımlılıkları iki yönlü olarak ileri ve geri yönde öğrenebilmeyi sağlamaktadır. Hem önceki hem de sonraki bağlamı her bir zaman adımda dikkate alması, modelin daha doğru tahmin gerçekleştirmesine imkan tanımaktadır. Bi-LSTM modeli yapısında çift ayrı LSTM katmanı bulundurur. Katman çiftlerinden biri girdiyi zaman adımı sırası ile ileri yönde işlerken, diğeri ise girdiyi zaman adımı ters sırası ile geri yönde işlemektedir. Elde edilen çıktılar ise daha sonra birleştirilmektedir. Bu çift yönlü yapısı ile Bi-LSTM birçok uygulamada yüksek doğruluk ile kullanılabilmektedir.

2.3. Makine Öğrenmesi Algoritmaları

KNN, en çok kullanılan makine öğrenmesi algoritmalarındandır. Algoritma, kendisine en yakın k komşuya göre tahmin yapmaktadır. Komşuların belirlenmesinde yakınlık hesabı için kosinus ve Öklid mesafesi gibi uzaklık yöntemleri kullanılmaktadır (Dolgın vd. 2009). KNN, sınıflandırma ve regresyon problemleri için etkili yöntemlerden biridir.

DT, ters ağaç yapısına benzer. Verileri dallara ayıran yapısı ile karar verme süreci oluşturur ve bu sürecin sonunda bir tahmin (sınıflandırma/regresyon) gerçekleştirir (Özger 2023). Veriyi bölmeye karar, çeşitli ölçütlerle (bilgi kazancı, Gini indeksi gibi) göre yapılmaktadır. Örneğin bilgi kazancı en yüksek olan özellik, kök düğümde tutulur ve veriyi bölmek için kullanılan ilk kriterdir. Her bir özelliğin aldığı değerler dalları ifade eder ve her bir dalın sonunda bir karar noktası (iç düğüm) oluşturulur ya da yaprak yer alır. Yapraklar, ağacın en alt seviyesidir ve nihai tahmini sağlar (Ünalı ve Yalçın 2022).

RF, sınıflandırma ve regresyon amaçlı karar ağaçlarını kullanan bir topluluk (ensemble) yöntemi olarak bilinmektedir. Algoritmanın çalışma mantığı, veri kümelerinden rastgele oluşturulan her bir alt küme için DT meydana getirilmesine dayanır. Her bir DT tarafından üretilen tahminlere göre ağırlıklandırılmıştır ve elde edilen sonuç nihai tahmin olarak sunulur (Özger 2023, Yalçın vd. 2024).

3. Bulgular ve Tartışma

Çalışma kapsamında geliştirilen öğrenme modelleri, Google Colaboratory platformunda Python programla dili ile geliştirilmiştir. Pandas, NumPy, Keras (models, layers, callbacks), Matplotlib, Sklearn (metrics, model_selection, preprocessing, neighbors, tree, ensemble) ve Mlxtend kütüphaneleri kullanılmıştır.

Sinir ağları, sayısal girdiler gerektirdiği için veri setinde yer alan kategorik veriler (protocol_type, flag, service, target) sayısal değerlere dönüştürmüştür. Daha sonra bütün değerler, 0 ile 1 arasında olacak şekilde normalize edilmiştir. Veri seti, eğitim ve test veri seti olmak üzere 80:20 oranında ikiye ayrılmıştır. Bununla birlikte KNN, DT ve RF modelleri için 5 katlı çapraz doğrulama (cross validation) yöntemi uygulanmıştır. KNN için k komşu sayısı, Elbow yöntemi ile 5 olarak elde edilmiştir. Denemeler sonucunda DT ve RF için maksimum derinlik (max_depth) 5 ve RF içinde oluşturulacak ağaç sayısı (n_estimators) 40 olarak belirlenmiştir. Çalışmada Basit RNN, LSTM ve Bi-LSTM yöntemleri kullanılarak 3 farklı RNN derin öğrenme modeli tasarlanmıştır

ve tasarlanan RNN modellerine ilişkin detaylar ise Çizelge 1'de verilmiştir. Her bir RNN modeli, model ile aynı isimli katman ve bir yoğun (dense) katmandan oluşmaktadır. Çizelge 1'de her bir katmandaki nöron, eğitilebilir (trainable) ve toplam (total) parametre sayısı (params) görülebilmekte- dir. Katmanlarda Adam optimize edici, sigmoid aktivasyon

fonksiyonu ve ikili çapraz entropi kaybı (binary crossentropy loss) kullanılmıştır.

Geliştirilen tüm modeller için elde edilen test karmaşıklık matrisleri, Şekil 3'te sunulmuştur. Test veri setinin 79452 adeti saldırısı, 19353 adeti ise normal trafik verilerinden oluş-

Çizelge 1. Tasarlanan RNN model mimarileri.

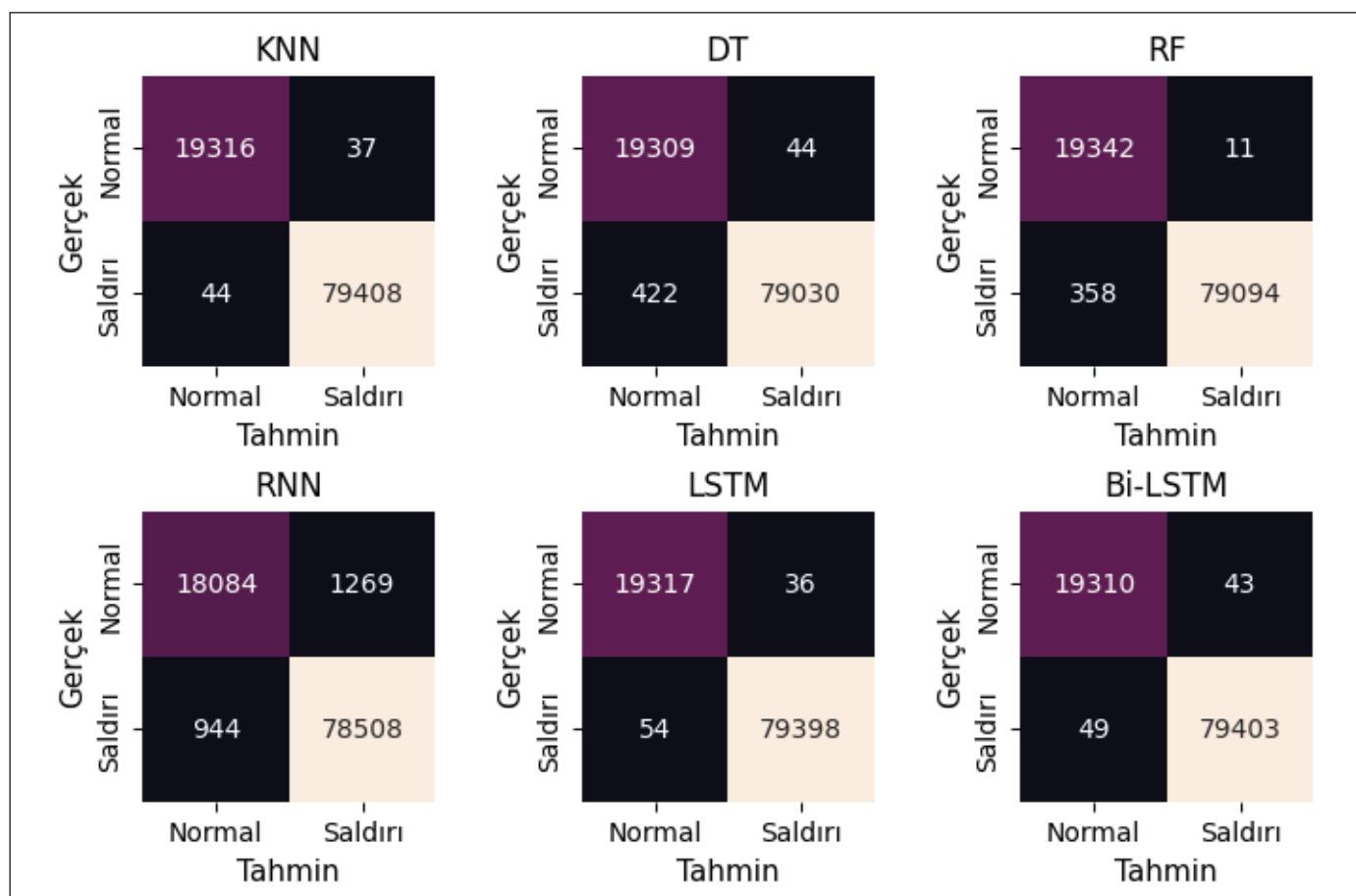
Model	Mimari
Basit RNN	<pre> Model: "sequential" Layer (type) Output Shape Param # ===== simple_rnn (SimpleRNN) (None, 100) 10200 dense (Dense) (None, 1) 101 ===== Total params: 10301 (40.24 KB) Trainable params: 10301 (40.24 KB) Non-trainable params: 0 (0.00 Byte) </pre>
LSTM	<pre> Model: "sequential_2" Layer (type) Output Shape Param # ===== lstm_1 (LSTM) (None, 50) 10400 dense_2 (Dense) (None, 1) 51 ===== Total params: 10451 (40.82 KB) Trainable params: 10451 (40.82 KB) Non-trainable params: 0 (0.00 Byte) </pre>
Bi-LSTM	<pre> Model: "sequential_1" Layer (type) Output Shape Param # ===== bidirectional (Bidirection (None, 100) 20800 al) dense_1 (Dense) (None, 1) 101 ===== Total params: 20901 (81.64 KB) Trainable params: 20901 (81.64 KB) Non-trainable params: 0 (0.00 Byte) </pre>

maktadır. Karmaşıklık matrisleri analiz edildiğinde; saldırı örneklerinden 79408'i KNN tarafından doğru şekilde sınıflandırılmıştır. Yüksek duyarlılıkla saldırıların tespitini gerçekleştiren diğer bir yöntem Bi-LSTM olmuştur ve saldırıya ilişkin örneklerin 79403'ünü doğru tespit etmiştir. RF, normal trafiğe ilişkin örneklerin sadece 11'ini yanlış şekilde saldırı olarak nitelendirmiştir. Bununla birlikte saldırıya ilişkin 358 örneği de normal olarak tahmin etmiştir.

Model performanslarını karşılaştırmak için doğruluk, kesinlik, duyarlılık, F1 ölçütü ve yanlış tespit oranı hesaplanmış-

tır. Her bir modele ilişkin performans sonuçları Çizelge 2'de sunulmuştur. Sonuçlar incelendiğinde, bütün modellerin %97.76 ve üzeri sınıflandırma doğruluğu sunduğu görülmektedir. KNN ve Bi-LSTM, %99.94 ile en yüksek tespit oranına (duyarlılığı) sahiptir.

Çalışma sonuçları, literatürde aynı veri seti üzerinde yapılan benzer amaçlı çalışmalar ile karşılaştırılmıştır (Çizelge 3). Çakır ve Angin (2021)'nin çalışmalarında en yüksek doğrulukla saldırı tespiti LSTM yöntemi ile elde edilmiştir. Bununla birlikte LSTM kullanılarak elde edilen sınıflandır-



Şekil 3. Karmaşıklık matrisleri.

Çizelge 2. Model performans sonuçları.

Model	Doğruluk	Kesinlik	Duyarlılık	F1-ölçütü	Yanlış Tespit Oranı
Basit RNN	0.9776	0.9841	0.9881	0.9861	0.0656
LSTM	0.9991	0.9995	0.9993	0.9994	0.019
Bi-LSTM	0.9991	0.9995	0.9994	0.9994	0.0022
KNN	0.9992	0.9995	0.9994	0.9995	0.0019
DT	0.9953	0.9994	0.9947	0.9971	0.0023
RF	0.9963	0.9999	0.9955	0.9977	0.0006

Çizelge 3. Aynı veri seti üzerinde literatür karşılaştırması.

Referans	Yöntem	Doğruluk	Kesinlik	Duyarlılık	F1-ölçütü	Yanlış Tespit Oranı
Bu çalışma	Basit RNN	0.9776	0.9841	0.9881	0.9861	0.0656
	LSTM	0.9991	0.9995	0.9993	0.9994	0.019
	Bi-LSTM	0.9991	0.9995	0.9994	0.9994	0.0022
	KNN	0.9992	0.9995	0.9994	0.9995	0.0019
	RF	0.9963	0.9999	0.9955	0.9977	0.0006
Çakır ve Angin 2021	FCN	0.935	0.927	0.992	0.958	-
	LSTM	0.942	0.939	0.989	0.963	
	TCN	0.941	0.939	0.988	0.963	
Gao vd. 2021	FNN	-	~0.9911	~0.8763	~0.9253	-
	LSTM		0.95±0.01	0.84±0.02	0.88±0.01	
Iwendi vd. 2020	AdaBoost+RF	0.9908	0.9910	0.9910	0.9910	0.009
	Bagging+RF	0.9940	0.9940	0.9940	0.9990	0.0057
Liu ve Zhang 2020	CNN	0.9802	0.9998	0.9981	0.9989	0.02

ma sonuçları incelendiğinde bu çalışmada, (Çakır ve Angin 2021) ve (Gao vd. 2021) çalışmalarından daha yüksek başarı sağlanmıştır. Yanlış tespit oranı açısından en başarılı model, 0.0006 ile bu çalışmada sunulan RF modeli olmuştur. Iwendi ve diğerleri (2020) tarafından önerilen Bagging+RF yaklaşımı da düşük yanlış tespit oranına (0.0057) sahiptir. Çizelge 3'te verilen aynı veri seti kullanılarak yapılan çalışmalar incelendiğinde, en yüksek duyarlılığa sahip modeller ise bu çalışmada sunulan Bi-LSTM (0.9994) ve RF (0.9955) modelleridir.

Çalışma kapsamında KDD'99 veri setinin farklı versiyonları üzerine yapılan çalışmalar da incelenmiştir. Saldırı tespit için LSTM yaklaşımının benimsendiği NSL-KDD veri seti üzerinde yapılan bir çalışmada (Kasongo 2023) %88.13 doğruluk, KDD'99 veri seti üzerinde yapılan bir diğer çalışmada (Laghrissi vd. 2021) %99.49 doğruluk elde edilmiştir. Bi-LSTM kullanan bir saldırı tespit çalışmasında (Pooja ve Shrinivasacharya 2021) ise KDD'99 veri seti için %99 doğruluk sağlanmıştır. Alenazi ve Mishra tarafından önerilen XGBoost modeli ile KDD'99 veri setinde %99.98 ve NSL-KDD veri setinde %99.97 ise doğruluk sağlanmıştır (Alenazi ve Mishra 2024). En yüksek doğrulukla saldırı tespitinin XGBoost modeli tarafından sunulduğu görülmüştür.

4. Sonuç ve Öneriler

Bu çalışmada önerilen modellerin başarısını incelemek için saldırı tespiti alanındaki çalışmalarla yoğunlukla kullanılmış temel kıyaslama (benchmark) veri setlerinden biri olan %10 KDD'99 veri seti kullanılmıştır. Çalışmamızda modellerin uygulandığı bu veri seti sınırlı sayıda saldırı kategorisi

icermektedir. Önerilen modeller çok basamaklı saldıruları içeren farklı bir veri seti üzerine uygulandığında modellere ilişkin başarımın daha net bir şekilde gözlemleneceği Çakır ve Angin (2021)'nin çalışmasında sonuçlar kısmında verilmiştir. Bu araştırmada incelenen modeller ele alınarak başarıyı kıyaslaması yapıldığında KNN, daha yüksek bir test doğruluğu (%99.92), duyarlılık (%99.94) ve F1-ölçütü (%99.95) sunmuştur.

Önerilen modeller, siber güvenliğin sağlanması noktasında siber saldırıların tespit edilmesinde yardımcı olabilir. Bununla birlikte siber güvenlik, teknolojinin gelişmesiyle birlikte sürekli olarak değişen bir alan olduğundan, siber tehditlere karşı savunma stratejilerini sürekli olarak güncellemek ve iyileştirmek önemlidir.

KDD'99 veri setinin, makine öğrenmesi yöntemleri için sınırlamalarının üstesinden gelmek amacıyla Tavallae ve diğerleri (2009) tarafından NSL-KDD veri seti tanıtılmıştır. Bu nedenle gelecek çalışmada, önerilen yöntemler daha kapsamlı ve farklı veri setleri üzerinde test edilebilir. Gelecek çalışmada, %10 KDD'99 veri seti üzerinde topluluk öğrenme yöntemlerinin başarımı detaylı olarak değerlendirilebilir. Ayrıca bu çalışma, saldırısı tespiti için çoklu sınıflandırma yapılacak şekilde genişletilebilir.

Yazar katkıları

Nesibe Yalçın: Çalışmayı planlamış ve tasarlamış, veri setini düzenlemiş, deneyleri gerçekleştirmiş, sonuçları analiz etmiş ve makaleyi yazmıştır, **Semih Çakır:** Sonuçları analiz etmiş ve makaleyi yazmıştır, **Sibel Ünalı:** Sonuçları değerlendirmiştir ve makaleyi yazmıştır.

5. Kaynaklar

- Alenazi M., Mishra, S.** 2024. Cyberattack detection and classification in IIoT systems using XGBoost and Gaussian Naïve Bayes: A comparative study. *Eng. Technol. Appl. Sci. Res.*, 14, 4, 15074-15082. Doi: 10.48084/etasr.7664
- Bouktif, S., Fiaz, A., Ouni, A., Serhani, MA.** 2020. Multi-sequence LSTM-RNN deep learning and metaheuristics for electric load forecasting. *Energies*, 13, 391. Doi: 10.3390/en13020391
- Cakir, S., Toklu, S., Yalcin, N.** 2020. RPL attack detection and prevention in the Internet of Things networks using a GRU based deep learning. *IEEE Access*, 8, 183678-183689. Doi: 10.1109/ACCESS.2020.3029191
- Çakır, B., Angın, P.** 2021. Zamansal evrişimli ağlarla siber saldırı tespiti: karşılaştırmalı bir analiz. *Avrupa Bilim ve Teknoloji Dergisi*, 22, 204-211. Doi: 10.31590/ejosat.848784)
- Dolgun, MÖ., Özdemir, T., Oğuz, D.** 2009. Veri madenciliğinde yapısal olmayan verinin analizi: metin ve web madenciliği. *İstatistikçiler Dergisi*. (2), s.48-58.
- Gao, J., Gan, L., Buschendorf, F. et al.** 2021. Omni SCADA intrusion detection using deep learning algorithms. *IEEE Internet of Things Journal*, 8(2), 951-961. Doi: 10.1109/JIOT.2020.3009180
- Graves, A., Schmidhuber, J.** 2005. Framewise phoneme classification with bidirectional LSTM and other neural network architectures. *Neural Netw.*, 18(5-6), 602-610. Doi: 10.1109/ijcnn.2005.1556215
- Hochreiter, S., Schmidhuber, J.** 1997. Long Short-Term Memory. *Neural Comput.* 9(8), 1735-1780. Doi: 10.1162/neco.1997.9.8.1735
- Iwendì, C., Khan, S., Anajemba, JH., Mittal, M., Alenezi, M., Alazab, M.** 2020. The use of ensemble models for multiple class and binary class classification for improving intrusion detection systems. *Sensors*, 20, 2559. Doi: 10.3390/s20092559
- İlgün, EG., Samet, R.** 2024. Veri setine uygulanan ön işlemler ile makine öğrenimi yöntemi kullanılarak geliştirilen saldırısı tespit modellerinin performanslarının artırılması. *Gazi Üniversitesi Mühendislik Mimarlık Fakültesi Dergisi*, 39(2), 679-692.
- Kasongo, SM.** 2023. A deep learning technique for intrusion detection system using a Recurrent Neural Networks based framework. *Comput. Commun.*, 199, 113-125. Doi: 10.1016/j.comcom.2022.12.010
- Liu, G., Zhang, J.** 2020. CNID: research of network intrusion detection based on convolutional neural network. *Discrete Dynamics in Nature and Society*, 2020(1), 4705982.
- Laghrissi, F., Douzi, S., Douzi, K., Hssina, B.** 2021. Intrusion detection systems using long short-term memory (LSTM). *J. Big Data*, 8, 65(1-16). Doi: 10.1186/s40537-021-00448-4
- Mikolov, T., Karafiat, M., Burget, L., Černocký, J., Khudanpur, S.** 2010. Recurrent neural network based language model. 11th Annual Conference of the International Speech Communication Association - Interspeech 2010, Japan, 1045-1048. Doi: 10.21437/Interspeech.2010-343
- Özger, F.** 2023. Makine öğrenmesi algoritmalarının hibrit yaklaşımı ile ağ anomalisi tespiti. Yüksek lisans tezi, Sakarya Uygulamalı Bilimleri Üniversitesi, s.18-19.
- Pooja, TS., Shrinivasacharya, P.** 2021. Evaluating neural networks using Bi-Directional LSTM for network IDS (intrusion detection systems) in cyber security. *Global Transitions Proceedings*, 2(2), 448-454. Doi: 10.1016/j.gltcp.2021.08.017
- Schuster, M., Paliwal, KK.** 1997. Bidirectional recurrent neural networks. *IEEE Trans. Signal Process.*, 45(11), 2673-2681. Doi: 10.1109/78.650093
- Şeker, A., Diri, B., Balık, HH.** 2017. Derin öğrenme yöntemleri ve uygulamaları hakkında bir inceleme. *GJES*, 3(3), 47-64.
- Tavallaei, M., Bagheri, E., Lu, W., Ghorbani, AA.** 2009. A detailed analysis of the KDD CUP 99 data set. 2009 IEEE Symposium on Computational Intelligence for Security and Defense Applications, Ottawa, ON, Canada, 1-6. Doi: 10.1109/CISDA.2009.5356528
- Thant, YM., Su Thwin, MM., Htwe, CS.** 2023. IoT network intrusion detection using long short-term memory recurrent neural network. 2023 IEEE Conference on Computer Applications (ICCA), Yangon, Myanmar, 334-339. Doi: 10.1109/ICCA51723.2023.10182005
- UCI KDD Archive.** 1999. KDD Cup 1999 Data. Available on April 2024, <https://kdd.ics.uci.edu/databases/kddcup99/kddcup99.html>
- Ünalı, S., Yalçın, N.** 2022. Hava kirliliğinin makine öğrenmesi tabanlı tahmini: Başakşehir örneği. *Mühendislik Bilimleri ve Araştırmaları Dergisi*, 4(1), 35-44. Doi:10.46387/bjesr.1055946
- World Economic Forum (WEF).** 2024. Global Risks Report 2024. https://www3.weforum.org/docs/WEF_The_Global_Risks_Report_2024.pdf
- Yalçın, N., Çakır, S., Ünalı, S.** 2024. Attack detection using artificial intelligence methods for SCADA security. *IEEE Internet Things J.* Doi: 10.1109/JIOT.2024.3447876



Investigation of a New Blade Design to Improve the Efficiency of an Axial Fan Used in an Underground Mine

Bir Yeraltı Madeninde Kullanılan Eksenel Fanın Verimliliğini Artırmak İçin Yeni Bir Kanat Tasarımının Araştırılması

Güneyhan Taşkaya *, Beytullah Erdoğan*

Zonguldak Bülent Ecevit University, Engineering Faculty, Mechanical Engineering of Department, Zonguldak, Türkiye

Abstract

The blade geometry of a 40 cm diameter axial fan with a front stator cylindrical duct used in the ventilation of an underground mine is redesigned. The Computer Aided Design (CAD) geometry of the existing fan was extracted and all parameters were analysed. Keeping the geometrical characteristics of the real fan constant, a redesign was made according to the system requirements and a new blade profile was selected to provide the required lifting force. In addition to National Advisory Committee for Aeronautics (NACA) 747A315 and NACA 6412 airfoils, Computational Fluid Dynamics (CFD) analysis of NACA 63-412 airfoil was performed and airfoil performance ratios (C_L/C_D) were determined. The rotor geometry designed using the NACA 63-412 airfoil and the existing fan geometry were combined in CAD environment. The CFD results of the new fan were compared with those of the existing fan. The CFD results of the new fan were compared with the existing case. Accordingly, in the existing fan, at 3700, 4000, 4700 rpm and a constant flow rate of 2 kg/s, 25%, 37.5% and 43.5% performance increases were obtained with mass flow rates of 2.5, 2.75, 2.87 kg/s respectively in the new fan design.

Keywords: Airfoil, axial fan, CFD, fan blades, rotor, ventilation.

Öz

Bir yeraltı madeninin havalandırılmasında kullanılan 40 cm çapındaki ön statorlu silindirik kanallı eksenel fanın kanat geometrisi yeniden tasarlanmıştır. Mevcut fanın Bilgisayar Destekli Tasarım (CAD) geometrisi çıkarılmış ve tüm parametreler analiz edilmiştir. Gerçek fanın geometrik özellikleri sabit tutularak sistem gereksinimlerine göre yeniden bir tasarım yapılmış ve gerekli kaldırma kuvvetini sağlayacak yeni bir kanat profili seçilmiştir. Ulusal Havacılık Danışma Komitesi (NACA) 747A315 ve 6412 kanat profillerine ek olarak NACA 63-412 kanat profilinin Hesaplama Akışkanlar Dinamigi (HAD) analizi yapılmış ve kanat performans oranları (C_L/C_D) belirlenmiştir. NACA 63-412 kanat profili kullanılarak tasarlanan rotor geometrisi ile mevcut fan geometrisi CAD ortamında birleştirilmiştir. Yeni fanın CFD sonuçları mevcut fanın sonuçları ile karşılaştırılmış ve yeni fanda farklı dönüş hızlarında kütlesel debide %45'e varan bir artış sağlanmıştır. Buna göre mevcut fanda 3700, 4000, 4700 devir/dakika ve 2 kg/s sabit debide yeni fan tasarımında 2.5, 2.75, 2.87 kg/s kütle debileri ile sırasıyla %25, %37.5 ve %43.5 performans artışları elde edilmiştir.

Anahtar Kelimeler: Airfoil, eksenel fan, HAD, fan kanatları, rotor, havalandırma.

1. Introduction

Underground mining is undoubtedly very important in terms of the economic and strategic position of states and their competition with each other. Sustainable underground

mining is only possible by providing favorable conditions for safe access and extraction. Safe access to the mine is largely dependent on ventilation. The evacuation of toxic gases that threaten the health and safety of workers in mines, spontaneously or during mining activities, and keeping the accumulated explosive and flammable gases at the desired amounts are provided by the ventilation system. In addition, a ventilation system is needed to disperse mine dust, to ensure the correct operation of machinery and equipment, and to control temperature and humidity to increase worker comfort. In order to fulfil all these conditions,

*Corresponding author: beytullah.erdogan@beun.edu.tr

Güneyhan Taşkaya orcid.org/0000-0003-3267-6091

Beytullah Erdoğan orcid.org/0000-0002-6120-9196



This work is licensed by "Creative Commons Attribution-NonCommercial 4.0 International (CC BY NC)".

the ventilation system is expected to operate 24 hours a day. This results in a very high consumption of electrical energy. The rapid development of needs and technology has made it necessary to use limited energy resources more carefully and effectively. Less energy consumption increases environmental sustainability by reducing the carbon footprint, as well as reducing costs, enabling technological progress and enabling countries and organizations to compete with each other. Therefore, energy efficiency is a fundamental energy policy element for all countries. For this reason, considering that one third of the electricity demand of a typical mining operation is caused by the ventilation system, it is aimed to minimize the losses in the system, device and process and to obtain the same system output with less energy consumption (Panigrahi and Mishra 2014).

The necessity of high efficiency of the components used in ventilation increases the importance of studies to improve the performance of axial fans, one of the most important components of the system. Axial fans have a wide range of applications such as aircraft engines, heat exchangers, cooling of computers, heating-cooling-air conditioning installations of industrial processes, tunnel and mine ventilation and their physical properties (blade profile, number of blades, hub geometry, etc.) vary according to the needs of the application in which they are used. In underground mine ventilation, where the need for fresh air is at the forefront, directing blades that protect the fan from mine dust and at the same time distribute the air evenly can be preferred at the fan inlet, as well as at the fan outlet or at both inlet and outlet of the fan. The air coming axially to the fan gains kinetic energy during its movement on the rotor blades. The directing blades of the fan ensure that the air flow is directed uniformly towards the rotor. The efficiency of the fan depends on how much kinetic energy is generated, how low the rotor losses can be kept and how much of this kinetic energy is converted into static pressure. Therefore, the calculation of blade angles, determination of the number of blades and selection of blade profiles are very important in fan efficiency (Çakır 2018). Until recently, the effects of certain parameters such as radial distribution of Euler work, blade load, blade profile, blade tip clearance, number of blades, ratio of hub radius to tip radius of the fan on axial fan performance have been demonstrated and accordingly, axial fan efficiencies have increased. With the increase in computer speed and capacities after 1980s, Computational Fluid Dynamics (CFD) has been widely used in studies to improve the performance of axial fans. The cheap and fast CFD method has enabled the determination of the effects

of new parameters on axial fan performance, which are difficult and costly to investigate by experimental methods (İlikan 2014).

Keklikoğlu (2019), developed an application code for fan design using some empirical equations in order to examine the effects of all parameters of axial fan design. The results obtained by performing experiments in the test setup prepared according to Air Movement and Control Association (AMCA) standards with the new prototype produced by making a sample design were compared with the results obtained with ANSYS-CFX software. According to the experimental and numerical results of the study, a new design code was developed for the designers as the pressure difference and volumetric flow rate values were quite close (Keklikoğlu 2019). Jung and Joo (2019) examined the effect of fan inlet core length on the efficiency of the fan in their study with the axial fan of an outdoor unit air conditioner. They determined that the vortex occurring at the edge of the fan hub inlet affects the attack edge of the blade and causes yield loss. If the input core length is shorter than a certain value, the loss increases, but the rounded corner shape improves the situation. The results showed that the efficiency increases at certain inlet hub length due to the interaction between the hub vortex and the blade (Jung and Joo 2019). İlikan (2014), investigated the effects of airfoil arrangement patterns on fan performance and three-dimensional flow structure. When the results of the CFD solutions made with the frozen rotor approach are compared with the experimental results, no significant changes are observed in the performance values, but differences are observed in the design flow rates. It is observed that shifting the fan blades backwards reduces the total pressure and efficiency of the fan at low flow rates, while it has no effect at design flow rates and high flow rates. The main novelty of this study is the demonstration that the unstable region in the performance curve of axial fans is completely eliminated by the application of positive translation to the fan blades, and thus the stable operating region is significantly expanded (İlikan 2014). Çakır (2018), carried out two-stage CFD studies with stator axial fan. In the first stage of the study, the effects of rotor-stator interaction surface models on fan performance were compared. At a single rotational speed, the static pressure and flow rate values were closer to each other in the stationary impeller and mixing surface models, but remained lower than the experimental results. It was observed that the time transformation method was closer to the experimental results. In the second stage of the study, two different models were created by applying 300 shifts to

the rotor airfoils forward and backward in the chord direction. In a study using a mixing surface model, it was concluded that forward shifting relatively increases fan efficiency compared to rearward shifting (Çakır 2018). Park et al. (2019), investigated the effect of reducing tip leakage flows on the efficiency of an axial flow fan used in an air conditioning outdoor unit. They aimed to prevent tip leakage flows and related vortices by coating the casing of the axial fan. With a CFD study at 154.000 Reynolds number, they concluded that reducing tip leakage flows increases efficiency by reducing total pressure loss (Park et al. 2019). Galpin et al. (2017) compared the total pressure and efficiency results obtained from time-independent and time-dependent CFD analyses with experimental results using a single-stage transonic compressor with 20 rotor and 43 stator blades. Mixing surface model was used for time independent solution and time transform model was used for time dependent solution. In order to understand the uncertainties of the flow in advance and to establish a solution system, they first analyzed the flow on the rotor. They found that the mixing surface model gives results almost as consistent as the time transformation and that the gain is not so good compared to the mixing surface when the cost of the time transformation method is considered (Galpin et al 2017). Tonello et al. (2017), performed time-independent CFD analyses on the Franscis-99 turbine using open-source software. When they compared the results obtained from the study in which they applied the $k-\omega$ (omega) Shear Stress Transport (SST) turbulence model (partial load, high load and best efficiency point) with the experimental results, they found that the mixing surface model has no advantage over the standing wheel method in predicting the flow inside the emitter and the general characteristics of the turbine. When the rotor-stator interactions where the losses are intense are examined, it is argued that the mixing surface will be more effective, this is due to the lack of rotor-stator interaction in the emitter (Tonello et al. 2017). Castegnaro (2017) worked on the design of low-speed axial fans in which three important parameters (blade profile, stiffness ratio and insertion angle) provide the required pressure difference with the highest efficiency. He stated that there are methodological differences between traditional blade design methods of axial fans and that these differences are caused by these three parameters. Three different rotors with a diameter of 315 mm were used in the study. In one of the models, British airfoil C4 and American airfoil NACA 65 series fans were compared by considering the angle of insertion. The second study was carried out according to the

stiffness distribution and the third according to the Reynolds numbers. According to the results of the study, it was stated that C4 airfoil showed higher performance than NACA 65 airfoils and C4 airfoil is the most ideal airfoil in axial fan applications (Castegnaro 2017). When designing the airfoils of turbomachinery and aircraft, it is of great importance to increase efficiency in the application. Blade efficiency is highly dependent on the on-wing flows. A high wing performance ratio, characterized by a high lift coefficient and low drag coefficient ratio, contributes to increased efficiency. Çoban (2019), conducted a CFD study with new geometries obtained by changing the geometric properties of the NACA 0018 airfoil in order to increase the performance ratio (C_L/C_D) in wings, and compared the wing performances with experimental results. Of the 3 geometries used, the first is a 165 mm long standard NACA 0018, the second is a new profile derived from NACA 0018 with a gap cut into the upper surface, and the third is another NACA 0018 wing variation with 66% of the trailing edge cut off at the vet length. Reynolds number between 20.000 - 100.000 and angle of attack between 0°-15° values. As a result, the streamlines and pressure contours of the airfoils were visually compared at the same Reynolds number at different angles of attack and at different Reynolds numbers, at the same angle of attack. The lift coefficient (C_L), resistance coefficient (C_D) and the ratio of lift coefficient to resistance coefficient (C_L/C_D) between airfoils and between different airfoils are given in the study. According to the results of the study, opening steps and gaps on the airfoil affected the flow, but this effect was not favorable in the lift coefficient compared to the standard airfoil geometry. In addition, the hollow model performed better than the stepped model, and it was found that the drag coefficient performance decreased while the lift coefficient performance increased in all models as the Reynolds numbers increased (Çoban 2019). Dilmaç (2019), conducted a series of analyses to prove that the performance of wind turbines can be improved by thickening the trailing edge of the airfoil geometry symmetrically and asymmetrically and at certain rates. As a result of the aerodynamic analyses, the aerodynamic performance of the NACA 4415 airfoil at 10° angle of attack was increased by 5% by thickening the airfoil by 2% just below the vet exit edge. After determining the optimum thickness, 2D analyses were performed at $Re=124.000$ at angles of attack between 00-180, and as a result, the C_L coefficient of the new variation was better, while the C_D coefficient was close in both profiles. By applying 3D CFD analysis to 2 geometries with a rotor diameter of 1,44 m, which he produced and

tested in the wind tunnel, he obtained 4,42 Nm torque with NACA 4415 and 5,12 Nm torque with the second thickened variation (Dilmaç 2019) Korkmaz (2018), suggested that changing the airfoil shape increases the efficiency by delaying flow separation at different speeds and angles of attack. According to the results of CFD analyses of NACA 4412 and NACA 63-215 profiles with 2 new profiles obtained by changing the x/c ratio (the ratio of the distance of the maximum blade thickness point from the edge of attack to the length of the vet), it was seen that the new airfoils increased the maximum performance ratio. Thus, by delaying the flow separation between 2-4 degrees, it was able to postpone the stall due to the sudden decrease in the lift coefficient (Korkmaz 2018). Bacak (2016), obtained characteristic and performance curves from CFD analyses of an axial fan and determined the optimum operating range of the fan. He compared these results with the results obtained from Wing Fan's test bench built according to AMCA 210 standard. The maximum allowable angle of attack was verified by analyzing the velocity profile around the airfoil of an axial fan (Bacak 2016). Fan et al. (2020), investigated the effects of rotation, displacement and translation methods applied to the fan blades on the aerodynamic and structural performance of the fan. The variation of the wing geometry was performed with a Free Form Deformation (FFD) approach. According to the results obtained from CFD analyses, rotation and scrolling methods are relatively more efficient on the aerodynamic performance of the fan. At different operating conditions, the effect of rotation on the efficiency did not always tend to increase. The excessive rotational effect at low flow rates caused the total pressure differential of the fan to drop sharply. According to the optimization results, rotation caused maximum stress on the wing, while the backward displacement reduced the stress on the wing surface. Up to 15% improvement in the total pressure difference was achieved with the blades formed by rotation and sliding methods (Fan et al. 2020). Bakhtar et al. (2024) has examined various add-on designs to reduce noise generated by axial fans. Their research focuses on understanding how different attachments to axial fans affect aerodynamic noise. Eight distinct design cases have been evaluated, including the extension of outlet and inlet ducts, the use of Chevron nozzles, the placement of spherical balls inside the fan in staggered and straight patterns, the application of a wavy inner wall treatment, and combinations of some of these designs. To analyze the effects of these designs on noise, CFD and acoustic analyses were conducted using Ansys

Fluent 2022 R1 software. The results obtained indicate that all design modifications reduced noise levels and suggest that these designs could contribute to the development of quieter fans suitable for various environments (Bakhtar et al. 2024).

Fernando and Mudunkotuwa (2021), designed a biologically-derived modification with the aim of achieving a major reduction in fuel costs and environmental impacts by reducing frictional resistance. The experimental results of the NACA 0012 airfoil were used as a reference. They investigated four different types of modifications which are lighter than the original wing. By comparing the numerical results with experimental results, they found two bio-inspired wing shapes that are more efficient than the original wing and can be incorporated into the future aerospace industry (Fernando and Mudunkotuwa 2021). Drwiega et al. (2019) discussed current research and development projects carried out within the European project to improve the effectiveness of auxiliary ventilation in underground mines. These projects are generally studies to improve the parameters affecting the fan efficiency by modifying the rotor blades. The rotor blades and modifications used in the study were obtained by printing from 3D printing. Both aerodynamic and structural performance results were obtained by CFD and Finite Element Method (FEM) analyses on the existing and modified wings. By comparing the fan characteristic graphs before and after the modification, it was observed that the pressure difference, power and efficiency were increased in the modified fan (Drwiega et al. 2019). Fakhari and Mrad (2024), conducted an optimization study of an axial flow fan used in underground mine ventilation using the parameters of angle of attack, tip clearance, speed, hub to tip ratio and number of blades. By comparing the experimental results with the results obtained from CFD analysis, they stated that by reducing the number of blades and tip span, a performance increase of 9% was achieved and confirmed the experimental results with an error rate of less than 5% (Fakhari and Mrad 2024). NACA airfoils in order to propose an airfoil for use in underground mine ventilation fans Panigrahi and Mishra (2014), conducted CFD analyses with 6 different in 2014. By determining the lift and drag ratios of the wings at different angles of attack, the maximum aerodynamic performance ratios were compared. At 150 angles of attack, they found that the profile with the highest performance ratio was NACA 747A315. (Panigrahi and Mishra 2014). Kong et al. (2023) optimized the blade geometry of low-pressure axial flow

fans to enhance their aerodynamic performance. Traditional design theories often fall short in addressing the complexity of 3D internal flows, leading to suboptimal blade profiles and spanwise distribution. To address this, he developed a surrogate-assisted multi-objective optimization process, supported by CFD methods, to determine the optimal blade shape under two typical operating conditions. Sixteen parameters were selected, and response functions were constructed using kriging models, followed by a multi-objective genetic algorithm to identify the best solutions. The results indicate that efficiency can be improved by %1,26 under low mass flow conditions and by %5,47 under high mass flow conditions. The optimization also led to a better distribution of low-pressure zones along the blade leading edge and a reduction in tip leakage vortex intensity. This study presents a successful approach for optimizing fan blade geometry (Kong et al. 2023).

Hassen (2021), focused on developing new blade types for underground mine ventilation fans, arguing that higher efficiency can be achieved with a more uniform flow distribution. For this purpose, firstly, performance comparison studies were carried out with CFD using NACA747A315 and NACA 6412 profiles. Since it achieved higher efficiency, the NACA 6412 profile continued its studies. With the analyses performed at 30°-40° angles of attack with 4 different designs, namely fixed vane, tapered vane, skewed vane and tapered skewed vane, the flow velocity, homogeneity and efficiency of the designs were investigated. He stated that high homogeneity and efficiency do not necessarily mean high system efficiency and these two parameters should be evaluated together with system efficiency (Hassen 2021). Krasyuk and Kosykh (2023) address the aerodynamic design of axial fans by utilizing an impeller and an inlet guide vane to reverse the direction of airflow. This process involves stopping the rotation of the impeller while allowing the guide vane to rotate, aiming to enhance fan efficiency in reverse mode. The authors have developed a novel blade angle analysis method to identify airflow parameters under reversal conditions. Furthermore, they delineate the parametric regions in which the proposed reversal approach is effective. A design of a fan exhibiting similar performance curves in both forward and reverse airflow is undertaken. The swirl ratios of the flow within the guide vane are correlated with the axial velocity ratios, based on the geometrical similarity of the blade profiles of the impeller and guide vane at an average radius (Krasyuk and Kosykh 2023).

In the aforementioned literature studies to improve the performance of axial fans, some researchers have focused on the optimization of all parameters required for fan design (Keklikoğlu 2019, Bacak 2016, Fakhari and Mrad 2024) while others have focused on the airfoils, arguing that the fan efficiency is largely dependent on the flows over the blade. Axial fan performance has been improved by many studies such as the application of shifting and translation methods on airfoils (Çakır 2018, İlikan 2014, Fan et al. 2020), changing the geometric properties on the existing airfoil (Çoban 2019, Dilmaç 2019, Korkmaz 2018), Drwiega et al. 2019) comparing the performance of different airfoils (Panigrahi and Mishra 2014, Hassen 2021). However, very few of them are related to axial fans used in underground mine ventilation (Panigrahi and Mishra 2014, Fakhari and Mrad 2024, Hassen 2021) and more studies are needed in this field.

The innovative aspect of this study compared to other studies is that it contributes to energy efficiency by improving the performance of a fan used in a real mining operation, and at the same time, an alternative blade profile is presented to increase the efficiency of axial fans used in underground mine ventilation. CAD geometry of the existing fan was extracted, all parameters were analyzed and CFD analysis was performed. When the ventilation systems used in underground mining were investigated to be used in the blade design of the existing fan, NACA 747A315, NACA 6412 blades were used (Panigrahi and Mishra 2014, Hassen 2021) and blade performance comparison studies of NACA 63-412 blades were carried out as an alternative to these blades. The mass flow rates of the polluted air drawn from the mine at different speeds and at the same pressure difference values of the new fan created with the alternative blade with the highest blade performance ratio were compared. In this study, the blade geometry of the pre-stator cylindrical ducted axial fan used in the ventilation of an underground mining operation in Zonguldak Mining Basin was redesigned due to low efficiency.

2. Material and Methods

Axial fans used in underground mine ventilation have stator blades to distribute the air evenly and these blades can be preferred in front of the rotor to protect the fan from the adverse conditions of the mine environment (Çengel and Cimbala 2018). The air coming to the fan in axial direction is directed towards the rotor blades by the stator blades and its pressure is increased by being compressed by the rotor

blades. Thus, the air is displaced in the desired direction. The axial fan whose specifications are given in Table 1 is used in the ventilation of a real mine operation.

Table 1. Technical and geometrical characteristics of the existing fan with Ø400 mm used in the mine.

Parameter	Property
Weight and Power	60 kg and 9 HP
Air Pipe Diameter	400 mm
Operating Pressure	4-6 bar
Air Output Speed	15 m/s
Volumetric Flow	143 m ³ /min
Air Consumption at Normal Pressure	175 m ³ /min
Number of Revolution	3700 - 4700 rpm
Pressing Height	20 mmwc (milimeter water column)
Hub Diameter	200 mm
Number of Rotor Blades	6 pieces
Number of Stator Blades	6 pieces

In order to increase the efficiency of the fan, firstly, all design parameters of the fan were reviewed by applying the classical axial fan design method. Considering the design conditions specified in the fan catalogue, lift coefficients and drag coefficients were determined according to the stiffness values calculated for the hub end and middle layers of the blade (Keklikoglu 2019). The rotor blades of the fan rotate with the flywheel around it and there is no blade end gap (Figure 1). Certain parameters such as fan diameter, hub-tip ratio, number of blades, blade angle, vet length were found to be suitable for the design and it was decided to redesign the blade geometry by selecting a new blade profile.

2.1. Analytical Approach

The methods and techniques applied should be given in an understandable way. It should be supported by previous references. Statistical models and methods of analysis should be clearly stated.

Air enters the airfoil at the attack edge and leaves the wing at the trailing edge (Figure 2). The hump part of the airfoil is referred to as the low-pressure zone or suction edge, and

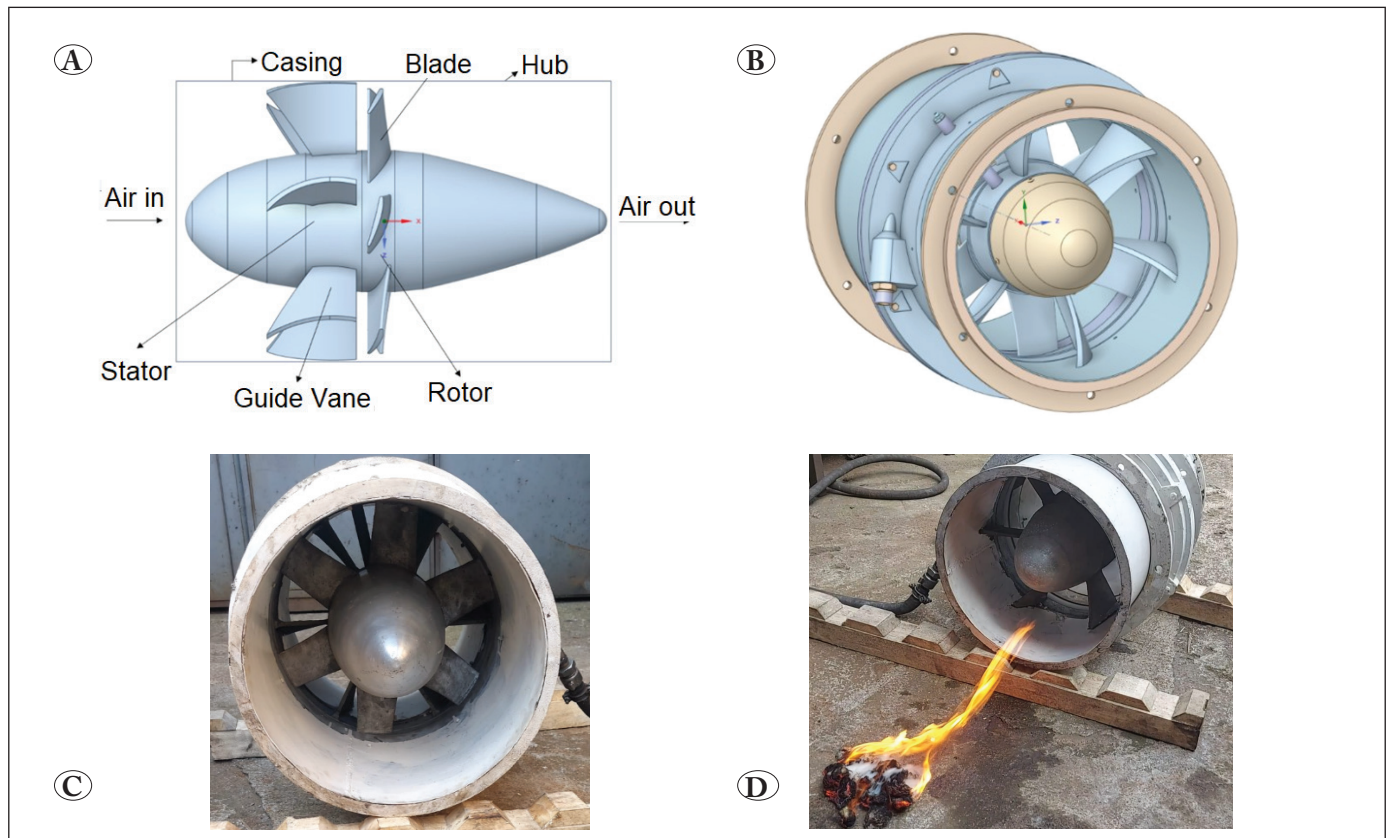


Figure 1. Side view (A) and isometric view (B) of the fan created by software, real fan image (C) and the flow direction (D) of the fan used in the underground mine.

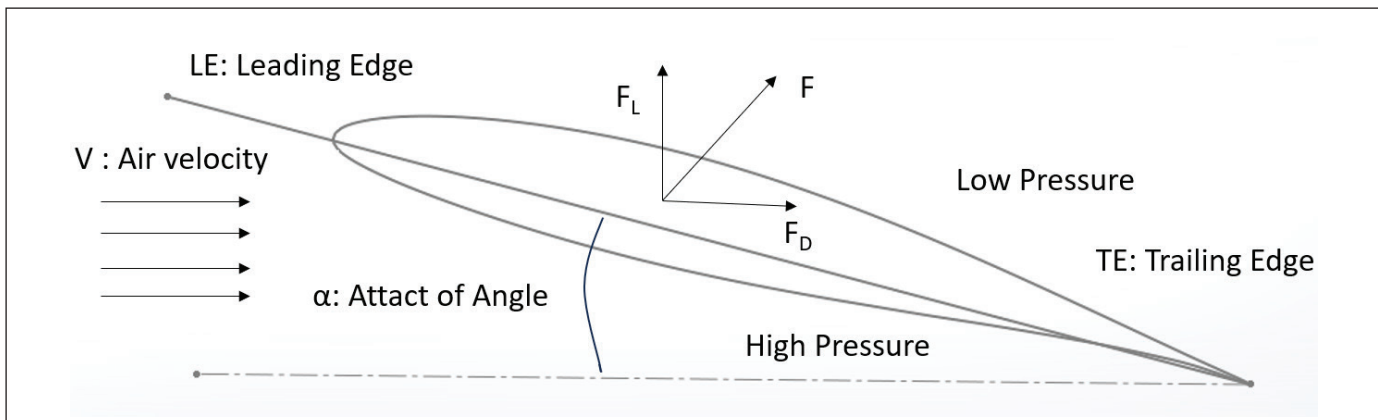


Figure 2. Forces acting on the airfoil (Yılmaz et al. 2018).

the hollow part is referred to as the high pressure zone or compression edge. The angle between the direction of arrival of the air to the wing and the wing is called the angle of attack. The lift coefficient increases until the optimum value of the angle of attack. When the angle of attack reaches a certain value, the lift coefficient becomes maximum and starts to decrease rapidly after this value. The fan switches to unstable operation. This condition can also be expressed as stopping the fan. In order to prevent unstable operation in fans, it is necessary to determine at which value of the angle of attack the lift coefficient reaches its maximum value and the angle of attack should be kept below this value (İlukan 2014, Köse 2018).

The high lift airfoil blades provide an increase in static pressure, while the low drag force (F_D) helps to achieve lower power consumption, thus increasing fan efficiency. Therefore, in the selection of the airfoil, it is not sufficient only to have high lift coefficients of the wings. Drag coefficients should also be low. The ratio of the lift coefficient of an airfoil to the drag coefficient (C_L/C_D) is called the airfoil performance ratio and when comparing airfoils, the airfoil with the maximum performance ratio represents the highest efficiency. C_L and C_D are given by equation (1) and (2) (İlukan 2014, Keklikoğlu 2019).

$$C_L = \frac{F_L}{0,5\rho V^2 A} \quad (1)$$

$$C_D = \frac{F_D}{0,5\rho V^2 A} \quad (2)$$

F_L : Buoyancy force (N)

ρ : Density (kg/m^3)

V: Velocity (m/s)

A: Wing projection area (m^2)

F_D : Drag force (N)

When designing axial fans, a preliminary design process is initiated and the design approach is determined by using the desired results as initial parameters (flow rate (Q , m^3/s), total pressure difference (ΔP , Pa) and speed (n, rpm)) (İlukan 2014). For this, the solidity value of the blade is needed. The solidity value (is given by equation (3)).

$$\sigma = \frac{c}{s} \quad (3)$$

c: Chord distance (m)

s: Pitch distance (m)

Here "c" is the vet length (m) and refers to the distance between the LE (air's leading edge of the wing) end and the TE (the trailing edge of the wing where the air leaves) end of the wing. The distance "s", which is the distance between the two wings, is called the pitch distance (m).

Solidity value (σ) is an important parameter that determines the design approach in axial fans. When the solidty value is below 0,7, the isolated blade approach is used, when it is above 1 (one), the stepped blade approach is used, and for values in between, the mixed approach, which is a combination of both isolated and stepped approaches, is preferred (Castegnaro 2017). In the isolated blade approach, the interaction of the pressure fields of the blades with each other is ignored. In the stepped approach, the actual lift coefficient starts to change as the solidity value increases and this cannot be ignored because it reduces the fan efficiency (Keklikoğlu 2019).

Axial are designed by the classical method (İlukan 2014, Keklikoğlu 2019, Fakhari and Mrad 2024). The number

of graphs and equations used in the method is quite large. The axial fan geometry varies according to the needs of the system in which the fan will be used. In this part of the study, the methodology of the parts specific to the front stator axial fan is mainly included. Inlet and outlet vector analyses and inlet and outlet velocity triangles of front stator axial fans are given in Figure 3. The inlet and outlet angles of the stator are expressed as α_1 and α_2 .

$$V_a = \frac{Q}{A} \quad (4)$$

Q : Flow rate (m^3/s).

A : Cross-sectional area perpendicular to the flow direction (m^2).

Where is the vertical cross-sectional area through which the flow passes, " V_a " is the axial velocity (m/s).

In the Figure 3, "U" is the tangential velocity (m/s), "w" is the angular velocity (rad/s) and "r" is the radius of the fan (m). The relative speed "W" (m/s) is equal to the difference between the absolute speed and the tangential speed. " V_{2u} " is the tangential component of the absolute speed at the rotor inlet and is an important parameter that determines the inlet blade angle (β_1) given by equation (6) (Köse 2018).

$$U = w.r = \frac{\pi.D.n}{60} \quad (5)$$

U : Tangential velocity (m/s)

w : Angular velocity (rad/s)

r : Radius (m)

D : Diameter (m)

n : Revolutions per minute (rpm)

$$\tan \beta_1 = \frac{U + V_{2u}}{V_a} \quad (6)$$

V_{2u} : The tangential component of the absolute speed at the rotor inlet (m/s)

V_a : Axial velocity (m/s)

If the output blade angle β_2 (0) at the output edge of the rotor is β_2 (0), it is expressed as in equation (7).

$$\tan \beta_2 = \frac{U}{V_a} \quad (7)$$

U : Tangential velocity (m/s)

V_a : Axial velocity (m/s)

The relative flow velocities (W_1 and W_2) at the inlet and outlet of the rotor are given in equations (8) and (9).

$$W_1 = \frac{V_a}{\cos \beta_1} \quad (8)$$

$$W_2 = \frac{V_a}{\cos \beta_2} \quad (9)$$

V_a : Axial velocity (m/s)

The average blade angles and average relative flow velocities at the inlet and outlet of the rotor are given by equations (10) and (11).

$$\tan \beta_m = \frac{\tan \beta_1 + \tan \beta_2}{2} \quad (10)$$

β_1 : Wing entry angle

β_2 : Wing exit angle

$$W_m = \frac{V_a}{\cos \beta_m} \quad (11)$$

β_m : Average wing angle

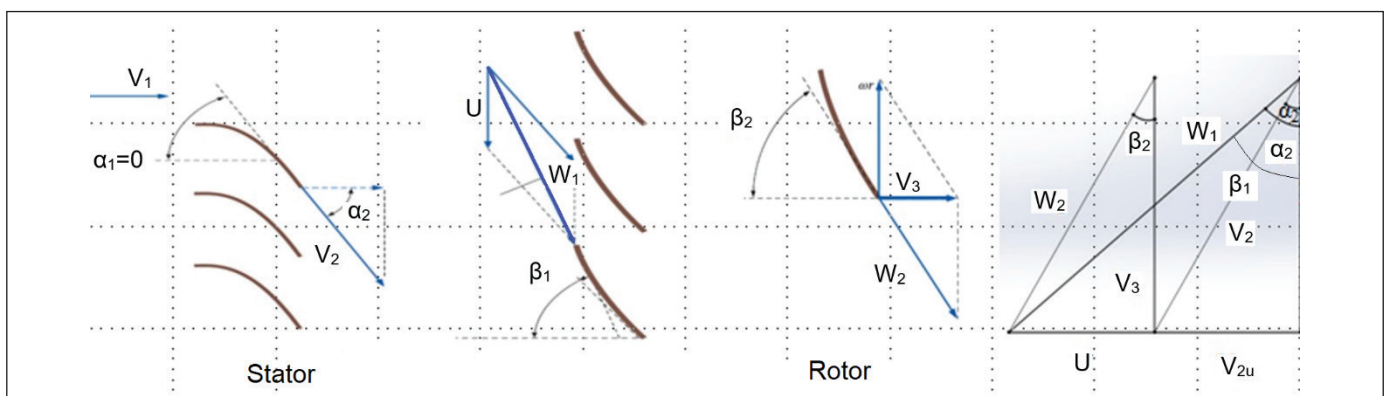


Figure 3. Vector analysis and speed triangles of axial fans with front stator (Çengel and Cimbala 2018).

W_m : Average relative flow velocity (m/s)

V_a : Axial velocity (m/s)

The useful power is the product of the flow rate of the fan and the total pressure difference as given by equation (12) and its unit is Watt. The delivered power is equal to the product of torque and angular velocity as expressed by equation (13).

$$W_{hydraulic\ power} = Q \cdot \Delta P_t \quad (12)$$

ΔP_t : Total pressure difference (Pa)

$$W_{shaft\ power} = w \cdot \tau \quad (13)$$

τ : Torque (Nm)

w: Angular velocity (rad/s)

In axial fans, the tangential velocities at inlet and outlet are equal and the shaft power can be calculated directly from equation (14). Here “ \dot{m} ” is the mass flow rate (kg/s).

$$W_{shaft\ power} = \dot{m} \cdot U \cdot V_{2u} \quad (14)$$

\dot{m} : Mass flow rate (kg/s)

U: Tangential velocity (m/s)

V_{2u} : The tangential component of the absolute speed at the rotor inlet (m/s)

The efficiency of axial fans (η) is defined as the ratio of the useful load to the delivered power as given by equation (15) (Çengel and Cimbala 2018).

$$\eta = \frac{Q \cdot \Delta P_t}{\dot{m} \cdot U \cdot V_{2u}} \quad (15)$$

Q: Flow rate (m³/s)

ΔP_t : Total pressure difference (Pa)

\dot{m} : Mass flow rate (kg/s)

U: Tangential velocity (m/s)

V_{2u} : The tangential component of the absolute speed at the rotor inlet (m/s)

2.2. Numerical Approach

In recent years, numerical methods have been used more and more compared to experimental methods because they are more economical and save time. With the computational fluid dynamics method, it is possible to quickly simulate complex geometries and systems.

Here the solution of two equations characterizing the flow is needed. One of them is the continuity equation expressing

the conservation of mass (16) and the other is the Navier-Stokes equation derived from Newton's law of motion (17).

$$\frac{\partial \rho}{\partial t} + \frac{\partial}{\partial x_i} (\rho u_i) = 0 \quad (16)$$

$$\frac{\partial}{\partial t} (\rho u_i) + \frac{\partial}{\partial x_i} (\rho u_j u_i) = - \frac{\partial p}{\partial x_i} + \frac{\partial}{\partial x_j} \left(\mu_{eff} \left(\frac{\partial u_i}{\partial x_j} + \frac{\partial u_j}{\partial x_i} \right) \right) + S_{u_i} \quad (17)$$

P: Pressure (Pa)

μ : Dynamic viscosity (Pa.s)

t: Time (s)

u: Velocity vector (m/s)

i: The velocity component of the physical quantity in the x direction in the Cartesian coordinate system (m/)

j: The velocity component of the physical quantity in the x direction in the Cartesian coordinate system (m/s)

r: Density (kg/m³)

p: Pressure (Pa)

x: Position vector (m)

S: Discretisation term

In Equation 16, t is the time, u is the velocity vector and x is the position vector. The lower index i represents the velocity component of the physical quantity in the Cartesian coordinate system. In Equation 17, P represents pressure and μ represents dynamic viscosity. A source term is added to the momentum equation, denoted by the mass forces (e.g. gravitational force), S.

In this study was carried out with ANSYS Fluent 2022 R1 software, which uses the finite volume method as a discretization method. With this software, which allows to determine the fluid dynamic forces and pressure distribution acting on the airfoil, firstly a validation study was carried out and then 3D CFD analyses of NACA 747A315, NACA 6412 and NACA 63-412 airfoils were performed and airfoil performance ratios were determined. The blade with the highest blade performance ratio was compared with the flow rate and pressure difference results determined by the analyses of the existing fan geometry.

2.2.1. Validation Study

For the validation study, a study was selected from the literature in which the performance ratio comparison was performed by 3D CFD analysis of airfoils (Fernando and

Mudunkotuwa 2021). In this study, a validation study comparing the experimental results of NACA 0012 with the results of CFD analysis is taken as a reference. The analysis geometry was obtained by taking the NACA 0012 airfoil profile coordinates from the Airfoil Tools official website and using the Design Modular CAD programme in the ANSYS Fluent interface (Yılmaz et al. 2018). As boundary condition, velocity inlet is modelled as velocity inlet 30 m/s, total pressure at the outlet is "0" Pa and wing surface is modelled as wall boundary condition Figure 4(a). The mesh structure of the analysis geometry was created using ANSYS Meshing. For the precise solution of the boundary layer on the wing surface, the thickness of the first cell was

chosen to be $y+ < 1$ and the $k-\omega$ SST turbulence model was used as the turbulence model (Luo et al. 2017). The number of elements used was kept around 1 million by adhering to the study. The network structure is given in Figure 4(b).

The graph of the C_D values obtained by CFD analysis and the C_D values obtained by experimental results are given in Figure 5.

Table 2 shows the C_L and C_D values obtained experimentally and numerically at different angle of attack values. As a result of the verification study, it is seen that similar results are obtained with the reference study (Figure 6). The reference study (Fernando and Mudunkotuwa 2021) for validation

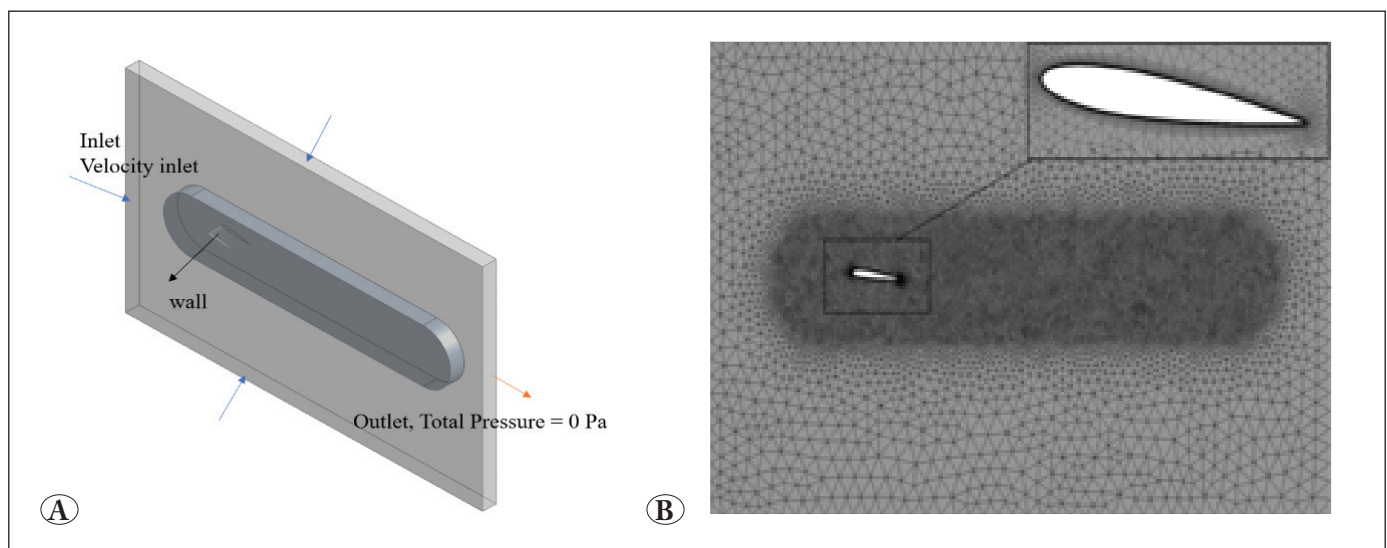


Figure 4. Mathematical representation of boundary condition (A), Network structure of the verification analysis geometry at 7° attack angle (B).

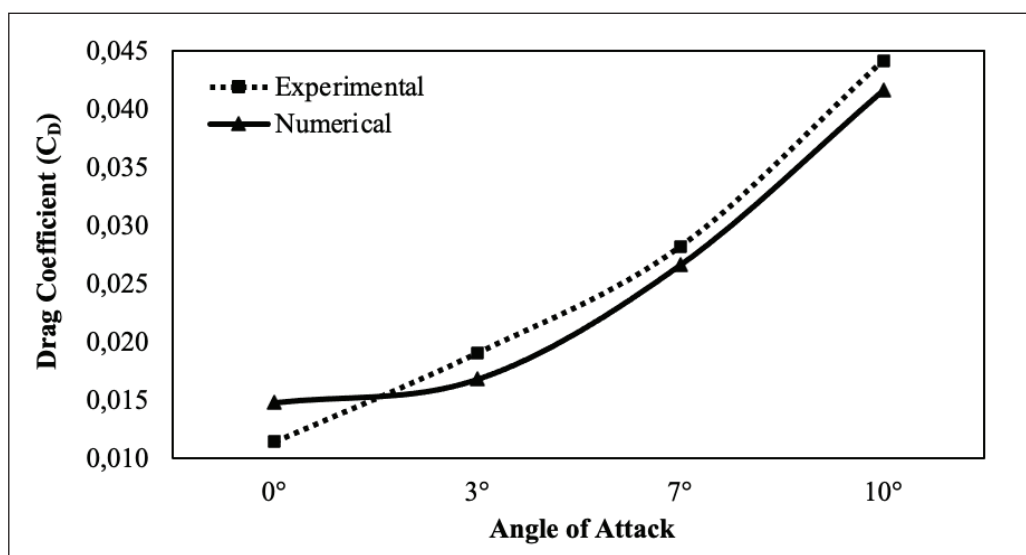
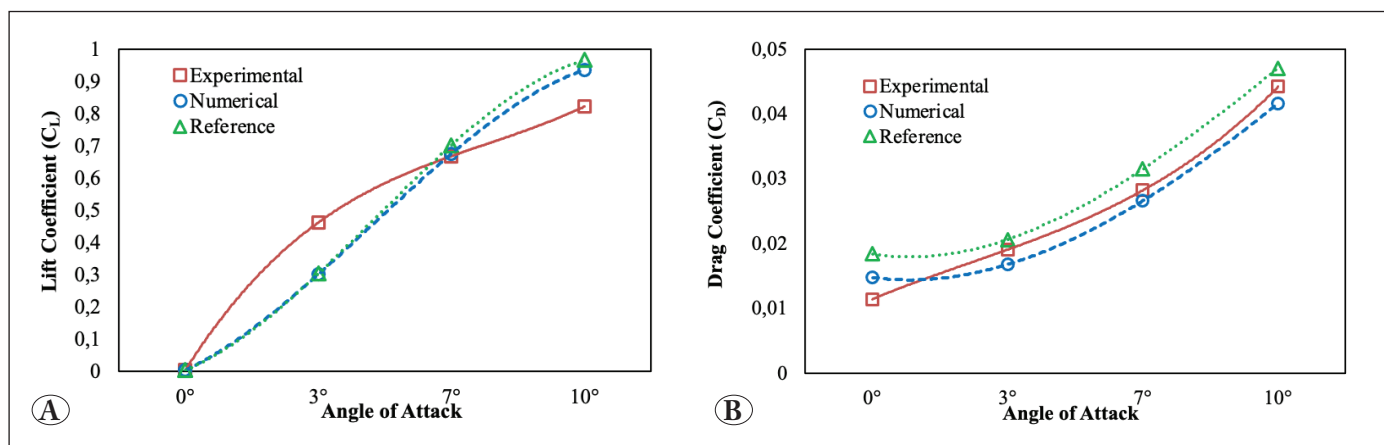


Figure 5. CFD analysis result comparison graph of the validation study with experimental results.

Table 2. Validation results of the NACA 0012 3D.

Angle of Attack	Experimental Results		Numerical Results		Error (%)			
	Lift Coeff. (C_L)	Drag Coeff. (C_D)	Lift Coeff. (C_L)	Drag Coeff. (C_D)	Lift Coeff. (C_L)	Drag Coeff. (C_D)	Lift Coeff. ($C_{L_{ref}}$)	Drag Coeff. ($C_{D_{ref}}$)
0°	-0.0039	0.0114	-0.0031	0.0147	20.63	29.23	15.43	61.18
3°	0.4619	0.0190	0.3011	0.0167	34.82	12.03	34.38	8.15
7°	0.6677	0.0282	0.6751	0.0265	1.12	5.73	5.10	11.60
10°	0.8220	0.0441	0.9350	0.0415	13.75	5.86	17.46	6.43

**Figure 6.** CFD analysis result comparison graph of experimental, numerical and reference studies **A)** Lift coefficient (C_L) comparison. **B)** Drag coefficient (C_D) comparison.

converges to the experimental values with a large error rate. In our study, convergence was obtained with similar error rates. However, the authors of reference study reached acceptable error rates (5%-10%) with 7° angle of attack and they continued their study with 7° angle of attack. It can be clearly seen that our error rate at 7° is lower than the reference study.

2.2.1. CFD Analysis

In this study, in order to propose a new blade profile as an alternative to the two blade profiles proposed in the literature for underground mine fans to be used in the blade design of the axial fan currently used in the underground mine, 3D CFD analyses of the profiles were performed and C_L/C_D values were compared. After transferring the coordinates of the airfoils to the Desing Modular, a 3D airfoil geometry was obtained by creating a surface and giving depth. In the validation study, the flow volume was obtained by giving depth to the flow area formed around the airfoil in accordance with the flow volume geometry used as a reference. In over-wing flows, the flow characteristics change abruptly on and around the wing surface. In order to

accurately observe the effects of flow separation, especially at the trailing edge, a more precise solution should be provided in these areas. For this purpose, a body of influence (boi) geometry is added around the wing geometry up to a certain distance. Thus, the flow volume is prepared in a structure that is denser around the airfoil and becomes sparser as it moves away from the airfoil.

The mesh structure was obtained using Fluent Meshing, which allows to obtain much higher quality mesh structures with the same or less number of elements. In order to better analyze the flow variations on the wing surface and near the surface, a boi geometry was created around the wing (Figure 7). In order to solve the boundary layer around the airfoil correctly, the height of the first cell was determined as 6×10^{-6} m to fulfil the condition $y^+ < 1$ and 15 prismatic layers were built on the boundary layer. For each profile, the optimum number of meshes was determined by performing an independence study from the mesh structure as coarse, medium and fine at a fixed attack angle (Figure 8). The DELL Precision 7670 mobile workstation with 12th generation i9 processor and 32 GB RAM was used in the analysis.

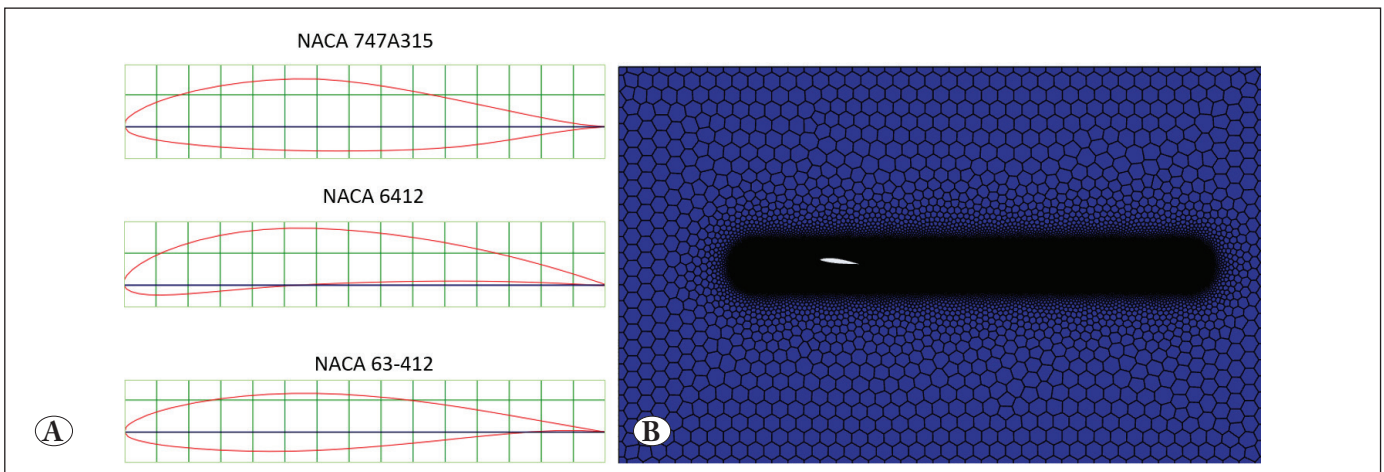


Figure 7. The airfoil shapes (A) and the mesh structure (B) of the analysis geometry for which the performance ratios are compared.

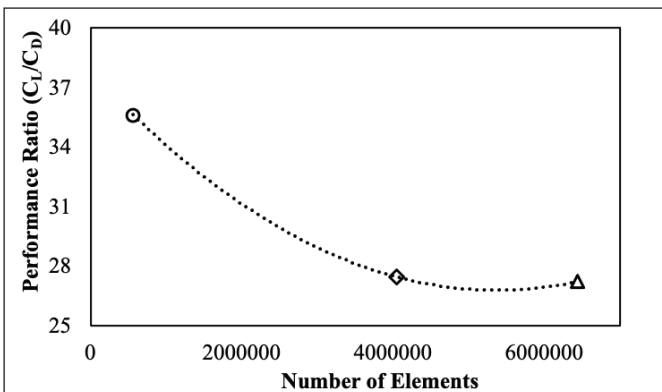


Figure 8. Optimum mesh count graph for NACA 63-412 airfoil.

The analysis is performed in a time-independent manner, as is commonly done in literature studies (Çakır 2018, İllikan 2014, Keklikoğlu 2019, Galpin et al. 2017, Tonello et al 2017). A k- ω SST turbulence model is chosen to provide a precise solution of the flow separation. Air of constant density ($\rho=1,225 \text{ kg/m}^3$, $\mu=1,8853 \times 10^{-5} \text{ Pa.s}$) was used as the fluid. The fluid velocity is 30 m/s and the analysis is performed parametrically at different angles of attack ($1^\circ, 3^\circ, 5^\circ, 7^\circ, 9^\circ, 11^\circ$). As boundary conditions, velocity inlet boundary condition, total pressure outlet boundary condition and wall boundary condition were applied. After selecting the blade profile with the highest performance, the new blade geometry (Figure 9), which was designed by taking into account the geometric features of the existing fan, was assembled to the existing fan in CAD environment and CFD analyses were performed.

The fan flow volume geometry is composed of 4 parts: inlet, stator, rotor and outlet. The rotor volume is modelled as

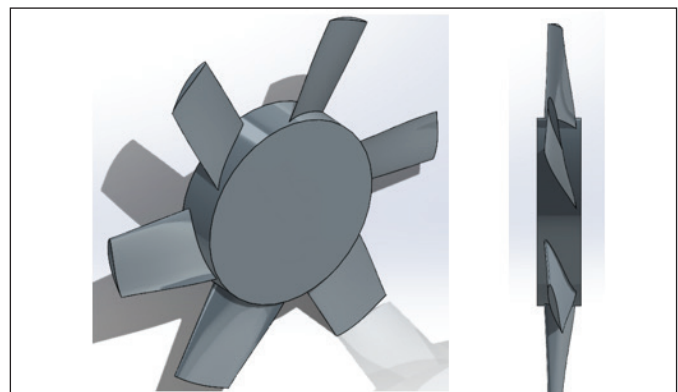


Figure 9. New wing design created with NACA 63-412, isometric view (left) and side view (right).

rotating and the other volumes are modelled as stationary volumes. In axial fan analysis, Multiple Reference Frame (MRF) method is used to model rotating and stationary volumes (İllikan 2014, Keklikoğlu 2019). The modelling of the rotor and stator interface in the fan considered as a reference is done by the frozen rotor method since this study is a comparison study (Çakır 2018). The analysis conditions are provided in Table 3.

The mesh structure was created in the Fluent Meshing interface. For both fans, solutions were made independent of the network by solving in different network structures as coarse, medium, fine. In the network structure, poly hexcore elements are preferred, which allow the creation of high quality network geometry. Smooth boundary layer definition was used on the wall surfaces (Figure 10). The minimum orthogonal quality value of the network structure using approximately 8 million elements is 0,3, the maximum

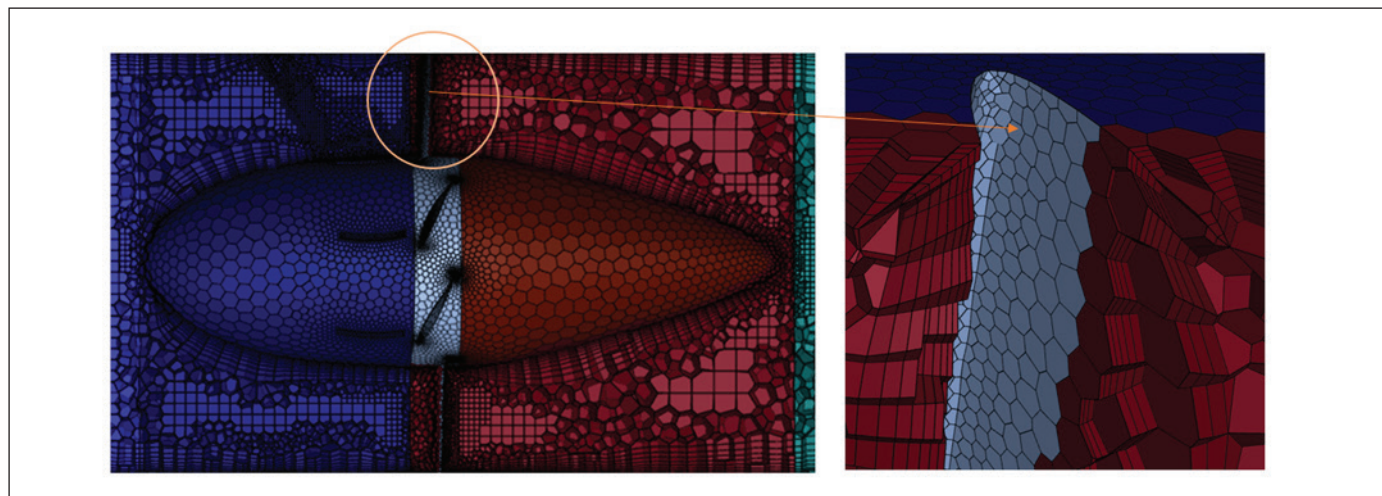


Figure 10. Fluent meshing of the new fan and a close-up view of the boundary layer around the blade.

Table 3. Analysis conditions.

General	Pressure Based, Steady
Model	k- ω SST, Production Limiter
Material	20 °C air, $\rho=1,204 \text{ kg/m}^3$, $\mu=1,825 \times 10^{-5} \text{ kg/m.s}$
Cell Zone Condition	MRF, Frozen Rotor, Rotating-Domain, 4000 rpm
Boundary Condition	Inlet: Mass Flow 2 kg/s, Outlet: 0 Pa
Method	Coupled, Second Order

aspect ratio value is 56 and the maximum skewness value is 0.7.

When Figure 10 is analyzed, it is seen that the maximum performance ratios of NACA 6412 and NACA 63-412 airfoils are reached at 3° attack angle. The NACA 747A315 airfoil reaches maximum performance at 5° angle of attack, but its performance at this angle of attack is lower than the other two airfoils.

3. Results and Discussion

This section is presented in two stages. The Stage 1 includes the results of the performance ratio comparison studies between the airfoils for the blade design of the existing fan. Stage 2 includes the results of the comparison of the CFD analyses of the new fan geometry and the existing fan geometry obtained by mounting the new blade designed with the blade profile with the highest performance among the blade profiles we tested to the existing fan in CAD environment.

3.1. Wing Profile Performance Ratio Comparison Study

After determining the lift coefficient required by the system (Table 4), it is crucial to correctly select the airfoil that will provide this lift coefficient. All 3 airfoils provide the lift coefficient required by the system. However, which one will perform better in the system is determined by the blade performance ratio.

With 3 different wing geometries NACA 747A315, NACA 6412 and NACA 63-412, C_L and C_D values were calculated at 6 different angles of attack ($\alpha=1-11^\circ$) and C_L/C_D ratios are given in Table 5. As a result of the CFD analyses performed with these airfoils, it was found that the airfoil performance ratio of NACA 6412 was higher than the NACA 747A315 airfoil, and the NACA 63-412 airfoil had the highest performance ratio.

The performance ratios of the airfoils are given in Figure 11. In the first stages of this study, the performance analysis of the existing fan airfoil and the NACA 747A315 airfoil was compared by CFD and found to be very close to each other. In the second stage of the study, airfoils with higher performance ratios were investigated, and there was no need to compare with the existing airfoil due to the information obtained from the first stage.

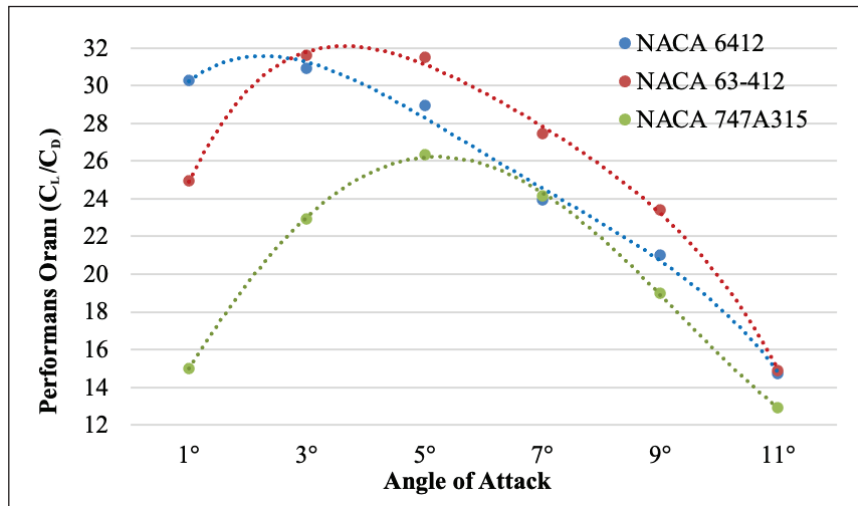
The distribution of the velocity vectors of the airfoils at an angle of attack of 7°, the velocity profiles around the airfoils (left) and the velocity contours (right) are shown in Figure 12. A uniformly distributed velocity profile is observed on the surface of the blades. Looking at the trailing edge of the profiles, NACA 63-412 is the profile where the flow separation starts the latest. Looking at the C_L graphs of the

Table 4. The stiffness value of the system and the theoretical lift coefficient calculated according to the velocity triangles.

Airfoil	Solidity (σ)	Absolute Speed (V_{2u}) (m/s)	Entry Wing Angle (β_1)	Exit Wing Angle (β_2)	Avg. Wing Angle (β_m)	Entry Rel. Flow Vel. (W_1) (m/s)	Exit Rel. Flow Vel. (W_1) (m/s)	Avg. Rel. Flow Vel. (W_1) (m/s)	Lift Coeff. (C_L)
Hub	0.84	26.25	78.03	71.36	75.36	72.06	46.93	59.21	0.99
Mid	0.49	17.50	79.90	77.33	78.72	85.20	68.38	76.40	0.82
Tip	0.34	13.13	81.64	80.43	81.03	102.66	90.20	95.80	0.60

Table 5. Performance ratio results of airfoils.

Attack Angle	NACA 6412	NACA 747A315	NACA 63-412
	Performance Ratio (C_L/C_D)	Performance Ratio (C_L/C_D)	Performance Ratio (C_L/C_D)
1°	30.30	15.00	24.95
3°	30.93	22.94	31.61
5°	28.93	26.36	31.51
7°	23.92	24.15	27.45
9°	21.03	18.99	23.42
11°	14.75	12.98	14.86

**Figure 11.** Performance ratio comparisons of airfoils.

airfoils at different angles of attack (Figure 13), it is seen that the C_L values reach their maximum value at 11°. In this study, the maximum angle of attack required in the system does not exceed 10°. Although the C_L value of the NACA 63-412 airfoil is lower than NACA 6412, its performance is higher because of its lower C_D value.

3.2. Comparison of Existing Fan and New Fan

Considering the catalogue values (Table 1), the axial fan currently used in a real underground mining operation is

expected to provide a flow rate of 2.87 kg/s between 3700-4700 rpm. According to CFD analyses (Table 6), the existing fan reaches a flow rate of 2.87 kg/s at a speed of 4700 rpm between these speeds. When the CFD analysis results of the new fan created with the fan blade designed using the NACA 63-412 airfoil, which shows the highest performance (Table 6), it is seen that it can provide a flow rate of 2.87 kg/s with a speed of 3700 rpm. Figure 14 and Figure 15 show that the desired flow rate and pressure differential can be achieved at lower speeds with the new

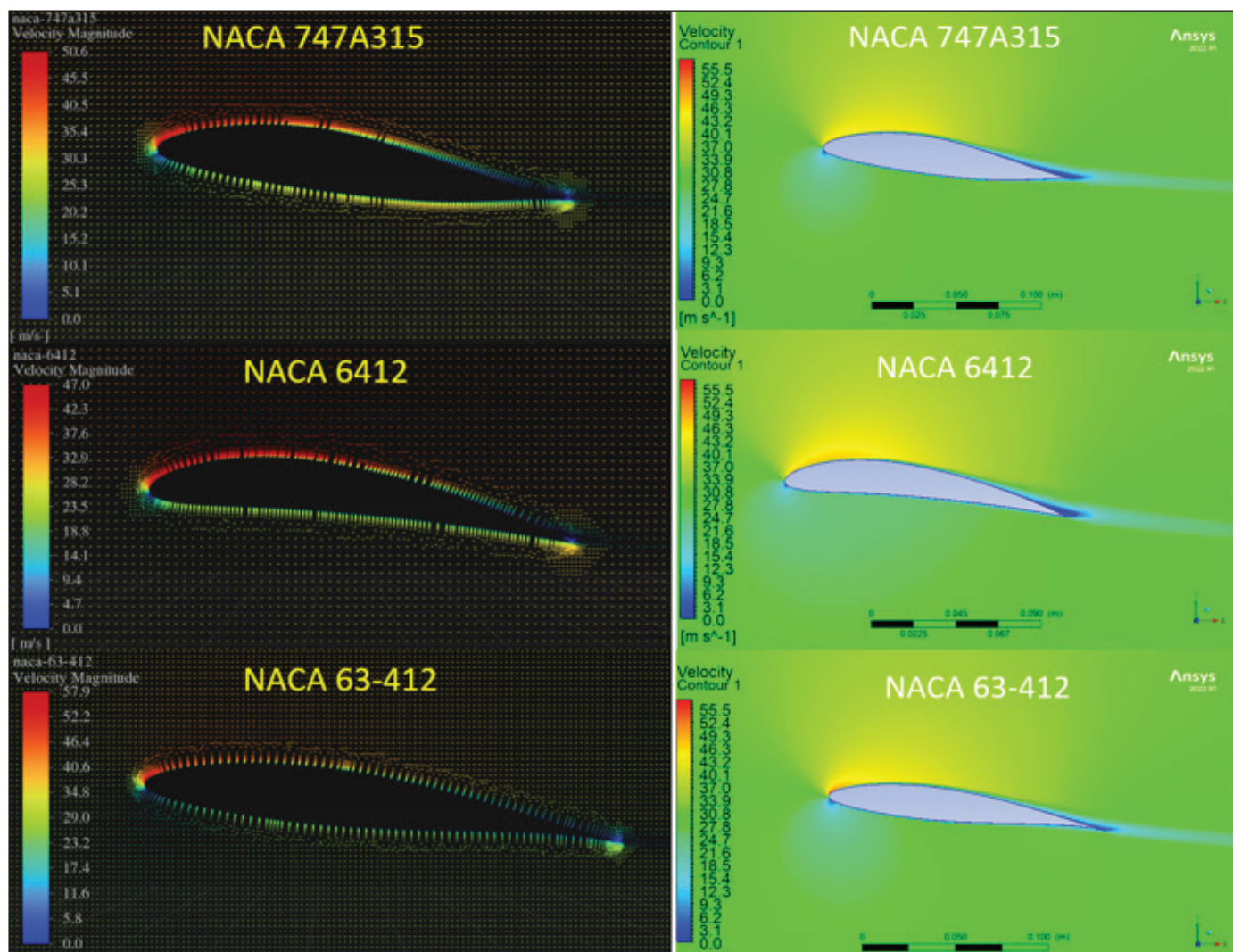


Figure 12. Velocity vectors and velocity contours of the wing blades.

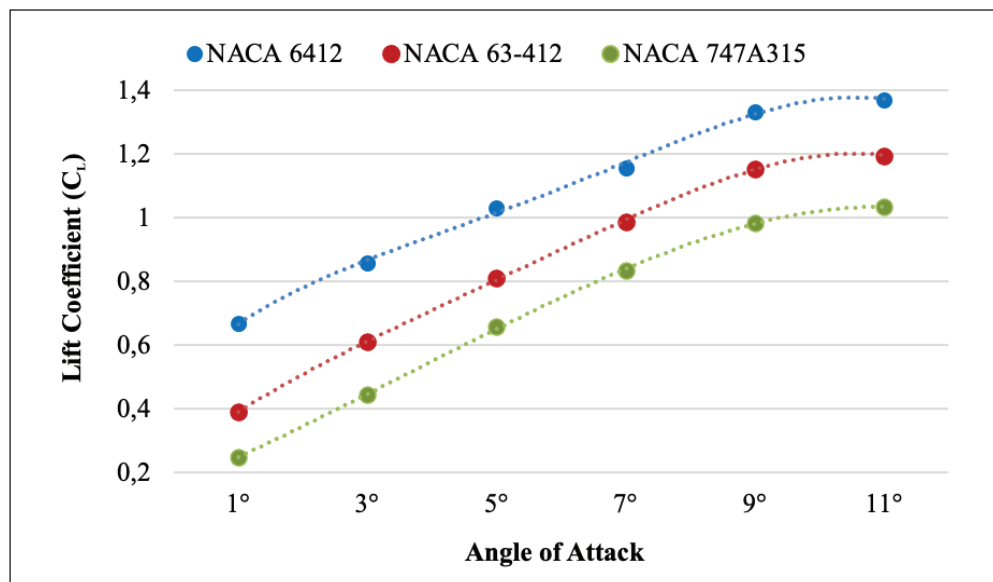


Figure 13. Comparison of values of airfoils at different angles of attack.

Table 6. CFD analysis results of the existing and new fan in the range of 3700-4700 rpm.

Number of revolutions (n) (rev/min)	Current Fan		New Fan	
	Mass Flow (\dot{m}) (kg/s)	Total Pressure Difference (ΔP) (Pa)	Mass Flow (\dot{m}) (kg/s)	Total Pressure Difference (ΔP) (Pa)
3700	1	347	1	503
3700	1.5	328	2.3	333
3700	2*	176	2.5*	221
4000	2*	275	2	685
4000	2.2	189	2.5	383
4000	2.4	81	2.75*	233
4700	2*	511	2.5	834
4700	2.5	312	2.75	649
4700	2.75	163	2.87*	580

*The results obtained in the new design at constant mass flow rate and different rotational speeds of the existing fan shows the mass flow rate values.

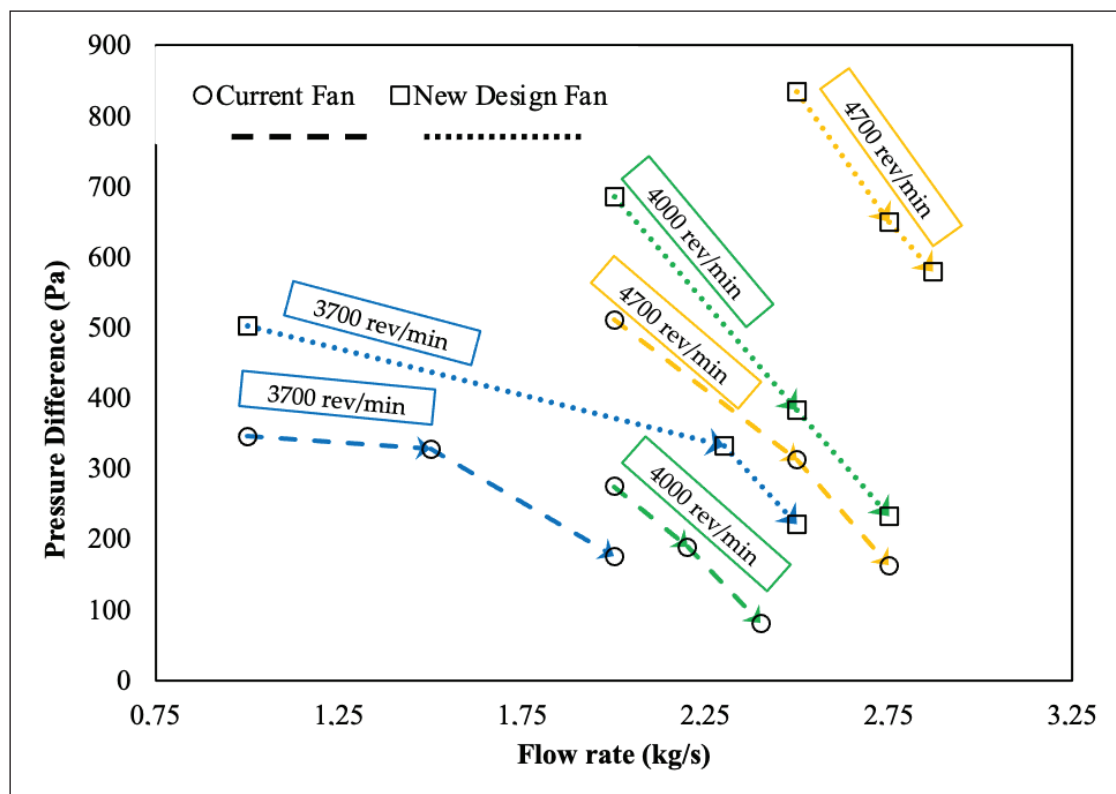


Figure 14. Flow-pressure graph of the existing fan and the new fan at 3700-4700 rpm.

fan, which can pump a flow rate of 2.87 kg/s at 4700 rpm with a pressure difference of 580 Pa, and its performance superiority over the existing fan.

At 4000 rpm-2 kg/s operating conditions, the flow rate of the new fan increased between 25%-435% compared to the existing fan (Table 7).

4. Conclusion and Suggestions

In this study, in order to increase the efficiency of the fan used in the ventilation of a real underground mining operation, a new blade profile that can be an alternative to the blades recommended to be used in underground mine fan blades in the literature is proposed. A new rotor blade was designed

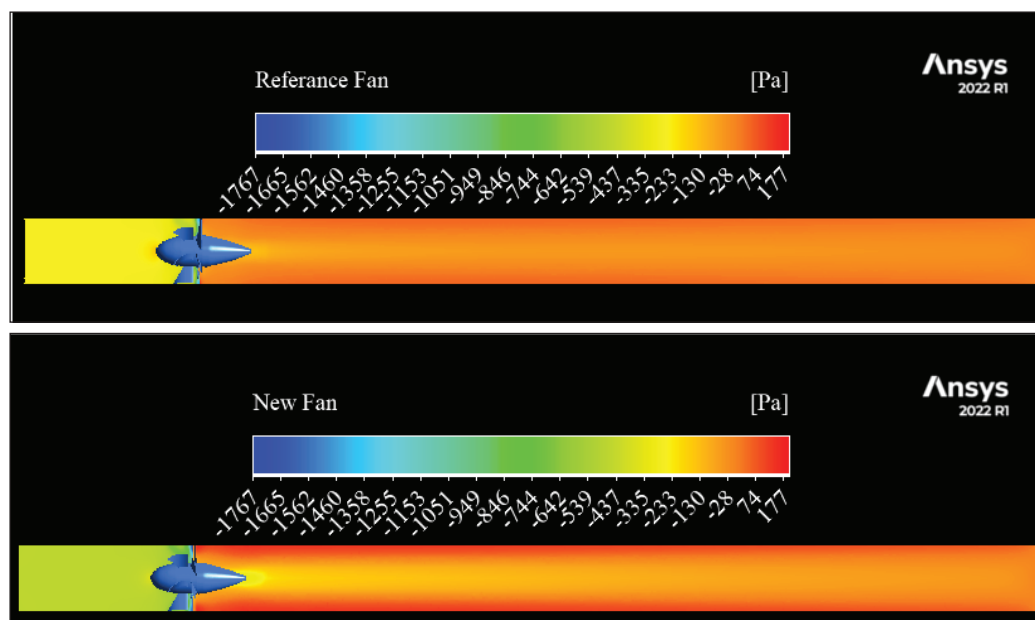


Figure 15. Comparison of the pressure contours of the existing fan and the new fan at 4000 rpm and 2 kg/s flow rate.

Table 7. Improvement in the constant flow rate value in the range of 3700–4700 rpm for the existing fan.

Number of revolutions (n) (rev/min)	Current Fan		New Fan		Increase (%)
	Mass Flow (\dot{m}) (kg/s)	Total Pressure Difference (ΔP) (Pa)	Mass Flow (\dot{m}) (kg/s)	Total Pressure Difference (ΔP) (Pa)	
3700	2	176	2.5	221	25.00%
4000	2	275	2.75	233	37.50%
4700	2	511	2.87	489	43.50%

with the profile with the highest performance and the results of CFD analyses of the reference fan and the new fan were compared with each other. According to the results of CFD analyses performed with NACA 747A315, NACA 6412 and NACA 63-412, NACA 63-412 has the highest wing performance ratio. NACA 6412 performed better than NACA 747A315, confirming the work of Hassen (2021).

In order to see the change in flow rate and pressure difference of NACA 63-412 in the existing fan, CFD analyses of the new fan, which was designed by adhering to the geo-metrical characteristics of the fan, showed that the new fan reached higher flow rates at the same pressure difference at 3700–4700 rpm. Under 4000 rpm-2 kg/s operating conditions, the flow rate of the new fan increased between 25% and 43.5% compared to the existing fan.

In this study, the improved fan was designed to provide the flow rate (2.87 kg/s) specified in the technical catalogue of

the product at the desired pressure difference (330 Pa) and at the lowest possible speed (3700 rpm), but it was observed that the new fan was slightly below these requirements. It is thought that the reason for this is related to the stator geometry and blade angles and that studies on this fan should continue with the stator part of the fan.

Author contribution: Conceptualization, Güneyhan Taşkaya (G.T.) and Beytullah Erdoğan (B.E.); methodology, G.T. and B.E.; software, G.T.; validation, G.T.; formal analysis, G.T.; investigation, G.T. and B.E.; resources, G.T. and B.E.; data curation, G.T. and B.E.; writing-original draft preparation, G.T., B.E. and G.T.; writing-review and editing, G.T., B.E.; visualization, G.T.; supervision, B.E. All authors have read and agreed to the published version of the manuscript.

Nomenclature	
F_L	Buoyancy Force (N)
F_D	Drag Force (N)
C_L	Lift Coefficient
C_D	Drag Coefficient
C_L/C_D	Performance Ratio
ρ	Density (kg/m^3)
V_a	Axial Velocity (m/s)
Q	Volumetric Flow Rate (m^3/s)
ΔP_t	Total Pressure Difference (Pa)
μ	Dynamic Viscosity (Pa.s)
c	Chord Length (m)
s	Pitch Distance (m)
β_1	Wing Entry Angle
β_m	Avarege Wing Angle
β_2	Wing Exit Angle
W_1	Entery Relative Flow Velocity (m/s)
W_m	Average Relative Flow Velocity (m/s)
W_2	Exit Relative Flow Velocity (m/s)
U	Tangential Velocity (m/s)
V_{2u}	Absolute Velocity (m/s)
η	Hydraulic Efficiency
\dot{m}	Mass Flow Rate (kg/s)
τ	Tork (Nm)
$W_{\text{shaft,power}}$	Shaft Power (kW)
σ	Solidity
t	Time (s)
u	Velocity Vector (m/s)
i	The velocity (x) Component (m/s)
j	The velocity (y) Component (m/s)
x	Position Vector (m)
S	Discretisation Term
n	Number Of Revolutions (rev/min)
w	Angular Velocity (m/s)

5. References

- Bacak, A.** 2016. Experimental and numerical analysis of axial fan performance analysed by methods. MSc Thesis, Department of Mechanical Engineering, Gebze Technical University, 57 s.
- Bakhtar, H., Alsahafi, N., Almehmadi, M. et al.** 2024. Flow-induced noise and vibration in axial fan: a case study. Journal of Umm Al-Qura University for Engineering and Architecture.1, 1-18, Doi:10.1007/s43995-024-00079-9
- Castegnaro, SA.** 2017. Critical Analysis of the Differences Among Design Methods for Low-Speed Axial Fans. Proceedings of the ASME Turbo Expo., 26-30, USA. Doi: 10.1115/GT2017-64276
- Çakır, ET.** 2018. Effects of rotor-stator interaction surface modelling and shifting of airfoils on the performance of axial fans. MSc Thesis, Department of Mechanical Engineering, Istanbul Technical University, 97 s.
- Çengel, YA., Cimbala, JM.** 2018. Fluid Mechanics, Fundamental and Applications, Turbomachinery (4th ed). McGraw-Hill, New York, 825-827 pp.
- Çoban, M.** 2019. Flow separation on an airfoil on a wing control by opening gap. MSc Thesis, Department of Mechanical Engineering, Sivas Cumhuriyet University, 126 s.
- Dilmaç, E.** 2019. Naca 4415 wind turbine blade the effect of the edge of the fingertip on the profile analysis. MSc Thesis, Department of Mechanical Engineering, Konya Technical University, 99 s.
- Drwiega, A., Szelka, M., Turewicz, A.** 2019. Improvement of auxiliary ventilation efficiency in underground workings. IOP Con-fERENCE Series: Earth and Environmental Science, 261(1). Doi:10.1088/1755-1315/261/1/012007.
- Fakhari, SM., Mrad, H.** 2024. Optimization of an axial-flow mine ventilation fan based on effects of design parameters. Results in Eng. 21, 101662. Doi:10.1016/j.rineng.2023.101662.
- Fan, C., Adjei, AR., Wu, Y., Wang, A.** 2020. Parametric study on the aerodynamic performance of a ducted-fan rotor using free-form method. Aerospace Science and Technology. 101, 105842. Doi:10.1016/j.ast.2020.105842.
- Fernando, VN., Mudunkotuwa, DY.** 2021. Bio-Inspired Aircraft Wing Modification Analysis in ANSYS Fluent. 10th International Conference on Information and Automation for Sustainability, Negombo, Sri Lanka, 11-13. Doi:10.1109/ICIAfS52090.2021.9605821
- Galpin, P., Hansen, T., Scheuerer, G., Kelly, R., Hickman, A., Jemcov, A., Morris, SC.** 2017. Validation of transonic axial compressor stage unsteady state rotor-stator simulations. Proceedings of the ASME Turbo Expo, 26-30, USA,
- Hassen, AE.** 2021. Flow characterization in mine ventilation fan blade design using CFD. Journal of Sustainable Mining. 20, 144–156. Doi:10.46873/2300-3960.1063.
- İlikan, NA.** 2014. Blade profile arrangement of axial fans effects on performance. PhD Thesis, Department of Mechanical Engineering, Istanbul Technical University, 212 s.
- Jung, JH., Joo, WG.** 2019. The effect of the entrance hub geometry on the efficiency in an axial flow fan. Intern. Journal of Refrigeration. 101, 90-97. Doi:10.1016/j.ijrefrig.2019.02.026.
- Keklikoğlu, ÖH.** 2019. Design, construction and performance evaluation of axial flow fans. MSc Thesis, Department of Mechanical Engineering, Middle East Technical University, 127 s.
- Kong, C., Wang, M., Jin, T. et al.** 2023. The blade shape optimization of a low-pressure axial fan using the surrogate-based multi-objective optimization method. Journal of Mechanical Science and Technology. 37, 179–189. Doi:10.1007/s12206-022-1219-y.

- Korkmaz, Ü.** 2018. Adjustable wing design to delay stall. MSc Thesis, Aircraft and Aerospacing Engineering, Gaziantep University, 51 s.
- Köse, Ö.** 2018. Axial gas turbines wing parameters analysis. MSc Thesis, Mechanical Engineering Department, Iskenderun Technical University, 76 s.
- Krasyuk, AM., Kosykh, PV.** 2023. Aerodynamic Design of Axial Fan with Guide Vane for Reverse Air Flow. Journal of Mining Science. 59, 424-432. Doi:10.1134/S1062739123030092.
- Luo, D., Huang, D., Sun, X., Chen, X., Zheng, ZA.** 2017. Computational Study on the Performance Improvement of Low-Speed Axial Flow Fans with Microplates. Journal Applied Fluid Mechanics. 10, 1735-3645. Doi:10.29252/JAFM.73.245.27492.
- Panigrahi, DC., Mishra, DP.** 2014. CFD Simulations for the Selection of an Appropriate Blade Profile for Improving Energy Efficiency in Axial Flow Mine Ventilation Fans. Journal of Sustainable Mining. 13, 15-21. Doi:10.7424/jsm140104.
- Park, K., Choi, H., Choi, S., Sa, Y.** 2019. Effect of a casing fence on the tip-leakage flow of an axial flow fan. International Journal of Heat and Fluid Flow. 77, 157-170. Doi:10.1016/j.ijheatfluidflow.2019.04.005.
- Tonello, N., Eudel, Y., Meux, L., Ferrand, M.** 2017. Frozen Rotor and Sliding Mesh Models Applied to the 3D Simulation of the Francis 99 Tokke Turbine with Code Saturne. Journal of Physics Conference Series. 782, 012009. Doi:10.1088/1742-6596/782/1/01200.
- Yılmaz, M., Köten, H., Çetinkaya, E., Coşar, ZA.** 2018. A Comparative CFD analysis of NACA0012 and NACA4412 airfoils. Journal of Energy Systems. 2, 145–159. Doi:10.30521/jes.454193.



Kestel Bölgesinde (Kadınhanı-Konya) Yetişen Bazı Makromantarların Antimikrobiyal Aktivitelerinin Araştırılması

Investigation of the Antimicrobial Activities of Some Macrofungi Growing in the Kestel Region (Kadınhanı-Konya)

Aysegül Yaprak¹, Sinan Alkan², Erdoğan Güneş¹, Giyasettin Kaşik¹

¹Selçuk University, Science Faculty, Department of Biology, Konya, Türkiye

²Selçuk University, Çumra School of Applied Sciences, Organic Agriculture Administration Department, Konya, Türkiye

Öz

Bu araştırma Beykavağı (Kadınhanı-Konya) yöresinde Kestel ormanlarında yaygın olarak yetişen bazı makrofungusların antimikrobiyal aktivitelerini belirlemek amacıyla gerçekleştirilmiştir. Kullanılan materyal; *Boletopsis leucomelaena* (Pers.) Fayod, *Infundibulicybe geotropa* (Bull.) Harmaja, *Lactarius sanguifluus* (Paulet) Fr., *Russula delica* Fr., *Rhizopogon roseolus* (Corda) Th. Fr. türlerine ait bazidiyokarplardır. Elde edilen metanol ekstraktları DMSO (Dimetil sulfoxid)’da çözülmüş 25 mg/ml olarak hazırlanarak, on bir mikroorganizma suşuna karşı test edilmiştir. Test suşları olarak; *Escherichia coli* ATCC 25922, *Pseudomonas aeruginosa* ATCC, 27853, *Klebsiella pneumoniae* ATCC 70603, Metisilin dirençli *Staphylococcus aureus* (MRSA) ATCC 43300, *Bacillus cereus* ATCC 11778, *Salmonella enteritidis* ATCC 13076, *Sarcina lutea* ATCC 9341, *Salmonella typhimurium* NRRLE 4463, *Citrobacter freundii*, *Enterococcus faecalis* ATCC 29212, *Candida albicans* NRRL Y-417 olmak üzere on tane bakteri suşu ve bir maya suşu kullanılmıştır. Antimikrobiyal aktiviteyi tespit için Sıvı Mikrodilüsyon ve Agar Disk Difüzyon teknikleri uygulanmıştır. Araştırmada negatif(-) kontrol olarak DMSO, pozitif(+) kontrol olarak da ticari gentamisin kullanılmıştır. Çalışmada belirlenen sonuçlara göre, *B. leucomelaena* özütünün her iki teknikte de yalnızca *E. coli* suşuna antibakteriyel bir aktivite göstermediği, mikrodilüsyon tekniğinde ise test edilen tüm bakteri suşlarına 1.56 – 0.39 mg/ml dozlarında etkili olduğu, en yüksek aktivitesinin ise 0.39 mg/ml dozunda *S. aureus* suşunda gerçekleştiği tespit edilmiştir. Disk difüzyon tekniğinde ise en yüksek aktivite *S. aureus* ile *S. lutea*’da belirlenmiştir. *I. geotropa* ve *R. roseolus*’un bazı suşlara karşı antimikrobiyal etki gösterdiği görülmüştür. Gerçekleştirilen uygulamalarda en yüksek antimikrobiyal aktivitenin *B. leucomelaena* türünde olduğu belirlenmiştir.

Anahtar Kelimeler: Antimikrobiyal aktivite, agar disk difüzyon, sıvı mikrodilüsyon, makrofungus.

Abstract

This research was carried out to determine the antimicrobial activities of some macrofungi commonly growing in Kestel forests in the Beykavağı (Kadınhanı-Konya) region. For the materials, basidiocarps belonging to the species *Boletopsis leucomelaena* (Pers.) Fayod, *Infundibulicybe geotropa* (Bull.) Harmaja, *Lactarius sanguifluus* (Paulet) Fr., *Russula delica* Fr., *Rhizopogon roseolus* (Corda) Th. Fr. were used. There relevant materials were subjected to methanol extraction and then were dissolved in DMSO (Dimethyl sulfoxide). The solutions prepared at 25 mg/ml were assayed against eleven microbial strains. For test strains, *Escherichia coli* ATCC 25922, *Pseudomonas aeruginosa* ATCC, 27853, *Klebsiella pneumoniae* ATCC 70603, Methicillin-resistant *Staphylococcus aureus* (MRSA) ATCC 43300, *Bacillus cereus* ATCC 11778, *Salmonella enteritidis* ATCC 13076, *Sarcina lutea* ATCC 9341, *Salmonella typhimurium* NRRLE 4463, *Citrobacter freundii*, *Enterococcus faecalis* ATCC 29212 ten bacterial strains, including, *Candida albicans* NRRL Y-417,

*Sorumlu yazarın e-posta adresi: giyasettin@selcuk.edu.tr

Aysegül Yaprak orcid.org/0000-0003-1444-1926

Sinan Alkan orcid.org/0000-0001-7725-1957

Erdoğan Güneş orcid.org/0000-0003-2833-5710

Giyasettin Kaşik orcid.org/0000-0001-8304-6554



and one yeast strain were used. Antimicrobial activity was determined using liquid microdilution and agar disc diffusion techniques. Out of the experimental groups, commercially available gentamicin has been used as a positive (+) control and DMSO as a negative (-) control. Accordingly *B. leucomelaena* extract did not show antibacterial activity only against the *E. coli* strain in both techniques, it was effective against all bacterial strains tested in the microdilution technique at doses of 1.56 - 0.39 mg/ml, and at the dose of 0.39 mg/ml. The highest activity was found against *S. aureus*. In the disc diffusion technique, the highest activity was detected in *S. aureus* and *S. lutea*. It has been observed that *I. geotropa* and *R. roseolus* have antimicrobial effects against some strains. In the applications carried out, it was determined that the highest antimicrobial activity was in the *B. leucomelaena* species.

Keywords: Antimicrobial activity, agar disk diffusion, liquid microdilution, macrofungus.

1. Giriş

Mantarlar fotosentez yapamadıkları için dışarıdan besin alarak beslenirler, yani heterotrofurlar. Gidalarını hücre periferinde parçaladıktan sonra absorbsiyonla hücreye alırlar. Misel veya hif olarak bilinen hücreleri içerirler. Bu hücreler miselyumu, ortam koşulları oluşursa miselyum da gelişerek fruktifikasyon organını meydana getirir (Kaşik 2010).

Günümüzde ise makrofungusların fruktifikasyon organlarının gıda olarak değerlendirilmesi dışında mantarlar kefir, ekmek, bira, kahve ve çay gibi gıda maddelerinin üretilmesinde, bunlardan başka fruktifikasyon organları veya doğrudan mantarın metabolitleri ilaç olarak da kullanılabilirliktedir (Kaşik 2010). Bunun dışında kimya ve gıda sanayisinde itaconik asit, fumarik, glukonik ve sitrik asit ile invertaz, selülaz, lipaz, proteaz, pektinaz, amiloglukosidaz ve alfa-amilaz gibi enzimlerin elde edilmesinde mantarlar kullanılmaktadır. Mantarların üretikleri vitamin ve mikrotoksinler gibi sağlık açısından büyük önem taşıyan sekonder metabolitler sağlık sektörü açısından değerlidir (Sümer 2006, Kaşik 2010, Kavanagy 2014).

Mantarlar yüzyıllardır çeşitli medeniyetlerde besin olarak (Pekşen ve Kaplan, 2017) özellikle Uzak Doğu ülkelerinde bir gıda maddesi ve doğal ilaç kaynağı olarak tüketilmektedir. (Kalyoncu vd. 2008). Besin değerlerinin yanı sıra mantarlar, doğada organik madde yıkımında rol aldıklarından yetişikleri substrat içeriğine bağlı olarak bünyelerinde ve bulundukları ortamın içerisinde değişime neden olurlar (Sevindik vd. 2016).

Antimikrobiyal etki çalışmalarında farklı test tekniklerinin ve test mikroorganizmalarının kullanıldığı ancak bu test teknikleri içinde en uygun ve güvenilir tekniğin Disk Difüzyon Yöntemi olduğu ifade edilmektedir (Dülger vd. 1998, Dülger ve Arslan 1999). Çeşitli makrofungusların antimikrobiyal aktivite çalışmalarında üzerine farklı test mikroorganizmaları üzerine değişik çözgenlerden hazırlanan özütlерinin değişik etkiler oluşturdukları ortaya çıkarılmakla beraber, Disk Difüzyon Metodu kullanımlarında etanol ekstrelerinden daha iyi sonuç alındığı belirtilmektedir (Be-

nedict ve Brady 1972, Gücin ve Tamer 1986, Isaacson ve Platt 1989).

Makrofunguslar konusunda antimikrobiyal aktivite çalışmaları oldukça yoğunlaşmıştır. Rougieux (1963), *Terfezia boudieri* Chatin'den hazırlanmış olan özütlерin göz içi ve gözün kornea infeksiyonlarının amili *S. aureus*'un gelişimini engellediğini saptamasıyla mantarların antimikrobiyal etki çalışmaları adına dikkat çeken ilk çalışmayı yapmıştır. Coletto vd. (1994), 34 Basidiomycetes türü, Smânia vd. (1995), *Ganoderma applanatum* (Pers.) Pat.'türü, Dülger vd. (1998), *Macrolepiota procera* (Scop.) Singer türü, Dülger ve Arslan (1999), *Coriolus versicolor* (L. ex Fr.) Quel.'türü, Dülger ve Şen (1999), *Russula delica* Fr. türü, Dülger vd. (1999), *Tricholoma terreum* (Fr) Kummer'türü, Gerasimenya vd. (2002), Rusya'nın Moskova şehri dolaylarında toplamış oldukları *Pleurotus ostreatus* (Jacq.) P. Kumm.'türü, Efremenkova vd. (2003), *Coprinus* cinsinin Rusya'nın farklı yerlerinden topladıkları 6 farklı türü, Solak vd. (2006), *Clitocybe alexandri* (Gill.) Konr. ile *Rhizophagus roseolus* (Corda) Th. Fr.'türleri, Yamaç ve Bilgili (2006), 10 farklı makrofungus türü, Demirhan vd. (2007), *Pleurotus floridanus* Singer, *Schizophyllum commune* Fr. ve *Helvella leucomelaena* (Pers.) Nannf.'türleri, Türkoglu vd. (2007), *Russula delica* Fr. türü, Yaltıraç vd. (2009) *Russula delica*, Altuner ve Akata (2010), *Infundibulicybe geotropa* (Bull.) Harmaja, *Lactarius deliciosus* (L.) Gray, *Lactarius controversus* Pers., ve *Phellinus hartigii* (Allesch. ve Schnabl) Pat. türleri, Kalyoncu vd. (2010), bazı yabani makrofungus misellerinin üzerinde, Bekçi vd. (2011), *Morchella elata* Fr., *Morchella conica* Krombh, *Terfezia claveryi* Chatin türleri, Karaca vd. (2017), *Lentinula edodes* (Berk.) Sing. (Shiitake), *Lactarius deliciosus* ve *Ganoderma lucidum* (Curtis) P. Karst. türleri, Eren ve Akyüz (2018), *Terfezia boudieri*, *Picoa juniperi* Vittad., *Picoa lefebvrei* (Pat.) Maire, *Pleurotus ostreatus*, *P. floridanus*, *P. sajor-caju* (Fr.) Singer, *P. eryngii* (DC.) Quél. ve *Agaricus bisporus* (J.E. Lange) Imbach türleri, İnci ve Kırbağ (2018), *Terfezia claveryi* türü, İnci vd. (2019), *H. leucomelaena* türü hakkında antimikrobiyal özelliklerile ilgili çalışmalar yapılmışlardır. Çalışmaların genel sonuçlarına bakıldığında mantarların farklı seviyelerde antimikrobiyal etkiye sahip oldukları görülmüştür.

Kadınhanı'nda, ormanlık bölgelerin az olması mantar çeşitliliğini de sınırlandırmaktadır. Bu nedenle mantarların sıklıkla yetiştiği yer Kestel/Beykavağı yöresidir. Kestel bölgesinde halen yoğun şekilde su tutma kapasitesine sahip büyük bir yapay gölet bulunmaktadır. Bu sayede bölgenin iklim şartları da her geçen yıl değişerek alanın bitki örtüsü üzerinde de olumlu yönde etkilemektedir. Bölgedeki engebeli arazide yaygın bitki türleri olarak *Pinus nigra* Arn. subsp. *pallasiana* (Lamb.) Holmboe, *Sorbus torminalis* (L.) Crantz var. *torminalis*, *Juniperus foetidissima* Willd., *Quercus pubescens* Willd., *Cistus laurifolius* L., *Quercus ithaburensis* Decne. subsp. *macrolepis* (Kotschy) Hedge ve Yalt., *Cotoneaster nummularia* Fish. ve Mey., *Juniperus oxycedrus* L. subsp. *oxycedrus*, ağaç ve ağaççıkları, dere kenarlarında *Salix* sp. ve *Populus* sp. gibi ağaçları görmek mümkündür (Küçüködük vd. 2002, Küçüködük vd. 2023, Alkan vd. 2023). Kestel yöresindeki ormanlarda mantarlar ile ilgili olarak bir yüksek lisans tezi (Erdoğan, 2004) ile Pekak vd. 2011 ve Aydemir vd. 2022 çalışmaları yapılmıştır. Kestel ormanlarında yapılan çalışmalarda iki sınıf, 27 familyaya dağılan 106 takson belirlenmiştir. En fazla temsil edilen taksonun *Tricholomataceae* familyası olduğu belirtilmiştir (Erdoğan, 2004). Kestel yöresinde belirlenen bazı makrofunguslar ile ilgili antibakteriyel ve antifungal çalışmaların olmadığından dolayı bu araştırma Kestel (Beykavağı-Kadınhanı-Konya) ormanında yaygın olarak yetişen bazı yenen makrofungusların antibakteriyel ve antifungal aktivitelerini belirlemek amacıyla gerçekleştirılmıştır.

2. Gereç ve Yöntem

Araştırma için gerekli mantar örnekleri sonbahar mevsiminde Kestel bölgesinde (Beykavağı-Kadınhanı-Konya) yapılan arazi çalışması ile elde edilmiştir. Arazi çalışmalarında tespit edilen mantar örneklerinin bulunduğu koordinatları belirlenip, fruktifikasyon organları alüminyum folyoya sarılarak, muhafaza altına alınmıştır. Elde edilen mantar örneklerinin ekolojik ve morfolojik karakterlerinin yanı sıra habitat özellikleri ve elde edilen diğer veriler kaydedilmiştir. Her mantar örneği numaralandırılmıştır. Fungaryuma alüminyum folyo içinde getirilen makrofungus örneklerinin mikroskopik ve makroskopik özellikleri incelenerek ve mevcut kaynaklar yardımıyla (Breitenbach ve Kranzlin 1986, Ellis ve Ellis 1990, Breitenbach ve Kranzlin 1991, Gerhardt 1997, Breitenbach ve Kranzlin 2005, Kranzlin 2005) teşhisleri yapılmıştır. Elde edilen mantarların fungaryum örnekleri Selçuk Üniversitesi Mantarcılık Uygulama ve Araştırma Merkezi Müdürlüğü Fungaryumu'nda arşivlenmiştir.

Mantar özütlerinin hazırlanmasında dimetil sülfoxit ve metanol çözümleri, antimikrobiyal etki ve bakteri kültürlerinin hazırlanması çalışmalarının değerlendirilmesinde Mueller-Hinton Broth ve Mueller-Hinton Agar besiyerleri kullanılmıştır. Ekstrelerin antimikrobiyal etkilerinin araştırıldığı çalışmalarla kontrol amaçlı Gentamisin (Genta®), ekstrelerin ve kontrol antibiotiğinin sulandırılmasında Phosphate Buffered Saline (PBS) tabletleri, mikroorganizmaların canlılığını göstermek için 2,3,5- Trifentetrazol-5-klorid (TTC) kullanılmıştır (Zengin vd, 2015).

Kullanılan çözümlerin özellikleri; Metanol (CH_3OH , kaynama noktası 64.6 °C, donma noktası -98 °C,), Dimetil sülfoxit (DMSO) [$(\text{CH}_3)_2\text{SO}$, kaynama noktası 189 °C, donma noktası -20 °C,] olarak belirtilmiştir (Uyar 1992).

Mantar ekstrelerinin antimikrobiyal etkilerinin belirlenmesi adına yapılmış çalışmalarla hayvan, insan ile gıdalar üzerinde patojen olan mikroorganizmalar tercih edilmiştir. Çalışmada *Escherichia coli* ATCC 25922, *Pseudomonas aeruginosa* ATCC, 27853, *Klebsiella pneumoniae* ATCC 70603, Metilsilin dirençli *Staphylococcus aureus* (MRSA) ATCC 43300, *Bacillus cereus* ATCC 11778, *Salmonella enteritidis* ATCC 13076, *Sarcina lutea* ATCC 9341, *Salmonella typhimurium* NRRLE 4463, *Citrobacter freundii*, *Enterococcus faecalis* ATCC 29212, *Candida albicans* NRRL Y-417 olmak üzere on tane bakteri suyu ve bir maya suyu kullanılmış olup, antimikrobiyal çalışma Selçuk Üniversitesi Fen Fakültesi Biyoloji Bölümü, Mikrobiyoloji Araştırma Laboratuvarı'nda gerçekleştirilmiştir.

2.1. Mantar Ekstraktlarının Hazırlanması

Araziden toplanılan mantarlar temizlenip kurutulmaya tabi tutulmuş, kurutulan mantar örnekleri mekanik bir öğütücü yardımıyla öğütülmüştür. Daha sonra ekstraksiyon işlemi Soxhlet cihazında (QUALITEC) yapılmıştır. Hassas terazide (KERN PLJ) 5 g tartılan numuneler, 100 ml metanol çözgeninin kullanıldığı Soxhlet cihazında 50 °C'de 4 saat süreyle ekstraksiyon işlemeye tabi tutularak, özütleri elde edilmiştir. Elde edilen özütler Whatman No:1 filtre kağıdından geçirilerek filtre edilmiş ve daha sonra da azaltılmış basınç altında 50 °C'de rotary evaporatörde (ISOLAB) evapore edilmeye başlanmıştır. 64.5 °C'de çözücü ekstraktan ayrılmaya başlamıştır. Kalan çözümlünün uçması için ekstraktlar 48 saat etüde 40 °C'de bekletilmiştir. Bu işlemin ardından -20 °C'de dondurucuda saklanmıştır. Ekstreler antimikrobiyal etkileri yönünden inceleneceği sırada, Disk Difüzyon ve Sıvı Mikrodilüsyon yönteminde kullanılmak üzere DMSO'da çözülmüş 25 mg/ml olacak şekilde stokları hazırlanmış ve stoklar enjektör filtrelerden geçirilerek steril

edilmişlerdir ve kullanımlana kadar + 4 °C de saklanmışlardır (Zengin vd, 2015).

2.2. Besiyerlerin Hazırlanması

Antimikrobiyal aktivitenin belirlenmesi amacıyla kullanılan Sıvı Mikrodilüsyon tekniğinde Mueller-Hinton Broth besiyeri, disk difüzyon tekniğinde ise Mueller-Hinton Agar kullanılmıştır. Bakterilerin canlandırılmasında ise Brain Heart Infüzyon Broth (BHIB) besiyeri tercih edilmiştir. Brain Heart Infüzyon Broth (BHIB) ve Mueller-Hinton Broth besiyeri saf suda eritildikten sonra otoklavda 121 °C'de 15 dk. steril edilmiştir.

2.3. Antibakteriyel Aktivitenin Belirlenmesi

2.3.1. Disk Difüzyon Yöntemi

Öncelikle Stok bakteri ve maya suşları derin dondurucudan çıkarılmıştır. Suşlar inoküle edildikten sonra 37°C'de 18-24 saat inkübe edilerek taze kültürleri hazırlanmıştır. Kültürlerin yoğunluğu McFarland standart bulanıklık derecesine göre 0.5 olacak şekilde Densimat (Biosan) dansitometre cihazında ayarlanarak bakteriyel süspansiyon hazırlanmıştır. Daha sonra bakteri kültür solüsyonlarından 100 µl alınarak besiyerlerinin üzerine yayılmıştır. Daha önceden hazırlanan kendi çözücü içinde 25 mg/ml olan her ekstraktın steril solüsyonları 6 mm çapında steril antibiyotik diskler 20'ser µl emdirilerek, 37°C'de 18-24 saat inkübe edilmiştir. Daha sonrasında oluşan inhibisyon tabakalarının çapı ölçülerek kayıt işlemi yapılmıştır(Sökmen vd. 1999)

2.3.2. Sıvı Mikrodilüsyon Yöntemi

96 kuyucuklu mikrotitrasyon plakların her bir kuyucوغuna, hazırlanan Mueller-Hinton Besiyeri'nden 100'er µl dağıtıldıktan sonra stok haldeki ekstraktlardan plakların ilk kuyucuklarına 100'er µl konulmuştur. Daha sonra ilk kuyucuktan başlanılarak 100 µl'lik hacimler alınıp, bir sonraki kuyucuga ilave edilerek yarı yarıya sulandırmaları yapılmıştır. 0.5 McFarland bulanıklığında bakteri süspansiyonları hazırlanmış, gerekli sulandırma yapılarak her kuyucuktaki inokulumun son konsantrasyonu 5×10^5 kob/ml olacak şekilde her kuyucuga 100 µl eklenmiştir. Plakların son kuyucوغuna kontrol amaçlı herhangi bir kültür ya da ekstract konulmamıştır. Son olarak Plaklar 18-24 saat 37°C'de inkübe edilmiştir. İnkübasyon süresi bitiminde kuyucuklara 20 µl 2,3,5-trifeniltetrazolyum klorid eklenilerek 30 dk. daha inkübasyona bırakılmıştır. Plaklarda gözle görülür bir üreme olmamış, pembe kırmızı renkli olmayan son kuyucuk mini-

Cizelge 1. Tespit edilen makrofungusların sistematigi ve lokaliteleri.

Tür ismi	Türkçe Bilimsel İsmi (Sesli vd. 2020)	Sistematigi	Toplama Tarihi, Substrat, Koordinat	Fungaryum Numarası
<i>B. leucomelaena</i>	Karadibidelik	Bankeraceae, Thelephorales, <i>Agaricomycetes</i> , <i>Agaricomycotina</i> , <i>Basidiomycota</i> , <i>Myceteae</i> (Fungi)	10.11.2020 Karışık Orman 38°08'10.69"K 32°15'34.26"D	FN5416
<i>I. geotropa</i>	Etçe	Incertae sedis, <i>Agaricales</i> ,	09.11.2020 Karışık Orman 38°08'20.99"K 32°15'23.00"D	FN5415
<i>L. sanguifluus</i>	Solgunkanlıca	<i>Russulaceae</i> , <i>Russulales</i> ,	09.11.2020 Karışık Orman 38°08'22.45"K 32°15'24.67"D	FN5414
<i>R. roseolus</i>	Altavşanböbreği	<i>Rhizopogonaceae</i> , <i>Boletales</i> ,	10.11.2020 Karışık Orman 38°07'20.79"K 32°15'38.34"D	FN5418
<i>R. delica</i>	Akçıntılar	<i>Russulaceae</i> , <i>Russulales</i> ,	10.11.2020 Karışık Orman 38°08'11.04"K 32°15'29.05"D	FN5417

mum inhibisyon konsantrasyonu (MİK) olarak belirlenmiştir (Zengin vd., 2015).

3. Bulgular

Yapılan arazi çalışmalarında Kestel (Kadınhanı-Konya) ormanında yaygın olarak bulunan mantar örneklerinin teşhis sonucunda *Boletopsis leucomelaena* (Pers.) Fayod, *Infundibulicybe geotropa* (Bull.) Harmaja, *Lactarius sanguifluus* (Pouillet) Fr., *Russula delica* Fr. ve *Rhizopogon roseolus* (Corda) Th. Fr. türleri tespit edilmiştir (Şekil 1, Çizelge 1).

Çalışmada Kestel (Kadınhanı-Konya) bölgesinde yaygın olarak yetiştiği tespit edilen makrofungalardan *B. leucomelaena*, *I. geotropa*, *L. sanguifluus*, *R. roseolus* ve *R. delica* türlerinin metanol ekstraktlarının Sıvı Mikrodilüsyon metodunda elde edilen antimikrobiyal aktivite sonuçları Çizelge 2'de,

Disk Difüzyon metodundaki antimikrobiyal aktivite sonuçları ise Çizelge 3'de verilmiştir.

4. Tartışma

Çalışmada elde edilen bulgular literatür ile karşılaştırılmıştır. *Russula delica* ile yapılan antimikrobiyal aktivite çalışmalarında (Dülger ve Şen, 1999), mantarın başta *Corynebacterium xerosis* CCM 2824 ve *Listeria monocytogenes* ATCC 19117 olmak üzere bazı Gram pozitif ve Gram negatif bakteriler ile bazı mayalara özellikle *Kluyveromyces fragilis* üzerine bir antimikrobiyal etki içerdigini belirlemiştir. Başka bir çalışmada ise, Türkoglu vd. (2007) tarafından *R. delica*'nın antimikrobiyal etkisi, Agar Disk Difüzyon metodunda yedi Gram(-), altı Gram (+) bakteri ile bir maya üzerine incelenmiştir. *R. delica* Gram negatif bakterilere karşı etkili



Şekil 1. Arazi çalışmalarında tespit edilen ve materyal olarak kullanılan makrofungalardır.

olmadığı, *Micrococcus luteus* ve *Micrococcus flavus*' un da içinde bulunduğu Gram pozitif bakterilere karşı yüksek inhibe edici etki gösterdiği gözlenmiştir. Zonların maksimum değerlerinin 15 – 20 mm civarında olduğu tespit edilmiştir. Yine Yaltrak vd. (2009) *R. delica*'nın antimikrobiyal ve antioksidan etkilerini araştırdıkları çalışmada, kullanılan dokuz mikroorganizma suşuna karşı antimikrobiyal etkisinin olduğunu tespit etmişlerdir.

R. delica ile yaptığımız çalışmada ise; kullandığımız test mikroorganizmalarına karşı potansiyel bir antibakteriyel ve antifungal bir aktiviteye sahip olmadığı belirlenmiştir (Çizelge 2). *R. delica*'nın, farklı çalışmalarında antimikrobiyal etki gösterdiği aynı türe ait farklı suşlara çalışmamızda etki göstermediği tespit edilmiştir.

Solak vd. (2006), çalışmalarında *Clitocybe alexandri* ve *R. roseolus*'un farklı çözgenler kullanılarak hazırlanmış özütlerinin Agar Disk Difüzyon tekniği ile bazı mikroorganizmalar üzerine çalışıkları bir çalışmada ise her iki mantarın metanolik ekstrelerinin *E. coli* (15-13 mm), *Bacillus subtilis* (25-18 mm) ve *Enterobacter aerogenes* (25-16 mm)'e karşı antimikrobiyal etkisi saptamışlardır. Aynı zamanda *C. alexandri*'nin etilasetat özütünün *Saccharomyces cerevisiae* (12 mm) ve *C. albicans* (14 mm) mayaları üzerine etkisinin bulunduğu belirtmişlerdir.

R. roseolus özütü ile çalışmamızda ise, Mikrodilüsyon teknlığında *C. freundii*, *E. faecalis* ve *S. lutea* suşlarına karşı sırasıyla 1.56, 0.78 ve 0.39 mg/ ml dozlarında antibakteriyel aktivite tespit edilirken, en etkili olduğu suş ise 0.19 mg/ ml dozuyla *S. aureus* olduğu belirlenmiştir. Yine bu özütün her iki teknikte de antifungal bir aktiviteye sahip olmadığı görülmüştür (Çizelge 2, 3).

Altuner ve Akata (2010), bazı makrofungus ekstraktlarının antimikrobiyal aktivitesi isimli çalışmalarında, *I. geotropa*, *Lactarius controversus* Pers., *L. deliciosus* ve *Phellinus hartigii* (Allesch. & Schnabl) Pat. türlerine ait antimikrobiyal etkileri incelemiştir. Netice olarak, *Shigella flexneri* üzerine tüm ekstrelerin, *P. hartigii* hariç tüm ekstrelerin *P. aeruginosa* üzerine antibakteriyel etkiye sahip oldukları gözlemlenmiştir.

I. geotropa özütünün ise test edilen mikroorganizmalar arasında yalnızca *C. freundii* suşuna Sıvı Mikrodilüsyon teknlığında 1.56 mg/ml dozunda antimikrobiyal aktivite gösterdiği görülmüştür (Çizelge 2).

Lactarius sanguifluus özütü sonuçları incelendiğinde ise her iki teknikte de test edilen mikroorganizmalara karşı potansiyel bir antibakteriyel ve antifungal aktiviteye sahip olmadığı belirlenmiştir (Çizelge 2, 3).

Elde edilen literatür taramasında *B. leucomelaena* ekstraktı ile ilgili bir bulguya rastlanmamıştır.

Çizelge 2. Sıvı Mikrodilüsyon yöntemindeki sonuçlar (mg/ml).

Test mikroorganizmaları	<i>B. leucomelaena</i>	<i>I. geotropa</i>	<i>L. sanguifluus</i>	<i>R. delica</i>	<i>R. roseolus</i>
<i>E. coli</i> ATCC 25922	-	-	-	-	-
<i>Pseudomonas</i> ATCC 27853	0.78	-	-	-	-
<i>K. pneumonia</i> ATCC 70603	1.56	-	-	-	-
<i>Metisilin dirençli S. aureus (MSSA)</i> ATCC 43300	0.39	-	-	-	0.19
<i>S. enteritidis</i> ATCC 13076	1.56	-	-	-	-
<i>S. lutea</i> ATCC 9341	0.78	-	-	-	0.39
<i>E. faecalis</i> ATCC 29212	1.56	-	-	-	0.78
<i>S. typhimurium</i> NRRLE 4463	1.56	-	-	-	-
<i>B. cereus</i> ATCC 11778	1.56	-	-	-	-
<i>C. freundii</i>	0.78	1.56	-	-	1.56
<i>C. albicans</i> NRRL Y-417	1.56	-	-	-	-

Çizelge 3. Disk Difüzyon yöntemindeki sonuçlar(Zon çapları mm).

Test mikroorganizmaları	B. leucomelaena	I. geotropa	L. sanguifluus	R.delica	R. roseolus	Gentamisin
<i>E. coli</i> ATCC 25922	-	-	-	-	-	23
<i>Pseudomonas</i> ATCC 27853	7	-	-	-	-	22
<i>K. pneumonia</i> ATCC 70603	-	-	-	-	-	15
Metisilin dirençli <i>S.aureus</i> (MSSA) ATCC 43300	10	-	-	-	8	24
<i>S. enteritidis</i> ATCC 13076	-	-	-	-	-	25
<i>S.lutea</i> ATCC 9341	10	-	-	-	-	24
<i>E.faecalis</i> ATCC 29212	7	-	-	-	7	20
<i>S. typhimurium</i> NRRLE 4463	-	-	-	-	-	21
<i>B. cereus</i> ATCC 11778	-	-	-	-	-	23
<i>C. freundii</i>	-	-	-	-	-	23
<i>C. albicans</i> NRRL Y-417	-	-	-	-	-	25

Çalışmamızın sonuçlarına göre, *B. leucomelaena* ekstraktının her iki teknikte yalnızca *E. coli*'ye karşı antibakteriyel bir aktivite göstermediği, Mikrodilüsyon tekniğinde çalışmada test edilen bakteri suşlarının tümüne 1.56 – 0.39 mg/ml dozlarında etkili olduğu, en yüksek aktivitenin ise 0.39 mg/ml dozunda *S. aureus*'a karşı olduğu belirlenmiştir (Çizelge 2).

İncelenen beş makrofungus türünden *B. leucomelaena* ve *R. roseolus* türlerinin test mikroorganizmaları üzerinde antimikrobiyal etkisinin olduğu tespit edilmiştir. Diğer mantar türlerinden edilen ekstraktların etkisi gözlenmemiştir (Çizelge 2,3). Bu durumun suşların farklı direnç seviyelerinden ve kullanılan yöntemden kaynaklandığı varsayılmıştır.

Test mikroorganizmalarına antimikrobiyal aktivite göstermeyen mantar türleri besin olarak değerlendirilmekte olup, farklı çözücü ile elde edilmiş özütlerin farklı mikroorganizmalar açısından etkileri araştırılabilir. Çalışmada antimikrobiyal etkisi tespit edilen makrofungusların antibakteriyel özellikleri dikkate alınarak sağlık sektöründe potansiyel kaynak olarak değerlendirilmesi ve benzer çalışmalar için literatür veri kaynağı olarak kullanılması uygun olacaktır.

5. Teşekkür

Bu çalışma Selçuk Üniversitesi BAP Koordinatörlüğünde desteklenmiş olup, teşekkürlerimizi sunarız(Proje No: 20201060).

Yazarlık Katkı Beyanı

Yazar 1: Çalışmanın tüm aşamalarına katkısı vardır.

Yazar 2: Arazi çalışmaları, tür teşhisleri ve ekstract elde edilmesi

Yazar 3: Antimikrobiyal denemelerin yapılması

Yazar 4: Fikir sahibi ve tüm aşamaların gerçekleştirilmesi

Etik Standartlar Bildirgesi

Yazarlar tüm etik standartlara uyduklarını beyan ederler.

Çıkar Çatışması Beyanı

Yazarların bu makalenin içeriğiyle ilgili olarak beyan edecekleri hiçbir çıkar çatışması yoktur.

6. Kaynaklar

Alkan, S., Kaşık, G., ÖzTÜRK, C. 2023. Beykavağı/Kestel mantarları. Sayfa :19-33, "Kadınhanı İlçesi Çevre, Şehircilik ve İklim Değişikliği", ISBN: 978-625-00-1834-7 (Editörler; Küçükdağ, Y., Özcan, K., Arabacı, C.), Optimum Basım San. Ve Tic. Ltd. Şti. İstanbul.

Altuner, EM., Akata, I. 2010. Antimicrobial activity of some macrofungi extracts. Sakarya Üniversitesi Fen Bilimleri Dergisi, 14 (1), 45-49.

- Aydemir, RB., Kaşık, G., Öztürk, C., Alkan, S. 2022.** Kestel bölgesinde(Kadınhanı-Konya) yaygın olarak bulunan bazı makromantolarların mineral kompozisyonu. Mantar Dergisi, Aralık 13 (Özel Sayı)4-58. <https://doi.org/10.30708/mantar.1206667>.
- Bekçi, H., Altınsoy, B., Karakaya, S., Onbaşılı, D., Yuvalı Çelik, G. 2011.** Kastamonu yöresinden toplanan bazı makrofungusların antimikrobiyal aktivitesi. Kastamonu Üniversitesi Orman Fakültesi Dergisi, 11 (2), 18-10.
- Benedict, RG., Brady, LR. 1972.** Antimicrobial activity of mushroom metabolites. Journal Of Pharmaceutical Sciences, 61 (11), 1820-1821. <https://doi.org/10.1002/jps.2600611130>
- Breitenbach J., Kranzlin, F. 1986.** Fungi of Switzerland, Volume 2. Verlag Mykologia CH-6000 Luzern 9, Switzerland.
- Breitenbach J., Kranzlin, F. 1991.** Fungi of Switzerland, Volume 3., Verlag Mykologia CH-6000 Luzern 9, Switzerland.
- Breitenbach J., Kranzlin, F. 2005.** Fungi of Switzerland, Volume 5. Verlag Mykologia CH-6000 Luzern 9, Switzerland.
- Coletto, MAB., Pizzinat, M., Rossi, M. 1994.** Antibiotic activity in basidiomycetes. VII. Antibiotic activity of mycelia and cultural filtrates. Allionia, 32 (79-83). <https://doi.org/10.4308/hjb.17.2.63>
- Demirhan, A., Yeşil, ÖF., Yıldız, A., Gül, K. 2007.** Bazı makrofungus türlerinin antimikrobiyal aktiviteleri üzerine bir araştırma. Fırat Üniversitesi Fen Ve Müh. Bil. Dergisi, 19 (4), 425-433. <https://doi.org/10.30708/mantar.451294>
- Dülger, B., Yılmaz, F., Gücin, F. 1998.** *Macrolepiota procera* (Scop. Ex.Fr.) Sing. makrofungusunun antimikrobiyal aktivitesi. Kükkem Dergisi, 21 (1), 7-12.
- Dülger, B., Arslan, Ü. 1999.** *Coriolus versicolor* (L. Ex Fr.) Quel. makrofungusunun antimikrobiyal aktivitesi, Tr. J. Of Biology, 23 (385-392).
- Dülger, B., Şen, F. 1999.** *Russula delica* Fr. makrofungusunun antimikrobiyal aktivitesi. Tr.J. Of Biology, 23, 127-133. <https://journals.tubitak.gov.tr/biology/vol23/iss1/14>
- Dülger, B., Yılmaz, F., Gücin, F. 1999.** *Tricholoma terreum* (Fr.) Kummer "Cincile" makrofungusunun antimikrobiyal aktivitesi. Çev-Kor, 30 (8), 13-17.
- Efremenkova, OV., Ershova, EY., Tolstych, IV., Zenkova, VA., Dudnik, YV. 2003.** Antimicrobial activity of medicinal mushrooms from the genus Coprinus (Fr.) S. F. Gray (Agaricomycetidae). International Journal of Medicinal Mushrooms, 5, 37-41. DOI: 10.1615/InterJMedicMush.v5.i1.50
- Ellis, MB., Ellis, JP. 1990.** Fungi without gills (Hymenomycetes and Gasteromycetes). London, Chapman And Hill.
- Eren, A., Akyüz, M. 2018.** Bazı makrofungus misellerinin antimikrobiyal aktivitelerinin belirlenmesi. Mantar Dergisi, 9 (2), 196-205. Doi:[10.30708/mantar.451294](https://doi.org/10.30708/mantar.451294)
- Gerasimena, VP., Efremenkova, OV., Kamzolkina, OV., Bogush, TA., Tolstych, IV., Zenkova, VA. 2002.** Antimicrobial and antitoxic action of edible and medicinal mushroom *Pleurotus ostreatus* (Jacq.: Fr.) Kumm. extracts. International Journal of Medicinal Mushrooms, 4 (127-132). DOI: 10.1615/IntJMedMushr.v4.i2.50
- Gerhardt, E. 1997.** Der große BLV pilz führer für unterwegs. München, BLV.
- Gücin, F., Tamer, AÜ. 1986.** *Terfezia boudieri* Chatin " Domalan " nin antibiyotik aktivitesi üzerinde invitro arastirmalar. VIII. Ulusal Biyoloji Kongresi; Zooloji, Hidrobiyoloji, Temel Ve Endüstriyel Mikrobiyoloji Tebligleri, 107-113.
- İnci, Ş., Kırbağ, S. 2018.** *Terfezia claveryi* Chatin'in besinsel içeriği, antioksidan ve antimikrobiyal aktivitesi. Artvin Çoruh Üniversitesi, Orman Fakültesi Dergisi, 19 (2), 132-143. <https://doi.org/10.17474/artvinofd.375460>
- İnci, Ş., Dalkılıç, L., Dalkılıç, S., Kırbağ, S. 2019.** *Helvella leucomelaena* (Pers.) Nannf.'nin antimikrobiyal ve antioksidan etkisi. Artvin Çoruh Üniversitesi Orman Fakültesi Dergisi, 20 (2), 249-253. <https://doi.org/10.17474/artvinofd.601528>
- Isaacson, DM., Platt, TB. 1989.** Methods for bioassay of antibiotics. in: Practical Handbook of Microbiology, U.S.A., Harper And Coolins, P. 621-630.
- Kalyoncu, F., Oskay, M., Kalmış, E. 2010.** Bazı yabani makrofungus misellerinin antimikrobiyal aktivitelerinin belirlenmesi. Mantar Dergisi, 1 (1), 1-8.
- Kalyoncu, F., Kalmış, E., Solak, M. 2008.** Bazı makrofungus türlerine ait misellerin farklı kültür ortamlardaki gelişim hızlarının belirlenmesi, Süleyman Demirel Üniversitesi Fen Bilimleri Enstitüsü Dergisi, 12 (2).
- Karaca, B., Akata, I., Cihan, AÇ. 2017.** *Lentinus edodes*, *Lactarius delicious* ve *Ganoderma lucidum*'un antibiyofilm ve antimikrobiyal etkinlikleri. Kastamonu Üniversitesi Orman Fakültesi Dergisi, 17 (4), 660-668. <https://doi.org/10.17475/kastorman.341971>
- Kaşık, G. 2010.** Mantar bilimi. Marifet Matbaa Ve Kağıtçılık.
- Kavanagy, K. 2014.** Fungi Biology and Applications. (çeviri editörü: Ünal Özakça D.) Wiley-Blackwell,
- Kranzlin, F. 2005.** Fungi of Switzerland. Volume 6. Verlag Mykologia CH-6000 Luzern 9, Switzerland.
- Küçüködük, M., Ketenoglu, O., Serin, M., Şanda, MA. 2002.** Beykavağı (Kestel) Dağı (Kadınhanı-Konya) ve Çevresinin Vejetasyonu, Selçuk Üniversitesi Fen Fakültesi Fen Dergisi, 1, 19, 51-61.
- Küçüködük, M., Ketenoglu, O., Serin, M., Şanda, MA. 2023.** Beykavağı/Kestel'in Orman ve Step Vejetasyonu. Sayfa 5-18, "Kadınhanı İlçesi Çevre, Şehircilik ve İklim Değişikliği", ISBN: 978-625-00-1834-7 (Editörler;Küçükdağ,Y.,Özcan, K., Arabacı, C.), OPTIMUM Basım San. ve Tic. Ltd. Şti. İstanbul.

- Pekak, C., Kaşık, G., Eroğlu, G.** 2011. Chemical composition of two *Lactarius* species of wild growing in Kestel Kadınhanı-Konya district. Mantar Dergisi, Nisan-Ekim 2(1-2)57-61.
- Pekşen, A., Kaplan, M.** 2017. Ordu ilinin ekonomik öneme sahip yenilebilen doğa mantarları, Akademik Ziraat Dergisi, 6, 335-342.
- Rougieux, R.** 1963. Actions antibiotiques et stimulantes de la truffe du desert (*Terfezia boudieri*). Ann. Inst. Pasteur, 105, 315-318.
- Sesli, E., Asan, A., Selçuk, F., Abacı Günyar, Ö., Akata, I., Akgül, H., Aktaş, S., Alkan, S., Allı, H., Aydoğdu, H., Berikten, D., Demirel, K., Demirel, R., Doğan, HH., Erdoğdu, M., Ergül, CC., Eroğlu, G., Giray, G., Halik Uztan, A., Kabaktepe, Ş., Kadaifçiler, D., Kalyoncu, F., Karaltı, İ., Kaşık, G., Kaya, A., Keleş, A., Kirbağ, S., Kivanç, M., Ocak, İ., Ökten, S., Özkal, E., Öztürk, C., Sevindik, M., Şen, B., Şen, İ., Türkkekul, İ., Ulukapı, M., Uzun, Y., Uzun, Y., Yoltaş, A.** 2020. Türkiye mantarları listesi. Nurtan Ambalaj ve Matbaacılık San. Ve Tic. A.Ş., Ali Nihat Gökyiğit Vakfı Yayınları, P. 1177.
- Sevindik, M., Akgül, H., Günal, S., Doğan, M.** 2016. Pleurotus ostreatus' un doğal ve kültür formlarının antimikrobiyal aktiviteleri ve mineral madde içeriklerinin belirlenmesi, Kastamonu University Journal of Forestry Faculty, 16 (1). <https://doi.org/10.17475/kujff.27130>
- Smânia, A., Delle Monache, F., Smânia, E., Gil, M., Benchetrit, L., Cruz, F.** 1995. Antibacterial activity of a substance produced by the fungus *Pycnoporus sanguineus* (Fr.) Murr. Journal of Ethnopharmacology, 45(3), 177-181.[https://doi.org/10.1016/0378-8741\(94\)01212-i](https://doi.org/10.1016/0378-8741(94)01212-i)
- Solak, MH., Kalmış, E., Sağlam, H., Kalyoncu, F.** 2006. Antimicrobial activity of two wild mushrooms *Clitocybe alexandri* (Gill.) Konr. and *Rhizopogon roseolus* (Corda) T.M. fries collected from Turkey. Phytother. Res., 20, 1085-1087. DOI: 10.1002/ptr.2002
- Sökmen, A., Jones, BM., Erturk, M.** 1999. The in vitro antibacterial activity of Turkish medicinal plants, Journal of ethnopharmacology, 67 (1), 79-86. DOI: 10.1016/s0378-8741(98)00189-5
- Sümer, S.** 2006. Genel mikoloji. İstanbul, Nobel Yayın Dağıtım.
- Türkoğlu, A., Duru, ME., Mercan, N.** 2007. Antioxidant and antimicrobial activity of *Russula delica* Fr. an edible wild mushroom. Eurasian Journal of Analytical Chemistry, 2 (1), 54-67. DOI: 10.12973/ejac/78055
- Uyar, T.** 1992. Organik kimya. Güneş Kitabevi.
- Yaltrıak, T., Aslim, B., Öztürk, S., Allı, H.** 2009. Antimicrobial and antioxidant activities of *Russula delica* Fr.. Food and Chemical Toxicology, 47, 2052-2056. <https://doi.org/10.1016/j.fct.2009.05.029>
- Yamaç, M., Bilgili, F.** 2006. Antimicrobial activities of fruit bodies and/or mycelial cultures of some mushroom isolates. Pharmaceutical Biology, 44 (9), 660-667. <https://doi.org/10.1080/13880200601006897>
- Zengin, G., Sarıkürkü, C., Güneş, E., Uysal, A., Ceylan, R., Uysal, S., Güngör, H., Aktümsek, A.** 2015. Two Ganoderma species: profiling of phenolic compounds by HPLC-DAD, antioxidant, antimicrobial and inhibitory activities on key enzymes linked to diabetes mellitus, Alzheimer's disease and skin disorders, Food & Function, 6 (8), 2794-2802. <https://doi.org/10.1039/c5fo00665a>

Makalenin Adı:**Yazarların adı (makaledeki sırayla):**

Biz aşağıda imzaları bulunan yazarlar, sunduğumuz makalenin orijinal olduğunu; başka bir dergiye yayınlanmak üzere verilmediğini, daha önce yayınlanmadığını, eğer, tümüyle ya da bir bölümü yayınlandı ise yukarıda adı geçen dergide yayınlanabilmesi için gerekli her türlü iznin alındığını ve orijinal telif hakkı devri formu ile birlikte *Karaelmas Fen ve Mühendislik Dergisi Editörlüğü*'ne gönderildiğini garanti ederiz.

Makalenin telif hakkından feragat etmeyi kabul ederek sorumluluğu üstlenir ve imza ederiz.

Bu vesileyle makalenin telif hakkı Zonguldak Bülent Ecevit Üniversitesi'ne devredilmiştir.

Karaelmas Fen ve Mühendislik Dergisi Editörlüğü makalenin yayınlanabilmesi konusunda yetkili kılınmıştır. Bununla birlikte yazarların aşağıdaki hakları saklıdır:

1. Telif Hakkı dışında kalan patent vb. bütün tescil edilmiş haklar.
2. Yazarın gelecekteki kitaplar ve dersler gibi çalışmalarında; makalenin tümü ya da bir bölümünü ücret ödemeksiz kullanma hakkı.
3. Makaleyi satmamak koşulu ile kendi amaçları için çoğaltma hakkı.

Bütün yazarlar tarafından imzalanmak üzere:

Yazar Adı : (Yazarlar sırayla yazılacaktır)

Tarih : .../.../.....

İmza :

Yazar Adı :

Tarih : .../.../.....

İmza:

Yazar Adı :

Tarih : .../.../.....

İmza:

Yazar Adı :

Tarih : .../.../.....

İmza:

Yazar Adı :

Tarih : .../.../.....

İmza:

Yazar Adı :

Tarih : .../.../.....

İmza:

Makaleyi gönderen sorumlu yazarın;

Adı-Soyadı:

Yazışma Adresi : (**Sorumlu yazarın ait posta gönderim adresi**)

Telefonu : (**Sorumlu yazarla ulaşılabilcek telefon numarası**)

Belge Geçer : (**Sorumlu yazarla ulaşılabilcek faks numarası**)

E-posta : (**Sorumlu yazarın e-mail adresi**)

Manuscript Title:

Full names of all authors (in order to appear on manuscript)

The undersigned authors, we guarantee that our submitted manuscript is original work; it has not been published and is not being submitted or considered for publication elsewhere, if, in whole or part of the publication of the magazine was published for the above-mentioned receipt of all necessary permits and was sent to *Editorial Office of Karaelmas Fen ve Mühendislik Dergisi* with copyright transfer form.

We agree to waive the right to assume the responsibility of the copyright of the article and thank signature.

This article is hereby transferred to the copyright of Zonguldak Bülent Ecevit University.

Karaelmas Fen ve Mühendislik Dergisi Editor of the publication of the article is authorized.

However, the authors reserve the following rights:

1. All proprietary rights Copyright outside, such as patent.
2. to use, free of charge, all parts of this article for the author's future works in books, lectures.
3. the right to reproduce the article for their own purposes provided the copies are not offered for sale.

To be signed by all authors:

Author Name : **(The authors will be written in the order)** Date : .../.../..... Signature :

Author Name : Date : .../.../..... Signature :

Author Name : Date : .../.../..... Signature :

Author Name : Date : .../.../..... Signature :

Author Name : Date : .../.../..... Signature :

Author Name : Date : .../.../..... Signature :

Corresponding author's

Name-Surname:

Address : **(Corresponding author's mail address)**

Phone : **(Corresponding author's contact phone number)**

Fax : **(Corresponding author's contact fax number)**

E-mail : **(Corresponding author's e-mail address)**